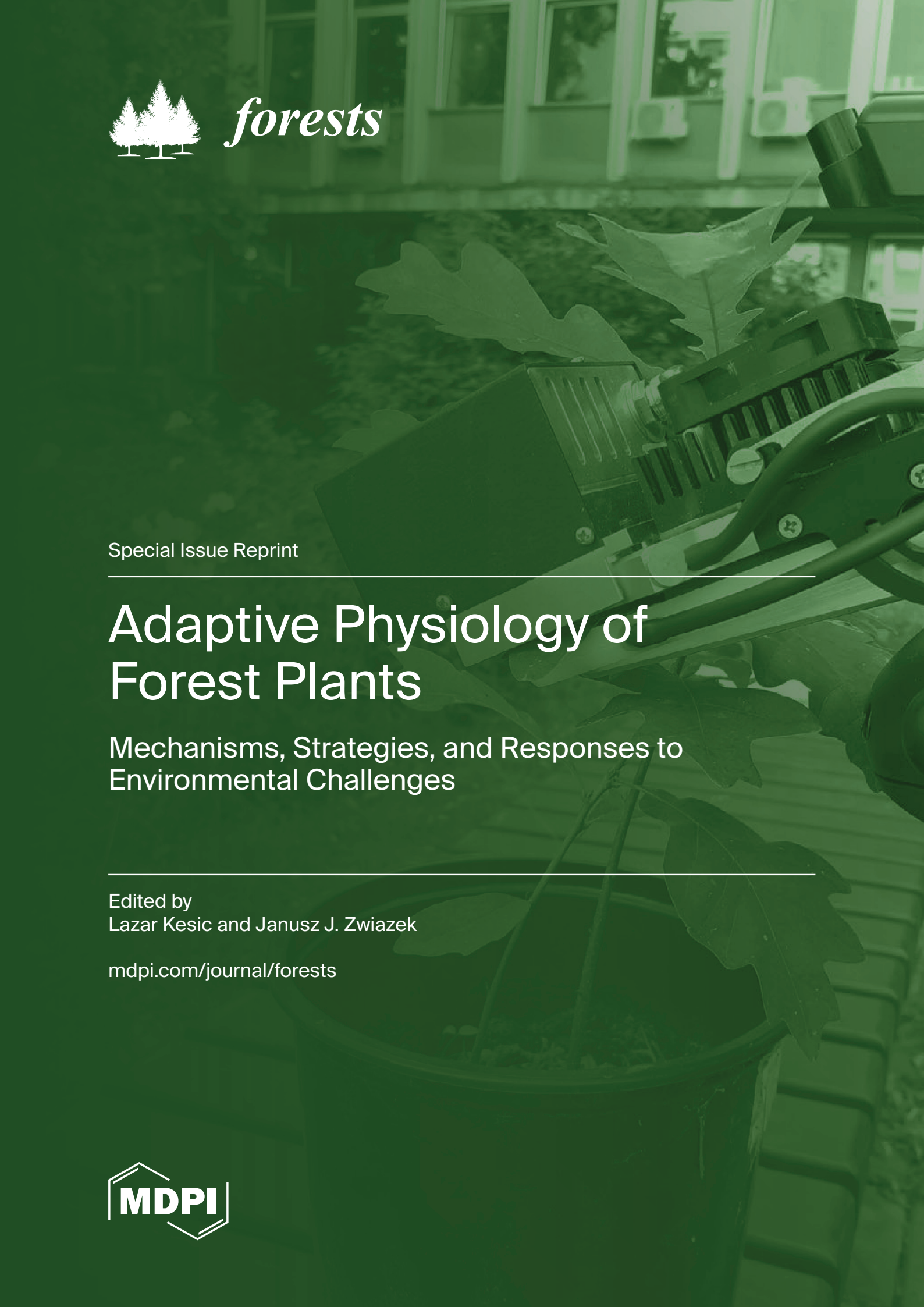


forests

Special Issue Reprint

Adaptive Physiology of Forest Plants

Mechanisms, Strategies, and Responses to Environmental Challenges

Edited by
Lazar Kesic and Janusz J. Zwiazek

mdpi.com/journal/forests

MDPI

Adaptive Physiology of Forest Plants: Mechanisms, Strategies, and Responses to Environmental Challenges

Adaptive Physiology of Forest Plants: Mechanisms, Strategies, and Responses to Environmental Challenges

Guest Editors

Lazar Kesic
Janusz J. Zwiazek

MDPI

Basel • Beijing • Wuhan • Barcelona • Belgrade • Novi Sad • Cluj • Manchester

Guest Editors

Lazar Kesic
Institute of Lowland Forestry and Environment (ILFE)
University of Novi Sad
Novi Sad
Serbia

Janusz J. Zwiazek
Department of Renewable Resources
University of Alberta
Edmonton
Canada

Editorial Office
MDPI AG
Grosspeteranlage 5
4052 Basel, Switzerland

This is a reprint of the Special Issue, published open access by the journal *Forests* (ISSN 1999-4907), freely accessible at: https://www.mdpi.com/journal/forests/special_issues/445M2751L0.

For citation purposes, cite each article independently as indicated on the article page online and as indicated below:

Lastname, A.A.; Lastname, B.B. Article Title. *Journal Name* **Year**, *Volume Number*, Page Range.

ISBN 978-3-7258-8991-4 (Hbk)
ISBN 978-3-7258-8992-1 (PDF)
https://doi.org/10.3390/books978-3-7258-8992-1

Cover image courtesy of Lazar Kesic
Leaf gas exchange measurement in Quercus robur

© 2026 by the authors. Articles in this reprint are Open Access and distributed under the Creative Commons Attribution (CC BY) license. The reprint as a whole is distributed by MDPI under the terms and conditions of the Creative Commons Attribution-NonCommercial-NoDerivs (CC BY-NC-ND) license (https://creativecommons.org/licenses/by-nc-nd/4.0/).

Contents

About the Editors . . . . . **vii**

Preface . . . . . **ix**

Lazar Kesić and Janusz J. Zwiazek
Adaptive Physiology of Forest Plants: Mechanisms, Strategies, and Responses to Environmental Challenges
Reprinted from: *Forests* **2026**, *17*, 735, https://doi.org/10.3390/f17070735 . . . . . **1**

Lazar Kesić, Vladimir Višacki, Lazar Pavlović, Olivera Kalozi, Martina Zorić, Saša Kostić and Saša Orlović
Assessment of Tree Physiological Performance in Urban and Park Environments Using Leaf Gas Exchange and Satellite-Based Vegetation Metrics
Reprinted from: *Forests* **2026**, *17*, 647, https://doi.org/10.3390/f17060647 . . . . . **7**

Željko Škvorc, Saša Bogdan, Ida Katičić Bogdan, Daniel Krstonošić and Krunoslav Sever
Functional Acclimation of *Quercus robur* from Nine European Provenances to Repeated Drought Events
Reprinted from: *Forests* **2026**, *17*, 636, https://doi.org/10.3390/f17060636 . . . . . **25**

Ling Xia, Peichun Li, Wenxiu Li, Meng Wang, Xiaoyu Liang and Yu Zhang
Integrative Structural, Physiological, and Transcriptomic Analyses Reveal Key Determinants of Anthracnose Resistance in Rubber Tree (*Hevea brasiliensis*)
Reprinted from: *Forests* **2026**, *17*, 629, https://doi.org/10.3390/f17050629 . . . . . **42**

Jiefei Nai, Wanpeng He, Tieming Ma, Xidong Han, Zhenxing Luo, Xinyu Li, et al.
Impact of Melatonin on Antioxidant Enzymes and Soluble Metabolites in Salt–Alkali-Stressed Poplar (*Populus* spp.): A Comparative Study of Pretreatment and Post-Treatment Effects
Reprinted from: *Forests* **2026**, *17*, 373, https://doi.org/10.3390/f17030373 . . . . . **57**

Ukhan Jeong, Dohee Kim, Sohyun Kim, Jiyeon Park, Seung Hyun Han and Eun Ju Cheong
Linking Leaf Angle to Physiological Responses for Drought Stress Detection: Case Study on *Quercus acutissima* Carruth. in Forest Nursery
Reprinted from: *Forests* **2026**, *17*, 348, https://doi.org/10.3390/f17030348 . . . . . **76**

Lucia Mondanelli, Claudia Cocozza, Barbara Mariotti and Alberto Maltoni
Shoot Vigour, Leaf Water Status and Physiological Traits of Mature *Castanea sativa* Mill. Trees Along the Canopy Vertical Gradient
Reprinted from: *Forests* **2026**, *17*, 173, https://doi.org/10.3390/f17020173 . . . . . **92**

Qi Lin, Wanju Feng, Man Tang, Mengqiu Chen, Xun Song, Lin Wu, et al.
Organ-Specific Gene Expression and Metabolite Accumulation in *Fargesia rufa* in Response to an Altitudinal Gradient
Reprinted from: *Forests* **2026**, *17*, 167, https://doi.org/10.3390/f17020167 . . . . . **102**

Hong-Yong Wang, Xing-Ju Liu, Meng-Zhen Yin, Sheng-Jia Cui, Hai-Yong Liang and Zhen-Hua Xu
Transcriptomic Analysis of Anthocyanin Degradation in *Salix alba* Bark: Insights into Seasonal Adaptation and Forestry Applications
Reprinted from: *Forests* **2025**, *16*, 1598, https://doi.org/10.3390/f16101598 . . . . . **119**

Jorge Palomo-Kumul, Mirna Valdez-Hernández, Gerald A. Islebe, Edith Osorio-de-la-Rosa, Gabriela Cruz-Piñon, Francisco López-Huerta and Raúl Juárez-Aguirre
Hydro-Functional Strategies of Sixteen Tree Species in a Mexican Karstic Seasonally Dry Tropical Forest
Reprinted from: *Forests* **2025**, *16*, 1535, https://doi.org/10.3390/f16101535 . . . . . **137**

Andrea Pogányová, Djordje P. Božović, Martin Bačkor, Michal Goga, Marián Tomka and Marko S. Sabovljević
Effect of Lead on the Physiological Parameters and Elemental Composition of *Pinus sylvestris* L. and *Picea abies* (L.) H. Karst Seedlings
Reprinted from: *Forests* **2025**, *16*, 990, https://doi.org/10.3390/f16060990 . . . . . **160**

Anita Gurung, Benjamin Wagner, Elizabeth C. Pryde, Craig R. Nitschke and Stefan K. Arndt
Functional Traits Associated with Drought Tolerance Exhibit Low Variability in 21 Provenances of a Montane Tree Species—*Eucalyptus delegatensis*
Reprinted from: *Forests* **2025**, *16*, 898, https://doi.org/10.3390/f16060898 . . . . . **174**

Kaijie Yang, Yifei Cai, Xiaoya Li, Weiwei Cong, Yiming Feng and Feng Wang
Seasonal Variations in the Relationship Between Canopy Solar-Induced Chlorophyll Fluorescence and Gross Primary Production in a Temperate Evergreen Needleleaf Forest
Reprinted from: *Forests* **2025**, *16*, 893, https://doi.org/10.3390/f16060893 . . . . . **194**

Xueying Wang, Peifang Chong, Xinguang Bao and Feng Zhang
The Effects of Inoculation with Rhizosphere Phosphate-Solubilizing Bacteria on the Growth and Physiology of *Reaumuria soongorica* Seedlings Under NaCl Stress
Reprinted from: *Forests* **2025**, *16*, 591, https://doi.org/10.3390/f16040591 . . . . . **209**

Hanbing Leng, Lingyan Zhou and Wei Yan
Variations in Leaf Photosynthesis and Its Limitations at Different Canopy Positions in Mature Camphor Trees
Reprinted from: *Forests* **2025**, *16*, 581, https://doi.org/10.3390/f16040581 . . . . . **226**

Wenlong Sun, Luyu Qi, Haonan Chen, Yixin Song, Jiaqi Jiang, Puyi Zhang, et al.
Mycorrhization of *Quercus dentata* Seedlings with *Laccaria bicolor* Enhances Salt Tolerance of Plants Only Under Relatively Moderate Soil Salinity Level
Reprinted from: *Forests* **2025**, *16*, 413, https://doi.org/10.3390/f16030413 . . . . . **245**

About the Editors

Lazar Kesic

Lazar Kesic is a Research Associate at the Institute of Lowland Forestry and Environment, University of Novi Sad, Serbia. His research is primarily focused on plant physiology in forest and urban ecosystems, with a particular emphasis on plant ecophysiology and leaf gas exchange. His work investigates the physiological mechanisms underlying plant responses to changing environmental conditions and both biotic and abiotic stress factors, contributing to a better understanding of plant adaptation, productivity, and resilience.

Throughout his scientific career, Dr. Kesić has been actively involved in experimental and field-based research addressing a wide range of ecological and environmental challenges. In addition to his expertise in plant physiological processes, he has participated in studies examining the application of phytoremediation techniques for the reclamation and ecological restoration of landfill sites and other degraded environments. His research combines physiological measurements with ecological approaches to evaluate plant performance and the potential of vegetation-based solutions for ecosystem restoration.

Dr. Kesić's broader research interests include plant–environment interactions, forest ecology, urban forestry, ecophysiology, environmental monitoring, and sustainable ecosystem management. His work aims to bridge fundamental plant physiology with applied environmental research, providing scientific knowledge that supports biodiversity conservation, climate change adaptation, and the development of nature-based solutions for restoring and managing forest and urban landscapes. He has contributed to numerous national and international research projects and has authored and co-authored scientific publications in the fields of plant physiology, forestry, and environmental sciences.

Janusz J. Zwiazek

Janusz J. Zwiazek is a Professor of Plant Physiology in the department of Renewable Resources of the University of Alberta in Edmonton, Canada. His research interests are stress physiology of forest plants; the role of aquaporins in the regulation of water and gas transport; the effects of salinity, drought and other environmental stresses on the function and structure of plants; stress resistance, revegetation of sites affected by salinity and high soil pH; physiological, biochemical and structural adaptations of plants to stress; tree improvement and stress conditioning; and the structure and function of cell membranes.

Preface

This Reprint brings together a collection of research papers focused on recent advances in the understanding of plant physiological responses to environmental conditions and stress factors. The contributions cover a broad range of topics, including plant ecophysiology, leaf gas exchange, forest and urban ecosystems, and sustainable approaches to environmental restoration, reflecting current developments in these research areas.

The primary aim of this Reprint is to provide readers with a comprehensive overview of recent scientific findings while highlighting the importance of integrating physiological, ecological, and environmental perspectives in plant science. The selected papers demonstrate how physiological measurements can improve our understanding of plant performance under changing environmental conditions and contribute to the development of effective management and restoration strategies.

The motivation for preparing this Reprint stems from the growing need to better understand plant responses to global environmental challenges, including climate change, urbanization, and soil degradation. Advances in plant physiology and environmental sciences have generated valuable knowledge that can support sustainable ecosystem management and nature-based solutions for environmental restoration.

This Reprint is intended for researchers, graduate students, environmental scientists, forest managers, and professionals working in plant physiology, forestry, ecology, and related disciplines. It is hoped that the collected contributions will serve as a useful scientific resource, stimulate further interdisciplinary research, and encourage the application of current knowledge to both fundamental and applied environmental challenges.

Lazar Kesic and Janusz J. Zwiazek
Guest Editors

forests

MDPI

Editorial

Adaptive Physiology of Forest Plants: Mechanisms, Strategies, and Responses to Environmental Challenges

Lazar Kesić [1,*] and Janusz J. Zwiazek [2]

[1] Institute of Lowland Forestry and Environment (ILFE), University of Novi Sad, 21000 Novi Sad, Serbia
[2] Department of Renewable Resources, University of Alberta, 442 Earth Sciences Bldg., Edmonton, AB T6G 2E3, Canada
* Correspondence: kesic.lazar@uns.ac.rs

1. Introduction

Forest plants inhabit environments where water availability, temperature, and other abiotic factors vary across seasons, years, and locations, often acting simultaneously rather than independently. As long-lived and sessile organisms, trees cannot avoid unfavorable conditions and instead rely on physiological adjustment, acclimation, and adaptive strategies to maintain function under stress [1,2]. Consequently, adaptive physiology plays a central role in forest productivity, resilience, and ecosystem functioning under climate change [3].

A major challenge in understanding forest responses is that environmental stress rarely occurs in isolation. Drought and heat frequently interact, influencing carbon assimilation, hydraulic function, growth, and survival in ways that vary among species, developmental stages, and environmental histories [2,4,5]. These interactions can alter forest dynamics and ecosystem performance, emphasizing the need for mechanistic approaches to stress physiology [6].

Within this context, forest adaptation can be viewed through three interconnected dimensions: mechanisms, strategies, and responses. Mechanisms include processes such as stomatal regulation, hydraulic transport, carbon balance, and temperature acclimation; strategies encompass drought avoidance, drought tolerance, and other water-use adaptations; while responses represent observable changes in photosynthesis, respiration, transpiration, growth, biomass allocation, and mortality risk [7,8].

Among environmental drivers, drought has emerged as one of the most important causes of forest decline and tree mortality worldwide. Hydraulic failure is widely recognized as a major mechanism of drought-induced mortality, whereas the role of carbon starvation appears more species- and context-dependent [3]. Heat stress further compounds these effects by reducing photosynthesis, increasing oxidative damage, and intensifying water deficits, particularly when occurring simultaneously with drought [4,5].

With increasing urbanization and the growing impacts of climate change, water scarcity has become a major constraint affecting the health and performance of urban trees. Previous studies conducted in urban environments have demonstrated that drought stress induces substantial changes in tree physiological functioning, primarily through alterations in gas exchange and chlorophyll fluorescence parameters. Reductions in stomatal conductance, transpiration, and photosynthetic activity are commonly accompanied by adjustments in photochemical and non-photochemical energy dissipation processes, reflecting species-specific strategies for coping with water limitation [9]. In addition to drought, trees are frequently exposed to heavy metal contamination originating from traffic

emissions, industrial activities, and other anthropogenic sources [10], which can further impair physiological processes such as photosynthesis and stomatal regulation [11]. In urban roadside environments, naturally occurring drought and pollution pressures have been shown to trigger significant physiological and morphological adjustments, with the magnitude of responses varying among species and local site conditions [12].

Importantly, adaptive physiology also includes recovery and acclimation processes. Recovery rates often differ among physiological functions, while temperature acclimation and intraspecific variation can enhance resilience to changing environmental conditions [8,13,14]. Together, these mechanisms and strategies determine the capacity of forest trees to survive, recover, and persist under increasingly variable climates, although significant challenges remain in understanding how multiple stressors interact across biological and ecological scales [2].

Forest ecosystems represent highly dynamic systems in which plants are continuously exposed to a wide range of abiotic and biotic stressors, further intensified by ongoing climate change. The studies included in this Special Issue highlight the diversity and complexity of adaptive physiological and molecular mechanisms that underpin plant survival, performance, and resilience under environmental constraints. Bringing together 15 articles authored by 95 researchers from nine countries—Serbia, Croatia, China, the Republic of Korea, Italy, Mexico, Slovakia, Australia, and Canada—this collection advances our understanding of how forest plants respond to changing environments. By integrating research on stress tolerance, resource acquisition, and ecosystem responses, this collection advances our understanding of how trees cope with changing conditions and maintain functionality. Collectively, the findings presented here provide valuable insights for predicting forest responses to future environmental change and for informing conservation and management strategies aimed at sustaining forest health and stability.

2. Functional Strategies of Trees Under Environmental Change: Integrating Photosynthetic Dynamics, Water Relations, and Secondary Metabolism

Recent research in plant physiology increasingly points toward a common conclusion: tree responses to environmental variability cannot be understood through isolated physiological traits alone. Instead, photosynthetic performance, water-use strategies, secondary metabolism, and structural organization operate as interconnected components of a dynamic adaptive system. Across diverse ecosystems—from temperate coniferous forests and Mediterranean oak populations to tropical dry forests and urban green infrastructure—emerging evidence highlights the importance of multi-scale integration in explaining plant resilience and productivity under changing environmental conditions.

A prominent research direction concerns the seasonal reorganization of the photosynthetic apparatus and its dependence on environmental conditions. Studies combining physiological measurements with remote sensing approaches demonstrate that photosynthetic activity is not merely a function of instantaneous environmental drivers but follows predictable seasonal trajectories shaped by light availability, temperature, and water balance. The observed coupling between solar-induced chlorophyll fluorescence (SIF) and gross primary productivity (GPP) in temperate evergreen conifer forests illustrates the potential of remotely sensed signals to capture seasonal changes in ecosystem carbon uptake with considerable temporal precision [15]. Such findings reinforce the growing role of Earth observation technologies in bridging leaf-level physiological processes and ecosystem-scale carbon dynamics.

At the same time, investigations within tree canopies challenge the traditional assumption that canopy photosynthesis can be represented as a homogeneous process. Evidence

https://doi.org/10.3390/f17070735

from mature camphor and chestnut trees demonstrates substantial vertical heterogeneity in photosynthetic performance, water status, and nutrient allocation [16,17]. Highly illuminated upper canopy leaves do not necessarily exhibit the greatest photosynthetic capacity, particularly when nitrogen limitation or hydraulic constraints become dominant. Consequently, canopy architecture emerges not merely as a structural characteristic but as a critical determinant of physiological function. These studies collectively suggest that understanding carbon assimilation requires explicit consideration of spatial variation within individual trees.

Tree performance under environmental stress depends on the combination of species, treatment, and site conditions. In the poplar study, exogenous melatonin improved salt–alkali stress tolerance by enhancing plant growth, antioxidant enzyme activity, and osmoregulatory capacity, with pretreatment and post-treatment both offering benefits [18]. The conifer study showed that low-level lead exposure produced species-specific responses, with *Picea abies* displaying greater physiological stability while *Pinus sylvestris* accumulated more lead in its tissues, which may be relevant for phytoremediation [19]. The alpine ash paper found little variation in drought-related traits among 21 provenances and concluded that there is likely no "superior" provenance based on drought-adapted traits alone [20]. The mycorrhizal study further showed that L. bicolor can support *Q. dentata* under moderate salinity, but may worsen nutrient stress, water stress, and Na[+] toxicity under high salinity, meaning its usefulness depends on soil conditions [21]. Accumulating evidence indicates that plant tolerance to salinity is strongly influenced by interactions with rhizosphere microorganisms capable of enhancing nutrient availability and regulating physiological responses to stress. In particular, phosphate-solubilizing bacteria have been recognized as important components of plant adaptation mechanisms, contributing to improved phosphorus acquisition, growth performance, and stress tolerance under saline conditions [22].

Water availability remains one of the most powerful drivers of physiological and structural adaptation. However, recent studies indicate that drought resistance should be viewed not as a single trait but as a suite of alternative adaptive strategies. Research on European provenances of sessile oak revealed that repeated drought events primarily elicited divergence in morphological characteristics rather than gas-exchange responses, indicating that long-term adaptation may be embedded within structural traits such as leaf morphology and stomatal organization [23]. Similar conclusions emerge from investigations of tropical dry-forest species, where contrasting combinations of hydraulic safety, wood density, and water-storage capacity define distinct ecological strategies along a continuum from conservative to acquisitive resource use [24].

This perspective is particularly relevant in anthropogenically modified environments. Urban ecosystems expose trees to novel combinations of thermal stress, altered hydrology, and soil and air pollution. Studies of urban trees have consistently shown reduced photosynthetic activity, stomatal conductance, and transpiration in boulevard trees compared with the trees growing in less stressful park environments [25]. Such findings emphasize that urbanization affects entire physiological syndromes rather than isolated functional traits. Likewise, investigations of morphological responses to drought suggest that leaf angle monitoring could be implemented to provide a useful operational indicator of stress, although it merely reflects the ongoing physiological adjustments and could not serve as a reliable early-warning signal [26].

Another emerging theme concerns the central role of secondary metabolism in linking acclimation, defense, and seasonal transitions. Recent transcriptomic studies reveal that flavonoid and phenylpropanoid pathways function as major regulatory hubs through which plants coordinate responses to both environmental and biotic stressors. Seasonal

https://doi.org/10.3390/f17070735

anthocyanin degradation in willow bark involves extensive transcriptional regulation associated with redox homeostasis, hormone signaling, and phenolic metabolism [27]. Similarly, resistance mechanisms against anthracnose disease in rubber trees rely on coordinated activation of antioxidant systems, structural defenses, and phenylpropanoid biosynthesis [28]. Although these systems differ markedly in biological context, they converge on common metabolic networks that facilitate resource allocation between growth, protection, and environmental adaptation.

Importantly, several studies demonstrate that adaptive responses are highly organ-specific. Research on *Fargesia rufa* illustrates how leaves and rhizomes may pursue fundamentally different metabolic strategies under the same environmental gradient, with leaves exhibiting metabolic conservation while rhizomes increase storage and secondary metabolite production [29]. Similar patterns of functional specialization are evident within tree canopies, where upper and lower crown positions often differ substantially in resource allocation and physiological activity [16,17]. These findings underscore an increasingly recognized principle in plant ecology: adaptation is frequently achieved through internal division of labor among organs and tissues rather than through uniform whole-plant responses.

Beyond their biological implications, these studies collectively highlight a methodological transition toward integrative research frameworks. The combination of physiological measurements, remote sensing technologies, transcriptomics, metabolomics, structural trait analysis, and ecological modeling is transforming our understanding of plant function. SIF-based monitoring enables scaling from leaf physiology to ecosystem productivity [15], while satellite-derived indicators facilitate assessment of urban tree health across broad spatial extents [25]. Concurrently, transcriptomic approaches provide unprecedented insight into the regulatory mechanisms underlying stress acclimation and defense responses [28].

Taken together, the emerging literature suggests three overarching lessons. First, resilience and productivity are inherently context-dependent properties shaped by interactions among species identity, organ function, canopy structure, and environmental conditions [16,17,25]. Second, structural and morphological traits often provide more robust indicators of long-term adaptation than instantaneous physiological measurements alone [23,24]. Third, future advances in both ecological research and ecosystem management will depend increasingly on integrative monitoring systems that connect local physiological observations with scalable, non-destructive, and remotely sensed indicators [15,25,26].

3. Conclusions

The studies collected in this Special Issue demonstrate that plant adaptation to environmental change is governed by the integration of physiological, morphological, biochemical, and molecular processes operating across multiple organizational scales. Together, they show that resilience cannot be explained by individual traits alone, but rather emerges from coordinated interactions among photosynthetic regulation, water-use strategies, secondary metabolism, and structural organization.

A recurring message across the contributions is that plant responses are highly context-dependent, varying among species, populations, organs, and environmental conditions. Drought, heat, seasonal transitions, urban stressors, and biotic challenges trigger diverse yet interconnected adaptive pathways that influence carbon assimilation, resource allocation, defense, and recovery. These findings reinforce the view of trees as dynamic systems capable of continuously adjusting their functional strategies in response to changing environments.

The Special Issue also highlights the growing importance of integrative research approaches that combine field physiology, structural trait analysis, omics technologies, and

https://doi.org/10.3390/f17070735

remote sensing. Such frameworks are essential for linking mechanistic understanding with ecosystem-scale monitoring and prediction.

As climate change increases the frequency and intensity of environmental stressors, advancing our understanding of adaptive physiology will be critical for improving forest conservation, management, and restoration. Future research should focus on integrating responses across biological scales and stress types to better predict the resilience and functioning of forest ecosystems in a rapidly changing world.

Author Contributions: Conceptualization, L.K.; writing—original draft preparation, L.K.; writing—review and editing, L.K. and J.J.Z. All authors have read and agreed to the published version of the manuscrip.

Funding: This research received no external funding.

Acknowledgments: We would like to sincerely thank all authors who contributed their work to this Special Issue. We are also deeply grateful to the reviewers for their insightful comments and valuable suggestions, which have significantly improved the quality of the published papers.

Conflicts of Interest: The authors declare no conflicts of interest.

References

1. Bussotti, F.; Pollastrini, M. Plant Stress Revisiting the Concept of Stress in Forest Trees at the Time of Global Change and Issues for Stress Monitoring. *Plant Stress* **2021**, *2*, 100013. [CrossRef]
2. Niinemets, Ü. Forest Ecology and Management Responses of Forest Trees to Single and Multiple Environmental Stresses from Seedlings to Mature Plants: Past Stress History, Stress Interactions, Tolerance and Acclimation. *For. Ecol. Manag.* **2010**, *260*, 1623–1639. [CrossRef]
3. Adams, H.D.; Zeppel, M.J.B.; Anderegg, W.R.L.; Hartmann, H.; Landhäusser, S.M.; Tissue, D.T.; Huxman, T.E.; Hudson, P.J.; Franz, T.E.; Allen, C.D.; et al. A Multi-Species Synthesis of Physiological Mechanisms in Drought-Induced Tree Mortality. *Nat. Ecol. Evol.* **2017**, *1*, 1285–1291. [CrossRef] [PubMed]
4. Teskey, R.; Wertin, T.; Bauweraerts, I.; Ameye, M.; Mcguire, M.A.; Steppe, K. Responses of Tree Species to Heat Waves and Extreme Heat Events. *Plant Cell Environ.* **2015**, *38*, 1699–1712. [CrossRef] [PubMed]
5. Reich, P.B.; Sendall, K.M.; Stefanski, A.; Rich, R.L.; Hobbie, S.E.; Montgomery, R.A. Boreal Tree Species Depend on Soil Moisture. *Plant Cell Environ.* **2018**, *38*, 1699–1712.
6. Rennenberg, H.; Loreto, F.; Polle, A.; Brilli, F.; Fares, S.; Beniwal, R.S.; Gessler, A. Physiological Responses of Forest Trees to Heat and Drought. *Plant Biol.* **2006**, *8*, 556–571. [CrossRef] [PubMed]
7. Volaire, F. A Unified Framework of Plant Adaptive Strategies to Drought: Crossing Scales and Disciplines. *Glob. Change Biol.* **2018**, *24*, 2929–2938. [CrossRef] [PubMed]
8. Sendall, K.M.; Reich, P.B.; Zhao, C.; Jihua, H.; Wei, X.; Rice, K.; Rich, R.L.; Montgomery, R.A. Acclimation of Photosynthetic Temperature Optima of Temperate and Boreal Tree Species in Response to Experimental Forest Warming. *Glob. Change Biol.* **2014**, *21*, 612–625. [CrossRef] [PubMed]
9. Vastag, E.; Orlović, S.; Kesić, L.; Karaklić, V.; Lapin, K.; Vukmirović, A.; Višacki, V.; Stojnić, S. Physiological Responses of Tilia Tomentosa, Liriodendron Tulipifera, and Liquidambar Styraciflua to Urban Stress: Implications for Roadside Tree Selection. *Trees For. People* **2026**, *26*, 101316. [CrossRef]
10. Kalozi, O.; Kebert, M.; Orlovi, S. *Populus* × *Euramericana* Accumulates More Organic Pollutants (PAHs and PCBs), While *P. nigra* 'Italica' Absorbs More Heavy Metals. *Plants* **2025**, *14*, 1445. [CrossRef] [PubMed]
11. Kesić, L.; Kovačević, B.; Milović, M.; Poljaković-Pajnik, L.; Pekeč, S.; Višacki, V.; Orlović, S. Physiological Responses of Poplar and Willow Clones Grown in Pot Trials on Soil from Landfills. *Topola* **2024**, *82*, 55–63. [CrossRef]
12. Vastag, E.; Kesi, L.; Cocozza, C.; Karakli, V.; Višacki, V.; Ili, M. Leaf Functional Traits and Water-Use Strategies of Two Riparian Tree Species in an Urban Environment. *Forests* **2026**, *17*, 339. [CrossRef]
13. Ruehr, N.K.; Grote, R.; Mayr, S.; Arneth, A. Beyond the Extreme: Recovery of Carbon and Water Relations in Woody Plants Following Heat and Drought Stress. *Tree Physiol.* **2019**, *39*, 1285–1299. [CrossRef] [PubMed]
14. Isaac-renton, M.; Montwé, D.; Hamann, A.; Treydte, K.; Spiecker, H.; Cherubini, P. Maladapted to Drought. *Nat. Commun.* **2018**, *9*, 5254. [CrossRef] [PubMed]
15. Yang, K.; Cai, Y.; Li, X.; Cong, W.; Feng, Y. Seasonal Variations in the Relationship Between Canopy Solar-Induced Chlorophyll Fluorescence and Gross Primary Production in a Temperate Evergreen Needleleaf Forest. *Forests* **2025**, *16*, 893. [CrossRef]

16. Leng, H.; Zhou, L. Variations in Leaf Photosynthesis and Its Limitations at Different Canopy Positions in Mature Camphor Trees. *Forests* **2025**, *16*, 581. [CrossRef]
17. Mondanelli, L.; Cocozza, C.; Mariotti, B.; Maltoni, A. Shoot Vigour, Leaf Water Status and Physiological Traits of Mature Castanea Sativa Mill. Trees Along the Canopy Vertical Gradient. *Forests* **2026**, *17*, 173. [CrossRef]
18. Nai, J.; He, W.; Ma, T.; Han, X.; Luo, Z.; Li, X.; Sun, J.; Zhao, X. Impact of Melatonin on Antioxidant Enzymes and Soluble Metabolites in Salt—Alkali-Stressed Poplar (*Populus* spp.): A Comparative Study of Pretreatment and Post-Treatment Effects. *Forests* **2026**, *17*, 373. [CrossRef]
19. Pogányová, A.; Božović, D.P.; Bačkor, M.; Goga, M.; Tomka, M. Effect of Lead on the Physiological Parameters and Elemental Composition of *Pinus sylvestris* L. and *Picea abies* (L.) H. Karst Seedlings. *Forests* **2025**, *16*, 990. [CrossRef]
20. Gurung, A.; Wagner, B.; Pryde, E.C.; Nitschke, C.R. Functional Traits Associated with Drought Tolerance Exhibit Low Variability in 21 Provenances of a Montane Tree Species—Eucalyptus Delegatensis. *Forests* **2025**, *16*, 898. [CrossRef]
21. Sun, W.; Qi, L.; Chen, H.; Song, Y.; Jiang, J.; Zhang, P.; Wang, B.; Wang, Q.; Meng, G.; Ji, T.; et al. Mycorrhization of Quercus Dentata Seedlings with Laccaria Bicolor Enhances Salt Tolerance of Plants Only Under Relatively Moderate Soil Salinity Level. *Forests* **2025**, *16*, 413. [CrossRef]
22. Wang, X.; Chong, P.; Bao, X.; Zhang, F. The Effects of Inoculation with Rhizosphere Phosphate- Solubilizing Bacteria on the Growth and Physiology of Reaumuria Soongorica Seedlings Under NaCl Stress. *Forests* **2025**, *16*, 591. [CrossRef]
23. Škvorc, Ž.; Bogdan, S.; Bogdan, I.K.; Krstonošić, D.; Sever, K. Functional Acclimation of Quercus Robur from Nine European Provenances to Repeated Drought Events. *Forests* **2026**, *17*, 636. [CrossRef]
24. Palomo-kumul, J.; Valdez-hernández, M.; Islebe, G.A.; Osorio-de-la-rosa, E.; Cruz-piñon, G.; López-huerta, F.; Juárez-aguirre, R. Hydro-Functional Strategies of Sixteen Tree Species in a Mexican Karstic Seasonally Dry Tropical Forest. *Forests* **2025**, *16*, 153. [CrossRef]
25. Kesic, L.; Višacki, V.; Pavlovi, L.; Kalozi, O.; Zori, M.; Kosti, S. Assessment of Tree Physiological Performance in Urban and Park Environments Using Leaf Gas Exchange and Satellite-Based Vegetation Metrics. *Forests* **2026**, *17*, 647. [CrossRef]
26. Jeong, U.; Kim, D.; Kim, S.; Park, J.; Han, S.H.; Cheong, E.J. Linking Leaf Angle to Physiological Responses for Drought Stress Detection: Case Study on *Quercus acutissima* Carruth. in Forest Nursery. *Forests* **2026**, *17*, 647. [CrossRef]
27. Wang, H.; Liu, X.; Yin, M.; Cui, S.; Liang, H.; Xu, Z. Transcriptomic Analysis of Anthocyanin Degradation in Salix Alba Bark: Insights into Seasonal Adaptation and Forestry Applications. *Forests* **2025**, *16*, 1598. [CrossRef]
28. Xia, L.; Li, P.; Li, W.; Wang, M.; Liang, X. Integrative Structural, Physiological, and Transcriptomic Analyses Reveal Key Determinants of Anthracnose Resistance in Rubber Tree (*Hevea brasiliensis*). *Forests* **2026**, *17*, 629. [CrossRef]
29. Lin, Q.; Feng, W.; Tang, M.; Chen, M.; Song, X.; Wu, L.; Zhao, X.; Long, Z. Organ-Specific Gene Expression and Metabolite Accumulation in Fargesia Rufa in Response to an Altitudinal Gradient. *Forests* **2026**, *17*, 167. [CrossRef]

Disclaimer/Publisher's Note: The statements, opinions and data contained in all publications are solely those of the individual author(s) and contributor(s) and not of MDPI and/or the editor(s). MDPI and/or the editor(s) disclaim responsibility for any injury to people or property resulting from any ideas, methods, instructions or products referred to in the content.

forests

MDPI

Article

Assessment of Tree Physiological Performance in Urban and Park Environments Using Leaf Gas Exchange and Satellite-Based Vegetation Metrics

Lazar Kesić [1], Vladimir Višacki [1,*], Lazar Pavlović [2], Olivera Kalozi [2], Martina Zorić [1], Saša Kostić [1] and Saša Orlović [1,2]

[1] Institute of Lowland Forestry and Environment (ILFE), University of Novi Sad, 21000 Novi Sad, Serbia; kesic.lazar@uns.ac.rs (L.K.); martinazoric@uns.ac.rs (M.Z.); sasa.kostic@uns.ac.rs (S.K.); sasao@uns.ac.rs (S.O.)
[2] Department of Fruit Growing, Viticulture, Horticulture, and Landscape Architecture, Faculty of Agriculture, University of Novi Sad, 21000 Novi Sad, Serbia; lazar.pavlovic@polj.edu.rs (L.P.); olivera.kalozi@polj.edu.rs (O.K.)
* Correspondence: vladimir.visacki@uns.ac.rs

Abstract

Urbanization significantly alters microclimatic and environmental conditions, thereby affecting the physiological functioning of urban trees. This study aimed to evaluate whether leaf-level physiological measurements and satellite-based remote sensing indicators consistently detect similar physiological response patterns across contrasting urban and park environments in Novi Sad, Serbia, using three tree species (*Platanus* × *acerifolia*, *Celtis australis*, and *Tilia tomentosa*). Leaf gas exchange parameters, including stomatal conductance (g_s), net photosynthesis (A), transpiration rate (E), water use efficiency (WUE), and intercellular CO_2 concentration (Ci), were measured using a CIRAS-3 portable photosynthesis system. Satellite-derived variables included vegetation indices (NDVI, NDRE, NDMI) and land surface temperature (LST), which were used to construct proxy indicators of physiological processes. Results revealed consistent differences between urban and park environments, with urban conditions associated with reduced photosynthetic activity, stomatal conductance, and transpiration, alongside increased physiological stress. These patterns were consistently captured by satellite-derived proxies, demonstrating strong agreement in the direction of physiological responses across species and environments. Species-specific responses were evident, with *P.* × *acerifolia* showing the highest sensitivity to urban conditions, *C. australis* exhibiting intermediate responses, and *T. tomentosa* suggesting comparatively greater tolerance. The integration of leaf-level measurements with satellite-derived proxies provides a robust framework for scaling physiological processes and monitoring urban tree performance, highlighting the potential of remote sensing for assessing urban vegetation stress and supporting evidence-based urban forestry management.

Keywords: leaf gas exchange; urban forestry; remote sensing proxies; urban heat stress; vegetation indices

1. Introduction

Rapid urban expansion has fundamentally transformed land surface properties and local atmospheric conditions, resulting in pronounced alterations of energy balance, hydrological cycling, and air quality [1,2]. These modifications, in combination with increased concentrations of atmospheric pollutants and altered vapor pressure deficit (VPD), impose

substantial physiological constraints on urban vegetation, particularly on tree species that are integral to ecosystem functioning and urban ecosystem services [3,4].

Leaf-level physiological processes, especially gas exchange traits such as stomatal conductance (g_s), net photosynthetic rate (A), and transpiration rate (E), represent highly sensitive and mechanistically informative indicators of plant responses to environmental stressors [5]. Empirical evidence consistently demonstrates that urban trees frequently exhibit reduced g_s and photosynthetic capacity compared to individuals in park or peri-urban environments, largely as a consequence of stomatal limitation induced by elevated VPD, thermal stress, and pollutant deposition [6]. These constraints often translate into altered water use efficiency (WUE), which may increase under moderate stress due to stronger reductions in transpiration relative to photosynthesis, although prolonged exposure typically results in net declines in carbon assimilation and growth potential [7].

In parallel with in situ physiological measurements, satellite-derived vegetation indices such as the Normalized Difference Vegetation Index (NDVI) and Enhanced Vegetation Index (EVI) have emerged as robust proxies for assessing vegetation vigor, canopy structure, and photosynthetic activity at broader spatial and temporal scales [8,9]. These indices, derived from spectral reflectance characteristics in the red and near-infrared bands, have been widely applied in urban ecological research to quantify spatial gradients of vegetation health and detect early signs of stress, including defoliation and chlorophyll degradation [10]. Notably, recent advances in remote sensing technologies, including hyperspectral imaging and airborne laser scanning, have further enhanced the capacity to resolve fine-scale variation in urban canopy condition with increasing accuracy [11].

The integration of leaf-level gas exchange measurements with satellite-based vegetation metrics represents a major methodological advancement for the multiscale assessment of tree physiological performance [12]. Gas exchange measurements provide high-resolution insight into instantaneous physiological functioning, capturing key processes such as carbon assimilation, stomatal regulation, and transpiration. However, their spatial coverage is inherently limited. In contrast, remote sensing approaches enable continuous, spatially explicit monitoring of vegetation dynamics across heterogeneous urban landscapes [13,14]. Despite their clear complementarity, these approaches are still rarely integrated within a unified analytical framework. Most studies continue to rely on either field-based physiological measurements or remote sensing data independently, which restricts the ability to link mechanistic understanding with large-scale ecosystem patterns and limits the development of predictive models for urban tree performance [15].

Urban environments impose a unique combination of abiotic stressors that fundamentally alter the conditions under which trees grow and function. Compared to peri-urban or natural forest ecosystems, urban trees are exposed to elevated air and surface temperatures, modified radiation regimes due to shading and heat trapping, restricted soil volumes, and highly variable water availability influenced by impervious surfaces and management practices. These factors directly regulate leaf gas exchange processes—including stomatal conductance (g_s), photosynthetic rate (A), transpiration (E), water use efficiency (WUE), and intercellular CO_2 concentration (Ci)—which ultimately determine tree growth, survival, and ecosystem service provision [6]. Importantly, urban tree cooling depends not only on structural attributes such as canopy size and shading capacity, but also on physiological processes, particularly transpiration, which is tightly controlled by stomatal behavior and environmental conditions [16]. Consequently, interpreting differences between contrasting urban habitats, such as street canyons and park environments, requires a detailed understanding of the interactions between microclimate, plant hydraulics, and stomatal regulation [17,18].

https://doi.org/10.3390/f17060647

Street canyons and park habitats represent contrasting urban microecosystems that differ substantially in microclimatic characteristics and the intensity of anthropogenic influence [1,18]. Street canyons are typically exposed to higher levels of anthropogenic stress, including intensive vehicular traffic, elevated emissions of atmospheric pollutants, noise, artificial surface heating, and soil degradation caused by urban infrastructure and human activities [19,20]. In addition, these environments are characterized by a pronounced urban heat island effect, reduced air circulation and turbulence due to dense building structures, increased soil compaction, and limited water availability [19]. In contrast, park habitats generally provide more favorable thermal and hydrological conditions, greater vegetation cover, higher relative air humidity, improved soil properties, and lower levels of anthropogenic disturbance and air pollution [21]. Such environmental differences can strongly affect plant physiological processes, particularly stomatal conductance and gas exchange, since elevated temperature, drought stress, and pollutant exposure may induce partial or complete stomatal closure, thereby reducing transpiration, CO_2 assimilation, and photosynthetic efficiency [22]. Therefore, the comparison of these two habitat types is scientifically important because it enables the evaluation of plant physiological responses and adaptive capacity under different levels of anthropogenic and environmental stress within urban ecosystems.

Species-specific variability represents an additional layer of complexity in understanding urban tree responses. Numerous studies have demonstrated that tree species differ markedly in their tolerance to heat, drought, and pollution, with some taxa maintaining relatively stable gas exchange rates under stress, while others exhibit strong physiological downregulation [6,14]. These differences are closely associated with intrinsic functional traits, including stomatal regulation strategies (isohydric vs. anisohydric behavior), leaf morphology, hydraulic architecture, and biochemical limitations of photosynthesis [23,24]. Such interspecific variation has important implications for urban forest management, as species selection directly influences ecosystem resilience and the capacity of urban green infrastructure to mitigate climate extremes [25]. Furthermore, metrics such as water use efficiency (WUE), which reflect the balance between carbon gain and water loss, are not uniform across scales or methodologies, complicating comparisons between field measurements and remote sensing products [26]. Long-term observations indicate increasing WUE in many forest systems, although the underlying mechanisms—whether driven by enhanced photosynthesis or reduced stomatal conductance—vary depending on species and environmental conditions [27,28].

Remote sensing offers a powerful pathway for scaling physiological processes from the leaf to canopy and landscape levels, although it does not directly measure gas exchange parameters. Instead, it captures state variables such as canopy reflectance, land surface temperature, and vegetation structure, which can be linked to physiological functioning through biophysical models and empirical relationships [29,30]. Thermal remote sensing is particularly valuable, as canopy temperature integrates the balance between sensible and latent heat fluxes, providing an indirect but robust indicator of stomatal regulation and transpiration [31]. Increases in canopy temperature are commonly associated with reduced transpiration and stomatal closure, enabling the detection of plant water stress [32,33]. At the same time, optical remote sensing provides complementary information on canopy structure and photosynthetic capacity. Red-edge spectral indices have been shown to outperform traditional vegetation indices in capturing variability in gross primary productivity (GPP), particularly in relation to chlorophyll dynamics [34,35]. Additionally, solar-induced chlorophyll fluorescence (SIF) has emerged as a promising proxy for photosynthetic activity, although its ability to capture stomatal responses under stress conditions remains limited [35–38]. The primary objective of this study was to inte-

grate leaf-level physiological measurements with satellite-based remote sensing indicators in order to evaluate whether both approaches consistently detect similar physiological response patterns across contrasting urban environments. The study examined differences among tree species, between site types (urban street versus urban park), and between two measurement periods, thereby capturing spatial and temporal variability in environmental conditions. Furthermore, the study aimed to test whether relationships between thermal and optical remote sensing signals and leaf physiological parameters—well established in agricultural and forest ecosystems—are transferable to heterogeneous urban environments. In addition, the study evaluated how contrasting urban habitat conditions were associated with differences in stomatal conductance, photosynthesis, and transpiration across site types. Finally, it explored the potential utility of temperature-based indicators, such as land surface temperature (LST), relative to greenness-based vegetation indices for detecting physiological stress in urban trees.

Due to the inherent spatial and temporal scale differences between instantaneous leaf-level measurements and satellite-derived observations, the objective of this study is not to establish direct predictive relationships between terrestrial and remote sensing variables. Instead, the study focused on assessing the conceptual and directional consistency of ecological response patterns detected by terrestrial and satellite-based approaches across contrasting urban environments.

2. Materials and Methods

2.1. Study Area and Experimental Design

Novi Sad has a temperate continental climate (Köppen–Geiger classification: Cfb), characterized by warm summers and moderately cold winters. The mean annual air temperature is approximately 11 °C, while mean annual precipitation ranges from approximately 580 to 700 mm, with precipitation maxima typically occurring during late spring and early summer [39]. Seasonal climatic conditions are additionally influenced by regional air circulation patterns, including the Košava wind during autumn and winter periods. The research aimed to evaluate the physiological responses of selected tree species under contrasting environmental conditions, with a particular focus on the influence of urban stress factors.

Three commonly planted urban tree species were selected for the study: *P.* × *acerifolia*, *C. australis*, and *T. tomentosa*. These species were chosen due to their widespread use in urban greening and their presumed differences in tolerance to environmental stressors [40].

For each species, two types of sites were defined: (i) urban locations situated along roads with intensive traffic, representing environments exposed to pronounced anthropogenic stress, including elevated levels of air pollutants, higher temperatures associated with the urban heat island effect, and potential water deficit; and (ii) park locations characterized by reduced anthropogenic pressure, more favorable microclimatic conditions, and generally improved soil and moisture regimes (Figure 1, Table 1).

The study included three different parks and three distinct high-traffic streets within the city of Novi Sad. Environmental conditions within each habitat type were relatively comparable, as all selected parks and street canyon sites were located within the same urban area and exposed to similar climatic conditions. Although some degree of local microenvironmental variability is inevitable in urban ecosystems, the selected sites shared comparable levels of urban influence, vegetation structure, and environmental exposure, allowing meaningful comparisons between the two habitat types. The selected species differed among individual parks and streets, ensuring that each site represented a specific combination of environmental conditions and tree species. Specifically, *T. tomentosa* (●) was sampled along Bulevar cara Lazara as an urban site, while its park counterpart was located

at Petrovaradin Fortress. *P.* × *acerifolia* (■) was studied in the urban conditions of Futoška Street, with the park site located at the Štrand locality. The third species, *C. australis* (▼), was investigated along Radnička Street as an urban environment, while its park trees were located in Limanski Park.



Figure 1. Spatial Distribution of Study Sites (*P.* × *acerifolia* (■); *T. tomentosa* (●); *C. australis* (▼); green—parks; orange—urban environments).

Table 1. Coordinates of the investigated locations.

Study Sites	Latitude	Longitude
●	45.2527	19.8652
●	45.2451	19.8463
■	45.2361	19.8445
■	45.2516	19.8374
▼	45.2395	19.8408
▼	45.2485	19.8461

Such an experimental design enables a comparative assessment of species-specific adaptive responses and provides a basis for evaluating their suitability for urban environments under increasing environmental stress.

2.2. Physiological Measurements

Physiological measurements were conducted in situ on fully developed, sun-exposed leaves of selected tree species during the peak growing season, under stable and non-

limiting weather conditions to minimize short-term environmental variability. Measurements were conducted twice during 2022 (in July and August). Special care was taken to select leaves without any visible signs of chlorosis, mechanical damage, or disease symptoms, ensuring that all measurements reflected optimal physiological status. At each sampling site, both in urban and park environments, physiological measurements were conducted on five individual trees per species.

Measurements were performed using a CIRAS-3 portable photosynthesis system (Amesbury, MA, USA) during the morning hours, between 9:00 a.m. and 11:00 a.m., to capture optimal physiological activity. To maintain uniform environmental conditions during measurements, a constant photosynthetically active radiation (PAR) level of 1000 μmol m^{-2} s^{-1} and an atmospheric CO_2 concentration of 390 μmol mol^{-1} were applied.

Gas exchange parameters, including net photosynthetic rate (A), transpiration rate (E), and stomatal conductance (g_s), were determined using a portable photosynthesis system under ambient light and CO_2 conditions. Care was taken to ensure consistent measurement conditions across all sampling sites, including leaf position, orientation, and measurement timing.

Water use efficiency (WUE) was calculated as the ratio of net photosynthetic rate to transpiration rate (A/E), providing an integrated indicator of the balance between carbon assimilation and water loss. This parameter is particularly relevant for assessing plant performance under conditions of environmental stress, such as those present in urban ecosystems.

2.3. Remote Sensing Data Sources and Preprocessing

Satellite-derived variables were obtained and processed using the Google Earth Engine (GEE) platform. The analysis integrated data from multiple satellite systems, including Sentinel-2, Landsat 8 and 9, and MODIS products, in order to capture vegetation status, water availability, and thermal conditions over time.

Optical data were derived from the Sentinel-2 MultiSpectral Instrument (MSI) (European Space Agency—ESA, Paris, France), using the surface reflectance product (COPERNICUS/S2_SR_HARMONIZED). Images were filtered by date and spatial extent and further constrained by scene-level cloudiness, with a maximum cloud cover threshold of 50%. Cloud and cirrus contamination were removed using the QA60 band, applying bitmask filtering for cloud (bit 10) and cirrus (bit 11). In addition, the Scene Classification Layer (SCL) was used to exclude cloud shadows, medium- and high-probability clouds, cirrus, and snow/ice pixels.

From the cloud-masked Sentinel-2 imagery, several vegetation indices were calculated. The Normalized Difference Vegetation Index (NDVI) was computed using near-infrared (Band 8) and red (Band 4) reflectance. The Normalized Difference Red Edge Index (NDRE) was calculated using near-infrared (Band 8) and red-edge bands (Band 5). The Normalized Difference Water Index (NDWI) was calculated using green (Band 3) and near-infrared (Band 8) bands following the McFeeters formulation. The Normalized Difference Moisture Index (NDMI) was calculated using near-infrared (Band 8) and shortwave infrared (Band 11) reflectance.

Thermal data were obtained from Landsat 8 and Landsat 9 Collection 2 Level-2 products. Cloud, shadow, and snow pixels were removed using the QA_PIXEL band. Land surface temperature (LST) was derived from the ST_B10 thermal band using standard radiometric conversion. Digital numbers were converted to temperature in Kelvin using the scaling factor (0.00341802) and additive constant (149.0) and subsequently converted to degrees Celsius by subtracting 273.15.

Ecosystem-scale variables were obtained from MODIS products. Gross primary productivity (GPP) was derived from the MOD17A2HGF dataset and scaled using a factor of 0.0001. Evapotranspiration (ET) was obtained from the MOD16A2GF dataset and scaled by 0.1. These datasets were temporally matched using inner joins based on acquisition time, and water use efficiency (WUE) was calculated as the ratio of GPP to ET (GPP/ET).

To reduce noise and harmonize temporal resolution across datasets, all satellite variables were aggregated into fixed time intervals using a compositing approach. Composite images were generated at regular intervals (10- or 15-day steps, depending on configuration) by averaging all available observations within each time window. For each composite, metadata were retained, including the number of observations contributing to the composite for each sensor. The compositing approach was applied to minimize cloud contamination, reduce short-term variability, and improve temporal comparability between satellite-derived indicators and field-based physiological measurements. For each time step, data from Sentinel-2, Landsat, and MODIS were merged into a single multi-band image. Sentinel-2 indices, Landsat-derived LST, and MODIS-derived GPP, ET, and WUE were combined to create a unified dataset representing vegetation condition and environmental stress.

Spatial sampling was performed at predefined point locations representing individual trees. To reduce single-pixel noise and spatial misalignment, a buffer of 5 m was applied around each point. Mean values of all variables were extracted within the buffered area using a spatial reducer.

The resulting dataset consisted of time series of satellite-derived variables for each sampling point, including NDVI, NDRE, NDWI, NDMI, LST (°C), GPP, ET, and WUE, along with temporal metadata (start and end date of each composite interval).

Based on the extracted satellite variables, proxy indicators of plant physiological processes were constructed.

Derivation of Remote Sensing Proxies

The proxy variables used in this study were based on established thermal and optical remote sensing indices commonly associated with canopy productivity, vegetation water status, and thermal stress. In the present study, these variables were interpreted as ecophysiological indicators of physiological response patterns within the specific context of urban environmental stress assessment, rather than as direct physiological retrieval products or calibrated biophysical models.

The photosynthesis proxy (A_proxy) was derived from vegetation indices sensitive to chlorophyll content and canopy productivity, primarily NDRE and NDVI, assuming that higher values correspond to increased photosynthetic activity.

The stomatal conductance proxy (g_s_proxy) was derived from a combination of canopy water status and thermal conditions, using NDMI as an indicator of water availability and LST as an indicator of heat stress, where higher NDMI and lower LST correspond to higher stomatal conductance. G_s_proxy was inferred from the relationship between NDMI and LST, representing canopy water availability and thermal stress conditions.

The transpiration proxy (E_proxy) was primarily derived from land surface temperature (LST), with additional contextual support from evapotranspiration (ET) data obtained from MODIS products. Importantly, E_proxy does not represent direct transpiration flux. Instead, it should be interpreted as a temperature-driven indicator of evaporative demand and thermal stress conditions. Higher values reflect increased thermal load and atmospheric demand, which are associated with reduced stomatal conductance and lower actual transpiration at the leaf level. Therefore, E_proxy was interpreted as an inverse proxy of transpiration.

https://doi.org/10.3390/f17060647

Water use efficiency (WUE_proxy) was derived from MODIS-based estimates as the ratio of GPP to ET, representing the efficiency of carbon assimilation relative to water use.

The intercellular CO_2 proxy (Ci_proxy) was estimated indirectly from the relationship between photosynthetic activity and thermal stress, combining NDRE and LST signals, where higher values reflect reduced CO_2 assimilation and increased physiological stress. Ci_proxy was interpreted as an indirect indicator derived from the relationship between NDRE and LST.

2.4. Statistical Analysis

2.4.1. Statistical Analysis for Terrestrial Data

The statistical analyses were performed using repeated-measures analysis of variance (ANOVA) to assess temporal variation in the examined parameters, followed by Tukey's HSD test for post hoc comparisons between measurement times. The analysis was designed to identify statistically significant differences (1) between park and urban sites, (2) among species, (3) in the interaction between species and locality, and (4) across measurement times, at a significance level of $p < 0.05$.

All statistical analyses were conducted using STATISTICA 14.0.0 software (TIBCO Software Inc., Palo Alto, CA, USA).

2.4.2. Statistical Evaluation of Site Effects on Satellite-Derived Proxies

For each sampling point and time period, satellite-derived variables were aggregated, and mean values were calculated for the corresponding observation periods. Differences between environments were quantified as follows:

$$\Delta = \text{Urban} - \text{Park}$$

where negative values indicate lower proxy values in urban environments, and positive values indicate higher values.

To assess the statistical significance of differences between site types, Welch's *t*-test was applied independently for each species and proxy variable. This test was selected because it does not assume equal variances between groups and is robust for datasets with unequal sample sizes. For each comparison, the null hypothesis assumed no difference between urban and park conditions. In addition to Welch's *t*-test, effect sizes were calculated using Cohen's d to evaluate the magnitude and ecological relevance of differences between urban and park environments.

Statistical significance was evaluated using the following thresholds: * $p < 0.05$, ** $p < 0.01$, *** $p < 0.001$.

Results were visualized using heatmaps, where each cell represents the mean difference (Urban − Park) for a given species and proxy variable, with significance levels indicated by asterisks.

In addition to significance testing, species-specific responses to urban conditions were evaluated by calculating the magnitude of change as the mean absolute difference:

$$|\Delta| = |\text{Urban} - \text{Park}|$$

This metric was used to compare the relative sensitivity of species to environmental stress, where smaller values indicate higher tolerance and larger values indicate greater sensitivity.

All satellite data processing, including cloud masking, index calculation, temporal compositing, and spatial sampling, was performed within the Google Earth Engine (GEE) platform. For each sampling point, time-series data were extracted and exported as tabular

datasets (CSV format) containing vegetation indices, land surface temperature, and MODIS-derived variables, together with temporal metadata.

The exported datasets were subsequently processed and analyzed outside of GEE using Python 3.14 software (Python Software Foundation, Wilmington, DE, USA), where statistical analyses and visualizations were conducted (pandas 3.0, numpy 2.4, scipy 1.17, and matplotlib 3.10).

Statistical analysis was performed to evaluate differences between urban and park environments for each species and satellite-derived proxy variable.

3. Results

3.1. Effects of Species, Environmental Conditions, and Measurement Time on Leaf Gas Exchange Parameters

The repeated-measures ANOVA results show that all measured variables (Ci, A, E, g_s, and WUE) changed significantly over time (factor Repeated, $p < 0.001$), indicating temporal variation across measurements.

Ci showed a significant species effect (F = 28.23, $p < 0.001$), while the environmental treatment was not significant (F = 0.50, $p = 0.48$), and there was no species × environment interaction (F = 0.03, $p = 0.97$). Thus, Ci differs among species and over time but does not respond to the environmental treatment, nor does the treatment effect depend on species (Table 2).

Table 2. F-test based on the ANOVA for repeated measurement for the examined leaf gas exchange parameters.

	Ci **µmol mol^{-1}**		**A** **µmol m^{-2} s^{-1}**		**E** **mmol m^{-2} s^{-1}**		**g_s** **mmol m^{-2} s^{-1}**		**WUE** **mmol m^{-2} s^{-1}**	
	F	***p***	**F**	***p***	**F**	***p***	**F**	***p***	**F**	***p***
Repeated	38.81	0.00	228.82	0.00	500.20	0.00	126.82	0.00	179.19	0.00
Species (A)	28.23	0.00	0.24	0.78	18.3	0.00	20.15	0.00	11.34	0.00
Environment (B)	0.50	0.48	9.32	0.00	0.91	0.34	10.38	0.00	6.24	0.01
Interaction A × B	0.03	0.97	7.31	0.00	2.55	0.08	10.24	0.00	2.39	0.09

F stands for F-value and *p* stands for *p*-value.

Photosynthetic rate A did not differ among species (F = 0.24, $p = 0.78$) but was significantly affected by environment (F = 9.32, $p < 0.001$) and showed a significant species × environment interaction (F = 7.31, $p < 0.001$). This indicates that the environmental effect on A depends on species; post hoc tests are needed to identify which species and treatments differ (Table 2).

Transpiration E differed among species (F = 18.30, $p < 0.001$) and varied over time, while the main effect of environment was not significant (F = 0.91, $p = 0.34$). The species × environment interaction for E was significant (F = 2.55, $p = 0.08$), suggesting a possible trend but not a statistically significant interaction at $\alpha = 0.05$ (Table 2).

Stomatal conductance g_s showed significant main effects and interaction: species (F = 20.15, $p < 0.001$), environment (F = 10.38, $p < 0.001$), and species × environment (F = 10.24, $p < 0.001$). This indicates that environmental effects on g_s differ by species; pairwise comparisons should be performed to identify specific differences (Table 1).

Water use efficiency (WUE) differed among species (F = 11.34, $p < 0.001$) and was affected by environment (F = 6.24, $p = 0.01$). The species × environment interaction was not significant at $\alpha = 0.05$ (F = 2.39, $p = 0.09$) but shows a trend (Table 2).

The results of the post hoc test indicated statistically significant differences between the two measurements for all analyzed leaf gas exchange parameters. The values of intercellular CO_2 concentration (Ci), net photosynthetic rate (A), transpiration rate (E), and

stomatal conductance (g_s) were significantly higher during the first measurement compared to the second measurement. In contrast, water use efficiency (WUE) was significantly higher during the second measurement than the first measurement (Table 3). These results indicate pronounced differences in the physiological responses of plants between the two measurement times.

Table 3. Result of Tukey's post hoc test.

Period of Measurments	I	II	I	II	I	II	I	II	I	II
Parameters	Ci	Ci	A	A	E	E	g_s	g_s	WUE	WUE
Mean	431.62 [a]	276.80 [b]	8.43 [a]	5.59 [b]	6.97 [a]	1.71 [b]	100.59 [a]	58.49 [b]	1.59 [b]	3.49 [a]

Values with the same letter are not significantly different according to Tukey's HSD test for $\alpha = 0.05$.

3.2. Urban Effects on Satellite-Derived Physiological Proxies

Satellite-derived proxy variables revealed consistent and statistically significant differences between urban and park environments across all studied species (Figure 2). Overall, both terrestrial measurements and satellite-derived proxies consistently indicated reduced physiological performance and increased stress under urban conditions, with comparable directional response patterns among species.

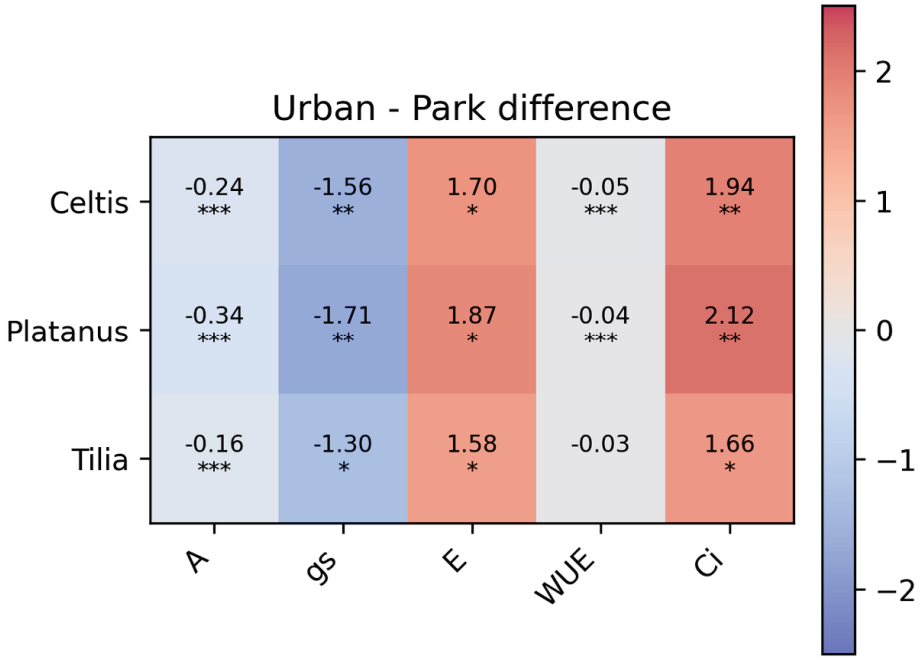


Figure 2. Differences between urban and park environments (Urban − Park) for satellite-derived physiological proxies across three tree species (*C. australis*, *P. acerifolia*, and *T. tomentosa*). Values shown in the heatmap represent signed mean differences (Δ = Urban − Park), where negative values (blue) indicate lower values in urban environments and positive values (red) indicate higher values. Statistical significance of differences between site types was assessed using Welch's *t*-test and is indicated as follows: * $p < 0.05$, ** $p < 0.01$, *** $p < 0.001$. The transpiration proxy (E_proxy) is primarily derived from land surface temperature (LST) and interpreted in the context of evapotranspiration (ET); higher values correspond to increased thermal stress and reduced actual transpiration.

3.2.1. Differences Between Urban and Park Environments

Net photosynthesis (A_proxy) was consistently lower in urban environments for all species, with negative Δ values indicating reduced photosynthetic activity under urban con-

ditions. These differences were statistically significant for all species ($p < 0.001$), indicating a strong and consistent urban effect (Figure 2).

Stomatal conductance (g_s_proxy) followed a similar pattern, showing significantly lower values in urban environments across all species. The magnitude of reduction was consistent and statistically significant ($p < 0.001$), suggesting reduced stomatal activity under increased environmental stress (Figure 2).

In contrast, intercellular CO_2 proxy values (Ci_proxy) were consistently higher in urban environments for all species, with positive Δ values and strong statistical significance ($p < 0.001$). This pattern indicates reduced CO_2 assimilation efficiency and increased physiological stress (Figure 2).

The transpiration proxy (E_proxy), derived primarily from land surface temperature (LST) and interpreted in conjunction with evapotranspiration (ET), showed higher values in urban environments across all species. These differences were statistically significant ($p < 0.001$). Given that E_proxy is derived from land surface temperature and represents a stress-related signal, higher values indicate increased evaporative demand and reduced actual transpiration (Figure 2).

Water use efficiency (WUE_proxy) was generally lower in urban environments, with negative Δ values observed across species. These differences were statistically significant, although with smaller effect sizes compared to other variables, indicating a moderate reduction in efficiency under urban conditions (Figure 2). Effect-size analysis confirmed that most urban–park differences were not only statistically significant but also associated with moderate to large standardized effects. The strongest effects were observed for A_proxy, while g_s_proxy, E_proxy, and Ci_proxy showed medium to large effects during the growing season. Although WUE_proxy differences were statistically significant, their ecological interpretation was treated cautiously due to the small absolute magnitude of change.

3.2.2. Species-Specific Responses

Although all species exhibited consistent directional responses to urban conditions, the magnitude of these responses differed among species.

P. × acerifolia showed the largest deviations between urban and park environments across all proxy variables, indicating the strongest response to urban stress. *C. australis* exhibited intermediate changes, while *T. tomentosa* consistently showed the smallest differences between environments. These patterns were consistent across all proxy variables, indicating that *T. tomentosa* was the least affected by urban conditions, while *P. × acerifolia* was the most sensitive (Figure 2).

Across all species, urban environments were associated with:

- Reduced photosynthetic activity (A_proxy);
- Reduced stomatal conductance (g_s_proxy);
- Reduced water use efficiency (WUE_proxy);
- Increased intercellular CO_2 (Ci_proxy);
- Increased stress-related transpiration proxy (E_proxy).

These results demonstrate a consistent and coherent physiological response to urban conditions captured by satellite-derived proxies.

4. Discussion

4.1. Physiological Responses of Tree Species to Contrasting Urban and Park Environments

The obtained results demonstrate that both species identity and environmental conditions play a key role in shaping leaf gas exchange responses, with additional modulation by temporal variation. The significant effect of species observed across all parameters indi-

cates pronounced inherent physiological differences among *T. tomentosa*, *C. australis*, and *P.* × *acerifolia*. These differences likely reflect variation in photosynthetic capacity, stomatal regulation, and water use strategies, which together determine how species respond to environmental constraints.

Overall, the obtained results indicate consistent differences in physiological responses between trees growing in street canyons and those in park habitats. Trees exposed to street canyon conditions generally exhibited reduced stomatal conductance and gas exchange intensity, suggesting a stronger influence of urban environmental stress. In contrast, individuals located in park habitats maintained comparatively higher physiological activity under more favorable microclimatic conditions. Additionally, temporal variation between the two measurement periods indicated seasonal changes in plant physiological performance, likely associated with differences in temperature, water availability, and atmospheric conditions during the study period. These findings collectively support the conclusion that contrasting urban habitats significantly influence plant physiological responses and adaptive capacity.

The absence of a significant environmental effect on Ci, despite its pronounced variation among species, suggests that intercellular CO_2 concentration is largely governed by intrinsic physiological traits rather than direct environmental control. However, the significant species × environment interaction indicates that environmental conditions modulate Ci indirectly through species-specific responses [41]. The consistently higher Ci observed in *P.* × *acerifolia*, particularly under urban conditions, may indicate reduced carboxylation efficiency or biochemical limitations of photosynthesis, resulting in a mismatch between CO_2 supply and assimilation. Such a response is commonly associated with stress conditions, where metabolic constraints, rather than stomatal limitation, dominate the regulation of photosynthesis [24,42]. In contrast, lower Ci values in *T. tomentosa* and *C. australis* suggest a more efficient coordination between stomatal conductance and carbon fixation [42,43].

Photosynthetic rate, transpiration, and stomatal conductance were strongly influenced by environmental conditions, with significantly higher values recorded in park environments. This pattern indicates that park habitats provide more favorable microclimatic conditions, including improved water availability, lower temperatures, and reduced pollutant load, which collectively enhance physiological activity [35]. The significant species × environment interaction observed for A and g_s further suggests that the magnitude of these responses is species dependent. For example, *C. australis* exhibited the highest photosynthetic rates and transpiration, particularly under park conditions, indicating a high degree of physiological plasticity and the ability to maximize carbon gain under favorable conditions. Conversely, reductions in A and g_s under urban conditions, especially in *T. tomentosa*, suggest a stronger sensitivity to environmental stress [44,45].

Although E was significantly affected by both species and environment, the lack of significant interaction indicates a relatively consistent response pattern across species. This suggests that, while absolute transpiration rates differ, the direction of change between urban and park environments is similar among species, likely reflecting a common response to environmental drivers such as vapor pressure deficit or soil moisture availability [46–48].

Water use efficiency showed significant differences among species but was not significantly influenced by environmental conditions, indicating that intrinsic species traits play a dominant role in determining water use strategies. The higher WUE observed in *P.* × *acerifolia* suggests a more conservative water use strategy, which may confer a competitive advantage under water-limited or stressful urban conditions. In contrast, lower WUE values in *T. tomentosa* may indicate a strategy oriented toward higher gas exchange rates at the expense of water conservation [49,50].

The repeated-measures ANOVA further revealed pronounced temporal variation in all examined parameters, emphasizing the importance of measurement timing in physiological

assessments. The observed decline in Ci, A, E, and g_s during the second measurement, accompanied by a significant increase in WUE, suggests a shift toward more conservative water use behavior over time. This pattern is indicative of progressive environmental stress, such as increasing temperature or decreasing water availability, leading to partial stomatal closure and reduced carbon assimilation [38,49].

Importantly, the significant species × environment interactions observed for A and g_s in the repeated-measures analysis indicate that temporal dynamics are not uniform across species. This suggests that different species employ distinct acclimation strategies over time, with some maintaining higher physiological activity under changing conditions, while others exhibit stronger reductions in gas exchange as a protective response [51,52]. Species like ash (*Fraxinus chinensis*) maintain higher A and photosynthetic capacity under combined pavement and drought compared to ginkgo (*Ginkgo biloba*), which shows greater reductions [52]. Although the interaction effects for E and WUE were not statistically significant, the observed patterns may suggest subtle species-specific temporal adjustments that could become more pronounced under prolonged stress conditions. Protective stomatal closure may reduce g_s and E in susceptible species during prolonged stress, while more tolerant species (e.g., *Gleditsia triacanthos*, *Pyrus calleryana*, *Platanus* × *hispanica*) may sustain higher g_s and adjust by dissipating excess light energy without complete stomatal closure [53].

4.2. Remote Sensing Proxies and Their Agreement with Leaf-Level Measurements

The comparison between satellite-derived physiological proxies and leaf-level gas exchange measurements revealed a high degree of conceptual and directional agreement across both environmental gradients and species-specific responses. Although remote sensing proxies do not directly measure physiological processes, the observed patterns closely mirrored those obtained from in situ measurements, supporting their applicability for large-scale monitoring of tree physiological performance.

Across all species, both approaches consistently indicated that urban environments impose significant physiological constraints. Leaf-level measurements showed reduced net photosynthesis (A), stomatal conductance (g_s), and transpiration (E) under urban conditions, accompanied by increased intercellular CO_2 concentration (Ci), suggesting limitations in carbon assimilation [54]. These patterns are consistent with previous leaf-level physiological studies reporting reduced gas exchange and stomatal activity in urban trees exposed to thermal and atmospheric stress [6,14]. These patterns were strongly reflected in the satellite-derived proxies, where A_proxy and g_s_proxy were significantly lower in urban environments, while Ci_proxy and E_proxy were higher.

The agreement between methods is particularly notable for variables directly linked to stomatal regulation and thermal stress. The increase in E_proxy in urban environments, derived primarily from land surface temperature (LST), corresponds well with the observed decrease in actual transpiration (E) measured at the leaf level. This apparent contradiction is physiologically consistent, as higher canopy temperatures indicate reduced latent heat flux due to stomatal closure, leading to increased thermal stress despite lower actual water loss. These relationships between canopy temperature, stomatal conductance, and transpiration have been well documented in thermal remote sensing studies [25,47]. In this context, E_proxy effectively captures evaporative demand rather than transpiration itself, highlighting the importance of interpreting thermal signals as inverse indicators of physiological activity.

Similarly, the increase in Ci_proxy under urban conditions aligns with measured increases in Ci, suggesting that satellite-based indicators combining spectral and thermal information can successfully capture limitations in CO_2 assimilation. This reflects a decou-

pling between stomatal conductance and photosynthetic capacity under stress conditions, where biochemical limitations become more pronounced, as reported in studies examining stress-induced photosynthetic constraints [17,33].

Species-specific responses were also consistently detected by both approaches. *P.* × *acerifolia* exhibited the largest differences between urban and park environments in both leaf-level measurements and satellite-derived proxies, indicating a strong sensitivity to urban stress. In contrast, *T. tomentosa* showed the smallest changes across environments, suggesting higher tolerance. *C. australis* displayed intermediate responses, consistent with its relatively high physiological plasticity observed in gas exchange measurements. These findings are in agreement with previous studies demonstrating interspecific variability in drought tolerance and stomatal regulation strategies in urban trees [14,16].

The consistency in species ranking between methods is particularly important, as it demonstrates that remote sensing proxies are capable not only of detecting general environmental effects but also of resolving interspecific differences in stress responses. This supports their use in urban forestry for species selection and performance assessment at spatial scales not achievable through field measurements alone. Similar conclusions have been reported in remote sensing-based vegetation monitoring studies, integrating remote sensing and physiological data for vegetation monitoring [12,13].

4.3. Limitations of the Remote Sensing Approach, Implications and Synthesis

Despite the overall agreement between satellite-derived proxies and leaf-level measurements, several limitations should be acknowledged. Remote sensing proxies represent integrated canopy-level signals and do not directly measure leaf-level physiological processes [22,23]. Consequently, relationships between proxies and gas exchange parameters are inherently indirect and may be influenced by canopy structure, background reflectance, and spatial heterogeneity.

The temporal resolution of satellite data, based on composited observations, may not fully capture short-term physiological dynamics or diurnal variability observed at the leaf level. This temporal mismatch introduces uncertainty when comparing instantaneous field measurements with temporally aggregated satellite signals.

Furthermore, the transpiration proxy (E_proxy), derived primarily from land surface temperature, reflects thermal and evaporative stress rather than actual transpiration flux. Although this approach is widely used in remote sensing studies, it requires careful interpretation, particularly when directly comparing satellite-derived indicators with leaf-level transpiration measurements. The spatial resolution of satellite data may introduce mixed-pixel effects, especially in heterogeneous urban environments, where individual tree crowns can be influenced by surrounding surfaces such as soil, grass, or built structures [25].

Despite these limitations, the strong agreement between satellite-derived proxies and leaf-level measurements demonstrates that remote sensing approaches can reliably capture key physiological responses of urban trees to environmental stress. The ability to reproduce both the direction and relative magnitude of differences between urban and park environments, as well as species-specific responses, highlights the robustness of the proxy-based approach. Importantly, the consistency in relative response patterns among species observed in both datasets indicates that remote sensing may help identify differences in stress responses among urban tree species. This is particularly relevant for urban forestry applications, where large-scale monitoring and species selection are critical. Because tree species were sampled across distinct urban and park locations rather than replicated within identical site conditions, species-specific responses should be interpreted cautiously, as they may partially reflect unmeasured site-related environmental variability.

https://doi.org/10.3390/f17060647

Due to the spatial and temporal scale mismatch between instantaneous physiological measurements and temporally aggregated satellite observations, direct quantitative correspondence between field and remote sensing variables should not be expected. Additionally, the heterogeneous structure of urban landscapes may introduce mixed-pixel effects within moderate-resolution satellite imagery, potentially incorporating signals from impervious surfaces, bare soil, and shaded areas surrounding tree canopies. The absence of detailed environmental covariate measurements (e.g., air temperature, vapor pressure deficit, soil moisture, and pollution intensity) represents an important limitation of the present study and restricts mechanistic interpretation of the observed physiological responses. Therefore, remotely sensed variables should be interpreted as ecological indicators of physiological response patterns rather than direct equivalents of instantaneous leaf-level measurements. Nevertheless, the integration of satellite-based indicators with physiological measurements provides a valuable framework for linking leaf-level processes with landscape-scale assessments of urban vegetation stress [55]. Such an approach may support more efficient monitoring, management, and selection of urban tree species under changing environmental conditions [56].

5. Conclusions

The results clearly indicate that park environments support higher physiological performance, while urban conditions impose constraints that limit gas exchange and promote more conservative water use strategies. Among the studied species, *C. australis* appears to exhibit greater physiological plasticity and responsiveness to favorable conditions, whereas *P.* × *acerifolia* shows traits associated with stress tolerance, particularly in maintaining higher WUE and Ci under urban conditions. *T. tomentosa*, on the other hand, appears to be more sensitive to environmental stress, as indicated by stronger reductions in gas exchange parameters. These findings highlight the importance of species-specific traits in determining plant performance in urban ecosystems and provide valuable insights for the selection of species in urban greening and climate adaptation strategies. In addition to leaf-level physiological measurements, satellite-derived proxies consistently reproduced the observed patterns of physiological responses across both environmental gradients and species. The agreement between field measurements and remote sensing indicators supports that proxy-based approaches can reliably capture reductions in photosynthetic activity, stomatal conductance, and transpiration, as well as increases in physiological stress under urban conditions. Importantly, both approaches identified similar species-specific responses, with *P.* × *acerifolia* showing the highest sensitivity and *T. tomentosa* the lowest. These findings demonstrate that remote sensing can effectively upscale leaf-level physiological processes and provide a robust tool for monitoring urban tree performance across larger spatial scales. This study demonstrates that satellite-based proxies not only complement field-based physiological measurements but also consistently capture comparable physiological response patterns across environments and species.

Author Contributions: Conceptualization, S.K. and M.Z.; methodology, L.K.; software, L.K. and V.V.; validation, V.V. and L.K.; investigation, L.K., O.K. and V.V.; data curation, L.K. and V.V.; writing—original draft preparation, L.K. and V.V.; writing—review and editing, L.K., V.V., L.P. and S.O.; visualization, L.K., O.K. and V.V.; supervision, S.O.; project administration, S.K.; funding acquisition, S.O. All authors have read and agreed to the published version of the manuscript.

Funding: This research has been supported by the Ministry of Science, Technological Development, and Innovation of the Republic of Serbia (Contract No. 451-03-33/2026-03/200197) and by the Provincial Secretariat for Higher Education and Scientific Research through the project 'Influence of specific factors in urban environment on alley trees vitality' (Contract No. 003085367 2024 09418 003 000 000 001/2).

Data Availability Statement: All data are included in the manuscript. Further inquiries can be directed at the author and corresponding author.

Acknowledgments: The authors would like to thank the Public Utility Company "Gradsko zelenilo Novi Sad" for their support and assistance during the research.

Conflicts of Interest: The authors declare no conflicts of interest.

References

1. Piracha, A.; Chaudhary, M.T. Urban Air Pollution, Urban Heat Island and Human Health: A Review of the Literature. *Sustainability* **2022**, *14*, 9234. [CrossRef]
2. Pacheco, P.; Mera, E.; Fuentes, V. Intensive Urbanization, Urban Meteorology and Air Pollutants: Effects on the Temperature of a City in a Basin Geography. *Int. J. Environ. Res. Public Health* **2023**, *20*, 3941. [CrossRef] [PubMed]
3. Yuan, W.; Zheng, Y.; Piao, S.; Ciais, P.; Lombardozzi, D.; Wang, Y.; Ryu, Y.; Chen, G.; Dong, W.; Hu, Z.; et al. Increased Atmospheric Vapor Pressure Deficit Reduces Global Vegetation Growth. *Sci. Adv.* **2019**, *5*, eaax1396. [CrossRef] [PubMed]
4. Patel, S. The Potential for Urban Vegetation to Mitigate Ambient Air Pollution Threats to Public Health. *Topophilia* **2020**, 53–62. [CrossRef]
5. Muhammad, I.; Shalmani, A.; Ali, M.; Yang, Q.H.; Ahmad, H.; Li, F.B. Mechanisms Regulating the Dynamics of Photosynthesis Under Abiotic Stresses. *Front. Plant Sci.* **2021**, *11*, 615942. [CrossRef]
6. Winbourne, J.B.; Jones, T.S.; Garvey, S.M.; Harrison, J.L.; Wang, L.; Li, D.; Templer, P.H.; Hutyra, L.R. Tree Transpiration and Urban Temperatures: Current Understanding, Implications, and Future Research Directions. *Bioscience* **2020**, *70*, 576–588. [CrossRef]
7. Guo, F.; Jin, J.; Yong, B. Responses of Forest Water-Use Efficiency to Growing Season Length Across Eastern China. In *Proceedings of the IGARSS 2019–2019 IEEE International Geoscience and Remote Sensing Symposium, Yokohama, Japan, 28 July–2 August 2019*; IEEE: New York, NY, USA, 2019; pp. 7399–7402.
8. Xue, J.; Su, B. Significant Remote Sensing Vegetation Indices: A Review of Developments and Applications. *J. Sens.* **2017**, *2017*, 1353691. [CrossRef]
9. Xu, X.; Tang, Y.; Qu, Y.; Zhou, Z.; Hu, J. Global Vegetation Photosynthetic Phenology Products Based on Modis Vegetation Greenness and Temperature: Modeling and Evaluation. *Remote Sens.* **2021**, *13*, 5080. [CrossRef]
10. Sun, Y.; Qin, Q.; Ren, H.; Zhang, T.; Chen, S. NoRed-Edge Band Vegetation Indices for Leaf Area Index Estimation From Sentinel-2/MSI Imagery. In *Proceedings of the IEEE Transactions on Geoscience and Remote Sensing*; IEEE: New York, NY, USA, 2020; pp. 826–840.
11. Zhang, Y.; Shao, Z. Assessing of Urban Vegetation Biomass in Combination with LiDAR and High-Resolution Remote Sensing Images. *Int. J. Remote Sens.* **2021**, *42*, 964–985. [CrossRef]
12. Oivukkamäki, J.; Aalto, J.; Pfündel, E.E.; Tian, M.; Zhang, C.; Grebe, S.; Salmon, Y.; Hölttä, T.; Porcar-Castell, A. Integrating Leaf Gas Exchange and Chlorophyll Fluorescence to Reveal the Long-Term Regulation of Photosynthesis in Situ. *bioRxiv* **2023**. [CrossRef]
13. Damm, A.; Paul-Limoges, E.; Kükenbrink, D.; Bachofen, C.; Morsdorf, F. Remote Sensing of Forest Gas Exchange: Considerations Derived from a Tomographic Perspective. *Glob. Change Biol.* **2020**, *26*, 2717–2727. [CrossRef] [PubMed]
14. Marchin, R.M.; Backes, D.; Ossola, A.; Leishman, M.R.; Tjoelker, M.G.; Ellsworth, D.S. Extreme Heat Increases Stomatal Conductance and Drought-Induced Mortality Risk in Vulnerable Plant Species. *Glob. Change Biol.* **2022**, *28*, 1133–1146. [CrossRef]
15. Liu, Y.; Zhao, D.; Zhang, Y.; Zhang, Z. Global 0.1-Degree Monthly Mean Hourly Total Canopy Solar-Induced Chlorophyll Fluorescence Dataset Derived from Random Forest. *Remote Sens.* **2025**, *17*, 3429. [CrossRef]
16. Konarska, J.; Uddling, J.; Holmer, B.; Lutz, M.; Lindberg, F.; Pleijel, H.; Thorsson, S. Transpiration of Urban Trees and Its Cooling Effect in a High Latitude City. *Int. J. Biometeorol.* **2015**, *60*, 159–172. [CrossRef]
17. Hang, J.; Chen, G. Xperimental Study of Urban Microclimate on Scaled Street Canyons with Various Aspect Ratios. *Urban Clim.* **2022**, *46*, 101299. [CrossRef]
18. Gebert, L.L.; Coutts, A.M.; Tapper, N.J. The Influence of Urban Canyon Microclimate and Contrasting Photoperiod on the Physiological Response of Street Trees and the Potential Benefits of Water Sensitive Urban Design. *Urban For. Urban Green.* **2019**, *40*, 152–164. [CrossRef]
19. Wu, Q.; Huang, Y.; Irga, P.; Kumar, P.; Li, W.; Wei, W.; Kyong, H.; Lei, C.; Zhou, J.L. Synergistic Control of Urban Heat Island and Urban Pollution Island Effects Using Green Infrastructure. *J. Environ. Manag.* **2024**, *370*, 122985. [CrossRef]
20. Bright, V.B.; Bloss, W.J.; Cai, X. Urban Street Canyons: Coupling Dynamics, Chemistry and within-Canyon Chemical Processing of Emissions. *Atmos. Environ.* **2013**, *68*, 127–142. [CrossRef]
21. Liu, H.; Shen, Y. The Impact of Green Space Changes on Air Pollution and Microclimates: A Case Study of the Taipei Metropolitan Area. *Sustainability* **2014**, *6*, 8827–8855. [CrossRef]

22. Lima, W.D.P.; Jarvis, P.; Rhizopoulou, S. Stomatal responses of Eucalyptus species to elevated CO_2 concentration and drought stress. *Sci. Agric.* **2003**, *60*, 231–238. [CrossRef]
23. Leuschner, C.; Wedde, P.; Lübbe, T. The Relation between Pressure–Volume Curve Traits and Stomatal Regulation of Water Potential in Five Temperate Broadleaf Tree Species. *Ann. For. Sci.* **2019**, *76*, 60. [CrossRef]
24. Chen, Z.; Li, S.; Wan, X.; Liu, S. Strategies of Tree Species to Adapt to Drought from Leaf Stomatal Regulation and Stem Embolism Resistance to Root Properties. *Front. Plant Sci.* **2022**, *13*, 926535. [CrossRef]
25. Wan, H.; McLaughlin, D.; Shao, Y.; van Eerden, B.; Ranganathan, S. Remotely-Sensed Evapotranspiration for Informed Urban Forest Management. *Landsc. Urban Plan.* **2021**, *210*, 104069. [CrossRef]
26. Puchi, P. One Metric, Many Meanings: Reconciling Water Use Efficiency Definitions. 2025, pp. 1–12. Available online: https://essopenarchive.org/doi/full/10.22541/essoar.176340163.39240299 (accessed on 8 April 2026).
27. Guerrieri, R.; Belmecheri, S.; Ollinger, S.V.; Asbjornsen, H.; Jennings, K.; Xiao, J.; Stocker, B.D.; Martin, M.; Hollinger, D.Y.; Bracho-Garrillo, R.; et al. Disentangling the Role of Photosynthesis and Stomatal Conductance on Rising Forest Water-Use Efficiency. *Proc. Natl. Acad. Sci. USA* **2019**, *116*, 16909–16914. [CrossRef] [PubMed]
28. Palandrani, C.; Motta, R.; Cherubini, P.; Čurović, M.; Dukić, V.; Tonon, G.; Ceccon, C.; Peressotti, A.; Alberti, G. Role of Photosynthesis and Stomatal Conductance on the Long-Term Rising of Intrinsic Water Use Efficiency in Dominant Trees in Three Oldgrowth Forests in Bosnia-Herzegovina and Montenegro. *IForest* **2021**, *14*, 53–60. [CrossRef]
29. Chen, J.M.; Liu, J. Evolution of Evapotranspiration Models Using Thermal and Shortwave Remote Sensing Data. *Remote Sens. Environ.* **2020**, *237*, 111594. [CrossRef]
30. Derardja, B.; Khadra, R.; Abdelmoneim, A.A.A.; El-Shirbeny, M.A.; Valsamidis, T.; De Pasquale, V.; Deflorio, A.M.; Volden, E. Advancements in Remote Sensing for Evapotranspiration Estimation: A Comprehensive Review of Temperature-Based Models. *Remote Sens.* **2024**, *16*, 1927. [CrossRef]
31. Hou, M.; Tian, F.; Zhang, T.; Huang, M. Evaluation of Canopy Temperature Depression, Transpiration, and Canopy Greenness in Relation to Yield of Soybean at Reproductive Stage Based on Remote Sensing Imagery. *Agric. Water Manag.* **2019**, *222*, 182–192. [CrossRef]
32. Mayanja, I.K.; Yun, H.; Bailey, B.N. Automated Calibration of Stomatal Conductance Models from Thermal Imagery by Leveraging Synthetic Images Generated from Helios 3D Biophysical Model Simulations. *J. Exp. Bot.* **2026**, *77*, 312–329. [CrossRef] [PubMed]
33. Qiu, G.Y.; Yu, X.; Wen, H.; Yan, C. An Advanced Approach for Measuring the Transpiration Rate of Individual Urban Trees by the 3D Three-Temperature Model and Thermal Infrared Remote Sensing. *J. Hydrol.* **2020**, *587*, 125034. [CrossRef]
34. Lin, S.; Li, J.; Liu, Q.; Li, L.; Zhao, J.; Yu, W. Evaluating the Effectiveness of Using Vegetation Indices Based on Red-Edge Reflectance from Sentinel-2 to Estimate Gross Primary Productivity. *Remote Sens.* **2019**, *11*, 1303. [CrossRef]
35. Cheng, R. Solar-Induced Chlorophyll Fluorescence (SIF): Towards a Better Understanding of Vegetation Dynamics and Carbon Uptake in Arctic-Boreal Ecosystems. *Curr. Clim. Change Rep.* **2024**, *10*, 13–32. [CrossRef]
36. Qin, J.; Deng, Z.; Wang, S.; Chen, J.; Fu, P.; Huang, C. A Review on Solar-Induced Chlorophyll Fluorescence of Vegetation and Its Ecological Process Modeling. *Ecol. Front.* **2026**, *46*, 55–67. [CrossRef]
37. Pilipović, A.; Headlee, W.L.; Zalesny, R.S.; Pekeč, S.; Bauer, E.O. Water Use Efficiency of Poplars Grown for Biomass Production in the Midwestern United States. *GCB Bioenergy* **2022**, *14*, 287–306. [CrossRef]
38. Wang, Z.; Slot, M.; Wang, C. Decoupling of Stomatal Conductance, Transpiration and Photosynthesis in Terrestrial Plants under Elevated Temperature: A Meta-Analysis. *Nat. Commun.* **2026**, *17*, 1528. [CrossRef] [PubMed]
39. Dunji, J.; Miloševi, D.; Savi, S. Air Humidity Characteristics in "Local Climate Zones" of Novi Sad (Serbia) Based on Long-Term Data. *ISPRS Int. J. Geo-Inf.* **2021**, *10*, 810. [CrossRef]
40. Kostić, S.; Kebert, M.; Teslić, N.; Stojanović, D.B.; Zorić, M.; Kovačević, B.; Orlović, S. Polycyclic Aromatic Hydrocarbon (PAH) Phytoaccumulation in Urban Areas by *Platanus* × *acerifolia*, *Celtis australis*, and *Tilia grandifolia* Leaves and Branches. *Environ. Sci. Pollut. Res.* **2024**, *31*, 31273–31286. [CrossRef]
41. Stojanović, M.; Jocher, G.; Kowalska, N.; Szatniewska, J.; Zavadilová, I.; Urban, O.; Čáslavský, J.; Horáček, P.; Acosta, M.; Pavelka, M.; et al. Disaggregation of Canopy Photosynthesis among Tree Species in a Mixed Broadleaf Forest. *Tree Physiol.* **2024**, *44*, tpae064. [CrossRef]
42. Pellegrini, E.; Francini, A.; Lorenzini, G.; Nali, C. Ozone, CO_2 Assimilation and PSII Function in Urban Trees: The Case of Tilia Americana. *Acta Hortic.* **2010**, *881*, 539. [CrossRef]
43. García-Sánchez, I.E.; Barradas, V.L.; de León Hill, C.A.P.; Esperón-Rodríguez, M.; Pérez, I.R.; Ballinas, M. Effect of Heavy Metals and Environmental Variables on the Assimilation of CO_2 and Stomatal Conductance of Ligustrum Lucidum, an Urban Tree from Mexico City. *Urban For. Urban Green.* **2019**, *42*, 72–81. [CrossRef]
44. Zhao, D.; Lei, Q.; Shi, Y.; Wang, M.; Chen, S.; Shah, K.; Ji, W. Role of Species and Planting Configuration on Transpiration and Microclimate for Urban Trees. *Forests* **2020**, *11*, 825. [CrossRef]
45. Levinsson, A.; Emilsson, T.; Sjöman, H.; Wiström, B. Using Stomatal Conductance Capacity during Water Stress as a Tool for Tree Species Selection for Urban Stormwater Control Systems. *Urban For. Urban Green.* **2024**, *91*, 128164. [CrossRef]

46. Rahman, M.A.; Moser, A.; Rötzer, T.; Pauleit, S. Comparing the Transpirational and Shading Effects of Two Contrasting Urban Tree Species. *Urban Ecosyst.* **2019**, *22*, 683–697. [CrossRef]
47. Markus Anys, M.W. Controls on Tree Transpiration Dynamics in an Urban Environment. *Agric. For. Meteorol.* **2025**, *372*, 110726. [CrossRef]
48. Abbes, A.B.; Jarray, N.; Farah, I.R. Advances in Remote Sensing Based Soil Moisture Retrieval: Applications, Techniques, Scales and Challenges for Combining Machine Learning and Physical Mode. *Artif. Intell. Rev.* **2024**, *57*, 224. [CrossRef]
49. Chaves, M.M.; Pereira, J.S.; Maroco, J.; Rodrigues, M.L.; Ricardo, C.P.P.; Osório, M.L.; Carvalho, I.; Faria, T.; Pinheiro, C. How Plants Cope with Water Stress in the Field. Photosynthesis and Growth. *Ann. Bot.* **2002**, *89*, 907–916. [CrossRef]
50. Arsenov, D.; Borišev, M.; Nikolić, N.; Horak, R.; Pajević, S. Physiological and Biochemical Indicators of Urban Environmental Stress in Tilia, Celtis, and Platanus: A Functional Trait-Based Approach. *Plants* **2025**, *14*, 3451. [CrossRef] [PubMed]
51. Kullberg, A.T.; Slot, M.; Feeley, K.J. Thermal Optimum of Photosynthesis Is Controlled by Stomatal Conductance and Does Not Acclimate across an Urban Thermal Gradient in Six Subtropical Tree Species. *Plant Cell Environ.* **2023**, *46*, 831–849. [CrossRef]
52. Wang, X.M.; Wang, X.K.; Su, Y.B.; Zhang, H.X. Land Pavement Depresses Photosynthesis in Urban Trees Especially under Drought Stress. *Sci. Total Environ.* **2019**, *653*, 120–130. [CrossRef]
53. Swoczyna, T.; Kalaji, H.M.; Pietkiewicz, S.; Borowski, J. Ability of Various Tree Species to Acclimation in Urban Environments Probed with the JIP-Test. *Urban For. Urban Green.* **2015**, *14*, 544–553. [CrossRef]
54. Liu, M.; Wang, H.; Liu, X.; Liu, B.; Chen, X.; Zhang, Q.; Meng, Z. Integration of Carbon Dioxide Concentration in a Simplified Process-Based Model for Evapotranspiration Estimation in an Old-Growth Forest. *For. Ecol. Manag.* **2022**, *520*, 120392. [CrossRef]
55. Stojanović, D.; Orlović, S.; Zlatković, M.; Kostić, S.; Vasić, V.; Miletić, B.; Kesić, L.; Matović, B.; Božanić, D.; Pavlović, L.; et al. Climate Change within Serbian Forests: Current State and Future Perspectives. *Topola* **2021**, *208*, 39–56. [CrossRef]
56. Tanovski, V.; Matović, B.; Kesić, L.; Stojanović, D. A Review of the Influence of Climate Change on Coniferous Forests in the Balkan Peninsula. *Topola* **2022**, *210*, 41–64. [CrossRef]

Disclaimer/Publisher's Note: The statements, opinions and data contained in all publications are solely those of the individual author(s) and contributor(s) and not of MDPI and/or the editor(s). MDPI and/or the editor(s) disclaim responsibility for any injury to people or property resulting from any ideas, methods, instructions or products referred to in the content.

forests

MDPI

Article

Functional Acclimation of *Quercus robur* from Nine European Provenances to Repeated Drought Events

Željko Škvorc, Saša Bogdan, Ida Katičić Bogdan, Daniel Krstonošić and Krunoslav Sever *

Faculty of Forestry and Wood technology, University of Zagreb, Svetošimunska 23, HR-10000 Zagreb, Croatia; zskvorc@sumfak.hr (Ž.Š.); sbogdan@sumfak.unizg.hr (S.B.); ikaticic@sumfak.hr (I.K.B.); dkrstonosic@sumfak.hr (D.K.)

* Correspondence: ksever@sumfak.hr; Tel.: +385-1-235-2521

Abstract

Forest tree provenances have evolved diverse and complex mechanisms to acclimate to changes in environmental conditions. Pedunculate oak (*Quercus robur* L.), along with other European tree species, is increasingly exposed to the adverse effects of climate change, particularly prolonged drought periods and severe drought stress. Understanding the species' capacity to acclimate to expected environmental changes requires knowledge of key functional traits linked to drought tolerance, such as leaf structure and gas exchange. To explore the acclimation mechanisms of pedunculate oak provenances to repeated drought events, a study was conducted under controlled conditions with plants from nine provenances spanning a north–south gradient across eastern Europe, from Estonia to Italy. The study consisted of two parts: first, leaf structural traits were analyzed after three years of experimentally induced drought by comparing drought and control treatments; second, both treatments were subjected to subsequent drought to analyze differences in gas exchange trait responses. Results demonstrated ecotypic differentiation among provenances in morphological, but not in gas exchange traits, suggesting that provenance adaptedness to drier habitats is more closely associated with structural than physiological traits. Provenances originating from drier habitats showed lower specific leaf area but also different acclimation to repeated drought events, including a stronger reduction in stomatal density and a smaller increase in leaf dry matter content, compared to provenances from more humid habitats. Gas exchange acclimation occurred through a shift in the strategy of photosynthesis down-regulation. These findings emphasize the importance of investigating multiple functional traits rather than focusing solely on individual key traits.

Keywords: pedunculate oak; field trial; climate; ecotypic adaptedness; stress memory; leaf morphology; photosynthesis

1. Introduction

Extreme climatic events associated with climate change, including the increasing frequency and intensity of droughts, pose significant challenges to tree species in forest ecosystems [1]. Trees, as long-lived organisms, have evolved complex mechanisms to acclimate their responses to environmental changes, including drought episodes, over their lifespans. Acclimation modifies plant physiology and morphology to enhance tolerance or improve fitness in response to periodic environmental changes [2]. Many studies have demonstrated that plants subjected to repeated stressful events exhibit a key acclimation mechanism known as stress memory [3]. This concept suggests that previous exposure to

stressors, such as drought, can adjust a plant's physiological or morphological response to subsequent stress events, potentially leading to increased tolerance or sensitivity [4,5]. Stress memory has been explored in the context of drought hardening of planted forest seedlings through controlled water deficit treatments in nurseries. The positive outcomes of drought hardening are mostly attributed to modifications in morpho-physiological traits, such as reduced water demand due to decreased foliage area, increased leaf sclerophylly, and enhanced osmotic regulation [5,6]. The expression of drought memory varies depending on each species' ecological adaptations and the specific morpho-physiological traits being examined. These differences are linked to factors such as species-specific water-use strategies, root system architecture, and inherent physiological plasticity [7].

Forest tree species distributed across diverse environmental conditions have been subjected to differential selective pressures throughout their evolutionary history. Long-term selection has led to genetic differentiation and the development of varied acclimation mechanisms among provenances due to local adaptedness. Local adaptedness implies that genotypes achieve better fitness in their local environments compared to genotypes from other provenances [8]. Elucidating variation in acclimation mechanisms for key functional traits, along with disentangling adaptive responses of major forest tree species to recurrent drought events, is crucial for understanding their adaptation to a changing climate. These insights can help to define conservation strategies for potentially endangered populations and guide adaptive forest management practices. It enables matching genetic material to site-specific conditions, increasing survival rates and promoting resilience under future climate scenarios [9].

Pedunculate oak (*Quercus robur* L.) is a widespread European temperate tree species with a broad ecological amplitude, although it generally prefers fertile and moist habitats. It is a dominant species in various forest communities at low-mid elevations and is one of the most economically valuable hardwoods in Europe [10,11]. Recently, oak forests, along with other forest ecosystems across Europe, have been increasingly affected by climate change, particularly through prolonged drought periods and severe drought stress. Such events negatively impact the overall fitness of forest tree species [12–14].

Oaks are generally considered relatively drought-tolerant, exhibiting high plasticity in traits such as leaf morphology, wood anatomy, root structure, and the ability to recover CO_2 assimilation following periods of water deficiency [15–17]. Consequently, climate change may enhance the competitiveness of European oaks compared to less drought -tolerant species such as beech and lime [18,19]. However, changing conditions could also lead to the partial competitive exclusion of pedunculate oak by closely related species such as *Q. petraea* and *Q. pubescens*, which are better adapted to drought and high temperatures [16,20].

To understand the capacity of pedunculate oak to adapt in a timely manner to expected environmental changes, it is essential to examine key functional traits related to drought tolerance, such as stomatal density, leaf structure, and stomatal conductance. However, knowledge about the genetic basis and intraspecific variation in these traits in oaks remains limited [21,22]. As widespread species, European oaks experience diverse environmental conditions across their distribution range [11] and possess high genetic diversity, leading to significant population differentiation in many adaptive traits [23].

To address these goals, we established a pedunculate oak provenance trial using plants originating from nine provenances along an eastern European north–south gradient, spanning Estonia to Italy. Experimental drought treatments were applied to study their acclimation mechanisms. Over three growing seasons (2015–2017), half of the plants from each provenance were subjected to drought (Drought Treatment—DT), while the other half were maintained under well-watered conditions (Control Treatment—CT). In the final

growing season (2018), all plants in both treatments were exposed to drought to study photosynthetic acclimation to subsequent stress.

The study consisted of two parts: (I) an analysis of leaf functional traits after three years of drought by comparing drought and control treatments at the start of the 2018 growing season, and (II) an examination of gas exchange responses to subsequent drought during the 2018 growing season. The study aimed to investigate (1) how different pedunculate oak provenances acclimate leaf structural traits (specific leaf area—SLA, leaf dry matter content—LDMC, stomatal density—SD) following long-term (three years) experimentally induced drought, and (2) how these provenances acclimate gas exchange traits (net CO_2 assimilation rate—A, transpiration rate—E, stomatal conductance—g_s) in response to subsequent drought stress. We hypothesize that long-term experimentally induced drought leads to functional acclimation of leaf structural traits in the studied pedunculate oak provenances. Furthermore, repeated drought exposure enhances drought tolerance as reflected in gas exchange traits, enabling previously drought-treated plants to maintain higher A, E, and g_s during subsequent drought stress compared with control plants.

2. Materials and Methods

2.1. Plant Material and Provenance Origin

The study was conducted on a provenance trial established at the nursery of the Croatian Forest Research Institute (45.66896 N, 15.64269 E; 141 m a.s.l.). Plants were grown from acorns collected in autumn 2013 beneath the crowns of at least 10 randomly selected mature trees (spaced at least 100 m apart) from nine pedunculate oak stands (provenances). These provenances were distributed along a latitudinal gradient in Europe, from Estonia to Italy (Table 1 and Figure 1). Acorns were sown in pots filled with nursery substrate, and germinated seedlings were transplanted in spring 2014 into 50 L PVC pots filled with homogenized natural soil extracted from a local pedunculate oak forest (soil type: gleysol; pH = 7.6; texture: silty loam). During the 2014 growing season, plants were exposed to natural weather conditions and regularly watered to ensure acclimatization and survival. Further details on plant material and the provenance trial can be found in Čehulić et al. [24].

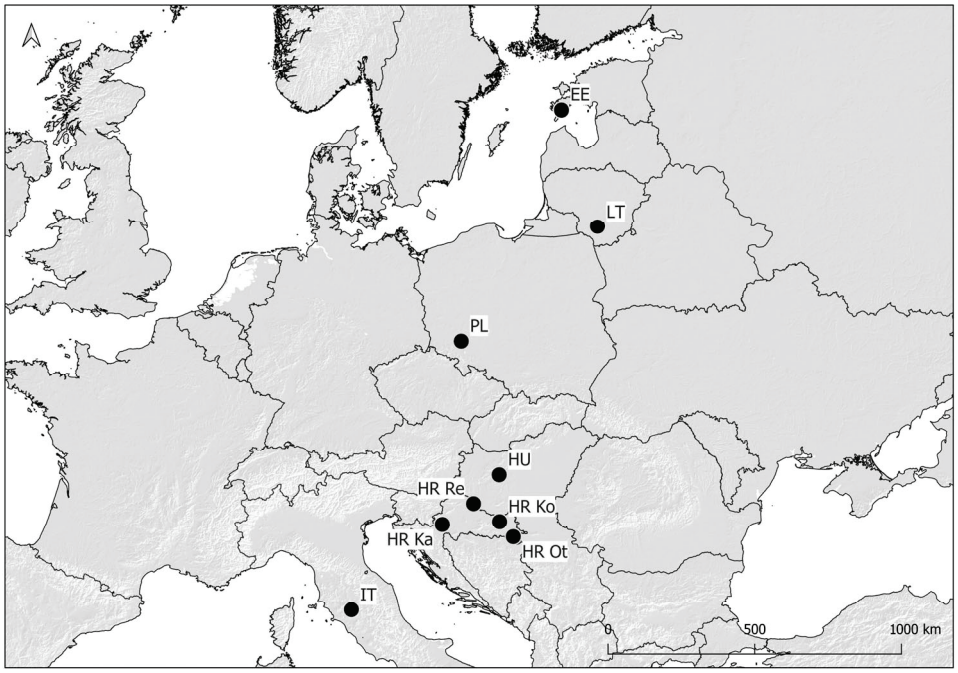


Figure 1. Location of acorn collection sites. The provenance labels correspond to Table 1.

https://doi.org/10.3390/f17060636

Table 1. Location and climate of acorn collection sites. Mean annual temperature (MAT), mean annual precipitation (MAP), mean growing season precipitation (MGSP) and number of investigated plants in control (CT) and drought (DT) treatment.

Provenance	Latitude N	Longitude E	MAT (°C)	MAP (mm)	MGSP (mm)	CT	DT
Estonia—EE	58.23852	22.44289	6.7	607	281	26	27
Lithuania—LT	54.53798	23.81118	6.9	612	358	15	14
Poland—PL	51.19030	16.54901	9.0	520	386	9	9
Hungary—HU	47.02512	18.26350	11.5	546	357	22	24
Croatia (Repaš)—HR Re	46.13976	17.09161	11.4	781	515	23	24
Croatia (Koška)—HR Ko	45.56973	18.23556	11.6	719	463	28	28
Croatia (Karlovac)—HR Ka	45.49489	15.70838	11.8	969	632	23	23
Croatia (Otok)—HR Ot	45.09425	18.82152	11.8	745	471	27	28
Italy—IT	42.75538	11.91804	14.6	670	460	14	15

MAT, MAP and MGSP were generated with ClimateEU software (version 4.63) for the period 1983–2013 [25].

2.2. Experimental Design and Growth Conditions

During the 2015 growing season, plants were grown in a greenhouse. For the next three growing seasons (2016–2018), plants were moved outdoors (Figure S1).

On 15 March 2015, potted plants were transferred to a greenhouse equipped with a ventilation and cooling system to prevent excessive atmospheric moisture and overheating. Pots were arranged into two groups representing control treatment (CT) and drought treatment (DT). Plants were randomly arranged within treatments, with each provenance represented by 9 to 28 plants (Table 1), depending on acorn germination and seedling survival rates in 2014.

In the CT group, plants were watered with 4 L of water per pot every three days using an automated drip irrigation system from 1 April to 31 October 015. The amount of water applied was calculated to maintain the soil near field capacity. In the DT group, plants were deprived of water from 1 April to 21 July 2015, until the volumetric soil water content (SWC) approached the permanent wilting point, and about 50% of plants exhibited visible drought stress symptoms (leaf curling and yellowing). From 22 July to 31 October 2015, DT plants were watered similarly to CT plants. During the winter of 2015/2016, all plants were moved outdoors and exposed to natural winter conditions.

Due to unexpectedly vigorous plant growth in the greenhouse, which threatened to reach the ceiling, the trial was relocated outdoors for the remaining study duration (2016–2018). The arrangement of plants within and between treatments remained consistent. To prevent natural precipitation from entering the pots, polystyrene panels were fitted around the plant stems, sealed with polyurethane foam and duct tape (Figure S1). Plants were watered with 4 L of water per pot every three days. During the 2016 and 2017 growing seasons, DT plants were deprived of water from 20 June to 16 July, when visual symptoms of drought stress appeared. From 16 July to 31 October in both years, DT plants were watered as in the CT group. During the winter periods of 2016/2017 and 2017/2018, polystyrene panels were removed, and plants were exposed to natural winter conditions.

In the final growing season of 2018, all plants from both treatments were subjected to drought from 20 June to 18 July until visible drought stress symptoms appeared (Figure 2). Throughout the study (2015–2018), SWC in pots was measured using 54 sensors (EC-5 soil water sensors; Decagon Devices, Inc., Pullman, WA, USA) connected to data loggers (ECH2O, Decagon Devices, Inc., Pullman, WA, USA). Sensors were placed at a depth of 15–20 cm in three randomly selected pots per provenance within each treatment. SWC in CT pots was maintained at 40%–50%, corresponding approximately to field capacity, while SWC in DT pots dropped to 16%–20% during drought periods, corresponding

approximately to the permanent wilting point, both determined for the soil used in the experiment (Figure 2).

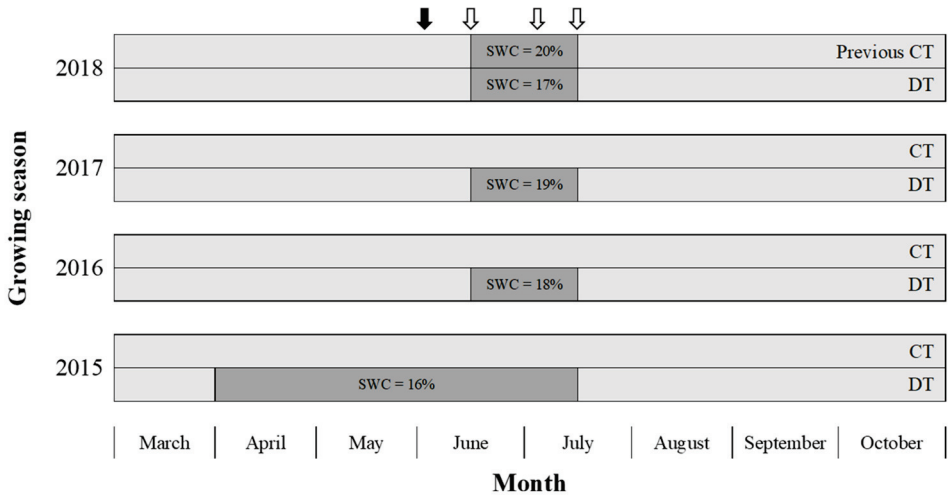


Figure 2. Water regimes in the control (CT) and drought (DT) treatments during the four consecutive growing seasons 2015–2018. Duration of drought periods marked as dark grey polygons in DT and in the previous control treatment for the last season 2018 (previous CT). Relative values in dark grey polygons indicate the lowest mean values of volumetric soil water content (SWC) during the drought period. Light grey colour in CT and DTs indicates the periods when the plants were regularly watered, with variation in SWC in the range from 40% to 50%. The black arrow indicates the date of leaf sampling for measurements of leaf structural traits (1 June 2018). White arrows indicate dates of leaf water potential and gas exchange measurements at the beginning (20 June 2018), in the middle (5 July 2018), and at the end (18 July 2018) of the drought period.

2.3. Leaf Structural Traits

Leaf samples were collected on 1 June 2018, from regularly watered and drought -treated plants that had been exposed to their respective treatments during the 2015–2017 growing seasons. Three fully expanded, healthy leaves were sampled per plant. Accordingly, a total of 561 leaves from 187 plants were sampled in the CT, and 576 leaves from 192 plants were sampled in the DT. Leaves were rehydrated in the dark for 24 h before fresh mass was measured. Leaf area was determined using a desktop scanner (150 dpi) and analyzed with WINFOLIA 2001 software (Regent Instruments Inc., Quebec, QC, Canada). Dry mass was measured after drying leaves for 72 h at 60 °C. Specific leaf area (SLA, m^2/kg) was calculated as the ratio of leaf area to dry mass. Leaf dry matter content (LDMC, mg/g) was calculated as the ratio of dry mass to fresh mass. To determine the number of stomata, each sampled leaf was covered with a thin layer of clear fingernail polish in the area between two veins on the lower epidermis. A short strip of clear tape was used to transfer the imprint to a microscope slide. Stomatal counts were made at five different locations (each with an area of 1 mm^2) on each previously prepared microscope slide/imprint using a microscope OLYMPUS BX41 (Olympus Corporation, Tokyo, Japan) with magnification of 100×. Stomatal density (SD, stomata/mm^2) was calculated as the number of stomata per leaf area. All individual leaf data were averaged per plant.

2.4. Measurements of Leaf Water Potential and Gas Exchange Traits

Pre-dawn leaf water potentials and gas exchange were measured on all plants in the trial three times during the 2018 growing season: at the beginning (20 June), middle (5 July), and end (18 July) of the drought period. Measurements were conducted on DT plants (previously exposed to drought) and CT plants (experiencing drought for the first time) (Figure 2). Pre-dawn leaf water potential was measured using a Scholander pressure

https://doi.org/10.3390/f17060636

chamber (M600; Mosler Tech Support, Berlin, Germany). Measurements of the instantaneous rate of net CO_2 assimilation (A) and H_2O transpiration (E), as well as stomatal conductance (g_s), were carried out using a portable photosynthesis system LCpro+ (ADC BioScentific Ltd., Hoddesdon, UK) equipped with a broadleaf cuvette. All measurements were taken between 10:00 AM and 3:00 PM. The conditions inside the cuvette were kept constant at 400 ppm CO_2, a photon flux density of 1000 µmol m^{-2} s^{-1} and an air temperature of 25 ± 2 °C. The cuvette with a leaf enclosed was equilibrated for 1 min before a reading.

2.5. Statistical Analysis

Differences between treatments and provenances for all analyzed variables were tested using the Analysis of Covariance (ANCOVA) procedure of Statistica software package [26]. Initial (measured in January 2015) and final (measured in January 2018) plant heights were included as covariates in the models analyzing leaf structural traits and gas exchange traits, respectively. Covariates were included because of their potential influence on studied traits and also to minimize potential maternal effects [27]. Although interactions involving the covariate were initially tested, only the interaction between treatments and provenances was retained in the final model. Normality of model residuals and homogeneity of variances were assessed visually using quantile-quantile plots and residuals versus fitted values plots. Significant differences among treatments and provenances were evaluated using Fisher's LSD post hoc tests at $p < 0.05$.

Plasticity in leaf structural traits was calculated as the difference between control and drought treatment means for each provenance. The relationship between all measured variables (including plasticity) and climatic conditions of the sampled provenances was assessed for both treatments separately, using a Pearson correlation coefficient.

3. Results

3.1. Leaf Structural Trait Responses After Three Years of Drought Treatment

Plants exposed to drought for three consecutive years (2015, 2016 and 2017) did not change SLA in the subsequent year 2018 compared to the control plants (Table 2, Figure 3a). However, regardless of the different water treatments, a clear differentiation of provenances was observed (Tables 2 and S3). SLA showed a significant relationship with the mean growing season precipitation of the provenance origin. SLA increases with MGSP, with the lowest SLA values in Estonian provenance and the highest values in Croatian provenances, especially Otok and Repaš (Figure 4).

Table 2. Effects of treatment, provenance and interaction treatment × provenance on specific leaf area (SLA), leaf dry matter content (LDMC) and stomatal density (SD) as calculated with the ANCOVA procedure. Covariates: initial plant height.

Trait	Value	Treatment	Provenance	Treatment × Provenance	Initial Height
SLA (m^2/kg)	F	0.04	10.41	0.53	1.62
	p	0.851	**<0.001**	0.834	0.204
	η^2p	<0.001	0.189	0.012	0.004
LDMC (mg/g)	F	15.24	2.89	1.13	0.20
	p	**<0.001**	**0.003**	0.340	0.660
	η^2p	0.041	0.061	0.024	<0.001
SD (mm^{-2})	F	11.40	6.72	1.00	7.35
	p	**<0.001**	**<0.001**	0.438	**0.009**
	η^2p	0.027	0.178	0.025	0.012

Bolded values indicate significant effects at $p < 0.05$.

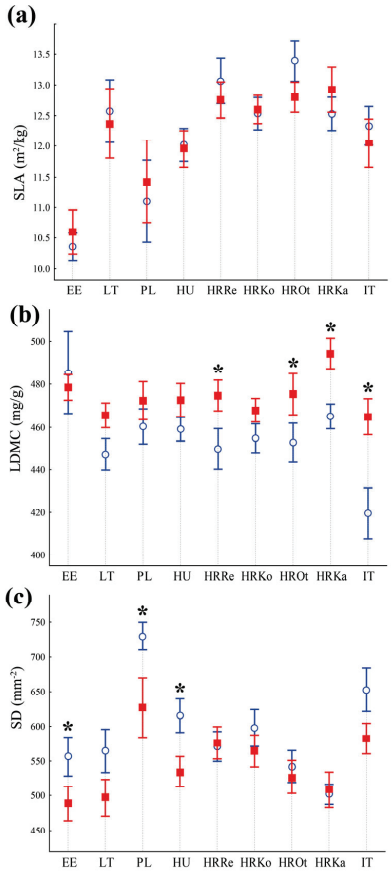


Figure 3. Provenance means for (**a**) specific leaf area (SLA), (**b**) leaf dry matter content (LDMC) and (**c**) stomatal density (SD) control (empty blue circles) and drought (filled red rectangles) treatments. Vertical bars indicate ± SE. Significant differences between control and drought treatment for each provenance are indicated with * at $p < 0.05$.

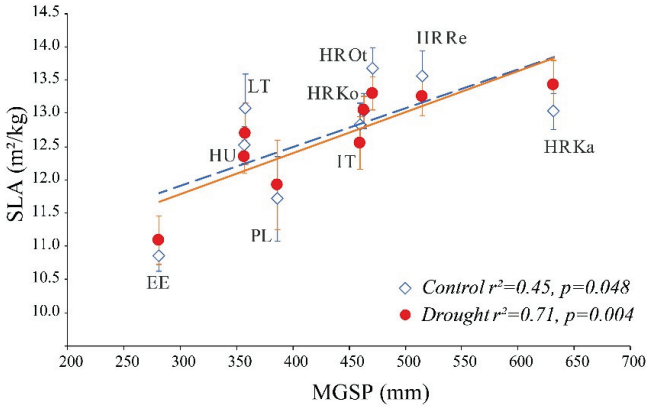


Figure 4. Relationship between the mean growing season precipitation (MGSP) of provenance origin and specific leaf area (SLA). Points represent provenance means for control treatment (empty blue rectangles) and drought treatment (filled red circles). The regression line is shown as a dashed blue line for the control and as a solid red line for the drought treatment. Vertical bars indicate ± SE.

On the other hand, the effect of both the drought treatment and provenance was significant for LDMC and SD (Table 2). Although the interaction between treatment and provenance was not statistically significant for LDMC and SD (Table 2), we observed visual trends suggesting that drought-treated plants tended to exhibit increased LDMC in wetter provenances (e.g., Italy and Croatian sites), and reduced SD in some drier provenances (e.g., Estonia, Poland, Hungary) (Figure 3b,c). These trends should be interpreted cautiously as exploratory observations rather than statistically confirmed differences.

Contrary to SLA, the provenances mean LDMC and SD values are not related to the MGSP (Table S1). However, plasticity of LDMC was related to MGSP, with the lower difference between the control and drought treatments in Estonian and Polish provenances and the higher in Italian and Croatian provenances, especially Karlovac (Figures 3b and S4a). In a similar way, plasticity of SD was related to MGSP, but contrary to the higher difference between the control and drought treatments in Polish, Estonian and Hungarian provenances and the lower in Croatian provenances (Figures 3c and S4b).

3.2. Response of Gas Exchange Traits of Previously Controlled and Drought-Treated Plants to Subsequent Drought in 2018

On 20 June, at the beginning of the subsequent drought period in 2018, when the plants had not yet experienced drought stress, significant differences in g_s, A and E (gas exchange traits) between drought and control treatment were not observed (Table 3). It indicates that experimentally induced drought for the three previous and consecutive years, 2015, 2016 and 2017, did not have a negative impact on gas exchange traits of the investigated plants. Before the onset of drought stress on 20 June 2018, significant provenance differentiation was observed only for A (Table 3), with the highest mean values for EE and the lowest for HR Ot and HR Re (Table S3). However, no clear pattern of this differentiation was found. Moreover, the relation between gas exchange traits on 20 June and MGSP was weak and not significant (Table S1).

Table 3. Effects of treatment, provenence and interaction treatment × provenance on leaf water potential (Ψ), rate of net CO_2 assimilation (A), stomatal conductance (g_s) and rate of transpiration (E) measured at the beginning (20 June), in the middle (5 July) and on the end (18 July) of the drought period in growing season 2018, as calculated with ANCOVA procedure. Covariates: plant height at the beginning of subsequent drought treatment in 2018.

Date	Trait	Values	Treatment	Provenance	Treatment × Provenances	Height
June 20th	Ψ (MPa)	F	5.23	0.91	2.02	0.01
		p	0.049	0.513	0.050	0.921
		η^2p	0.022	0.039	0.083	<0.001
	A (μmol CO_2 m^{-2} s^{-1})	F	0.43	5.51	0.35	1.99
		p	0.513	**<0.001**	0.944	0.159
		η^2p	0.001	0.109	0.008	0.005
	g_s (mol H_2O m^{-2} s^{-1})	F	3.01	1.06	0.35	2.17
		p	0.084	0.394	0.943	0.141
		η^2p	0.008	0.023	0.008	0.006
	E (mol H_2O m^{-2} s^{-1})	F	0.39	0.98	0.26	1.09
		p	0.535	0.453	0.978	0.298
		η^2p	0.001	0.021	0.005	0.003
5 July	Ψ (MPa)	F	24.08	2.12	2.84	0.25
		p	**<0.001**	**0.046**	**0.009**	0.613
		η^2p	0.040	0.069	0.094	<0.001
	A (μmol CO_2 m^{-2} s^{-1})	F	57.79	8.11	1.34	0.02
		p	**<0.001**	**<0.001**	0.224	0.884
		η^2p	0.138	0.152	0.028	<0.001
	g_s (mol H_2O m^{-2} s^{-1})	F	68.59	3.97	1.83	5.55
		p	**<0.001**	**0.003**	**0.048**	**0.019**
		η^2p	0.160	0.062	0.039	0.015
	E (mol H_2O m^{-2} s^{-1})	F	16.52	2.52	0.93	6.45
		p	**<0.001**	**0.011**	0.493	**0.012**
		η^2p	0.044	0.055	0.020	0.017

https://doi.org/10.3390/f17060636

Table 3. *Cont.*

Date	Trait	Values	Treatment	Provenance	Treatment × Provenances	Height
18 July	Ψ (MPa)	F	9.26	3.85	1.18	5.46
		p	**0.003**	**<0.001**	0.313	**0.021**
		η^2p	0.049	0.148	0.050	0.030
	A (µmol CO_2 m^{-2} s^{-1})	F	32.93	5.10	1.12	1.92
		p	**<0.001**	**<0.001**	0.351	0.167
		η^2p	0.084	0.102	0.024	0.005
	g_s (mol H_2O m^{-2} s^{-1})	F	31.52	4.00	0.52	0.79
		p	**<0.001**	**<0.001**	0.841	0.376
		η^2p	0.080	0.081	0.011	0.002
	E (mol H_2O m^{-2} s^{-1})	F	24.08	5.23	0.29	0.29
		p	**<0.001**	**<0.001**	0.970	0.588
		η^2p	0.063	0.104	0.006	<0.001

Bolded values indicate significant effects at $p < 0.05$.

On 5 July 2018, following two weeks of experimentally induced drought, a significant difference in Ψ was observed between treatments (Table 3). However, Ψ was significantly lower in drought-treated plants than in previously control plants only for HU and HR Ko provenances (Figure 5a). On that date, the average Ψ of all provenances in both treatments was around −0.5 MPa (Figure 5a), and soil moisture significantly decreased compared to the beginning of the treatment (Figure S3).

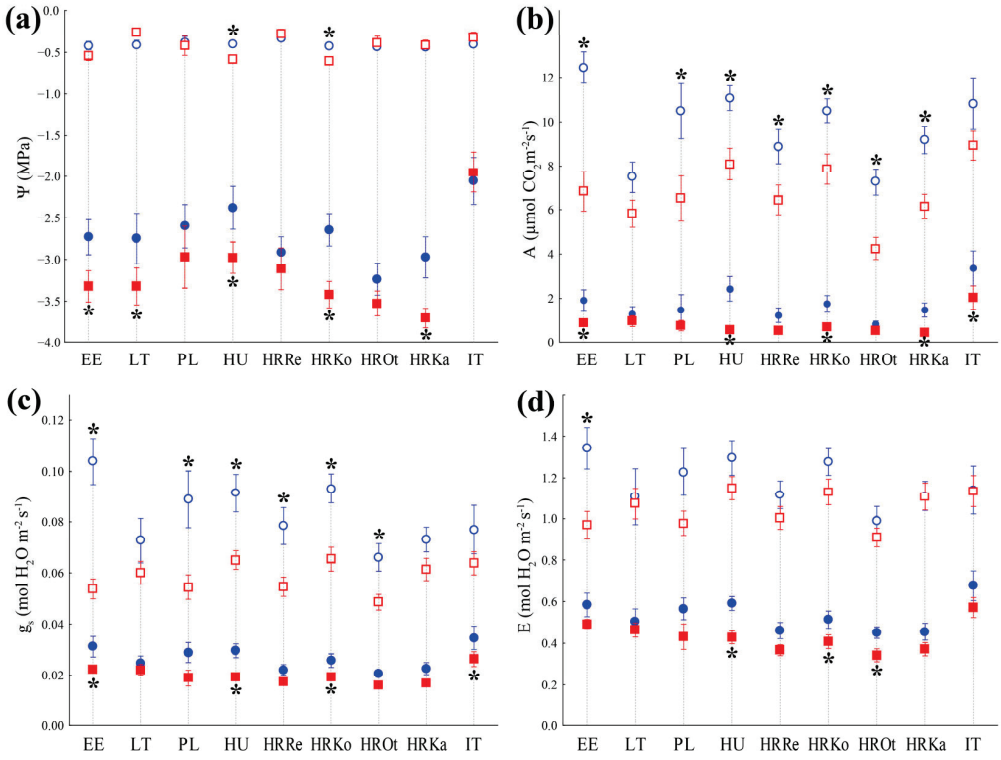


Figure 5. Provenance means ± SE for (**a**) leaf water potential (Ψ), (**b**) rate of CO_2 net assimilation (A), (**c**) stomatal conductance (g_s) and (**d**) rate of transpiration (E) measured in the middle (5 July, upper and empty circles and rectangles) and on the end (18 July, lower and filled circles and rectangles) of the drought period in growing season 2018 in previously control (blue circles) and drought (red rectangles) treatments. Significant differences between the previously control and drought treatment for each measurement date are indicated with * at $p < 0.05$.

Despite the favourable water potential, a reduction in g_s, E and A was observed, with drought-treated plants exhibiting a more pronounced reduction compared to the previous control (Table 3). These results for g_s and E were significantly influenced by the height of the plants at the onset of the subsequent drought treatments, with higher plants generally exhibiting lower g_s and E (Table 3, Figure S2).

On 18 July 2018, after four weeks of experimentally induced drought, a strong decline of Ψ below −2.5 MPa was recorded for all provenances, except the Italian provenance, where it was around −2.0 MPa (Figure 5a), indicating quite severe drought stress of all investigated plants. However, on 18 July 2018, Ψ in drought-treated plants was lower than in previously control plants in all provenances (Figure 4).

After four weeks of experimentally induced drought, g_s, E, and A further decreased to very low levels, leading to a reduction in the difference between drought-treated and previously control plants (Figure 5b–d). The observed population differentiation for gas exchange traits (Table 3) was not related to the MGSP of provenance origin (Table S1).

4. Discussion

4.1. Leaf Structural Trait Responses After Three Years of Drought Treatment

We found no SLA adjustments in pedunculate oak in response to three consecutive years of drought compared to control plants (Table 2), which is consistent with results reported for other deciduous oak species (*Q. petraea*, *Q. robur*, *Q. pubescens*) in a previous study [28]. On the contrary, evergreen oaks in experimental field trials show a highly plastic response in SLA that adjusts to interannual precipitation variations [27,29,30]. Our results confirm that, compared with evergreen oaks, deciduous oak species display lower plasticity in SLA and rely more on other morphological and physiological traits to cope with drought [31].

Our results revealed strong ecotypic differentiation in SLA (Table 2), which was expected for provenances originating from climatically diverse regions along the studied latitudinal gradient. This differentiation was primarily associated with the amount of precipitation during the growing season. Provenances from sites with lower precipitation exhibited lower SLA compared to those from wetter habitats (Figure 4). These are northern provenances characterized by very short growing seasons (e.g., EE) or provenances characterized by generally low total precipitation (e.g., HU), both of which result in lower precipitation during the growing season and overall higher physiological aridity. SLA commonly decreases with decreasing rainfall in oaks [27,30,32,33], as well as in other tree species [34,35], although such a relationship has not always been observed [36]. Since different provenances are adapted to their original environmental conditions, the observed provenance differentiation may be attributed, at least partially, to ecotypic adaptedness to varying climatic conditions. Lower SLA as an adaptation to arid habitat conditions is consistent with the hypothesis that drought tolerance evolves to enhance fitness in low -water environments [29,33]. Sclerophyllous leaves with reduced SLA confer an advantage by enabling plants to maintain photosynthetic activity and carbon assimilation during extended drought periods [37,38].

Unlike SLA, drought memory effects were evident in other structural traits (Table 2). After three consecutive years of drought, a significant overall increase in LDMC and a reduction in SD were observed across provenances (Table 2). While the interaction terms were not statistically significant, visual trends suggest that provenances from drier habitats tended to show lower SD, and wetter provenances tended to show higher LDMC under drought conditions (Figure 3b,c). These patterns may reflect different acclimation strategies, but should be viewed as indicative rather than conclusive, given the absence of significant

https://doi.org/10.3390/f17060636

interaction effects. Furthermore, plasticity (the difference between control and drought-hardened plants) decreases with increasing habitat aridity (Figure S4).

These findings indicate that drought-adapted provenances tend to have less plasticity in LDMC due to their inherently sclerophyllous leaves, which is consistent with previous research [39]. They already have more sclerophyllous leaves, so it can be assumed that further sclerophyllization could reduce mesophyll conductance and photosynthetic efficiency due to decreased cell wall permeability to CO_2 [40]. For this reason, there is a trade-off in dry-adapted provenances, and they reduce SD to a greater extent. The reduction in SD in response to repeated drought is a common adjustment mechanism of plants that try to improve water use efficiency [41].

The contrasting responses of SLA and LDMC to drought in our experiment are not unexpected, as these traits are functionally distinct. SLA and its reciprocal counterpart LMA are composite traits related to two variables: leaf tissue density (LD) and leaf thickness (LT), and can be expressed by the following equation: $SLA = 1/(LT \times LD)$ [42,43]. LT and LD can vary independently along different environmental gradients [40,44,45]. Conversely, LDMC is closely related to LD [46]. Since LDMC differentiation among provenances was not correlated with habitat aridity (Figure 3b), it is likely that the observed SLA reduction with increasing aridity was driven by increases in LT rather than LD.

Our results suggest that memory response to repeated drought of studied pedunculate oak provenances and their adaptedness to dry habitat conditions with regard to the morphological functional leaf traits takes place according to two different scenarios in accordance with the leaf economic spectrum theory [47,48]. Adaptedness of provenances to dry habitat conditions is achieved by decreasing SLA associated with an increase in leaf mesophyll thickness and the amount of photosynthetically active tissues [47,49]. This leads to a greater capacity for C assimilation per unit leaf area and enables compensation for a shorter favourable season caused by a higher duration of stressful climatic events such as aridity or cold [31]. In contrast, provenances' memory response to repeated drought is associated with an increase in LDMC (Figure 3b), i.e., LD. Higher LD is usually associated with thicker cell walls, higher vein density or the presence of sclerenchyma, giving more structural resistance to the leaf cells necessary under drought stress events [40,44–46]. In this way, the increase in LD has a protective role against intense drought climatic stresses because this ensures a longer lifespan of such leaves, compensating for the lower C assimilation rate caused by reducing the efficiency of photosynthesis due to a reduction in cell wall permeability to CO_2 [31,50].

A limitation of our study is that we described habitat aridity using a climatic variable that quantifies the amount of precipitation during the growing season (Table 1). This variable effectively reflects the severity of environmental conditions as it integrates two key climatic drivers affecting plant fitness: the amount of precipitation and the length of the favourable growing season. Our findings indicate that adaptedness and acclimation mechanisms are differentiated based on the severity of environmental conditions. Provenances with more arid and stressful climates, such as HU, where low precipitation results from a continental climate, or EE, where prolonged cold periods shorten favourable seasons, show distinct differentiation (Table 1). In contrast, less arid provenances are characterized by higher precipitation and longer favourable growing seasons. However, the moisture levels in lowland habitats, where pedunculate oak commonly occurs, are also significantly influenced by proximity to watercourses and groundwater levels. To better understand the underlying drivers of intraspecific variability, future research should include variables that more comprehensively characterize the aridity of habitats where different provenances are found.

https://doi.org/10.3390/f17060636

4.2. Response of Gas Exchange Traits of Previously Controlled and Drought-Treated Plants to Subsequent Drought in 2018

Drought limits photosynthesis through both stomatal closure and metabolic impairment, though the relative contributions of these mechanisms are often unclear [51]. In our study, the observed decline in net CO_2 assimilation rate (A) during the final experimental year, as a response to repeated drought in the preceding three years, was primarily due to stomatal limitation, as A decreased in parallel with stomatal conductance (g_s) (Figure 4). This response is consistent with the general pattern of drought-induced photosynthetic limitation observed in many tree species, including *Quercus robur* [16,52].

However, plants that experienced drought in previous years changed the dynamics of the down-regulation of g_s. Even with a minor reduction in leaf water potential, when plants were not under severe drought stress (Figure 5a), they significantly reduced g_s to conserve water, leading to a simultaneous reduction in A due to decreased CO_2 uptake. In contrast, control plants maintained higher g_s (and consequently A) under moderate water stress, only reducing g_s sharply when water potential dropped below a critical threshold (~−2.0 MPa, Figure 5). These findings suggest that the investigated plants, as a physiological response to repeated drought stress (acclimation), changed the strategy of photosynthetic down-regulation. In drought-hardened plants, stomata appeared to become more sensitive, resulting in a shift from anisohydric toward more isohydric stomatal regulation. It has been suggested that anisohydric species such as oaks exhibit plasticity in leaf biophysical properties and may shift along the iso/anisohydric continuum depending on developmental stage and environmental conditions [53,54]. Consequently, acclimated plants appeared to prioritize hydraulic safety over carbon gain by reducing g_s and A under relatively moderate water deficits. Numerous plant traits may underlie these changes in stomatal behaviour, including phytohormonal signalling (ABA), hydraulic traits (e.g., embolism resistance, turgor loss point, and water potential at stomatal closure), and structural investment traits such as wood density, SLA, and leaf carbon content [53].

Although g_s showed significant differentiation among provenances on 5 July (Table 3), this differentiation was weak under drought conditions, as g_s values were reduced to similar levels across provenances (Figure 5c, Table S3). However, in previously controlled plants subsequently exposed to drought stress, clear differentiation among provenances was evident in the degree of g_s reduction. This differentiation was not associated with the local habitat conditions of the provenances (Table S1) but appeared to be linked to plant size, represented here by plant height at the onset of the subsequent drought treatment (significant effect of plant height for g_s and E on 5 July, Table 3).

Provenances with smaller reductions in g_s had lower mean plant heights (Figures 5c and S2), which also influenced patterns of differentiation in A and E (Figures 5b,d and S2). Smaller plants, with lower total leaf area, depleted soil water more slowly in the restricted pot volume, resulting in less pronounced reductions in g_s. However, in acclimated plants, plant size had less impact, as they responded to soil drying by rapidly reducing g_s (Figure 5c).

Stomata often close in response to soil drying before significant changes in leaf water potential occur, driven by drought-induced root-to-leaf signalling [55]. This mechanism was evident in our study (Figures 5c and S3).

Although the experimental design and pot traits in this study were chosen in line with positive experiences in designing drought experiments [56], the use of pots likely influenced some results, particularly the pattern of provenance differentiation in gas exchange traits under subsequent drought. This is a consequence of the prolonged duration of the experiment and the use of a woody species that grew significantly during this period (Figure S2). Generally, it can be suggested that the use of pots in our field trial

may have amplified the observed acclimatization effect, as it is known that the effect is significantly more pronounced in pot-based experiments [57], probably due to restriction of root exploration, which limits access to moist soil layers and increases reliance on physiological mechanisms and carbon allocation changes induced by conditioning [58].

The differences observed on 18 July between drought-treated and previously control plants for Ψ and gas exchange traits may initially appear unexpected. Drought-treated plants, which had closed their stomata earlier and more extensively, exhibited lower Ψ along with reduced gas exchange traits (Table 3, Figure 5). This suggests that repeated drought exposure may have caused damage to their vascular system and/or roots. As a result, these plants, despite reducing g_s more than control plants, were less effective at maintaining favourable Ψ.

Previous drought exposure can significantly reduce the capacity of roots to absorb water after stress cessation [57]. Additionally, xylem conductivity may be reduced due to embolism, which does not fully recover in the following season after the stress ends [59].

4.3. Relationship Between Structural Leaf Traits and Gas Exchange Traits

SLA is a key anatomical trait, and according to expectations based on the leaf economic spectrum, there is a positive relation between SLA and mass-based net CO_2 assimilation across species at the global scale [47]. However, the relationships between SLA and area-based net CO_2 assimilation are less clear and could be influenced by different physiological and structural traits [49]. Alonso-Forn et al. [49] observed a negative relationship between SLA and area-based net CO_2 assimilation among deciduous oak species (the general relationship considering both deciduous and evergreen oak species was not significant).

The relationship between SLA and net CO_2 assimilation within single oak species is less studied, but a negative relationship has been reported for a few evergreen oak species [30,60,61], which is congruent with our results (Table S2). However, according to expectations based on the leaf economic spectrum, low SLA should constrain photosynthesis due to a higher investment in non-photosynthetic tissues and a reduction in mesophyll conductance to CO_2, limiting the efficiency of the photosynthesis [47,62]. No significant relation between A and leaf density or LDMC (Table S1) suggests that the negative relationship between SLA and area-based photosynthetic rate observed in our study can be attributed to the thicker mesophyll of leaves with lower SLA, which leads to the accumulation of photosynthetically active biomass per unit leaf area. A similar relationship between mesophyll leaf thickness and area-based photosynthesis was also observed by Niinemets [60] in *Q. ilex* and Ramírez-Valiente et al. [30] in *Q. oleoides*. The pattern of intraspecific relationships among photosynthesis, SLA and other structural traits in *Q. robur,* as well as in other deciduous oaks, should be investigated in more detail.

5. Conclusions

Our results suggest that drought hardening of young pedunculate oak trees induces alterations in leaf physiological and morphological traits, leading to a more efficient drought response and enhancing the capacity to acclimate to harsh environmental conditions and climate change. Morphological trait acclimation to repeated drought involved adjustments in stomatal density and leaf dry matter content, while gas exchange trait acclimation occurred through a shift in the strategy of photosynthesis down-regulation. This supports the application of drought hardening practices in forest nurseries aimed at improving drought resilience and enhancing plant survival and performance under dry conditions in the field. Furthermore, our results revealed ecotypic differentiation among pedunculate oak provenances in morphological but not in gas exchange traits, indicating that adaptedness to drier conditions is primarily linked to leaf structural traits rather than physiological traits.

https://doi.org/10.3390/f17060636

The identified ecotypic differentiation is reflected in the lower specific leaf area of provenances originating from drier habitats. In addition, these provenances exhibited different acclimation to repeated drought events, including a stronger reduction in stomatal density and a smaller increase in leaf dry matter content, compared to provenances from more humid habitats. Pedunculate oak has evolved diverse multiple mechanisms of acclimation and adaptation to drought stress, which underscore the necessity of investigating multiple functional traits rather than focusing on individual key traits. A comprehensive approach allows us to better understand the complex patterns of adaptation and acclimation in forest trees, offering critical insights for their conservation and management in the face of future climate change. Understanding intraspecific variability is particularly important for defining effective management strategies and optimizing the use of reproductive material under changing environmental conditions. To achieve this, future research in field trials should integrate a broader range of functional traits, such as leaf turgor loss point, leaf carbon content, wood density and xylem embolism resistance, to provide a more complete picture of the underlying mechanisms. Such work will enhance our ability to develop strategies for sustaining forest ecosystems in an increasingly unpredictable climate.

Supplementary Materials: The following supporting information can be downloaded at: https://www.mdpi.com/article/10.3390/f17060636/s1, Figure S1: Investigated plants in greenhouse at the beginning of the experiment, during the first growing season 2015 on April 1st (a) and July 1st (b), as well as outside (c) during the next three growing seasons 2016, 2017 and 2018, when the wetting of the soil with natural precipitation was prevented by polystyrene panels (d); Figure S2: Provenance means for initial plant height; Figure S3: Provenance means ± SE for relative soil water content; Figure S4: Relationship between mean growing season precipitation of provenance origin and plasticity; Table S1: Pearson pairwise correlation coefficients and level of significance between mean provenance SLA, LDMC, SD, rate of net CO_2 assimilation, stomatal conductance and rate of transpiration and mean growing season precipitation; Table S2: Pearson pairwise correlation coefficients among specific leaf area, leaf dry matter content and stomatal density on the one hand (morphological traits) and rate of net CO_2 assimilation, stomatal conductance and rate of transpiration on the other hand (physiological traits); Table S3: Provenance means and significant differences among provenances calculated using Fisher's LSD post hoc tests.

Author Contributions: Conceptualization, Ž.Š., K.S. and S.B.; methodology, Ž.Š., K.S. and S.B.; investigation, D.K. and I.K.B.; writing—original draft preparation, Ž.Š.; writing—review and editing, K.S. and S.B.; All authors have read and agreed to the published version of the manuscript.

Funding: This study was funded by the European Union from source 581—Recovery and Resilience Mechanism (NextGenerationEU) under project "Genetic, phenotypic and ecological characterization of forest reproductive material sources of economically important oaks—ŠRMQuercus, FŠDT11001", which is currently being conducted at the University of Zagreb, Faculty of Forestry and Wood Technology.

Data Availability Statement: The data presented in this study are available on request from the corresponding author.

Conflicts of Interest: The authors declare no conflicts of interest.

References

1. Bréda, N.; Huc, R.; Granier, A.; Dreyer, E. Temperate forest trees and stands under severe drought: A review of ecophysiological responses, adaptation processes and long-term consequences. *Ann. For. Sci.* **2006**, *63*, 625–644. [CrossRef]
2. Taiz, L.; Zeiger, E.; Møller, I.M.; Murphy, A. *Plant Physiology and Development*, 6th ed.; Sinauer Associates Incorporated: Sunderland, MA, USA, 2015.
3. Fleta-Soriano, E.; Munné-Bosch, S. Stress memory and the inevitable effects of drought: A physiological perspective. *Front. Plant Sci.* **2016**, *7*, 171549. [CrossRef] [PubMed]

4. Alves, R.D.F.B.; Menezes-Silva, P.E.; Sousa, L.F.; Loram-Lourenço, L.; Silva, M.L.F.; Almeida, S.E.S.; Silva, F.G.; Farnese, F.S. Evidence of drought memory in Dipteryx alata indicates differential acclimation of plants to savanna conditions. *Sci. Rep.* **2020**, *10*, 16455. [CrossRef]
5. Pritzkow, C.; Szota, C.; Williamson, V.; Arndt, S.K. Previous drought exposure leads to greater drought resistance in eucalypts through changes in morphology rather than physiology. *Tree Physiol.* **2021**, *41*, 1186–1198. [CrossRef] [PubMed]
6. Villar-Salvador, P.; Planelles, R.; Oliet, J.; Peñuelas-Rubira, J.L.; Jacobs, D.F.; González, M. Drought tolerance and transplanting performance of holm oak (*Quercus ilex*) seedlings after drought hardening in the nursery. *Tree Physiol.* **2004**, *24*, 1147–1155. [CrossRef]
7. Toca, A.; Gonzalez-Benecke, C.A.; Nelson, A.S.; Jacobs, D.F. Drought memory expression varies across ecologically contrasting forest tree species. *Environ. Exp. Bot.* **2025**, *231*, 106094. [CrossRef]
8. Kawecki, T.J.; Ebert, D. Conceptual issues in local adaptation. *Ecol. Lett.* **2004**, *7*, 1225–1241. [CrossRef]
9. George, J.P.; Theroux-Rancourt, G.; Rungwattana, K.; Scheffknecht, S.; Momirovic, N.; Neuhauser, L.; Weißenbacher, L.; Watzinger, A.; Hietz, P. Assessing adaptive and plastic responses in growth and functional traits in a 10-year-old common garden experiment with pedunculate oak (*Quercus robur* L.) suggests that directional selection can drive climatic adaptation. *Evol. Appl.* **2020**, *13*, 2422–2438. [CrossRef] [PubMed]
10. Ellenberg, H. *Vegetation Ecology of Central Europe*, 4th ed.; Cambridge University Press: Cambridge, UK, 2009; p. 756.
11. Eaton, E.; Caudullo, G.; Oliveira, S.; de Rigo, D. *Quercus robur* and Quercus petraea in Europe: Distribution, habitat, usage and threats. In *European Atlas of Forest Tree Species*; San-Miguel-Ayanz, J., de Rigo, D., Caudullo, G., Houston Durrant, T., Mauri, A., Eds.; Publ. Off. EU: Luxembourg, 2016; p. e01c6df+.
12. Lindner, M.; Maroschek, M.; Netherer, S.; Kremer, A.; Barbati, A.; Garcia-Gonzalo, J.; Seidl, R.; Delzon, S.; Corona, P.; Kolström, M.; et al. Climate change impacts, adaptive capacity, and vulnerability of European forest ecosystems. *For. Ecol. Manag.* **2010**, *259*, 698–709. [CrossRef]
13. Hlásny, T.; Mátyás, C.; Seidl, R.; Kulla, L.; Merganičová, K.; Trombik, J.; Dobor, L.; Barcza, Z.; Konôpka, B. Climate change increases the drought risk in Central European forests: What are the options for adaptation? *C. Eur. For. J.* **2014**, *60*, 5–18. [CrossRef]
14. Hanel, M.; Rakovec, O.; Markonis, Y.; Máca, P.; Samaniego, L.; Kyselý, J.; Kumar, R. Revisiting the Recent European Droughts from a Long-Term Perspective. *Sci. Rep.* **2018**, *8*, 9499. [CrossRef]
15. Kleinschmit, J. Intraspecific variation of growth and adaptive traits in European oak species. *Ann. Sci. For.* **1993**, *50*, 166–185. [CrossRef]
16. Arend, M.; Brem, A.; Kuster, T.M.; Gunthardt-Goerg, M.S. Seasonal photosynthetic responses of European oaks to drought andelevated daytime temperature. *Plant. Biol.* **2013**, *15*, 169–176. [CrossRef]
17. Vukmirović, A.; Škvorc, Ž.; Bogdan, S.; Krstonošić, D.; Bogdan, I.K.; Karažija, T.; Bačurin, M.; Brener, M.; Sever, K. Photosynthetic Response to Phosphorus Fertilization in Drought-Stressed Common Beech and Sessile Oak from Different Provenances. *Plants* **2024**, *13*, 2270. [CrossRef]
18. Schroeder, H.; Nosenko, T.; Ghirardo, A.; Fladung, M.; Schnitzler, J.P.; Kersten, B. Oaks as beacons of hope for threatened mixed forests in Central Europe. *Front. For. Glob. Change* **2021**, *4*, 670797. [CrossRef]
19. Kasper, J.; Leuschner, C.; Walentowski, H.; Petritan, A.M.; Weigel, R. Winners and losers of climate warming: Declining growth in Fagus and Tilia vs. stable growth in three Quercus species in the natural beech–oak forest ecotone (western Romania). *For. Ecol. Manag.* **2022**, *506*, 119892. [CrossRef]
20. Alexandre, H.; Truffaut, L.; Klein, E.; Ducousso, A.; Chancerel, E.; Lesur, I.; Dencausse, B.; Louvet, J.-M.; Napveu, G.; Torres-Ruiz, J.M.; et al. How does contemporary selection shape oak phenotypes? *Evol. Appl.* **2020**, *13*, 2772–2790. [CrossRef] [PubMed]
21. Bresson, C.C.; Vitasse, Y.; Kremer, A.; Delzon, S. To what extent is altitudinal variation of functional traits driven by genetic adaptation in European oak and beech? *Tree Physiol.* **2011**, *31*, 1164–1174. [CrossRef]
22. Torres-Ruiz, J.M.; Kremer, A.; Carins Murphy, M.R.; Brodribb, T.; Lamarque, L.J.; Truffaut, L.; Bonne, F.; Ducousso, A.; Delzon, S. Genetic differentiation in functional traits among European sessile oak populations. *Tree Physiol.* **2019**, *39*, 1736–1749. [CrossRef]
23. Kremer, A. Evolutionary responses of European oaks to climate change. *Ir. For.* **2010**, *67*, 53–66.
24. Čehulić, I.; Sever, K.; Katičić Bogdan, I.; Jazbec, A.; Škvorc, Ž.; Bogdan, S. Drought impact on leaf phenology and spring frost susceptibility in a *Quercus robur* L. provenance trial. *Forests* **2019**, *10*, 50. [CrossRef]
25. Marchi, M.; Castellanos-Acuña, D.; Hamann, A.; Wang, T.; Ray, D.; Menzel, A. ClimateEU, scale-free climate normals, historical time series, and future projections for Europe. *Sci. Data* **2020**, *7*, 428. [CrossRef] [PubMed]
26. TIBCO Software Inc. *Data Science Workbench*; version 14; TIBCO Software Inc.: San Ramon, CA, USA, 2020; Available online: http://tibco.com (accessed on 14 May 2026).
27. Ramírez-Valiente, J.A.; Sánchez-Gómez, D.; Aranda, I.; Valladares, F. Phenotypic plasticity and local adaptation in leaf ecophysiological traits of 13 contrasting cork oak populations under different water availabilities. *Tree Physiol.* **2010**, *30*, 618–627. [CrossRef] [PubMed]

28. Günthardt-Goerg, M.S.; Kuster, T.M.; Arend, M.; Vollenweider, P. Foliage response of young central European oaks to air warming, drought and soil type. *Plant Biol.* **2013**, *15*, 185–197. [CrossRef]
29. Ramírez-Valiente, J.A.; Valladares, F.; Delgado, A.; Nicotra, A.B.; Aranda, I. Understanding the importance of intrapopulation functional variability and phenotypic plasticity in *Quercus suber*. *Tree Genet. Genomes* **2015**, *11*, 35. [CrossRef]
30. Ramírez-Valiente, J.A.; Center, A.; Sparks, J.P.; Sparks, K.L.; Etterson, J.R.; Longwell, T.; Pilz, G.; Cavender-Bares, J. Population-level differentiation in growth rates and leaf traits in seedlings of the neotropical live oak Quercus oleoides grown under natural and manipulated precipitation regimes. *Front. Plant Sci.* **2017**, *8*, 585. [CrossRef]
31. Sancho-Knapik, D.; Escudero, A.; Mediavilla, S.; Scoffoni, C.; Zailaa, J.; Cavender-Bares, J.; Álvarez-Arenas, T.G.; Molins, A.; Alonso-Forn, D.; Ferrio, J.P.; et al. Deciduous and evergreen oaks show contrasting adaptive responses in leaf mass per area across environments. *New Phytol.* **2021**, *230*, 521–534. [CrossRef]
32. Bruschi, P. Geographical variation in morphology of Quercus petraea (Matt.) Liebl. as related to drought stress. *Plant Biosyst.* **2010**, *144*, 298–307. [CrossRef]
33. Ramírez-Valiente, J.A.; Valladares, F.; Sánchez-Gómez, D.; Delgado, A.; Aranda, I. Population variation and natural selection on leaf traits in cork oak throughout its distribution range. *Acta Oecol.* **2014**, *58*, 49–56. [CrossRef]
34. Fonseca, C.R.; Overton, J.M.; Collins, B.; Westoby, M. Shifts in trait-combinations along rainfall and phosphorus gradients. *J. Ecol.* **2000**, *88*, 964–977. [CrossRef]
35. Marchin, R.M.; Sage, E.L.; Ward, J.K. Population-level variation of Fraxinus americana (white ash) is influenced by precipitation differences across the native range. *Tree Physiol.* **2008**, *28*, 151–159. [CrossRef]
36. Aranda, I.; Castro, L.; Alía, R.; Pardos, J.A.; Gil, L. Low temperature during winter elicits differential responses among populations of the Mediterranean evergreen cork oak (*Quercus suber*). *Tree Physiol.* **2005**, *25*, 1085–1090. [CrossRef]
37. Dudley, S.A. Differing selection on plant physiological traits in response to environmental water availability: A test of adaptive hypotheses. *Evolution* **1996**, *50*, 92–102. [CrossRef]
38. Dudley, S.A. The response to differing selection on plant physiological traits: Evidence for local adaptation. *Evolution* **1996**, *50*, 103–110. [CrossRef]
39. Anderegg, L.D.; Loy, X.; Markham, I.P.; Elmer, C.M.; Hovenden, M.J.; HilleRisLambers, J.; Mayfield, M.M. Aridity drives coordinated trait shifts but not decreased trait variance across the geographic range of eight Australian trees. *New Phytol.* **2021**, *229*, 1375–1387. [CrossRef] [PubMed]
40. Niinemets, Ü. Components of leaf dry mass per area-thickness and density-alter leaf photosynthetic capacity in reverse directions in woody plants. *New Phytol.* **1999**, *144*, 35–47. [CrossRef]
41. Bertolino, L.T.; Caine, R.S.; Gray, J.E. Impact of stomatal density and morphology on water-use efficiency in a changing world. *Front. Plant Sci.* **2019**, *10*, 225. [CrossRef]
42. Witkowski, E.T.F.; Lamont, B.B. Leaf specific mass confounds leaf density and thickness. *Oecologia* **1991**, *88*, 486–493. [CrossRef] [PubMed]
43. John, G.P.; Scoffoni, C.; Buckley, T.N.; Villar, R.; Poorter, H.; Sack, L. The anatomical and compositional basis of leaf mass per area. *Ecol. Lett.* **2017**, *20*, 412–425. [CrossRef]
44. Niinemets, Ü. Global-scale climatic controls of leaf dry mass per area, density, and thickness in trees and shrubs. *Ecology* **2001**, *82*, 453–469. [CrossRef]
45. Poorter, H.; Niinemets, Ü.; Poorter, L.; Wright, I.J.; Villar, R. Causes and consequences of variation in leaf mass per area (LMA): A meta-analysis. *New Phytol.* **2009**, *182*, 565–588. [CrossRef] [PubMed]
46. Shipley, B.; Vu, T.-T. Dry matter content as a measure of dry matter concentration in plants and their parts. *New Phytol.* **2002**, *153*, 359–364. [CrossRef]
47. Wright, I.J.; Reich, P.B.; Westoby, M.; Ackerly, D.D.; Baruch, Z.; Bongers, F.; Cavender-Bares, J.; Chapin, T.; Cornelissen, J.H.C.; Diemer, M.; et al. The worldwide leaf economics spectrum. *Nature* **2004**, *428*, 821–827. [CrossRef]
48. Shipley, B.; Lechowicz, M.J.; Wright, I.; Reich, P.B. Fundamental trade-offs generating the worldwide leaf economics spectrum. *Ecology* **2006**, *87*, 535–541. [CrossRef]
49. Alonso-Forn, D.; Sancho-Knapik, D.; Ferrio, J.P.; Peguero-Pina, J.J.; Bueno, A.; Onoda, Y.; Cavender-Bares, J.; Niinemets, Ü.; Jansen, S.; Riederer, M.; et al. Revisiting the functional basis of sclerophylly within the leaf economics spectrum of oaks: Different roads to Rome. *Curr. For. Rep.* **2020**, *6*, 260–281. [CrossRef]
50. Turner, I.M. Sclerophylly: Primarily Protective? *Funct. Ecol.* **1994**, *8*, 669. [CrossRef]
51. Flexas, J.; Gallé, A.; Galmés, J.; Ribas-Carbo, M.; Medrano, H. The response of photosynthesis to soil water stress. In *Plant Responses to Drought Stress: From Morphological to Molecular Features*; Aroca, R., Ed.; Springer: Berlin/Heidelberg, Germany, 2012; pp. 129–144. [CrossRef]
52. Rennenberg, H.; Loreto, F.; Polle, A.; Brilli, F.; Fares, S.; Beniwal, R.S.; Gessler, A. Physiological responses of forest trees to heat and drought. *Plant Biol.* **2006**, *8*, 556–571. [CrossRef]

53. Chen, Z.; Li, S.; Wan, X.; Liu, S. Strategies of tree species to adapt to drought from leaf stomatal regulation and stem embolism resistance to root properties. *Front. Plant Sci.* **2022**, *13*, 926535. [CrossRef]
54. Meinzer, F.C.; Woodruff, D.R.; Marias, D.E.; Smith, D.D.; McCulloh, K.A.; Howard, A.R.; Magedman, A. L Mapping 'hydroscapes' along the iso- to anisohydric continuum of stomatal regulation of plant water status. *Ecol. Lett.* **2016**, *19*, 1343–1352. [CrossRef]
55. Medrano, H.; Escalona, J.M.; Bota, J.; Gulías, J.; Flexas, J. Regulation of photosynthesis of C3 plants in response to progressive drought: Stomatal conductance as a reference parameter. *Ann. Bot.* **2002**, *89*, 895–905. [CrossRef] [PubMed]
56. Turner, N.C. Imposing and maintaining soil water deficits in drought studies in pots. *Plant Soil* **2019**, *439*, 45–55. [CrossRef]
57. Puértolas, J.; Villar-Salvador, P.; Andivia, E.; Ahuja, I.; Cocozza, C.; Cvjetković, B.; Devetaković, J.; Diez, J.J.; Fløistad, I.S.; Ganatsas, P.; et al. Die-hard seedlings. A global meta-analysis on the factors determining the effectiveness of drought hardening on growth and survival of forest plantations. *For. Ecol. Manag.* **2024**, *572*, 122300. [CrossRef]
58. Moler, E.R.V.; Nelson, A.S. Perspectives on drought preconditioning treatments with a case study using western larch. *Front. Plant Sci.* **2021**, *12*, 741027. [CrossRef]
59. Klein, T.; Zeppel, M.J.; Anderegg, W.R.; Bloemen, J.; De Kauwe, M.G.; Hudson, P.; Ruehr, N.K.; Powel, T.L.; Arx, G.; Nardini, A. Xylem embolism refilling and resilience against drought-induced mortality in woody plants: Processes and trade-offs. *Ecol. Res.* **2018**, *33*, 839–855. [CrossRef]
60. Niinemets, Ü. Is there a species spectrum within the world-wide leaf economics spectrum? Major variations in leaf functional traits in the Mediterranean sclerophyll Quercus ilex. *New Phytol.* **2015**, *205*, 79–96. [CrossRef] [PubMed]
61. Škvorc, Ž.; Lisica, L.; Zorić, V.; Bačurin, M.; Sever, K. Functional differentiation of holm oak provenances in the east Adriatic coast. *Šumar. List.* **2021**, *145*, 415–420. [CrossRef]
62. Niinemets, Ü.; Díaz-Espejo, A.; Flexas, J.; Galmés, J.; Warren, C.R. Role of mesophyll diffusion conductance in constraining potential photosynthetic productivity in the field. *J. Exp. Bot.* **2009**, *60*, 2249–2270. [CrossRef]

Disclaimer/Publisher's Note: The statements, opinions and data contained in all publications are solely those of the individual author(s) and contributor(s) and not of MDPI and/or the editor(s). MDPI and/or the editor(s) disclaim responsibility for any injury to people or property resulting from any ideas, methods, instructions or products referred to in the content.

forests

MDPI

Article

Integrative Structural, Physiological, and Transcriptomic Analyses Reveal Key Determinants of Anthracnose Resistance in Rubber Tree (*Hevea brasiliensis*)

Ling Xia [1], Peichun Li [1], Wenxiu Li [2], Meng Wang [1], Xiaoyu Liang [1,*] and Yu Zhang [1,*]

[1] State Key Laboratory of Tropical Crop Breeding, Sanya Institute of Breeding and Multiplication, School of Tropical Agriculture and Forestry, Hainan University, Sanya 572025, China; 994480@hainanu.edu.cn (L.X.)
[2] Zhanjiang Experimental Station, Chinese Academy of Tropical Agricultural Sciences, Zhanjiang 524091, China
* Correspondence: liang2017@hainanu.edu.cn (X.L.); yuzhang_rain@163.com (Y.Z.)

Abstract

Anthracnose, caused by *Colletotrichum* spp., is a major foliar disease limiting rubber tree (*Hevea brasiliensis*) productivity. To uncover resistance mechanisms, we compared resistant and susceptible germplasm using an integrated framework combining leaf structural analysis, physiological defense profiling, and transcriptome sequencing. Resistant germplasm exhibited lower stomatal density and more compact mesophyll, likely restricting pathogen entry and within-leaf spread. Following inoculation, resistant accessions showed stronger antioxidant responses, with higher activities of superoxide dismutase (SOD) and peroxidase (POD), and elevated phenylpropanoid-related enzymes, including polyphenol oxidase (PPO) and phenylalanine ammonia-lyase (PAL), peaking at 24–48 h post inoculation. These responses were accompanied by enhanced reactive oxygen species (ROS) accumulation (H_2O_2) but reduced lipid peroxidation (malondialdehyde), indicating efficient oxidative stress regulation. Microscopic observation revealed delayed infection progression and postponed differentiation of infection structures in resistant germplasm. Transcriptomic analysis further demonstrated that differentially expressed genes were mainly enriched in pathways related to signal transduction and secondary metabolism, particularly phenylpropanoid metabolism and related secondary metabolic pathways. Together, these results suggest that anthracnose resistance is mediated by coordinated structural barriers, redox homeostasis, and transcriptional regulation of defense networks. This study provides a mechanistic framework for resistance-oriented breeding and the utilization of resistant germplasm in rubber tree.

Keywords: *Hevea brasiliensis*; anthracnose; disease resistance; leaf structure; ROS; phenylpropanoid metabolism

1. Introduction

Natural rubber is an essential industrial raw material, and rubber tree (*Hevea brasiliensis*) is the primary commercial source, contributing more than 90% of global natural rubber production [1,2]. Anthracnose is among the most destructive foliar diseases constraining rubber plantations worldwide [3]. It can infect leaves, shoots, fruits, and green bark tissues, causing defoliation, dieback, and yield losses, and may trigger severe production reductions under epidemic conditions [4,5]. Anthracnose is mainly caused by species in the genus *Colletotrichum*, particularly members of the *C. gloeosporioides* species complex, which exhibit diverse infection strategies and pathogenicity [6].

Deploying resistant germplasm is widely considered the most effective and environmentally sustainable strategy for anthracnose management [7]. However, research on rubber tree has largely emphasized resistance screening and identification, whereas systematic side-by-side comparisons between resistant and susceptible germplasm remain limited. Consequently, the biological basis underlying resistance divergence is still insufficiently resolved, which constrains resistance breeding and mechanism-based management. Plant resistance to foliar pathogens relies on coordinated responses across structural, physiological, and molecular levels [8]. Structural traits, including stomatal features and internal leaf anatomy, can influence pathogen entry and colonization. Because stomata serve as natural entry points for many foliar pathogens, stomatal density can affect infection efficiency [9]. Moreover, leaf tissue organization and compactness may modulate intercellular space availability and thereby alter pathogen proliferation [10]. In addition, internal leaf structure, including tissue organization and compactness, can affect pathogen colonization by modulating intercellular space [11]. Nevertheless, the extent to which these structural traits contribute to anthracnose resistance in rubber tree remains unclear.

At the physiological level, defense responses are closely linked to reactive oxygen species (ROS) metabolism and secondary metabolite biosynthesis. ROS such as hydrogen peroxide (H_2O_2) can act as defense signals, whereas excessive ROS accumulation may cause oxidative damage [12]. Antioxidant enzymes including superoxide dismutase (SOD) and peroxidase (POD) contribute to ROS homeostasis, while enzymes related to phenylpropanoid metabolism, such as phenylalanine ammonia-lyase (PAL) and polyphenol oxidase (PPO), promote the biosynthesis of lignin and flavonoids [13,14]. Resistant plants often exhibit stronger antioxidant capacity and more active secondary metabolism than susceptible ones [15]. At the molecular level, transcriptome analysis has provided important insights into plant–pathogen interactions. Comparative studies between resistant and susceptible genotypes have revealed that plant defense involves multiple signaling pathways, including MAPK cascades, plant hormone signaling, and secondary metabolism pathways [16,17]. Although transcriptomic studies have been conducted in several crops, integrative analyses combining structural, physiological, and molecular perspectives remain limited in rubber tree.

Therefore, we performed a comprehensive comparative analysis of resistant versus susceptible rubber tree germplasm in response to anthracnose infection. By integrating structural characterization, physiological profiling, and transcriptomic analyses, this study aims to identify key resistance-associated differences and provide a mechanistic basis for resistance breeding in rubber tree.

2. Materials and Methods

2.1. Plant Materials and Pathogen

Rubber tree (*Hevea brasiliensis*) germplasm accessions used in this study were obtained from the germplasm nursery of the Zhanjiang Experimental Station, Chinese Academy of Tropical Agricultural Sciences (Zhanjiang, Guangdong, China). Six rubber tree germplasm accessions (ZhanShi 477-6, RO42, Reyan 879, ZhanShi 327-20, ZhanShi 5006, and Reyan 73397) were selected based on previous evaluations and used for comparative analysis in this study. The pathogen used for inoculation was *Colletotrichum siamense* strain M-2, isolated and maintained in our laboratory.

2.2. Pathogen Culture, Inoculation, and Resistance Evaluation

The *C. siamense* M-2 strain was initially grown on potato dextrose agar (PDA) at 28 °C in the dark for 3–4 days. Subsequently, three mycelial plugs (~2 mm in diameter) taken from the colony edge were inoculated into 100 mL of potato dextrose broth (PDB) and incubated

https://doi.org/10.3390/f17050629

at 28 °C with constant shaking at 125 rpm for 3–4 days to promote conidial formation. The suspension was filtered through four layers of sterile gauze and centrifuged at 2000 rpm for 5 min. The conidia were resuspended in sterile water and adjusted to 1×10^6 conidia mL^{-1} using a hemocytometer, with 0.02% Tween-80 added to improve dispersion. Healthy leaves at the color-change stage (i.e., transitional leaves shifting from light green to fully expanded mature green) were collected, washed with sterile water, and air-dried. No mechanical wounding was applied prior to inoculation. Leaves were placed in plastic boxes lined with moist gauze, and petioles were wrapped with wet cotton to maintain humidity. Inoculation was performed using two methods: (i) spray inoculation, in which conidial suspension was evenly sprayed onto both leaf surfaces using a handheld sprayer, to evaluate disease index and observe infection processes under conditions mimicking natural infection; (ii) drop inoculation, in which 5 μL of suspension was applied to both sides of the leaf using a micropipette, to measure lesion diameter and provide a more direct assessment of resistance differences among germplasm groups. After inoculation, leaves were incubated at 28 °C under relative humidity > 90%. A mock inoculation using sterile water containing 0.02% Tween-80 was included as the control treatment. Each treatment included 12 leaves with three biological replicates, and measurements were performed in triplicate. Disease symptoms were evaluated at 3 days post inoculation. Lesion diameter was measured using the cross method, and disease severity was assessed on a 0–5 scale based on lesion coverage, where 0 indicates no visible symptoms and 5 indicates severe infection (>50% of leaf area affected), according to the agricultural industry standard (NY/T 3518-2019). The disease index was subsequently calculated to classify resistance levels [18].

2.3. Analysis of Leaf Structural Characteristics

Leaf structural traits were analyzed using leaves from all six germplasm accessions at the same developmental stage. Stomatal characteristics were determined using the nail polish imprint method on the abaxial leaf surface. Imprints were observed under a light microscope, and stomatal density was calculated from 10 randomly selected fields per sample. Stomatal length and width were measured for 10 stomata per field, and stomatal aperture area was calculated as S = (length × width × $\pi/4$). Leaf anatomical structures were examined using paraffin-embedded sections fixed in 50% FAA solution for 24 h. Sections were stained with safranin–fast green and scanned for analysis. Thickness of the upper epidermis (UET), palisade tissue (PT), spongy tissue (ST) and lower epidermis (LET) and total leaf thickness (LT) were measured. Derived indices were calculated as follows: cell tightness ratio (CTR) = PT/LT; spongy ratio (SR) = ST/LT; and palisade-to-spongy ratio (P/S) = PT/ST. Measurements were performed on 10 fields per sample with three replicates, with each measurement performed in triplicate.

2.4. Physiological and Biochemical Assays

Resistant (ZhanShi 477-6) and susceptible (ZhanShi 5006) germplasm accessions were selected for physiological analysis. Leaves were inoculated as described above, with sterile water used as a control. Samples were collected at 0, 12, 24, 48, and 72 h post inoculation. For enzyme extraction, 0.5 g of leaf tissue was homogenized in 5 mL pre-cooled phosphate buffer (PBS, pH 7.8) and centrifuged at 8500 rpm at 4 °C for 20 min. The supernatant was collected as a crude enzyme extract and used for the determination of SOD, POD, PPO, and PAL activities [19]. SOD activity was determined using the nitroblue tetrazolium (NBT) method and measured at 560 nm after 20 min illumination (4000 lux). POD activity was measured using guaiacol as substrate, and absorbance was recorded at 470 nm every 1 min. PPO activity was determined using catechol as substrate at 525 nm. PAL activity was measured at 290 nm using L-phenylalanine as substrate after incubation at 30 °C for 30 min.

https://doi.org/10.3390/f17050629

For H_2O_2 determination, 0.2 g of leaf tissue was homogenized in acetone and reacted with titanium sulfate, and absorbance was measured at 425 nm. MDA content was determined using thiobarbituric acid (TBA) reaction and measured at 532 and 600 nm [20]. Enzyme activities were expressed on a fresh weight basis (U g^{-1} FW), and H_2O_2 and MDA contents were expressed as μmol g^{-1} FW and nmol g^{-1} FW, respectively. Each treatment included three biological replicates, and measurements were performed in triplicate.

2.5. Infection Process Observation

Leaves from resistant and susceptible germplasm were sampled at 0, 2, 4, 12, 24, 36, 48, 72, and 96 h post inoculation. Leaf segments (2 cm × 2 cm) were decolorized in a solution of 0.15% trichloroacetic acid and chloroform (5:1, v/v) for 12 h. After washing, samples were stained with 1% Congo red under vacuum for 10 min and incubated for 2 h. Fungal infection structures, including conidia, germ tubes, appressoria, and penetration pegs, were observed under a light microscope. At least 200 conidia were counted per sample (n = 3 biological replicates), with each measurement performed in triplicate.

2.6. RNA Sequencing and Data Analysis

Leaf samples from resistant and susceptible rubber tree germplasm were collected at 0 and 24 h post inoculation and immediately stored at −80 °C. Total RNA was extracted, and cDNA libraries were prepared for RNA sequencing by a commercial provider. Subsequent steps, including library construction, alignment of reads to the reference genome, quantification of gene expression, and functional enrichment analyses, were carried out by Gene Denovo Biotechnology Co. (Guangzhou, China) following standard protocols [21]. The raw RNA-seq datasets have been deposited in the National Center for Biological Information (CNCB, https://www.cncb.ac.cn/, accessed on 1 April 2026), China, under BioProject accession PRJCA060963. After quality filtering, clean reads were mapped to the rubber tree reference genome (ASM3005281v1) using HISAT2. Gene expression levels were calculated as fragments per kilobase of transcript per million mapped reads (FPKM). Differentially expressed genes (DEGs) were determined with DESeq2 using thresholds of $|\text{fold change}| > 2$ and a false discovery rate (FDR) < 0.05.

2.7. Statistical Analysis

Statistical analyses were performed using SPSS software (version 13.0; SPSS Inc., Armonk, NY, USA). Differences were considered statistically significant at $p < 0.05$. All results are presented as the mean of at least three independent replicates.

3. Results

3.1. Evaluation of Anthracnose Resistance in Rubber Tree Germplasm

Significant variation in anthracnose resistance was observed across the six rubber tree germplasm accessions under artificial inoculation (Table 1). Reyan 879, Zhanshi 477-6, and RO42 were classified as resistant (R), with lesion diameters ranging from 0.24 to 0.81 cm and disease index values between 10.67% and 14.67%. In contrast, Reyan 73397 and Zhanshi 327-20 were categorized as susceptible (S), showing larger lesion diameters (1.00–1.09 cm) and higher disease index values (32.00%–37.33%). Zhanshi 5006 exhibited the highest lesion diameter (1.17 cm) and disease index (49.33%), and was classified as highly susceptible (HS). Overall, resistant germplasm developed significantly smaller lesions and lower disease index values than susceptible germplasm, indicating robust phenotypic divergence in anthracnose response.

https://doi.org/10.3390/f17050629

Table 1. Resistance evaluation of rubber tree germplasm to anthracnose.

Germplasm Name	Lesion Diameter (cm)	Disease Index (%)	Resistance Level
Zhanshi 477-6	0.29 ± 0.06 d	10.67	R
Reyan 879	0.24 ± 0.08 d	13.33	R
RO42	0.81 ± 0.17 c	14.67	R
Reyan 73397	1.09 ± 0.03 ab	32.00	S
Zhanshi 327-20	1.00 ± 0.07 bcd	37.33	S
Zhanshi 5006	1.17 ± 0.08 a	49.33	HS

Values are mean ± standard deviation (SD). Different letters indicate significant differences at $p < 0.05$ (Tukey's test). R, resistant; S, susceptible; HS, highly susceptible.

3.2. Differences in Leaf Structural Traits Between Resistant and Susceptible Rubber Tree Germplasm

To compare the leaf structural characteristics of resistant and susceptible rubber tree germplasm, six accessions were systematically analyzed. The results showed that stomatal density in resistant germplasm was significantly lower than that in susceptible germplasm, whereas stomatal length, width, and opening area did not exhibit consistent variation patterns between resistant and susceptible groups (Figure 1A; Table 2). Correlation analysis further revealed a significant positive relationship between disease index and stomatal density (R^2 = 0.7397; Figure 1B).

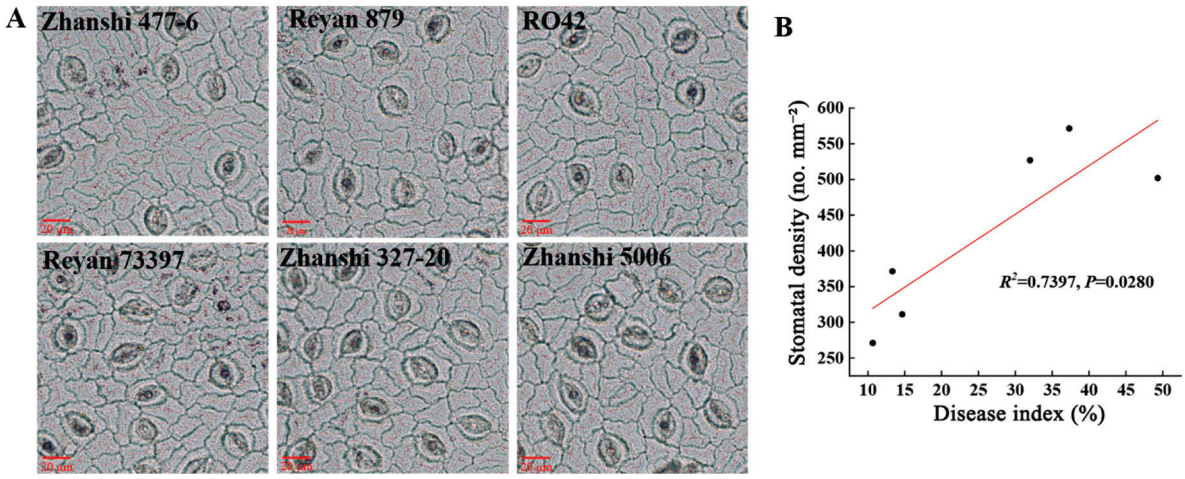


Figure 1. Stomatal characteristics and their relationship with anthracnose disease index in rubber tree germplasm. (**A**) Representative stomatal micrographs of six rubber tree germplasm accessions. Stomata are distributed on the abaxial leaf surface and exhibit elliptical openings. Scale bars = 20 μm. (**B**) Correlation between stomatal density and disease index. Stomatal density is positively correlated with disease index (R^2 = 0.7397, p = 0.0280).

Table 2. Stomatal characteristics in leaves of resistant and susceptible germplasm.

Germplasm Name	Stomatal Density (no. mm^{-2})	Stomatal Width (μm)	Stomatal Length (μm)	Stomatal Opening Area (μm^2)
Zhanshi 477-6	270.99 ± 7.77 b	8.43 ± 0.37 b	15.93 ± 0.43 ab	107.4 ± 6.67 bc
Reyan 879	371.35 ± 35.34 b	8.48 ± 0.32 b	15.11 ± 0.51 ab	102.42 ± 6.11 bc
RO42	311.13 ± 16.79 b	9.38 ± 0.26 ab	15.62 ± 0.34 ab	115.46 ± 4.48 abc
Reyan 73397	526.92 ± 21.64 a	9.84 ± 0.27 a	17.67 ± 0.34 a	136.89 ± 5.03 a
Zhanshi 327-20	571.29 ± 13.78 a	8.61 ± 0.24 b	14.67 ± 0.29 c	99.65 ± 3.99 c
Zhanshi 5006	501.82 ± 16.79 a	9.33 ± 0.30 ab	14.68 ± 0.41 bc	123.1 ± 5.73 ab

Values are mean ± standard deviation (SD). Different letters indicate significant differences at $p < 0.05$ (Tukey's test).

In terms of leaf anatomical structure, no significant differences were observed in the thickness of the upper epidermis, lower epidermis, palisade tissue, or spongy tissue or total leaf thickness between resistant and susceptible germplasm (Figure 2A; Table 3). In contrast, the palisade-to-spongy ratio (P/S) and cell tightness ratio (CTR) were significantly higher in resistant germplasm, whereas the spongy ratio (SR) was significantly lower compared with susceptible germplasm. Further correlation analysis indicated that the disease index was positively correlated with SR (R^2 = 0.6778), but negatively correlated with P/S (R^2 = 0.6665) and CRT (R^2 = 0.7181) (Figure 2B).

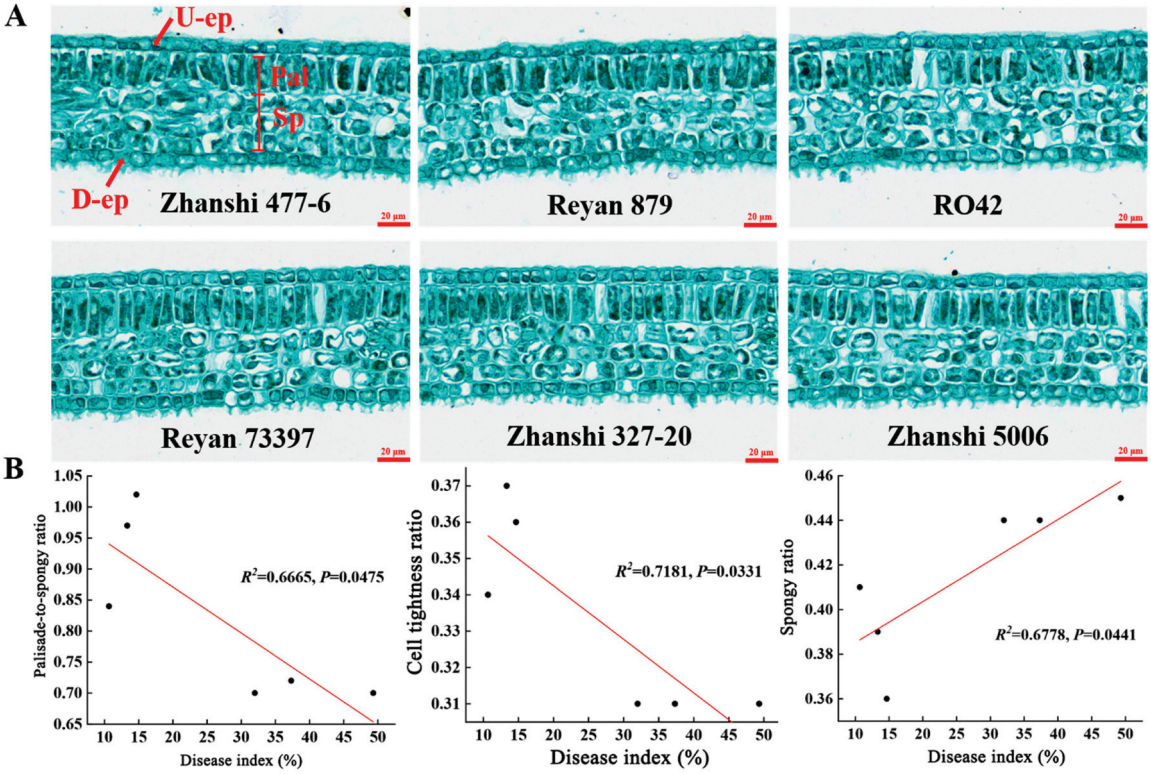


Figure 2. Leaf anatomical structure and its relationship with anthracnose disease index in rubber tree germplasm. (**A**) Representative transverse sections of leaves from six rubber tree germplasm accessions. U-ep, upper epidermis; Pal, palisade tissue; Sp, spongy tissue; D-ep, lower epidermis. Scale bars = 20 μm. (**B**) Correlation analysis between anatomical structural parameters and disease index.

Table 3. Leaf anatomical characteristics of resistant and susceptible rubber tree germplasm.

Germplasm Name	Upper Epidermis Thickness (μm)	Palisade Tissue Thickness (μm)	Spongy Tissue Thickness (μm)	Lower Epidermis Thickness (μm)	Leaf Thickness (μm)	Palisade-to-Spongy Ratio	Cell Tightness Ratio	Spongy Ratio
Zhanshi 477-6	10.60 ± 1.37 ab	27.93 ± 3.17 b	33.41 ± 2.39 b	10.06 ± 0.89 ab	82.01 ± 3.95 b	0.84 ± 0.13 b	0.34 ± 0.03 b	0.41 ± 0.03 b
Reyan 879	10.76 ± 1.37 a	33.75 ± 3.39 a	35.01 ± 3.28 ab	11.22 ± 4.12 a	90.74 ± 6.29 a	0.97 ± 0.13 a	0.37 ± 0.03 a	0.39 ± 0.03 c
RO42	9.51 ± 1.35 c	23.72 ± 2.41 d	23.41 ± 2.81 c	8.84 ± 1.11 b	65.48 ± 5.11 d	1.02 ± 0.13 a	0.36 ± 0.03 a	0.36 ± 0.03 d
Reyan 73397	10.02 ± 1.09 abc	23.31 ± 1.55 d	33.82 ± 3.07 b	9.00 ± 0.97 b	76.14 ± 3.71 c	0.70 ± 0.08 c	0.31 ± 0.02 c	0.44 ± 0.02 a
Zhanshi 327-20	9.78 ± 0.91 bc	25.66 ± 2.25 c	36.63 ± 2.75 a	9.74 ± 1.23 b	81.81 ± 3.79 b	0.70 ± 0.08 c	0.31 ± 0.02 c	0.45 ± 0.02 a
Zhanshi 5006	10.1 ± 0.80 abc	24.61 ± 1.69 cd	34.5 ± 1.61 b	9.17 ± 0.70 b	78.37 ± 1.84 c	0.72 ± 0.07 c	0.31 ± 0.02 c	0.44 ± 0.02 a

Values are presented as mean ± standard deviation (SD). Different lowercase letters within a column indicate significant differences at $p < 0.05$ (Tukey's test).

3.3. Temporal Changes in Defense-Related Enzyme Activities and Oxidative Stress Indicators

Following anthracnose inoculation, the activities of SOD, POD, PPO, and PAL exhibited dynamic changes in both resistant and susceptible germplasm (Figure 3). Overall, enzyme activities were induced after inoculation, with more pronounced increases observed in the resistant germplasm Zhanshi 477-6 (R) compared with the susceptible germplasm

Zhanshi 5006 (S), particularly at peak stages (24–48 h post inoculation). Specifically, SOD activity in resistant germplasm increased rapidly and reached a peak at 24 h, followed by a gradual decline, whereas susceptible germplasm showed a relatively moderate increase. POD activity exhibited a similar early induction pattern, with resistant germplasm peaking at 24 h, although susceptible germplasm showed a delayed peak at 48 h. PPO and PAL activities were also significantly elevated in resistant germplasm, particularly at 24–48 h, with higher peak levels than those observed in susceptible germplasm. Quantitatively, enzyme activities in resistant germplasm were generally higher than those in susceptible germplasm, with differences of approximately 20%–80% depending on the time point.

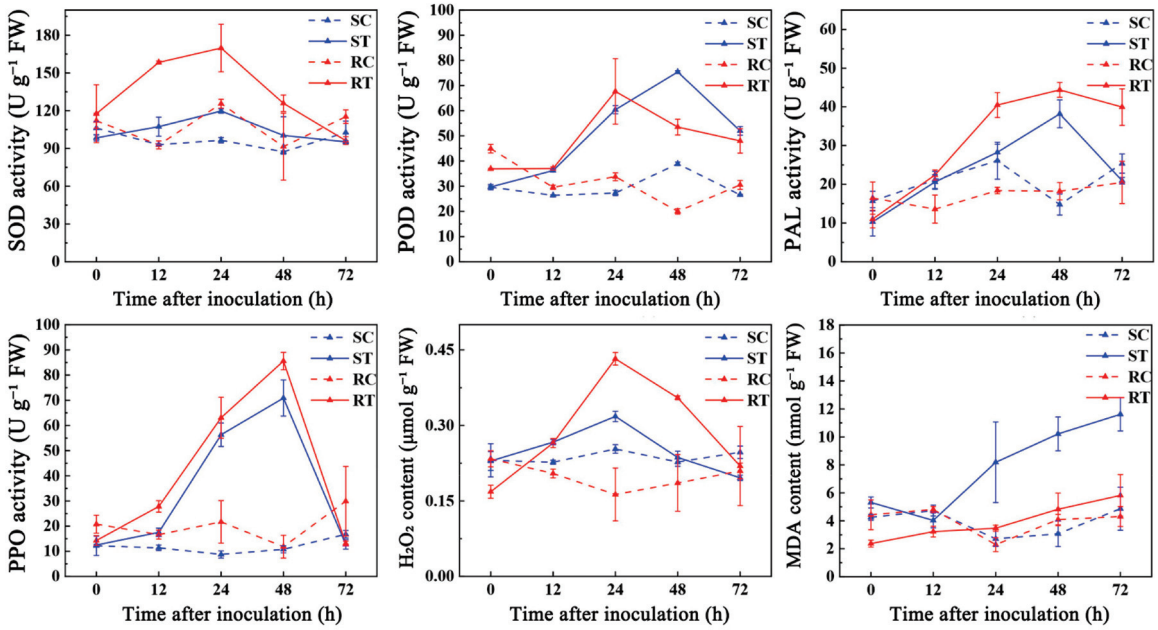


Figure 3. Temporal dynamics of defense-related enzyme (SOD, POD, PPO, and PAL) activities and oxidative stress indicators (H_2O_2 and MDA) in resistant and susceptible rubber tree germplasm after anthracnose inoculation. Changes in SOD, POD, PAL, and PPO activities, as well as H_2O_2 and MDA contents, in rubber tree germplasm at different time points after inoculation with *C. siamense*. SC, susceptible control (Zhanshi 5006 without inoculation); ST, susceptible treatment (Zhanshi 5006 inoculated with *C. siamense*); RC, resistant control (Zhanshi 477-6 without inoculation); RT, resistant treatment (Zhanshi 477-6 inoculated with *C. siamense*).

In addition, oxidative stress indicators showed distinct temporal patterns. H_2O_2 content increased rapidly after inoculation and reached higher levels in resistant germplasm at early stages (12–24 h), whereas susceptible germplasm exhibited comparatively lower accumulation. In contrast, malondialdehyde (MDA) content increased more markedly in susceptible germplasm, while remaining lower in resistant germplasm at later stages (48–72 h), indicating reduced membrane lipid peroxidation.

3.4. Temporal Progression of Infection and Infection Structure Differentiation in Resistant and Susceptible Rubber Tree Germplasm

Clear differences in infection progression were observed between resistant and susceptible rubber tree germplasm after inoculation with *Colletotrichum siamense* (Figure 4). Disease symptoms appeared at 48 hpi in resistant leaves, whereas susceptible leaves showed earlier symptom development at 36 hpi. Resistant leaves exhibited only slight chlorosis with limited lesion expansion, while susceptible leaves displayed rapid lesion development at later stages (48–96 hpi). Infection structure analysis indicated a similar early progression in both germplasm groups, with conidia dominating at 2 hpi and germ

https://doi.org/10.3390/f17050629

tubes and appressoria becoming predominant at 4–12 hpi. However, at later stages, penetration pegs accumulated more rapidly in susceptible germplasm, reaching 65% and 73% at 24 and 36 hpi, respectively, compared with 25% and 46% in resistant germplasm, indicating a faster transition to host penetration in susceptible leaves.

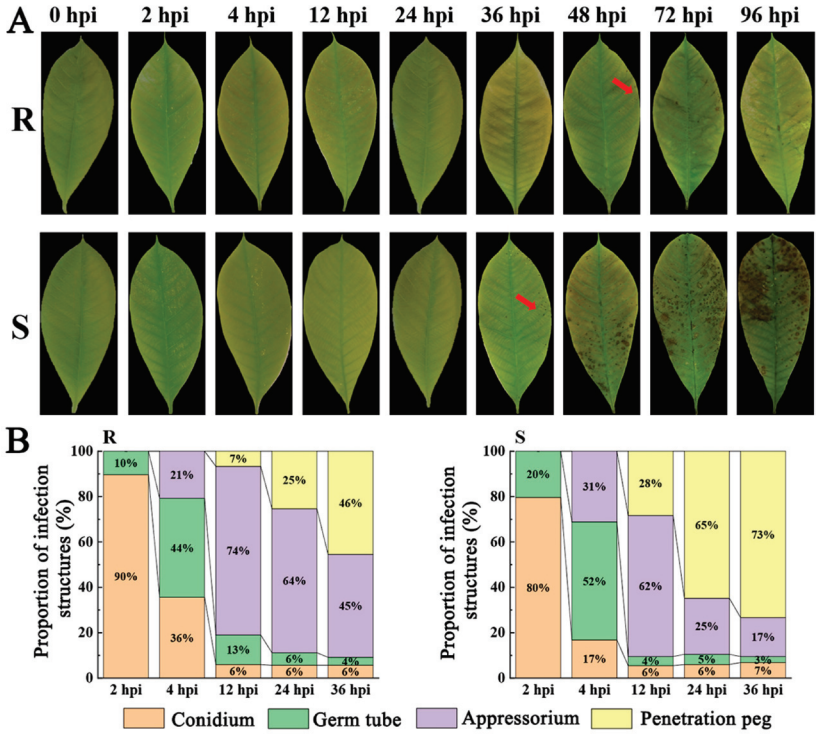


Figure 4. Infection process and infection structure dynamics in resistant and susceptible rubber tree germplasm after inoculation with *C. siamense.* (**A**) Disease development in resistant (R, Zhanshi 477-6) and susceptible (S, Zhanshi 5006) rubber tree leaves at different time points after inoculation (0–96 hpi). Red arrows indicate typical disease symptoms. (**B**) Proportion of infection structures at different time points (2–36 hpi), including conidia, germ tubes, appressoria, and penetration pegs.

3.5. Transcriptomic Variation and Differential Gene Expression Analysis Between Resistant and Susceptible Germplasm

Principal component analysis (PCA) revealed a clear separation among samples (Figure 5A), with PC1 explaining 85.5% of the total variance and PC2 explaining 6.2%. Biological replicates within each group clustered closely, indicating high reproducibility. Resistant (R0 and R24) and susceptible (S0 and S24) samples were distinctly separated along PC1, suggesting substantial transcriptional divergence between the two germplasm groups. In addition, samples at different time points exhibited directional shifts, indicating dynamic transcriptional responses following infection.

Differential expression analysis identified large numbers of differentially expressed genes (DEGs) across all comparisons (Figure 5B). In the R0 vs. R24 comparison, 3453 genes were upregulated and 4627 were downregulated. In S0 vs. S24, 4079 upregulated and 4585 downregulated genes were detected. In S0 vs. R0, 2747 genes were upregulated and 1707 were downregulated, while in S24 vs. R24, 2946 genes were upregulated and 1689 were downregulated. Overall, time-course comparisons (R0 vs. R24 and S0 vs. S24) showed higher numbers of DEGs than genotype comparisons, indicating stronger transcriptional reprogramming during infection.

Venn diagram analysis further revealed both shared and specific DEG patterns. For upregulated genes (Figure 5C), 67 genes were commonly upregulated across all four comparisons, while each comparison also contained a large number of unique DEGs,

including 1187 in R0 vs. R24 and 1103 in S24 vs. R24. Similarly, for downregulated genes (Figure 5D), 26 genes were shared among all comparisons, whereas 1520 and 755 genes were uniquely regulated in R0 vs. R24 and S24 vs. R24, respectively.

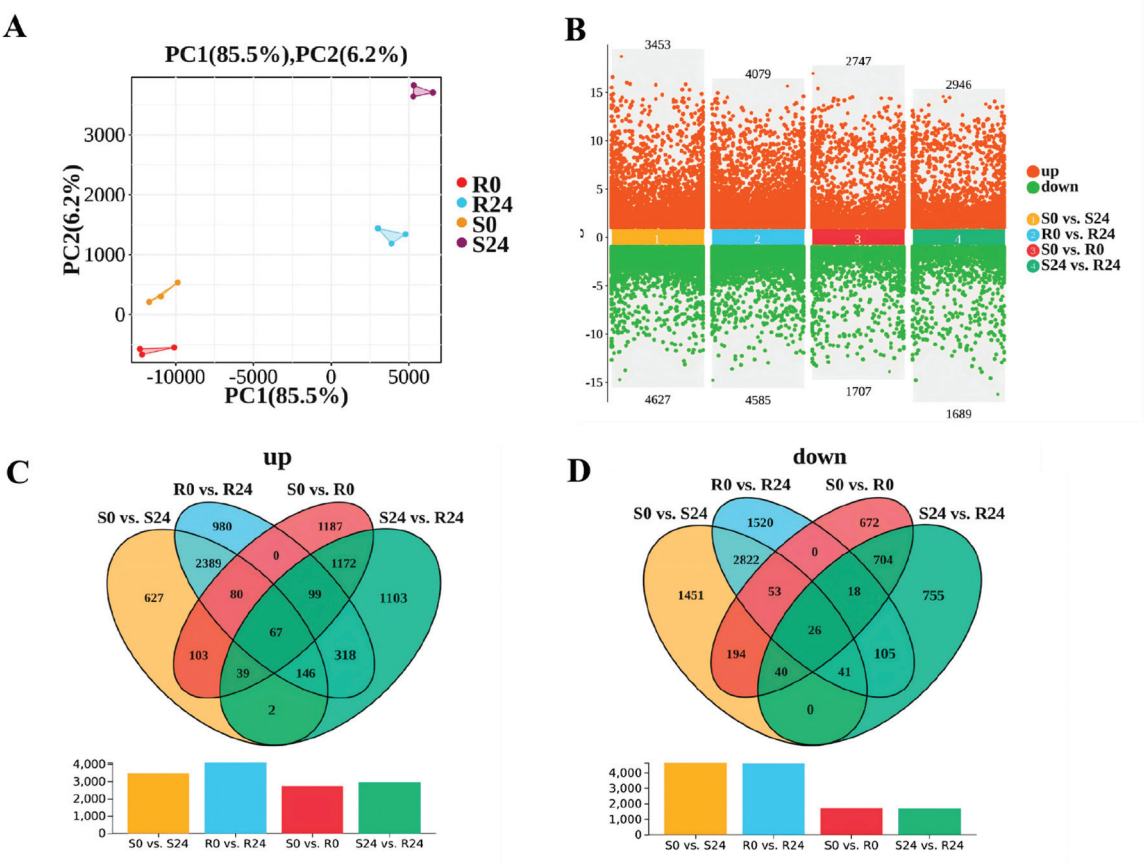


Figure 5. Transcriptome profiling and differential gene expression analysis in resistant and susceptible rubber tree germplasm following anthracnose infection. (**A**) Principal component analysis (PCA) of transcriptome data from resistant (R) and susceptible (S) rubber tree germplasm at different time points after inoculation. PC1 and PC2 explain 85.5% and 6.2% of the total variance, respectively. (**B**) Distribution of differentially expressed genes (DEGs) in pairwise comparisons, including R0 vs. R24, S0 vs. S24, S0 vs. R0, and S24 vs. R24. Red and green dots represent upregulated and downregulated genes, respectively. (**C**,**D**) Venn diagrams showing the overlap of upregulated (**C**) and downregulated (**D**) DEGs among different comparisons. Numbers indicate shared and unique DEGs in each comparison. R0 and R24 represent resistant germplasm (Zhanshi 477-6) at 0 and 24 h post inoculation (hpi), respectively; S0 and S24 represent susceptible germplasm (Zhanshi 5006) at 0 and 24 hpi, respectively.

3.6. Enrichment Analysis of Resistance-Related Pathways and Key Genes

Differentially expressed genes (DEGs) were detected between resistant and susceptible germplasm prior to pathogen infection, indicating inherent transcriptional differences (Figure 6). GO enrichment analysis showed that these DEGs were mainly associated with chloroplast/plastid components (GO:0009570; GO:0009532), ATPase and hydrolase activities (GO:0016887; GO:0016818), and small molecule metabolic processes (GO:0036094; GO:0006082). KEGG enrichment analysis revealed that these genes were primarily involved in secondary metabolite biosynthesis, flavonoid biosynthesis, phenylpropanoid biosynthesis, and glutathione metabolism pathways.

At 24 h post inoculation (hpi), DEGs between resistant and susceptible germplasm (S24 vs. R24) were further analyzed. Among the top 20 enriched GO terms, 18 were classified as molecular function (MF), and 2 as cellular component (CC). These terms

were mainly enriched in nucleotide binding (ATP/ADP/purine; GO:0005524), protein kinase activity (GO:0004672), phosphotransferase activity (GO:0016773), and catalytic activity, indicating active energy metabolism and phosphorylation-mediated signaling. KEGG analysis showed enrichment in secondary metabolite biosynthesis, phenylpropanoid biosynthesis, flavonoid biosynthesis, and plant hormone signal transduction pathways. Notably, the number of upregulated genes associated with the phenylpropanoid pathway increased markedly at 24 hpi, with its enrichment ranking rising from 18th at 0 h to 3rd at 24 h, suggesting that this pathway plays a key role in resistance.

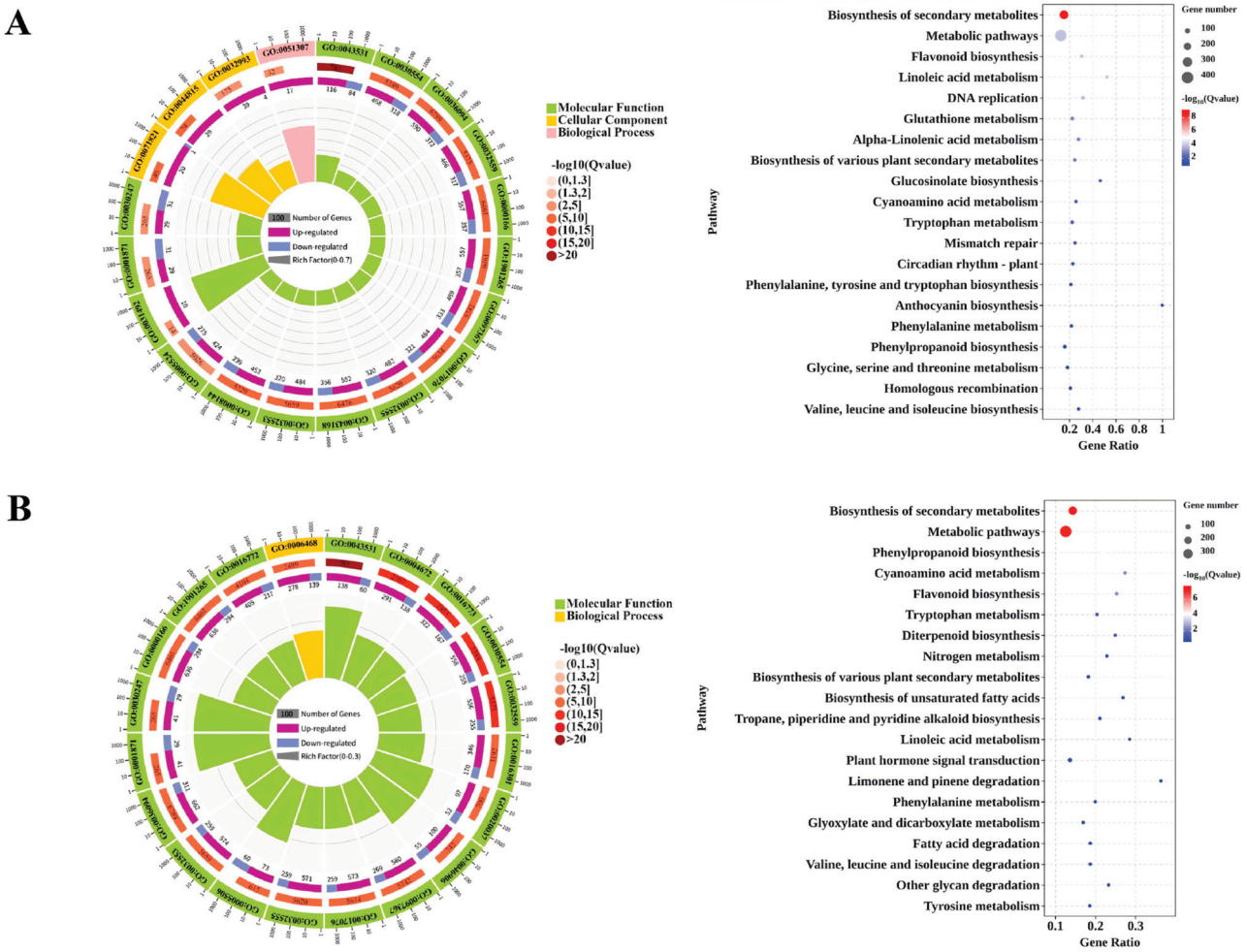


Figure 6. GO and KEGG enrichment analysis of differentially expressed genes between resistant and susceptible rubber tree germplasm at 0 and 24 h post inoculation with *C. siamense* (top 20 terms). (**A**) GO and KEGG enrichment analysis of differentially expressed genes (DEGs) between resistant (R) and susceptible (S) germplasm at 0 h post inoculation (hpi). (**B**) GO and KEGG enrichment analysis of DEGs between R and S germplasm at 24 hpi. For GO analysis, enriched terms are categorized into molecular function (MF), biological process (BP), and cellular component (CC). The circular plots display the number of DEGs, the proportion of up- and downregulated genes, and the enrichment significance indicated by −log10(Q value). For KEGG analysis, the dot plots show the top 20 enriched pathways. The size of each dot represents the number of genes, and the color indicates the enrichment significance (−log10(Q value)). R and S represent resistant (Zhanshi 477-6) and susceptible (Zhanshi 5006) rubber tree germplasm, respectively.

Further analysis of germplasm-specific DEGs revealed distinct patterns (Figure 7). Specifically upregulated DEGs in resistant germplasm were significantly enriched in GO terms related to protein kinase activity (GO:0004672), protein phosphorylation (GO:0006468), phosphotransferase activity (GO:0016773), and ATP binding (GO:0005524), all of which are as-

sociated with signal transduction processes. KEGG pathways were significantly enriched in MAPK signaling, plant hormone signal transduction, plant–pathogen interaction, and phenylpropanoid biosynthesis pathways. In contrast, specifically downregulated DEGs in susceptible germplasm were enriched in similar signaling-related GO terms, as well as membrane (GO:0016020), cell wall (GO:0005618), and glycosyltransferase activity (GO:0046527). KEGG pathways included plant hormone signal transduction, photosynthesis, brassinosteroid biosynthesis, and phenylpropanoid biosynthesis. Overall, these results indicate that differences in signaling pathways and secondary metabolism, particularly phenylpropanoid biosynthesis, are closely associated with resistance to anthracnose in rubber tree germplasm.

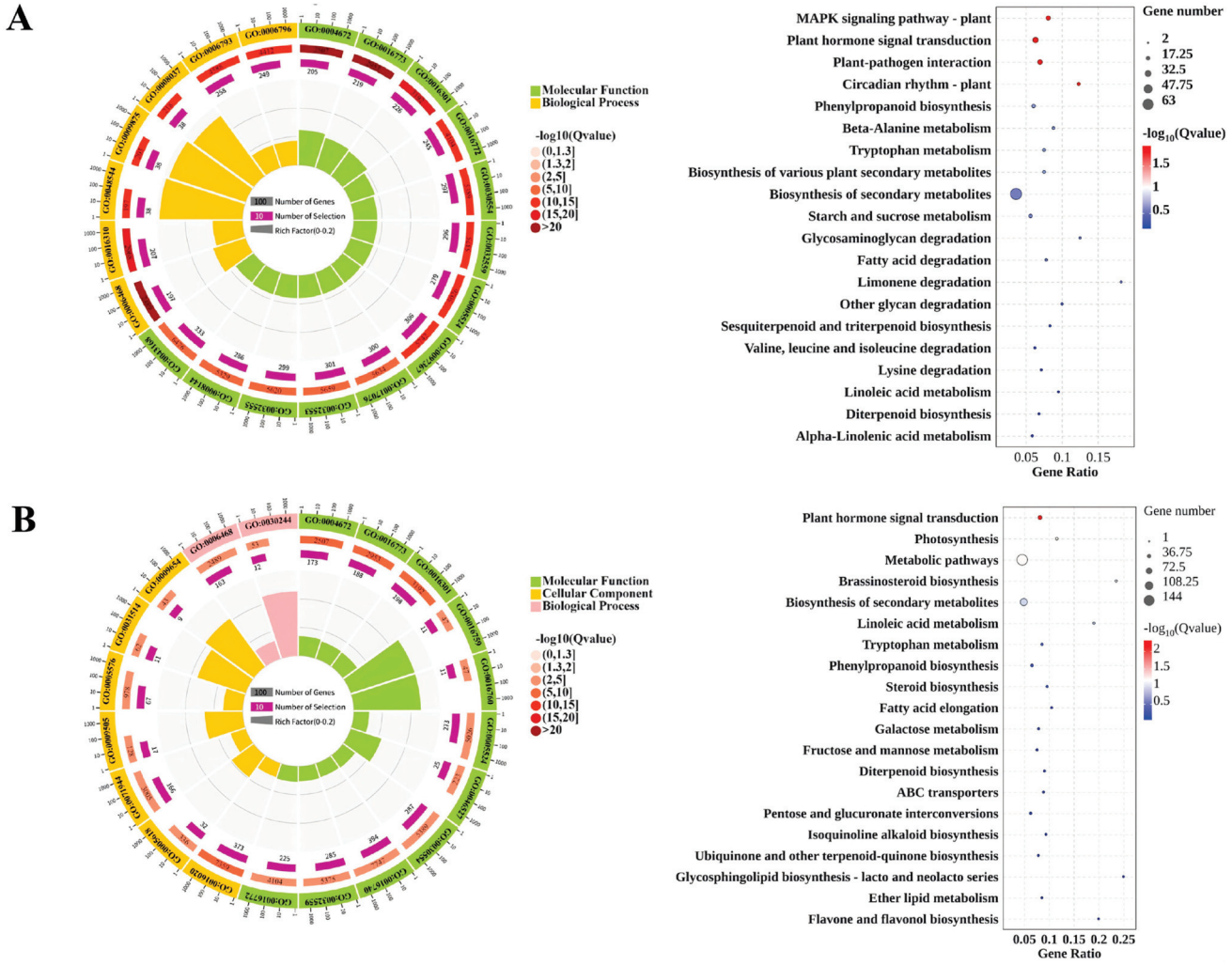


Figure 7. GO and KEGG enrichment analysis of specifically upregulated genes in resistant germplasm and specifically downregulated genes in susceptible germplasm following anthracnose infection (top 20 terms). (**A**) GO and KEGG enrichment analysis of specifically upregulated differentially expressed genes (DEGs) in resistant germplasm (R). (**B**) GO and KEGG enrichment analysis of specifically downregulated DEGs in susceptible germplasm (S). For GO analysis, enriched terms are classified into molecular function (MF), biological process (BP), and cellular component (CC). The circular plots display the number of genes, the number of selected DEGs, and the enrichment significance indicated by −log10(Q value). For KEGG analysis, the dot plots present the top 20 enriched pathways. Dot size represents gene number, and color indicates enrichment significance (−log10(Q value)). R and S represent resistant (Zhanshi 477-6) and susceptible (Zhanshi 5006) rubber tree germplasm, respectively.

https://doi.org/10.3390/f17050629

4. Discussion

Improved resistance to anthracnose may help maintain leaf integrity and photosynthetic capacity, thereby contributing to yield stability in rubber tree. The present study revealed clear phenotypic variation in anthracnose resistance among rubber tree germplasm groups, as reflected by lesion diameter and disease index. The consistency between these two indicators suggests that they reliably represent disease severity and can be used for resistance evaluation. The range of responses from resistant to highly susceptible germplasm suggests that anthracnose resistance is a complex trait influenced by multiple genetic and physiological factors [22,23]. This variation among germplasm groups provides a valuable basis for investigating the structural, physiological, and molecular mechanisms that underlie resistance.

Leaf structural traits constitute the first barrier against pathogen invasion. Stomata, as natural entry sites for *Colletotrichum*, can directly influence infection efficiency [24]. In this study, resistant germplasm exhibited significantly lower stomatal density, which positively correlated with disease index, suggesting that reduced stomatal density may limit pathogen entry and initial colonization. Although individual tissue thickness did not differ significantly, composite structural parameters—including P/S, CRT, and SR—showed strong correlations with disease index. Resistant germplasm displayed higher P/S and CRT and lower SR, indicating a more compact leaf architecture. Consistent with previous studies, increased tissue compactness can restrict hyphal penetration and intercellular colonization, thereby limiting pathogen spread and disease severity [25,26]. These findings highlight the combined contribution of stomatal traits and internal tissue organization to anthracnose resistance.

Physiological responses further contribute to disease resistance. ROS act as both signaling molecules and mediators of oxidative stress [27]. In this study, resistant germplasm exhibited stronger induction of defense-related enzymes (SOD, POD, PPO, and PAL), accompanied by higher early H_2O_2 accumulation and lower MDA levels, indicating more effective regulation of redox homeostasis. SOD and POD are involved in ROS scavenging, whereas PPO and PAL participate in phenolic metabolism and defense compound synthesis [21,28]. Previous studies have shown that maintaining a balance between ROS production and scavenging is critical for effective plant defense [29,30]. These findings suggest that coordinated antioxidant and metabolic responses enhance resistance by limiting oxidative damage and promoting defense activation.

The infection process further supports these observations. Although early infection stages, including conidial germination and appressorium formation, were similar between resistant and susceptible germplasm, significant differences emerged at later stages. Penetration structures developed more rapidly and reached higher proportions in susceptible germplasm, and disease symptoms appeared earlier than in resistant germplasm. This indicates that resistance mainly operates by restricting pathogen penetration and post-penetration colonization rather than inhibiting early infection events. This pattern is consistent with the infection strategy of *Colletotrichum* species, which rely on appressorium-mediated penetration and subsequent colonization for successful infection [31].

Transcriptomic analysis revealed substantial differences between resistant and susceptible germplasm at both constitutive and inducible levels. The presence of DEGs at 0 hpi suggests that resistant germplasm may maintain a primed defense state, which has been widely recognized as an important component of plant immunity [32]. After infection, particularly at 24 hpi, DEGs were significantly enriched in pathways related to signal transduction, including protein kinase activity, MAPK signaling, and plant hormone signaling. MAPK cascades play central roles in plant immune responses by integrating

external signals and activating downstream defense pathways [33]. These results indicate that rapid signal perception and transduction are essential for resistance.

Among the enriched pathways, phenylpropanoid biosynthesis showed a marked increase after infection. This pathway is responsible for the production of lignin and phenolic compounds, which contribute to structural reinforcement and antimicrobial defense [34]. Recent studies have further highlighted the importance of phenylpropanoid metabolism and flavonoid biosynthesis in plant resistance to *Colletotrichum* species [35–37]. The consistent enrichment of this pathway suggests that it plays a central role in rubber tree resistance to anthracnose. Furthermore, differences in the regulation of this pathway between resistant and susceptible germplasm indicate that variation in secondary metabolism may be a key factor determining resistance. Further validation of candidate genes using independent approaches such as qRT-PCR will be conducted in future studies to confirm their roles in anthracnose resistance.

Taken together, the results indicate that anthracnose resistance in rubber tree is associated with multiple interacting factors. Resistant germplasm is characterized by reduced stomatal density, more compact leaf structure, stronger activation of defense-related enzymes, and more dynamic transcriptional responses. These traits likely act in a coordinated manner to reduce pathogen entry, limit colonization, and enhance defense capacity, whereas susceptible germplasm exhibits weaker structural and physiological defenses, leading to more rapid disease development.

5. Conclusions

This study provides an integrated comparison of resistant and susceptible rubber tree germplasm under anthracnose challenge. Resistant germplasm is characterized by (i) lower stomatal density and more compact mesophyll architecture, (ii) stronger antioxidant and phenylpropanoid-associated enzyme responses coupled with reduced oxidative damage, (iii) delayed infection progression and postponed differentiation of infection structures, and (iv) distinct constitutive and inducible transcriptome programs enriched in signaling and phenylpropanoid-related pathways. These multilayered traits collectively contribute to restricting pathogen entry, colonization, and symptom development, and offer mechanistic clues and candidate genes for resistance-oriented rubber tree breeding.

Author Contributions: L.X.: Writing—original draft, Formal analysis, Data curation; P.L.: Formal analysis, Data curation; W.L.: Data curation; M.W.: Methodology; X.L.: Writing—review and editing, Conceptualization, Funding acquisition. Y.Z.: Writing—review and editing, Funding acquisition. All authors have read and agreed to the published version of the manuscript.

Funding: This work was supported by the Project of Hainan Province "Nanhai New Star" Technology Innovation Talent Platform (NHXXRCXM202310), the Project of Sanya Yazhou Bay Science and Technology City (SCKJ-JYRC-2023-22), Hainan Provincial Natural Science Foundation of China (326MS0039), and the Modern Agro-industry Technology Research System (CARS-33-BC1).

Data Availability Statement: Data will be made available on request.

Conflicts of Interest: The authors declare that they have no conflicts of interest.

References

1. Tang, C.; Yang, M.; Fang, Y.; Luo, Y.; Gao, S.; Xiao, X.; An, Z.; Zhou, B.; Zhang, B.; Tan, X.; et al. The rubber tree genome reveals new insights into rubber production and species adaptation. *Nat. Plants* **2016**, *2*, 16073. [CrossRef]
2. Tang, C.; Wu, S.; Shi, M.; Li, Z.; Li, H.; Ma, X.; Luo, Y.; Gao, S.; Xiao, X.; An, Z.; et al. Genomic insight into domestication of rubber tree. *Nat. Commun.* **2023**, *14*, 4651. [CrossRef]
3. Oghama, O.E.; Omorusi, E.S.; Osazuwa, V.I. Selected leaf diseases of rubber: Symptoms and control—A review. *J. Appl. Sci. Environ. Manag.* **2023**, *27*, 2369–2373. [CrossRef]

4. Liu, X.; Li, B.; Cai, J.; Zheng, X.; Feng, Y.; Huang, G. *Colletotrichum* species causing anthracnose of rubber trees in China. *Sci. Rep.* **2018**, *8*, 10435. [CrossRef]
5. Liu, Y.; Shi, Y.; Zhuo, D.; Yang, T.; Dai, L.; Li, L.; Zhao, H.; Liu, X.; Cai, Z. Characterization of *Colletotrichum* causing anthracnose on rubber trees in Yunnan: Two new records and two new species from China. *Plant Dis.* **2023**, *107*, 3037–3050. [CrossRef]
6. Liang, X.; Peng, Y.; Zou, L.; Wang, M.; Yang, Y.; Zhang, Y. Baseline sensitivity of penthiopyrad against *Colletotrichum gloeosporioides* species complex and its efficacy for the control of *Colletotrichum* leaf disease in rubber tree. *Eur. J. Plant Pathol.* **2020**, *158*, 965–974. [CrossRef]
7. Sobha, S.; Rekha, K.; Uthup, T.K. Biotechnological advances in rubber tree (*Hevea brasiliensis* Muell. Arg.) breeding. In *Advances in Plant Breeding Strategies: Industrial and Food Crops*; Al-Khayri, J.M., Jain, S.M., Johnson, D.V., Eds.; Springer: Cham, Switzerland, 2019; Volume 6, pp. 179–236.
8. Kaur, S.; Samota, M.K.; Choudhary, M.; Pandey, A.K.; Sharma, A.; Thakur, J. How do plants defend themselves against pathogens—Biochemical mechanisms and genetic interventions. *Physiol. Mol. Biol. Plants* **2022**, *28*, 485–504. [CrossRef]
9. Jian, Y.; Gong, D.; Wang, Z.; Liu, L.; He, J.; Han, X.; Tsuda, K. How plants manage pathogen infection. *EMBO Rep.* **2024**, *25*, 31–44. [CrossRef] [PubMed]
10. Hou, S.; Rodrigues, O.; Liu, Z.; Shan, L.; He, P. Small holes, big impact: Stomata in plant–pathogen–climate epic trifecta. *Mol. Plant* **2024**, *17*, 26–49. [CrossRef]
11. Chaudhry, V.; Runge, P.; Sengupta, P.; Doehlemann, G.; Parker, J.E.; Kemen, E. Shaping the leaf microbiota: Plant-microbe-microbe interactions. *J. Exp. Bot.* **2021**, *72*, 36–56. [CrossRef] [PubMed]
12. Haghpanah, M.; Namdari, A.; Kaleji, M.K.; Nikbakht-Dehkordi, A.; Arzani, A.; Araniti, F. Interplay between ROS and hormones in plant defense against pathogens. *Plants* **2025**, *14*, 1297. [CrossRef] [PubMed]
13. Zhai, S.; Guo, H.; Sun, T.; Guo, M.; Chen, J.; Cao, J.; Yang, W.; Chen, G. 3-Methyl-1-Butanol enhances postharvest resistance of red grapes to *Botrytis cinerea* by activating phenylpropanoid metabolism and antioxidant defences. *Plant Biotechnol. J.* **2025**, *24*, 2673–2684. [CrossRef] [PubMed]
14. Dong, B.; Da, F.; Chen, Y.; Ding, X. Melatonin treatment maintains the quality of fresh-cut *Gastrodia elata* under low-temperature conditions by regulating reactive oxygen species metabolism and the phenylpropanoid pathway. *Int. J. Mol. Sci.* **2023**, *24*, 14284. [CrossRef]
15. Dumanović, J.; Nepovimova, E.; Natić, M.; Kuča, K.; Jaćević, V. The significance of reactive oxygen species and antioxidant defense system in plants: A concise overview. *Front. Plant Sci.* **2021**, *11*, 552969. [CrossRef]
16. Geng, X.; Gao, Z.; Zhao, L.; Zhang, S.; Wu, J.; Yang, Q.; Liu, S.; Chen, X. Comparative transcriptome analysis of resistant and susceptible wheat in response to Rhizoctonia cerealis. *BMC Plant Biol.* **2022**, *22*, 235. [CrossRef] [PubMed]
17. Xu, B.; Qi, G.; Liu, X.; Yuan, C.; Wang, Y.; Li, Y.; Zhang, J.; Zhao, H.; Dong, Y. Transcriptome analysis reveals key pathways and regulatory networks involved in soybean's early resistance to *Peronospora manshurica*. *BMC Plant Biol.* **2025**, *25*, 1316. [CrossRef]
18. *NY/T 3518-2019*; Technical Code for Monitoring Pests of Tropical Crops—Anthracnose of Rubber Tree. Ministry of Agriculture and Rural Affairs of the People's Republic of China: Beijing, China, 2019. (In Chinese)
19. Deenamo, N.; Kuyyogsuy, A.; Khompatara, K.; Chanwun, T.; Ekchaweng, K.; Churngchow, N. Salicylic acid induces resistance in rubber tree against *Phytophthora palmivora*. *Int. J. Mol. Sci.* **2018**, *19*, 1883. [CrossRef]
20. Li, D.; Xia, Z.; Wang, X.; Yang, H.; Li, Y. Melatonin enhances drought tolerance by regulating the genes underlying photosynthesis and antioxidant defense in rubber tree (*Hevea brasiliensis*) seedlings. *Plants* **2025**, *14*, 2243. [CrossRef]
21. Han, C.; Su, Z.; Zhao, Y.; Li, C.; Guo, B.; Wang, Q.; Liu, F.; Zhang, S. Uncovering the mechanisms underlying pear leaf apoplast protein-mediated resistance against *Colletotrichum fructicola* through transcriptome and proteome profiling. *Phytopathol. Res.* **2024**, *6*, 3. [CrossRef]
22. Mulube, M.; Hamabwe, S.; Kuwabo, K.; Chinji, M.; Nkandela, M.; Botha, J.; Mwense, B.; Tembo, L.; Lungu, D.; Mukuma, C.; et al. Mapping of quantitative trait locus for resistance to anthracnose in a population derived from genotypes PI 527538 and Ervilha of common bean. *Front. Plant Sci.* **2025**, *16*, 1691703. [CrossRef]
23. Kadege, E.L.; Venkataramana, P.B.; Assefa, T.; Ndunguru, J.C.; Rubyogo, J.C.; Mbega, E.R. Characterization of phenotypic traits associated with anthracnose resistance in selected common bean (*Phaseolus vulgaris* L.) breeding material. *Heliyon* **2024**, *10*, e26917. [CrossRef]
24. Ren, J.; Pu, J.; Yu, J.; Huang, Y.; Shan, N.; Sun, J.; Chen, A.; Wang, S.; Zhou, Q.; Luo, S. Evaluation of anthracnose-resistant greater yam and the mechanism of abscisic acid-mediated disease resistance. *Trop. Plants* **2025**, *4*, e021. [CrossRef]
25. Engelsdorf, T.; Will, C.; Hofmann, J.; Schmitt, C.; Merritt, B.B.; Rieger, L.; Frenger, M.S.; Marschall, A.; Franke, R.B.; Pattathil, S.; et al. Cell wall composition and penetration resistance against the fungal pathogen *Colletotrichum higginsianum* are affected by impaired starch turnover in *Arabidopsis* mutants. *J. Exp. Bot.* **2017**, *68*, 701–713. [CrossRef]
26. Mittler, R.; Zandalinas, S.I.; Fichman, Y.; Van Breusegem, F. Reactive oxygen species signalling in plant stress responses. *Nat. Rev. Mol. Cell Biol.* **2022**, *23*, 663–679. [CrossRef]

27. Rao, M.J.; Duan, M.; Zhou, C.; Jiao, J.; Cheng, P.; Yang, L.; Wei, W.; Shen, Q.; Ji, P.; Yang, Y.; et al. Antioxidant defense system in plants: Reactive oxygen species production, signaling, and scavenging during abiotic stress-induced oxidative damage. *Horticulturae* **2025**, *11*, 477. [CrossRef]
28. Liang, X.; Qiu, Y.; Jian, S.; Hu, M.; Zhang, S.; Wang, M.; Zhang, Y. Potassium phosphite effectively controls rubber tree anthracnose by inhibiting melanin biosynthesis of*Colletotrichum siamense*. *Pestic. Biochem. Physiol.* **2025**, *215*, 106648. [CrossRef] [PubMed]
29. Alam, P.; Faizan, M.; Arif, Y.; Azzam, M.M.; Hayat, S.; Afzal, S.; Albalawi, T. Reactive oxygen species: Balancing agents in plants. *Front. Plant Sci.* **2025**, *16*, 1713590. [CrossRef]
30. Wang, Y.; Ji, D.; Chen, T.; Li, B.; Zhang, Z.; Qin, G.; Tian, S. Production, signaling, and scavenging mechanisms of reactive oxygen species in fruit–pathogen interactions. *Int. J. Mol. Sci.* **2019**, *20*, 2994. [CrossRef]
31. Usman, H.; Hussain, M.; Karim, M.; Nizamani, M.; Mubeen, M.; Hussain, S.; Kamran, A.; Wang, Y.; Liu, F. *Colletotrichum*: A versatile fungal genus with diverse infection strategies, host interactions, and management challenges. *Phytopathol. Res.* **2026**, *8*, 6. [CrossRef]
32. Yang, Z.; Zhi, P.; Chang, C. Priming seeds for the future: Plant immune memory and application in crop protection. *Front. Plant Sci.* **2022**, *13*, 961840. [CrossRef]
33. Zhang, M.; Zhang, S. Mitogen-activated protein kinase cascades in plant signaling. *J. Integr. Plant Biol.* **2022**, *64*, 301–341. [CrossRef]
34. Yadav, V.; Wang, Z.; Wei, C.; Amo, A.; Ahmed, B.; Yang, X.; Zhang, X. Phenylpropanoid Pathway Engineering: An Emerging Approach towards Plant Defense. *Pathogens* **2020**, *9*, 312. [CrossRef]
35. Xing, F.; Zhang, L.; Ge, W.; Fan, H.; Tian, C.; Meng, F. Comparative transcriptome analysis reveals the importance of phenylpropanoid biosynthesis for the induced resistance of 84K poplar to anthracnose. *BMC Genom.* **2024**, *25*, 306. [CrossRef]
36. Liu, Y.; Song, Q.; Yin, F.; Liang, Y.; Song, M.; He, M.; Shuai, L. *Colletotrichum capsici*-Induced disease development in postharvest pepper associated with cell wall metabolism and phenylpropanoid metabolism. *Horticulturae* **2025**, *11*, 794. [CrossRef]
37. Jiang, L.; Wu, P.; Yang, L.; Liu, C.; Guo, P.; Wang, H.; Wang, S.; Xu, F.; Zhuang, Q.; Tong, X.; et al. Transcriptomics and metabolomics reveal the induction of flavonoid biosynthesis pathway in the interaction of *Stylosanthes–Colletotrichum gloeosporioides*. *Genomics* **2021**, *113*, 2702–2716. [CrossRef]

Disclaimer/Publisher's Note: The statements, opinions and data contained in all publications are solely those of the individual author(s) and contributor(s) and not of MDPI and/or the editor(s). MDPI and/or the editor(s) disclaim responsibility for any injury to people or property resulting from any ideas, methods, instructions or products referred to in the content.

forests

MDPI

Article

Impact of Melatonin on Antioxidant Enzymes and Soluble Metabolites in Salt–Alkali-Stressed Poplar (*Populus* spp.): A Comparative Study of Pretreatment and Post-Treatment Effects

Jiefei Nai [1], Wanpeng He [1], Tieming Ma [1], Xidong Han [2], Zhenxing Luo [2], Xinyu Li [3], Jiatong Sun [4] and Xiyang Zhao [1,*]

[1] Jilin Provincial Key Laboratory of Tree and Grass Genetics and Breeding, College of Forestry and Grassland, Jilin Agricultural University, Xincheng Street No. 2888, Changchun 130118, China; naijiefei@163.com (J.N.); 13369401916@163.com (W.H.); tiemingart@jlau.edu.cn (T.M.)
[2] Baicheng Academy of Forestry, Baicheng 137000, China; xidong@163.com (X.H.); luozhenxing@163.com (Z.L.)
[3] Institute of Information, Liaoning Academy of Agricultural Sciences, Shenyang 110161, China; lixy@163.com
[4] Liaoning Institute of Forest Management, Shenyang 110161, China; sunjtt89@163.com
* Correspondence: zhaoxyphd@163.com

Abstract

Melatonin plays a crucial role in modulating plant stress responses; however, its potential for mitigating salt–alkali stress remains incompletely understood. This study evaluates the efficacy of exogenous melatonin in alleviating moderate salt–alkali stress (120 mM) in poplar (*Populus davidiana* × *P. bolleana* 'Baicheng Shanxinyang No. 1') seedlings, investigating both pre- and post-stress treatments across a concentration range of 0–1000 μM. Physiological and morphological parameters, including chlorophyll content, antioxidant enzyme activities, and osmolyte accumulation, were analyzed to assess stress responses. Under salt–alkali stress, seedlings exhibited elevated stress markers and osmolyte levels, reflecting activated stress responses. Melatonin at concentrations of 200–400 μM was the most effective in mitigating stress, significantly enhancing antioxidant enzyme activities such as superoxide dismutase (SOD) and catalase (CAT), restoring chlorophyll content, and reducing oxidative damage markers such as malondialdehyde (MDA). It also regulated osmotic balance in leaves, indicating improved cellular stability under stress. Notably, post-stress application required slightly higher melatonin concentrations to achieve comparable recovery, highlighting the critical influence of application timing. These findings provide valuable insights for optimizing melatonin use to improve poplar growth in saline–alkali environments and support molecular breeding efforts aimed at developing salt–alkali-tolerant poplar varieties.

Keywords: melatonin; salt–alkali stress; antioxidant enzymes; soluble metabolites; poplar plant

1. Introduction

Soil salinization, exacerbated by human activities and climate change, poses a critical threat to global agriculture. Recent studies indicate that over half of the world's arable land is at risk of salinization and desertification [1], with the FAO reporting more than 1.4 billion hectares affected by salinity, alkalinity, or their combined effects. These conditions generate saline–alkali stress, a synergistic phenomenon where salt and alkali stresses coexist, inflicting greater harm on plants than either stress alone. Saline–alkali stress

damages plants through four primary mechanisms: osmotic stress oxidative stress [2], osmotic stress [3], ion toxicity [4], and high pH stress [5]. Elevated sodium ion (Na^+) concentrations and high alkaline pH disrupt cellular functions, impair water uptake, and interfere with essential metabolic processes [6,7]. High salt levels increase soil osmotic pressure, inducing "physiological drought", a condition in which plants cannot absorb water despite its presence. This leads to cellular dehydration, wilting, and, in severe cases, death [8]. Moreover, saline–alkali conditions destabilize the redox balance in plant cells, triggering excessive production of reactive oxygen species (ROS). The overaccumulation of ROS damages cellular structures, exacerbates oxidative stress, and further compromises plant health. These multifaceted stressors collectively reduce agricultural productivity, underscoring the urgency of developing adaptive strategies to mitigate soil degradation and enhance crop resilience.

Melatonin (MEL) functions as a potent antioxidant in plants, effectively mitigating oxidative damage by scavenging reactive oxygen species (ROS) and maintaining cellular redox balance [9]. However, under stress conditions, the excessive accumulation of reactive oxygen species (ROS) disrupts chlorophyll (Chl) structure, impairs light absorption, and reduces photosynthetic efficiency. In addition, ROS-induced lipid peroxidation generates toxic by-products such as malondialdehyde (MDA), which further inhibit growth and physiological performance in species such as poplar [10]. To counteract these detrimental effects, plants activate a range of defense mechanisms, including the upregulation of antioxidant enzymes such as superoxide dismutase (SOD), peroxidase (POD), and catalase (CAT). Additionally, they enhance the accumulation of osmolytes, including soluble sugars (sSUG) and soluble proteins (sPRO), to mitigate oxidative and osmotic stress [11,12].

Poplar (*Populus* L.), a keystone genus in the *Salicaceae* family, is a high-value domesticated tree cultivated globally for woody biomass production, with plantations spanning ~31.4 million hectares. Comprising over 100 classified species such as *Tacamahaca* and *Aigeiros* [13], poplar is prized for its rapid growth, stress resilience, and ecological versatility, making it vital for industrial timber and reforestation [14]. However, sensitivity to soil conditions, especially salt–alkali stress, is a major limitation for agricultural and forestry productivity. This stress disrupts ion balance, damages cell membranes, and interferes with photosynthesis and metabolic processes, often resulting in stunted growth or plant death [15].

While melatonin (MEL) has been shown to enhance antioxidant enzyme activity and soluble metabolites in poplar trees under salt stress, its effectiveness in addressing the more complex and ecologically significant combined salt–alkali stress remains largely unexplored. To date, few studies have examined the effects of melatonin on the hybrid poplar *Populus cathayana* × *canadensis* 'Xinlin 1' under combined salt–alkali stress [16,17]. However, further research is essential to fully understand the effects of melatonin before and after exposure to salt and alkali stress. The objective of this study is to investigate the effects of exogenous melatonin on key physiological and biochemical parameters, including chlorophyll (Chl) content, malondialdehyde (MDA) levels, soluble sugars (sSUG), soluble proteins (sPRO), and the activity of antioxidant enzymes (SOD, POD, CAT) under salt and alkali stress. The effects of different concentrations of melatonin on the growth and physiology of plants were analyzed, and a melatonin concentration which could promote the accumulation of plant biomass, reduce the damage of cell membranes, enhance the regulation ability of antioxidant systems, and significantly alleviate the damage caused by saline alkali stress on plants was obtained. At the same time, two different application methods of melatonin were compared to confirm that the best planting method of this material in saline–alkali soil was to carry out melatonin pretreatment in advance. The results are expected to inform

https://doi.org/10.3390/f17030373

strategies for cultivating poplars in saline and alkaline soils, thereby supporting sustainable timber production and environmental restoration.

2. Materials and Methods

2.1. Plant Material and Treatments

In this study, we selected *Populus davidiana* × *P. bolleana* 'Baicheng Shanxinyang No. 1' developed by the Baicheng Forestry Research Institute in Jilin Province, China.

A pot experiment was conducted as follows. First, a layer of non-woven fabric was placed at the bottom of each plastic pot. Sterilized peat soil and vermiculite were then mixed in a 3:1 ratio to prepare the potting substrate. The plastic pots measured 20 cm in both height and upper diameter, with the substrate filled to the rim. One- or two-year-old seedlings free of pests and diseases with an average diameter of 0.8–1.0 cm and a height exceeding 30 cm (average 38–40 cm) were selected for the experiment.

2.2. Experimental Design

The experiment consisted of two main groups: one received melatonin treatment prior to salt–alkali stress, while the other was exposed to salt–alkali stress before melatonin treatment. Each group was further divided into six treatments based on different melatonin concentrations. For each treatment, six pots were placed in the same tray, with these six pots serving as replicates for that treatment. Melatonin was obtained from Shanghai Macklin Biochemical Technology Co., Ltd. (Shanghai, China) with a purity of 98%. For preparation, melatonin was first dissolved in 1 mL of 95% alcohol and then diluted with distilled water to achieve six different concentrations: 0, 200, 400, 600, 800, and 1000 μM (0 μM consisted of only 1 mL of alcohol and distilled water). In this experiment, 0 μM served as the control group (CK), and the alcohol content in all melatonin solutions was maintained below 0.1%. The six concentrations of exogenous melatonin were applied to the leaves using an agricultural lithium battery high-pressure cyclone sprayer (Dv0.5 < 500 μm) (Chaonongli Sprayer (Chaonongli (Zhejiang) Intelligent Technology Co., Ltd., Ningbo, China)). 120 mM NaCl solutions and 120 mM Na_2CO_3 solutions were prepared using distilled water (NaCl and Na_2CO_3 were sourced from Shanghai Macklin Biochemical Technology Co., Ltd. (Shanghai, China), with a purity of 99.5%). The above two solutions were mixed at a ratio of 1:1 by volume to form a mixed salt solution (κ = 18.74 mS/cm, Ph = 10.74) (mixed salt solutions of other concentrations can also be prepared according to this method). In order to better simulate the local soil environment of Baicheng City (pH 7.5~8.5), the pH of the soil in each pot was detected. The detection site in the pot was 7 cm from the soil in the pot. Five sites were set up in each pot to be assayed. Distilled water was added to the test sites until the bottom was in a muddy state. The pH meter probe was inserted to check the soil pH in the pot, and we waited until the average pH in each pot reached 8.0 (κ = 1.87 mS/cm).

During the experiment, when the subjects were subjected to saline–alkali stress, each sample received 100 milliliters of a 120 mM/L NaCl and Na_2CO_3 compound stress solution and a nutrient solution. When treated with melatonin, six concentrations of exogenous melatonin solution were sprayed onto the leaves with an air atomizing nozzle to ensure that the entire leaf was covered.

During the sampling process, the second topmost leaf of each sample was collected, followed by sampling every 4 days for 5 rounds. Fresh samples were frozen in liquid nitrogen immediately after collection and then stored at −80 °C in a refrigerator until use. The specific treatment duration is shown in Figure 1.

https://doi.org/10.3390/f17030373

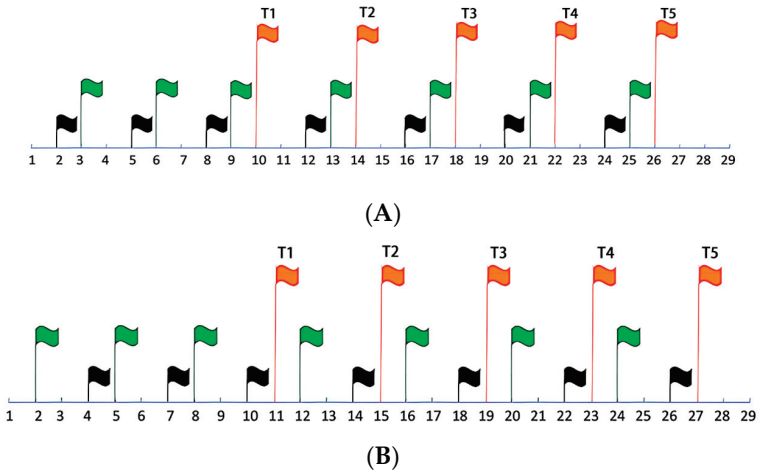


Figure 1. Schematic representation of the experimental setup: black flags indicate samples treated with melatonin (applicable to all concentrations), green flags indicate samples exposed to NaCl and Na_2CO_3, and orange flags indicate points of sample collection. T1 to T5 denote the timing and order of sample collection. (**A**) Melatonin treatment followed by saline–alkali stress; (**B**) First, saline–alkali stress and then melatonin treatment.

2.3. Index Determination

In the experiment, we utilized kits provided by Beijing BOX Biotechnology Co., Ltd. (Beijing, China) to measure the activities of SOD, POD, CAT, and the contents of MDA, Pro, soluble sugars, soluble proteins, and chlorophyll (see Appendix A for the article number and principle of the kit). The specific measurement process was as follows:

First, the samples (30 Hz, 90 s) were ground to powder using a grinder (MM400, Retsch) (Retsch, Diisseldorf, Germany). Then, 100 mg of the powder was weighed from each sample and dissolved in 1.2 mL of a 70% methanol solution. The supernatant was extracted using a centrifuge (12,000 rpm, 20 min). Then, it was pre-coated with SOD, POD, CAT, MDA, Pro, soluble proteins and soluble sugars. Firstly, the sample (30 Hz, 90 s) was ground into powder using a grinder (MM400, Retsch, Dieseldorf, Germany). Then, 100 milligrams of powder from each sample were weighed and then dissolved in 1.2 milliliters of 70% methanol solution. The supernatant was extracted using a centrifuge (12,000 rpm, 20 min). Then, the supernatant was transferred to the corresponding reagent for reaction. After the reaction was completed, the reaction solution was added to the micropores, and the absorbance (outer diameter value) of the corresponding nanometer wavelength was measured using a microplate reader (Infinite F50) (Tecan Group Ltd., Männedorf, Switzerland).

The conductivity of the samples was measured with a DDSJ-308F conductivity meter (Rex Electric Chemical, Shanghai, China).

2.4. Data Analysis

All indicators were derived from the average values of six biological replicates. Statistical analyses were performed using Microsoft Excel 2017 and SPSS 23 software. All data are presented as mean ± standard error (SE). To assess significant differences among the indicators, we applied two-way ANOVA with a significance level set at 0.05, and the analysis was conducted using ggplot2 (v3.5.0) in R [18].

3. Results

3.1. Effects of Saline–Alkali Stress on Poplar Plant Without Melatonin Treatment

The experiment investigated the effects of mixed salt–alkali stress on annual potted poplar cuttings using treatments of 0, 40, 80, 120, and 160 mM NaCl and Na_2CO_3. Plant

growth indicators were generally suppressed, as shown in Figure 2A–D. Interestingly, leaf area and plant height increased at 160 mM (Figure 2A,D), suggesting a potential reallocation of resources in response to partial mortality. However, increasing stress levels began to inhibit plant height and leaf area at 120 mM (Figure 3) while simultaneously elevating physiological parameters, including antioxidant enzyme activities, malondialdehyde (MDA), soluble sugars, soluble proteins, and conductivity in the second apical leaf, accompanied by a decrease in chlorophyll content (Figure 4A–H). Notably, antioxidant enzyme activities peaked at 120 mM before sharply declining, whereas chlorophyll content consistently decreased with rising stress. These results indicate that 120 mM represents the optimal stress threshold for poplar seedlings, beyond which growth is suppressed and physiological and biochemical defenses are negatively affected.

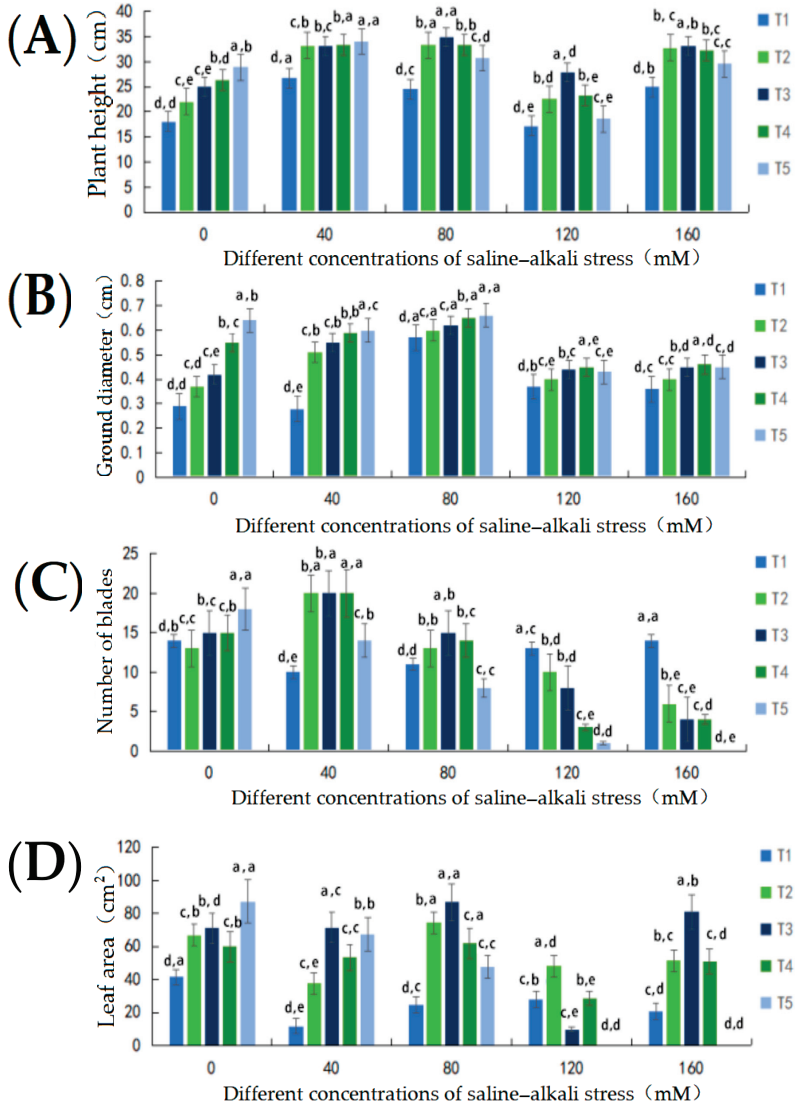


Figure 2. Effects of different salt and alkali treatments on the growth characteristics of *Populus davidiana* × *P. bolleana* 'Baicheng Shanxinyang No. 1'. (**A**) plant height; (**B**) ground diameter; (**C**) number of leaves; (**D**) leaf area. T1—5 days, T2—10 days, T3—15 days, T4—20 days, T5—25 days. All data are presented as mean ± standard error (±SE); error bars represent standard errors (n = 6, with six biological replicates set for each treatment). For two-way ANOVA, the letters on the left represent the detection phase ($p < 0.05$), and the letters on the right represent the experimental concentrations ($p < 0.05$), according to the Duncan test.

https://doi.org/10.3390/f17030373

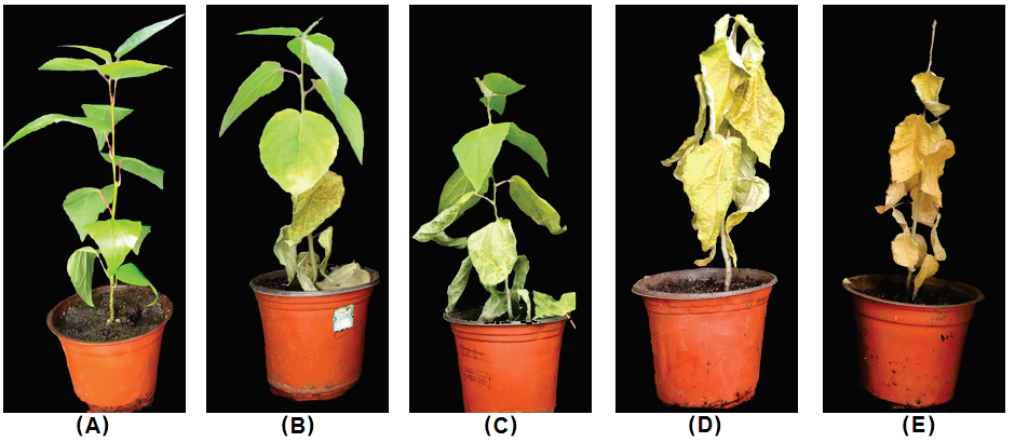


Figure 3. Effects of different salt and alkali treatments on the morphology of *Populus davidiana* × *P. bolleana* 'Baicheng Shanxinyang No. 1'. (**A**–**E**) represent 0, 40, 80, 120, and 160 Mm NaCl-Na_2CO_3 mixed salt–alkali treatment, respectively.

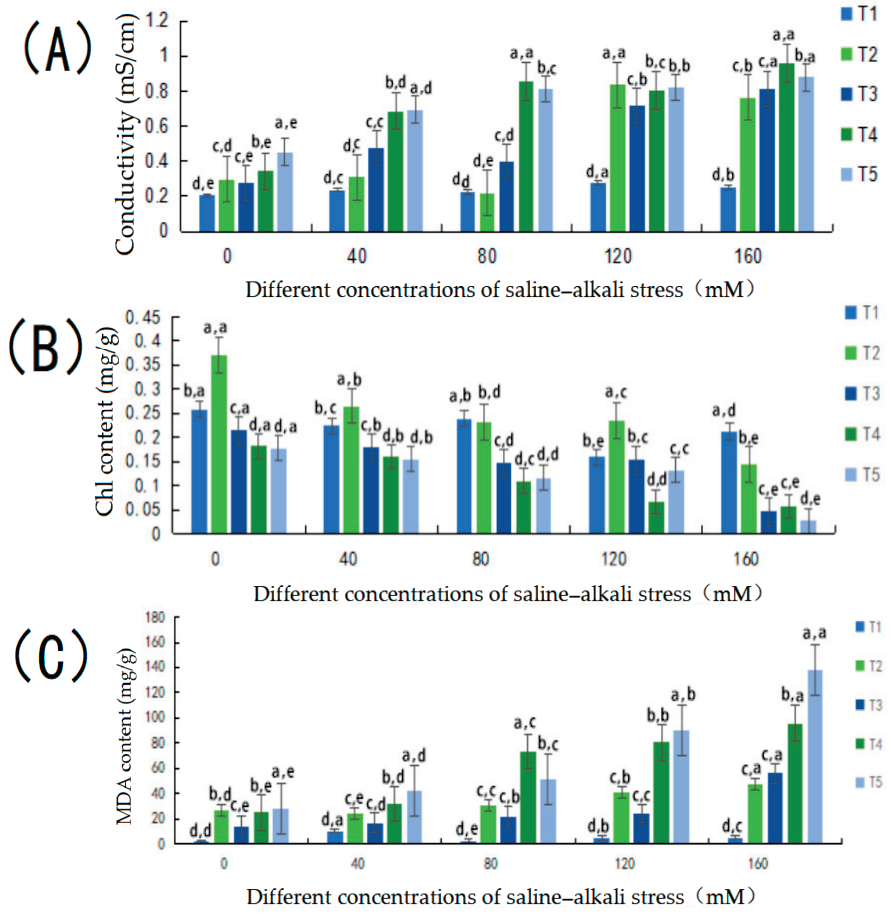


Figure 4. *Cont.*

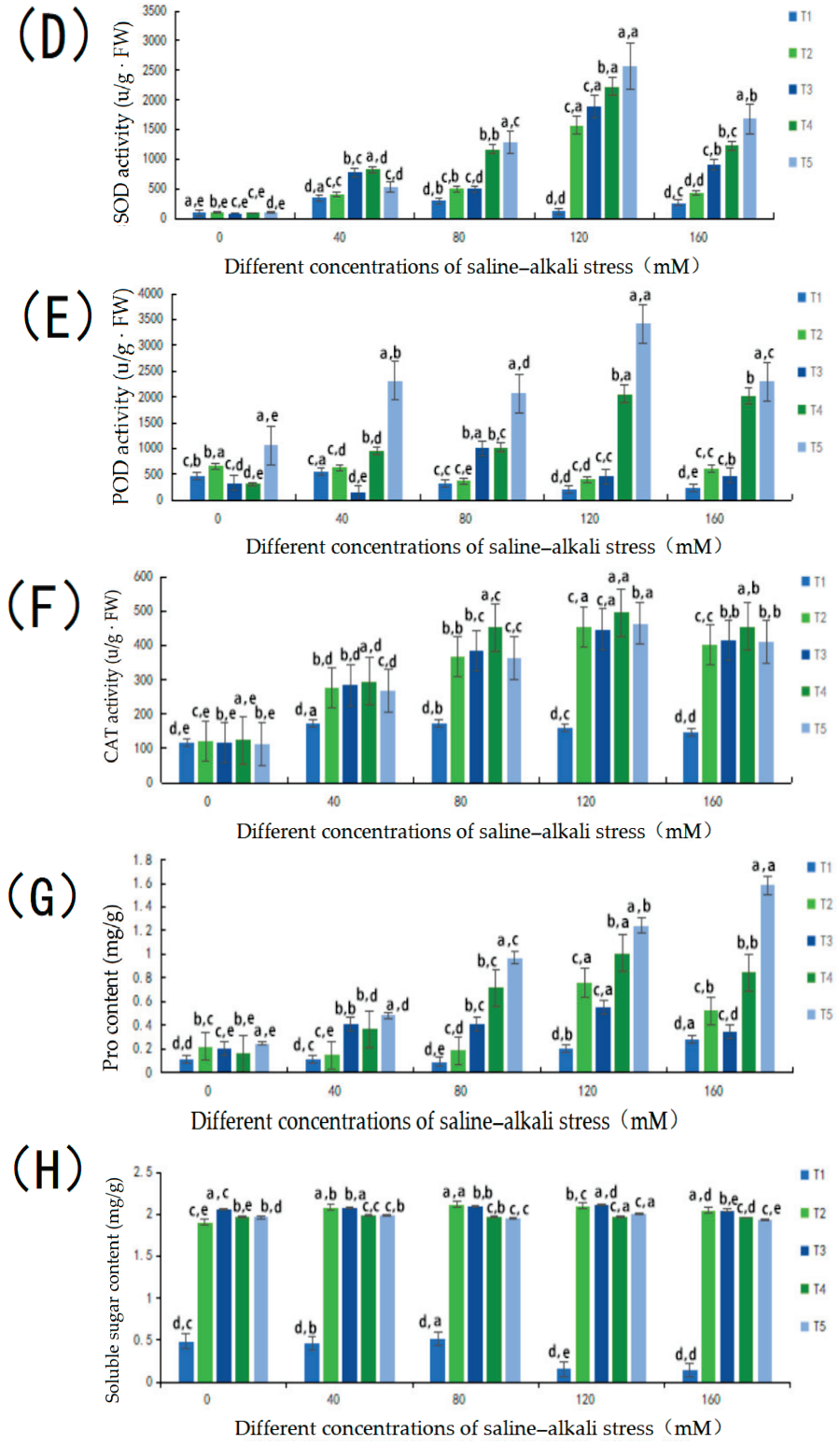


Figure 4. Effects of salt–alkali treatment with different concentrations on physiological indexes of *Populus davidiana* × *P. bolleana* 'Baicheng Shanxinyang No. 1': (**A**) electrical conductivity; (**B**) chlorophyll content; (**C**) malondialdehyde content; (**D**) superoxide dismutase activity; (**E**) peroxidase activity; (**F**) catalase activity; (**G**) soluble protein content; (**H**) soluble sugar content. T1—5 days, T2—10 days, T3—15 days, T4—20 days, T5—25 days. All data are presented as mean ± standard error (±SE), error bars represent standard errors (n = 6, with six biological replicates set for each treatment). For two-way ANOVA, the letters on the left represent the detection phase ($p < 0.05$), and the letters on the right represent the experimental concentrations ($p < 0.05$), according to the Duncan test.

https://doi.org/10.3390/f17030373

3.2. Effect of Melatonin Pretreatment on Saline–Alkali Stressed Poplar Plant

Populus davidiana × *P. bolleana* 'Baicheng Shanxinyang No. 1' plants were pretreated with melatonin at concentrations of 0, 200, 400, 600, 800, or 1000 μM for 24 h, followed by exposure to 120 mM mixed saline–alkali stress. Morphological and physiological parameters were measured every two days starting at one day post-stress induction. As shown in Figures 5 and 6, melatonin application significantly increased leaf number under stress compared to the stress-only control, with the most obvious effect observed at 400 μM during the T1 and T2 stages (10 and 14 days). This concentration optimally alleviated stress impacts, while efficacy declined at higher doses (1000 μM). In contrast, melatonin pretreatment did not statistically alter ground diameter, plant height, or leaf area. These findings suggest that low melatonin concentrations enhance saline–alkali stress resistance in poplar primarily through modulating leaf development rather than overall growth metrics.

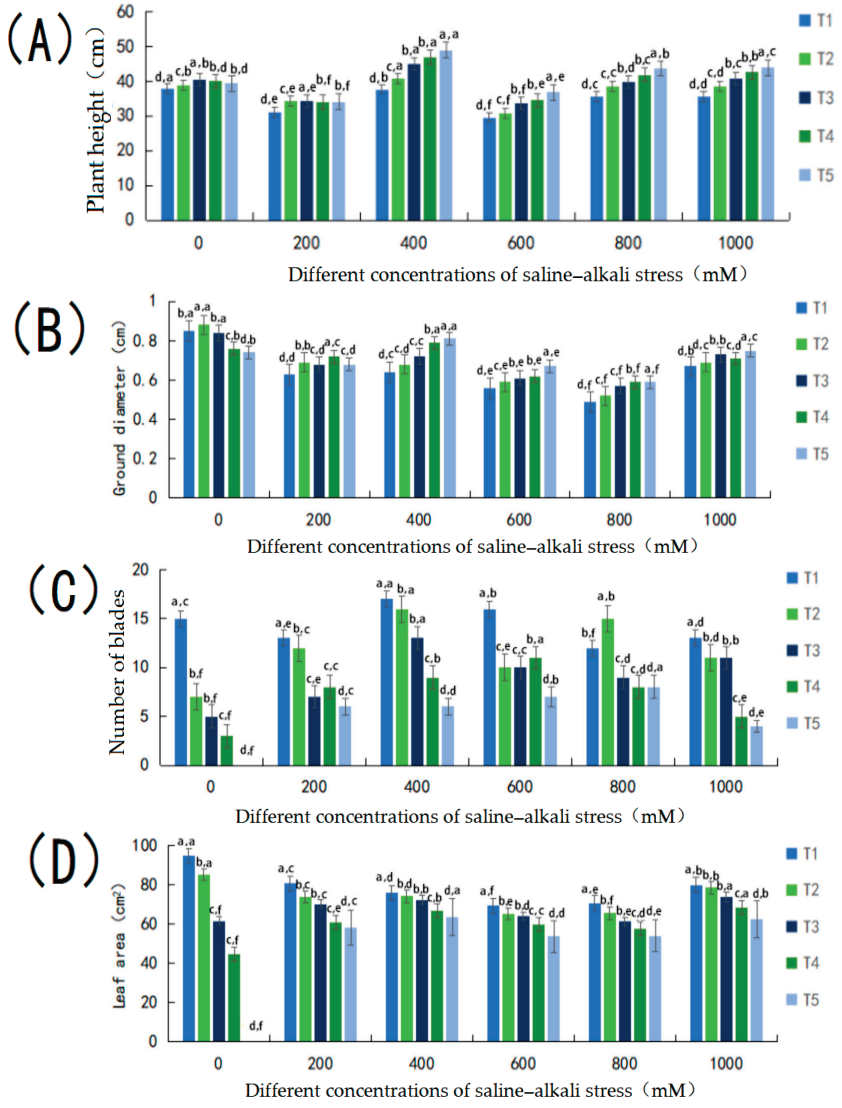


Figure 5. Effects of melatonin pretreatment on morphological indexes of *Populus davidiana* × *P. bolleana* 'Baicheng Shanxinyang No. 1' under saline–alkali stress (**A**) plant height; (**B**) ground diameter; (**C**) number of leaves; (**D**) leaf area. T1—10 days, T2—14 days, T3—18 days, T4—22 days, T5—26 days. All data are presented as mean ± standard error (±SE), error bars represent standard errors ($n = 6$, with six biological replicates set for each treatment). For two-way ANOVA, the letters on the left represent the detection phase ($p < 0.05$), and the letters on the right represent the experimental concentrations ($p < 0.05$).

https://doi.org/10.3390/f17030373

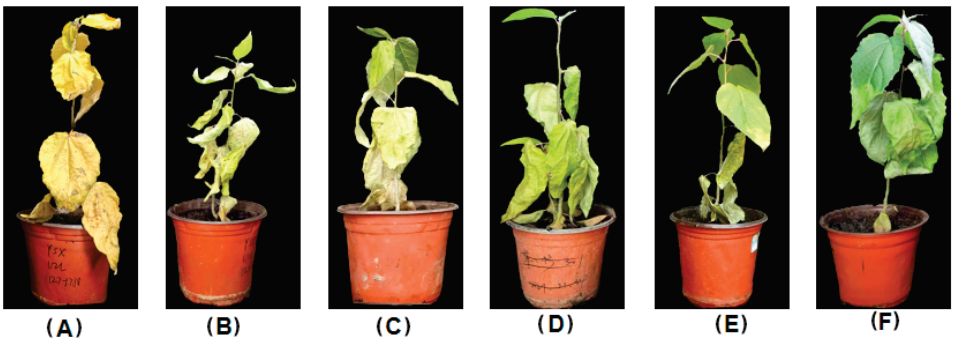


Figure 6. Effects of different melatonin pretreatments on the morphology traits of *Populus davidiana* × *P. bolleana* 'Baicheng Shanxinyang No. 1' under saline–alkali stress. (**A**–**F**) represent 0, 200, 400, 600, 800 and 1000 μM melatonin pretreatment, respectively.

Notably, as illustrated in Figure 7D,E, the activities of SOD and CAT exhibited a biphasic response to melatonin concentration. These activities increased at lower concentrations, reached a peak at 200 μM, and then decreased at higher concentrations (≥400 μM). In contrast, POD activity initially decreased at melatonin concentrations below 200 μM but increased at higher concentrations (Figure 7C), potentially reflecting its dual role in stress adaptation and alternative signaling pathways.

Furthermore, the dynamic changes in soluble metabolites, including sugars and proteins, across the experimental groups at different time points are depicted in Figure 7F,G. Melatonin's influence on osmolyte synthesis was found to be concentration-dependent, exhibiting a biphasic effect: lower concentrations (200 μM) suppressed the accumulation of soluble sugars and proteins, while higher concentrations (≥400 μM) significantly enhanced their production. This suggests that melatonin's role in osmoregulation is dose-specific, likely mediated by its dual function as both a signaling molecule and a stress modulator. The 200 μm melatonin pretreatment was proved to be the best concentration to alleviate plant stress symptoms.

To further evaluate these effects, we systematically analyzed MDA and chlorophyll dynamics across the experimental groups, as shown in Figure 7B. Specifically, MDA levels decreased progressively with increasing melatonin dosage, indicating that exogenous melatonin effectively preserved membrane integrity by reducing ROS-induced lipid degradation. In addition, chlorophyll content, an essential indicator of photosynthetic capacity, also displayed a biphasic response. While no statistically significant changes in chlorophyll levels were observed during pretreatment (Figure 7A), the concentration of 200 μM was noted for its optimal stress-alleviating effect. However, at concentrations exceeding 200 μM, chlorophyll levels declined, indicating potential phytotoxicity or resource reallocation resulting from excessively high melatonin doses.

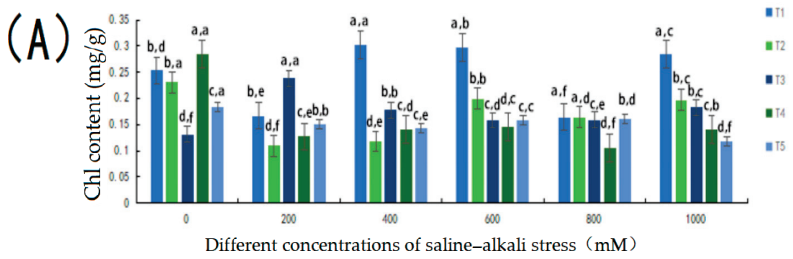


Figure 7. *Cont*.

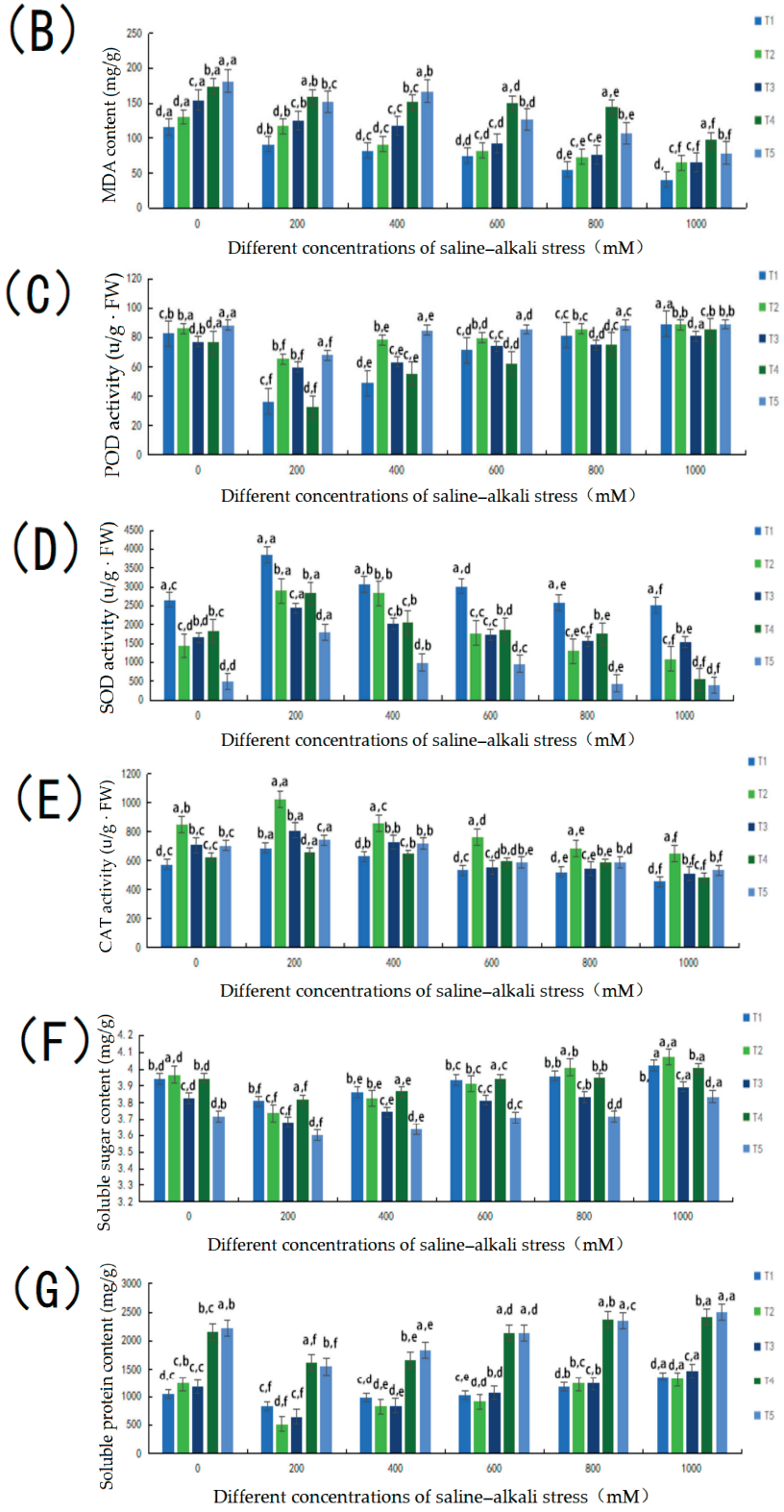


Figure 7. Effects of different concentrations of melatonin pretreatment on physiological characteristics of *Populus davidiana* × *P. bolleana* 'Baicheng Shanxinyang No. 1'. (**A**) chlorophyll content (**B**) malondialdehyde content (**C**) peroxidase activity (**D**) superoxide dismutase activity (**E**) catalase activity (**F**) soluble sugar content. (**G**) soluble protein content. T1—10 days, T2—14 days, T3—18 days, T4—22 days, T5—26 days. All data are presented as mean ± standard error (±SE), error bars represent standard errors (n = 6, with six biological replicates set for each treatment). For two-way ANOVA, the letters on the left represent the detection phase ($p < 0.05$), and the letters on the right represent the experimental concentrations ($p < 0.05$), according to the Duncan test.

3.3. Effect of Melatonin Post-Treatment on Saline–Alkali Stressed Poplar Plant

Following exposure to 120 mM mixed saline–alkali stress, poplar seedlings were treated with melatonin at concentrations of 0, 200, 400, 600, 800, and 1000 μM, and morphological and physiological parameters were assessed. Phenotypic analyses revealed pronounced stress-induced reductions in leaf number and leaf area (Figures 8 and 9), indicative of growth inhibition. Melatonin treatment counteracted these effects in a dose-dependent manner. Seedlings treated with 400–1000 μM melatonin showed significant increases in leaf number and expanded leaf area compared to untreated controls, with consistent stress-mitigating effects across this concentration range. Interestingly, 200 μM melatonin reduced leaf number relative to controls despite promoting an increase in leaf area, highlighting a concentration-dependent variation in morphological responses.

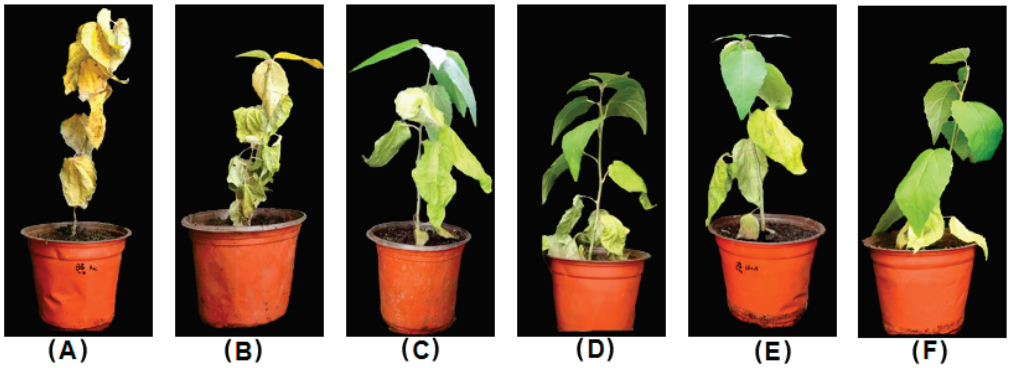


Figure 8. Effects of different concentrations of melatonin on the morphology of *Populus davidiana* × *P. bolleana* 'Baicheng Shanxinyang No. 1' under saline–alkali stress. (**A**–**F**) represent 0, 200, 400, 600, 800 and 1000 μM melatonin treatment, respectively.

Notably, Figure 10 illustrates the temporal variations in antioxidant enzyme activities (SOD, CAT, and POD) across experimental groups under different melatonin treatments. Over the treatment period, SOD and CAT activities exhibited a progressive decline in all groups. However, melatonin application at 200 μM significantly attenuated this reduction, with SOD and CAT levels remaining markedly higher than those in the untreated control group. Specifically, SOD activity peaked during the T1 phase (10 days), while CAT activity reached its maximum value of 1034.18 U/g in the T2 phase (14 days) under the 200 μM treatment (Figure 10C,E). In contrast to SOD and CAT, peroxidase (POD) in the 200 μM melatonin group displayed comparatively lower POD levels than other melatonin-treated groups. Meanwhile, higher melatonin concentrations (600–1000 μM) showed no statistically significant differences in POD activity relative to the control group (Figure 10D).

We also analyzed temporal changes in MDA and chlorophyll content across experimental groups, as shown in Figure 10A,B. MDA levels, a biomarker of oxidative lipid damage, exhibited a biphasic trend in all groups, initially rising before declining post-treatment. Notably, the 1000 μM melatonin group demonstrated the most pronounced stress-alleviating effect, with MDA accumulation reduced to the lowest observed levels at 200 μM. In parallel, chlorophyll content exhibited a distinct dose-dependent pattern. Under 200 μM melatonin treatment, chlorophyll concentrations reached their minimum values; however, a progressive recovery was noted at higher doses (400–1000 μM). This recovery was particularly evident during the T1 phase (10 days), where chlorophyll levels rebounded significantly.

Furthermore, we analyzed osmotic regulators; Figure 10F,G illustrates the temporal dynamics of osmotic regulator content (soluble sugars and proteins) across experimental groups exposed to varying concentrations of melatonin. Soluble sugar levels reached their lowest point on day 25 across all melatonin-treated groups, with the 200 μM group record-

https://doi.org/10.3390/f17030373

ing the minimum value (3.61 mg g^{-1}). Similarly, under the 200 μM melatonin treatment, soluble protein content dropped to minimal levels of 821.5 μg g^{-1} and 658.2 μg g^{-1} on days 14 and 18, respectively. Importantly, melatonin concentration had a dose-dependent effect on osmotic regulator accumulation. The 200 μM and 400 μM groups consistently showed significantly lower average soluble sugar and slightly reduced protein levels compared to the control group. Conversely, higher melatonin doses (800–1000 μM) resulted in moderately increased osmotic regulator content relative to the control, although these differences were less obvious.

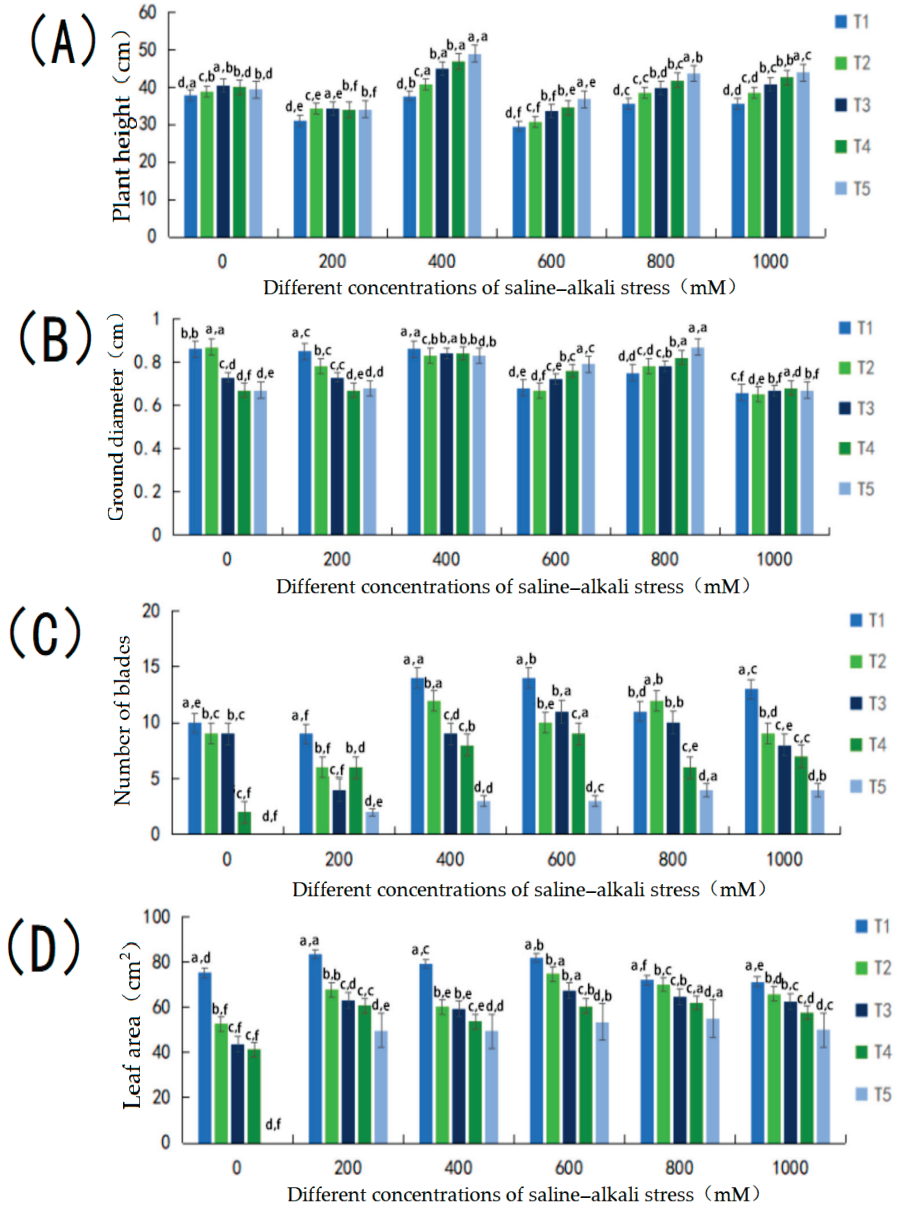


Figure 9. Effects of different concentrations of melatonin on the growth characteristics of *Populus davidiana* × *P. bolleana* 'Baicheng Shanxinyang No. 1' after salt and alkali stress. (**A**). plant height (**B**). ground diameter (**C**). number of leaves (**D**). leaf area. T1—11 days, T2—15 days, T3—19 days, T4—23 days, T5—27 days. All data are presented as mean ± standard error (±SE), error bars represent standard errors (n = 6, with six biological replicates set for each treatment). For two-way ANOVA, the letters on the left represent the detection phase ($p < 0.05$), and the letters on the right represent the experimental concentrations ($p < 0.05$), according to the Duncan test.

https://doi.org/10.3390/f17030373

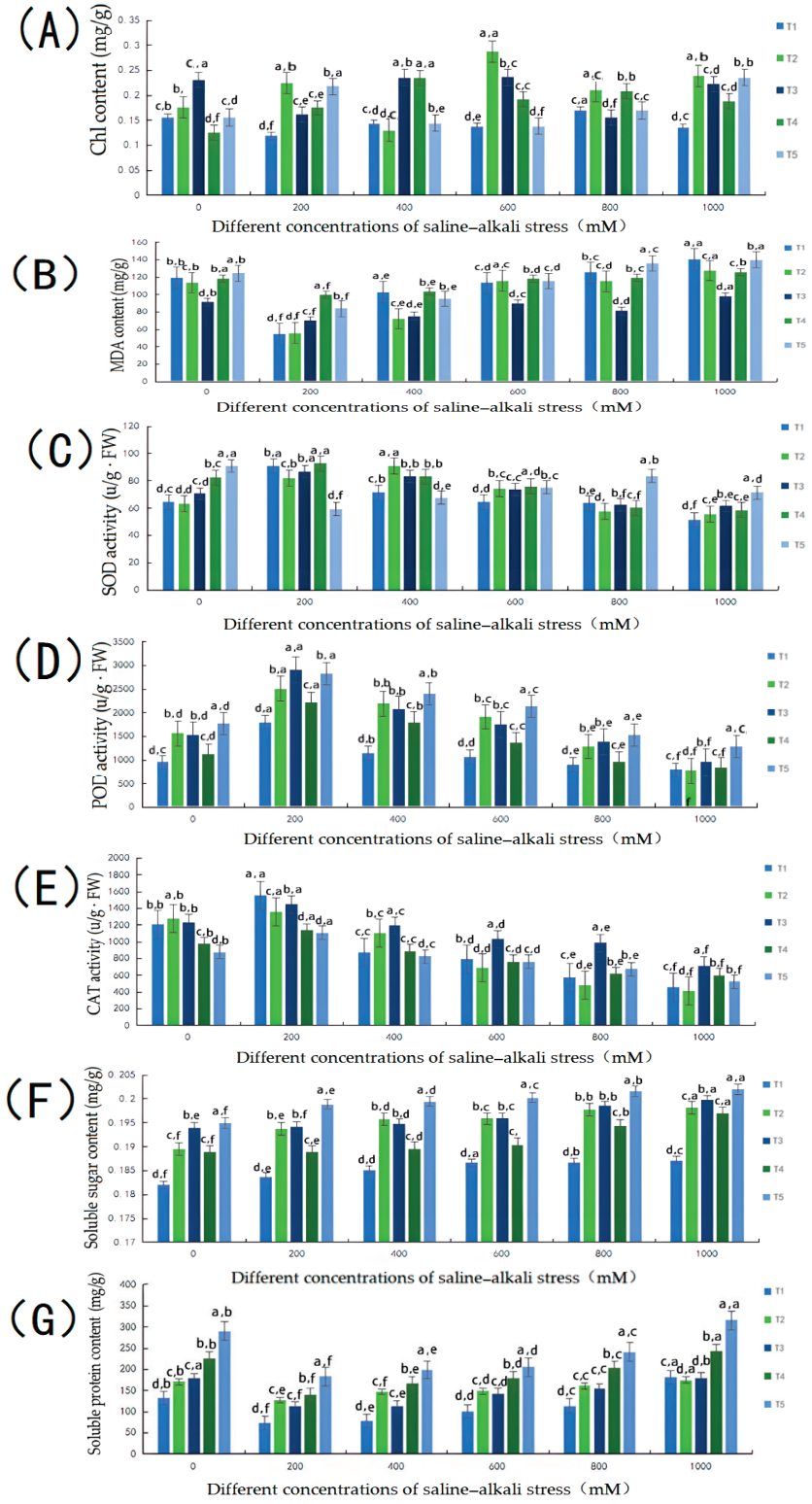


Figure 10. Effects of different concentrations of melatonin treatment on physiological characteristics of *Populus davidiana* × *P. bolleana* 'Baicheng Shanxinyang No. 1' after salt and alkali stress (**A**). chlorophyll content; (**B**). malondialdehyde content; (**C**). peroxidase activity; (**D**). superoxide dismutase activity; (**E**). catalase activity; (**F**). soluble sugar content; (**G**). soluble protein content. T1—11 days, T2—15 days, T3—19 days, T4—23 days, T5—27 days. All data are presented as mean ± standard error (±SE), error bars represent standard errors (n = 6, with six biological replicates set for each treatment). For two-way ANOVA, the letters on the left represent the detection phase ($p < 0.05$), and the letters on the right represent the experimental concentrations ($p < 0.05$), according to the Duncan test.

https://doi.org/10.3390/f17030373

4. Discussion

4.1. Background, Purpose and Significance of the Study

Among numerous abiotic stresses, salt–alkali stress is one of the most common environmental factors restricting plant growth and development. Long-term exposure to salt–alkali stress can adversely affect plant physiological functions. Melatonin is a multifunctional signaling molecule with the dual capacity to regulate growth dynamics and enhance resilience to abiotic stress [19].

This study systematically investigates the role of melatonin in alleviating salt–alkali stress in poplar (*Populus* spp.), with a focus on its regulatory effects on antioxidant enzyme activity and soluble metabolite profiles. To assess melatonin's stress-mitigating potential, a two-phase experimental design was employed: (1) an initial screening of salt–alkali stress intensity using a range of concentrations (0, 40, 80, 120, 160 mM), and (2) the subsequent application of melatonin at varying doses (0, 200, 400, 600, 800, 1000 μM) under both pre- and post-treatment schedules. The initial stress assessment identified 120 mM as the threshold concentration causing significant physiological disruption (Figure 4), which was subsequently adopted as the baseline stress condition, consistent with previous studies [17]. This concentration was subsequently applied to assess melatonin's efficacy in alleviating stress when administered either before or after exposure to stress. The dual experimental approach comparing stress-only conditions with melatonin-augmented interventions provides a comprehensive understanding of how melatonin influences stress adaptation in poplar.

4.2. Regulation of Melatonin on Antioxidant Enzyme Activity in Poplar

Saline–alkali stress primarily damages plants by disrupting cell membrane integrity and promoting reactive oxygen species (ROS) accumulation. Plants mitigate these effects through antioxidant enzymes such as SOD, CAT, and POD. In this study, melatonin pretreatment enhanced salt–alkali tolerance in poplar seedlings by modulating antioxidant enzyme activity. Under stress, SOD and CAT activities increased (Figure 4D,F) and were further elevated following melatonin application.

Enzyme responses showed a concentration-dependent biphasic pattern. The activities of SOD and CAT peaked at 200 μM melatonin (Figure 7D,E), reflecting enhanced ROS scavenging and a higher upregulation of antioxidant defenses. At higher concentrations ($\geq$400 μM), osmotic imbalance and ROS rebound dominated, and enzyme upregulation was insufficient to prevent membrane and metabolic damage, leading to reduced activity. POD activity initially decreased at 200 μM and rebounded at higher concentrations (Figure 7C), highlighting its complex role in stress signaling. These findings align with previous studies demonstrating that exogenous melatonin can enhance SOD and CAT activity in stressed poplar and apple plants, reducing oxidative damage and stabilizing cell membranes [17,18]. Notably, while post-treatment melatonin slightly increased CAT and POD activities, SOD activity remained unchanged at lower doses, and all enzymes declined at higher concentrations, emphasizing the critical role of dosage optimization. Similarly, managing melatonin as a pretreatment notably improves the salinity tolerance of poplar seedlings. This enhancement is achieved through efficiently scavenging of ROS and improvement of cellular membrane stability, thereby effectively reducing oxidative damage caused by salt [17]. Interestingly, a recent study on the transcriptome and metabolome shown of poplar seedlings has demonstrated that melatonin affects genes and metabolites associated with stress tolerance, with findings indicating that lower concentrations (100 μM) are supported by recent multi-omics studies [16,20]. Furthermore, prior research has shown that melatonin treatment significantly enhances the salt and drought tolerance of rice plants. This effect is realized by strengthening antioxidant defense mechanisms and

https://doi.org/10.3390/f17030373

upregulating stress-responsive genes, including *OsSOS*, *OsNHX*, *OsHSF*, and *OsDREB*, in rice [21]. Notably, we strongly suggest prioritizing the identification of regulatory genes underlying stress response pathways in poplar plants subjected to abiotic stressors. Similarly, our results align with earlier research indicating that low levels of exogenous melatonin can significantly enhance antioxidant enzyme activity in *Triticum aestivum* and *Pennisetum glaucum* when exposed to salt or drought stress [19,22]. These findings collectively highlight melatonin's potential as a priming agent to enhance stress tolerance, though its concentration-specific effects require further mechanistic investigation.

4.3. Effects of Melatonin on Morphological Indexes of Poplar

Melatonin pretreatment induced distinct morphological responses in poplar seedlings exposed to salt–alkali stress. Plants treated with 400 μM melatonin exhibited significant increases in leaf number and expanded leaf area compared to untreated controls, demonstrating consistent stress-mitigating effects at this concentration (Figure 2C,D). Interestingly, pretreatment with 200 μM melatonin resulted in a reduction in leaf number relative to controls, despite an increase in leaf area, indicating a dose-dependent variation in physiological responses. Furthermore, recent studies have reported that low concentrations of melatonin pretreatment (100 μM) can promote plant growth and alleviate the adverse effects of saline–alkali stress in tomato plants [23]. Furthermore, an early study on cotton (*Gossypium hirsutum*) demonstrated that the combined stress of salt and drought results in a significant reduction in plant growth and chlorophyll content [24].

In contrast, the post-stress application of melatonin produced distinct effects. Under salt–alkali stress, leaf number increased significantly compared to controls exposed only to stress, with the greatest alleviation observed at 400 μM across different growth stages. Higher concentrations, such as 1000 μM, were less effective. Notably, melatonin pretreatment did not significantly affect stem diameter, plant height, or overall leaf area, although subtle similarities between pre- and post-treatment responses were observed. Seedlings exposed to saline–alkali stress showed increases in plant height, stem diameter, leaf number, and leaf area, suggesting that higher melatonin doses may be required post-stress to fully mitigate damage, as stress conditions elevate physiological demands.

These findings highlight the nuanced role of melatonin dosage and timing in modulating morphological adaptations. Optimal stress alleviation was achieved at intermediate concentrations (400 μM), whereas excessive doses reduced beneficial effects. Overall, the results indicate that melatonin's effectiveness in enhancing salt–alkali tolerance depends on balancing its regulatory influence on growth with its capacity to counteract stress-induced oxidative and ionic imbalances.

4.4. Introduction to Research and Discussion

This study revealed the dose-dependent effects of melatonin on osmoregulation in poplar seedlings under salt–alkali stress. Lower melatonin concentrations (200 μM) suppressed the accumulation of soluble sugars and proteins during pretreatment, whereas higher concentrations (≥400 μM) significantly enhanced their production, highlighting melatonin's dual role as both a signaling molecule and a stress modulator in osmoregulation. Notably, the 200 μM pretreatment emerged as the optimal dose for improving stress resilience despite its inhibitory effect on osmolyte levels. A similar pattern was observed following salt–alkali stress: seedlings treated with 200 μM or 400 μM melatonin exhibited consistently lower soluble sugar levels and slightly reduced protein content compared to untreated controls. These findings are consistent with previous work by Song et al. (2022) [17], which demonstrated that low concentrations of exogenous melatonin can significantly influence osmoregulatory activity in plants.

https://doi.org/10.3390/f17030373

Saline–alkaline stress triggers initial root-derived stress signals that disrupt aboveground plant growth by degrading photosynthetic pigments, accelerating leaf senescence, and reducing photosynthetic capacity. Exogenous melatonin application mitigates these effects by slowing chlorophyll decline and preserving membrane integrity in poplar plants [19]. In this study, we confirmed that melatonin pretreatment significantly reduced MDA levels, a marker of oxidative membrane damage, with the lowest MDA observed at 200 μM. A recent study has demonstrated that pretreatment with melatonin reduces MDA content in rice plants under salt stress [25]. Conversely, post-stress melatonin supplementation showed concentration-dependent efficacy: MDA levels decreased progressively with higher doses, with the 1000 μM treatment group showing the most significant alleviation of oxidative stress. In parallel, pretreatment with melatonin did not statistically alter chlorophyll levels; however, post-treatment application under stress revealed a dose-dependent recovery. At 200 μM, chlorophyll concentrations dropped to minimal levels, yet higher doses (400–1000 μM) induced progressive recovery, particularly during the T2 phase (14 days), where chlorophyll rebounded significantly. This suggests that post-stress conditions require higher melatonin concentrations to counteract severe oxidative damage as stress intensifies physiological demands. Notably, melatonin's ability to stabilize membranes and scavenge free radicals aligns with previous findings [16,17,23], where lower concentrations (100 μM) alleviated stress by reducing cellular damage. Our results highlight melatonin's dual role in osmoregulation and antioxidant defense, demonstrating optimal efficacy at 400–1000 μM post-stress. This concentration enhances the synthesis of photosynthetic pigments and enhances resilience by counteracting chlorophyll degradation and oxidative damage [26]. These findings emphasize the significance of dosage and timing in melatonin's protective function, indicating its potential as a targeted intervention for enhancing plant tolerance under saline–alkaline stress.

5. Conclusions

Overall, we evaluated two different melatonin application strategies: pretreatment before exposure to saline–alkali conditions and post-treatment after planting in saline–alkali soil. The aim was to identify an effective growth approach for poplar trees in saline–alkali environments and reduce the challenges associated with soil amelioration. Our findings demonstrate that exogenous melatonin is a promising strategy for enhancing salt–alkali stress tolerance in poplar seedlings. It notably improves plant growth, antioxidant enzyme activity (SOD, CAT), and osmoregulatory capacity, collectively enhancing ROS scavenging and restoring the growth and development of salt–alkali-stressed seedlings by strengthening physiological and morphological resistance. While pretreatment offers a cost-effective approach to bolster stress resistance, post-treatment supplementation also alleviates stress effects, further enhancing tolerance and reducing potential agricultural losses. These dual-phase benefits underscore melatonin's versatility as a protective agent, providing both preventive and reparative mechanisms to mitigate stress-induced damage, as illustrated in the proposed model (Figure 11).

https://doi.org/10.3390/f17030373

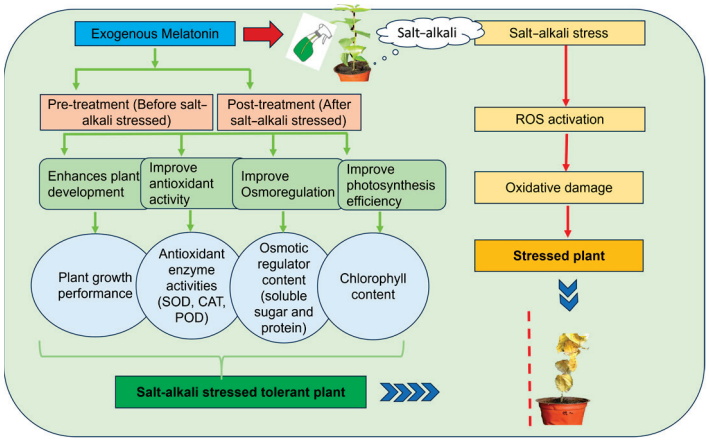


Figure 11. Proposed model for the response of *Populus davidiana* × *P. bolleana* 'Baicheng Shanxinyang No. 1' to melatonin under salt–alkali stress.

Author Contributions: Conceptualization, J.N. and X.Z.; methodology, J.N. and X.Z.; validation, W.H. and X.Z.; formal analysis, J.N., X.Z., W.H., T.M., X.H., Z.L., X.L. and J.S.; data curation, J.N. and X.Z.; writing original draft preparation, J.N., X.H., X.L. and J.S.; writing review and editing, J.N., W.H., T.M., Z.L., X.L. and J.S.; visualization, X.Z.; project administration, X.Z.; funding acquisition X.Z. All authors have read and agreed to the published version of the manuscript.

Funding: We are grateful to the researchers who are contributing to this field. This paper was funded by the Scientific Research Project of the Education Department of Jilin Province (JJKH20250597KJ).

Data Availability Statement: Research data are available upon request from the corresponding author.

Conflicts of Interest: The authors declare no conflicts of interest.

Appendix A

Name	Catalog Number	Principle
Superoxide dismutase (SOD) kits	AKAO001M-50S	The reaction system of xanthine and xanthine oxidase produces superoxide anion (O_2^-), which reduces nitroblue tetrazolium to form formazan. The product has a characteristic absorption peak at 560 nm. SOD activity is characterized by changes in absorbance.
Peroxidase (POD) kits	AKAO005M	Peroxidase catalyzes the oxidation of guaiacol by H_2O_2 to produce brown 4-hydroxyphenol. The product has a characteristic absorption peak at 470 nm. POD activity is characterized by changes in absorbance.
Catalase (CAT) kits	AKAO003-2M	H_2O_2 oxidizes MoO_4^{2-} to MoO_5^{2-}, which accepts electrons from hydroxide ions, dehydrates and condenses to form a stable yellow complex $(H_2MoO_4 \cdot \times H_2O)_n$. The product has a characteristic absorption peak at 405 nm. CAT activity is characterized by changes in absorbance.
Malondialdehyde (MDA) kits	AKFA013M	Under acidic and high-temperature conditions, malondialdehyde reacts with thiobarbituric acid (TBA) to form a red product. MDA content is quantified by absorbance values at 532 nm, 450 nm, and 600 nm.

Name	Catalog Number	Principle
Proline (Pro) kits	AKAM003M	Proline is extracted by sulfosalicylic acid and reacts with acidic ninhydrin to form a red substance. After extraction with toluene, proline content is quantified by absorbance at 520 nm.
Soluble sugar kits	AKPL008M	Under sulfuric acid, sugars dehydrate to form furfural or hydroxymethylfurfural, which condenses with anthrone to form a blue-green derivative. The product has a characteristic absorption peak at 620 nm. Soluble sugar content is quantified by changes in absorbance.
Soluble protein kits	AKPR001M	Proteins form a purple complex with biuret reagent in a strong alkaline solution. The product has a characteristic absorption peak at 540 nm. Soluble protein content is quantified by changes in absorbance.
Chlorophyll kits	AKPL003M	Chlorophyll a and chlorophyll b have characteristic absorption peaks at 663 nm and 645 nm, respectively. Contents of chlorophyll a, chlorophyll b, and total chlorophyll are calculated using empirical formulas.

References

1. Tarolli, P.; Luo, J.; Park, E.; Barcaccia, G.; Masin, R. Soil salinization in agriculture: Mitigation and adaptation strategies combining nature-based solutions and bioengineering. *iScience* **2024**, *27*, 108830. [CrossRef]
2. Xu, Z.; Wang, F.; Ma, Y.; Dang, H.; Hu, X. Transcription Factor SlAREB1 Is Involved in the Antioxidant Regulation under Saline-Alkaline Stress in Tomato. *Antioxidants* **2022**, *11*, 1673. [CrossRef]
3. Hongna, C.; Junmei, S.; Leyuan, T.; Xiaori, H.; Guolin, L.; Xianguo, C. Exogenous Spermidine Priming Mitigates the Osmotic Damage in Germinating Seeds of *Leymus chinensis* Under Salt-Alkali Stress. *Front. Plant Sci.* **2020**, *12*, 701538. [CrossRef]
4. Fan, Y.; Shen, W.-Y.; Vanessa, P.; Cheng, F.-Q. Synergistic effect of Si and K in improving the growth, ion distribution and partitioning of *Lolium perenne* L. under saline-alkali stress. *J. Integr. Agric.* **2021**, *20*, 1660–1673. [CrossRef]
5. Wang, Y.; Wang, J.; Guo, D.; Zhang, H.; Che, Y.; Li, Y.; Tian, B.; Wang, Z.; Sun, G.; Zhang, H. Physiological and comparative transcriptome analysis of leaf response and physiological adaption to saline alkali stress across pH values in alfalfa (*Medicago sativa*). *Plant Physiol. Biochem.* **2021**, *167*, 140–152. [CrossRef] [PubMed]
6. Zhang, H.; Yu, F.; Xie, P.; Sun, S.; Qiao, X.; Tang, S.; Chen, C.; Yang, S.; Mei, C.; Yang, D. A $G\gamma$ protein regulates alkaline sensitivity in crops. *Science* **2023**, *379*, eade8416. [CrossRef] [PubMed]
7. Zhao, C.; Zhang, H.; Song, C.; Zhu, J.K.; Shabala, S. Mechanisms of Plant Responses and Adaptation to Soil Salinity. *Innovation* **2020**, *1*, 100017. [CrossRef] [PubMed]
8. Wei, T.-J.; Li, G.; Cui, Y.-R.; Xie, J.; Gao, X.-A.; Teng, X.; Zhao, X.-Y.; Guan, F.-C.; Liang, Z.-W. Variation Characteristics of Root Traits of Different Alfalfa Cultivars under Saline-Alkaline Stress and their Relationship with Soil Environmental Factors. *Phyton* **2024**, *93*, 29–43. [CrossRef]
9. Khan, T.A.; Saleem, M.; Fariduddin, Q. Recent advances and mechanistic insights on melatonin-mediated salt stress signaling in plants. *Plant Physiol. Biochem.* **2022**, *188*, 97–107. [CrossRef]
10. Harfouche, A.; Meilan, R.; Altman, A. Molecular and physiological responses to abiotic stress in forest trees and their relevance to tree improvement. *Tree Physiol.* **2014**, *34*, 1181–1198. [CrossRef]
11. Qi, W.; Wang, F.; Ma, L.; Qi, Z.; Liu, S.; Chen, C.; Wu, J.; Wang, P.; Yang, C.; Wu, Y. Physiological and biochemical mechanisms and cytology of cold tolerance in *Brassica napus*. *Front. Plant Sci.* **2020**, *11*, 1241. [CrossRef]
12. Zhao, L.; Yang, T.; Xing, C.; Dong, H.; Qi, K.; Gao, J.; Tao, S.; Wu, J.; Wu, J.; Zhang, S.; et al. The β-amylase PbrBAM3 from pear (*Pyrus betulaefolia*) regulates soluble sugar accumulation and ROS homeostasis in response to cold stress. *Plant Sci.* **2019**, *287*, 110184. [CrossRef]
13. Müller, N.A.; Kersten, B.; Leite Montalvão, A.P.; Mähler, N.; Bernhardsson, C.; Bräutigam, K.; Carracedo Lorenzo, Z.; Hoenicka, H.; Kumar, V.; Mader, M.; et al. A single gene underlies the dynamic evolution of poplar sex determination. *Nat. Plants* **2020**, *6*, 630–637. [CrossRef] [PubMed]
14. Guo, Y.; Wang, S.; Yu, K.; Wang, H.L.; Xu, H.; Song, C.; Zhao, Y.; Wen, J.; Fu, C.; Li, Y.; et al. Manipulating microRNA miR408 enhances both biomass yield and saccharification efficiency in poplar. *Nat Commun.* **2023**, *14*, 4285. [CrossRef]

15. Mei, X.; Dai, T.; Shen, Y. Adaptive strategy of *Nitraria sibirica* to transient salt, alkali and osmotic stresses via the alteration of Na+/K+ fluxes around root tips. *J. For. Res.* **2023**, *34*, 425–432. [CrossRef]
16. Li, Y.; Song, R.; Cai, K.; Pang, Z.; Qian, C.; Xu, S.; Zhang, Y.; Bai, H.; Zhan, W.; Xiao, R. Exploring the molecular mechanisms of melatonin-induced tolerance to salt-alkali stress in *Populus cathayana* × *canadansis* 'Xinlin 1'. *Ind. Crops Prod.* **2024**, *215*, 118638. [CrossRef]
17. Song, R.; Ritonga, F.N.; Yu, H.; Ding, C.; Zhao, X. Effects of exogenous antioxidant melatonin on physiological and biochemical characteristics of *Populus cathayana* × *canadansis* 'xin lin 1'under salt and alkaline stress. *Forests* **2022**, *13*, 1283. [CrossRef]
18. Zhang, Z.; Liu, L.; Li, H.; Zhang, S.; Fu, X.; Zhai, X.; Yang, N.; Shen, J.; Li, R.; Li, D. Exogenous melatonin promotes the salt tolerance by removing active oxygen and maintaining ion balance in wheat (*Triticum aestivum* L.). *Front. Plant Sci.* **2022**, *12*, 787062. [CrossRef]
19. Mc Carthy, D.J.; Campbell, K.R.; Lun, A.T.; Wills, Q.E. Scater: Pre-processing quality control, normalization and visualization of single-cell RNA-seq data in R. *Bioinformatics* **2017**, *33*, 1179–1186. [CrossRef]
20. Xian, X.; Zhang, Z.; Wang, S.; Cheng, J.; Gao, Y.; Ma, N.; Li, C.; Wang, Y. Exogenous melatonin strengthens saline-alkali stress tolerance in apple rootstock M9-T337 seedlings by initiating a variety of physiological and biochemical pathways. *Chem. Biol. Technol. Agric.* **2024**, *11*, 58. [CrossRef]
21. Duan, W.; Lu, B.; Liu, L.; Meng, Y.; Ma, X.; Li, J.; Zhang, K.; Sun, H.; Zhang, Y.; Dong, H. Effects of exogenous melatonin on root physiology, transcriptome and metabolome of cotton seedlings under salt stress. *Int. J. Mol. Sci.* **2022**, *23*, 9456. [CrossRef]
22. Khan, Z.; Jan, R.; Asif, S.; Farooq, M.; Jang, Y.-H.; Kim, E.-G.; Kim, N.; Kim, K.-M. Exogenous melatonin induces salt and drought stress tolerance in rice by promoting plant growth and defense system. *Sci. Rep.* **2024**, *14*, 1214. [CrossRef] [PubMed]
23. Awan, S.A.; Khan, I.; Rizwan, M.; Brestic, M.; Wang, X.; Zhang, X.; Huang, L. Exogenous melatonin regulates the expression pattern of antioxidant-responsive genes, antioxidant enzyme activities, and physio-chemical traits in pearl millet under drought stress. *J. Plant Growth Regul.* **2024**, *43*, 1061–1075. [CrossRef]
24. Dou, J.; Tang, Z.; Yu, J.; Wang, G.; An, W.; Zhang, Y.; Yang, Q. Effects of exogenous melatonin on the growth and photosynthetic characteristics of tomato seedlings under saline-alkali stress. *Sci. Rep.* **2025**, *15*, 5172. [CrossRef] [PubMed]
25. Ibrahim, W.; Qiu, C.W.; Zhang, C.; Cao, F.; Shuijin, Z.; Wu, F. Comparative physiological analysis in the tolerance to salinity and drought individual and combination in two cotton genotypes with contrasting salt tolerance. *Physiol. Plant.* **2019**, *165*, 155–168. [CrossRef]
26. Ubaidillah, M.; Farooq, M.; Kim, K.-M. Enhancing salt tolerance in rice genotypes through exogenous melatonin application by modulating growth patterns and antistress agents. *Sci. Rep.* **2024**, *14*, 25217. [CrossRef]

Disclaimer/Publisher's Note: The statements, opinions and data contained in all publications are solely those of the individual author(s) and contributor(s) and not of MDPI and/or the editor(s). MDPI and/or the editor(s) disclaim responsibility for any injury to people or property resulting from any ideas, methods, instructions or products referred to in the content.

forests

MDPI

Article

Linking Leaf Angle to Physiological Responses for Drought Stress Detection: Case Study on *Quercus acutissima* Carruth. in Forest Nursery

Ukhan Jeong [1,2], Dohee Kim [2], Sohyun Kim [2], Jiyeon Park [2], Seung Hyun Han [1,*] and Eun Ju Cheong [2,*]

[1] Forest Technology and Management Research Center, National Institute of Forest Science, Pocheon 11186, Republic of Korea; uki7291@korea.kr
[2] College of Forest and Environmental Science, Kangwon National University, Chuncheon 24341, Republic of Korea; dohee373@gmail.com (D.K.); rlathgus0613@naver.com (S.K.); jiyoun0401@naver.com (J.P.)
* Correspondence: foresthsh@korea.kr (S.H.H.); ejcheong@kangwon.ac.kr (E.J.C.)

Abstract

Due to climate change, seedling damage caused by drought stress is expected to increase in both afforestation sites and nurseries. Therefore, to ensure stable seedling production under high-temperature conditions and to cultivate seedlings with enhanced drought tolerance through hardening treatments, the development of an effective irrigation system is required. Conventional physiological methods for non-destructive drought detection, such as chlorophyll fluorescence and leaf temperature measurements, require expensive and manual operation, thereby limiting their real-time applicability in forest nurseries. This study evaluated the applicability of using image-based leaf angle measurements for drought stress detection in *Quercus acutissima* Carruth. seedlings. One-year-old seedlings were grown under two water regimes—well-watered (CT: control) and unwatered (DT: drought)—through Day 8. Statistical analyses (RMANOVA) revealed that changes in the leaf angle parameter PMD–MD (the difference between the previous and current measurement days) showed treatment effects similar to those of the physiological responses ΦNO (quantum yield of non-regulated energy dissipation) and qL (fraction of open PSII reaction centers) to drought on Day 6. Leaf angle reflected drought stress but did not precede physiological changes, indicating its role as a complementary rather than an early indicator. Multiple regression models identified AT (air temperature), SM (soil moisture), Fm′ (maximum fluorescence in the light-adapted state), and VPD (vapor pressure deficit) as the main factors influencing leaf angle variation. Although leaf angle was affected by combined environmental stresses such as high temperature, it was less sensitive to heat stress than physiological responses based on RMANOVA results. These results indicate the potential of image-based leaf angle measurements for drought stress detection. To establish plant-based smart irrigation systems, future studies should validate and refine this approach using larger datasets.

Keywords: *Quercus acutissima*; forest nursery; tree physiology; drought stress; seedling hardening; image-based leaf angle; smart irrigation system

1. Introduction

Recent climate change-driven increases in temperature and the frequency of localized heavy rainfall have intensified environmental stress on reforestation species, raising the

potential for severe damage [1–4]. In particular, drought stress can have a critical impact on the survival of young seedlings planted in open-field conditions [5,6]. Such stress leads to physiological impairments, including reduced water-use efficiency, stomatal closure, and suppression of photosynthesis, and in extreme cases, can result in mortality [7]. However, in sites such as high-altitude or sloped terrains, the installation and maintenance of irrigation systems is challenging, and the ability to respond promptly to weather fluctuations is limited. Therefore, the establishment of seedling production systems that enhance stress adaptability is required to ensure stable rooting and growth.

Conventional forest nursery systems have limited capacity to cope with climate change, and even within the same species, survival rates can vary substantially depending on the planting site conditions. To overcome these challenges, precision nursery technologies that induce stress tolerance from the early growth stage or preselect seedlings with proven resilience are required. In particular, hardening treatments—controlled drought exposure during nursery production—have been reported as an effective strategy for improving drought tolerance [8–11]. Such treatments can be implemented more efficiently using ICT-based smart nursery systems capable of environmental monitoring and automated irrigation control [12–14]. However, compared to agricultural crops, forest seedlings have different production cycles and economic scales, making direct application of existing smart-farm technologies costly and technically challenging. Consequently, foundational research is needed to guide the development of smart nursery systems tailored to reforestation seedlings.

Non-destructive physiological measurement methods, such as chlorophyll fluorescence and leaf temperature, can detect drought stress earlier than visible symptoms like leaf browning or wilting [15,16]. However, these methods require expensive equipment and manual operation, limiting their real-time applicability in conventional nursery systems. Determining the optimal irrigation timing before drought stress reaches a physiological limit is crucial for effective management, and monitoring changes in leaf angle offers a promising approach. Leaf angle is known to be a physical adaptive strategy to environmental stress factors such as light, heat, and water availability [17]. Under drought stress, stomatal closure and reduced turgor pressure cause leaf wilting, which can be detected before irreversible damage occurs. However, continuous and precise manual measurement of leaf angle in nurseries is impractical.

Recent advances in image-based plant phenotyping have enabled automated monitoring of plant architecture and stress responses under controlled environments, including deep learning-based trait extraction, computer vision analysis of leaf structural characteristics, and high-throughput imaging for continuous monitoring of plant growth dynamics [18–20]. In particular, image-based monitoring of leaf angle has emerged as a low-cost, non-contact approach for assessing plant physiological status [21–25]. Leaf angle holds strong potential as an indirect indicator of drought-induced physiological and morphological changes in leaves. Previous studies conducted mainly on mature trees in ecological and physiological contexts have shown that leaf angle responds to changes in plant water status and canopy light-avoidance strategies [17,26–31]. However, applications to forest seedlings in nursery environments remain limited [32–34]. It is still unclear whether such drought-induced leaf angle responses are consistently expressed during early developmental stages, how closely image-derived leaf angle metrics correspond to conventional physiological indicators, and how early these changes can be detected before visible wilting occurs.

Because early detection and proactive irrigation management could substantially improve seedling survival and water-use efficiency, this study conducted a pilot experiment on one-year-old *Quercus acutissima* Carruth. seedlings to (1) quantify drought-induced changes in leaf angle derived from image analysis, and (2) evaluate the relationships

https://doi.org/10.3390/f17030348

between leaf angle and simultaneously measured physiological parameters, including their temporal sensitivity relative to conventional stress indicators. By integrating low-cost imaging with physiological measurements under controlled drought treatments, this work provides a proof-of-concept for incorporating leaf angle-based monitoring into smart nursery irrigation systems for reforestation seedlings.

2. Materials and Methods

2.1. Plant Materials

One-year-old *Q. acutissima* seedlings used in this study were produced in the greenhouse of the Forest Technology and Management Research Center (37°45′39″ N, 127°10′13″ E). In April 2024, seeds were sown in containers (top Ø6.4 cm × bottom Ø4.2 cm × height 14 cm, cell volume 320 mL, 24 cells per container) filled with growth medium composed of peat moss, perlite, and vermiculite at a 1:1:1 (*v*/*v*) ratio. Irrigation was applied daily at 20 L m^{-2} via sprinkler system. Fertilization was applied once per week using 1 g L^{-1} (1000 ppm) solution of MultiFeed 19 (19N:19P_2O_5:19K_2O; Haifa Chemicals, Haifa, Israel). From June until the start of the experiment, seedlings were transferred to the greenhouse of Kangwon National University, College of Forest and Environmental Sciences (37°52′00″ N, 127°44′51″ E) and acclimated under the same irrigation regime.

2.2. Experimental Conditions

Seedlings were randomly assigned to control (CT, n = 7) and drought treatment (DT, n = 6) groups while ensuring sufficient leaf numbers for parametric statistical analyses, and were positioned at 3 different orientations within the greenhouse so that each image frame contained 4–5 seedlings against a black background board. CT received 2.35 L of water per container, applied directly to the soil with a watering can between 11:00 AM and 12:00 PM daily. DT was applied by withholding irrigation starting on July 1 (Day 1). Air temperature (AT), air humidity (AH), and solar radiation (SR) in the greenhouse were recorded every 10 min using Juns OL sensors (PurumBio, Suwon, Korea). Soil temperature (ST) and soil moisture (SM) were measured by inserting temperature sensor (S-SMDM005, Onset, Bourne, MA, USA) and moisture sensor (S-TMB-M002, Onset, Bourne, MA, USA) into the growth medium. Data were collected at 30 min intervals using Hobo micro station (H21-USB, Onset, Bourne, MA, USA).

During the experiment, alternating sunny, cloudy, and rainy days resulted in considerable day-to-day variability in AH, AT, and SR values (Figure 1A). Among the measurement days, Day 4 was the only day with clear weather, recording the lowest AH (59.43%) and the highest AT (33.93 °C) and SR (220.39 W m^{-2}) during the experimental period. From BD (before drought) to Day 8, the drought treatment consistently maintained higher ST than the control (average 5.13 ± 2.23 °C) (Figure 1B). The SM of the control remained at 25.30 ± 1.32% from BD to Day 8, whereas the SM of the drought treatment continuously declined, reaching 2.19 ± 0.56% on Day 4 and converging to permanent wilting point thereafter.

https://doi.org/10.3390/f17030348

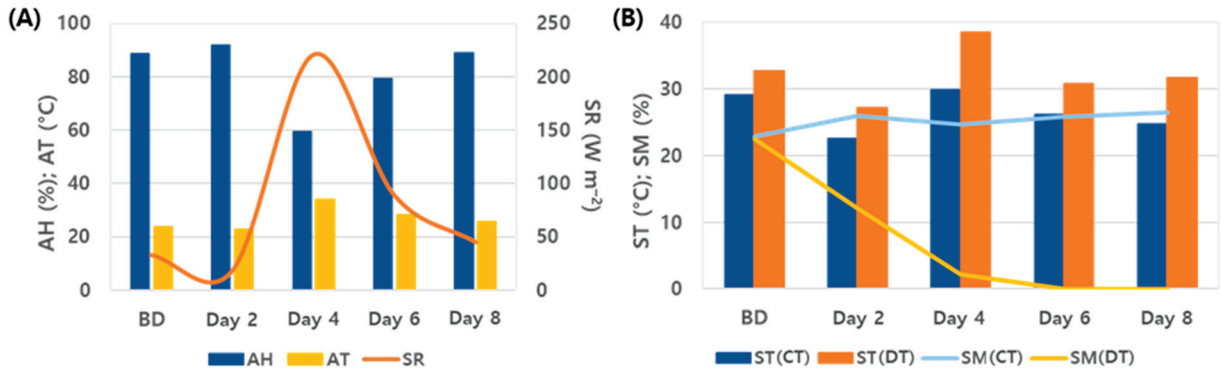


Figure 1. Overview of growth conditions during the experimental period. (**A**) Climatic conditions; (**B**) Soil conditions. AT: air temperature, AH: air humidity, SR: solar radiation, ST: soil temperature, SM: soil moisture, BD: before drought, CT: control, DT: drought.

2.3. Physiological Measurements

Prior to measurements, leaves (n = 37) from each treatment (CT and DT) that were measurable for leaf angle in the images were labeled. The labeled leaves were repeatedly measured by tracking the same leaves over time, ensuring consistency between physiological measurements and leaf angle assessments. The measured parameters included chlorophyll index (SPAD), chlorophyll fluorescence (Fm′: maximum fluorescence in light-adapted state; Fo′: minimum fluorescence in light-adapted state; Fv′/Fm′: maximum quantum yield of PSII in light-adapted state; ΦII: quantum yield of PSII; ΦNO: quantum yield of non-regulated energy dissipation; ΦNPQ: quantum yield of regulated energy dissipation; qL: fraction of open PSII reaction centers), vapor pressure deficit (VPD), and crop water stress index (CWSI). SPAD and chlorophyll fluorescence were measured with MultispeQ V2.0 device (PhotosynQ, East Lansing, MI, USA) between 12:00 PM and 6:00 PM. Leaf temperature data for VPD and CWSI calculations were collected using thermal camera (PI 160i, Optris, Berlin, Germany) positioned 2–3 m from the seedlings, with 10 min recordings taken daily (Figure 2A). The equations for calculating VPD and CWSI followed Gardner et al. [35], Stull [36], Grossiord et al. [37], and Zhou et al. [38] (Equations (1) and (2)).

$$VPD = 0.6108 \times exp\left(\frac{17.27Tl}{Tl + 237.3}\right) - (0.6108 \times exp(\frac{17.27Ta}{Ta + 237.3}) \times \frac{AH}{100}) \quad (1)$$

$$CWSI = \frac{(Tl - Ta) - (Tlw - Taw)}{(Tld - Tad) - (Tlw - Taw)} \quad (2)$$

Tl refers to leaf temperature, Ta to air temperature, Tlw to minimum leaf temperature, Tld to maximum leaf temperature, Taw to minimum air temperature, and Tad to maximum air temperature.

2.4. Leaf Angle Measurements

Leaf angle was measured using time-lapse camera (ATL200S, Afidus, New Taipei City, Taiwan) that captured RGB images (16:9 ratio) at 10 min intervals. To capture all labeled leaves within a single frame, images were taken from a height of 70 cm above the base of the target pot and 60 cm away from the seedlings. To minimize image distortion, all wide-angle, digital zoom, image stabilization, and auto-exposure optimization functions were disabled. RGB images were analyzed in ImageJ ver. 1.53k (NIH, Bethesda, MD, USA) to extract leaf angle data. Leaf angle was defined as the internal angle formed between horizontal reference line drawn from the petiole and line from the petiole to the leaf tip, measured using the angle tool in the software (Figure 2B). Leaves pointing upward were assigned angles between 0° and +90°, while downward-facing leaves were assigned between −90°

https://doi.org/10.3390/f17030348

and 0°. Collected leaf angle data were processed into leaf angle parameters according to Equations (3)–(5).

$$\text{leaf angle ranges divided into six intervals (STx): } -90° \leq \text{ST1} < -60°,\ -60° \leq \text{ST2} < -30°,\ -30° \leq \text{ST3} < 0°,\ 0° \leq \text{ST4} < +30°,\ +30° \leq \text{ST5} < +60°,\ +60° \leq \text{ST6} \leq +90° \quad (3)$$

$$\Delta\text{leaf angle (BD–MD): difference between measurements before drought and the current measurement day} \quad (4)$$

$$\Delta\text{leaf angle (PMD–MD): difference between the previous measurement day and the current measurement day} \quad (5)$$

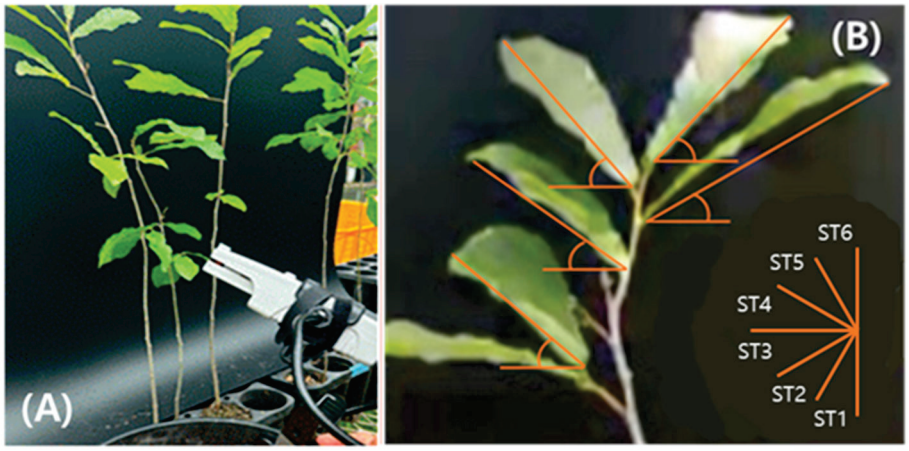


Figure 2. Physiological measurement and leaf angle monitoring for *Q. acutissima* seedlings. (**A**) Physiological measurement using MultispeQ; (**B**) RGB image-based leaf angle monitoring.

2.5. Statistical Analyses

Prior to statistical analysis, the environmental and leaf angle datasets were matched to the physiological data at 1 h intervals based on the timestamps recorded by the instruments. To assess the effects of DT on temporal and treatment-based variations in physiological parameters and leaf angle, two-way repeated measures analysis of variance (RMANOVA) was performed. Post hoc pairwise t-tests with Bonferroni correction ($p < 0.05$) were used. Stepwise multiple regression analysis was conducted to identify factors determining leaf angle variation, with leaf angle parameters as dependent variables and physiological parameters as independent variables (enter: $p < 0.05$, remove: $p > 0.10$). Multicollinearity among predictors was checked using tolerance and variance inflation factor (VIF) values. Principal component analysis (PCA) was performed to visualize variations in physiological and leaf angle characteristics across measurement days and to identify contributing factors. RMANOVA and regression analyses were conducted using SPSS ver. 26 (IBM, Armonk, NY, USA). PCA was performed in Python ver. 3.11 using the scikit-learn PCA module ver. 1.3.0, with StandardScaler applied to normalize all numerical data to account for differences in variable scales. Results were visualized as score plots for PC1 and PC2 using matplotlib ver. 3.7.2, and variable contributions were displayed as loading vectors.

3. Results

3.1. Physiological Responses

Physiological parameters showing an interaction effect were Fm′ ($p < 0.05$), ΦNO ($p < 0.01$), SPAD ($p < 0.01$), and CWSI ($p < 0.05$) (Table 1). Except for CWSI, all showed main effect for day ($p < 0.01$). The parameters that showed main effect for treatment were Fo′ ($p < 0.01$), Fm′ ($p < 0.001$), ΦNO ($p < 0.01$), qL ($p < 0.05$), and CWSI ($p < 0.01$).

Table 1. Results of two-way RMANOVA for physiology parameters.

Parameter		Sum of Square	df	Mean Square	F	*p*
Fo′	***D***	***9,039,198.58***	***2.46***	***3,677,270.36***	***190.34***	***<0.001***
	T	***2,169,069.76***	***1.00***	***2,169,069.76***	***11.849***	***<0.01***
	D × T	44,031.19	2.46	17,912.50	0.93	>0.05
Fm′	***D***	***208,508,197.18***	***2.16***	***96,431,192.15***	***137.57***	***<0.001***
	T	***30,413,395.13***	***1.00***	***30,413,395.13***	***15.17***	***<0.001***
	D × T	***5,333,267.68***	***2.16***	***2,466,537.85***	***3.52***	***<0.05***
Fv′/Fm′	***D***	***0.73***	***1.64***	***0.44***	***36.78***	***<0.001***
	T	0.02	1.00	0.02	1.79	>0.05
	D × T	0.06	1.64	0.04	3.14	>0.05
ΦII	***D***	***1.07***	***1.69***	***0.64***	***35.42***	***<0.001***
	T	<0.00	1.00	<0.00	<0.00	>0.05
	D × T	0.04	1.69	0.03	1.37	>0.05
ΦNO	***D***	***0.05***	***1.98***	***0.03***	***21.78***	***<0.001***
	T	***0.01***	***1.00***	***0.01***	***7.35***	***<0.01***
	D × T	***0.01***	***1.98***	***0.01***	***4.93***	***<0.01***
ΦNPQ	***D***	***1.60***	***1.62***	***0.99***	***38.34***	***<0.001***
	T	0.01	1.00	0.01	0.53	>0.05
	D × T	0.10	1.62	0.06	2.33	>0.05
qL	***D***	***0.19***	***2.24***	***0.09***	***6.14***	***<0.01***
	T	***0.08***	***1.00***	***0.08***	***4.84***	***<0.05***
	D × T	0.02	2.24	0.01	0.71	>0.05
SPAD	***D***	***200.06***	***2.05***	***97.49***	***21.1***	***<0.001***
	T	41.66	1.00	41.66	0.86	>0.05
	D × T	***66.37***	***2.05***	***32.34***	***7.00***	***<0.01***
VPD	***D***	***153.96***	***1.44***	***106.73***	***419.34***	***<0.001***
	T	0.50	1.00	0.5	3.00	>0.05
	D × T	1.29	1.44	0.89	3.51	>0.05
CWSI	D	0.73	1.27	0.57	2.8	>0.05
	T	***0.36***	***1***	***0.36***	***7.75***	***<0.01***
	D × T	***1.12***	***1.27***	***0.88***	***4.31***	***<0.05***

Two-way RMANOVA was conducted, followed by pairwise *t*-tests with Bonferroni correction for post hoc analysis ($p < 0.05$). Greenhouse–Geisser correction was applied for sphericity. Bold and italic indicate statistically significant effect. D: main effect for day, T: main effect for treatment, D × T: interaction effect between day and treatment, Fo′: minimum fluorescence in light-adapted state, Fm′: maximum fluorescence in light-adapted state, Fv′/Fm′: maximum quantum yield of PSII in light-adapted state, ΦII: quantum yield of PSII, ΦNO: quantum yield of non-regulated energy dissipation, ΦNPQ: quantum yield of regulated energy dissipation, qL: fraction of open PSII reaction centers, SPAD: chlorophyll index, VPD: vapor pressure deficit, CWSI: crop water stress index.

Overall, chlorophyll fluorescence such as decreases in Fv′/Fm′ (CT: 0.57 ± 0.13; DT: 0.58 ± 0.15) and increases in ΦNPQ (CT: 0.40 ± 0.18; DT: 0.38 ± 0.22) indicated that both treatments showed sharp increase in stress on Day 4 (Tables 2 and 3). Except for Day 4, DT showed a consistent decreasing trend over time in certain physiological parameters Fv′/Fm′, ΦII, ΦNO, ΦNPQ (Table 3). In comparisons between treatments, Fo′ and Fm′ showed significant differences from Day 2 onward (except Fm′ on Day 4)

https://doi.org/10.3390/f17030348

($p < 0.05$). ΦNO (Day 6 ** CT: 0.19 ± 0.02, DT: 0.18 ± 0.02; Day 8 *** CT: 0.20 ± 0.02, DT: 0.17 ± 0.03) and qL (Day 6 * CT: 0.63 ± 0.11, DT: 0.67 ± 0.06; Day 8 ** CT: 0.64 ± 0.11, DT: 0.70 ± 0.05) also differed significantly between the two treatments from Day 6 onward.

Table 2. Statistical analysis results of physiology parameters among days in CT.

	Day 2	Day 4	Day 6	Day 8
Fo′	1555.76 ± 253.68 a **	1067.30 ± 235.62 c **	1302.97 ± 220.82 b ***	1351.68 ± 204.70 b *
Fm′	5147.79 ± 779.32 a *	2773.73 ± 1147.19 c	4275.41 ± 742.00 b ***	4742.26 ± 717.08 b ***
Fv′/Fm′	0.70 ± 0.03 b	0.57 ± 0.13 c	0.69 ± 0.03 b	0.71 ± 0.02 a
ΦII	0.60 ± 0.04 a	0.45 ± 0.15 b	0.58 ± 0.07 a	0.61 ± 0.07 a
ΦNO	0.19 ± 0.02 b	0.15 ± 0.05 c	0.19 ± 0.02 ab **	0.20 ± 0.02 a ***
ΦNPQ	0.21 ± 0.05 b	0.40 ± 0.18 a	0.23 ± 0.06 b	0.19 ± 0.06 c
qL	0.67 ± 0.07 a	0.61 ± 0.14 a	0.63 ± 0.11 a *	0.64 ± 0.11 a **
SPAD	28.33 ± 4.22 c	30.04 ± 4.24 a	29.19 ± 3.94 bc	29.81 ± 3.64 ab
VPD	0.14 ± 0.11 d	2.02 ± 0.52 a	0.35 ± 0.11 c	1.00 ± 0.48 b
CWSI	0.61 ± 0.31 a	0.54 ± 0.32 a	0.36 ± 0.18 a ***	0.38 ± 0.35 a

Mean ± SD ($n = 37$). Two-way RMANOVA was conducted, followed by pairwise t-tests with Bonferroni correction for post hoc analysis ($p < 0.05$). Differences in letters indicate the results of comparisons among days. The significance levels for comparisons with drought treatment on each day are indicated as follows: blank ($p > 0.05$), * ($p < 0.05$), ** ($p < 0.01$), *** ($p < 0.001$). Fo′: minimum fluorescence in light-adapted state, Fm′: maximum fluorescence in light-adapted state, Fv′/Fm′: maximum quantum yield of PSII in light-adapted state, ΦII: quantum yield of PSII, ΦNO: quantum yield of non-regulated energy dissipation, ΦNPQ: quantum yield of regulated energy dissipation, qL: fraction of open PSII reaction centers, SPAD: chlorophyll index, VPD: vapor pressure deficit, CWSI: crop water stress index.

Table 3. Statistical analysis results of physiology parameters among days in DT.

	Day 2	Day 4	Day 6	Day 8
Fo′	1386.63 ± 282.61 a **	901.14 ± 204.61 d **	1094.11 ± 243.10 c ***	1211.00 ± 264.06 b *
Fm′	4694.94 ± 919.99 a *	2449.97 ± 970.43 c	3491.91 ± 1062.68 b ***	3738.03 ± 1065.19 b ***
Fv′/Fm′	0.70 ± 0.03 a	0.58 ± 0.15 b	0.67 ± 0.07 ab	0.66 ± 0.10 b
ΦII	0.62 ± 0.04 a	0.47 ± 0.18 c	0.58 ± 0.08 b	0.57 ± 0.11 b
ΦNO	0.19 ± 0.02 a	0.16 ± 0.05 b	0.18 ± 0.02 a **	0.17 ± 0.03 ab ***
ΦNPQ	0.19 ± 0.04 b	0.38 ± 0.22 a	0.24 ± 0.10 b	0.26 ± 0.13 ab
qL	0.69 ± 0.09 a	0.62 ± 0.17 a	0.67 ± 0.06 a *	0.70 ± 0.05 a **
SPAD	29.14 ± 4.11 bc	31.97 ± 3.56 a	30.17 ± 3.29 b	29.09 ± 3.26 c
VPD	0.11 ± 0.10 d	1.97 ± 0.61 a	0.49 ± 0.12 c	1.27 ± 0.40 b
CWSI	0.57 ± 0.29 a	0.47 ± 0.20 a	0.58 ± 0.19 a ***	0.54 ± 0.31 a

Mean ± SD ($n = 37$). Two-way RMANOVA was conducted, followed by pairwise t-tests with Bonferroni correction for post hoc analysis ($p < 0.05$). Differences in letters indicate the results of comparisons among days. The significance levels for comparisons with control on each day are indicated as follows: blank ($p > 0.05$), * ($p < 0.05$), ** ($p < 0.01$), *** ($p < 0.001$). Fo′: minimum fluorescence in light-adapted state, Fm′: maximum fluorescence in light-adapted state, Fv′/Fm′: maximum quantum yield of PSII in light-adapted state, ΦII: quantum yield of PSII, ΦNO: quantum yield of non-regulated energy dissipation, ΦNPQ: quantum yield of regulated energy dissipation, qL: fraction of open PSII reaction centers, SPAD: chlorophyll index, VPD: vapor pressure deficit, CWSI: crop water stress index.

3.2. Leaf Angle Variation

Visual observation revealed that noticeable leaf inclination occurred on Day 8 (Figure 3). BD–MD exhibited significant interaction (day × treatment: F = 20.607, $p < 0.001$) and main effects (day: F = 8.307, $p < 0.01$; treatment: F = 11.730, $p < 0.01$), with significant differences between treatments observed from Day 8 (CT: −6.43 ± 3.67°, DT: 19.52 ± 3.95°; $p < 0.001$) (Figure 4A). PMD–MD showed both interaction effect (day × treatment: F = 4.687, $p < 0.05$) and main effect for treatment (F = 9.592, $p < 0.01$), with significant differences between treatments beginning on Day 6 (CT: −0.77 ± 0.60°, DT: 2.39 ± 0.96°; $p < 0.01$) (Figure 4B). Notably, on Day 4, Fv′/Fm′ decreased in both treatments, likely reflecting responses to heat stress, whereas leaf angle parameters re-

mained relatively stable (Figures 1A and 4A). By Day 6, meteorological conditions began to resemble those of the early experimental period, with SM reaching the permanent wilting point, the PMD–MD exhibited clear drought stress responses between treatments (Figures 1 and 4B). At the same time, from Day 6 onward, Fv′/Fm′ in the DT showed a more gradual increase followed by a steeper decline compared with the CT, indicating a more pronounced drought stress effect. In DT, ST1 and ST2, which were within the negative angle range, exhibited an upward trend over time (Figure 5), with ST2 showing the greatest increase (Day 2: 18.9%, Day 4: 18.9%, Day 6: 24.3%, Day 8: 35.1%; y = 1.00x + 4.00). In contrast, ST5 showed the most pronounced decline (Day 2: 13.5%, Day 4: 16.2%, Day 6: 10.8%, Day 8: 5.4%; y = −0.56x + 7.03).

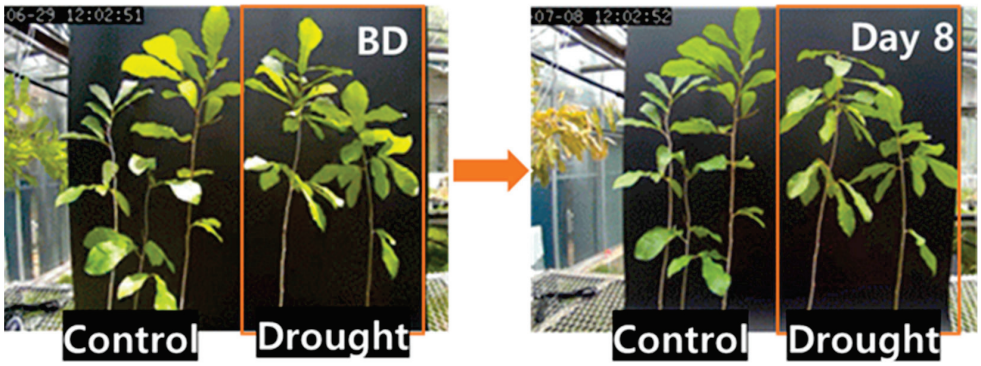


Figure 3. Monitoring of temporal change in leaf angle during the experimental period. BD: before drought.

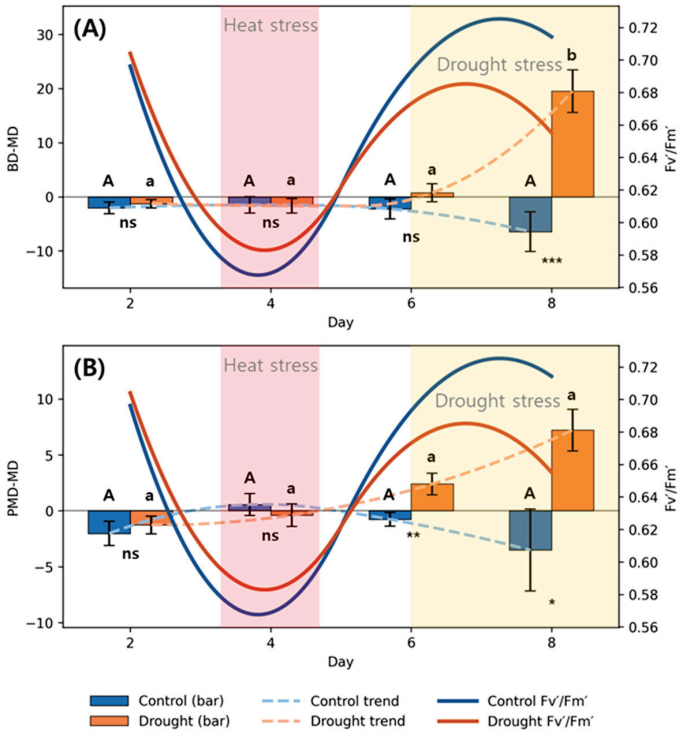


Figure 4. Statistical analysis results of leaf angle parameters by day and treatment. (**A**) BD–MD (difference between measurements before drought and the current measurement day); (**B**) PMD–MD (difference between the previous measurement day and the current measurement day). Bar graph represents mean and error bar indicates SE. Two-way RMANOVA was conducted, followed by pairwise t-tests with Bonferroni correction for post hoc analysis ($p < 0.05$). Uppercase letters indicate comparisons within control across days, while lowercase letters indicate comparisons within drought treatment across days. Significance levels for comparisons between the two treatments are denoted as follows: ns ($p > 0.05$), * ($p < 0.05$), ** ($p < 0.01$), *** ($p < 0.001$).

https://doi.org/10.3390/f17030348

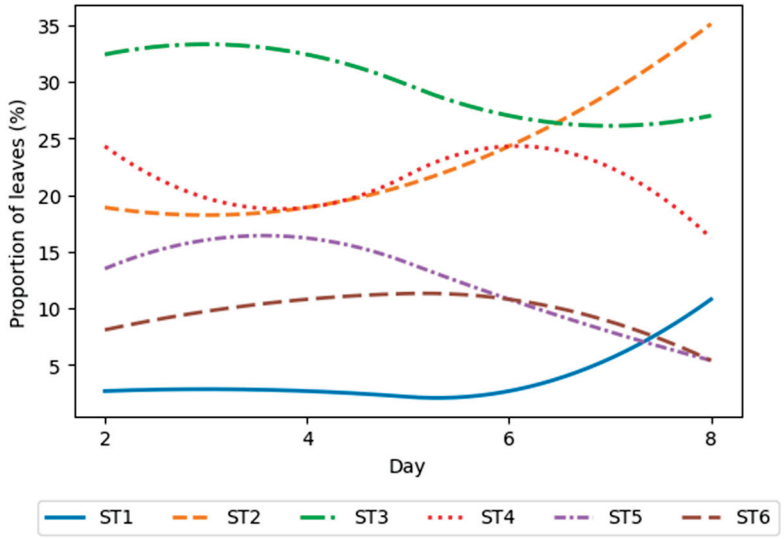


Figure 5. Temporal trends in the proportion of leaves across STx classes under drought treatment. STx leaf angle ranges divided into six intervals: $-90° \leq$ ST1 $< -60°$, $-60° \leq$ ST2 $< -30°$, $-30° \leq$ ST3 $< 0°$, $0° \leq$ ST4 $< +30°$, $+30° \leq$ ST5 $< +60°$, $+60° \leq$ ST6 $\leq +90°$.

3.3. Relationship Between Physiological and Leaf Angle Parameters

The BD–MD model (adjusted $R^2 = 0.389$) exhibited relatively higher stability in explanatory power compared to the PMD–MD model (adjusted $R^2 = 0.242$) (Tables 4 and 5). However, since both models had R^2 values below 0.5, they were appropriate for identifying general trends but could not be considered highly predictive. The addition of new variables contributed to an increase in explanatory power (Sig. F change < 0.05). The Durbin–Watson (DW) values were close to 2 indicating minimal autocorrelation. Significant variables selected in both models included SM, AT, Fm′, and VPD. Except for Fm′, most of these were environmental factors (AT, VPD, SM), which were identified as key drivers influencing leaf angle. In particular, AT (BD–MD standardized coefficient $\beta = -1.079$; PMD–MD standardized coefficient $\beta = -0.672$) exerted the strongest influence (negative) on both leaf angle parameters. On Day 8, PCA revealed a clear separation between CT and DT primarily along PC1, which accounted for 33.0% of the total variance (Figure 6). This separation was mainly driven by strong loadings of chlorophyll fluorescence and leaf angle parameters. In contrast, PC2 (19.3% of the variance) was dominated by atmospheric-related variables such as AH, SR, AT, VPD, and CWSI.

Table 4. Stepwise multiple regression model results for leaf angle parameter BD-MD.

	R^2	Adjusted R^2	F change	Sig. F change	DW
BD-MD	0.409	0.389	6.973	0.009	2.197
	β	**Standardized coefficient β**	***p*-value**	**Tolerance**	**VIF**
intercept	138.799	-	<0.001	-	-
SM	−1.249	−0.384	<0.001	0.665	1.504
AT	−4.208	−1.079	<0.001	0.279	3.588
VPD	11.454	0.565	<0.001	0.351	2.853
Fm′	−0.005	−0.386	<0.001	0.592	1.688
CWSI	−13.213	−0.204	<0.01	0.694	1.441
equation	$Y = 138.799 - 1.249 \times SM - 4.208 \times AT + 11.454 \times VPD - 0.005 \times Fm' - 13.213 \times CWSI$				

BD-MD: difference between measurements before drought and the current measurement day, SM: soil moisture, AT: air temperature, VPD: vapor pressure deficit, Fm′: maximum fluorescence in light-adapted state, CWSI: crop water stress index.

https://doi.org/10.3390/f17030348

Table 5. Stepwise multiple regression model results for leaf angle parameter PMD-MD.

	R^2	Adjusted R^2	F change	Sig. F change	DW
PMD-MD	0.263	0.242	4.746	0.031	2.112
	β	**Standardized coefficient β**	***p*-value**	**Tolerance**	**VIF**
intercept	44.965	-	<0.001	-	-
SM	−0.651	−0.403	<0.001	0.667	1.499
AT	−1.302	−0.672	<0.001	0.374	2.675
Fm′	−0.002	−0.305	<0.01	0.646	1.548
VPD	2.336	0.232	<0.05	0.455	2.200
equation	$Y = 44.965 - 0.651 \times SM - 1.302 \times AT - 0.002 \times Fm' + 2.336 \times VPD$				

PMD-MD: difference between the previous measurement day and the current measurement day, SM: soil moisture, AT: air temperature, VPD: vapor pressure deficit, Fm′: maximum fluorescence in light-adapted state.

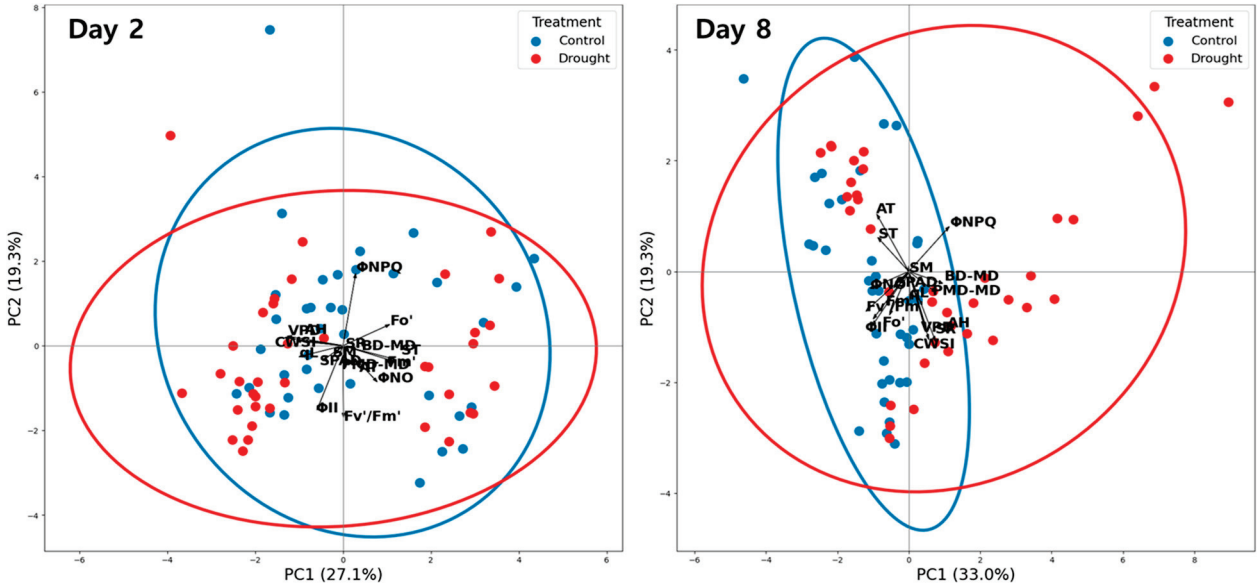


Figure 6. PCA results by experimental day. AT: air temperature, AH: air humidity, SR: solar radiation, ST: soil temperature, SM: soil moisture, Fo′: minimum fluorescence in light-adapted state, Fm′: maximum fluorescence in light-adapted state, Fv′/Fm′: maximum quantum yield of PSII in light-adapted state, ΦII: quantum yield of PSII, ΦNO: quantum yield of non-regulated energy dissipation, ΦNPQ: quantum yield of regulated energy dissipation, qL: fraction of open PSII reaction centers, SPAD: chlorophyll index, VPD: vapor pressure deficit, CWSI: crop water stress index.

4. Discussion

4.1. Physiological Responses of Q. acutissima to Drought Stress

In contrast to this study, previous studies have shown that 1–2-year-old *Q. acutissima* seedlings can survive beyond 30 days of drought treatment [39–42]. Up to 30 days of drought, no significant differences in chlorophyll content between irrigated and drought-treated seedlings have been observed, and chlorophyll fluorescence responses also showed minimal variation [39,42]. Before rewatering, leaves exhibited visible wilting, but recovery was observed following rewatering [42,43]. Thermal imaging further confirmed that leaf temperatures returned to pre-drought levels after rewatering [42]. Although the seedlings did not die, leaf abscission occurred progressively over time, while surviving leaves tended to recover in photosynthetic parameters [43]. These studies consistently indicate that, even under DT, SM levels remained higher than in this study, and recovery upon rewatering was possible as long as SM did not reach permanent wilting point. According to Lim et al. [39],

SM dropped below 1% after 30 days, after which drought stress responses were detected in chlorophyll fluorescence (Fv/Fm). This is consistent with the findings of this study, in which drought stress symptoms appeared when SM approached permanent wilting point. Further investigation is therefore required to determine whether leaf recovery can occur following rewatering once SM has reached permanent wilting point.

Even when leaf recovery was slow, Wang et al. [41] reported that stem starch concentrations increased 60 days after defoliation, suggesting an enhancement of drought tolerance through resource reallocation strategies. Liu et al. [44] observed that nutrient supplementation under drought conditions mitigated structural damage to leaves and maintained physiological functions, thereby alleviating drought stress. According to Li et al. [40], hardening treatment in *Q. acutissima* improved drought readaptation capacity by enhancing photosynthetic performance, activating carbon consumption reduction strategies, and increasing the fine-to-coarse root ratio. From physiological perspective, such effects could reduce leaf mortality, mitigate growth reduction, and enhance the feasibility of leaf-based drought stress detection.

In this context, the decline of SM to levels approaching the permanent wilting point in this study represents an extreme condition that is unlikely to occur frequently under natural field environments. Nevertheless, such moisture depletion provides important insight into the physiological limits and response thresholds of seedlings and becomes increasingly relevant under climate change scenarios characterized by more frequent drought events, elevated temperatures, and high VPD. In particular, containerized seedlings and recently planted seedlings with restricted rooting volumes may be more vulnerable to rapid SM depletion, and the findings of this study may contribute to the development of irrigation management strategies aimed at preventing irreversible stress.

4.2. Potential Applications of Leaf Angle Measurement

This study confirmed that changes in leaf angle closely align with physiological responses of seedlings to drought stress. On Day 6 of the no-irrigation treatment, significant differences between treatments were observed not only in ΦNO and qL but also in PMD–MD (CT: $-0.77 \pm 0.60^{\circ}$, DT: $2.39 \pm 0.96^{\circ}$), confirming a drought stress response. The numerical range of this leaf angle parameter may serve as a reference threshold for identifying no-irrigation conditions, provided that measurements are conducted using the same methodological approach as in this study. On Day 4 of experiment, physiological responses exhibited greater sensitivity to light and heat stress, whereas leaf angle did not show pronounced response to these factors. This suggests that leaf angle may be less influenced by light and heat stress and therefore could serve as more reliable indicator for detecting drought stress. Although AT exhibited the strongest standardized coefficient in the regression model, this inconsistency likely stems from differences in analytical approaches between treatment-based post hoc and regression analyses using continuous environmental variables. The relatively large variability (particularly on Day 8) in leaf angle among individual leaves may have contributed to weaker statistical significance in day-to-day differences compared with treatment-based differences. This characteristic was also reflected in the relatively low R^2 values observed in the regression models. In nursery environments, seedlings are inherently influenced by a complex interplay of factors, including water status, tissue elasticity, and leaf position. Therefore, expecting high explanatory power from a limited set of variables may not fully reflect realistic conditions. Accordingly, this (preliminary) study focused more on identifying significant parameters and exploring response trends rather than achieving high explanatory power per se. From this perspective, the results provide ecophysiologically meaningful insights into leaf angle research.

https://doi.org/10.3390/f17030348

Leaf angle is known to significantly influence various physiological processes, including suppression of excessive light saturation, prevention of leaf temperature rise, protection of the photosynthetic apparatus, activation of the xanthophyll cycle, and improvement of photosynthetic efficiency [45]. In some species, inherent leaf angles serve as an adaptive strategy for enhancing survival [29]. Under nursery conditions, seedlings with positive mean leaf angle exhibited significantly improved physiological responses even under reduced irrigation, whereas those with negative mean leaf angle required greater irrigation inputs [32,33]. In conifers such as larch, upper needles exhibited more rapid wilting response compared to broadleaved species, and drought stress symptoms were detectable earlier than physiological changes [34]. In *Larix kaempferi*, needles wilted at night under drought stress but recovered by the following morning, indicating a clear irrigation threshold and supporting the applicability of leaf angle-based monitoring. In contrast, such pronounced movements were less evident in *Q. acutissima*, suggesting that identifying appropriate re-irrigation thresholds may require further investigation. These findings underscore the importance of incorporating morphology-derived traits into leaf angle-based monitoring strategies to reflect species-specific differences.

For more practical applications, the approach proposed by Jeong et al. [34] could be integrated with software (e.g., PlantCV) capable of detecting canopy leaf area or morphology-derived traits based on leaf angle dynamics and automatically collecting quantitative data. Moreover, images can now be easily captured using smartphones, and app-based developments are underway to extract leaf area and related phenotypes from such images [23,46]. If these low-cost image acquisition and measurement technologies are coupled with automated analytical processes, they could ultimately be integrated into cost-effective automated irrigation systems [47].

Recent advances in machine learning and deep learning techniques have enhanced the precision of image-based leaf angle analysis [23,24]. For example, Qi et al. [23] applied Pyramid Convolutional Neural Network (PCNN) to smartphone images of *Euonymus japonicus* Thunb., effectively estimating leaf azimuth with high accuracy, as indicated by strong R^2 values, thus demonstrating its field applicability. Several other studies have also reported methods for measuring leaf angle distributions in various plant and crop species [21,22]. Jiang et al. [25] developed the Auto-LIA (leaf inclination angle) system, which integrates RGB imaging with computer vision techniques to achieve fully automated LIA measurement based on leaf–plant connectivity and 3D spatial information. This approach offers advantages of low cost and high precision, highlighting its potential for plant physiological monitoring and phenotyping. Furthermore, leaf angle datasets can be utilized for calibration modeling to improve measurement accuracy, and the data collected in this study are also expected to contribute to the development of future application technologies [33,48].

4.3. Limitation and Future Study

The relatively small sample size should be acknowledged as a primary limitation of this study. Although the repeated measures design partially enhanced analytical sensitivity by incorporating temporal data from labeled leaves, the limited number of independent seedlings may have constrained statistical power.

Genetic factors may also have contributed to variability, as seedlings were derived from open-pollinated seed sources and genetic variation was not strictly controlled. This variability may have influenced drought tolerance and leaf angle responses, highlighting the need for genetically uniform materials or explicit consideration of genetic effects in future studies.

In addition, this study was conducted only during July, corresponding to the active growth stage, and therefore did not account for seasonal variation or differences among leaf developmental stages. Previous studies have reported seasonal shifts in mean leaf angle [17,30], suggesting that temporal variability should be incorporated into future analyses. Increasing the number of replicates across different time periods and constructing separate datasets based on leaf position and environmental conditions would allow more robust modeling of leaf angle dynamics.

Despite these constraints, this study identified correlations and temporal trends in leaf angle responses under drought stress. The findings provide a preliminary experimental framework for designing more robust studies, including variation in seasonal timing and irrigation intensity. To enhance practical applicability, future research should extend analyses from individual leaves to containerized seedlings and larger plant populations, enabling evaluation of morphological patterns derived from leaf angle variation. With larger datasets, it may be possible to define threshold ranges associated with the onset of wilting and implement precision rewatering strategies based on real-time monitoring. The dataset generated in this study also provides foundational information for the development and validation of predictive models, including linear mixed modeling approaches.

5. Conclusions

This study explored the feasibility of image-based leaf angle monitoring for detecting drought-induced changes in one-year-old *Q. acutissima* container seedlings grown under controlled nursery conditions. From Day 6 of DT onward, leaf angle (PMD–MD) and physiological parameters (ΦNO and qL) exhibited comparable treatment-related differences, confirming that leaf angle reflected drought stress responses. However, leaf angle changes did not precede physiological responses, and the present experimental conditions did not allow for definitive validation of its early detection capability. Regression analyses indicated that SM and AT contributed to leaf angle variation. However, the relatively low R^2 values suggest limited predictive power.

Overall, this study provides preliminary evidence that leaf angle monitoring may function as a complementary indicator of drought stress rather than a substitute for physiological measurements. Future studies should validate these findings using larger datasets, across multiple seasonal conditions, and in different species. In this context, the integration of image-based monitoring into smart irrigation systems should be considered a long-term research direction rather than an immediate practical application.

Author Contributions: Conceptualization, U.J., S.H.H. and E.J.C.; methodology, U.J.; validation, U.J. and D.K.; formal analysis, U.J. and D.K.; investigation, U.J., D.K., S.K. and J.P.; resources, S.H.H.; data curation, U.J. and D.K.; writing—original draft preparation, U.J.; writing—review and editing, U.J.; visualization, U.J.; supervision, U.J. and E.J.C.; project administration, E.J.C.; funding acquisition, S.H.H. All authors have read and agreed to the published version of the manuscript.

Funding: This research was funded by the National Institute of Forest Science, grant number SC0300-2023-01-2024.

Data Availability Statement: The original contributions presented in this study are included in the article. Further inquiries can be directed to the corresponding authors.

Conflicts of Interest: The authors declare no conflicts of interest.

Abbreviations

The following abbreviations are used in this manuscript:

CT	Control
DT	Drought treatment
AT	Air temperature
AH	Air humidity
SR	Solar radiation
ST	Soil temperature
SM	Soil moisture
Fo′	Minimum fluorescence in light-adapted state
Fm′	Maximum fluorescence in light-adapted state
Fv′/Fm′	Maximum quantum yield of PSII in light-adapted state
ΦII	Quantum yield of PSII
ΦNO	Quantum yield of non-regulated energy dissipation
ΦNPQ	Quantum yield of regulated energy dissipation
qL	Fraction of open PSII reaction centers
SPAD	Chlorophyll index
VPD	Vapor pressure deficit
CWSI	Crop water stress index
STx	Leaf angle ranges divided into six intervals
BD–MD	Difference between measurements before drought and the current measurement day
PMD–MD	Difference between the previous measurement day and the current measurement day

References

1. Arnell, N.W.; Lowe, J.A.; Challinor, A.J.; Osborn, T.J. Global and regional impacts of climate change at different levels of global temperature increase. *Clim. Change* **2019**, *155*, 377–391. [CrossRef]
2. Menezes-Silva, P.E.; Loram-Lourenço, L.; Alves, R.D.F.B.; Sousa, L.F.; Almeida, S.E.D.S.; Farnese, F.S. Different ways to die in a changing world: Consequences of climate change for tree species performance and survival through an ecophysiological perspective. *Ecol. Evol.* **2019**, *9*, 11979–11999. [CrossRef] [PubMed]
3. Park, J.H.; Jung, S.Y.; Lee, K.S.; Lee, H.S. The Characteristics and survival rates of evergreen broad-leaved tree plantations in Korea. *J. Korean Soc. For. Sci.* **2019**, *108*, 513–521. [CrossRef]
4. Fowler, H.J.; Ali, H.; Allan, R.P.; Ban, N.; Barbero, R.; Berg, P.; Blenkinsop, S.; Cabi, N.S.; Chan, S.; Dale, M.; et al. Towards advancing scientific knowledge of climate change impacts on short-duration rainfall extremes. *Philos. Trans. Math. Phys. Eng. Sci.* **2021**, *379*, 20190542. [CrossRef]
5. Fisichelli, N.; Wright, A.; Rice, K.; Mau, A.; Buschena, C.; Reich, P.B. First-year seedlings and climate change: Species-specific responses of 15 North American tree species. *Oikos* **2014**, *123*, 1331–1340. [CrossRef]
6. Mechergui, T.; Pardos, M.; Jacobs, D.F. Effect of acorn size on survival and growth of *Quercus suber* L. seedlings under water stress. *Eur. J. For. Res.* **2021**, *140*, 175–186. [CrossRef]
7. Farooq, M.; Hussain, M.; Wahid, A.; Siddique, K.H.M. Drought stress in plants: An overview. Plant responses to drought stress: From morphological to molecular feature. In *Plant Responses to Drought Stress*; Aroca, R., Ed.; Springer: Berlin/Heidelberg, Germany, 2012; pp. 1–33.
8. Abdallah, M.B.; Methenni, K.; Nouairi, I.; Zarrouk, M.; Youssef, N.B. Drought priming improves subsequent more severe drought in a drought-sensitive cultivar of olive cv. *Chétoui. Sci. Hortic.* **2017**, *221*, 43–52. [CrossRef]
9. Lv, Z.; Zhang, H.; Huang, Y.; Zhu, L.; Yang, X.; Wu, L.; Chen, M.; Wang, H.; Jing, Q.; Shen, J.; et al. Drought priming at seedling stage improves photosynthetic performance and yield of potato exposed to a short-term drought stress. *Plant Physiol.* **2024**, *292*, 154157. [CrossRef]
10. Puértolas, J.; Villar-Salvador, P.; Andivia, E.; Ahuja, I.; Cocozza, C.; Cvjetković, B.; Devetaković, J.; Diez, J.J.; Fløistad, I.S.; Ganatsas, P.; et al. Die-hard seedlings. A global meta-analysis on the factors determining the effectiveness of drought hardening on growth and survival of forest plantations. *For. Ecol. Manag.* **2024**, *572*, 122300. [CrossRef]
11. Toca, A.; Gonzalez-Benecke, C.A.; Nelson, A.S.; Jacobs, D.F. Drought memory expression varies across ecologically contrasting forest tree species. *Environ. Exp. Bot.* **2025**, *231*, 106094. [CrossRef]
12. Et-Taibi, B.; Abid, M.R.; Boufounas, E.M.; Morchid, A.; Bourhnane, S.; Hamed, T.A.; Benhaddou, D. Enhancing water management in smart agriculture: A cloud and IoT-Based smart irrigation system. *Results Eng.* **2024**, *22*, 102283. [CrossRef]

13. Hong, S.; Park, S.; Youn, H.; Lee, J.; Kwon, S. Implementation of smart farm systems based on fog computing in artificial intelligence of things environments. *Sensors* **2024**, *24*, 6689. [CrossRef] [PubMed]
14. Younes, A.; Abou Elassad, Z.E.; El Meslouhi, O.; Abou Elassad, D.E.; Majid, E.D.A. The application of machine learning techniques for smart irrigation systems: A systematic literature review. *Smart Agric. Technol.* **2024**, *7*, 100425. [CrossRef]
15. Itam, M.; Hall, D.; Kramer, D.; Merewitz, E. Early detection of Kentucky bluegrass and perennial ryegrass responses to drought stress by measuring chlorophyll fluorescence parameters. *Crop Sci.* **2024**, *64*, 1015–1026. [CrossRef]
16. Yang, C.Y.; Zhang, Y.C.; Hou, Y.L. Assessing water status in rice plants in water-deficient environments using thermal imaging. *Bot. Stud.* **2025**, *66*, 6. [CrossRef]
17. Yang, X.; Li, R.; Jablonski, A.; Stovall, A.; Kim, J.; Yi, K.; Ma, Y.; Beverly, D.; Phillips, R.; Novics, K.; et al. Leaf angle as a leaf and canopy trait: Rejuvenating its role in ecology with new technology. *Ecol. Lett.* **2023**, *26*, 1005–1020. [CrossRef]
18. Tsaftaris, S.A.; Minervini, M.; Scharr, H. Machine learning for plant phenotyping needs image processing. *Trends Plant Sci.* **2016**, *21*, 989–991. [CrossRef] [PubMed]
19. Pound, M.P.; Atkinson, J.A.; Townsend, A.J.; Wilson, M.H.; Griffiths, M.; Jackson, A.S.; Bulat, A.; Tzimiropoulos, G.; Wells, D.M.; Murchie, E.H.; et al. Deep machine learning provides state-of-the-art performance in image-based plant phenotyping. *Gigascience* **2017**, *6*, gix083. [CrossRef]
20. Mertens, S.; Verbraeken, L.; Sprenger, H.; De Meyer, S.; Demuynck, K.; Cannoot, B.; Merchie, J.; De Block, J.; Vogel, J.T.; Bruce, W.; et al. Monitoring of drought stress and transpiration rate using proximal thermal and hyperspectral imaging in an indoor automated plant phenotyping platform. *Plant Methods* **2023**, *19*, 132. [CrossRef]
21. Zou, X.; Mõttus, M.; Tammeorg, P.; Torres, C.L.; Takala, T.; Pisek, J.; Mäkelä, P.; Stoddard, F.L.; Pellikka, P. Photographic measurement of leaf angles in field crops. *Agric. For. Meteorol.* **2014**, *184*, 137–146. [CrossRef]
22. Müller-Linow, M.; Pinto-Espinosa, F.; Scharr, H.; Rascher, U. The leaf angle distribution of natural plant populations: Assessing the canopy with a novel software tool. *Plant Methods* **2015**, *11*, 11. [CrossRef] [PubMed]
23. Qi, J.; Xie, D.; Li, L.; Zhang, W.; Mu, X.; Yan, G. Estimating leaf angle distribution from smartphone photographs. *IEEE Geosci. Remote Sens.* **2019**, *16*, 1190–1194. [CrossRef]
24. Kenchanmane Raju, S.K.; Adkins, M.; Enersen, A.; Santana de Carvalho, D.; Studer, A.J.; Ganapathysubramanian, B.; Schnable, P.S.; Schnable, J.C. Leaf Angle eXtractor: A high-throughput image processing framework for leaf angle measurements in maize and sorghum. *Appl. Plant Sci.* **2020**, *8*, e11385. [CrossRef]
25. Jiang, S.; Wu, X.; Wang, Q.; Pei, Z.; Wang, Y.; Jin, J.; Guo, Y.; Song, R.; Zang, L.; Liu, Y.J.; et al. Auto-LIA: The automated vision-based leaf inclination angle measurement system improves monitoring of plant physiology. *Plant Phenomics* **2024**, *6*, 0245. [CrossRef]
26. King, D.A. The functional significance of leaf angle in *Eucalyptus*. *Aust. J. Bot.* **1997**, *45*, 619–639. [CrossRef]
27. Ishida, A.; Toma, T.; Marjenah, M. Leaf gas exchange and cholorphyll fluorescence in relation to leaf angle, azimuth, and canopy position in the tropical pioneer tree, *Macaranga conifera*. *Tree Physiol.* **1999**, *19*, 117–124. [CrossRef]
28. Posada, J.M.; Lechowicz, M.J.; Kitajima, K. Optimal photosynthetic use of light by tropical tree crowns achieved by adjustment of individual leaf angles and nitrogen content. *Ann. Bot.* **2009**, *103*, 795–805. [CrossRef]
29. Mänd, P.; Hallik, L.; Peñuelas, J.; Kull, O. Electron transport efficiency at opposite leaf sides: Effect of vertical distribution of leaf angle, structure, chlorophyll content and species in a forest canopy. *Tree Physiol.* **2013**, *33*, 202–210. [CrossRef]
30. Raabe, K.; Pisek, J.; Sonnentag, O.; Annuk, K. Variations of leaf inclination angle distribution with height over the growing season and light exposure for eight broadleaf tree species. *Agric. For. Meteorol.* **2015**, *214*, 2–11. [CrossRef]
31. Hagemeier, M.; Leuschner, C. Functional crown architecture of five temperate broadleaf tree species: Vertical gradients in leaf morphology, leaf angle, and leaf area density. *Forests* **2019**, *10*, 265. [CrossRef]
32. Delgado, L.G.M.; da Silva, R.B.G.; Gabira, M.M.; Rodrigues, A.L.; Simões, D.; de Almeida, L.F.R.; da Silva, M.R. Mean leaf angles affect irrigation efficiency and physiological responses of tropical species seedling. *Forests* **2022**, *13*, 832. [CrossRef]
33. da Silva, R.B.G.; Simões, D.; Wendling, I.; do Prado, D.Z.; Sartori, M.M.P.; Bertholdi, A.A.D.S.; da Silva, M.R. Leaf Angle as a Criterion for Optimizing Irrigation in Forest Nurseries: Impacts on Physiological Seedling Quality and Performance after Planting in Pots. *Forests* **2023**, *14*, 1042. [CrossRef]
34. Jeong, U.; Kim, D.; Kim, S.; Han, S.H.; Cheong, E.J. Needle angle dynamics as a rapid indicator of drought stress in *Larix kaempferi* (Lamb.) Carrière: Advancing non-destructive imaging techniques for resilient seedling production. *Front. Plant Sci.* **2025**, *16*, 1550748. [CrossRef]
35. Gardner, B.R.; Nielsen, D.C.; Shock, C.C. Infrared thermometry and the crop water stress index. I. History, theory, and baselines. *J. Prod. Agric.* **1992**, *5*, 462–466. [CrossRef]
36. Stull, R.B. *Practical Meteorology: An Algebra-Based Survey of Atmospheric Science*; University of British Columbia: Vancouver, BC, Canada, 2015. [CrossRef]
37. Grossiord, C.; Buckley, T.N.; Cernusak, L.A.; Novick, K.A.; Poulter, B.; Siegwolf, R.T.; Sperry, J.S.; Mcdowell, N.G. Plant responses to rising vapor pressure deficit. *New Phytol.* **2020**, *226*, 1550–1566. [CrossRef]

38. Zhou, Z.; Majeed, Y.; Naranjo, G.D.; Gambacorta, E.M. Assessment for crop water stress with infrared thermal imagery in precision agriculture: A review and future prospects for deep learning applications. *Comput. Electron. Agric.* **2021**, *182*, 106019. [CrossRef]
39. Lim, H.; Kang, J.W.; Lee, S.; Lee, H.; Lee, W.Y. Growth and physiological responses of *Quercus acutissima* seedling under drought stress. *Plant Breed. Biotechnol.* **2017**, *5*, 363–370. [CrossRef]
40. Li, Q.; Liu, X.; Sun, X.; Zhao, M.; Liu, L.; Wang, N.; Gao, Q.; Fan, P.; Du, N.; Wang, H.; et al. Effects of drought hardening on the carbohydrate dynamics of *Quercus acutissima* seedlings under successional drought. *Front. Plant Sci.* **2023**, *14*, 1184584. [CrossRef]
41. Wang, N.; Song, M.; Zhang, Y.; Liu, X.; Wu, P.; Qi, L.; Song, H.; Du, N.; Wang, H.; Zheng, P.; et al. Physiological responses of *Quercus acutissima* and *Quercus rubra* seedlings to drought and defoliation treatments. *Tree Physiol.* **2023**, *43*, 737–750. [CrossRef]
42. Kim, T.L.; Oh, C.; Denison, M.I.J.; Natarajan, S.; Lee, K.; Lim, H. Transcriptomic and physiological responses of *Quercus acutissima* and *Quercus palustris* to drought stress and rewatering. *Front. Plant Sci.* **2024**, *15*, 1430485. [CrossRef]
43. Liu, D.; Guo, H.; Yan, L.P.; Gao, L.; Zhai, S.; Xu, Y. Physiological, photosynthetic and stomatal ultrastructural responses of *quercus acutissima* seedlings to drought stress and rewatering. *Forests* **2023**, *15*, 71. [CrossRef]
44. Liu, X.; Li, Q.; Sun, X.; Yi, S.; Wu, P.; Wang, N. Nutrition addition alleviates negative drought effects on *Quercus acutissima* seedlings. *For. Ecol. Manag.* **2024**, *562*, 121980. [CrossRef]
45. Liu, L.X.; Xu, S.M.; Woo, K.C. Influence of leaf angle on photosynthesis and the xanthophyll cycle in the tropical tree species *Acacia crassicarpa*. *Tree Physiol.* **2003**, *23*, 1255–1261. [CrossRef]
46. Müller-Linow, M.; Wilhelm, J.; Briese, C.; Wojciechowski, T.; Schurr, U.; Fiorani, F. Plant Screen Mobile: An open-source mobile device app for plant trait analysis. *Plant Methods* **2019**, *15*, 2. [CrossRef]
47. Ortiz, D.; Litvin, A.G.; Salas Fernandez, M.G. A cost-effective and customizable automated irrigation system for precise high-throughput phenotyping in drought stress studies. *PLoS ONE* **2019**, *13*, e0198546. [CrossRef]
48. Pisek, J.; Sonnentag, O.; Richardson, A.D.; Mõttus, M. Is the spherical leaf inclination angle distribution a valid assumption for temperate and boreal broadleaf tree species? *Agric. For. Meteorol.* **2013**, *169*, 186–194. [CrossRef]

Disclaimer/Publisher's Note: The statements, opinions and data contained in all publications are solely those of the individual author(s) and contributor(s) and not of MDPI and/or the editor(s). MDPI and/or the editor(s) disclaim responsibility for any injury to people or property resulting from any ideas, methods, instructions or products referred to in the content.

forests

MDPI

Article

Shoot Vigour, Leaf Water Status and Physiological Traits of Mature *Castanea sativa* Mill. Trees Along the Canopy Vertical Gradient

Lucia Mondanelli, Claudia Cocozza *, Barbara Mariotti and Alberto Maltoni

Department of Agriculture, Food, Environment and Forestry, University of Florence, 50121 Florence, Italy; lucia.mondanelli@unifi.it (L.M.); barbara.mariotti@unifi.it (B.M.); alberto.maltoni@unifi.it (A.M.)
* Correspondence: claudia.cocozza@unifi.it

Abstract

Climate change is increasingly exposing sweet chestnut (*Castanea sativa* Mill.) to more frequent and prolonged drought events, which can compromise growth and nut production, particularly in Mediterranean environments. Understanding how trees respond physiologically to ecological and environmental constraints requires a detailed analysis of their architectures. The aim of this study was to investigate how the shoot vigour and leaf water status of mature chestnut trees vary with height within the canopy. Three mature chestnut trees with distinct crown architectures were selected in a traditional chestnut orchard in Central Italy; the differences in crown structure reflected individual tree development under comparable pruning practices. Morphological traits, leaf water status, and physiological parameters related to chlorophyll were measured directly within the canopy by professional tree climbers, allowing access to both lower and upper shoots during the growing season of 2020. One tree, called "Tree 1," characterised by low bifurcation, with all epicormic shoot cluster (complexes) located on the two main branches and none on the main stem, showed partial vertical differences, mainly in water status and chlorophyll traits. "Tree 2", characterised by high bifurcation and shoots running along the main stem, exhibited clear vertical gradients: lower-canopy shoots had larger leaf areas and more dry mass, higher relative water content, and better photosynthetic performance index e values than upper shoots. At the end, "Tree 3", with the same architecture as Tree 1, displayed no consistent vertical trends. These findings indicate that individual tree architecture modulates hydraulic constraints and shoot vigour, even in hydraulically efficient epicormic branches. Although canopy access constraints limited the number of trees and measurements, this study—among the few to conduct in-canopy measurements on large, mature trees—provides valuable guidance for pruning and crown management, suggesting that lowering and simplifying the crown can enhance water-use efficiency, shoot vigour, and drought resilience in traditional and low-input chestnut orchards.

Keywords: canopy architecture; shoot vigour; hydraulic function; leaf water status; photosynthetic performance; vertical gradients; crown management

1. Introduction

Castanea sativa Mill., commonly known as sweet chestnut, is widespread throughout Europe and Western Asia and has historically been valued for its use in both timber and nut production [1]. The species has a long history of active cultivation, which has led to its

current establishment on sites characterised by a minimum rainfall that ranges between 600 and 800 mm and a mean annual temperature range of 8–15 °C across Central Europe [2]. In Europe, more than 2.5 million hectares are covered by chestnut forests, existing in natural, semi-natural, and managed stands—including orchards and plantations—where appropriate silvicultural practices are applied to sustain high levels of wood and fruit production. The Mediterranean basin represents the core cultivation area in Europe, with 89% of the distribution area concentrated in France and Italy, followed by Spain, Portugal, and Switzerland [2]. In Italy, chestnut forests occupy 778.475 ha [3] and have historically served as an essential economic resource for rural communities in the Apennine regions, where chestnut cultivation aimed at wood or nut production is deeply rooted in local tradition [4]. However, in recent years and with increasing frequency, field experience has shown numerous chestnut trees exhibiting desiccation in the upper branches of the canopy. In fact, recent studies have shown that climate change is increasingly exposing chestnut trees, growing in mountainous and hilly areas, to more frequent and prolonged drought events, whereas water availability was rarely a limiting factor in the past century [5–7]. Rising summer temperatures, reduced annual precipitation, and altered rainfall distribution are now negatively affecting the productivity of traditional rainfed chestnut orchards [5]. In particular, rainfall reduction during the summer and autumn has become a major constraint for chestnut growth and nut production, leading to significant economic losses for producers [8,9]. Overall, there is accumulating evidence indicating that chestnut is highly sensitive to summer droughts, which have become some of the primary threats causing substantial and often unexpected production losses in arid and semi-arid areas, including the Mediterranean region [10,11]. The vulnerability of Mediterranean systems to water scarcity is predicted to increase in the near future as a consequence of greater inter-annual rainfall variability and a greater frequency and intensity of extreme events such as droughts and heat waves [12,13]. In this context, the identification and implementation of adaptation aimed at enhancing the resilience of chestnut trees to water scarcity should be a key priority to maintain both the quality and quantity of production and protect water resources [13]. For these reasons and to increase production to answer the rising demand for sweet chestnut in Europe, some management practices are becoming essential [10]. These practices include fertilization, irrigation, and pruning [14]. While pruning has always been practised, today, it is complemented by mineral fertilisation and irrigation, mainly in more intensive systems to improve tree performance and nut quality [15–17]. However, traditionally managed chestnut orchards are an open forest habitat of anthropogenic origin characterised by a low-intensity management regime [18]. In fact, in the Mediterranean climate, spring precipitation is highly irregular, which makes it difficult to establish a fertilization program for chestnut orchards and, in particular, determine the best time to apply fertilizers [16]. In addition, irrigation is still barely employed in chestnut orchards due to many difficulties, like shortages of water (e.g., from artificial lakes or water reservoirs) for irrigation in typical chestnut cultivation areas (i.e., mountain-hills areas) [15]. Given these emerging constraints, it is therefore necessary to reconsider pruning strategies and canopy management techniques in chestnut orchards to improve water-use efficiency and enhance the trees' resilience to drought stress. Understanding how trees respond physiologically to ecological and environmental constraints requires a detailed analysis of their structural properties. As known from the literature, as a tree's height increases, its vertical structure imposes critical challenges for hydraulic functioning, as water must be transported over long xylem pathways to supply leaves at different heights [19,20]. According to the "hydraulic limitation hypothesis," increasing tree height increases hydraulic resistance, potentially reducing leaf-specific hydraulic conductance,

https://doi.org/10.3390/f17020173

stomatal conductance, and photosynthetic rates in upper-canopy leaves relative to those in lower canopy positions [21].

In this study, using tree architectures, we investigated how shoot vigour, leaf moisture, and chlorophyll traits of mature chestnut trees vary with height within the canopy using direct canopy access via tree climbing, an approach rarely applied to large, mature fruit trees. We hypothesised that lower and upper shoots differentiate such traits due to their positions within the canopy and, consequently, different exposure to environmental constraints. Specifically, under comparable light conditions, we expected lower shoots to display more favourable water statuses than those positioned in the upper canopy due to reduced hydraulic path length and lower tension along the soil–plant–atmosphere continuum.

2. Materials and Methods

2.1. Experimental Site

The experimental site is in an area in the upper valley of the Serchio river called Garfagnana, situated in north-west Tuscany in the province of Lucca in Central Italy. It is enclosed by two mountain ranges, which are significantly different from each other: the Apuan Alps in the West, facing the Tyrrhenian coast, and the Apennines in the east. The natural landscape of the valley is dominated primarily by chestnut (*Castanea sativa* Mill.) at up to approximately 1000 m a.s.l. Within this lower zone, Turkey oak (*Quercus cerris* L.) occurs sporadically, and hornbeam stands (*Ostrya carpinifolia* Scop. and *Carpinus betulus* L.) are occasionally present. In some places, there are large patches of invasive *Robinia pseudoacacia* L. At higher elevations, beech forests (*Fagus sylvatica* L.) predominate, extending up to about 1600 m a.s.l. On the western side of the valley, the proximity to the sea supports an Apuan flora that includes both alpine and Mediterranean elements. In this study, the chestnut orchard in Gello (Media Valle, right side of the Serchio Valley) (43°57′57.66″ N, 10°27′0.03″ E) was selected. It is a chestnut orchard that was recently restored after a period of abandonment in a flat area. The mean annual temperature in the area ranges from −4.4 to 20.9 °C, and the mean annual precipitation ranges from 481.6 to 2449.0 mm. During the summer in which the study was conducted, the Standardized Precipitation-Evapotranspiration Index (SPEI) was estimated to be 0.1 (https://climatedt.org/), indicating wet conditions and the absence of drought conditions. Soils vary from tropical red soils with low organic matter content to brown soils with high organic matter content. The chestnut orchard has a density of 120–130 trees/ha. All the trees were grafted at a young stage using the same local cultivar, "Carpinese," and are estimated to be between 80 and 150 years old, with diameters ranging from 50 to 90 cm and heights of 15 to 20 m.

2.2. Experimental Design, Sampling and Measurement

The investigation was conducted on three healthy mature trees, i.e., those that did not show symptoms of disease or pest attacks during the growing season. On each tree, all the measurements were performed on a variable number of epicormic complexes. In this study, the term epicormic complex refers to a cluster of orthotropic shoots originating from dormant buds that were activated following moderate/severe pruning [22]. Each complex consisted of two or more vertically oriented 1-year-old shoots emerging from the same trunk zone as a direct response to the same pruning intervention. Shoots had the same origin; they were characterised by ontogenetic juvenility and showed no variability in terms of physiological status. For this reason, epicormic complexes (hereafter referred to as "complexes") were used as consistent and comparable sampling units for assessing differences between canopy levels. Tree 1, Tree 2, and Tree 3 were individuals representing the two most common architectural types in the area. Trees 1 and 3 exhibited low bifurcation, with all complexes located on the two main branches and none on the main stem. In

https://doi.org/10.3390/f17020173

contrast, Tree 2 displayed high bifurcation and additional complexes along the main stem. Specifically, Tree 1 consisted of two branches, each bearing four complexes; Tree 2 had two branches plus complexes on the main stem; and Tree 3 had two branches, each with three complexes (Table 1).

Table 1. Architectures of the investigated trees, detailing the number of branches and of the complex within each branch, the height of the complex, and the length of the shoot.

Tree	Branch	Complex	Complex Height (m)	Shoot Length (cm)		
				Mean		st. er
1	1	1	10.17	52.83	±	13.70
		2	8.60	44.50	±	2.76
		3	6.53	42.17	±	10.45
		4	6.23	44.50	±	8.92
	2	5	11.13	44.75	±	8.61
		6	10.57	41.00	±	5.01
		7	7.30	57.44	±	7.83
		8	5.72	56.25	±	11.75
2	1	1	12.25	25.50	±	1.87
		2	11.94	68.20	±	11.81
	2	3	10.48	18.25	±	5.29
		4	9.41	37.60	±	6.03
	3 (main stem)	5	7.84	55.33	±	3.92
		6	4.88	58.67	±	7.06
		7	3.97	55.50	±	5.92
		8	2.57	74.50	±	20.58
3	1	1	11.10	34.17	±	9.47
		2	7.83	64.00	±	9.10
		3	5.01	44.00	±	11.02
	2	4	11.16	33.50	±	6.34
		5	6.55	39.50	±	2.84
		6	6.21	63.00	±	8.90

Complexes were characterised according to height, namely, the distance from the ground. For each tree, complexes were classified as either "upper" or "lower" based on this measurement. Specifically, upper complexes were those located above 10 m from the ground, whereas lower complexes were those positioned below 10 m. The length of each shoot in each complex was measured at DOY 218, when shoot elongation was completed (Table 1). A total of 91 shoots were taken into account and measured. Then, the leaves of the complexes were characterised in terms of morphology, leaf moisture, and chlorophyll traits. The performance at the complex level was monitored from June to September 2020, from Day of Year (DOY) 176 to DOY 260 for each tree. As the trees were tall (20–25 m), all the field measurements described were carried out by a tree climber.

2.2.1. Leaf Morphology

Three fully expanded leaves were randomly selected in each complex using destructive harvest during the survey at the beginning and end of the investigation period on DOY 176 and DOY 260. Leaf area was measured by selecting three leaves of different sizes (large, medium, and small) from a single complex at both time points. Immediately after being harvested, the leaves were weighed to prevent water loss and obtain the fresh mass (FM). Subsequently, leaves were immersed in water for 48 h to determine the fresh mass at full

https://doi.org/10.3390/f17020173

turgor (TM). After that, leaves were placed in an oven at a temperature of 75 °C until a constant dry mass (DM) was achieved. The leaf area (LA cm^2) was determined using Im [23]. Finally, the sclerophyll indices were calculated:

$$\text{Specific Leaf Area (SLA)} = \text{LA}/\text{DM}$$

$$\text{Leaf tissue density (D)} = (\text{DM}/\text{FM}) \times 1000$$

2.2.2. Leaf Moisture Indices

The leaf moisture indices were calculated using the same leaves and on the same date:

$$\text{Relative water content (RWC)} = (\text{FM} - \text{DM})/(\text{TM} - \text{DM}) \times 100$$

$$\text{Succulence (S)} = (\text{FM} - \text{DM})/\text{LA}$$

$$\text{Water content at saturation (WCS)} = (\text{TM} - \text{FM})/\text{DM}$$

$$\text{Water saturation deficit (WSD)} = (\text{TM} - \text{FM})/\text{TM} - \text{DM}) \times 100$$

2.2.3. Chlorophyll Traits

The total leaf chlorophyll content was estimated and chlorophyll fluorescence was measured on one fully expanded and exposed sun leaf from each shoot in each complex on the trees at DOY 176, 199, 218, 238, and 260. The chlorophyll content was estimated by using the SPAD (The Soil Plant Analysis Development) meter (Minolta-502), a hand-held chlorophyll meter that absorbs light wavelengths of 430–750 nm as it passes through leaves. Chlorophyll fluorescence was measured with a Hansatech Handy Plant Efficiency Analyzer (Handy PEA, Hansatech Instruments, King's Lynn, Norfolk, UK). Chlorophyll fluorescence was determined per complex on three leaves placed in the dark for 40 min using a clasp.

2.2.4. Statistical Analysis

Descriptive statistics, including means and standard errors, were calculated for all measured parameters. The normality of the data distribution was assessed using the Shapiro–Wilk test, and homogeneity of variances was evaluated with Levene's test. One-way ANOVA was conducted to examine the effects of shoot complexes height on leaf morphology, water-related indices, and physiological traits. When significant differences were detected, pairwise comparisons were performed using Tukey's post hoc test at a significance level of 0.05. All statistical analyses were carried out using OriginPro 8 (OriginLab Corporation, Northampton, UK).

3. Results

3.1. Leaf Morphology

The three trees showed distinct patterns in relation to height (Figure 1). Tree 1 displayed significant differences in SLA between the upper and lower complexes on DOY 260, with higher values in the lower complexes than in the upper ones. Tree 2 showed greater DM and LA in the lower complexes compared to the upper ones. Conversely, Tree 3 had greater DM and LA in the upper complexes than in the lower ones.

3.2. Leaf Moisture Indices

Regarding the leaf moisture indices, Tree 1 and Tree 2 showed higher RWC in the lower complexes than in the upper ones on DOY 260. On the same date, Tree 2 exhibited higher WSD values in the upper complexes than in the lower ones. No significant differences between lower and upper complexes were observed for Tree 3 (Figure 2).

https://doi.org/10.3390/f17020173

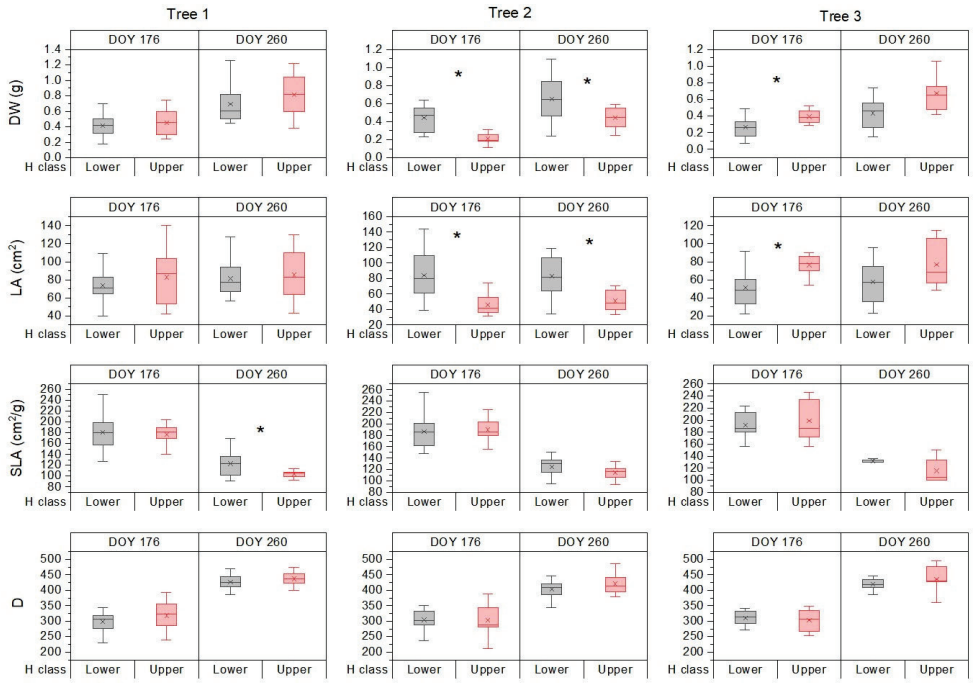


Figure 1. Box plots of dry mass (DM, g), leaf area (LA, cm^2), specific leaf area (SLA, cm^2/g), and leaf tissue density (D) for each tree on DOY 176 and DOY 260. Grey boxes indicate the lower complexes, and red boxes indicate the upper complexes. The box represents the interquartile range, containing the middle 50% of the data between the first and third quartiles; the whiskers show the minimum and maximum values that fall within 1.5 times the interquartile range from the quartiles; the horizontal line inside the box indicates the median (50th percentile) of the data; and the "x" symbol represents the mean value of the dataset. The effect of height was assessed using one-way ANOVA. Significance level of $p < 0.05$ (*) was used.

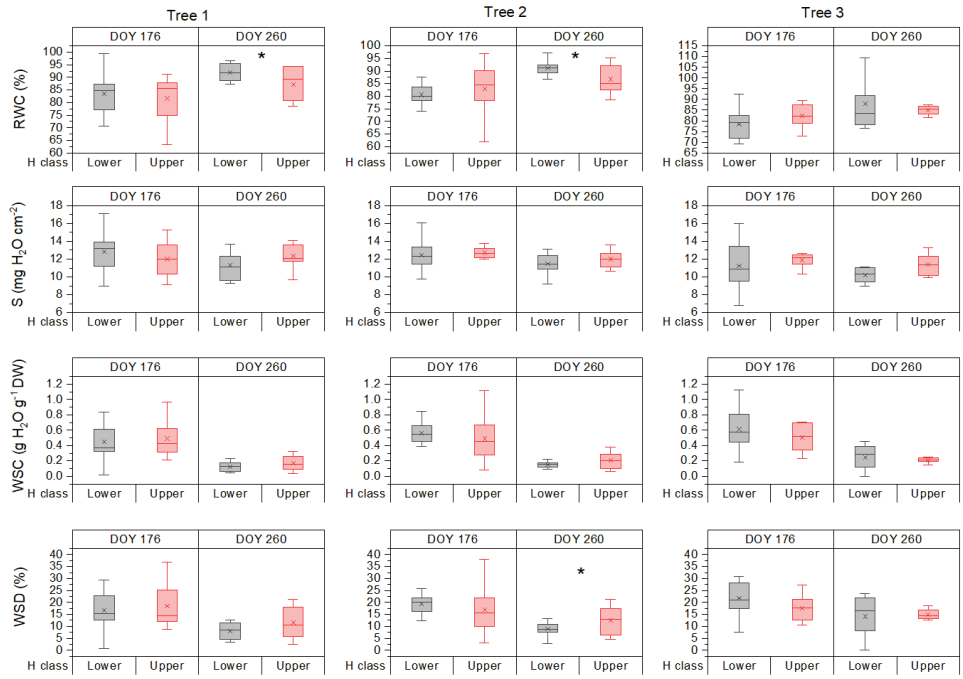


Figure 2. Effects of height class (lower vs. upper) on leaf moisture indices of three trees measured at two time points (DOY 176 and DOY 260). Boxplots represent relative water content (RWC%), succulence (S mg H_2O cm^2), water content at saturation (WCS g H_2O g^{-1} DM), and water saturation deficit (WSD %) for each tree. Grey boxes indicate the lower complexes, and red boxes indicate the upper complexes. The box represents the interquartile range, containing the middle 50% of the data

https://doi.org/10.3390/f17020173

between the first and third quartiles; the whiskers show the minimum and maximum values that fall within 1.5 times the interquartile range from the quartiles; the horizontal line inside the box indicates the median (50th percentile) of the data; and the "x" symbol represents the mean value of the dataset. The effect of height was assessed using one-way ANOVA. Significance was set at $p < 0.05$ (*).

3.3. Chlorophyll Traits

SPAD values were higher in the upper complexes on DOY 218 in Tree 1, whereas Fv/Fm was higher in the lower complexes on DOY 218 and 238 for Tree1 and Tree 3 (Figure 3). Tree 2 showed higher SPAD values in the lower complexes from DOY 176 to DOY 218, as well as a higher Pi_{ABS} on DOY 199, at the same canopy level (Figure 3).

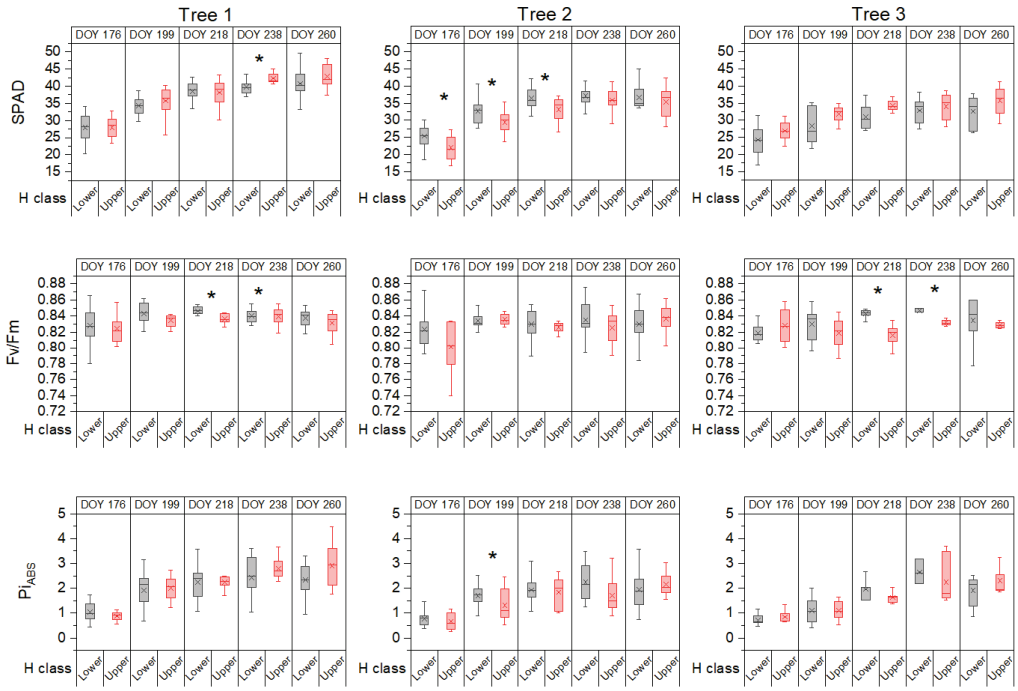


Figure 3. Effects of height class (lower vs. upper) on leaf physiology of three trees measured at five time points (DOY 176, 199, 218, 238, and 260). Boxplots represent chlorophyll index (SPAD), the ratio of the variable to maximum fluorescence (Fv/FM), and the performance index for photosynthesis (PiABS) for each tree. Grey boxes indicate the lower complexes, and red boxes indicate the upper complexes. The box represents the interquartile range, containing the middle 50% of the data between the first and third quartiles; the whiskers show the minimum and maximum values that fall within 1.5 times the interquartile range from the quartiles; the horizontal line inside the box indicates the median (50th percentile) of the data; and the "x" symbol represents the mean value of the dataset. The effect of height was assessed via one-way ANOVA. Significance level of $p < 0.05$ (*) was used.

4. Discussion

To our knowledge, this is the first study in which detailed morphological and physiological measurements of large, mature chestnut trees were performed directly within the canopy—made possible only through professional tree climbing—providing height-specific, in-canopy data that can offer practical, evidence-based guidance for pruning and crown management for traditional fruit orchards. The insights derived from this work are intended to provide practical, concrete, and applicable guidance for chestnut forest managers and pruning specialists. Overall, the measured morphological and physiological parameters did not reveal signs of stress in any of the investigated trees, as all values fell within ranges commonly associated with non-stressed conditions; this was expected given the climatic conditions in the study area during the year of investigation. The results indicated that the initial hypothesis was supported by Tree 2, partially supported by Tree

1, and not supported by Tree 3, highlighting the critical role of individual crown architecture in modulating hydraulic and physiological responses [24]. However, these results refer to non-stress environmental conditions and may differ under arid or drought-stress conditions. Tree 2, characterised by high bifurcation and the presence of lower clusters of replacement shoots along the main stem, showed a clear vertical gradient consistent across morphologies, water relations, and physiological traits. Lower-canopy epicormic shoots exhibited larger leaf area (LA) values, greater dry mass (DM), higher relative water content (RWC), and lower water saturation deficit (WSD), while upper-canopy shoots experienced hydraulic limitation and reduced physiological performance. Under drier or drought-stress conditions, the vertical gradient observed in Tree 2 may become more pronounced. Reduced soil water availability and increased evaporative demand could further exacerbate height-related hydraulic constraints, leading to stronger reductions in water status and physiological performance. Conversely, lower shoots, with shorter hydraulic pathways and closer connections to the main stem, may maintain comparatively better hydration and function. Such conditions are expected to reinforce the vertical differentiation observed under non-stress conditions. Tree 1, with low bifurcation and complexes restricted to the main branches, showed weaker vertical differentiation, with limited morphological differences (SLA) and a moderate advantage in water status (RWC) and photochemical efficiency (Fv/Fm) for lower-canopy shoots. This indicates a more homogeneous hydraulic architecture, in which height-related constraints are partially buffered. These results align with the concept that epicormic shoots may maintain relatively high hydraulic conductivity by connecting directly to lower-order axes with higher conductive capacity, such as the main stem, thereby shortening the length of the hydraulic path to the leaves [25]. However, our findings suggest there are different hydraulic strategies along the vertical profile of the tree: for Tree 2, shoot height from the ground clearly influenced shoot vigour. Increasing height still imposes hydraulic constraints, limiting leaf morphology, RWC, and chlorophyll traits, despite architectural compensation mechanisms. Tree 3, despite a similar degree of low bifurcation, did not show consistent vertical patterns in terms of morphology, water relations, or physiology, indicating an even more uniform water distribution within the crown, possibly due to differences in branch arrangement or hydraulic integration.

Therefore, if lower complexes show improved water relations, this will provide a strong rationale for developing pruning strategies aimed at lowering and re-structuring tree crowns to enhance tree vigour, improve canopy architecture, maximise fruit production, and increase chestnut trees' resilience to climate-change-induced drought. Overall, these initial results suggest that parties implementing pruning and canopy management strategies in chestnut orchards should consider tree-specific architectures: for trees resembling Tree 2, lowering the crown could enhance water relations and physiological performance, improving vigour and fruit production.

5. Conclusions

The investigation of morphological, physiological, and water-related traits of mature chestnut trees at different heights within the canopy necessarily requires the use of professional tree climbers. This methodological constraint inevitably limits both the number of measurements that can be performed and the number of individual trees that can be included, due to time and economic considerations. Therefore, in this study, the sample size of plant replicates was relatively small, constraining the extent to which the observed vertical patterns can be generalised or linked to specific architectural types. The observed patterns should be interpreted with caution when extrapolating them to broader populations or different environmental contexts. Therefore, the results should be regarded as exploratory and indicative of potential relationships between individual tree architectures

https://doi.org/10.3390/f17020173

and hydraulic or physiological function rather than as definitive evidence. Further investigations involving a larger number of trees within each architectural configuration and conducted across contrasting environmental conditions will be necessary to validate and extend these findings. Nevertheless, despite these constraints, the results provide valuable insights into within-canopy variability in adult sweet chestnut trees, a level of detail that can hardly be achieved in field studies of mature orchard systems. From a practical point of view, the observed height-related differences in hydraulic and physiological performance, particularly in relation to individual tree architecture, provide important insights regarding pruning strategies and canopy management in extensive chestnut orchards. Therefore, this study highlights that vertical variation in leaf morphology, water relations, and physiology is tree-specific, largely modulated by architectural traits, and provides a scientific rationale for adaptive pruning and canopy management strategies aimed at enhancing drought resilience and sustaining chestnut productivity under Mediterranean conditions.

Author Contributions: Conceptualization, C.C. and A.M.; methodology, C.C. and A.M.; formal analysis, investigation, and data curation, C.C., L.M., B.M. and A.M.; writing—original draft preparation, C.C. and L.M.; writing—review and editing, C.C., L.M., B.M. and A.M. All authors have read and agreed to the published version of the manuscript.

Funding: This research received no external funding.

Data Availability Statement: The data can be made available by the authors upon request.

Acknowledgments: The authors thank Fausto Palmerini (tree climber) for the field measurements.

Conflicts of Interest: The authors declare no conflicts of interest.

References

1. Chiriacò, M.V.; Samad, N.; Magnani, F.; Vianello, G.; Vittori-Antisari, L.; Mazzoli, I.; Ranieri, R.; Valentini, R. Ecophysiology of Mediterranean Chestnut (*Castanea sativa* Mill.) Forests: Effects of Pruning Studied through an Advanced IoT System. *Forests* **2024**, *15*, 1579. [CrossRef]
2. Conedera, M.; Tinner, W.; Krebs, P.; De Rigo, D.; Caudullo, G. *Castanea sativa* in Europe: Distribution, habitat, usage and threats. *Eur. Atlas For. Tree Species* **2016**, *78*, 79.
3. Gasparini, P.; Di Cosmo, L.; Floris, A.; De Laurentis, D. *Italian National Forest Inventory—Methods and Results of the Third Survey: Inventario Nazionale Delle Foreste e dei Serbatoi Forestali di Carbonio—Metodi e Risultati Della Terza Indagine*; Springer Nature: Cham, Switzerland, 2022.
4. Conedera, M.; Manetti, M.C.; Giudici, F.; Amorini, E. Distribution and Economic Potential of the Sweet Chestnut (*Castanea Sativa* Mill.) in Europe. *Ecol. Mediterr.* **2004**, *30*, 179–193. [CrossRef]
5. Perulli, G.D.; Boini, A.; Bresilla, K.; Morandi, B.; Grappadelli, L.C.; Manfrini, L. Growth Analysis of Sweet Chestnut Burr in Two Seasons with Differing Weather Conditions. *Italus Hortus* **2020**, *27*, 31–39. [CrossRef]
6. Freitas, T.R.; Santos, J.A.; Silva, A.P.; Fraga, H. Influence of Climate Change on Chestnut Trees: A Review. *Plants* **2021**, *10*, 1463, Correction in *Plants* **2022**, *11*, 1518. https://doi.org/10.3390/plants11111518. [CrossRef] [PubMed]
7. Conedera, M.; Krebs, P.; Gehring, E.; Wunder, J.; Hülsmann, L.; Abegg, M.; Maringer, J. How Future-Proof Is Sweet Chestnut (*Castanea sativa*) in a Global Change Context? *For. Ecol. Manag.* **2021**, *494*, 119320. [CrossRef]
8. Weise, K.; van der Maaten-Theunissen, M.; Seitz, G.; Keller, T.; van der Maaten, E. Future Suitability of Sweet Chestnut (*Castanea sativa* Mill.) Is Limited by Susceptibility to Drought. *Dendrochronologia* **2025**, *90*, 126299. [CrossRef]
9. Menéndez-Miguélez, M.; Álvarez-Álvarez, P.; Majada, J.; Canga, E. Effects of Soil Nutrients and Environmental Factors on Site Productivity in *Castanea sativa* Mill. Coppice Stands in NW Spain. *New For.* **2015**, *46*, 217–233. [CrossRef]
10. Zhang, C.; Moutinho-Pereira, J.M.; Correia, C.; Coutinho, J.; Gonçalves, A.; Guedes, A.; Gomes-Laranjo, J. Foliar Application of Sili-K® Increases Chestnut (*Castanea* Spp.) Growth and Photosynthesis, Simultaneously Increasing Susceptibility to Water Deficit. *Plant Soil* **2013**, *365*, 211–225. [CrossRef]
11. Conedera, M.; Barthold, F.; Torriani, D.; Pezzatti, G.B. Drought Sensitivity of *Castanea sativa*: Case Study of Summer 2003 in the Southern Alps. In *I Europeand Congress on Chestnut-Castanea*; Bounous, G., Beccaro, G.L., Eds.; ISHS: Brussels, Belgium, 2009.
12. Intergovernmental Panel on Climate Change (IPCC). *Climate Change 2022—Impacts, Adaptation and Vulnerability*; Cambridge University Press: Cambridge, UK, 2023. [CrossRef]

13. Tagliaferri, G.; Di Lonardo, S. Chestnut Management Practice as Tool for Natural and Cultural Landscaping. In *Biocultural Diversity in Europe*; Agnoletti, M., Emanueli, F., Eds.; Springer International Publishing: Cham, Switzerland, 2016; pp. 353–367. [CrossRef]
14. Martins, A.; Raimundo, F.; Borges, O.; Linhares, I.; Sousa, V.; Coutinho, J.P.; Gomes-Laranjo, J.; Madeira, M. Effects of Soil Management Practices and Irrigation on Plant Water Relations and Productivity of Chestnut Stands under Mediterranean Conditions. *Plant Soil.* **2010**, *327*, 57–70. [CrossRef]
15. Perulli, G.D.; Boini, A.; Morandi, B.; Grappadelli, L.C.; Manfrini, L. Irrigation Improves Tree Physiological Performances and Nut Quality in Sweet Chestnut. *Italus Hortus* **2022**, *29*, 156–169. [CrossRef]
16. Rodrigues, M.Â.; Grade, V.; Barroso, V.; Pereira, A.; Cassol, L.C.; Arrobas, M. Chestnut Response to Organo-Mineral and Controlled-Release Fertilizers in Rainfed Growing Conditions. *J. Soil. Sci. Plant Nutr.* **2020**, *20*, 380–391. [CrossRef]
17. Marques, T.; Ferreira-Pinto, A.; Fevereiro, P.; Pinto, T.; Gomes-Laranjo, J. Current Biological Insights of *Castanea sativa* Mill. to Improve Crop Sustainability to Climate Change. *Plants* **2025**, *14*, 335. [CrossRef] [PubMed]
18. Pezzi, G.; Buldrini, F.; Conedera, M.; Maresi, G.; Marzocchi, G.; Ferretti, F. Perception and Management of the Understorey Vegetation by Chestnut Growers: The Study Case of the Chestnut Orchards in the Bologna and Modena Apennines (Italy). *Rend. Lincei* **2025**, *36*, 697–712. [CrossRef]
19. Ryan, M.G.; Yoder, B.J. Hydraulic Limits to Tree Height and Tree Growth. *Bioscience* **1997**, *47*, 235–242. [CrossRef]
20. Cruiziat, P.; Cochard, H.; Améglio, T. Hydraulic Architecture of Trees: Main Concepts and Results. *Ann. For. Sci.* **2002**, *59*, 723–752. [CrossRef]
21. Becker, P.; Meinzer, F.C.; Wullschleger, S.D. Hydraulic Limitation of Tree Height: A Critique. *Funct. Ecol.* **2000**, *14*, 4–11. [CrossRef]
22. Fink, S. *Pathological and Regenerative Plant Anatomy*; Borntraeger: Sulzbach an der Murr, Germany, 1999.
23. Schneider, C.A.; Rasband, W.S.; Eliceiri, K.W. NIH Image to ImageJ: 25 Years of Image Analysis. *Nat. Methods* **2012**, *9*, 671–675. [CrossRef] [PubMed]
24. Gehring, E.; Pezzatti, G.B.; Krebs, P.; Mazzoleni, S.; Conedera, M. On the Applicability of the Pipe Model Theory on the Chestnut Tree (*Castanea sativa* Mill.). *Trees Struct. Funct.* **2015**, *29*, 321–332. [CrossRef]
25. Ishii, H.T.; Ford, E.D.; Kennedy, M.C. Physiological and Ecological Implications of Adaptive Reiteration as a Mechanism for Crown Maintenance and Longevity. *Tree Physiol.* **2007**, *27*, 455–462. [CrossRef] [PubMed]

Disclaimer/Publisher's Note: The statements, opinions and data contained in all publications are solely those of the individual author(s) and contributor(s) and not of MDPI and/or the editor(s). MDPI and/or the editor(s) disclaim responsibility for any injury to people or property resulting from any ideas, methods, instructions or products referred to in the content.

forests

MDPI

Article

Organ-Specific Gene Expression and Metabolite Accumulation in *Fargesia rufa* in Response to an Altitudinal Gradient

Qi Lin [1], Wanju Feng [1], Man Tang [2], Mengqiu Chen [2], Xun Song [2], Lin Wu [1], Xin Zhao [2,*] and Zhijian Long [2,*]

[1] Sichuan Academy of Giant Panda, Chengdu 610000, China; linjingxi07@126.com (Q.L.)
[2] College of Life Science and Agri-Forestry, Southwest University of Science and Technology, Mianyang 621000, China
* Correspondence: zhaoxin9@swust.edu.cn (X.Z.); long20053182@swust.edu.cn (Z.L.)

Abstract

Fargesia rufa, one of the main food bamboo species for giant pandas, exhibits significant changes in nutritional composition with altitudinal gradient. However, the molecular mechanisms underlying this adaptation and its impact on the foraging behavior of giant pandas remain unclear. In this study, metabolomic and transcriptomic analyses were integrated to compare gene expression and metabolite profiles in leaves and rhizomes of *F. rufa* collected from 1000 m and 2000 m altitudes. With increasing altitude, 710 metabolites were up-regulated and 1032 were down-regulated in the leaves of *F. rufa*, whereas 684 metabolites were up-regulated and 1342 were down-regulated in the rhizomes; only 629 differential metabolites were shared between the two organs. Further analyses revealed that *F. rufa* responds to altitudinal changes through organ-specific metabolic reprogramming: leaves adopt a "metabolic conservation" strategy, downregulating the majority of flavonoid and phenylpropanoid metabolites, while rhizomes take an "active storage" strategy, significantly enhancing secondary metabolite synthesis and starch accumulation. This functional differentiation is consistent with the biological roles of the organs: the metabolic simplification of leaves may enhance the palatability of high-altitude leaves, while the nutritional reserves in rhizomes support bamboo shoot emergence. This study reveals the molecular mechanisms of bamboo's altitudinal adaptation at the organ level, clarifies the intrinsic link between plant metabolism and animal diet, and provides a theoretical basis for giant panda habitat conservation.

Keywords: *Fargesia rufa*; altitudinal gradient; gene expression; metabolite accumulation; metabolomic and transcriptomic

1. Introduction

Fargesia rufa, as one of the main food bamboo species for giant pandas, is widely distributed in the mountainous areas surrounding the Sichuan Basin [1]. As a typical shallow-rooted, sympodial bamboo species, *F. rufa* possesses a relatively shallow root system, exhibiting high sensitivity to environmental factors such as soil moisture, temperature, and light. Consequently, its growth and development, population regeneration, and physiological metabolism are highly susceptible to micro-environmental changes within its habitat [2,3]. Notably, the sprouting pattern of *F. rufa* shows a distinct altitudinal gradient effect, that is, it sprouts successively from low to high altitudes. Furthermore, distinct differences exist in shoot growth rates, lignification processes, and nutrient accumulation across different altitudinal zones [4]. This unique ecological characteristic provides a natural and

ideal study system for systematically investigating the regulatory mechanisms of altitudinal gradients—which integrate multiple environmental factors such as low temperature, intense UV radiation, atmospheric pressure, and diurnal temperature fluctuations—on the bamboo metabolome and transcriptome [4,5].

The giant panda, a rare and endangered species endemic to China and a flagship species for global biodiversity conservation, has developed a highly specialized bamboo-dependent diet over its long evolutionary history, with bamboo constituting up to 99% of its natural diet [6]. This unique dietary specialization is not only a key adaptive strategy to its ecological environment but also tightly binds its survival status to the distribution, quality, and dynamic changes in bamboo resources. In its natural habitat, the giant panda exhibits refined selective foraging behavior: on one hand, it switches between bamboo species or different organs (shoots, leaves, culms) of the same species according to seasonal shifts; on the other hand, to track high-quality bamboo resources, it undertakes regular vertical migrations along altitudinal gradients for foraging, forming a distinctive ecological adaptation pattern [7,8]. Field telemetry observation data further confirm that the giant panda's feeding preferences show marked seasonal characteristics—prioritizing nutrient-rich shoots of different bamboo species in spring and summer, shifting to nutritionally stable leaves in autumn, and relying on fiber-rich culms for energy maintenance in winter. This series of feeding strategy adjustments is highly synchronized with changes in bamboo growth status induced by altitudinal variation [9]. In-depth analysis suggests that the essence of this specific foraging behavior is the giant panda's active adaptation to differences in the intrinsic nutritional components (such as proteins, soluble sugars) and metabolites (e.g., secondary metabolites) of bamboo driven by environmental changes, indicating a close ecological linkage between the two [10,11]. A metabolomics study based on 12 bamboo species revealed that high-altitude environments significantly increased the accumulation of flavonoids, while low-altitude environments increased the content of cinnamic acid derivatives, especially chlorogenic acids (CQAs) [12]. These metabolic changes may directly affect the nutritional value and palatability of bamboo, thereby guiding the feeding choices of giant pandas [13,14]. Previous studies have primarily focused on physiological responses and single-organ analyses. However, current research predominantly focuses on the overall physiological responses of bamboo or metabolic analyses of single organs (such as leaves). There remains a lack of systematic elucidation regarding the organ-specific regulatory mechanisms underlying altitude adaptation—particularly the synergistic and differential regulation between functionally distinct organs such as the photosynthetic organs (leaves) and the nutrient storage/propagation organs (rhizomes)—and the related molecular mechanisms are still unclear.

The impact of environmental factors on bamboo metabolism may be closely related to gene expression regulation [15,16]. Studies in *Phyllostachys heterocycla* var. pubescens have found that environmental factors regulate the biosynthesis of secondary cell walls by affecting the expression of key genes (such PAL, C4H) in the phenylpropanoid metabolic pathway [17]. Altitude changes, as comprehensive environmental alterations including low temperature, strong UV radiation, low oxygen, and temperature fluctuations, cause bamboo to precisely alter its metabolism to adapt to these changes [18,19]. For example, altitude changes affect flavonoid biosynthesis and plant hormone signal transduction in *Zanthoxylum planispinum* (*Z. planispinum*) var. *dintanensis*, with higher altitudes leading to more terpenoids and lower altitudes to more flavonoids and polyphenols [20]. Furthermore, studies have indicated that increasing altitude promotes the accumulation of soluble sugars (glucose, fructose, sucrose) within bamboo while reducing starch content. This shift in carbohydrate metabolism is likely an important strategy for bamboo to cope with low-temperature stress and maintain cellular osmotic pressure [21]. Transcriptome analysis

https://doi.org/10.3390/f17020167

of plants at different altitudes on the Tibetan Plateau shows that the phenylpropanoid biosynthesis pathway is significantly enriched across all altitudinal gradients, accompanied by the upregulation of secondary metabolites such as flavonoids and alkaloids, indicating that altitude changes activate this pathway to cope with strong UV radiation and low-temperature stress [22]. Although existing research has partially uncovered the patterns of how altitude affects bamboo metabolism and gene expression, the precise correlative mechanisms between gene expression patterns and metabolite synthesis in *F. rufa*—a core staple bamboo for giant pandas—across different altitudinal gradients remain unclear. There is a particular lack of systematic, multi-organ correlative analyses that integrate transcriptomic and metabolomic multi-omics data, making it difficult to comprehensively decipher its molecular regulatory network for altitude adaptation.

Based on this, the present study utilized the metabolomics and transcriptomics data of *F. rufa* leaves and rhizomes at altitudes of 1000 m and 2000 m to thoroughly elucidate the characteristics of gene expression changes in *F. rufa* caused by altitudinal differences; the impact of altitude on the accumulation of primary and secondary metabolites in *F. rufa*; and the relationships between metabolites and gene expression. This study will reveal the molecular mechanisms underlying the quality formation of the staple bamboo for giant pandas, providing a theoretical basis for the genetic breeding, habitat protection, and food resource management of the main food bamboo of giant pandas.

2. Materials and Methods

2.1. Plant Materials

F. rufa samples were collected from two distinct altitudes in the Tangjiahe Nature Reserve, Qingchuan County, Sichuan Province: 1000 m (the temperature at the time of sampling was 26 °C) and 2000 m (the temperature at the time of sampling was 20.8 °C) above sea level (a.s.l.). Sampling was carried out in mid-August 2025, the average air temperature within the region this month was 20 °C, the soil temperature at 10 cm depth was 17 °C, and the soil moisture content was approximately 65% (The mean annual temperature of the region is 16 °C, the average relative humidity is 72%, the annual frost-free period averages 243 days, and the mean annual precipitation is 1021.7 mm). Both bamboo leaves and rhizomes were sampled at each altitude, during sampling, individual samples were separated by at least 10 m; rhizomes from the same bamboo clump were collected 10–20 cm outward from the base of the culm to avoid resampling the same ramet. A total of 20 samples were collected, with five biological replicates for each tissue type at each altitude, ensuring a comprehensive representation of the natural variation. Samples were immediately frozen in liquid nitrogen and stored at −80 °C until further processing.

2.2. RT-qPCR

Total RNA was extracted from bamboo leaves and rhizomes using the TRIzol reagent according to the manufacturer's instructions, through sample lysis, phase separation, RNA precipitation, washing, and resuspension steps, followed by quality assessment for reverse transcription. cDNA synthesis and subsequent quantitation reverse transcription-PCR (RT-qPCR) were performed following the aforementioned protocol [23]. Taking UBQ (*TRINITY_DN1489_c0_g1*) as the internal reference, primers for the validation genes were designed with Primer 5.0. All samples were analyzed in three biological replicates. Gene expression in different leaves and rhizomes of *F. rufa* was quantified by RT-qPCR on the Applied Biosystems 7500 Real-Time PCR System. Target genes and their specific primers are listed in Supplementary Table S3. Relative expression levels were calculated using the $2^{(-\Delta\Delta Ct)}$ method with UBQ as the internal control [24].

https://doi.org/10.3390/f17020167

2.3. RNA Sequencing and Data Analysis

Total RNA was extracted from leaf and rhizome samples of *F. rufa* collected at 1000 m and 2000 m a.s.l. with the RNAprep Pure Plant Kit (Tiangen, Beijing, China) following the manufacturer's instructions; three biological replicates were prepared for each group. RNA concentration and purity were checked with a NanoDrop-2000 spectrophotometer, integrity was verified by 1% agarose-gel electrophoresis, and RQN (RNA Quality Number) values were determined on an Agilent 5300 Fragment Analyzer (Agilent Technologies, Santa Clara, CA, USA). For library construction, $\geq$1 μg of RNA with a concentration $\geq$ 30 ng μL^{-1}, RQN > 6.5 and $OD_{260/280}$ between 1.8 and 2.2 was required. Strand-specific RNA-seq libraries were prepared and sequenced on an Illumina platform by Majorbio Bio-Pharm Technology Co., Ltd. (Shanghai, China).

After sequencing, raw reads were filtered to remove adapters, poly-N stretches and low-quality sequences; all downstream analyses were based on the resulting high-quality clean data. Trim low-quality bases (Phred < 20) from the 3′ end; if any remaining base has a quality value < 10, discard the entire read. Remove reads with >10% ambiguous (N) bases. Discard sequences shorter than 20 bp after adapter clipping and quality trimming. Base-composition and quality-distribution statistics were calculated for every cycle to provide an overall view of sequencing and library quality. Clean reads from all samples were pooled and de novo assembled with Trinity (https://github.com/trinityrnaseq/trinityrnaseq/wiki, accessed on 16 October 2025). The assembly pipeline integrates three independent modules that process and splice large RNA-seq data sets; the primary contigs were subsequently filtered, optimized and re-evaluated. Finally, all unique transcripts were aligned against six public databases (NR, Swiss-Prot, Pfam, COG, GO and KEGG) to obtain comprehensive functional annotations, and the annotation results for each database were summarized.

To pinpoint the genes that are differentially expressed between distinct sample sets or groups, the abundance of each transcript was gauged utilizing the transcripts per million (TPM) metric. The RSEM tool [25] was employed to ascertain the levels of gene expression. The DESeq2 [26] and DEGseq methodologies [27] were subsequently applied to discern genes with notable expression disparities. Genes exhibiting a log2 fold change magnitude of 1 or greater, coupled with a false discovery rate (FDR) below 0.05 when using DESeq2, or beneath 0.001 for DEGseq, were categorized as significantly differentially expressed. Moreover, to elucidate the biological significance of these findings, functional enrichment analyses were conducted. These analyses, incorporating both Gene Ontology (GO) and Kyoto Encyclopedia of Genes and Genomes (KEGG) annotations, aimed to highlight the GO terms and metabolic pathways that were significantly overrepresented among the differentially expressed genes, with a Bonferroni-adjusted *p*-value threshold of less than 0.05 relative to the entire transcriptome. The GO enrichment analysis was executed using the Goatools package, while the KEGG pathway analysis was facilitated by Python 3.13.2's scipy library.

2.4. Metabolite Measurement and Analysis

The leaves and rhizomes of *F. rufa* were ground in liquid nitrogen and subsequently immersed in the extraction solvent for the extraction process. The metabolic profiling was performed using an ultra-performance liquid chromatography-tandem mass spectrometry system (UPLC-MS), and metabolites were identified based on the information from tandem mass spectrometry. The LC-MS analysis was performed on a Thermo Scientific UHPLC-Q Exactive HF-X system (Thermo Scientific, Waltham, MA, USA), consisting of an ultra-high-performance liquid chromatograph coupled to a Fourier-transform mass spectrometer. C18 column chromatographic conditions: ACQUITY UPLC BEH C18 column

https://doi.org/10.3390/f17020167

(100 mm × 2.1 mm i.d., 1.7 μm; Waters, Milford, MA, USA); mobile phase A: 2% acetonitrile in water (0.1% formic acid); mobile phase B: acetonitrile (0.1% formic acid); injection volume: 1 μL; column temperature: 40 °C. MS conditions: samples were ionized by electrospray and mass signals were acquired in both positive- and negative-ion modes. The acquired mass spectrometry data were subjected to principal component analysis (PCA) and sample correlation analysis to evaluate the reproducibility and degree of variation among samples. Following Worley & Powers (2016), we validated the use of VIP > 1 and $p < 0.05$ and further imposed a $|FC| \geq 2$ cut-off to highlight metabolites with biologically relevant changes. Orthogonal partial least squares discriminant analysis (OPLS-DA) was employed to analyze the metabolites and identify significantly different metabolites. The KEGG database was utilized for functional analysis of the differential metabolites to determine the specific biological pathways involved.

2.5. Statistical Analysis

Metabolomic analyses were carried out with five biological replicates; all other experiments were performed using three independent biological replicates. The presented values represent the mean ± standard error (S.E.) of at least three replicates. One-way analysis of variance (ANOVA) was performed to evaluate overall differences among groups. When the ANOVA revealed a significant effect ($p < 0.05$), Tukey's Honestly Significant Difference (HSD) post hoc test was applied for pairwise comparisons. Adjusted p-values < 0.05 were considered statistically significant. All analyses were conducted using GraphPad Prism 9.0.

3. Results

3.1. Metabolic Phenotype of F. rufa in Response to Altitude

To investigate how altitude shapes the metabolic composition of *F. rufa*—a key food source for giant pandas—we performed untargeted metabolomic profiling on leaves and rhizomes collected from 1000 m and 2000 m elevations. The rhizome, being the primary storage organ responsible for shoot germination (Supplementary Figure S1), was included to assess below-ground metabolic adaptation. Liquid chromatography-mass spectrometry (LC-MS) detected 2396 annotated secondary metabolites across all samples. Flavonoids constituted the most abundant class terpenoids (730 compounds, 30.45%), (704 compounds, 29.37%), followed by phenolic acids and derivatives (9.8%), and coumarins/lignans (3.67%). Minor yet ecologically relevant classes included tannins (0.71%), stilbenes (1.13%), and alkaloids (1.71%) (Figure 1A). The predominance of flavonoids and phenolic acids aligns with the high UV-B exposure and herbivore pressure typical of montane bamboos and establishes the first quantitative inventory of defensive chemistry in *F. rufa*.

Principal component analysis (PCA) of the metabolome clearly separated samples into four distinct groups: L-1000 m, L-2000 m, Rh-1000 m, and Rh-2000 m (Figure 1B). The first two principal components explained 62.7% and 8.36% of the total variance, respectively. Separation along PC1 was driven primarily by altitude, indicating that elevation exerts a stronger influence on metabolic profile than tissue type. Leaves clustered more tightly than rhizomes, suggesting that aerial organs maintain a more conserved metabolic architecture, whereas below-ground organs exhibit higher plasticity. A sample correlation heatmap confirmed strong reproducibility within biological replicates and clear metabolic divergence between altitude-organ groups (Figure 1C). Venn diagram analysis further identified a core set of 3951 metabolites common to all groups, alongside numerous altitude- and organ-specific metabolites (such as 28 unique to L-1000 m; 4198 shared between Rh-2000 m and Rh-1000 m) (Figure 1D). This pattern supports a hierarchical regulatory model in which altitude is the primary factor shaping metabolism, followed by tissue-specific modulation.

https://doi.org/10.3390/f17020167

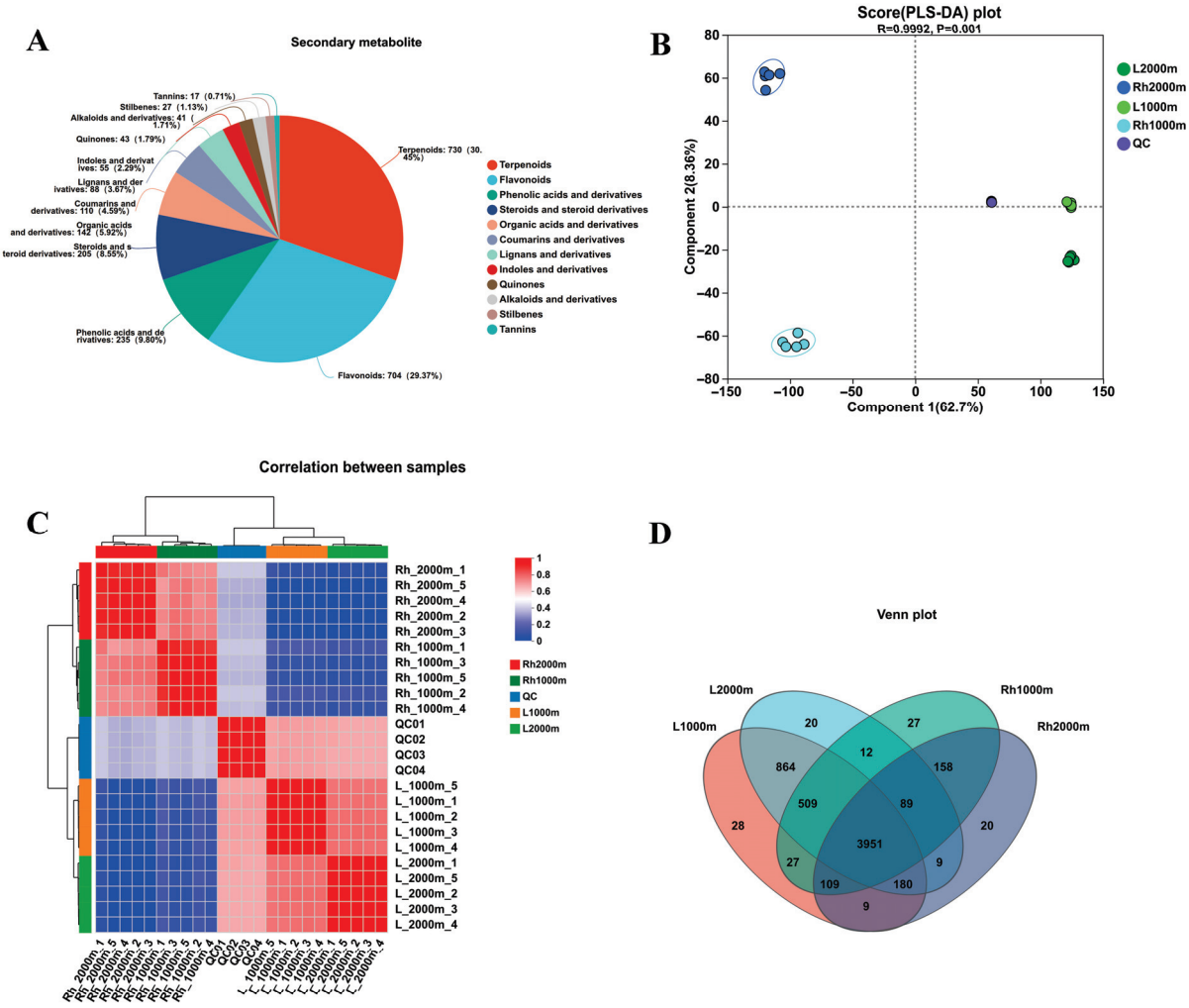


Figure 1. Metabolomic Analysis of *F. rufa* Leaves and Rhizomes at Altitudes of 1000 m and 2000 m. (**A**) Classification of secondary metabolites in bamboo leaves and rhizomes. The metabolites are displayed in descending order based on their quantities in the selected classifications (plant compound classification, primary plant classification, and secondary plant classification). The characteristics of the metabolites in each classification and their respective percentages are shown. In the pie charts, different colors represent different classifications, and the areas indicate the relative proportions of metabolites in each classification. (**B**) The composite PLS-DA score plot of the metabolomics data of *F. rufa* leaves and rhizomes. (**C**) The heatmap analysis of the correlation between samples indicates the degree of variation in the composition and abundance of metabolites among samples. The closer the correlation is to 1, the higher the similarity in metabolic composition and abundance between samples. (**D**) The Venn diagram analysis of the metabolomics data of bamboo leaves and rhizomes.

Collectively, these results indicate that *F. rufa* undergoes extensive metabolic reorganization in response to altitude, with rhizomes—particularly at high elevation—shifting resource allocation toward flavonoid and stilbene biosynthesis. This adjustment may enhance oxidative stress tolerance while concurrently altering tissue palatability, potentially influencing foraging behavior of giant pandas during their seasonal vertical migration.

3.2. Analysis of Differentially Expressed Metabolites in Bamboo Leaves and Rhizomes at Altitudes of 1000 m and 2000 m

To identify metabolites responsive to altitudinal variation, we conducted a differential abundance analysis comparing leaves and rhizomes from 1000 m and 2000 m. Metabolites with a variable importance in projection (VIP) > 1.0 and a *p*-value < 0.05 were considered significantly altered; fold-change (FC) thresholds were not pre-applied to capture broad

trends. Volcano plots revealed a pronounced bidirectional shift in metabolite abundance in both leaves and rhizomes with increasing altitude (Figure 2A,B). Quantitative analysis showed that in leaves (L2000 m vs. L1000 m), 710 metabolites were upregulated and 1032 were downregulated. In rhizomes (Rh2000 m vs. Rh1000 m), 684 metabolites increased and 1342 decreased (Figure 2C). The greater number of altered metabolites in rhizomes suggests a higher degree of metabolic reprogramming below ground, consistent with the role of rhizomes as integrated nutrient reservoirs and stress-responsive organs.

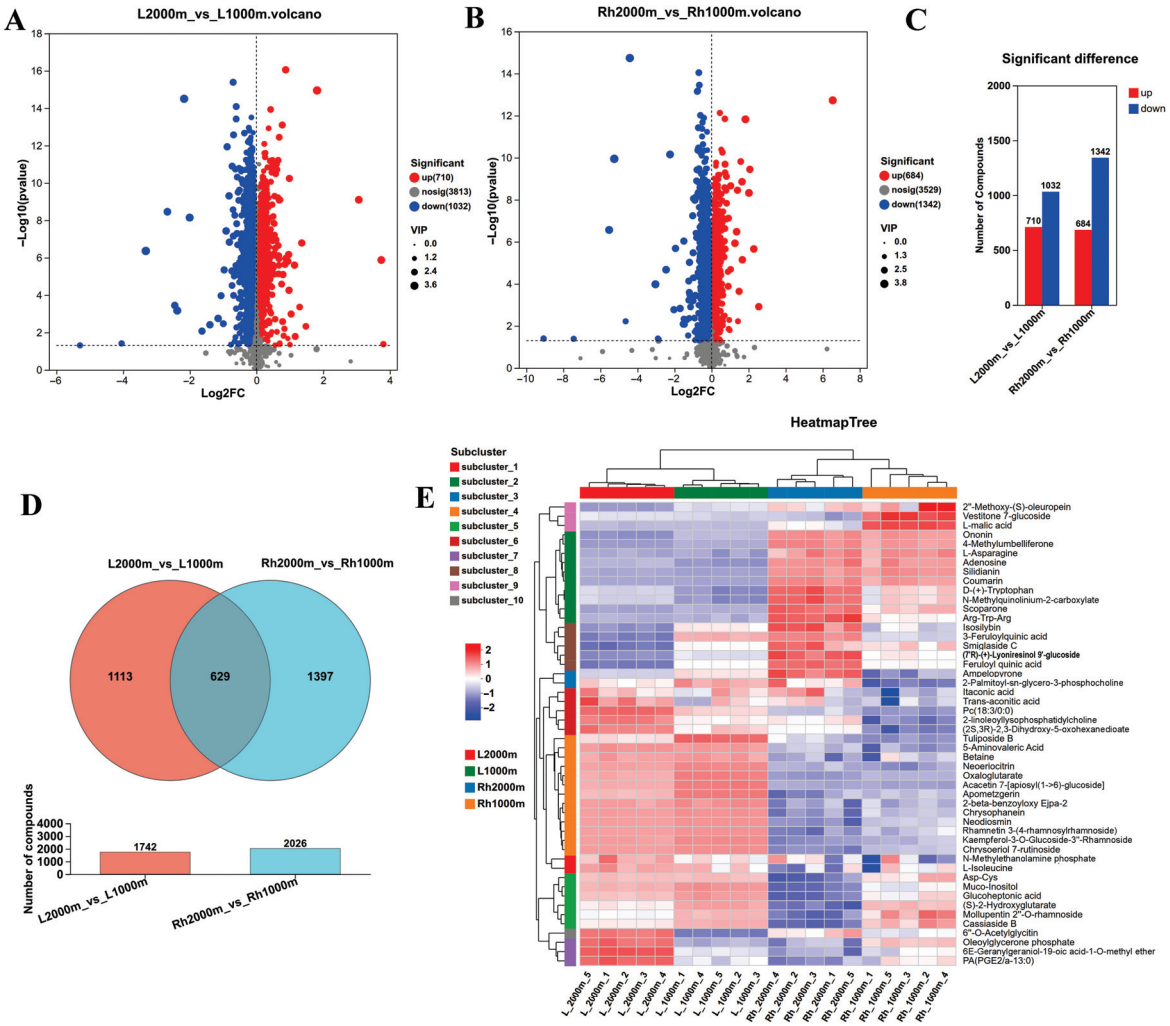


Figure 2. Analysis of differentially expressed metabolites in bamboo leaves and rhizomes at 2000 m and 1000 m. (**A**) Volcano plot of differential metabolites in bamboo leaves at different altitudes. (**B**) Volcano plot of differential metabolites in bamboo rhizomes at different altitudes. (**C**) Statistics of differentially expressed metabolites in bamboo leaves and rhizomes at different altitudes. (**D**) Venn diagram of differentially expressed metabolites in bamboo leaves and rhizomes at different altitudes. (**E**) Cluster analysis of differentially expressed metabolites in bamboo leaves and rhizomes at different altitudes. Each column in the figure represents a sample, and each row represents a metabolite. The colors in the figure indicate the relative expression levels of metabolites in the respective groups of samples. For specific trends in expression levels, please refer to the numerical annotations below the color bar in the lower right corner. The dendrogram on the left represents the clustering of metabolites, while the names of the metabolites are listed on the right. The closer the branches of two metabolites are, the more similar their expression levels are. The dendrogram above represents the clustering of samples, with the names of the samples listed below. The closer the branches of two samples are, the more similar the expression patterns of all metabolites in these samples are, that is, the more similar the trends in metabolite expression levels are.

https://doi.org/10.3390/f17020167

Venn analysis further highlighted the organ specificity of these responses (Figure 2D). While 629 differentially expressed metabolites were common to both leaves and rhizomes, 1113 were unique to leaves and 1397 were unique to rhizomes. This indicates that altitude regulates a core set of metabolic adaptations shared across tissues, superimposed upon extensive organ-specific adjustments. Together, these data underscore that altitude-driven metabolic remodeling in *F. rufa* is both profound and organ-preferential, with rhizomes undergoing particularly extensive reconfiguration—a pattern that is likely tied to their dual role in storage and stress tolerance.

A hierarchical clustering heatmap of the 50 most significantly altered metabolites further illustrated the structured reorganization of the *F. rufa* metabolome along the altitudinal gradient (Figure 2E). Metabolites with related biological functions or shared biosynthetic pathways clustered into distinct branches, indicating co-regulated metabolic modules. For instance, flavonoids—including neodiosmin, chrysoeriol 7-rutinoside, and alpha-hydrojuglone-4-glucoside—formed a coherent cluster, as did amino acid derivatives such as D-(+)-tryptophan and L-phenylalanine. Samples clustered primarily by altitude and secondarily by organ type. Leaves collected at 2000 m (L2000 m) grouped separately from their low-altitude counterparts (L1000 m), and a similar clear division was observed between rhizome samples from different elevations (Rh2000 m vs. Rh1000 m). This clustering pattern reinforces that altitude exerts a stronger organizing influence on metabolic variation than tissue identity, highlighting the specificity of altitudinal regulation in shaping the overall metabolomic landscape.

3.3. KEGG Pathway Enrichment Highlights Organ-Specific Metabolic Reprogramming

KEGG pathway enrichment analysis of altitude-responsive metabolites revealed distinct metabolic priorities in leaves and rhizomes of *F. rufa* (Figure 3A,B). In both organs, secondary metabolic pathways were prominently enriched, including "Phenylpropanoid biosynthesis," "Flavonoid biosynthesis," and "Flavone and flavonol biosynthesis." In leaves, significant enrichment was also observed in primary metabolic pathways such as "Phenylalanine, tyrosine and tryptophan biosynthesis" and "Starch and sucrose metabolism," suggesting an altitude-mediated trade-off between nutritional provision and stress adaptation. In contrast, rhizomes showed marked enrichment in pathways related to lipid-based signaling and defense, including "α-Linolenic acid metabolism," "Linoleic acid metabolism," and "Stilbenoid, diarylheptanoid and gingerol biosynthesis."

Corresponding to these pathway signatures, targeted analysis of key metabolites showed pronounced organ-specific accumulation patterns (Figure 3C). In leaves, the majority of phenylpropanoid and flavonoid derivatives, along with sucrose-related metabolites, were significantly lower at 2000 m compared to 1000 m. Only a limited set of stress-linked compounds—such as (3S)-3-Hydroxy-cyclocitral, specific iron-chelating deoxymugineic acids, the phytoalexin (−)-medicarpin-3-O-glucoside, and hydroxycinnamic acid amides (coumaroyl-agmatine and feruloyl-agmatine)—were upregulated. Conversely, rhizomes at high altitude exhibited a coordinated upregulation of the linoleic acid pathway (such as lecithin, crepenynate, arachidonate) and a broad suite of phenylpropanoid and flavonoid compounds (such as rutin, luteoloside, caffeic acid, caffeoyl quinic acid). This was accompanied by a metabolic shift from soluble monosaccharides toward significant starch accumulation. Collectively, these metabolite profiles reflect a functional division that supports both plant adaptation and consumer foraging: leaves reduce investment in generalized chemical defense at high altitude, potentially increasing their palatability to migrating giant pandas, whereas rhizomes enhance storage and stress-resilient compound biosynthesis, securing perennial survival and shoot vigor. This integrated response illustrates how metabolic

https://doi.org/10.3390/f17020167

plasticity in *F. rufa* supports ecological coexistence with a specialized herbivore through spatially structured resource allocation.

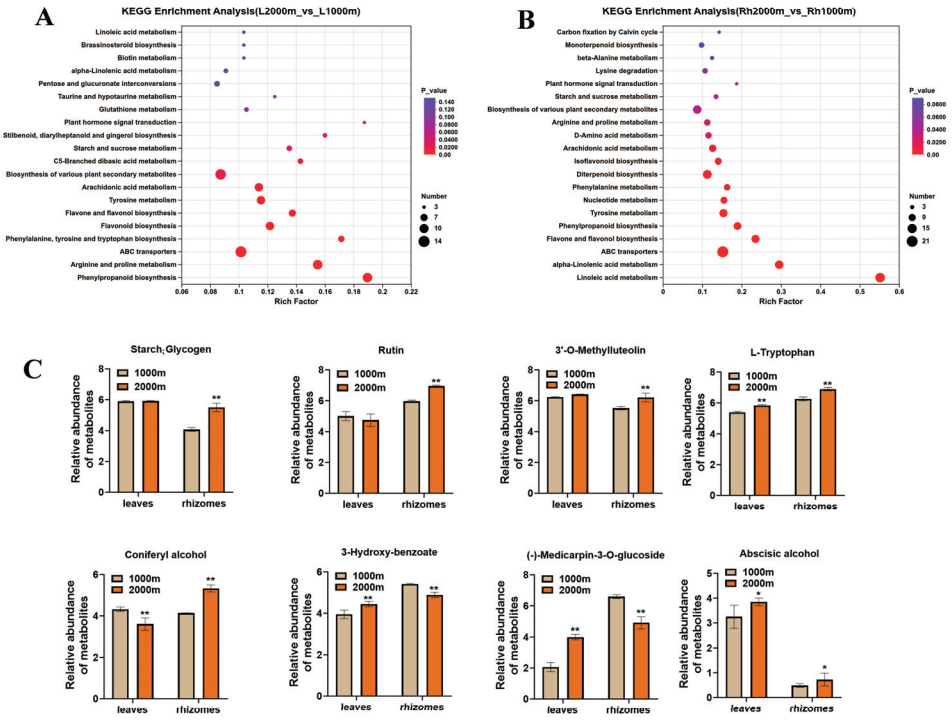


Figure 3. KEGG pathway enrichment analysis and expression abundance of some metabolites of differentially expressed metabolites in bamboo leaves and rhizomes at different altitudes. (**A**) KEGG pathway enrichment analysis of differentially expressed metabolites in bamboo leaves. (**B**) KEGG pathway enrichment analysis of differentially expressed metabolites in bamboo rhizomes. The horizontal axis represents the enrichment rate, calculated as num_in_study/num_in_pop; the vertical axis represents the KEGG pathways. The size of the bubble in the figure indicates the number of metabolites enriched in the pathway, and the color of the bubble represents the significance of the enrichment *p*-value. (**C**) Expression abundance of some phenylpropanoids, flavonoids, and sugar metabolism products. Error bars indicate the standard deviation obtained from five biological replicates. Stars indicate the significance of differences (* adjusted $p < 0.05$, ** adjusted $p < 0.01$).

3.4. Transcriptome Analysis of F. rufa Leaves and Rhizomes at Different Altitudes

To elucidate the transcriptional basis of altitude adaptation in *F. rufa*, we performed RNA-seq analysis on leaves and rhizomes collected from 1000 m and 2000 m (Supplementary Table S1). Sequencing of the 12 samples generated an average of 5.41 Gb clean data per sample, with Q30 scores exceeding 95.63%. De novo assembly using Trinity yielded 375,166 unigenes (530,488 transcripts) with an average N50 of 851 bp. Read mapping rates to this transcriptome reference ranged from 71.39% to 86.48%.

Functional annotation against GO, KEGG, EggNOG, NR, Swiss-Prot, and Pfam databases successfully assigned putative roles to 369,695 unigenes (Figure 4A). Sample correlation heatmap and principal component analysis confirmed high reproducibility among biological replicates and clear separation by both tissue type and altitude (Figure 4B,C). Venn analysis of expressed genes further highlighted distinct transcriptional landscapes: while 21,842 genes were constitutively expressed across all conditions, a substantial number exhibited tissue- and/or altitude-specific expression, underscoring pronounced transcriptomic plasticity in response to both developmental and environmental cues (Figure 4D). These foundational analyses establish a robust transcriptomic framework for subsequent investigation of altitude-responsive gene regulation in *F. rufa*.

https://doi.org/10.3390/f17020167

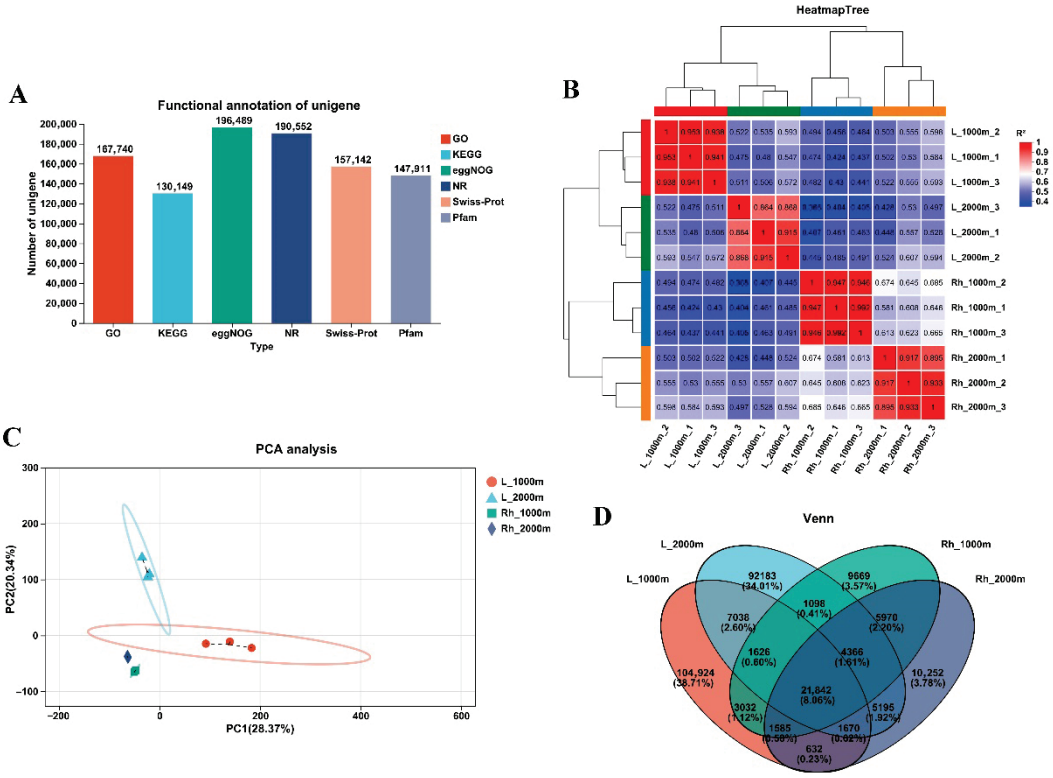


Figure 4. Transcriptome sequencing analysis of bamboo leaves and rhizomes of *F. rufa* at different altitudes. (**A**) Transcriptome Functional Annotation Results Table Based on Six Databases. (**B**) Correlation Analysis Among Transcriptome Samples. (**C**) PCA Among Transcriptome Samples (Supplementary Table S4). (**D**) Venn Analysis of Expressed Genes Among Transcriptome Samples.

3.5. Differential Expression Analysis of Transcriptomes of Bamboo Leaves and Rhizomes of F. rufa at Different Altitudes

To decipher the key transcriptional changes underlying altitudinal adaptation in *F. rufa*, we identified differentially expressed genes (DEGs) between 1000 m and 2000 m in leaves and rhizomes, followed by functional enrichment analysis. GO and KEGG classification of all DEGs revealed pronounced organ-specific functional signatures (Supplementary Figure S2). In leaves, GO terms were dominated by "cellular anatomical entity" and "cellular component," whereas rhizome DEGs were broadly enriched in "transferase activity," "kinase activity," and "protein kinase activity" (Figure 5A,B). KEGG pathway analysis further highlighted distinct metabolic priorities: leaf DEGs were notably enriched in "Protein processing in endoplasmic reticulum," "Pyruvate metabolism," "Oxidative phosphorylation," and "Biosynthesis of unsaturated fatty acids," reflecting active stress acclimation and energy remodeling. In rhizomes, the most significantly enriched pathways included "Biosynthesis of unsaturated fatty acids," along with other routes linked to nutrient assimilation and secondary metabolism (Figure 5C,D). These enrichment patterns align closely with the known physiological roles of each organ: leaves prioritize structural integrity and energy-dependent stress responses, while rhizomes enhance catalytic and biosynthetic capacity, supporting storage and defense. The clear divergence in enriched pathways underscores that altitude adaptation in *F. rufa* is mediated through highly tissue-specific transcriptional reprogramming, fine-tuned to the distinct functional demands of aerial and below-ground organs.

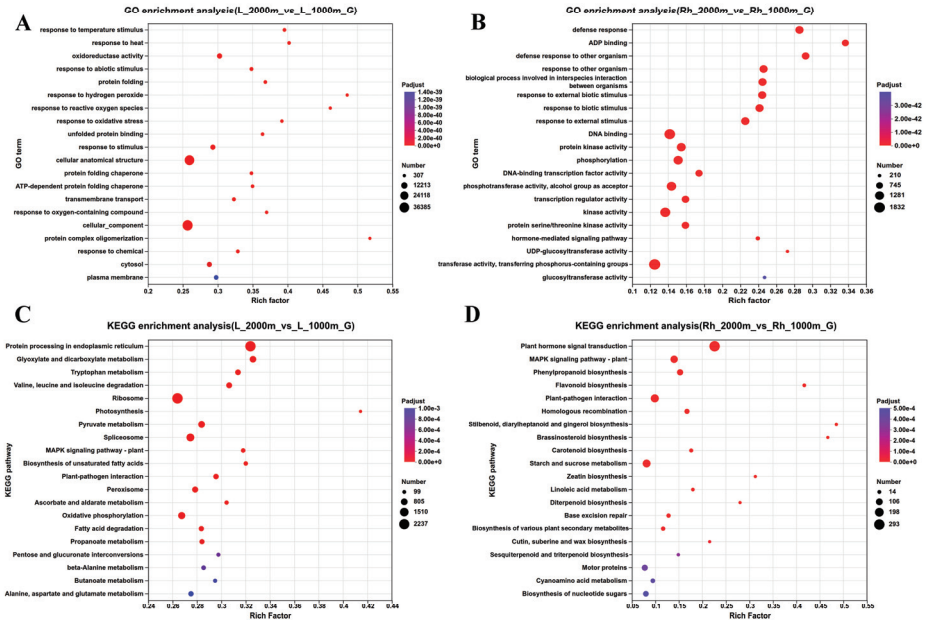


Figure 5. GO and KEGG enrichment analysis of DEGs in bamboo leaves and rhizomes at different altitudes. (**A**) GO enrichment analysis of DEGs in bamboo leaves of *F. rufa* at altitudes of 1000 m and 2000 m. (**B**) GO enrichment analysis of DEGs in bamboo rhizomes of *F. rufa* at altitudes of 1000 m and 2000 m. (**C**) KEGG enrichment analysis of DEGs in bamboo leaves of *F. rufa* at altitudes of 1000 m and 2000 m. (**D**) KEGG enrichment analysis of DEGs in bamboo rhizomes of *F. rufa* at altitudes of 1000 m and 2000 m.

3.6. Coordinated Transcriptional Regulation Underpins Organ-Specific Metabolic Adaptation

To resolve the transcriptional drivers of the observed metabolic shifts, we analyzed the expression of DEGs within three key altitude-responsive pathways: flavonoid biosynthesis, phenylpropanoid biosynthesis, and starch and sucrose metabolism (Supplementary Figure S3). Heatmap visualization revealed pronounced organ-specific expression patterns that aligned with our metabolomic data (Figure 6). In high-altitude leaves, most genes associated with flavonoid biosynthesis were downregulated, whereas their homologs were predominantly upregulated in high-altitude rhizomes (Figure 6A). This transcriptional divergence mirrored the organ-specific accumulation patterns of flavonoid metabolites. Similarly, genes in the upstream phenylpropanoid biosynthesis pathway were largely suppressed in high-altitude leaves but strongly induced in rhizomes (Figure 6B), directing metabolic flux differentially between organs. For starch and sucrose metabolism, expression of related genes was downregulated in leaves but markedly upregulated in rhizomes at high altitude (Figure 6C), consistent with the observed reallocation of carbon resources toward storage in below-ground tissues.

We further validated these expression trends using RT-qPCR on selected key genes from each pathway (Figure 7) and illustrated the interaction relationships between these genes and their corresponding metabolites (Supplementary Figure S4). The results confirmed that altitude induces opposite expression changes in leaves and rhizomes for flavonoid biosynthesis and stress hormone signaling genes, whereas some phenylpropanoid biosynthesis genes were upregulated in both organs. Genes involved in starch synthesis were preferentially enhanced in rhizomes but repressed in leaves at higher elevations. Collectively, these transcriptomic profiles demonstrate that altitude adaptation in *F. rufa* is orchestrated through complementary, organ-defined gene regulatory programs: leaves attenuate pathways for secondary metabolism and nutrient storage, while rhizomes activate them, thereby optimizing the dual needs of stress tolerance and resource sequestration in a vertically stratified environment.

https://doi.org/10.3390/f17020167

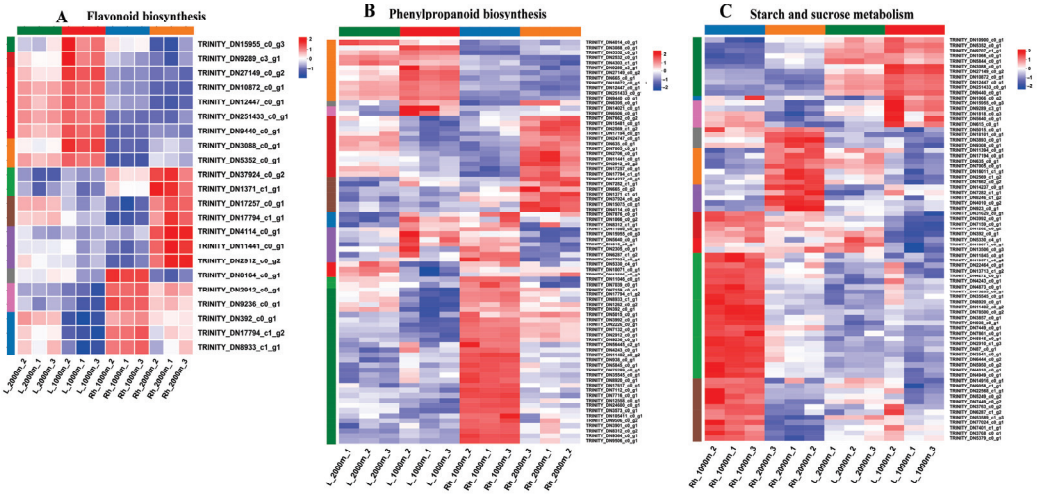


Figure 6. Heatmap of differentially expressed key genes in the metabolic pathways of flavonoid biosynthesis, starch and sucrose metabolism, and phenylpropanoid biosynthesis in bamboo leaves and rhizomes at altitudes of 1000 m and 2000 m. (**A**) Heatmap of key gene expression in the flavonoid biosynthesis pathway in bamboo leaves and rhizomes at different altitudes. (**B**) Heatmap of key gene expression in the starch and sucrose metabolism pathway in bamboo leaves and rhizomes at different altitudes. (**C**) Heatmap of key gene expression in the phenylpropanoid biosynthesis pathway in bamboo leaves and rhizomes at different altitudes. Detailed expression data are presented in Supplementary Table S3.

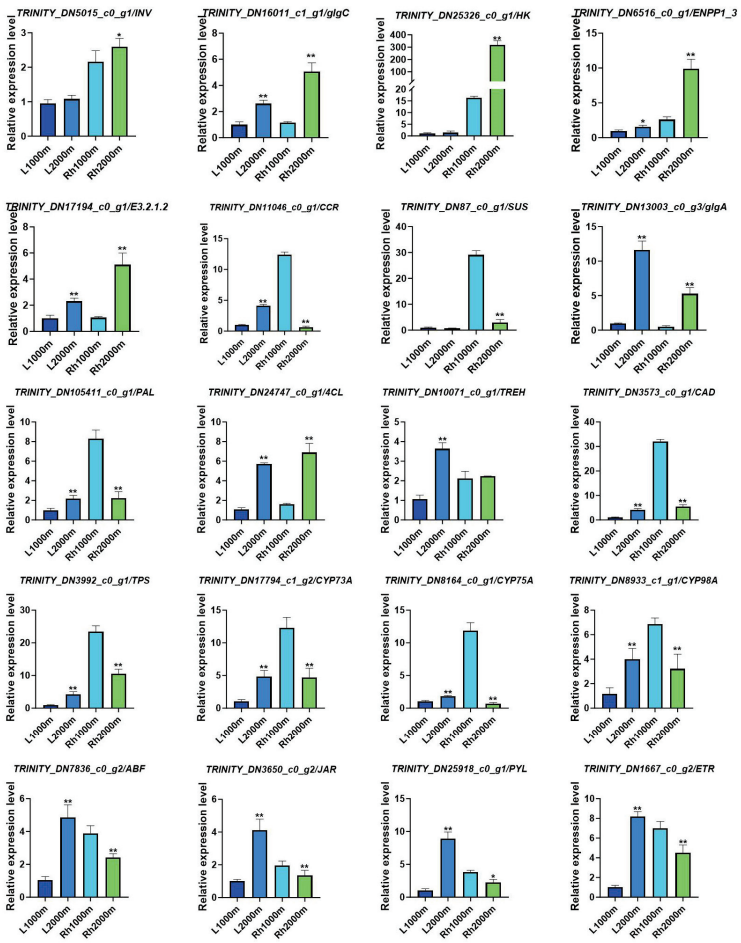


Figure 7. RT-qPCR analysis of key DEGs. key genes include those from the pathways: starch and sucrose metabolism (*TRINITY_DN25326_c0_g1*, *TRINITY_DN6516_c0_g1*, *TRINITY_DN17194_c0_g1*,

TRINITY_DN87_c0_g1, *TRINITY_DN13003_c0_g3*), phenylpropanoid biosynthesis (*TRINITY_DN11046_c0_g1*, *TRINITY_DN105411_c0_g1*, *TRINITY_DN24747_c0_g1*, *TRINITY_DN10071_c0_g1*, *TRINITY_DN3573_c0_g1*, *TRINITY_DN3992_c0_g1*) flavonoid biosynthesis (*TRINITY_DN17794_c1_g2*, *TRINITY_DN8164_c0_g1*, *TRINITY_DN8933_c1_g1*), stress hormone (ABA/JA/ETH) key genes (*TRINITY_DN7836_c0_g2*, *TRINITY_DN3650_c0_g2*, *TRINITY_DN25918_c0_g1*, *TRINITY_DN1667_c0_g2*), error bars represent the standard deviation obtained from at least three biological replicates. stars indicate significant differences (∗ adjusted $p < 0.05$, ∗∗ adjusted $p < 0.01$).

4. Discussion

This study reveals that *F. rufa* employs an organ-specific functional differentiation strategy to cope with altitudinal gradients, a mechanism that aligns with the seasonal foraging migration of the giant panda [28,29]. Integrated metabolomic and transcriptomic analyses demonstrate that at high altitude (2000 m), leaves shift toward a metabolically streamlined phenotype: sucrose metabolism and its key genes (such as SUS) are downregulated, and most phenylpropanoid/flavonoid pathway genes and metabolites are reduced, with only core stress-responsive compounds such as 3-hydroxybenzoate remaining elevated; these compounds enhance the fundamental stress tolerance of leaves by scavenging reactive oxygen species and stabilizing cellular structures [30]. In contrast, rhizomes adopt a resource-enhancing and defense-priming strategy, marked by accumulation of flavonoids (such as rutin, luteoloside), linoleic acid derivatives (such as lecithin), and starch, coupled with coordinated upregulation of the corresponding biosynthetic genes (Figures 2E and 3) [31]. This "leaves for foraging, rhizomes for survival" division of labor closely mirrors the giant panda's vertical foraging migration behavior. Giant pandas preferentially consume nutrient-rich leaves and shoots with low levels of defensive compounds in lower-altitude areas to meet their energy needs for growth and reproduction. In contrast, they rely on bamboo tissues with stronger chemical defenses but greater persistence in higher-altitude regions to sustain survival. This adaptive relationship clearly reveals the metabolic-genetic foundation of their long-term co-evolution.

Compared to traditional bamboo studies mentioned in the Introduction—which often focus on the physiological responses of single organs and lack integrated multi-omics analysis—this research achieves a dual breakthrough in both perspective and evidential support, thereby precisely addressing the research gap regarding the organ-specific molecular mechanisms of bamboo adaptation to altitude [3]. As noted in the Introduction, previous work has primarily examined physiological indicators (such as soluble sugar accumulation and flavonoid synthesis) in single organs of bamboo species like *P. heterocycla* var. pubescens and *Chimonobambusa quadrangularis*, or has only explored the correlation between flavonoid content in *F. rufa* and giant panda diet, without clarifying the molecular regulatory mechanisms driven by altitudinal gradients or the synergistic strategies across multiple organs [32,33]. Through comparative analysis of leaves and rhizomes, this study expands and refines the model of bamboo adaptation to altitude. While earlier research found that high-altitude leaves of *P. heterocycla* var. *pubescens* accumulate soluble sugars to enhance stress tolerance [33], it did not address the coordinated responses of belowground organs. In contrast, this study reveals for the first time an organ-specific regulation pattern of the phenylpropanoid pathway in *F. rufa*: downregulation in leaves to reduce metabolic costs, and upregulation in rhizomes to strengthen defense and storage. This pattern stands in sharp contrast to the organ-convergent adaptation observed in plants such as *Arabidopsis thaliana* and alpine rhododendrons [34–36], highlighting the unique altitudinal adaptation logic of the staple bamboo species for giant pandas (Figures 3, 5 and 6). Furthermore, the shift from monosaccharides to starch in rhizomes, supported by upregulated biosynthetic genes, corroborates the general plant strategy of converting soluble sugars to storage polysaccharides under stress [37,38], while specifying its role in below-ground resource al-

https://doi.org/10.3390/f17020167

location. These key genes—such as PAL, CHS, and INV—represent prime targets for future functional validation (Figure 7). Notably, enriched linoleic acid metabolism in high-altitude rhizomes, including elevated lecithin, provides new molecular insight into membrane stability and stress resilience in underground storage organs.

Ecologically, the organ-specific metabolic reprogramming of *F. rufa* is essentially a molecular adaptation to the "shooting altitudinal gradient effect" described in the Introduction, while also serving as a key signal regulating giant panda foraging decisions and habitat selection [8]. In conjunction with the giant panda's seasonal preferences for "shoots in spring/summer and leaves in autumn/winter" mentioned in the Introduction, we hypothesize that the reduced content of defensive secondary metabolites (such as flavonoids, phenolic acids) in high-altitude leaves not only enhances palatability and lowers digestive costs for giant pandas but also complements the stable levels of crude protein and amino acids characteristic of high-altitude leaves during summer and autumn. This provides an explanation for the panda's behavior of migrating to higher altitudes to feed on leaves during these seasons [39,40]. Conversely, the simultaneous accumulation of defensive metabolites and starch in high-altitude rhizomes serves a dual purpose: on one hand, it reserves energy and defensive substances for next year's shoot sprouting, ensuring population continuity; on the other hand, the low temperature and reduced light at high altitudes delay shoot emergence, creating a spatiotemporal pattern of "shoots emerging earlier at low altitudes and later at high altitudes." This aligns closely with the observed foraging pattern of giant pandas, which preferentially consume early-emerging shoots at lower altitudes before migrating to higher elevations, further supporting their co-evolutionary relationship. Of course, this hypothesis requires validation through field telemetry monitoring and controlled experiments [39]. As noted in the Introduction, altitude adaptation strategies vary among plants. This study also finds that orchids adapt to altitude through specific morphological and alkaloid-synthesis strategies [41], which differ markedly from the organ-functional differentiation strategy of *F. rufa*, reflecting the diversity of altitude adaptation across plant taxa. This tight coupling between tissue-specific metabolite landscapes and herbivore foraging behavior highlights a refined co-evolutionary adjustment: *F. rufa* optimizes its own altitudinal fitness through divergent organ strategies while generating a spatiotemporal gradient in food quality that guides panda resource use [42]. Future research should focus on addressing the "gap in integrated multi-omics studies" highlighted in the Introduction by pursuing two main avenues: first, conducting controlled feeding experiments to clarify the effects of specific metabolites (such as rutin, lecithin) on giant panda feeding preferences; second, utilizing tools such as gene editing and overexpression to validate the functions of key genes, thereby bridging molecular mechanisms with macro-foraging ecology. This will provide precise theoretical support for giant panda habitat conservation and staple bamboo resource management, ultimately fulfilling the research objective proposed in the Introduction: elucidating the "molecular mechanisms underlying the quality formation of the staple bamboo."

5. Conclusions

This study systematically elucidates that *F. rufa* employs an organ-specific metabolic reprogramming strategy to adapt to altitudinal variation. Specifically, leaves adopt a "metabolic economy" mode, downregulating the synthesis of phenylpropanoids and flavonoids, whereas rhizomes enhance the accumulation of phenylpropanoids and starch, forming an "active storage" pattern. This strategy not only ensures the plant's own altitudinal adaptation but also provides a molecular-level explanation for the vertical foraging migration of giant pandas. The metabolic simplification in high-altitude leaves may improve their palatability, while the accumulation of nutrients and defensive compounds in

rhizomes likely influences bamboo shoot quality. Together, these factors shape the seasonal foraging preferences of giant pandas. These findings reveal a novel mechanism by which plant metabolic plasticity drives "plant–animal" interactions, offering important theoretical insights for understanding species coevolution and informing targeted conservation strategies for giant panda habitats.

Supplementary Materials: The following supporting information can be downloaded at https://www.mdpi.com/article/10.3390/f17020167/s1, Figure S1: Observations on *F. rufa* at different altitudes; Figure S2: Functional annotation of differentially expressed genes in bamboo leaves and rhizomes at different altitudes; Figure S3: KEGG pathway maps; Figure S4: Interaction network between metabolites and key genes; Table S1: Sequencing data statistics of *F. rufa* leaves and rhizomes at different altitudes; Table S2: Metabolite expression table across different samples; Table S3: Pathway gene annotation and expression matrix; Table S4: Primers for key genes in the study; Table S5: PCA analysis data table.

Author Contributions: Conceptualization: Q.L., W.F., M.T. and X.Z.; methodology: Q.L., W.F., M.T., X.Z. and Z.L.; software: M.C., X.S., L.W. and X.Z.; validation: Q.L., X.Z. and Z.L.; formal analysis: Q.L., X.Z. and Z.L.; investigation: Q.L., X.Z. and Z.L.; resources: Q.L., X.Z. and Z.L.; data curation: Q.L., X.Z. and Z.L.; writing—original draft preparation: X.Z. and Z.L.; writing—review and editing: X.Z. and Z.L.; visualization: Q.L., X.Z. and Z.L.; supervision: X.Z. and Z.L.; project administration: Q.L., X.Z. and Z.L. All authors have read and agreed to the published version of the manuscript.

Funding: This research was funded by the "14th Five-Year" National Key Research and Development Program, High-efficiency Cultivation Technology of Bamboo Shoot Forest with Southwest Characteristics (2023YFD220120302), Sichuan Forestry and Grassland Technology Innovation Team (CXTD2025009), and the National Natural Science Foundation of China (32501608).

Data Availability Statement: The RNA-seq data are available in the database resources of the national genomics data center, China National Center for Bioinformation (GSA: CRA034565). The data presented in this study are available on request from the corresponding author.

Conflicts of Interest: The authors declare that there are no conflicts of interest regarding the publication of this paper.

References

1. Xiao, M. The Effect of Elevation on Population Characteristics and Agronomic Traits of *Fargesia rufa*. Master's Thesis, Xihua Normal University, Nanchong, China, 2024.
2. Liu, C.; Wang, Y.; Pan, K.; Jin, Y.; Liang, J.; Li, W.; Zhang, L.J. Photosynthetic carbon and nitrogen metabolism and the relationship between their metabolites and lipid peroxidation in dwarf bamboo (*Fargesia rufa* Yi) during drought and subsequent recovery. *Trees* **2015**, *29*, 1633–1647. [CrossRef]
3. Liu, C.; Wang, Y.; Pan, K.; Jin, Y.; Li, W.; Zhang, L.J. Effects of phosphorus application on photosynthetic carbon and nitrogen metabolism, water use efficiency and growth of dwarf bamboo (*Fargesia rufa*) subjected to water deficit. *Plant Physiol. Biochem.* **2015**, *96*, 20–28. [CrossRef] [PubMed]
4. Zhou, X.; Wang, J.; Zhang, H.; Wang, J.; Zhang, Y. Effect of elevated CO_2 and nitrogen deposition on leaf nutrient quality of *Fargesia rufa* Yi. *Acta Ecol. Sin.* **2012**, *32*, 7644–7653. [CrossRef]
5. Yang, S.H.; Shen, H.; Luo, H.B.; Su, H.S.; Zou, Q.; Yu, Y.H.; Chen, Y.N.; Yu, Y.S.; Hu, T.G.; Dong, X.; et al. The effect of near-freezing temperature storage on delaying postharvest lignification of *Dendrocalamus brandisii* shoots. *Food Sci.* **2024**, *45*, 216–225.
6. Wang, H.; Fu, W.J.; Tian, M.; Zhang, X. A diet diverse in bamboo parts is important for giant panda (*Ailuropoda melanoleuca*) metabolism and health. *Sci. Rep.* **2017**, *7*, 3377. [CrossRef]
7. Zhang, M.; Zhang, Z.; Li, Z.; Hong, M.; Zhou, X.; Zhou, S.; Zhang, J.; Hull, V.; Huang, J.; Zhang, H.J. Giant panda foraging and movement patterns in response to bamboo shoot growth. *Environ. Sci. Pollut. Res.* **2018**, *25*, 8636–8643. [CrossRef]
8. Liu, Y.; Liu, X.; Songer, M.; Wang, P.; Jiang, X.; Hong, X.; Chen, Q.J. The effect of elevation on structure and nutrition of staple food bamboo and seasonal distribution of giant pandas. *Acta Theriol. Sin.* **2016**, *36*, 24.
9. Jiang, C.; Li, Q.; Liu, L.; Zhou, J.; Chen, F.; Yang, Y.; Zhang, X.; Guo, A.J. Seasonal variation in nutritional components of ten potential edible bamboos for giant panda. *J. Nanjing For. Univ.* **2018**, *42*, 148–154.

10. Zhang, S.J. Technology, coupling mechanism between reproductive strategies and foraging behavior of giant pandas: Energy-nutrition-temperature correlation effect. *J. Sichuan For. Sci. Technol.* **2021**, *42*, 21–28.
11. Huang, G.; Wang, L.; Li, J.; Hou, R.; Wang, M.; Wang, Z.; Qu, Q.; Zhou, W.; Nie, Y.; Hu, Y.J. Seasonal shift of the gut microbiome synchronizes host peripheral circadian rhythm for physiological adaptation to a low-fat diet in the giant panda. *Cell Rep.* **2022**, *38*, 110203. [CrossRef]
12. Chitiva, L.C.; Lozano-Puentes, H.S.; Londoño, X.; Leão, T.F.; Cala, M.P.; Ruiz-Sanchez, E.; Díaz-Ariza, L.A.; Prieto-Rodríguez, J.A.; Castro-Gamboa, I.; Costa, G.M.J. Untargeted metabolomics approach and molecular networking analysis reveal changes in chemical composition under the influence of altitudinal variation in bamboo species. *Front. Mol. Biosci.* **2023**, *10*, 1192088. [CrossRef]
13. Chen, L.; Zhang, L.; Zhao, Y.; He, M.; Wu, H.; Wang, J.; Chen, Z.; Zhao, Y.; Shen, F.; Zhang, X. Impact of DNA methylation on digestive and metabolic gene expression in red pandas (*Ailurus fulgens*) during the transition from milk to bamboo diet. *BMC Genom.* **2025**, *26*, 404. [CrossRef] [PubMed]
14. Lin, D.; Jia, J.; Zhao, Z. Relationship between feeding tendency of giant panda and cellulose of edible bamboo. *J. Northeast For. Univ.* **2020**, *48*, 67–70.
15. Qian, Y.; Jia, J.; Chen, Z.; Wang, K.; Li, P.; Gao, P.; Ying, Y.; Shi, W.J. Environmental drivers and transcriptomic variations shaping Lei bamboo shoots across cultivation regions. *Front. Plant Sci.* **2025**, *16*, 1565665. [CrossRef]
16. Muhamed, A. RNA-seq Transcriptome Profiling of Ethiopian Lowland Bamboo (*Oxytenanthera abyssinica* (A. Rich) Munro) Under Drought and Salt Stresses and SSR Based Genetic Diversity Analysis of Ethiopian Highland Bamboo (*Arundinaria alpina* K. Schum). Ph.D. Thesis, Addis Ababa University, Addis Ababa, Ethiopia, 2019.
17. Peng, Z.; Lu, Y.; Li, L.; Zhao, Q.; Feng, Q.; Gao, Z.; Lu, H.; Hu, T.; Yao, N.; Liu, K.; et al. The draft genome of the fast-growing non-timber forest species moso bamboo (*Phyllostachys heterocycla*). *Nat. Genet.* **2013**, *45*, 456–461. [CrossRef]
18. Jing, X.; Cai, C.J.; Fan, S.H.; Liu, G.L.; Li, X.J. Research advances in ecological adaptability of bamboo under environmental stresses. *World For. Res.* **2018**, *31*, 36–41.
19. Pan, H.L.; Tian, Y.; Liu, X.L.; Cai, X.H.; He, F.; Li, M.H. Ecological responses of *Fargesia nitida* to altitude in the wolong nature reserve. *Ecol. Environ.* **2010**, *19*, 2832.
20. Wang, J.; Yang, M.; Huang, X.; Yu, Y.; Liao, S.; Yang, X.J. Response of leaf blade in *Zanthoxylum planispinum* var. *dintanensis* to different altitudes through integrated metabolomics and transcriptomics analysis. *S. Afr. J. Bot.* **2023**, *162*, 41–51. [CrossRef]
21. Xu, S.; Yang, L.T.; Chen, S.L.; Guo, Z.W.; Gu, R.; Zhang, C. Review on the formation of bamboo shoot palatability and its main influencing factors. *J. Zhejiang A F Univ.* **2021**, *38*, 403–411.
22. Chen, F.F.; Ji, Y.L.; Chen, Z.H.; Liu, T.L.; Liu, X. Transcriptome sequencing and expression analysis of *Batrachium bungei* (Steud.) L. liou at different altitudes based on RNA-seq in the Qinghai-Tibet plateau. *J. Plant Sci.* **2021**, *16*, 50–58.
23. Wang, P.; Guo, Y.; Chen, X.; Zheng, Y.; Sun, Y.; Yang, J.; Ye, N.J. Genome-wide identification of WOX genes and their expression patterns under different hormone and abiotic stress treatments in tea plant (*Camellia sinensis*). *Trees* **2019**, *33*, 1129–1142. [CrossRef]
24. Livak, K.J.; Schmittgen, T.D.J. Analysis of relative gene expression data using real-time quantitative PCR and the $2^{-\Delta\Delta CT}$ method. *Methods* **2001**, *25*, 402–408. [CrossRef]
25. Li, B.; Dewey, C.N.J. RSEM: Accurate transcript quantification from RNA-Seq data with or without a reference genome. *BMC Bioinform.* **2011**, *12*, 323. [CrossRef]
26. Love, M.I.; Huber, W.; Anders, S.J. Moderated estimation of fold change and dispersion for RNA-seq data with DESeq2. *BMC Biol.* **2014**, *15*, 550. [CrossRef]
27. Wang, L.; Feng, Z.; Wang, X.; Wang, X.; Zhang, X.J. DEGseq: An R package for identifying differentially expressed genes from RNA-seq data. *Bioinformatics* **2010**, *26*, 136–138. [CrossRef]
28. Wang, M.; Nie, Y.G.; Swaisgood, R.R.; Wei, W.; Zhou, W.L.; Zhang, G.M.; Wei, F.W.J. Stable seasonal migration patterns in giant pandas. *Zool. Res.* **2023**, *44*, 341. [CrossRef]
29. Zeng, Y.; Han, H.; Gong, Y.; Qubi, S.; Chen, M.; Qiu, L.; Huang, Y.; Zhou, H.; Wei, W.J. Feeding habits and foraging patch selection strategy of the giant panda in the Meigu Dafengding National Nature Reserve, Sichuan Province, China. *Environ. Sci. Pollut. Res.* **2023**, *30*, 49125–49135. [CrossRef]
30. Nehela, Y.; Taha, N.A.; Elzaawely, A.A.; Xuan, T.D.; Amin, M.A.; Ahmed, M.E.; El-Nagar, A.J. Benzoic acid and its hydroxylated derivatives suppress early blight of tomato (*Alternaria solani*) via the induction of salicylic acid biosynthesis and enzymatic and nonenzymatic antioxidant defense machinery. *J. Fungi* **2021**, *7*, 663. [CrossRef]
31. Jiang, Y.; Liu, Q.; Feng, S.G.; Zhou, D.Y.; Yu, Q. Effects of Environmental Factors on the Content of Flavonoids and Chlorogenic Acid in *Chrysanthemum morifolium* Ramat. *Chin. J. Mod. Appl. Pharm.* **2018**, *35*, 225–230.
32. Peng, X.; Teng, L.; Yan, X.; Zhao, M.; Shen, S.J. The cold responsive mechanism of the paper mulberry: Decreased photosynthesis capacity and increased starch accumulation. *BMC Genom.* **2015**, *16*, 898. [CrossRef] [PubMed]
33. Wang, H.; Guo, L.; Zha, R.; Gao, Z.; Yu, F.; Wei, Q.J. Histological, metabolomic and transcriptomic analyses reveal mechanisms of cold acclimation of the Moso bamboo (*Phyllostachys edulis*) leaf. *Tree Physiol.* **2022**, *42*, 2336–2352. [CrossRef]

34. Nong, M.L.; Luo, X.H.; Zhu, L.X.; Zhang, Y.N.; Dun, X.Y.; Huang, L.J. Insights into the adaptation to high altitudes from transcriptome profiling: A case study of an endangered species, *Kingdonia uniflora*. *Genes* **2023**, *14*, 1291. [CrossRef]
35. Ye, L.J.; Möller, M.; Luo, Y.H.; Zou, J.Y.; Zheng, W.; Liu, J.; Li, D.Z.; Gao, L.M.J. Variation in gene expression along an elevation gradient of *Rhododendron sanguineum* var. *haemaleum* assessed in a comparative transcriptomic analysis. *Front. Plant Sci.* **2023**, *14*, 1133065. [CrossRef]
36. Qi, X.; Zhang, Q.; He, Y.; Yang, L.; Zhang, X.; Shi, P.; Yang, L.; Liu, Z.; Zhang, F.; Liu, F.; et al. The Transcriptomic Landscape of Yaks Reveals Molecular Pathways for High Altitude Adaptation. *Genome Biol. Evol.* **2019**, *11*, 72–85. [CrossRef]
37. Dong, S.; Beckles, D.M. Dynamic changes in the starch-sugar interconversion within plant source and sink tissues promote a better abiotic stress response. *J. Plant Physiol.* **2019**, *234–235*, 80–93. [CrossRef]
38. Keller, I.; Rodrigues, C.M.; Neuhaus, H.E.; Pommerrenig, B. Improved resource allocation and stabilization of yield under abiotic stress. *J. Plant Physiol.* **2021**, *257*, 153336. [CrossRef] [PubMed]
39. Wang, L.; Yuan, S.; Nie, Y.; Zhao, J.; Cao, X.; Dai, Y.; Zhang, Z.; Wei, F. Dietary flavonoids and the altitudinal preference of wild giant pandas in *Fargesia* habitats of Foping National Nature Reserve, China. *Glob. Ecol. Conserv.* **2020**, *22*, e00981.
40. Wang, D.; Guo, Q.; Wang, X.; Liang, C.; Zhang, Y.J. Effects of different altitudes on the nutrient and amino acid contents of bamboo (*Fargesia denudata*), staple food of the Giant Panda, in Minshan, Sichuan, China. *Acta Ecol. Sin.* **2017**, *37*, 6440–6447. [CrossRef]
41. Feizi, F.; Zakizadeh, H.; Mirjalili, M.H. Altitudinal Effects on Morphology and Biochemistry of Native Iranian Orchids in Guilan, Iran: Insights into Adaptive Strategies and Conservation Priorities. *Russ. J. Plant Physiol.* **2024**, *71*, 217. [CrossRef]
42. Nie, Y.; Zhang, Z.; Raubenheimer, D.; Elser, J.J.; Wei, W.; Wei, F.J. Obligate herbivory in an ancestrally carnivorous lineage: The giant panda and bamboo from the perspective of nutritional geometry. *Funct. Ecol.* **2015**, *29*, 26–34. [CrossRef]

Disclaimer/Publisher's Note: The statements, opinions and data contained in all publications are solely those of the individual author(s) and contributor(s) and not of MDPI and/or the editor(s). MDPI and/or the editor(s) disclaim responsibility for any injury to people or property resulting from any ideas, methods, instructions or products referred to in the content.

forests

MDPI

Article

Transcriptomic Analysis of Anthocyanin Degradation in *Salix alba* Bark: Insights into Seasonal Adaptation and Forestry Applications

Hong-Yong Wang [1], Xing-Ju Liu [1], Meng-Zhen Yin [1], Sheng-Jia Cui [1], Hai-Yong Liang [1,2,*] and Zhen-Hua Xu [3,*]

[1] College of Forestry, Hebei Agricultural University, Baoding 071000, China; 17835714216@163.com (H.-Y.W.); 15175761562@163.com (X.-J.L.); 18833761082@163.com (M.-Z.Y.); cui112199@163.com (S.-J.C.)
[2] Key Laboratory of Germplasm Resources and Forest Protection, Baoding 071000, China
[3] Hebei Forests Tree Germplasm Innovation Center, Hebei Academy of Forestry and Grassland Sciences, Shijiazhuang 050000, China
* Correspondence: lianghy@hebau.edu.cn (H.-Y.L.); hblky303@126.com (Z.-H.X.)

Abstract: Anthocyanins, key flavonoid-derived secondary metabolites, not only confer diverse pigmentation but also function in photoprotection, antioxidative defense, and cold acclimation. In woody species, bark anthocyanin turnover is tightly linked to environmental adaptation, stress resilience, and ornamental traits, yet its molecular regulation remains largely unresolved. Here, we investigated *Salix alba* L. bark by integrating anthocyanin quantification, transcriptome profiling, and weighted gene co-expression network analysis (WGCNA) to dissect the temporal dynamics and regulatory architecture of anthocyanin degradation. Anthocyanin content peaked at D2 (late December 2024), declined through D3 (mid-January 2025) and D4 (mid-February 2025), and partially rebounded at D5 (early March 2025), coinciding with peak expression of structural genes *LAC1/2*, *POD1/2*, and *BGLU10*. These enzymes co-expressed with multiple transcription factors, including *MYB*, *bHLH*, and *WRKY* families, forming putative core modules. Functional enrichment indicated that differentially expressed genes were enriched in redox processes, glycoside hydrolysis, flavonoid metabolism, and hormone signaling, suggesting a degradation mechanism mediated by reactive oxygen species, glycosidic cleavage, and hormone–transcription factor interplay. This study provides the first comprehensive framework of bark anthocyanin degradation in white willow, advancing the understanding of pigment dynamics, gene–environment crosstalk, and breeding strategies for ornamental woody plants.

Keywords: *Salix alba*; anthocyanin degradation; bark pigmentation; transcriptome; WGCNA; transcription factors; seasonal adaptation

1. Introduction

Anthocyanins, as prominent secondary metabolites within the flavonoid (flavonoids) pathway, are widely accumulated in various plant organs, including leaves, stems, flowers, and fruits, where they impart red, blue, and purple pigmentation [1–3]. Beyond their role in coloration, anthocyanins play critical functions in photoprotection, reactive oxygen species (ROS) scavenging, osmotic adjustment, and cold acclimation, thereby contributing substantially to plant growth, development, and environmental adaptation [4,5]. In woody plants, anthocyanins are further implicated in xylem differentiation, bark pigmentation, ultraviolet defense, and pathogen resistance [6,7]. These multifaceted roles are not only indispensable for maintaining the stability of forest ecosystems but also hold significant im-

plications for forestry production, efficient utilization of woody resources, and sustainable forest management.

The biosynthetic pathway of anthocyanins has been systematically elucidated in model plants and fruit crops. Originating from phenylpropanoid metabolism, anthocyanins are synthesized through the sequential actions of structural genes such as *CHS*, *CHI*, *F3H*, *DFR*, *ANS*, and *UFGT* [8]. At the transcriptional level, the *MYB–bHLH–WD40* (MBW) complex precisely regulates the expression of these structural genes, enabling tissue-specific and developmental stage-dependent accumulation of anthocyanins [9,10]. In contrast, the molecular basis of anthocyanin degradation remains far less understood. Current evidence suggests that multiple enzymes play pivotal roles in this process: peroxidases (*PODs*) accelerate breakdown through reactive oxygen species, laccases (*LACs*) mediate oxidative polymerization, and β-glucosidases (*BGLUs*) cleave glycosidic bonds to reduce molecular stability, while polyphenol oxidases (*PPOs)* oxidize o-diphenols to quinone intermediates that subsequently react with anthocyanins [11], ultimately leading to color loss [12]. These enzymatic mechanisms have been experimentally validated in processes such as tomato (*Solanum lycopersicum*) fruit ripening and blueberry (*Vaccinium corymbosum*) postharvest storage [13,14]. Nevertheless, studies on anthocyanin degradation in woody plants, particularly in bark tissues, remain scarce.

The genus *Salix* (willows) comprises typical fast-growing tree species with wide distribution and is frequently used in bioenergy plantations, wetland restoration, and urban greening [15]. Transcriptomic studies in several *Salix* species have identified key structural genes and transcription factors associated with phenylpropanoid metabolism and flavonoid biosynthesis, such as *SaMYB4*, *SaMYB33*, and members of the *bHLH* family, which play important regulatory roles under environmental stresses including salinity–alkalinity, drought, and high light [16]. In closely related genera such as *Populus* (poplars) [17] and *Betula* (birches) [18], similar patterns of anthocyanin and flavonoid metabolism have been reported, with pigment dynamics in bark and leaves closely linked to ecological adaptation. As an important member of the willow genus, *Salix alba* L. is characterized by rapid growth and high biomass, making it well suited for energy plantations and ecological restoration [19]. Moreover, its bark exhibits seasonal variation in coloration, conferring ornamental value. Anthocyanins and related metabolites in *S. alba* not only contribute to stress responses and ecological adaptation [20] but may also affect wood quality, antioxidant capacity, and potential medicinal properties [21]. Therefore, a systematic elucidation of anthocyanin accumulation and degradation in *S. alba* bark will not only advance the understanding of pigment dynamics in woody plants but also provide novel strategies for forestry improvement and efficient utilization of woody resources.

The bark of white willow (*Salix alba*) exhibits a progressive shift in coloration from light to dark and subsequently to pale again across the growth season (D1–D5, corresponding to late November 2024, late December 2024, mid-January 2025, mid-February 2025, and early March 2025), reflecting a dynamic balance between anthocyanin accumulation and degradation [22]. Pigment degradation not only determines bark appearance and ornamental value but may also be closely linked to environmental adaptability and stress resistance [23]. Previous studies have demonstrated that elevated temperatures can markedly enhance the activities of peroxidases (*PODs*) and polyphenol oxidases (*PPOs*) [24], while ultraviolet radiation accelerates anthocyanin oxidation by promoting reactive oxygen species (ROS) accumulation [25]. In contrast, low temperatures suppress degradation and increase pigment stability [26]. Thus, elucidating the dynamic changes in bark pigmentation requires an integrated framework that considers the coordinated effects of enzymatic degradation, transcriptional regulation, and environmental signaling.

Building upon this background, the present study focused on the bark of white willow (*Salix alba*), integrating anthocyanin quantification, transcriptome sequencing, and weighted gene co-expression network analysis (WGCNA) to systematically identify candidate degradation-related enzyme genes (*POD*, *LAC*, *PPO*, and *BGLU*) together with their regulatory transcription factors, and to explore their associations with bark pigment dynamics. Through module–trait correlation analysis and functional annotation, this work elucidates the molecular basis of anthocyanin degradation in *S. alba* bark, providing a new perspective for studies on anthocyanin catabolism in willows and other woody plants. Moreover, these findings offer theoretical foundations for advancing the understanding of gene–environment interactions, constructing regulatory models of pigment dynamics, and supporting stress-resilient breeding as well as the sustainable management of bioenergy, ecological, and ornamental forests.

2. Results

2.1. Differential Anthocyanin Content in Salix alba Bark During Color Transitions

The anthocyanin content in the bark of *Salix alba* was quantified across five developmental stages (D1–D5). As shown in Figure 1, total anthocyanin levels reached a peak at stage D2, followed by a significant decline at D3, a further decrease to the lowest level at D4, and a slight rebound at D5, displaying an overall stage-dependent attenuation consistent with the phenotypic changes.

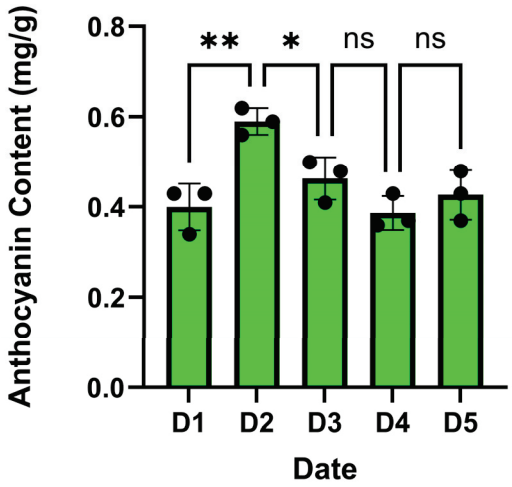


Figure 1. Anthocyanin content in the bark of *Salix alba* across five developmental stages (D1–D5). Data are presented as mean ± SD of three biological replicates, with individual replicate values shown as scatter points(black dots represent three biological replicates). Significant differences among stages were assessed using one-way ANOVA followed by Tukey's multiple comparison test (** $p < 0.01$, * $p < 0.05$, ns = not significant). Anthocyanin content is expressed as mg per gram of fresh weight (mg/g FW). The results show that anthocyanin content peaked at D2, decreased at D3 and D4, and partially rebounded at D5.

2.2. Transcriptome Sequencing and Assembly

To investigate the molecular mechanisms underlying anthocyanin degradation in *Salix alba* bark, high-throughput RNA sequencing (RNA-seq) was performed across five developmental stages (D1–D5). Each stage included three biological replicates, with each replicate composed of pooled bark tissues from 10 trees; no technical replicates were applied. Approximately 40.25–43.39 million raw reads were generated per library. After quality control, nearly 100% of clean reads were retained, with Q30 values exceeding 92% and GC contents of ~44%–45% (Table 1), indicating high sequencing quality suitable for subsequent differential expression and gene co-expression network analyses.

Table 1. Transcriptome sequencing data for the bark of *Salix alba*. Raw reads and clean reads indicate the number of sequencing reads before and after quality filtering, respectively. Q20 and Q30 represent the percentage of bases with Phred quality scores ≥ 20 and ≥30. GC content denotes the percentage of guanine and cytosine bases in clean reads. D1–D5 correspond to the five sampling stages, each with three biological replicates (e.g., D1-1 to D1-3).

Sample	Raw Reads	Clean Reads	Q20_Rate	Q30_Rate	GC_Content
D1-1	43,335,042	43,335,026	98.10%	94.82%	44.68%
D1-2	43,340,716	43,340,702	98.39%	95.60%	44.79%
D1-3	43,344,920	43,344,894	97.43%	93.09%	44.84%
D2-1	43,359,260	43,359,236	97.87%	94.27%	45.33%
D2-2	43,383,632	43,383,614	97.99%	94.51%	44.98%
D2-3	40,257,396	40,257,384	97.65%	93.60%	45.22%
D3-1	43,372,770	43,372,736	97.47%	93.14%	44.59%
D3-2	43,334,934	43,334,914	97.47%	93.20%	44.58%
D3-3	42,901,164	42,901,140	97.55%	93.37%	44.63%
D4-1	43,376,796	43,376,776	98.16%	95.00%	44.50%
D4-2	43,375,470	43,375,456	98.09%	94.74%	43.93%
D4-3	43,398,338	43,398,322	98.20%	95.06%	44.65%
D5-1	43,334,392	43,334,348	97.95%	94.46%	44.44%
D5-2	43,351,042	43,350,978	97.15%	92.67%	43.94%
D5-3	43,351,570	43,351,560	97.90%	94.21%	44.00%

2.3. Differentially Expressed Genes (DEGs) Analysis

Differentially expressed genes (DEGs) were identified using the DESeq2 algorithm with thresholds of $|\log_2\text{FoldChange}| \geq 1$ and adjusted $p < 0.05$. Although bark samples were collected across five developmental stages (D1–D5), particular attention was given to stages D2–D4, during which anthocyanin levels declined most rapidly, in order to capture transcriptional regulatory changes closely associated with pigment loss. A total of 627 upregulated and 175 downregulated genes were detected in the comparison between D2 and D3, while 265 upregulated and 283 downregulated genes were identified between D3 and D4 (Figure 2a). These findings suggest that bark pigment loss is accompanied by continuous and dynamic transcriptional reprogramming rather than a single discrete event, reflecting the progressive nature of anthocyanin degradation [22]. Venn diagram analysis revealed 83 DEGs shared between the two comparisons (Figure 2b), indicating that a set of common regulatory genes may play central roles in anthocyanin degradation in *S. alba* bark.

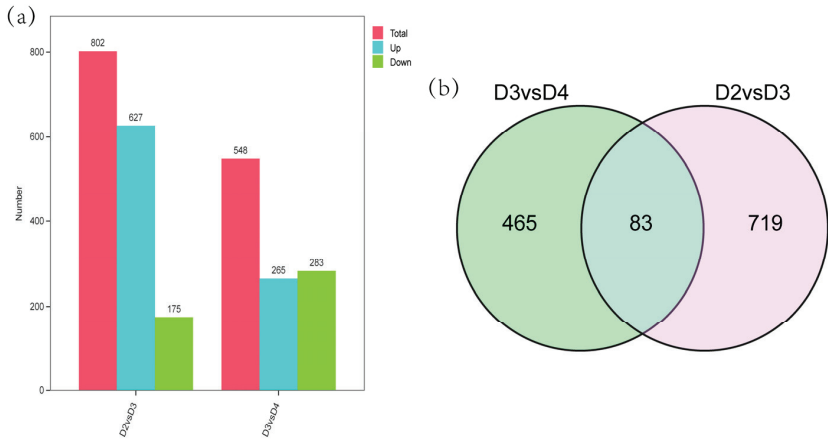


Figure 2. Differentially expressed genes (DEGs) associated with anthocyanin degradation in the bark of *Salix alba*. (**a**) Histogram showing the numbers of up- and down-regulated DEGs during the key degradation stages (D2–D4). (**b**) Venn diagram displaying the overlap of DEGs among these stages. DEGs were identified using DESeq2 with the thresholds of false discovery rate (FDR) < 0.05 and $|\log_2\text{FoldChange}| > 1$.

2.4. GO Enrichment Analysis of Common DEGs

To elucidate the potential functions of the 83 DEGs shared between the two comparisons, Gene Ontology (GO) enrichment analysis was conducted. These genes were predominantly associated with cellular components including the cell wall, apoplast, plasma membrane, and cell–cell junctions. In terms of molecular function, significant categories comprised DNA binding, transcription factor activity, hydrolase activity on glycosyl bonds, and oxidoreductase activity. At the biological process level, enrichment was observed in responses to oxidative stress, flavonoid metabolic process, cell wall organization, auxin-activated signaling, carbohydrate metabolism, and defense responses (Figure 3). Collectively, the GO terms indicated enrichment of the shared DEGs in categories related to cell structural organization, enzymatic activities, and stress- and metabolism-associated processes.

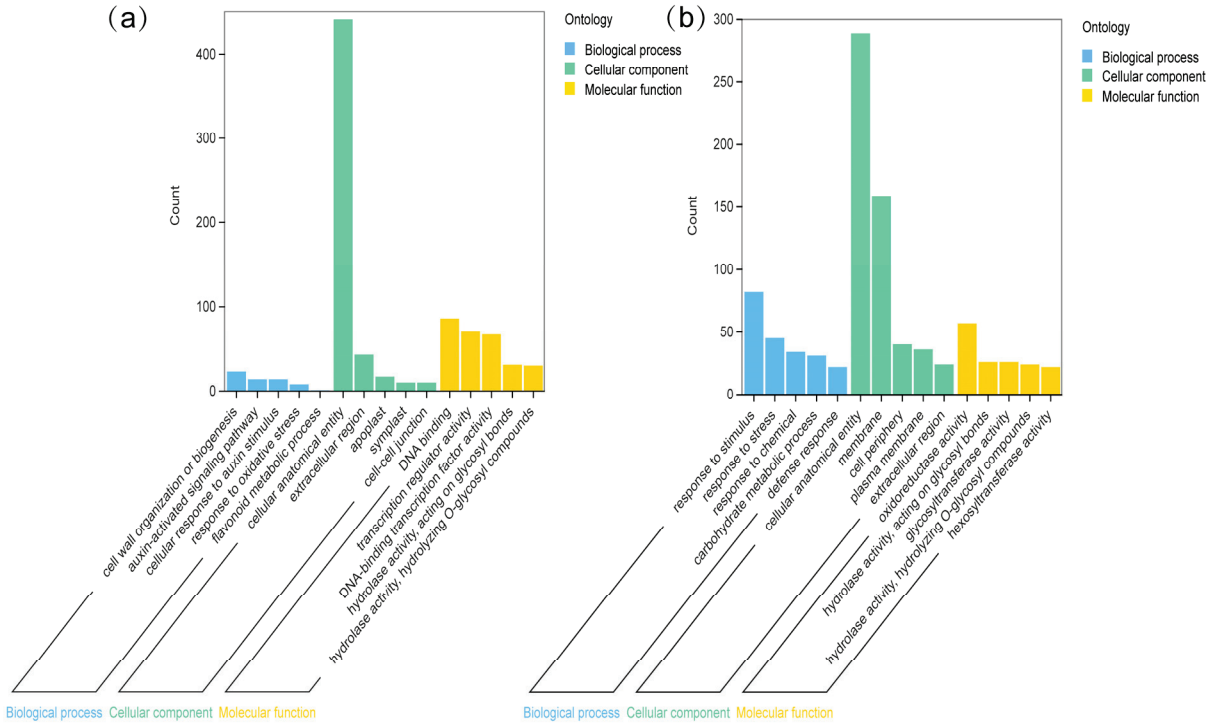


Figure 3. Gene Ontology (GO) enrichment analysis of differentially expressed genes (DEGs) during anthocyanin degradation in the bark of *Salix alba*. The top 10 significantly enriched GO terms for each stage comparison are shown. Analyses were conducted for D2 vs. D3 (**a**) and D3 vs. D4 (**b**), with enriched terms classified into three categories: biological process (BP), molecular function (MF), and cellular component (CC).

2.5. KEGG Pathway Enrichment Analysis of Common DEGs

Further KEGG pathway enrichment analysis revealed that the 83 shared DEGs were distributed across multiple metabolic and signaling pathways (Figure 4). In the metabolism category, significant enrichment was observed in phenylpropanoid biosynthesis, cysteine and methionine metabolism, cyanoamino acid metabolism, starch and sucrose metabolism, and glutathione metabolism, as well as in broad categories such as metabolic pathways and biosynthesis of secondary metabolites. In addition, several DEGs were assigned to environmental information processing pathways, including MAPK signaling and plant hormone signal transduction, while others were enriched in ABC transporters and peroxisome-related processes. At the organismal level, plant–pathogen interaction was also significantly represented. Collectively, these enriched pathways spanned primary metabolism, secondary metabolite biosynthesis, stress signaling, and transport processes.

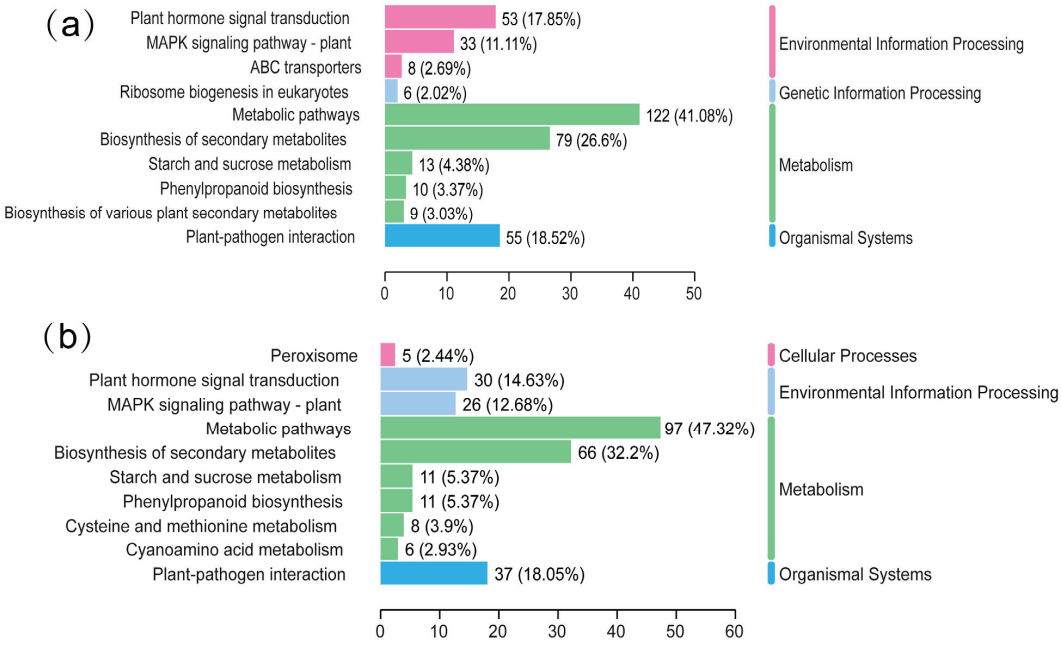


Figure 4. KEGG pathway enrichment analysis of differentially expressed genes (DEGs) during anthocyanin degradation in the bark of *Salix alba*. The top 10 significantly enriched pathways for each comparison are shown. Analyses were conducted for D2 vs. D3 (**a**) and D3 vs. D4 (**b**), with enriched pathways classified into major functional categories, including metabolism, cellular processes, and environmental information processing.

2.6. Transcription Factor Profiling Associated with Anthocyanin Degradation

Transcription factors (TFs) are central regulators of gene expression and play pivotal roles in plant growth, development, stress responses, and secondary metabolism. In the bark of *Salix alba*, a total of 2207 TFs were annotated, classified into 57 families. Among them, *MYB-related* (271) and canonical *MYB* (215) were the most abundant, followed by *C3H* (210), *bZIP* (111), *HB-other* (89), *HB-PHD* (87), and *bHLH* (53). Together, these results indicate that *MYB* and *C3H* families dominate the TF repertoire of *S. alba* bark, while diverse other families also contribute to transcriptional regulation during bark development (Figure 5).

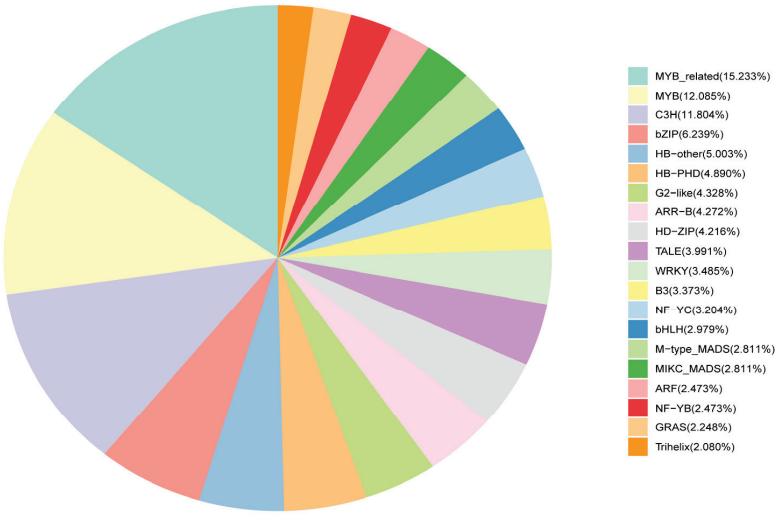


Figure 5. Identification and classification of transcription factors (TFs) in the bark of *Salix alba*. The pie chart illustrates the distribution of major TF families, with *MYB-related, MYB, and C3H* being the most abundant. Percentages indicate the relative proportion of each family among all identified TFs.The slight deviation from 100% is due to rounding of values and the partial display of top TF families.

2.7. Identification of Candidate Genes Involved in Anthocyanin Degradation

To identify structural enzymes potentially involved in anthocyanin degradation in *Salix alba* bark, we focused on differentially expressed genes (DEGs) annotated as laccases (*LAC*), peroxidases (*POD*), β-glucosidases (*BGLU10*), and polyphenol oxidases (*PPO*). Five candidate genes—*LAC1* (novel2814_c2_g9), *LAC2* (OIU76_005661_c2_g1), *POD1* (OIU76_024764_c3_g3), *POD2* (OIU76_030521_c3_g24), and *BGLU10* (OIU76_013561_c4_g11)—exhibited peak transcript levels at stage D4 (Figure 6). Although *PPO* did not show significant differential expression, it displayed dynamic transcriptional variation during stages D2–D4, suggesting a possible auxiliary role in anthocyanin metabolism.

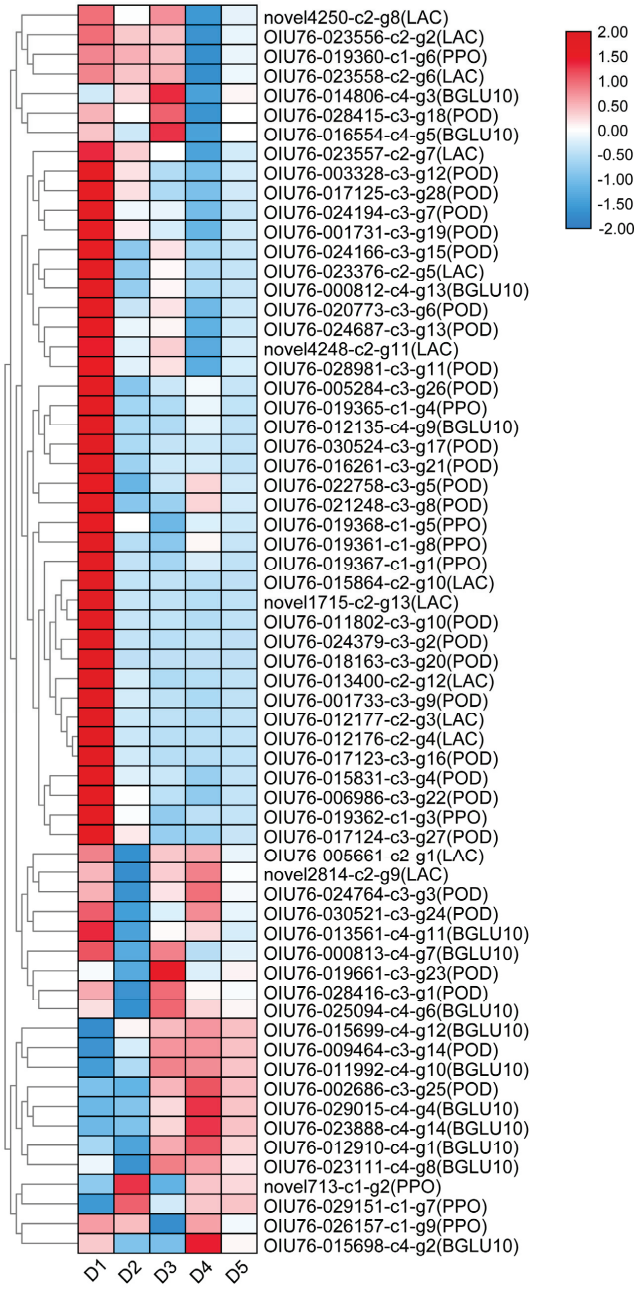


Figure 6. Expression heatmap of candidate anthocyanin-degrading enzyme genes in the bark of *Salix alba*. The heatmap depicts four enzyme families—laccases (*LAC*), peroxidases (*POD*), β-glucosidases (*BGLU*), and polyphenol oxidases (*PPO*)—across all samples. Color gradients from blue to red represent low to high expression levels based on FPKM values. Both genes and samples were hierarchically clustered to highlight similar expression patterns and potential co-expression relationships, providing a foundation for candidate gene identification and subsequent network analysis.

2.8. Weighted Gene Co-Expression Network Analysis (WGCNA)

To elucidate the potential regulatory framework underlying anthocyanin degradation in *Salix alba* bark, weighted gene co-expression network analysis (WGCNA) was conducted based on the RNA-seq dataset [27]. After removing low-variance genes, 20,874 annotated genes were retained by selecting the top 75% ranked by median absolute deviation (MAD) or those with MAD > 0.01, thereby improving network stability. Hierarchical clustering showed that no outlier samples were detected, confirming the consistency of biological replicates (Figure 7a). The optimal soft-thresholding power (β = 16) was determined using the pickSoftThreshold function, which yielded a scale-free topology fit index of $R^2 > 0.8$ and an average connectivity below 100 (Figure 7b), meeting the criteria for constructing biologically meaningful modules. Using the blockwise module detection method, 14 distinct co-expression modules were identified, each represented by a unique color (Figure 7c).

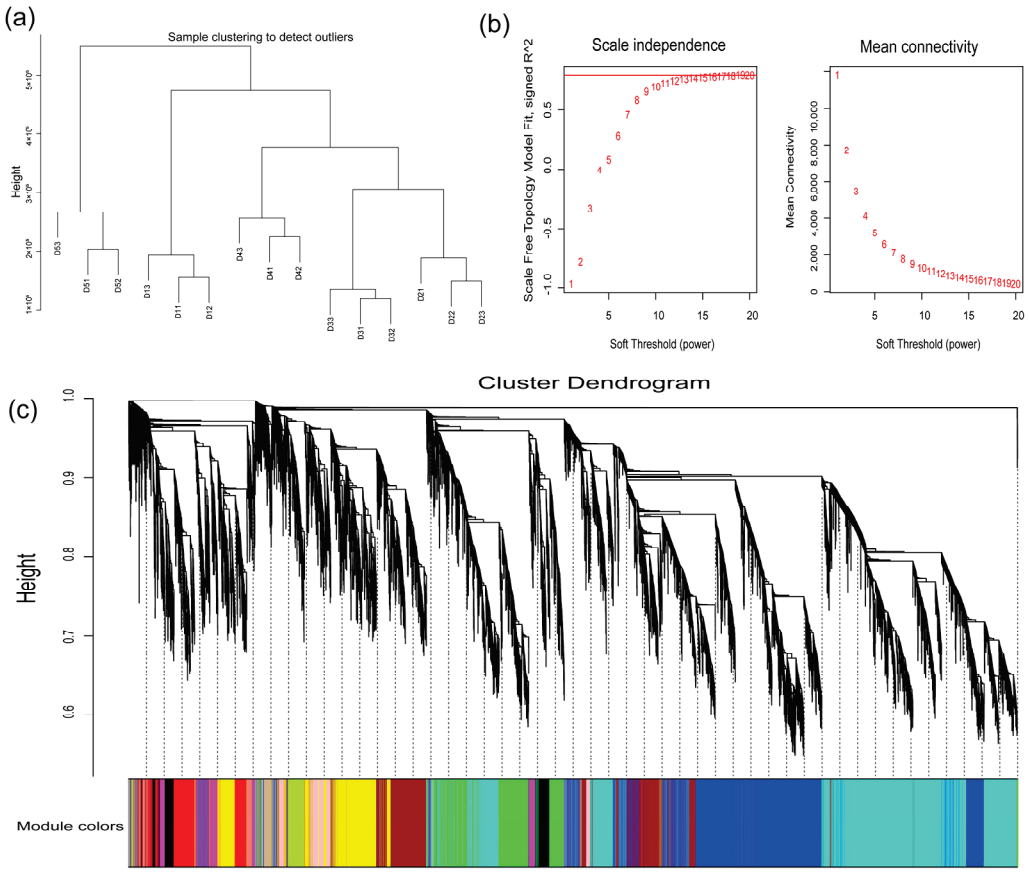


Figure 7. Construction of a weighted gene co-expression network (WGCNA) in the bark of *Salix alba*. (**a**) Sample clustering dendrogram of 15 biological samples used to evaluate sample similarity and identify potential outliers. (**b**) Soft-threshold analysis for determining the appropriate power value for network construction. (**c**) Gene clustering and module assignment, showing the grouping of genes into distinct co-expression modules, which serves as the basis for subsequent network analysis and module–trait association.Each color represents a distinct co-expression module identified by WGCNA.

Module sizes ranged from 120 genes in the salmon module to 6210 genes in the turquoise module (Figure 8a). To assess the relationship between gene modules and anthocyanin content, the phenotypic trait was binarized as high (purple stage = 1) and low (red stage = 0). Correlation analysis revealed that the brown module exhibited the strongest negative association with anthocyanin levels (r = –0.68, $p < 0.01$), indicating its potential involvement in pigment degradation (Figure 8b).

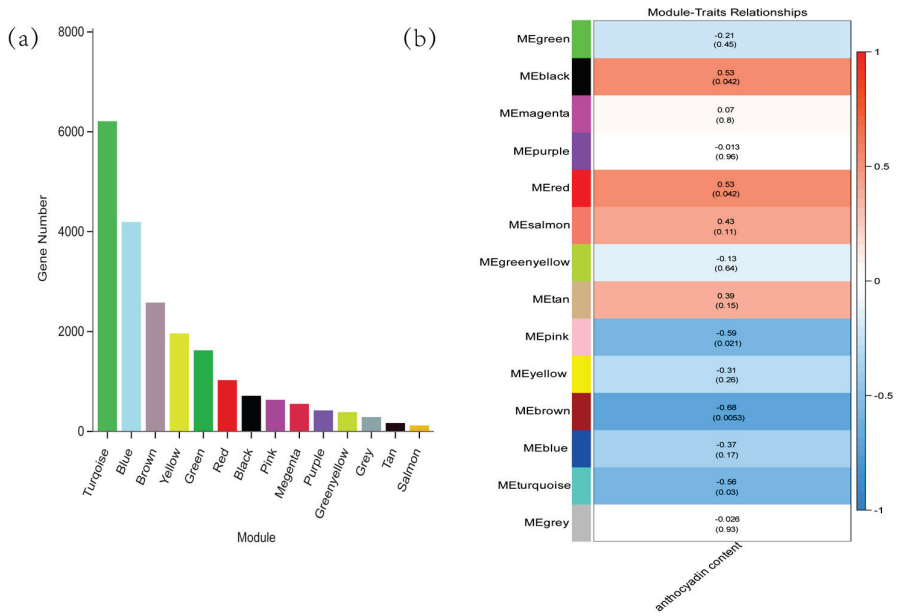


Figure 8. WGCNA module analysis in the bark of *Salix alba*. (**a**) Number of genes in 14 co-expression modules. (**b**) Module–trait correlation heatmap illustrating the associations between the 14 modules and anthocyanin content. Colors represent the magnitude and direction of Pearson correlation coefficients, with red indicating positive correlations and blue indicating negative correlations. This analysis highlights modules most strongly associated with anthocyanin dynamics, forming the basis for hub gene identification and subsequent co-expression network analysis.

Within the brown module, the gene OIU76_005661 emerged as a hub based on its high intramodular connectivity and an expression pattern closely paralleling the temporal decline in anthocyanin concentration. To visualize the underlying co-expression network, Cytoscape (version 3.10.1) was employed to construct a subnetwork containing 20,874 edges (with weight > 0.2). The top 50 genes ranked by degree centrality were extracted and plotted to highlight putative regulatory hubs (Figure 9).

2.9. Transcription Factor–Enzyme Co-Expression and Integrated Regulatory Framework of Anthocyanin Degradation

The five candidate genes (*LAC1*, *LAC2*, *POD1*, *POD2*, and *BGLU10*) exhibited significant co-expression patterns and, together with multiple transcription factors—particularly members of the *MYB*, *bHLH*, and *CAMTA* families—formed a putative core transcriptional regulatory module. To further dissect the regulatory hierarchy, the expression patterns of TFs identified from the transcriptome were compared with those of the key degradation-related genes, leading to the construction of a TF–target gene co-expression network (Figure 10). Within this network, *CAMTA* family TFs showed strong positive correlations with *LAC1*, *LAC2*, and *POD1*, suggesting their possible involvement in bark pigment metabolism via calcium signaling pathways. A *bHLH* TF exhibited a correlation coefficient of 0.91 with *POD1*, indicating a potentially crucial regulatory role within the TF–enzyme module [28]. In addition, *WRKY* TFs were also significantly co-expressed with *POD1* (r = 0.901), implying a role for *WRKYs* in the regulation of anthocyanin degradation [29]. Nevertheless, their precise functions and mechanisms of action require further validation through experimental approaches such as yeast one-hybrid (Y1H), chromatin immunoprecipitation (ChIP), or gene editing.

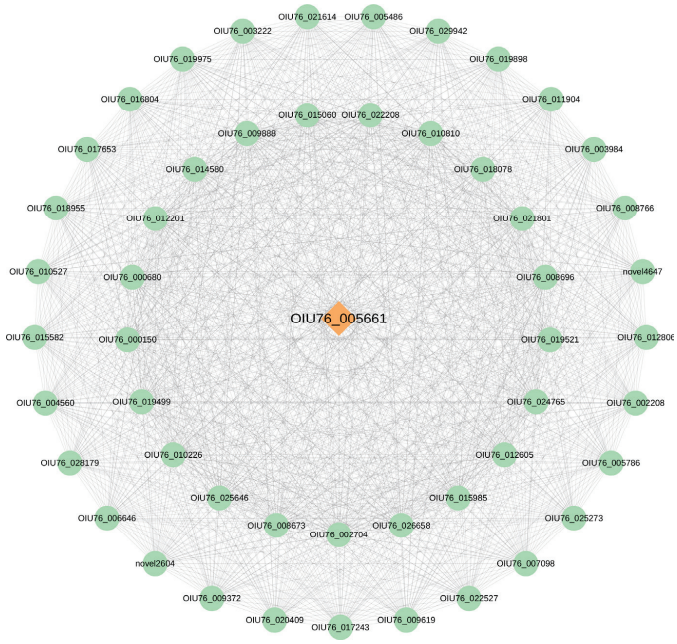


Figure 9. Co-expression network of the brown module identified by WGCNA in the bark of *Salix alba*. The network highlights candidate key genes potentially involved in anthocyanin degradation. The hub gene OIU76_005661 is represented by an orange diamond, showing high intramodular connectivity and a negative correlation with anthocyanin content. The top 50 genes ranked by degree centrality are displayed as green circles, forming a putative regulatory subnetwork. Only edges with weights > 0.2 are shown to emphasize strong co-expression relationships. Network visualization was performed using Cytoscape.

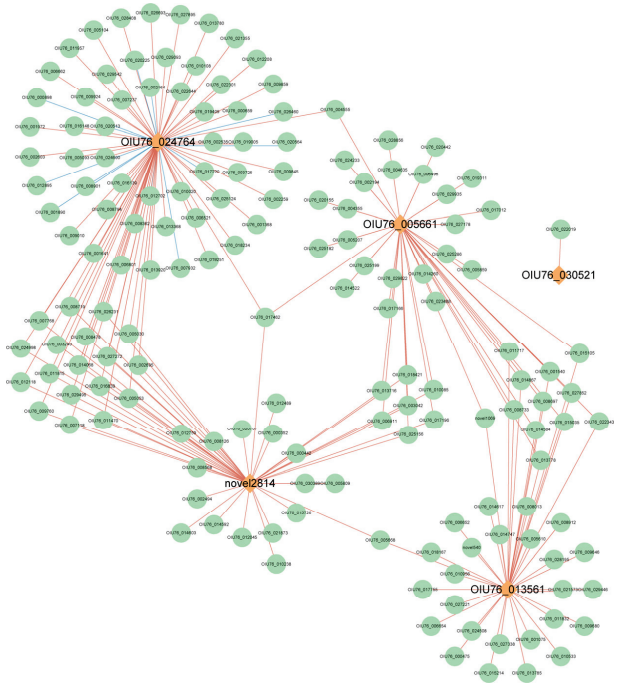


Figure 10. Co-expression network of anthocyanin degradation-related structural genes and transcription factors in the bark of *Salix alba*. Five key candidate enzyme genes (*LAC1, LAC2, POD1, POD2,* and *BGLU10*) are represented by orange diamonds, while transcription factors are depicted as green circles. Red edges indicate positive correlations and blue edges indicate negative correlations. The network reveals potential co-expression relationships between enzyme genes and transcription factors, including *MYB, bHLH, CAMTA*, and *WRKY*, suggesting that multi-level transcriptional regulation may underlie seasonal anthocyanin degradation in white willow bark.

3. Discussion

3.1. Spatiotemporal Dynamics of Anthocyanins in Bark and Ecological Implications

In this study, anthocyanin content in the bark of *Salix alba* exhibited pronounced stage-specific variation, with the peak and subsequent decline closely aligned with visible pigment fading. Such stage-dependent changes suggest that anthocyanin metabolism is tightly linked to seasonal development and environmental cues. This study demonstrates that anthocyanins in the bark of *Salix alba* exhibit pronounced spatiotemporal dynamics across developmental stages, indicating that their degradation is not merely a passive loss of pigments but rather a finely regulated metabolic process [30]. The stage-specific decline of anthocyanins during winter likely reflects adaptive strategies to low temperature, light variation, and seasonal stress conditions [31–33]. Beyond their conventional roles in photoprotection and antioxidative defense, the accumulation and degradation of anthocyanins may also contribute to the regulation of bark light absorption properties and antioxidant metabolism, thereby providing protective advantages under harsh winter environments [34,35]. Comparable seasonal dynamics of anthocyanins have been documented in other deciduous woody species, including willow (*Salix alba* spp.) [22], maple (*Acer* spp.) [34], and birch (*Betula* spp.) [36], where pigment accumulation and degradation are closely associated with bark light absorption, antifreeze protein activity, and osmotic adjustment. These findings suggest that anthocyanin degradation in bark represents an important metabolic strategy for seasonal environmental adaptation in woody plants. This interpretation also clarifies the biological significance of the observed up- and down-variation in anthocyanin content, linking pigment turnover to adaptive strategies under fluctuating seasonal conditions.

3.2. Candidate Enzyme Genes as Central Mediators of Anthocyanin Degradation

Transcriptome analysis revealed that *LAC1*, *LAC2*, *POD1*, *POD2*, and *BGLU10* were highly expressed during stages D2–D4, with peak levels coinciding with the period of anthocyanin decline, suggesting that these enzymes play central roles in the degradation process [37]. Among them, *LAC1/2* are likely to mediate anthocyanin oxidation [38], *POD1/2* contribute to oxidative degradation through the regulation of H_2O_2 and other reactive oxygen species [39], while *BGLU10* hydrolyzes anthocyanin glycosides [40], generating substrates that are more readily degraded. The expression of these enzymes may be influenced by environmental signals such as low temperature, light intensity, and spectral composition, thereby enabling functions related to photoprotection and thermal buffering. Similar enzyme-mediated degradation mechanisms have been observed in woody plants such as poplar (*Populus* spp.) [41], maple (*Acer* spp.) [42], and tea (*Camellia sinensis*) [43], indicating that bark anthocyanin degradation may represent a broadly conserved adaptive metabolic strategy. To further clarify the regulatory context of these enzyme genes, functional enrichment analysis was performed.

3.3. Functional Enrichment Reveals Multi-Layered Metabolic Regulation

Functional enrichment analysis indicated that the differentially expressed genes (DEGs) were predominantly associated with redox processes, hydrolase activity, glycosidic bond hydrolysis, flavonoid metabolism, and plant hormone signaling pathways. These enriched categories were broadly consistent with the regulatory patterns revealed by the co-expression networks of structural enzymes and transcription factors, suggesting that anthocyanin degradation is subject to multi-layered regulation. In this process, glycosidic hydrolysis may release substrates susceptible to degradation, while redox-related enzymes influence the progression of degradation by modulating local reactive oxygen species (ROS) levels [44]. In parallel, plant hormone signaling pathways—such as

AUX/IAA and ABA—may exert additional control through transcription factor-mediated regulation [45,46]. Similar associations between anthocyanin accumulation/degradation and environmental cues such as light, temperature, and seasonal signals have been reported in woody plants including camphor (*Cinnamomum camphora*) [47], birch (*Betula* spp.) [48], and oak *(Quercus* spp.) [49], highlighting the pivotal role of anthocyanin degradation in seasonal environmental adaptation and carbon allocation in woody species. Furthermore, metabolic reallocation may contribute to carbon storage during dormancy and provide energy during spring bud break, indicating that anthocyanin degradation is not merely a consequence of pigment metabolism but also an integral component of the ecological adaptation strategies of woody plants [50–53].

3.4. Transcription Factors and Co-Expression Networks in Regulatory Control

Weighted gene co-expression network analysis (WGCNA) revealed that multiple transcription factors (TFs), including *MYB*, *bHLH*, *WRKY*, *bZIP*, *HB-PHD*, *G2-like*, and *ARR-B*, exhibited co-expression patterns with structural enzymes, indicating that anthocyanin degradation is governed by a complex transcriptional regulatory network [54]. The *MYB/bHLH* complex within the MBW system may simultaneously regulate both biosynthetic and degradation-related genes, thereby maintaining the dynamic balance of bark coloration [55,56]. *WRKY* TFs are known to respond to oxidative stress and hormonal signaling [57], while *bZIP* and *HD-ZIP* TFs may integrate light and temperature signals to further regulate the expression of *LAC*, *POD*, and *BGLU* genes [58]. Similar phenomena have been reported in larch (*Larix* spp.) [59] and poplar (*Populus* spp.) [60], where *WRKY* TFs and peroxidase genes are co-upregulated during winter or under light stress, thereby coordinating local ROS regulation with anthocyanin degradation. These findings indicate that the dynamic variation in bark anthocyanins reflects not only a metabolic process but also the integrative capacity of woody plants to process environmental information. Building upon these observations, broader integration of transcription factor–enzyme modules highlights the multi-layered regulatory framework of anthocyanin degradation.

Collectively, the results indicate that anthocyanin degradation in *Salix alba* bark is likely governed by a multi-layered transcriptional regulatory system, encompassing both broad-spectrum transcription factors responsive to environmental cues and key regulators specifically targeting flavonoid metabolism. Comparable WGCNA-based co-expression regulatory networks have been reported in tea (Camellia sinensis) [61], grape (Vitis vinifera) [62], and litchi (Litchi chinensis) [63], suggesting that transcriptional reprogramming associated with pigment fading and senescence may be evolutionarily conserved across plant species. Together, these results suggest that *POD*, *LAC*, *BGLU10* and hub TFs (*MYB*, *bHLH*, *CAMTA*) form core regulatory modules underlying seasonal bark coloration in *S. alba*, highlighting anthocyanin degradation as a tightly coordinated and environmentally responsive process. Despite these advances, some important limitations should be acknowledged.

3.5. Limitations and Future Perspectives

It should be noted that although this study incorporated monthly climate background data (temperature and precipitation) from publicly available meteorological datasets, it did not directly measure environmental variables such as light intensity, spectral composition, or endogenous hormone levels. Therefore, the environmental responsiveness of anthocyanin dynamics in *Salix alba* bark remains to be further validated. Moreover, as this work focused on one-year-old shoots, the applicability of the findings to mature trees requires further confirmation. Nevertheless, by integrating evidence from ROS accumulation, antioxidant enzyme activity, and transcriptomic analyses, we propose that anthocyanin degradation may represent an adaptive strategy regulated through gene × en-

vironment interactions. Future research incorporating real-time environmental monitoring, endogenous hormone profiling, and functional validation approaches (e.g., CRISPR/Cas9 or transgenic experiments) will be critical to elucidate the precise roles of specific enzymes and transcription factors under natural conditions. Furthermore, additional studies should explore the potential functions of anthocyanin degradation in cold tolerance, light stress resistance, and pathogen defense of woody plants, thereby providing a robust molecular basis for ornamental tree breeding and sustainable forest management.

In summary, this study advances the current understanding of anthocyanin metabolism in *Salix alba* bark by linking pigment dynamics with structural enzymes (*LAC1/2*, *POD1/2*, and *BGLU10*), transcription factors, and their regulatory networks. The findings highlight the dynamic balance between anthocyanin biosynthesis and degradation and its potential roles in environmental adaptation, offering valuable insights into seasonal metabolic regulation, stress resilience, and ornamental trait improvement in woody plants. Future research should extend this framework to other deciduous tree species to further elucidate the general functions of anthocyanins in light acclimation, carbon allocation, stress resistance, and defense. Such efforts will provide a solid theoretical basis for forest ecology and functional genomics in woody species.

4. Materials and Methods

4.1. Plant Materials, Experimental Site, and Climate Background

Ten healthy one-year-old *Salix alba* plants propagated from the same batch of cuttings were cultivated at the Sanfen Experimental Base of Hebei Agricultural University, Baoding, China (115°24′56″ E, 38°48′35″ N). The region has a temperate monsoon climate with a mean annual temperature of ~12.5 °C and an average annual precipitation of ~550 mm, based on records from the Baoding Meteorological Station. To provide environmental context, monthly mean temperature and precipitation during the sampling period (November 2024–March 2025, corresponding to D1–D5) are summarized in Table 2. The soil type was classified as brown loam with a pH of 7.2–7.5. All plants were maintained under uniform silvicultural management, including standardized irrigation, fertilization, and pest control, to minimize confounding environmental variation.

Table 2. Monthly mean temperature (°C) and precipitation (mm/day) at the experimental site in Baoding, Hebei Province, China, during the sampling period (November 2024–March 2025; stages D1–D5). Climate data were obtained from the NASA POWER Climate Data Service (https://power.larc.nasa.gov) for the grid cell centered at 38.92°N, 115.68°E, and represent model-based reanalysis estimates rather than direct ground observations.

Stage	Month	Temperature (°C)	Precipitation (mm)
D1	Nov 2024	7.61	20.4
D2	Dec 2024	−0.45	1.6
D3	Jan 2024	−1.74	5.0
D4	Feb 2025	−0.60	0.6
D5	Mar 2025	7.78	4.7

4.2. Sampling Design and Sample Preparation

Sampling commenced on 23 November 2024 (D1) and was conducted every 25 ± 1 days across five stages (D1–D5), thereby covering developmental transitions from late autumn to early spring. The 25-day interval was determined based on preliminary observations of seasonal bark pigment variation to ensure the capture of critical stages of anthocyanin metabolism. At each stage, vigorous branches were collected from the sun-exposed side of current-year shoots (diameter 0.8–1.2 cm, length ~10 cm) of all 10 individuals to reduce intra-plant microenvironmental heterogeneity.

To establish three independent biological replicates at each stage, a pooled sampling strategy was adopted. For each replicate, equal bark segments from a randomly selected subset of the 10 individuals were combined, ensuring proportional representation of all plants. This design minimized individual-level variability while enhancing the robustness of stage-specific comparisons. Each pooled sample was divided into two portions, one for anthocyanin quantification and the other for transcriptomic sequencing. Immediately after harvest, samples were flash-frozen in liquid nitrogen and stored at –80 °C. Prior to analysis, the bark periderm was removed, and the underlying phloem tissue was collected, ground into fine powder under liquid nitrogen, and used for subsequent experiments.

4.3. Anthocyanin Quantification

Total anthocyanin content in bark tissues was quantified using acidified methanol extraction coupled with a modified spectrophotometric method. Approximately 0.1 g of phloem tissue, previously ground in liquid nitrogen, was extracted with 1 mL of acidified methanol (0.1% HCl, v/v) under dark conditions at 4 °C for 48 h to enhance the recovery of anthocyanins, including partially conjugated forms. The extracts were centrifuged at 12,000× g for 10 min at 4 °C, and the supernatant was collected for absorbance measurement at 530 nm and 657 nm using a UV–Vis spectrophotometer (UV-1800, Shimadzu, Kyoto, Japan). The corrected absorbance was calculated as $\Delta A = A530 - A657$.

The total anthocyanin content was determined according to the following equation:

$$Anthocyanin\ content\ (mg/g\ FW) = \frac{\Delta A \times 0.005 \times 1000 \times 445.2}{30200 \times 0.1}$$

In this formula, 0.005 L represents the extraction volume; 445.2 g·mol^{-1} corresponds to the molecular weight of cyanidin-3-galactoside; 30,200 L·mol^{-1}·cm^{-1} is its molar extinction coefficient; 0.1 g denotes the fresh weight of the sample; and 1000 is the conversion factor. The calculation was adapted from the pH differential method described by Giusti and Wrolstad (2001) (Current Protocols in Food Analytical Chemistry, John Wiley & Sons) with modifications to accommodate the experimental conditions, including detection wavelengths, sample mass, and extraction system [64].

4.4. RNA Extraction and Transcriptome Sequencing

Total RNA was extracted from ground phloem tissue using the Plant RNA Kit (Tiangen Biotech, Beijing, China) following the manufacturer's protocol. RNA quality was evaluated by 1.5% agarose gel electrophoresis, a NanoDrop 2000 spectrophotometer (Thermo Fisher Scientific, Waltham, MA, USA), and an Agilent 2100 Bioanalyzer (Agilent Technologies, Santa Clara, CA, USA). Samples with RNA integrity number (RIN) $\geq$ 7.0 and OD260/280 between 1.8 and 2.2 were used for library preparation.

RNA-seq libraries were prepared with the NEBNext® Ultra™ RNA Library Prep Kit (New England Biolabs, Ipswich, MA, USA) and sequenced on an Illumina NovaSeq 6000 platform (paired-end 2 × 150 bp) by Benagen Tech Solutions (Wuhan, China).

4.5. Transcriptome Data Processing and Co-Expression Network Analysis

Raw sequencing reads were processed with Fastp v0.23.2 to remove adapters and low-quality sequences. Clean reads were aligned to the *Salix alba* reference genome (GCA_029030765.1_ASM2903076v1) using HISAT2 v2.2.1. Transcript assembly and expression quantification were performed with StringTie v2.2.0, and expression levels were normalized as fragments per kilobase of transcript per million mapped reads (FPKM).

Differentially expressed genes (DEGs) were identified using DESeq2 v1.30.0 with thresholds of $|\log_2$ fold change$| \geq 1$ and adjusted $p < 0.05$. Functional annotation was

conducted via BLASTx searches against the NR, SwissProt, Pfam, GO, and KEGG databases. GO enrichment was performed using the topGO R package(version 2.52.0), and KEGG pathway enrichment with KOBAS 3.0.

For weighted gene co-expression network analysis (WGCNA), genes with FPKM < 1 in all samples were excluded. A soft-thresholding power (β) of 16 was chosen to approximate scale-free topology. Gene modules were identified using the blockwiseModules function with dynamic tree cutting, and Pearson correlation analysis was applied to assess module–trait associations using anthocyanin content as a quantitative trait. Hub genes were defined as those with module membership (kME) > 0.8.

4.6. Transcription Factor Annotation and Co-Expression Analysis

To identify transcription factors (TFs) potentially involved in anthocyanin degradation, all assembled unigenes were searched against the Plant Transcription Factor Database (PlantTFDB v5.0) using BLASTX with an E-value cutoff of 1×10^{-5}. In total, 2207 TFs were identified across 57 families, with *MYB* (n = 468) being the most abundant, followed by *bHLH*, *WRKY*, *C3H*, and *CAMTA*—families previously linked to flavonoid metabolism and abiotic stress responses.

For TF–target co-expression network construction, Pearson correlation coefficients were calculated between the expression profiles of TFs and differentially expressed genes (DEGs). Pairs with $|r| \geq 0.8$ and $p < 0.01$ were retained, and networks were visualized in Cytoscape v3.9.1. TFs co-expressed with candidate structural genes (peroxidases, laccases, β-glucosidases) or WGCNA-identified hub genes were prioritized as strong candidates for regulating anthocyanin catabolism in *Salix alba* bark.

4.7. Statistical Analysis

All experiments were performed with three biological replicates unless otherwise specified. Data are expressed as mean ± standard deviation (SD). Differences in anthocyanin content among developmental stages (D1–D5) were analyzed using one-way analysis of variance (ANOVA), followed by Tukey's honest significant difference (HSD) test for multiple comparisons at a significance level of $p < 0.05$. All statistical analyses were conducted using GraphPad Prism 9 (GraphPad Software, San Diego, CA, USA).

5. Conclusions

In conclusion, this study systematically elucidated the dynamics of anthocyanin degradation in the bark of *Salix alba* across different developmental stages. The results suggest that key structural enzymes, including *LAC1/2*, *POD1/2*, and *BGLU10*, together with multiple transcription factors such as *MYB*, *bHLH*, and *WRKY*, are potentially involved in this process, in close association with redox reactions, glycoside hydrolysis, flavonoid metabolism, and plant hormone signaling pathways. These findings provide important insights into the dynamic regulation of bark pigmentation and its underlying molecular networks in woody plants, although their precise functions still require further validation under natural environmental conditions. Overall, this study offers a scientific basis and preliminary clues for exploring the molecular mechanisms of anthocyanin degradation, as well as for advancing research on stress resilience and ornamental traits in woody species.

Author Contributions: Conceptualization, H.-Y.W.; formal analysis, H.-Y.W.; methodology, H.-Y.W.; investigation, H.-Y.W., M.-Z.Y. and S.-J.C.; resources, X.-J.L. and H.-Y.L.; data curation, H.-Y.W.; writing—original draft preparation, H.-Y.W.; writing—review and editing, H.-Y.L.; project administration, H.-Y.L. and Z.-H.X.; Funding acquisition, Z.-H.X. All authors have read and agreed to the published version of the manuscript.

Funding: This research was funded by Research and Application of Key Technology of Willow Flying Flocs Treatment (13000024P00141410178C).

Data Availability Statement: Data are contained within the article.

Conflicts of Interest: The authors declare no conflicts of interest.

References

1. Xu, L.; Wang, X. A Comprehensive Review of Phenolic Compounds in Horticultural Plants. *Int. J. Mol. Sci.* **2025**, *26*, 5767. [CrossRef]
2. Kuang, L.; Chen, J.; Bao, X.; Zhang, D.; Liu, J.; Wang, W.; Wei, Y.; Zong, C. Environmental and Phytohormonal Factors Regulating Anthocyanin Biosynthesis in Fruits. *Horticulturae* **2025**, *11*, 681. [CrossRef]
3. Câmara, J.S.; Locatelli, M.; Pereira, J.A.M.; Oliveira, H.; Arlorio, M.; Fernandes, I.; Perestrelo, R.; Freitas, V.; Bordiga, M. Behind the Scenes of Anthocyanins—From the Health Benefits to Potential Applications in Food, Pharmaceutical and Cosmetic Fields. *Nutrients* **2022**, *14*, 5133. [CrossRef] [PubMed]
4. Cheaib, A.; Mahmoud, L.M.; Vincent, C.; Killiny, N.; Dutt, M. Influence of Anthocyanin Expression on the Performance of Photosynthesis in Sweet Orange, *Citrus sinensis* (L.) Osbeck. *Plants* **2023**, *12*, 3965. [CrossRef] [PubMed]
5. Ashikhmin, A.; Bolshakov, M.; Pashkovskiy, P.; Vereshchagin, M.; Khudyakova, A.; Shirshikova, G.; Kozhevnikova, A.; Kosobryukhov, A.; Kreslavski, V.; Kuznetsov, V.; et al. The Adaptive Role of Carotenoids and Anthocyanins in *Solanum lycopersicum* Pigment Mutants under High Irradiance. *Cells* **2023**, *12*, 2569. [CrossRef] [PubMed]
6. Mohammed, H.A.; Khan, R.A. Anthocyanins: Traditional Uses, Structural and Functional Variations, Approaches to Increase Yields and Products' Quality, Hepatoprotection, Liver Longevity, and Commercial Products. *Int. J. Mol. Sci.* **2022**, *23*, 2149. [CrossRef]
7. Dabravolski, S.A.; Isayenkov, S.V. The Role of Anthocyanins in Plant Tolerance to Drought and Salt Stresses. *Plants* **2023**, *12*, 2558. [CrossRef]
8. Duan, X.; Wang, K.; Tang, R.; Liu, J.; Cheng, K.; Gao, G.; Wang, Y.; Qin, G. Recent advances in biosynthesis and regulation of strawberry anthocyanins. *Hortic. Res.* **2025**, *12*, uhaf135. [CrossRef]
9. Zhao, G.; Xiang, F.; Zhang, S.; Song, J.; Li, X.; Song, L.; Zhai, R.; Yang, C.; Wang, Z.; Ma, F.; et al. PbLAC4-like, activated by PbMYB26, related to the degradation of anthocyanin during color fading in pear. *BMC Plant Biol.* **2021**, *21*, 469. [CrossRef]
10. Wu, Y.; Han, T.; Lyu, L.; Li, W.; Wu, W. Research progress in understanding the biosynthesis and regulation of plant anthocyanins. *Sci. Hortic.* **2023**, *321*, 112374. [CrossRef]
11. Zhao, Y.W.; Wang, C.K.; Huang, X.Y.; Hu, D.G. Anthocyanin stability and degradation in plants. *Plant Signal. Behav.* **2021**, *16*, 1987767. [CrossRef] [PubMed]
12. Sun, T.; Wang, M.; Ren, H.; Xiong, Q.; Xu, J.; Yang, X.; Chen, Y.; Zhang, W. Comprehensive analysis of the physiological, metabolome, and transcriptome provided insights into anthocyanin biosynthesis and degradation of Malus crabapple. *Plant Physiol. Biochem.* **2025**, *223*, 109821. [CrossRef] [PubMed]
13. Ha, H.; Thuy, N. Kinetic study on peroxidase inactivation and anthocyanin degradation of black cherry tomatoes (*Solanum lycopersicum* cv. OG) during blanching. *Herba Pol.* **2021**, *67*, 60–69. [CrossRef]
14. Adhikari, J.; Araghi, L.R.; Singh, R.; Adhikari, K.; Patil, B.S. Continuous-Flow High-Pressure Homogenization of Blueberry Juice Enhances Anthocyanin and Ascorbic Acid Stability during Cold Storage. *J. Agric. Food Chem.* **2024**, *72*, 11629–11639. [CrossRef]
15. Achim, F.; Dinca, L.; Chira, D.; Raducu, R.; Chirca, A.; Murariu, G. Sustainable Management of Willow Forest Landscapes: A Review of Ecosystem Functions and Conservation Strategies. *Land* **2025**, *14*, 1593. [CrossRef]
16. Xin, Y.; Huang, R.; Xu, M.; Xu, L.A. Transcriptome-Wide Identification and Response Pattern Analysis of the Salix integra NAC Transcription Factor in Response to Pb Stress. *Int. J. Mol. Sci.* **2023**, *24*, 11334. [CrossRef]
17. Yang, Y.; Chen, M.; Zhang, W.; Zhu, H.; Li, H.; Niu, X.; Zhou, Z.; Hou, X.; Zhu, J. Metabolome combined with transcriptome profiling reveals the dynamic changes in flavonoids in red and green leaves of *Populus* × *euramericana* 'Zhonghuahongye'. *Front. Plant Sci.* **2023**, *14*, 1274700. [CrossRef]
18. Guo, S.; Wang, S.; Zhao, S.; Zhang, X.; Ji, X.; Yun, C.; Wu, S.; Takayoshi, K.; Wang, W.; Wang, H. Plant species richness regulated by geographical variation down-regulates triterpenoid compounds production and antioxidant activities in white birch bark. *Flora* **2023**, *305*, 152343. [CrossRef]
19. Almuktar, S.A.A.A.N.; Abed, S.N.; Scholz, M. Biomass Production and Metal Remediation by *Salix alba* L. and *Salix viminalis* L. Irrigated with Greywater Treated by Floating Wetlands. *Environments* **2024**, *11*, 44. [CrossRef]
20. Bajraktari, D.; Bauer, B.; Zeneli, L. Antioxidant Capacity of *Salix alba* (Fam. Salicaceae) and Influence of Heavy Metal Accumulation. *Horticulturae* **2022**, *8*, 642. [CrossRef]
21. Piątczak, E.; Dybowska, M.; Płuciennik, E.; Kośla, K.; Kolniak-Ostek, J.; Kalinowska-Lis, U. Identification and accumulation of phenolic compounds in the leaves and bark of *Salix alba* (L.) and their biological potential. *Biomolecules* **2020**, *10*, 1391. [CrossRef]

22. Zhou, J.; Guo, J.; Chen, Q.; Wang, B.; He, X.; Zhuge, Q.; Wang, P. Different color regulation mechanism in willow barks determined using integrated metabolomics and transcriptomics analyses. *BMC Plant Biol.* **2022**, *22*, 530. [CrossRef]
23. Zheng, L.; Jacquier, J.-C.; Harbourne, N. Preparation of Polyphenol-Rich Herbal Beverages from White Willow (*Salix alba*) Bark with Potential Alzheimer's Disease Inhibitory Activity In Silico. *Beverages* **2024**, *10*, 75. [CrossRef]
24. Rehman, R.N.U.; You, Y.; Zhang, L.; Goudia, B.D.; Khan, A.R.; Li, P.; Ma, F. High Temperature Induced Anthocyanin Inhibition and Active Degradation in *Malus profusion*. *Front. Plant Sci.* **2017**, *8*, 1401. [CrossRef]
25. Schumaker, B.; Mortensen, L.; Klein, R.R.; Mandal, S.; Dykes, L.; Gladman, N.; Rooney, W.L.; Burson, B.; Klein, P.E. UV-induced reactive oxygen species and transcriptional control of 3-deoxyanthocyanidin biosynthesis in black sorghum pericarp. *Front. Plant Sci.* **2024**, *15*, 1451215. [CrossRef]
26. Enaru, B.; Drețcanu, G.; Pop, T.D.; Stănilă, A.; Diaconeasa, Z. Anthocyanins: Factors Affecting Their Stability and Degradation. *Antioxidants* **2021**, *10*, 1967. [CrossRef]
27. Langfelder, P.; Horvath, S. WGCNA: An R package for weighted correlation network analysis. *BMC Bioinform.* **2008**, *9*, 559. [CrossRef]
28. An, J.P.; Wang, X.F.; Zhang, X.W.; Xu, H.F.; Bi, S.Q.; You, C.X.; Hao, Y.J. An apple MYB transcription factor regulates cold tolerance and anthocyanin accumulation and undergoes MIEL1-mediated degradation. *Plant Biotechnol. J.* **2020**, *18*, 337–353. [CrossRef] [PubMed]
29. Tao, H.; Gao, F.; Linying, L.; He, Y.; Zhang, X.; Wang, M.; Wei, J.; Zhao, Y.; Zhang, C.; Wang, Q.; et al. WRKY33 negatively regulates anthocyanin biosynthesis and cooperates with PHR1 to mediate acclimation to phosphate starvation. *Plant Commun.* **2024**, *5*, 100821. [CrossRef] [PubMed]
30. Liu, Y.; Tikunov, Y.; Schouten, R.E.; Marcelis, L.F.M.; Visser, R.G.F.; Bovy, A. Anthocyanin Biosynthesis and Degradation Mechanisms in Solanaceous Vegetables: A Review. *Front. Chem.* **2018**, *6*, 52. [CrossRef] [PubMed]
31. Zhang, Q.; Zhai, J.; Shao, L.; Lin, W.; Peng, C. Accumulation of Anthocyanins: An Adaptation Strategy of *Mikania micrantha* to Low Temperature in Winter. *Front. Plant Sci.* **2019**, *10*, 1049. [CrossRef]
32. Li, Z.; Ahammed, G.J. Plant stress response and adaptation via anthocyanins: A review. *Plant Stress* **2023**, *10*, 100230. [CrossRef]
33. He, Q.; Ren, Y.; Zhao, W.; Li, R.; Zhang, L. Low Temperature Promotes Anthocyanin Biosynthesis and Related Gene Expression in the Seedlings of Purple Head Chinese Cabbage (*Brassica rapa* L.). *Genes* **2020**, *11*, 81. [CrossRef] [PubMed]
34. Zhao, S.; Blum, J.A.; Ma, F.; Wang, Y.; Borejsza-Wysocka, E.; Ma, F.; Cheng, L.; Li, P. Anthocyanin Accumulation Provides Protection against High Light Stress While Reducing Photosynthesis in Apple Leaves. *Int. J. Mol. Sci.* **2022**, *23*, 12616. [CrossRef] [PubMed]
35. Hughes, N.M.; Neufeld, H.S.; Burkey, K.O. Functional role of anthocyanins in high-light winter leaves of the evergreen herb Galax urceolata. *New Phytol.* **2005**, *168*, 575–587. [CrossRef]
36. Yang, L.; Zhang, D.; Qiu, S.; Gong, Z.; Shen, H. Effects of environmental factors on seedling growth and anthocyanin content in *Betula* 'Royal Frost' leaves. *J. For. Res.* **2017**, *28*, 1147–1155. [CrossRef]
37. Zhang, A.; Yang, H.; Ji, S.; Tian, C.; Chen, N.; Gong, H.; Li, J. Metabolome and Transcriptome Analyses of Anthocyanin Accumulation Mechanisms Reveal Metabolite Variations and Key Candidate Genes Involved in the Pigmentation of *Prunus tomentosa* Thunb. Cherry Fruit. *Front. Plant Sci.* **2022**, *13*, 938908. [CrossRef]
38. Fang, F.; Zhang, X.L.; Luo, H.H.; Zhou, J.J.; Gong, Y.H.; Li, W.J.; Shi, Z.W.; He, Q.; Wu, Q.; Li, L.; et al. An Intracellular Laccase Is Responsible for Epicatechin-Mediated Anthocyanin Degradation in Litchi Fruit Pericarp. *Plant Physiol.* **2015**, *169*, 2391–2408. [CrossRef]
39. Zhang, Z.; Pang, X.; Xuewu, D.; Ji, Z.; Jiang, Y. Role of peroxidase in anthocyanin degradation in litchi fruit pericarp. *Food Chem.* **2005**, *90*, 47–52. [CrossRef]
40. Yuan, K.; Li, X.; Zeng, Y.; Liu, C.; Zhu, Y.; Hu, J.; Sun, J.; Bai, W. Chemical stability of carboxylpyranocyanidin-3-O-glucoside under β-glucosidase treatment and description of their interaction. *Food Chem.* **2024**, *447*, 138840. [CrossRef]
41. Tallis, M.J.; Lin, Y.; Rogers, A.; Zhang, J.; Street, N.R.; Miglietta, F.; Karnosky, D.F.; De Angelis, P.; Calfapietra, C.; Taylor, G. The transcriptome of Populus in elevated CO_2 reveals increased anthocyanin biosynthesis during delayed autumnal senescence. *New Phytol.* **2010**, *186*, 415–428. [CrossRef]
42. Wu, K.; Liu, Y.; Liu, J.; Ren, Y.; Liu, Y.; Sun, F.; Abozeid, A.; Tang, Z.; Mu, L. Comparison of Seasonally Adaptive Metabolic Response Strategies of Two Acer Species. *Forests* **2022**, *13*, 2141. [CrossRef]
43. Maritim, T.K.; Masand, M.; Seth, R.; Sharma, R.K. Transcriptional analysis reveals key insights into seasonal induced anthocyanin degradation and leaf color transition in purple tea (*Camellia sinensis* (L.) O. Kuntze). *Sci. Rep.* **2021**, *11*, 1244. [CrossRef] [PubMed]
44. Zoclanclounon, Y.A.B.; Rostás, M.; Chung, N.J.; Mo, Y.; Karlovsky, P.; Dossa, K. Characterization of Peroxidase and Laccase Gene Families and In Silico Identification of Potential Genes Involved in Upstream Steps of Lignan Formation in Sesame. *Life* **2022**, *12*, 1200. [CrossRef] [PubMed]
45. Huang, L.; Lin, B.; Hao, P.; Yi, K.; Li, X.; Hua, S. Multi-Omics Analysis Reveals That Anthocyanin Degradation and Phytohormone Changes Regulate Red Color Fading in Rapeseed (*Brassica napus* L.) Petals. *Int. J. Mol. Sci.* **2024**, *25*, 2577. [CrossRef]

46. Gao, C.; Sun, Y.; Li, J.; Zhou, Z.; Deng, X.; Wang, Z.; Wu, S.; Lin, L.; Huang, Y.; Zeng, W.; et al. High Light Intensity Triggered Abscisic Acid Biosynthesis Mediates Anthocyanin Accumulation in Young Leaves of Tea Plant (*Camellia sinensis*). *Antioxidants* **2023**, *12*, 392. [CrossRef]
47. Wu, X.; Li, Y.; Du, T.; Kang, L.; Pei, B.; Zhuang, W.; Tang, F. Transcriptome sequencing and anthocyanin metabolite analysis involved in leaf red color formation of *Cinnamomum camphora*. *Sci. Rep.* **2024**, *14*, 31470. [CrossRef]
48. Sirgedaitė-Šėžienė, V.; Čėsnienė, I.; Vaitiekūnaitė, D. Temporal Variations in Enzymatic and Non-Enzymatic Antioxidant Activity in Silver Birch (*Betula pendula* Roth.): The Genetic Component. *Forests* **2024**, *15*, 1262. [CrossRef]
49. Yang, X.; Yang, N.; Zhang, Q.; Pei, Z.; Chang, M.; Zhou, H.; Ge, Y.; Yang, Q.; Li, G. Anthocyanin Biosynthesis Associated with Natural Variation in Autumn Leaf Coloration in *Quercus aliena* Accessions. *Int. J. Mol. Sci.* **2022**, *23*, 12179. [CrossRef]
50. Pei, Z.; Huang, Y.; Ni, J.; Liu, Y.; Yang, Q. For a Colorful Life: Recent Advances in Anthocyanin Biosynthesis during Leaf Senescence. *Biology* **2024**, *13*, 329. [CrossRef]
51. Fermaniuk, C.; Fleurial, K.G.; Wiley, E.; Landhäusser, S.M. Large seasonal fluctuations in whole-tree carbohydrate reserves: Is storage more dynamic in boreal ecosystems? *Ann. Bot.* **2021**, *128*, 943–957. [CrossRef]
52. Bowling, D.R.; Schädel, C.; Smith, K.R.; Richardson, A.D.; Bahn, M.; Arain, M.A.; Varlagin, A.; Ouimette, A.P.; Frank, J.M.; Barr, A.G.; et al. Phenology of Photosynthesis in Winter-Dormant Temperate and Boreal Forests: Long-Term Observations From Flux Towers and Quantitative Evaluation of Phenology Models. *J. Geophys. Res. Biogeosci.* **2024**, *129*, e2023JG007839. [CrossRef]
53. Acharya, T.P.; Malladi, A.; Nambeesan, S.U. Sustained carbon import supports sugar accumulation and anthocyanin biosynthesis during fruit development and ripening in blueberry (*Vaccinium ashei*). *Sci. Rep.* **2024**, *14*, 24964. [CrossRef]
54. Xu, C.; Huang, H.; Tan, C.; Gao, L.; Wan, S.; Zhu, B.; Chen, D.; Zhu, B. Transcriptome and WGCNA Analyses Reveal Key Genes Regulating Anthocyanin Biosynthesis in Purple Sprout of Pak Choi (*Brassica rapa* L. ssp. chinensis). *Int. J. Mol. Sci.* **2024**, *25*, 11736. [CrossRef] [PubMed]
55. Broucke, E.; Dang, T.T.V.; Li, Y.; Hulsmans, S.; Van Leene, J.; De Jaeger, G.; Hwang, I.; Wim, V.d.E.; Rolland, F. SnRK1 inhibits anthocyanin biosynthesis through both transcriptional regulation and direct phosphorylation and dissociation of the MYB/bHLH/TTG1 MBW complex. *Plant J.* **2023**, *115*, 1193–1213. [CrossRef] [PubMed]
56. Cappellini, F.; Marinelli, A.; Toccaceli, M.; Tonelli, C.; Petroni, K. Anthocyanins: From Mechanisms of Regulation in Plants to Health Benefits in Foods. *Front. Plant Sci.* **2021**, *12*, 748049. [CrossRef] [PubMed]
57. Zhang, Z.; Chen, C.; Jiang, C.; Lin, H.; Zhao, Y.; Guo, Y. VvWRKY5 positively regulates wounding-induced anthocyanin accumulation in grape by interplaying with VvMYBA1 and promoting jasmonic acid biosynthesis. *Hortic. Res.* **2024**, *11*, uhae083. [CrossRef]
58. Gai, S.; Du, B.; Xiao, Y.; Zhang, X.; Turupu, M.; Yao, Q.; Wang, X.; Yan, Y.; Li, T. bZIP Transcription Factor PavbZIP6 Regulates Anthocyanin Accumulation by Increasing Abscisic Acid in Sweet Cherry. *Int. J. Mol. Sci.* **2024**, *25*, 10207. [CrossRef]
59. Wang, C.; Zhao, Q.; Zhang, L.; Zhang, H. Expression Pattern Analysis of Larch WRKY in Response to Abiotic Stress. *Forests* **2022**, *13*, 2123. [CrossRef]
60. Levée, V.; Major, I.; Levasseur, C.; Tremblay, L.; MacKay, J.; Séguin, A. Expression profiling and functional analysis of Populus WRKY23 reveals a regulatory role in defense. *New Phytol.* **2009**, *184*, 48–70. [CrossRef]
61. Xia, P.; Chen, M.; Chen, L.; Yang, Y.; Ma, L.; Bi, P.; Tang, S.; Luo, Q.; Chen, J.; Chen, H.; et al. Deciphering the Anthocyanin Metabolism Gene Network in tea plant(*Camellia sinensis*) through Structural Equation modeling. *BMC Genom.* **2024**, *25*, 1093. [CrossRef]
62. Fu, G.; Ren, Y.; Kang, J.; Wang, B.; Zhang, J.; Fang, J.; Wu, W. Integrative analysis of grapevine (*Vitis vinifera* L) transcriptome reveals regulatory network for Chardonnay quality formation. *Front. Nutr.* **2023**, *10*, 1187842. [CrossRef]
63. Hu, B.; Li, J.; Wang, D.; Wang, H.-C.; Yonghua, Q.; Hu, G.; Zhao, J. Transcriptome profiling of Litchi chinensis pericarp in response to exogenous cytokinins and abscisic acid. *Plant Growth Regul.* **2018**, *84*, 437–450. [CrossRef]
64. Giusti, M.M.; Wrolstad, R.E. Characterization and Measurement of Anthocyanins by UV-Visible Spectroscopy. *Curr. Protoc. Food Anal. Chem.* **2001**, *1*, F1.2.1–F1.2.13. [CrossRef]

Disclaimer/Publisher's Note: The statements, opinions and data contained in all publications are solely those of the individual author(s) and contributor(s) and not of MDPI and/or the editor(s). MDPI and/or the editor(s) disclaim responsibility for any injury to people or property resulting from any ideas, methods, instructions or products referred to in the content.

forests

MDPI

Article

Hydro-Functional Strategies of Sixteen Tree Species in a Mexican Karstic Seasonally Dry Tropical Forest

Jorge Palomo-Kumul [1], Mirna Valdez-Hernández [1,*], Gerald A. Islebe [1], Edith Osorio-de-la-Rosa [2], Gabriela Cruz-Piñon [3], Francisco López-Huerta [4] and Raúl Juárez-Aguirre [4]

[1] Herbario, Diversidad y Dinámica de Ecosistemas del Sureste de México, El Colegio de la Frontera Sur, Chetumal 77014, Quintana Roo, Mexico
[2] Departamento de Ciencias, Ingeniería y Tecnología, SECIHTI-Universidad Autónoma del Estado de Quintana Roo, Blv. Ignacio Comonfort S/N, Chetumal 77015, Quintana Roo, Mexico
[3] Laboratorio de Socioecosistemas Marinos y Costeros, Departamento Académico de Ciencias Marinas y Costeras, Universidad Autónoma de Baja California Sur, La Paz 23085, Baja California Sur, Mexico
[4] Facultad de Ingeniería Eléctrica y Electrónica, Universidad Veracruzana, Boca del Río 94294, Veracruz, Mexico
* Correspondence: mavaldez@ecosur.mx

Abstract: Seasonally dry tropical forests (SDTFs) are shaped by strong climatic and edaphic constraints, including pronounced rainfall seasonality, extended dry periods, and shallow karst soils with limited water retention. Understanding how tree species respond to these pressures is crucial for predicting ecosystem resilience under climate change. In the Yucatán Peninsula, we characterized sixteen tree species along a spatial and seasonal precipitation gradient, quantifying wood density, predawn and midday water potential, saturated and relative water content, and specific leaf area. Across sites, diameter classes, and seasons, we measured ≈4 individuals per species (n = 319), ensuring replication despite natural heterogeneity. Using a principal component analysis (PCA) based on individual-level data collected during the dry season, we identified five functional groups spanning a continuum from conservative hard-wood species, with high hydraulic safety and access to deep water sources, to acquisitive light-wood species that rely on stem water storage and drought avoidance. Intermediate-density species diverged into subgroups that employed contrasting strategies such as anisohydric tolerance, high leaf area efficiency, or strict stomatal regulation to maintain performance during the dry season. Functional traits were strongly associated with precipitation regimes, with wood density emerging as a key predictor of water storage capacity and specific leaf area responding plastically to spatial and seasonal variability. These findings refine functional group classifications in heterogeneous karst landscapes and highlight the value of trait-based approaches for predicting drought resilience and informing restoration strategies under climate change.

Keywords: plant hydraulics; precipitation gradient; wood density; water potential; functional traits; functional groups; drought resilience; restoration ecology

1. Introduction

Seasonally dry tropical forests (SDTFs) are among the most climatically constrained terrestrial ecosystems, characterized by marked intra-annual precipitation seasonality, extended dry periods, and high evaporative demand. Although they account for less than 42% of tropical forests globally, SDTFs are biodiversity hotspots and significant carbon reservoirs [1]. Climate projections indicate that these forests will experience increased drought frequency and altered rainfall regimes under global change [2,3], pushing many species toward their physiological limits, particularly in areas already subjected to prolonged water

deficits [4,5]. Projections of species distributions in Central America and southern Mexico suggest that 58%–67% of forest plant species will be classified as threatened by the IUCN by 2061–2080. This evidence highlights the significant impact of climate change on plant communities in water-limited tropical ecosystems [6].

Tree species inhabiting these environments display a wide spectrum of hydraulic and morphological strategies to cope with seasonal and interannual water deficits. Key traits include wood density (WD), vulnerability to xylem cavitation (P50), turgor loss point (Ψtlp), and sapwood capacitance, which together shape drought resistance [7–9]. High WD is generally associated with conservative water-use strategies and greater hydraulic safety, whereas low WD often corresponds to acquisitive strategies that maximize hydraulic efficiency at the cost of vulnerability [10–12]. Leaf-level traits such as specific leaf area (SLA) and relative water content (RWC), together with stem water storage capacity and stomatal regulation, further modulate drought tolerance [13,14].

Functional group classifications based on WD, xylem water potential, RWC, and phenology have been widely employed to identify patterns of water-use strategies in SDTFs [15–17]. These classifications, such as distinguishing drought-avoiding deciduous species from drought-tolerant evergreen species, provide a valuable framework for predicting species responses. At the same time, recent studies suggest that in heterogeneous karst environments, species with contrasting phenologies may occasionally converge in traits such as deep-water access [18–20]. Furthermore, inter- and intraspecific variability in rooting depth, water sources, and safety–efficiency trade-offs add complexity to these classifications [9,14,21]. Rather than diminishing their utility, such variability underscores the need to refine functional group schemes by identifying subgroups within traditional categories, which is a central contribution of the present study.

Integrating above- and below-ground traits provides a more robust framework for predicting community responses under changing climates [13,22]. In extensive SDTFs, acquisitive species with high stem and bark water storage can persist in drier sites by buffering short-term rainfall variability, while conservative species maintain lower vulnerability through tighter hydraulic safety margins [9,22]. Additional factors, such as plant–microbe interactions, may also enhance drought resistance—for example, endophytic fungi have been shown to improve water uptake efficiency and alter stomatal control in karst-adapted species [23].

In the Yucatán Peninsula, these climatic constraints are compounded by the presence of karst landscapes. Formed through the dissolution of carbonate rocks, karst terrains are characterized by shallow, rocky soils, low water-holding capacity, high infiltration rates, and extensive subterranean drainage [24,25]. These edaphic conditions severely limit surface water and nutrient retention, forcing trees to rely on deep water stored in fractures or aquifers, sometimes several meters below ground [17,19,20,26]. While groundwater access can buffer the impacts of seasonal drought, its availability is spatially heterogeneous, and the aquifer is increasingly threatened by salinization and contamination linked to land use change and anthropogenic pollution [27,28]. Also, such hydrological pressures are expected to interact with climate change to further constrain plant performance and forest resilience.

In this study, we examine 16 tree species from SDTFs on karst soils in the Yucatán Peninsula along a precipitation gradient. We quantify WD, xylem water potential, SLA, RWC, and saturated water content (SWC) to characterize species' positions along the conservative–acquisitive continuum, assess the reliability of functional group classifications in predicting water-use strategies, and identify trait combinations that underpin resilience in one of the most hydrologically challenging tropical forest environments.

2. Materials and Methods

2.1. Study Area

This study was carried out at three representative sites of seasonally dry tropical forests of the Yucatán Peninsula. In the Yucatán Peninsula, three seasons are present: the dry season, which runs from March to May, is characterized by high temperatures and sporadic rainfall; the rainy season, which runs from June to October, is characterized by high temperatures and constant rainfall; and the nortes season is characterized by lower temperatures and sporadic precipitation. In addition to the seasonal effect on water availability, we consider the spatial gradient of precipitation that can be observed from north to south of the Yucatán Peninsula [29]. The selected sites have a mean annual precipitation of 700, 1000, and 1200 mm (Figure 1).

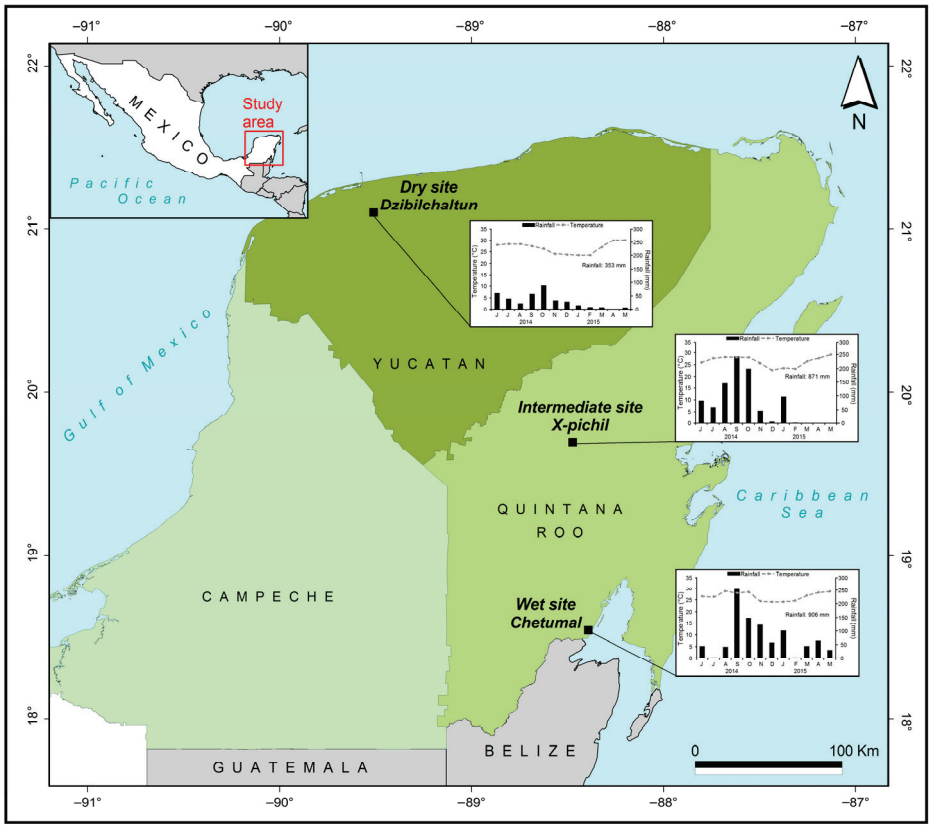


Figure 1. Geographic location of the three study sites in the Yucatán Peninsula, Mexico: dry site (Dzibilchaltún National Park; 21°05′ N, 89°35′ W; MAP 700 mm), intermediate site (X-pichil forest reserve; 19°41′ N, 88°22′ W; MAP 1000 mm), wet site (ECOSUR forest area in Chetumal; 18°32′ N, 88°15′ W; MAP 1200 mm). Ombrothermic diagrams correspond to the sampling period at each site.

The dry site is positioned in Dzibilchaltún National Park, located in the north of Yucatán state (21°05′ N, 89°35′ W), with a mean annual temperature of 25.8 °C and a mean annual precipitation (MAP) of 700 mm. The characteristic vegetation is low deciduous forest [17,30]. The soil is flat, shallow, dark or reddish in color, and calcareous, with several rocky outcrops [30].

The intermediate site is positioned in a forest reserve of the X-pichil community, located in the center of Quintana Roo state (19°41′ N, 88°22′ W), with a mean annual temperature of 26.4 °C and MAP of 1000 mm. Characteristic vegetation is semi-evergreen forest described in [31]. The soils are lithosols associated with rendzinas and luvisols [31].

The wet site is positioned in a forest area of the El Colegio de la Frontera Sur-Chetumal, located in the south of Quintana Roo state (18°32′ N, 88°15′ W), with a mean annual

temperature of 27 °C and MAP of 1200 mm. The characteristic vegetation is semi-evergreen forest (personal observation). The soils are lithosols associated with rendzinas and are shallow, with calcareous rocks in the lower part [32].

2.2. Species Analyzed

Sixteen tree species were analyzed; they were chosen considering a contrasting leaf phenology (evergreen or deciduous) and wood density differences. For classification purposes, species were grouped into three categories: light wood (<0.60 g cm^{-3}), soft wood (0.60–0.80 g cm^{-3}), and hard wood (>0.80 g cm^{-3}). These thresholds follow established ecological frameworks that link wood density to life-history strategies and hydraulic performance in tropical forests [33,34]. From each species, two diameter classes were selected (young < 10 cm and mature > 20 cm). A brief description of the species and a list of individuals used are presented in Table 1. All trees were selected without visible damage on stems or crown.

Table 1. Main characteristics of the species, grouped according to wood density, showing the number of individuals per species. Wet site (W, 1200 mm mean annual precipitation), intermediate site (I, 1000 mm mean annual precipitation), dry site (D, 700 mm mean annual precipitation), young stage (Y), mature stage (M). Asterisks indicate that trees were in homegardens.

Family	Species	Key	Fruit Type	Leaf Phenology	Individual					
					W		I		D	
					Y	M	Y	M	Y	M
Light-wood species										
Burseraceae	*Bursera simaruba* (L.) Sarg.	Bs	Drupe	D	4	4	4	4	4	4
Anacardiaceae	*Spondias* sp.	Sp	Drupe	D	0	4	4	4	0	4 *
Soft-wood species										
Apocynaceae	*Thevetia peruviana* (Pers.) K. Schum.	Tp	Drupe	E	4	4	4	4	3 *	0
Boraginaceae	*Cordia dodecandra* DC.	Cd	Drupe	D	4	4	4 *	3 *	4	2 *
Sterculiaceae	*Guazuma ulmifolia* Lam.	Gu	Capsule	D	4	4	0	0	4	4
Boraginaceae	*Ehretia tinifolia* L.	Et	Drupe	E	4	4	4 *	4 *	0	4
Leguminosae	*Piscidia piscipula* (L.) Sarg.	Pp	Pod	D	4	4	4	4	4	4
Ebenaceae	*Diospyros cuneata* Standl.	Dc	Drupe	E	0	0	4	0	4	4
Anacardiaceae	*Metopium brownei* (Jacq.) Urb.	Mb	Drupe	D	4	4	4	4	0	0
Polygonaceae	*Gymnopodium floribundum* Rolfe	Gf	Nut	E	0	0	4	4	4	4
Fabaceae	*Lysiloma latisiliquum* (L.) Benth.	Ly	Pod	D	4	4	4	4	4	4
Fabaceae	*Leucaena leucocephala* (Lam.) de Wit	Ll	Pod	D	4	4	4	4	4	4
Malpighiaceae	*Byrsonima crassifolia* (L.) Kunth	Bc	Drupe	D	4	4	4	4	0	4
Hard-wood species										
Moraceae	*Brosimum alicastrum* Sw.	Ba	Drupe	E	4	4	4 *	4 *	4 *	4 *
Sapotaceae	*Manilkara zapota* (L.) P. Royen	Mz	Drupe	E	4	4	4	4	2 *	3 *
Sapotaceae	*Chrysophyllum mexicanum* Brandegee ex Standl.	Cm	Drupe	E	4	4	4	4 *	2 *	4 *

2.3. Sampling Seasons

Samples were taken during the three seasons of the Yucatán Peninsula: dry, rainy, and nortes. The samples were taken in three or four days per site consecutively. The sampling of the rainy season was carried out from 29 October to 14 November 2014. For the nortes season, sampling was carried out from 9 to 20 January 2015, and the dry season was sampled from 31 March to 12 April 2015.

2.4. Morphophysiological Parameters

Water potential (Ψx): Measures were carried out with a Scholander pressure chamber (1505D, PMS Instrument, Albany, OR, USA) using three terminal twigs per individual, in four individuals per species, site, and per season. The terminal twigs were collected at half-canopy with a pruning stick; predawn water potential (Ψ_{pd}) was measured between 4:00 and 5:00; midday water potential (Ψ_{md}) was measured between 12:00 and 13:00. Immediately after their collection, the terminal twigs were deposited in hermetically sealed plastic bags and transported with ice in a refrigerator to avoid dehydration. The measurements were made in a maximum time of two hours. This protocol follows procedures previously applied and validated in SDTF studies of the Yucatán Peninsula [17,18], where no artefacts due to short-term transport were detected. Samples were consistently kept under cool and sealed conditions to minimize water loss, ensuring reliable Ψ measurements despite logistical constraints.

To integrate daily plant water dynamics, we also calculated the difference between midday and predawn water potential ($\Delta\Psi = \Psi_{md} - \Psi_{pd}$). This parameter is widely used as an indicator of transpiration demand and soil–plant water gradients, providing complementary insight into drought response strategies.

Wood samples: Samples for evaluating wood density (WD, g cm^{-3}), relative water content (RWC, %), and saturated water content (SWC, %) were collected with a core borer (wood cores: 5 mm diameter, ~30 mm long). Immediately after collection, the samples were placed in a microtube with a hermetic seal to prevent dehydration and were transported on ice to the laboratory. Each sample was weighed on an analytical balance (PA214C, OHAUS, Parsippany, NJ, USA) to obtain fresh weight. Subsequently, wood cores were placed in distilled water for 24 h to obtain weight at saturation. Finally, samples were dried in an oven at 80 °C for 24 h to obtain the dry weight. To ensure complete saturation, wood cores were submerged in distilled water for 24 h until no further weight increase was detected. For drying, samples were oven-dried at 110 °C for 24 h, until constant weight was achieved, following standard wood trait protocols. Only sapwood tissue was extracted and used for these analyses, while heartwood was explicitly avoided to prevent bias in water storage estimates. WD (g cm^{-3}) was estimated as the sample dry weight over the volume [35].

$$\text{SWC} = (\text{saturated weight} - \text{dry weight})/\text{dry weight} \times 100$$

$$\text{RWC} = (\text{fresh weight} - \text{dry weight})/(\text{saturated weight} - \text{dry weight}) \times 100$$

Specific leaf area (SLA): SLA was measured independently from wood traits. Ten exposed leaves and ten shaded leaves of four individuals per species per site and season were collected to evaluate specific leaf area. After collection, each leaf was photographed and marked to determine leaf area with Imagej 1.48 [36]. In the laboratory, leaves were dried at 80 °C for 48 h to obtain dry weight. The specific leaf area was calculated using leaf area and dry weight values according to [37].

Sampling sizes: In general, four individuals were sampled per species, diameter class, and site. However, depending on local availability, this number may have been lower in some cases. Exact replication by species, site, and size is presented in Table 1. These

differences reflect natural heterogeneity and the uneven distribution of individuals within SDTFs. Nevertheless, replication was sufficient to capture consistent patterns across traits and sites.

In cases where certain species could not be found across all sites, individuals from traditional Maya homegardens were also included. These homegardens, which often extend over areas of one hectare or more, are ecologically comparable to extensions of tropical dry forest and receive no irrigation, being fully dependent on natural precipitation. To verify that their inclusion did not bias water potential measurements (Ψ_{pd}, Ψ_{md}), a two-way ANOVA was performed considering microenvironment (natural forest vs. homegarden) and season (dry, rainy, nortes). No significant differences were detected, confirming the robustness of this approach. Per-figure and per-table sample sizes (n = 319) are reported in the corresponding captions.

2.5. Environmental Parameters

The meteorological data of wet and intermediate sites were obtained by the National Commission of Water; stations were located between 5 and 12 km away from the sites. For the wet site, data were obtained from a weather station located at the same site (WatchDog Serie 2000, Spectrum, Aurora, IL, USA).

2.6. Statistical Analysis

Considering that the selected species were selected when their wood density was inferred through their foliar phenology, to corroborate that there are significant differences in wood density between species, a multifactorial ANOVA was performed; species, sites (dry, intermediate, wet), and diameter classes (young < 10 cm and mature > 20 cm) were considered factors. To establish differences in Ψ_{pd}, Ψ_{md}, WD, RWC, SWC, and SLA, we used a multifactorial ANOVA; species, sites (dry, intermediate, wet), seasons (dry, rainy, nortes), and diameter classes (young < 10 cm and mature > 20 cm) were considered factors. In addition, the diurnal amplitude of water potential ($\Delta\Psi$) was calculated as the difference between predawn (Ψ_{pd}, maximum water potential) and midday (Ψ_{md}, minimum water potential), expressed as $\Delta\Psi = \Psi_{pd} - \Psi_{md}$, to evaluate the diurnal amplitude of plant water status. In addition, a post hoc Tukey HSD test was applied to determine significant differences. Some tree species could not be found in all sites and categories, so trees in homegardens were integrated. All trees present in homegardens were not irrigated and were located far from sources of additional water. To rule out the effect of a possible additional supply of water in individuals (Ψ_{pd}, Ψ_{md}), a two-way ANOVA was performed; microenvironment (natural conditions, homegarden) and season (dry, rainy, nortes) were considered as factors. To determine the effect of the environment on the physiological response, a Spearman correlation was performed. The environmental data (precipitation, average temperature, and vapor pressure deficit) were considered by station and site. For the physiological parameters (Ψ_{pd}, Ψ_{md}, $\Delta\Psi$, SWC, RWC, WD, SLA), the averages by species, station, and site were considered. Prior to the application of ANOVA, assumptions of normality and homogeneity of variances were tested using the Shapiro–Wilk and Levene's tests, respectively. When assumptions were not fully met, log- or square-root transformations were applied to improve data fit. All analyses were performed with Statistica 12 [38].

To identify functional groups, a principal component analysis (PCA) was performed using individual-level trait data (Ψ_{pd}, Ψ_{md}, $\Delta\Psi$, RWC, SWC, WD, SLA) collected across sites (dry, intermediate, wet) and seasons (rainy, nortes, dry). By incorporating all individuals rather than species means, the analysis captures both intraspecific variation and seasonal plasticity, avoiding artificial inflation of group separation and ensuring that ordination

patterns reflect the full range of observed trait responses. The PCA was conducted with PC-Ord 5.1 [39], and eigenvalues and loadings were used to identify the traits contributing most strongly to each axis.

3. Results

3.1. Wood Density

The wood density values defined three groups (Figure 2; F = 248.65, $p < 0.001$). The first group is species with low density or light wood (WD < 0.5 g cm^{-3}). In this group, *B. simaruba* and *Spondias* sp. were found. The second group is intermediate-wood-density or soft-wood species (WD = 0.5–0.7 g cm^{-3}). The species in this group are *D. cuneata*, *P. piscipula*, *C. dodecandra*, *M. brownei*, *G. ulmifolia*, *E. tinifolia*, *G. floribundum*, *L. latisiliquum*, *L. leucocephala*, *T. peruviana*, and *B. crassifolia*. In the third group, species with high wood density or hard wood (WD > 0.75 g cm^{-3}) are found. In this group, *B. alicastrum*, *C. mexicanum*, and *M. zapota* were found.

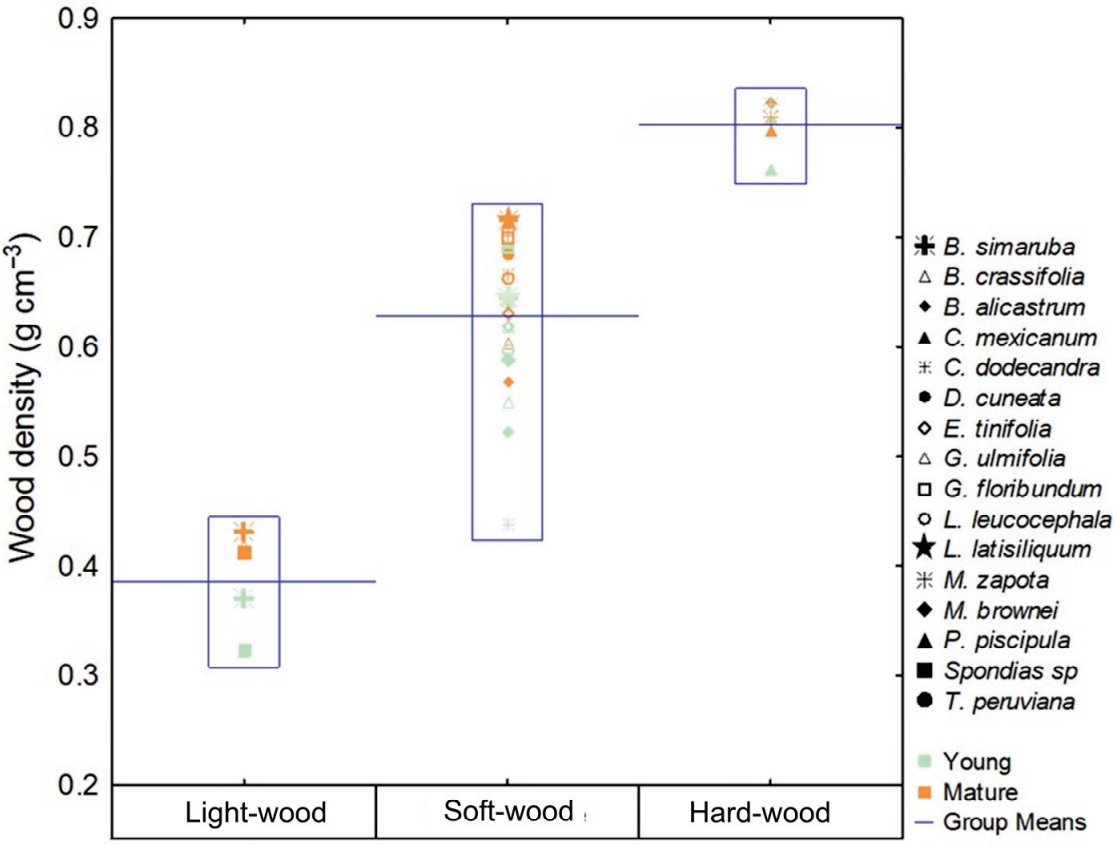


Figure 2. Wood density (WD, g cm^{-3}) groups for 16 tree species considering two diameter classes: young (<10 cm DBH) and mature (>20 cm DBH). Groups: light-wood (WD < 0.50 g cm^{-3}), soft-wood (0.50–0.74 g cm^{-3}), and hard-wood (>0.75 g cm^{-3}). Error bars indicate ± SE.

In the three wood density groups (light-wood, soft-wood, and hard-wood), the young stage has significant differences between sites (Table 2; F = 4.1784, $p < 0.01$). The dry site had lower precipitation and higher wood density. In the mature stage, only the soft-wood group shows significant differences between sites (Table 2; F = 8.6350, $p < 0.001$), and dry sites have the highest wood density values. No significant inter-seasonal differences in both stages are detected. Diametric classes give significant differences and were observed in the light-wood group (Table 2; F = 55.221, $p < 0.001$) and soft-wood group (Table 2; F = 112.27, $p < 0.001$), where the young stage has low wood density.

Table 2. Physiological parameters are grouped according to wood density, between sites, seasons, and diameter classes. Wet site (W), intermediate site (I), dry site (D), young stage (Y), mature stage (M), wood density (WD, g cm^{-3}), saturated water content (SWC, %), predawn water potential (Ψ_{pd}, MPa), midday water potential (Ψ_{md}, MPa), relative water content (RWC, %), specific leaf area (SLA, cm^2 g^{-1}), the hyphen represents absence of trees in the site, the asterisk represents absence of leaves of individuals in the site, n = 319.

	Site	Season	WD		SWC		Ψ_{pd}		Ψ_{md}		RWC		SLA	
			Y	M	Y	M	Y	M	Y	M	Y	M	Y	M
Light-wood species														
B. simaruba	W	rain	0.34	0.44	255	188	−0.39	−0.39	−0.61	−0.63	54	67	133	120
		dry	0.38	0.45	242	201	−0.45	−0.48	−0.99	−0.59	61	68	138	140
		nortes	0.35	0.42	319	230	−0.37	−0.37	−0.5	−0.52	41	60	127	123
	I	rain	0.34	0.39	287	227	−0.34	−0.45	−0.57	−0.7	36	51	129	128
		dry	0.38	0.44	242	173	−0.88	−0.87	−1.1	−1.08	50	60	122	124
		nortes	0.34	0.43	272	211	−0.46	−0.38	−0.5	−0.45	48	53	97	102
	D	rain	0.39	0.46	225	146	−0.33	−0.31	−0.81	−0.74	58	69	132	144
		dry	0.43	0.42	204	179	−1.02	−0.71	−1.3	−1.24	55	61	153	153
		nortes	0.41	0.43	188	200	−0.95	−0.84	−1.18	−0.61	61	63	*	131
Spondias sp.	W	rain	-	0.41	-	207	-	−0.13	-	−0.25	-	63	-	213
		dry	-	0.45	-	201	-	−0.48	-	−0.59	-	68	-	179
		nortes	-	0.42	-	230	-	−0.37	-	−0.52	-	60	-	*
	I	rain	0.29	0.42	305	196	−0.2	−0.18	−0.99	−1.05	45	56	184	184
		dry	0.32	0.43	285	175	−0.97	−0.59	−1.6	−1.5	48	63	239	236
		nortes	0.35	0.45	293	198	−0.25	−0.29	−0.86	−0.57	35	50	211	161
	D	rain	-	0.36	-	254	-	−0.31	-	−1	-	95	-	188
		dry	-	0.38	-	282	-	−0.81	-	−1.54	-	74	-	193
		nortes	-	0.43	-	201	-	−0.41	-	−0.75	-	89	-	199
Soft-wood species														
T. peruviana	W	rain	0.46	0.54	146	145	−1.16	−1.06	−1.75	−1.53	40	40	184	187
		dry	0.48	0.54	149	140	−1.67	−1.55	−2.14	−2.13	36	38	158	145
		nortes	0.46	0.55	176	135	−0.52	−0.49	−2.03	−1.82	33	42	166	147
	I	rain	0.55	0.61	134	115	−1.08	−1.01	−1.5	−1.75	42	41	172	149
		dry	0.57	0.63	112	109	−2.27	−1.9	−2.67	−2.29	35	39	136	137
		nortes	0.54	0.54	158	145	−1.39	−1.27	−1.66	−1.8	34	34	148	122
	D	rain	0.52	-	121	-	−0.82	-	−1.49	-	54	-	209	-
		dry	0.53	-	140	-	−1.9	-	−2.47	-	36	-	115	-
		nortes	0.56	-	116	-	−1.73	-	−2.19	-	48	-	150	-
L. leucocephala	W	rain	0.55	0.67	115	94.8	−0.71	−0.75	−1.12	−1.33	46	64	256	273
		dry	0.54	0.67	142	104	−0.76	−0.93	−1.63	−1.61	46	59	182	174
		nortes	0.6	0.66	129	107	−0.92	−0.96	−1.83	−1.69	49	71	197	203
	I	rain	0.6	0.64	110	97.2	−0.25	−0.12	−1.66	−1.64	48	53	355	293
		dry	0.61	0.66	116	97.6	−0.88	−0.85	−2.16	−2.16	38	45	179	172
		nortes	0.57	0.62	140	121	−0.37	−0.26	−1.09	−0.64	40	43	171	196
	D	rain	0.63	0.7	118	99	−0.32	−0.57	−0.96	−1.49	43	56	256	246
		dry	0.65	0.68	99.2	92.1	−2.98	−1.1	−3.78	−2.82	41	52	147	152
		nortes	0.61	0.67	115	104	−1.9	−1.59	−3.29	−3.31	39	55	167	147
P. piscipula	W	rain	0.66	0.71	108	81.3	−0.54	−0.49	−0.63	−0.57	72	74	132	134
		dry	0.64	0.72	114	105	−0.92	−1.08	−2.04	−1.8	67	72	88	111
		nortes	0.63	0.7	131	109	−0.81	−0.81	−1.36	−1.25	61	64	119	99
	I	rain	0.61	0.75	107	82.3	−0.25	−0.23	−0.86	−0.83	68	71	121	104
		dry	0.65	0.74	103	92.1	−0.7	−0.55	−2.15	−1.01	65	68	116	79
		nortes	0.64	0.68	124	122	−0.62	−0.6	−1	−0.84	63	68	112	94
	D	rain	0.63	0.7	109	87.8	−0.36	−0.39	−1.04	−0.92	65	56	117	101
		dry	0.67	0.73	108	96.1	−1.08	−0.93	−1.61	−1.7	60	65	109	109
		nortes	0.67	0.7	110	90.9	−0.87	−0.75	−1.9	−1.33	64	73	97	86
E. tinifolia	W	rain	0.63	0.65	111	111	−0.35	−0.48	−0.99	−0.89	61	63	173	148
		dry	0.64	0.67	112	106	−0.69	−0.9	−1.8	−1.56	67	67	152	145
		nortes	0.67	0.67	118	117	−0.51	−0.62	−1.13	−1.37	62	62	163	139
	I	rain	0.57	0.58	119	129	−0.6	−0.58	−1.68	−1.48	49	43	171	172
		dry	0.59	0.61	121	121	−0.66	−0.52	−2.01	−2.05	66	67	177	191
		nortes	0.61	0.61	125	123	−0.19	−0.15	−0.25	−0.28	68	66	141	151
	D	rain	-	0.63	-	105	-	−0.38	-	−1.15	-	57	-	133
		dry	-	0.6	-	107	-	−0.78	-	−1.62	-	64	-	160
		nortes	-	0.66	-	97.4	-	−1.09	-	−1.44	-	74	-	132
C. dodecandra	W	rain	0.69	0.7	105	104	−0.86	−0.81	−1.23	−1.25	65	65	104	87
		dry	0.69	0.7	104	98.2	−0.69	−0.62	−1.17	−1.07	65	66	148	125
		nortes	0.67	0.66	109	104	−0.63	−0.56	−1.09	−1	70	71	115	146
	I	rain	0.58	0.7	92.5	90.5	−0.97	−0.5	−1.95	−1.9	52	55	141	132
		dry	0.62	0.72	115	92.7	−1.21	−0.74	−2.47	−2.08	64	68	82	95
		nortes	0.57	0.68	146	94	−0.64	−0.43	−0.75	−0.65	65	73	150	187
	D	rain	0.62	0.72	107	86.2	−0.73	−0.73	−1.54	−1.97	61	52	100	114
		dry	0.61	0.72	127	98.5	−1.57	−1.08	−2.18	−1.58	54	60	153	99
		nortes	0.6	0.69	129	98.3	−1.28	−1.56	−2.03	−1.95	51	65	125	102

Table 2. *Cont.*

	Site	Season	WD		SWC		Ψ_{pd}		Ψ_{md}		RWC		SLA	
			Y	M	Y	M	Y	M	Y	M	Y	M	Y	M
G. floribundum	W	rain	0.67	0.69	107	101	−1.71	−1.21	−3.19	−2.81	54	52	180	157
		dry	0.7	0.71	98.4	92.7	−1.5	−1.27	−3.99	−3.08	59	63	126	113
		nortes	0.69	0.70	111	96.7	−1.99	−1.55	−3.5	−3.1	65	67	161	130
	D	rain	0.71	0.72	81	87.5	−0.65	−0.63	−2.33	−2.27	49	58	176	161
		dry	0.70	0.70	87.3	90.8	−2.31	−2.79	−4.5	−4.72	54	59	123	92
		nortes	0.70	0.71	88.7	92	−4.01	−3.45	−5.41	−4.33	59	66	144	159
L. latisiliquum	W	rain	0.41	0.55	205	130	−0.37	−0.31	−1.95	−2.43	65	70	74	72
		dry	0.36	0.63	254	111	−0.44	−0.47	−1.93	−1.71	56	76	154	145
		nortes	0.42	0.66	218	111	−0.48	−0.71	−2.23	−2.64	67	74	77	72
	I	rain	0.44	0.66	214	109	−0.77	−0.81	−2.65	−2.68	45	58	117	117
		dry	0.43	0.66	199	112	−0.99	−0.95	−2.19	−2.12	35	56	266	198
		nortes	0.40	0.66	248	116	−0.16	−0.21	−1.76	−0.82	42	61	147	94
	D	rain	0.43	0.73	198	92	−0.23	−0.32	−1.94	−2.37	65	67	156	112
		dry	0.47	0.72	161	86	−1.64	−1.95	−2.30	−2.94	32	55	183	87
		nortes	0.46	0.69	158	86	−2.74	−1.72	−3.92	−2.44	42	66	124	95
M. brownei	W	rain	0.59	0.67	143	97.4	−0.45	−0.48	−0.54	−0.49	57	62	107	112
		dry	0.62	0.67	123	111	−0.58	−0.58	−0.96	−0.81	57	66	93	93
		nortes	0.58	0.64	150	114	−0.52	−0.69	−0.84	−1.22	59	65	93	104
	I	rain	0.53	0.61	149	120	−0.43	−0.51	−0.62	−0.59	44	60	128	117
		dry	0.57	0.63	149	124	−0.77	−0.74	−1.86	−1.35	57	63	174	217
		nortes	0.63	0.65	137	127	−0.8	−0.78	−0.9	−0.85	53	60	116	102
G. ulmifolia	W	rain	0.62	0.64	102	97.3	−0.67	−0.79	−0.9	−0.93	53	59	205	220
		dry	0.57	0.66	126	95.2	−0.94	−1.07	−1.86	−2.25	52	64	166	195
		nortes	0.59	0.64	124	104	−0.89	−1.04	−1.46	−1.58	54	59	160	192
	D	rain	0.64	0.63	97.2	97.9	−0.42	−0.4	−1.27	−1.25	47	39	182	184
		dry	0.65	0.65	98.6	103	−2.37	−1.51	−2.5	−1.66	53	53	149	105
		nortes	0.65	0.65	101	97.9	−2.2	−1.92	−3.16	−3.23	57	57	161	151
D. cuneata	W	rain	0.69	-	91.8	-	−0.53	-	−2.11	-	42	-	93	-
		dry	0.70	-	88	-	−1.36	-	−3.62	-	56	-	76	-
		nortes	0.70	-	91.4	-	−1.1	-	−2.8	-	62	-	67	-
	D	rain	0.66	0.68	103	99.3	−0.59	−0.58	−1.96	−2.13	55	57	126	101
		dry	0.69	0.7	95	96.7	−3.57	−2.44	−5.3	−4.83	56	61	78	66
		nortes	0.70	0.69	97.5	104	−2.58	−2.07	−3.41	−3.06	62	63	84	76
B. crassifolia	W	rain	0.51	0.64	157	99.2	−0.18	−0.17	−1.11	−1	81	75	89	125
		dry	0.54	0.6	154	118	−0.3	−0.74	−1.26	−1.36	78	73	94	117
		nortes	0.51	0.59	161	120	−0.36	−0.3	−1.33	−1.09	84	77	96	134
	I	rain	0.5	0.66	166	114	−0.35	−0.3	−1.27	−1.37	70	75	132	130
		dry	0.53	0.64	155	116	−0.3	−0.43	−1.52	−1.41	59	65	111	127
		nortes	0.59	0.58	150	150	−0.15	−0.15	−0.71	−0.48	67	54	109	112
	D	rain	0.59	0.58	123	133	−0.41	−0.3	−1.32	−1.33	69	63	134	132
		dry	0.57	0.56	146	153	−0.71	−0.83	−1.56	−1.53	55	61	115	122
		nortes	0.6	0.57	128	132	−0.59	−0.58	−1.48	−1.19	67	72	115	114
Hard-wood species														
B. alicastrum	W	rain	0.78	0.83	84.9	74.9	−0.25	−0.23	−0.32	−0.35	54	52	111	115
		dry	0.77	0.85	89.6	66.3	−0.7	−0.59	−1.93	−1.55	56	54	112	113
		nortes	0.79	0.81	93.6	77.4	−0.49	−0.49	−0.6	−0.6	56	54	119	122
	I	rain	0.8	0.77	72.6	65.1	−0.44	−0.47	−0.56	−0.59	31	39	140	159
		dry	0.83	0.84	76.8	71.5	−0.97	−1.14	−2.27	−1.95	56	52	112	112
		nortes	0.8	0.81	83.8	73.6	−0.49	−0.39	−0.49	−0.45	64	66	116	120
	D	rain	0.82	0.82	66.6	64.1	−0.39	−0.41	−1.66	−1.58	42	39	135	134
		dry	0.83	0.84	67.8	70.3	−1.43	−1.43	−2.85	−3.23	47	49	100	104
		nortes	0.83	0.83	72.2	76.5	−0.75	−0.76	−0.79	−1	55	55	106	106
M. zapota	W	rain	0.79	0.73	80	80	−0.36	−0.45	−0.56	−0.44	58	58	106	110
		dry	0.8	0.77	91	97.3	−0.79	−0.86	−1.22	−1.38	62	60	98	103
		nortes	0.81	0.79	87.2	85.4	−1.19	−1.05	−2.04	−1.66	63	64	104	103
	I	rain	0.81	0.83	76.2	71	−0.67	−0.55	−1.3	−1.08	54	54	105	94
		dry	0.84	0.86	70.5	68.6	−0.95	−1.01	−1.92	−2.17	64	59	99	86
		nortes	0.85	0.86	75	71.9	−0.93	−0.84	−1.34	−1.49	69	67	92	91
	D	rain	0.84	0.82	66.6	63.5	−0.69	−0.67	−1.55	−1.64	57	55	89	87
		dry	0.83	0.82	69.8	73	−1.57	−1.45	−2.71	−3.17	56	56	53	84
		nortes	0.82	0.81	74.8	77.5	−1.15	−0.86	−1.92	−1.68	61	68	88	84
C. mexicanum	W	rain	0.79	0.81	75.5	67.5	−0.54	−0.59	−1.45	−1.12	68	67	109	110
		dry	0.75	0.79	90.5	79.5	−0.57	−0.72	−1.5	−1.7	65	66	104	98
		nortes	0.77	0.76	92.8	97.4	−0.61	−0.63	−1.43	−1.09	61	60	142	107
	I	rain	0.77	0.74	79.2	57.1	−0.34	−0.54	−1.04	−1.1	64	48	74	104
		dry	0.76	0.82	83.9	70.1	−0.87	−0.76	−1.56	−1.85	65	58	70	90
		nortes	0.73	0.83	96.7	68.7	−0.44	−0.36	−1.01	−0.47	69	71	72	108
	D	rain	0.73	0.83	74.9	80.7	−0.41	−0.58	−1.7	−1.44	38	56	98	112
		dry	0.78	0.81	85.1	61.6	−0.98	−1.06	−2.02	−2.11	61	59	82	80
		nortes	0.78	0.78	90.7	89.8	−0.74	−0.63	−1.45	−1.87	68	69	89	86

3.2. Water Potential

Changes in water potential by site, season, and diameter class (young and mature) will be discussed separately for each wood density group.

The light-wood group (*B. simaruba* and *Spondias* sp.) has high water potential values (~−1 MPa). The young stage Ψ_{pd} shows significant differences between sites (Figure 3a; F = 5.2062, $p < 0.01$); Ψ_{pd} is lower in the dry site, where there are lower precipitation values. For Ψ_{pd} in the mature stage, no significant differences are found (Figure 3b). In relation to seasonality, Ψ_{pd} in the dry season has the lowest values (Figure 3a,b; F = 50.948, $p < 0.001$). Ψ_{md} shows significant differences between sites for both the young and mature stages (Figure 4a,b; F = 9.7348, $p < 0.001$); at both stages, the Ψ_{md} was higher at the wet site (Figure 4a,b). Comparing diameter classes, Ψ_{md} registered in young and mature stages shows no significant differences (Table 2).

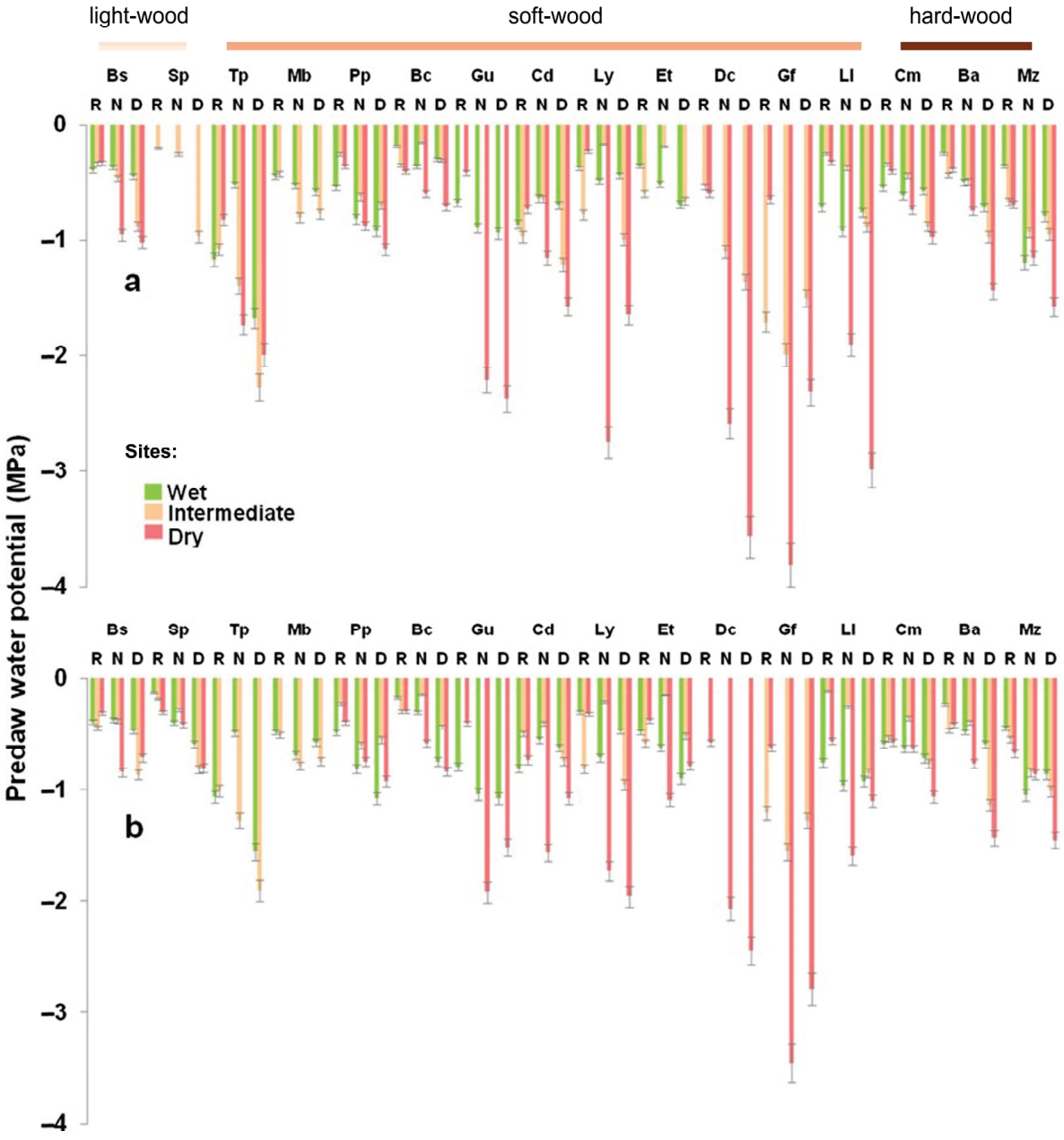


Figure 3. Predawn water potential (Ψ_{pd}, MPa) recorded for 16 tree species in the Yucatán Peninsula during the rainy season (R), nortes (N), and dry season (D). (**a**) Young stage; (**b**) mature stage. Values represent mean ± SE, $n = 319$.

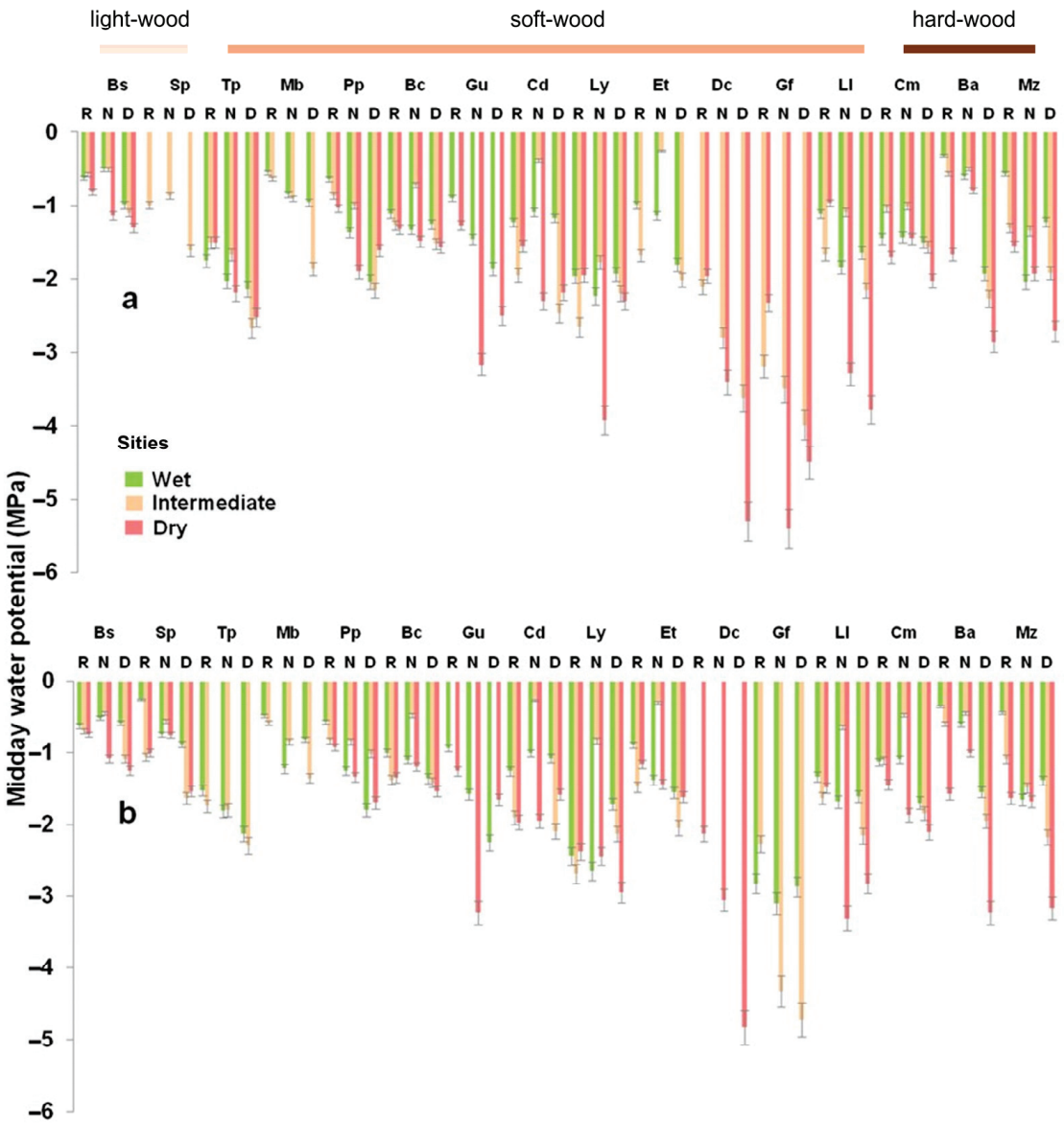


Figure 4. Midday water potential (Ψ_{md}, MPa) for 16 tree species during the rainy season (R), nortes (N), and dry season (D). (**a**) Young stage; (**b**) mature stage. Values are mean ± SE, n = 319.

The soft-wood group shows significant differences within the group (Figure 3a,b; F = 14.061, $p < 0.001$). Species that showed high Ψ_{pd} (>−1 MPa) were *C. dodecandra*, *P. piscipula*, *B. crassifolia*, *E. tinifolia*, *and M. brownei*. Species with low Ψ_{pd} were *G. ulmifolia*, *D. cuneata*, *G. floribundum*, *L. latisiliquum*, and *T. peruviana* (<−1 MPa). Those species showed significant differences in Ψ_{pd} between sites (Figure 3a,b; F = 58.942, $p < 0.001$), and the dry site had the lowest values. In relation to seasonality, the dry season showed the lowest Ψ_{pd} (Figure 3a,b; F = 41.701, $p < 0.001$). Between diameter classes, young and mature presented no differences. Likewise, Ψ_{md} of M. brownei shows high values (~−1 MPa; Figure 4b; F = 30.776, $p < 0.001$); *C. dodecandra*, *G. ulmifolia*, *P. piscipula*, *B. crassifolia*, and *E. tinifolia* can register water potential between −1 MPa and −2 MPa (Figure 4a,b), while *D. cuneata*, *G. floribundum*, *L. latisiliquum*, and *T. peruviana* may present values below −2 MPa (Figure 4a,b; F = 30.776, $p < 0.001$). The Ψ_{md} showed significant differences between sites (Figure 4a,b; F = 58.730, $p < 0.001$); dry sites showed the lowest values, and the dry season showed the lowest values (Figure 4a,b; F = 27.376, $p < 0.001$). For the diameter classes, the mature stage presents the highest values (Figure 4b; p = 5.2496, $p < 0.01$).

The hard-wood group with the species *C. mexicanum*, *B. alicastrum*, and *M. zapota* showed low values, but a high variation during the day. The juvenile and mature stage showed Ψ_{pd} (Figure 3a,b; F = 10.94, $p < 0.001$) and Ψ_{md} values (Figure 4a,b; F = 24.484, $p < 0.001$) that evidence significant differences between sites, with the driest site showing the lowest values.

Comparison Between Natural Conditions and Homegardens

C. dodecandra is the only species in the same diameter class with individuals in both homegardens and natural conditions. The variance analysis indicates that homegarden trees do not have a higher amount of water, since the Ψ_{pd} and Ψ_{md} traits, linked directly to the water status of individuals, showed no significant differences (Figure 5).

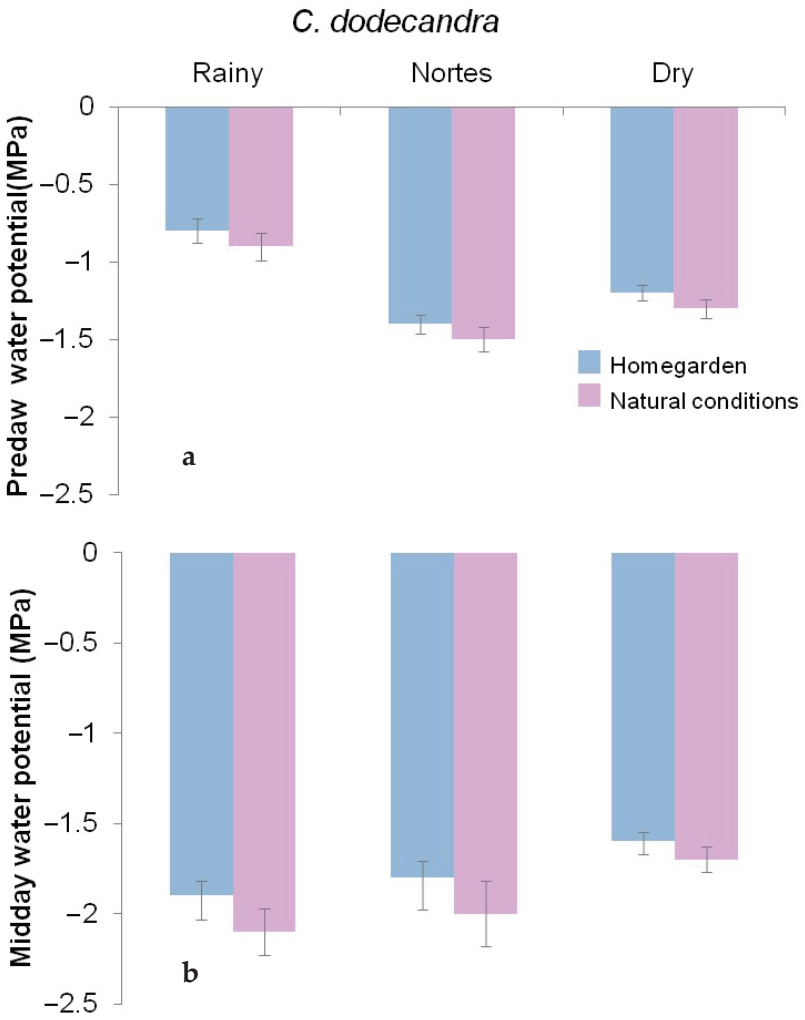


Figure 5. Water potential comparison of *Cordia dodecandra*, homegarden vs. natural conditions. (**a**) Predawn water potential (Ψ_{pd}), (**b**) midday water potential (Ψmd); error bars represent standard errors.

3.3. Saturated Water Content

The species with the highest saturated water content were *B. simaruba* and *Spondias* sp. (Figure 6; F = 695.99, $p < 0.001$), corresponding to the light-wood group with the lowest WD values. In this group, young individuals showed significant site-level differences (F = 11.685, $p < 0.001$), with the lowest values recorded in dry sites, and no seasonal differences were observed. Mature individuals did not differ significantly between sites or seasons. Across diameter classes, young trees consistently presented higher SWC than mature ones (Figure 6; F = 36.432, $p < 0.001$).

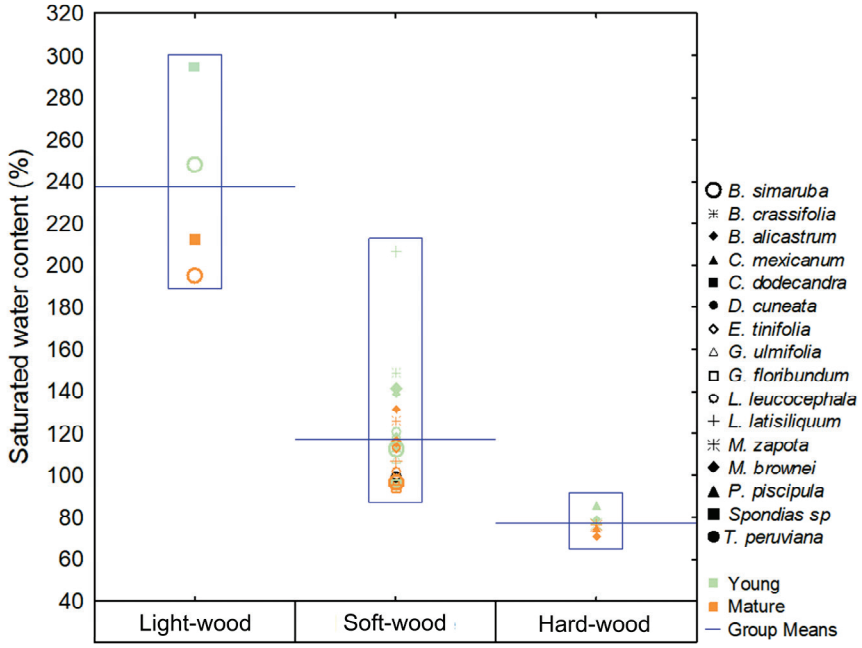


Figure 6. Saturated water content (SWC, %) for 16 tree species grouped by wood density classes and considering two diameter classes: young (<10 cm DBH) and mature (>20 cm DBH). Values are mean ± SE.

Soft-wood species (*C. dodecandra*, *P. piscipula*, *D. cuneata*, *G. floribundum*, *B. crassifolia*, *L. latisiliquum*, *L. leucocephala*, *E. tinifolia*, *M. brownei*, *G. ulmifolia*, and *T. peruviana*) showed intermediate SWC values (Figure 6; F = 695.99, $p < 0.001$). Both young and mature individuals differed significantly among sites (F = 17.645, $p < 0.001$), with the lowest values in dry sites. In mature trees, seasonal differences were also detected (F = 4.1120, $p < 0.05$), with the highest values recorded in the nortes season.

Hard-wood species (*B. alicastrum*, *M. zapota*, and *C. mexicanum*) exhibited the lowest SWC values (Figure 6; F = 695.99, $p < 0.001$). Significant differences between sites were observed for both diameter classes (F = 15.232, $p < 0.001$), with the wet site showing the highest values. Seasonal differences were also present (F = 9.7981, $p < 0.001$), with the nortes season showing the highest SWC. As in the other wood density groups, young trees exhibited higher SWC than mature ones (Figure 6; F = 10.697, $p < 0.001$).

3.4. Relative Water Content

Relative water content (RWC) varied markedly among species (Figure 7a; F = 34.043, $p < 0.001$). The highest values (>55%) were observed in *B. simaruba*, *Spondias* sp., *C. mexicanum*, *C. dodecandra*, *P. piscipula*, *D. cuneata*, *G. floribundum*, *B. crassifolia*, *L. latisiliquum*, *E. tinifolia*, and *M. brownei*, while the lowest corresponded to *T. peruviana* (<40%). Intermediate values (50–55%) were found *in B. alicastrum*, *M. zapota*, and *G. ulmifolia*. Across sites, RWC was consistently higher in wet forests (Figure 7b; F = 21.783, $p < 0.001$). Seasonal variation was also evident, with nortes registering the highest values (F = 8.5645, $p < 0.001$). These patterns are consistent with recent studies that highlight the importance of quantifying trait plasticity across environmental gradients [40]. Between diameter classes, the mature stage maintained higher RWC compared to young individuals (Figure 7b; F = 47.119, $p < 0.001$). Moreover, significant season × species interactions confirmed that RWC plasticity varied among taxa, with several species showing marked shifts across seasons, reflecting their ability to adjust water-use strategies to fluctuating environmental conditions.

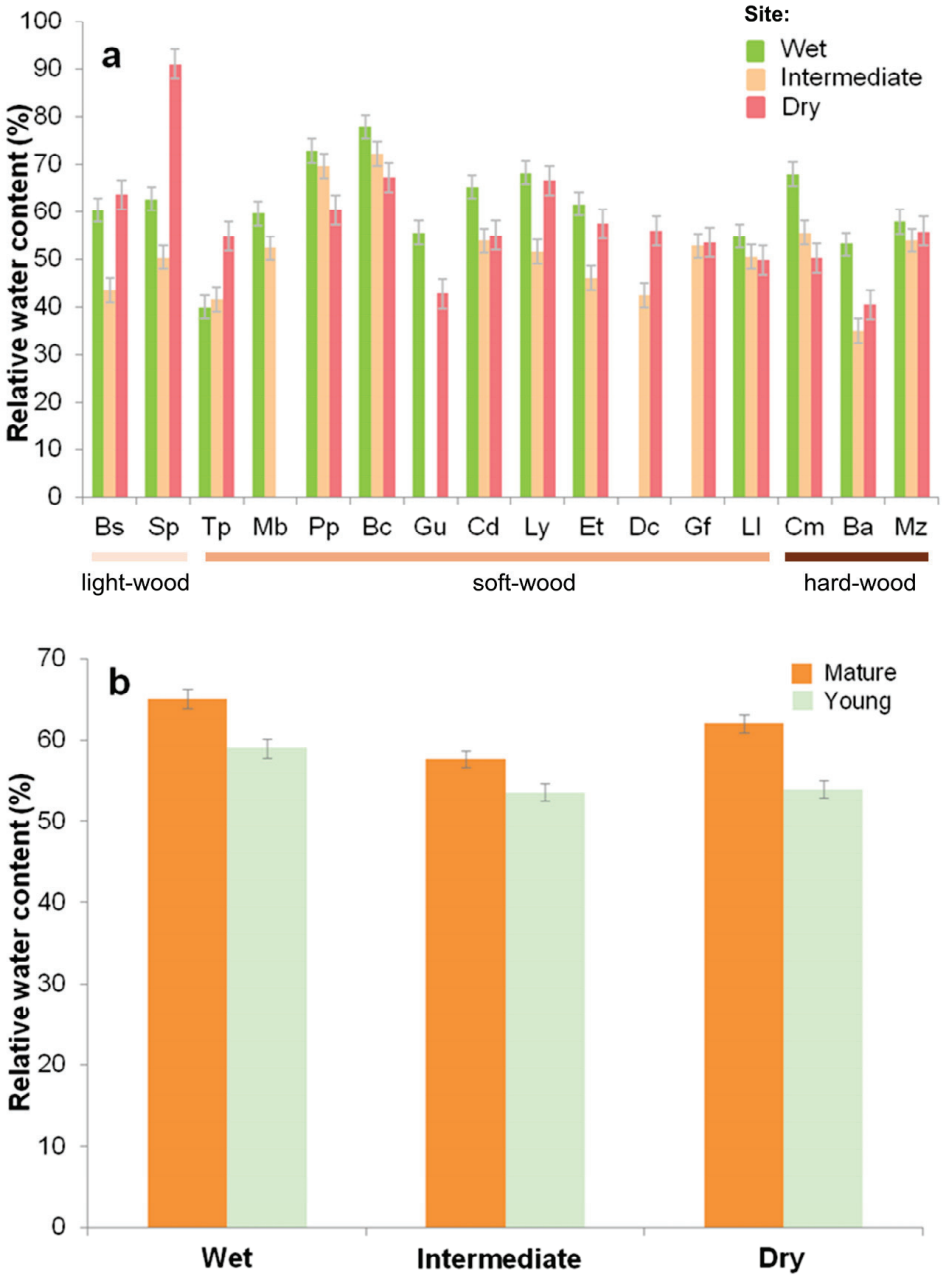


Figure 7. Relative water content (RWC, %) for 16 tree species of the Yucatán Peninsula. (**a**) Rainy season comparison among sites; (**b**) comparison between diameter classes and sites. Values are mean ± SE.

3.5. Specific Leaf Area

Species with the highest specific leaf area were *L. leucocephala* and *Spondias* sp. (Figure 8a; ~200 cm^2 g^{-1}) and showed significant differences between species (Figure 8a; F = 58.006, $p < 0.001$). Medium specific leaf area values were measured in *T. peruviana*, *G. ulmifolia*, *E. tinifolia*, and *G. floribundum* (140–170 cm^2 g^{-1}). A low specific leaf area was found in *B. alicastrum*, *B. simaruba*, *M. brownei*, *C. dodecandra*, and *L. latisiliquum* (120–140 cm^2 g^{-1}), and lower values were found in *B. crassifolia*, *C. mexicanum*, *M. zapota*, *P. piscipula*, and *D. cuneata* (<120 cm^2 g^{-1}). There are significant differences between sites (Figure 8b; F = 3.0510, $p < 0.05$); the dry site showed the lowest values. Regarding seasonality, the rainy season showed the highest specific leaf area (Figure 8b; F = 12.643, $p < 0.001$). Between diameter classes, no differences were found.

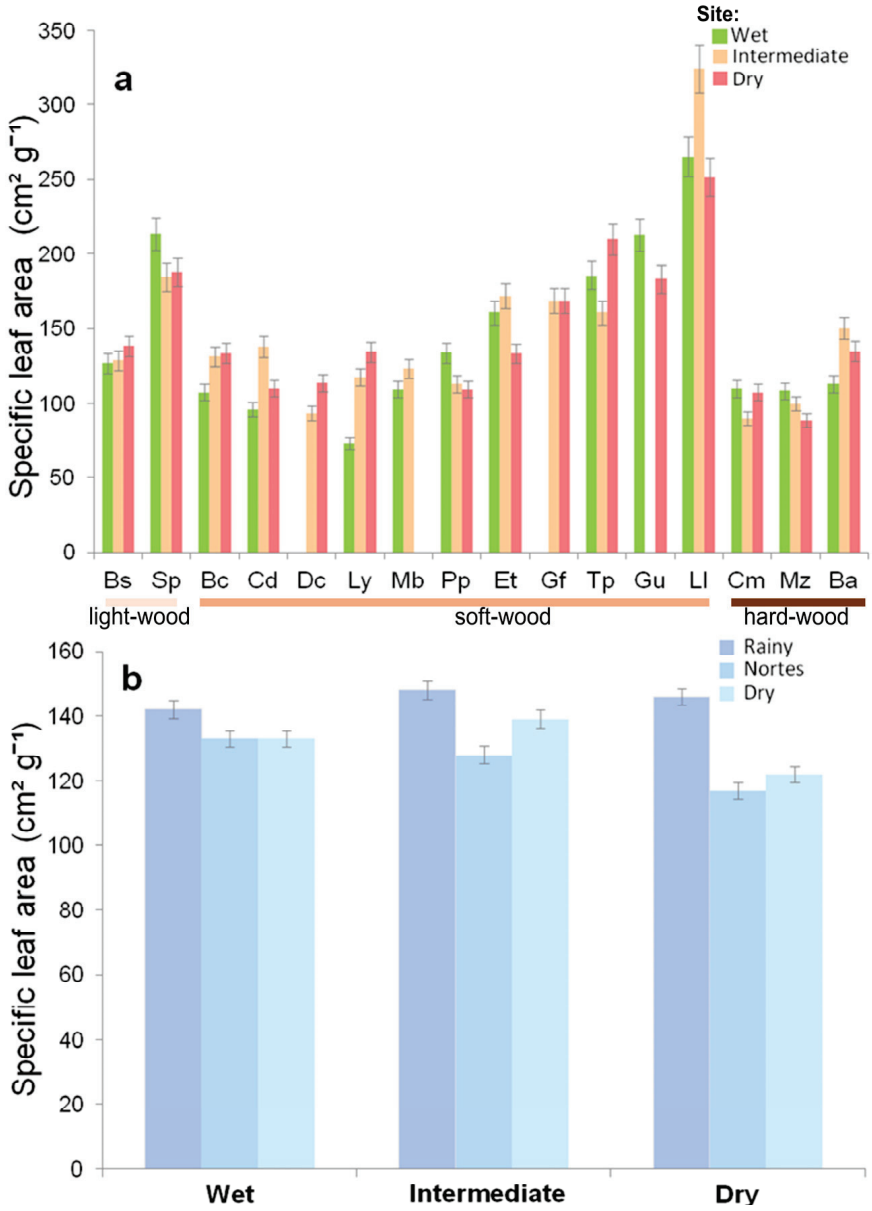


Figure 8. Specific leaf area (SLA) recorded for 16 tree species. (**a**) Rainy season comparison among sites. (**b**) comparison between seasons and sites. Values are mean ± SE.

3.6. Correlations Between Functional Traits and Environmental Factors

Although there was no strong correlation between the functional traits and the environmental factors, some of the correlations are significant (Table 3). We found a negative correlation of the water potential values (Ψ_{pd} and Ψ_{md}) with the temperature and the vapor pressure deficit, and a positive correlation with precipitation balances. SWC was negatively correlated with temperature and vapor pressure deficit, while WD was negatively correlated with precipitation. SLA, in contrast, showed a positive correlation with precipitation. Furthermore, SWC and RWC were positively correlated with Ψ_{pd} and Ψ_{md}, whereas RWC was negatively correlated with SWC (Table 3). WD correlated positively with RWC but negatively with Ψ_{pd}, Ψ_{md}, and SWC. These patterns indicate that wood density is a strong predictor of water storage capacity and leaf morphological adjustments. These results are summarized in Table 3 and highlight the role of wood density as a central integrator of water storage and leaf morphological traits. The broader implications of these correlations are further developed in the Discussion.

Table 3. Spearman correlation between biological variables and environmental factors for 16 tree species of the Yucatán Peninsula. a $p < 0.05$, b $p < 0.001$, c $p < 0.0001$.

Environmental Variables	**Biological Variables**							
	Temperature (°C)	Rainfall (mm)	VPD (kPa)	Ψ_{pd} (MPa)	Ψ_{md} (MPa)	SWC (%)	RWC (%)	WD (g cm^{-3})
Ψ_{pd} (MPa)	−0.1151 c	0.4919 c	−0.2572 c					
Ψ_{md} (MPa)	−0.2195 c	0.4151 c	−0.2136 c	0.6754 c				
SWC (%)	−0.0804 a	0.0522	−0.0966 b	0.2190 c	0.1966 c			
RWC (%)	−0.0708 a	−0.0420	0.0384	0.1613 c	0.1533 c	−0.0861 b		
WD (g cm^{-3})	0.0357	−0.0767 a	0.0447	−0.2009 c	−0.1535 c	−0.9231 c	0.1578 c	
SLA (cm^2 g^{-1})	0.0357	0.1080 c	−0.0337	0.0603	0.0513	0.3153 c	−0.2934 c	−0.4078 c

3.7. Functional Groups

PCA analysis explains 79% of the total variance. The first axis explains 53% of the variance and is determined mainly by ΔΨ (correlation coefficient: −0.82) and SWC (correlation coefficient: 0.86). The second axis explains 26% of the variance and is determined mainly by RWC (correlation coefficient: 0.75) and SLA (correlation coefficient: −0.51). This ordination was based on individual-level data across sites and seasons, ensuring that intraspecific variation and seasonal plasticity were represented. According to PCA, five functional groups were identified (Figure 9).

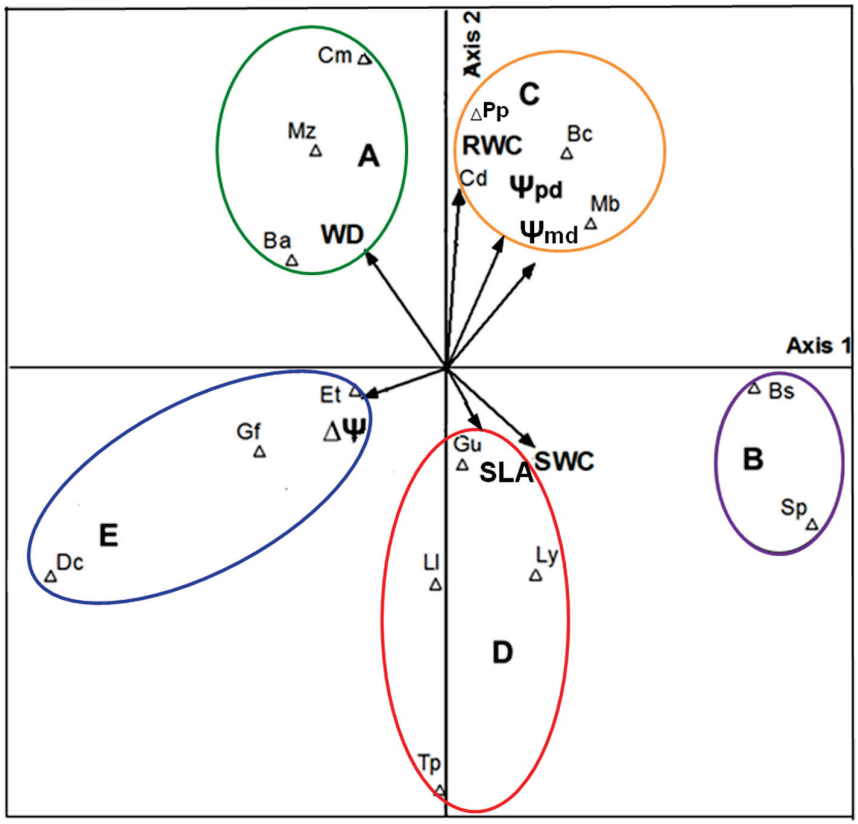


Figure 9. Principal component analysis (PCA) for 16 tree species during the dry season (n = 319), based on wood density (WD), saturated water content (SWC), predawn water potential (Ψ_{pd}), midday water potential (Ψ_{md}), relative water content (RWC), specific leaf area (SLA), and diurnal amplitude of water potential (ΔΨ). Functional groups identified: (A) hard-wood; (B) light-wood; (C) soft-wood with high RWC; (D) soft-wood with high SLA; (E) soft-wood tolerant to low water potentials. Symbols and colors indicate functional groups; percentages in axes labels represent variance explained.

The hard-wood group (A, Figure 9) comprises species with high WD (0.80 g cm^{-3} ± 0.010), low SWC (76.84% ± 1.35), low SLA (96.59 cm^2 g^{-1} ± 5.39), intermediate RWC values (58.22% ± 2.51), and the highest tolerance to low Ψ_{md} (−2.06 MPa ± 0.127).

The light-wood group (B, Figure 9) is characterized by species with low WD values (0.40 g cm^{-3} ± 0.004), high SWC values (220.13% ± 9.24), high Ψ_{md} values (~−1 MPa), and high SLA values (171.21 cm^2 g^{-1} ± 22.72).

The soft-wood group (C, Figure 9) comprises species with high RWC values and slight $\Delta\Psi$ values (−0.76 MPa ± 0.068), high Ψ_{pd} values (−0.77 MPa ± 0.097), and low Ψ_{md} values (−1.54 MPa ± 0.121). The soft-wood group with high SLA (D, Figure 9) further comprises the largest SWC values of the group (124.36% ± 11.236). The soft-wood group, highly tolerant to low water potentials (E, Figure 9), showed the lowest Ψ_{pd} values (−1.66 MPa ± 0.18) and Ψ_{md} values (−3.48 MPa ± 0.32) and highest $\Delta\Psi$ values (−1.81 MPa ± 0.152) throughout the day.

Loadings of the PCA are provided in Tables S1 and S2 (Supplementary Materials), highlighting $\Delta\Psi$ and SWC as the strongest contributors to the first axis and RWC and SLA to the second axis.

4. Discussion

The functional classification derived from our PCA (Figure 9) underscores the considerable diversity of hydraulic strategies among tree species in SDTFs on karst soils. The five groups identified—ranging from hard-wood species with high hydraulic safety to light-wood species with large water storage capacity—capture the continuum between conservative and acquisitive strategies under severe seasonal water limitation, reflecting both structural and physiological adjustments shaped by the dual constraints of climatic seasonality and karst edaphic conditions [20].

Hard-wood species (Group A), such as *Brosimum alicastrum*, *Chrysophyllum mexicanum*, and *Manilkara zapota*, exhibited high wood density, low saturated water content (SWC), and low specific leaf area, consistent with conservative water-use strategies. These traits are often associated with higher resistance to xylem cavitation as suggested by previous studies [41,42], although this relationship was not directly evaluated in our study. While low midday water potentials during the dry season align with high safety margins, some individuals maintained unexpectedly high values. One possible explanation is latex-mediated buffering, which has been observed in other latex-producing species [19,43]. It has been hypothesized that latex contributes to maintaining water status under drought stress [44]. Previous research has suggested that latex influences water relations in species such as *Hevea brasiliensis* during the dry season [43] and that laticiferous vessels provide osmotic adjustment [45]. In *Manilkara zapota*, latex production has been reported to vary with microenvironmental conditions [46]. However, direct measurements of latex production, vessel pressure, and osmotic potential are lacking. Therefore, this remains a hypothetical mechanism that requires direct experimental testing. Future studies that explicitly assess seasonal latex production and its physiological effects are needed to clarify its potential role in regulating water use and drought resilience in karst ecosystems. The ability of these species to access deep water sources, documented in *Brosimum alicastrum* [47], in *Manilkara zapota* [47], and more broadly across SDTF taxa [26], also contributes to their persistence in the driest sites.

Light-wood species (Group B), including *Bursera simaruba* and *Spondias* spp., displayed low wood density and high SWC, enabling them to sustain higher predawn and midday water potentials even during the dry season. The wood density values of *B. simaruba* (0.42 g cm^{-3}; Table 2) from the dry site are like the WD values (~ 0.4 g cm^{-3}) reported by [17,48]. For *Spondias* (WD = 0.38 g cm^{-3}), the results are similar compared to those reported by [49] in *Spondias mombin* (WD = 0.39 g cm^{-3}) in a dry tropical forest of Costa Rica. The group agrees with the findings of other studies like [15,17,50,51]. The species of this group have a high ability to store water in the stem and therefore suffer less variation

in water during the day [52]. These species can even present high water potential values (~−1 MPa) in the dry season [15,17]. Water stored in the stem can be quite abundant, and species can afford to flower during the dry season [17,49]. Deciduousness and shallow root growth after rainfall have been reported as drought-avoidance traits in SDTF species [53], although these aspects were not directly evaluated in our study. This is in line with reports from other SDTFs where stem water storage supports transpiration and reproduction during drought [14,15].

Species with soft wood density under high-humidity conditions behave as a single functional group, differentiated into three functional subgroups under dry-season conditions (Figure 9).

Soft-wood species with high RWC (Group C)—*Piscidia piscipula*, *Cordia dodecandra*, *Metopium brownei*, *Byrsonima crassifolia*—maintained relatively stable daily water potentials, likely due to efficient stomatal control, as observed in species initiating leaf flush during the dry season [54]. *B. crassifolia* trait values are similar to the data reported by [54] for the same species, which has high daily and seasonal water potential. Therefore, a constant water potential during the dry season, when new leaves are formed, could be explained by efficient stomatal control. This suggests greater stomatal sensitivity to moisture in young leaves than in mature leaves [54].

The high-SLA subgroup (Group D)—*Guazuma ulmifolia*, *Lysiloma latisiliquum*, *Leucaena leucocephala*, *Thevetia peruviana*—showed lower RWC but tolerated reduced Ψ_{md}, consistent with acquisitive strategies that balance photosynthetic gain with moderate hydraulic risk. Density values are higher than those obtained by [48] for *L. leucocephala* (WD = 0.65 g cm^{-3}; Table 2). In the case of *G. ulmifolia*, the observed low relative water content during the dry season may reflect additional physiological demands, potentially including reproductive activity, as has been documented for other SDTF species in the Yucatán Peninsula [17] and specifically reported for *G. ulmifolia* [55]. Although we do not present data on the phenology and reproductive status of the species in this study, this explanation constitutes an interesting hypothesis that we will test in the future to better understand the relationship between phenological investment and hydraulic regulation. Results of water potential and wood density in *G. ulmifolia* are like the values reported by [56]. Those data confirm the ability of this species to tolerate low water potential. Also, this response is consistent with [49], where in a dry tropical forest of Costa Rica, soft-wood group plants presented intermediate values in wood density and could tolerate low water potential and low relative water content.

The low-water-potential-tolerant subgroup (Group E)—*Diospyros cuneata*, *Ehretia tinifolia*, *Gymnopodium floribundum*—with evergreen or leaf-exchange phenology tolerated extreme midday water potentials (<−3 MPa) and exhibited traits associated with anisohydric regulation and deep rooting [4,57]. Also, it is necessary to consider that the three species of this functional group are evergreen or leaf-exchange species [17,47]. To maintain their phenological behavior, these species can develop large root systems and access underground water reserves to avoid dehydration [17,47,58]. These groups agree with those found by [17], where the group of evergreen soft-wood species presented relatively high values of relative water content. Likewise, these species show a high predawn water potential, even during the dry season. During the night, these species access deep water sources and recharge their water reserves for daytime use. In *D. cuneata*, a trait that could allow drought tolerance is the presence of sclerophyllous leaves [17], in addition to a combination with low stomatal conductivity and a deep root system [59]. These groups reflect the trade-offs between hydraulic safety and efficiency described by [9], where higher WD often limits storage but increases cavitation resistance, while lower WD supports higher capacitance at the expense of vulnerability.

Across groups, correlation analysis (Table 3) demonstrated strong coupling between climate drivers and hydraulic performance: water potentials were negatively related to temperature and vapor pressure deficit (VPD) and positively related to precipitation, while SWC declined with higher VPD. WD consistently emerged as a strong negative predictor of SWC, reinforcing its role as a structural constraint on water storage capacity [9,13]. SLA increased with precipitation, reflecting plasticity in leaf morphology along the gradient. These results align with recent syntheses that emphasize the integration of above- and below-ground traits for predicting drought responses in heterogeneous karst environments [20,22].

Nevertheless, we acknowledge that our environmental dataset was derived from regional meteorological stations and did not include direct measurements of soil moisture or groundwater availability. Therefore, the observed correlations should be interpreted as associations rather than strict causal relationships. Future studies incorporating local soil and hydrological monitoring will be essential to strengthen trait–environment inferences and refine our understanding of hydraulic responses in karst SDTFs.

In addition, we note that PCA and correlation analyses are exploratory tools that reveal patterns of association but cannot establish causality among traits and environmental variables. Accordingly, we interpret our findings as indicative linkages rather than mechanistic pathways. While our study did not calculate explicit plasticity indices, the observed patterns align with recent work stressing the value of quantifying trait flexibility across temporal and environmental gradients [40]. Future work incorporating structural equation modeling or path analysis, coupled with broader replication, will be necessary to test causal hypotheses more directly.

While our PCA and trait–environment correlations reveal meaningful associations, we recognize that the analysis is based on species means with uneven replication across sites and size classes. These constraints are inherent to field-based studies in natural SDTFs, where individual availability is heterogeneous and replication cannot be standardized as in nursery or common-garden experiments. For this reason, we interpret the observed patterns cautiously, emphasizing associations rather than direct causal mechanisms. Future studies employing hierarchical or mixed-effects approaches, together with expanded and more balanced sampling, will be essential to refine the relationships identified here and to further integrate variability across individuals and environments.

In karst landscapes, hydrological functioning is tightly coupled to below-ground architecture and access to fractured aquifers; these processes interact with above-ground functional traits to shape phenology and drought tolerance. Evidence from the Yucatán Peninsula shows that rooting distribution and source-water partitioning can strongly influence seasonal performance and life-history timing [17,26,47]. Incorporating such below-ground perspectives in future research will provide a more integrative understanding of hydraulic strategies and enhance predictions of species resilience across precipitation gradients in seasonally dry tropical forests on shallow karst soils.

Building on these ecological insights, from a restoration perspective, our classification provides concrete guidance for species selection in karst SDTFs. Hard-wood species (Group A, e.g., *Brosimum alicastrum* and *Manilkara zapota*) are especially suitable for the driest sites, where their deep-rooting capacity ensures access to fractured aquifers. Light-wood species (Group B, e.g., *Bursera simaruba* and *Spondias* spp.) can buffer drought through stem water storage and maintain reproductive activity during water scarcity. Soft-wood groups (Groups C–E) are ideal for mixed plantations that combine acquisitive and conservative strategies, thereby enhancing resilience through functional complementarity. Restoration efforts must also explicitly consider karst constraints such as shallow soils, spatially variable hydrological regimes, and aquifer connectivity. These practical implications are consistent

with recent syntheses on ecosystem processes in carbonate landscapes [60], underscoring the need to integrate trait-based frameworks into restoration planning under increasing hydroclimatic variability.

Due to natural heterogeneity and species availability, replication between sites was inevitably uneven. As shown in Table 1, sample sizes varied depending on species, site, and diameter class. Despite this variation, the consistency of trait patterns across sites lends robustness to our results. However, future studies with more balanced designs and hierarchical models will help to refine these conclusions.

Although this study examined only 16 tree species, it is one of the few studies with a complex field experimental design conducted on a precipitation gradient. The study considered species with contrasting leaf phenologies, wood density categories, and diameter classes. Therefore, it is one of the most extensive comparative datasets of hydrofunctional traits for SDTFs in Central America. However, we acknowledge that our sample comprises only a small percentage of the approximately 500 tree species in the regional flora. Consequently, it is highly likely that not all documented functional strategies have been identified. Future studies should expand taxonomic coverage to include less common and less accessible species. Building on the foundations laid here will provide a more complete picture of hydraulic and phenological diversity in seasonally dry tropical forests.

5. Conclusions

From a regional perspective, the limited availability of functional data underscores a critical knowledge gap in the Yucatán Peninsula, where only ~3% of the ~500 tree species have documented physiological traits and ~20% have recorded values of wood density (WD) [29,61]. Extrapolation from our dataset suggests that soft-wood species could represent approximately two-thirds (66%) of the flora, while hard-wood and light-wood species may comprise 26% and 8%, respectively. The predominance of soft-wood species, combined with substantial intragroup variability, highlights the limitations of relying exclusively on WD as a functional classifier in SDTFs.

In the context of projected increases in dry-season length and vapor pressure deficit, evergreen anisohydric species within Group E may face elevated vulnerability unless continuous access to deep groundwater is secured. By contrast, hard-wood species and light-wood species could maintain resilience through deep-water uptake and stem water storage, respectively, if aquifer integrity and quality are preserved.

From an applied perspective, the classification proposed here offers a mechanistic framework for species selection in restoration and climate adaptation strategies. In the driest environments, prioritizing taxa with wider hydraulic safety margins or enhanced storage capacity could increase establishment and survival under intensifying drought. In more mesic sites, combining acquisitive and conservative species may optimize productivity while buffering against interannual variability. Looking forward, future research should integrate long-term monitoring of plant water status, rooting profiles, and latex production, alongside continuous assessments of groundwater availability and quality, to refine projections of species resilience under increasingly variable hydroclimatic and edaphic conditions.

Supplementary Materials: The following supporting information can be downloaded at https://www.mdpi.com/article/10.3390/f16101535/s1: Table S1: Eigenvalues and percentage of variance explained by the principal components derived from functional trait data across sites and seasons; Table S2: Loadings of functional traits on the first two principal components (PC1 and PC2) derived from the dry-season dataset. Values in bold indicate traits with the highest contributions ($>|0.70|$) to axis separation.

Author Contributions: Conceptualization, M.V.-H.; methodology, M.V.-H. and J.P.-K.; software, validation, M.V.-H. and J.P.-K.; formal analysis, M.V.-H., J.P.-K., E.O.-d.-l.-R., G.A.I., G.C.-P., F.L.-H., and R.J.-A.; investigation, M.V.-H. and J.P.-K.; resources, M.V.-H.; data curation, M.V.-H. and J.P.-K.; writing—original draft preparation, M.V.-H., J.P.-K., and G.A.I.; writing—review and editing, M.V.-H., E.O.-d.-l.-R., and G.C.-P.; visualization, M.V.-H. and J.P.-K.; supervision, M.V.-H.; project administration, M.V.-H.; funding acquisition, M.V.-H. All authors have read and agreed to the published version of the manuscript.

Funding: This research was supported by Secretaria de Educación Pública-Consejo Nacional de Ciencia y Tecnología (177842). J. Palomo-Kumul received a fellowship from Consejo Nacional de Ciencia y Tecnología (307957).

Data Availability Statement: The original contributions presented in this study are included in the article and Supplementary Materials. Further inquiries can be directed to the corresponding author.

Acknowledgments: We thank Oscar Verduzco, Carlos Gómez, Vanessa Préfontaine, Eduardo Avilez, Yonathan Puc, Irving Ramírez, and Holger Weissenberger for support during the field work. We thank National Park Dzibilchaltún, Xpichil and El Colegio de la Frontera Sur, unidad Chetumal, and the homegarden owners in Xpichil and Dzibilchaltún for permission to conduct the field work.

Conflicts of Interest: The authors declare no conflicts of interest.

References

1. Murphy, P.G.; Lugo, A.E. Ecology of Tropical Dry Forest. *Annu. Rev. Ecol. Syst.* **1986**, *17*, 67–88. [CrossRef]
2. IPCC. Contribution of Working Groups I, II and III to the Sixth Assessment Report of the Intergovernmental Panel on Climate Change. In *Climate Change 2023: Synthesis Report*; Core Writing Team, Lee, H., Romero, J., Eds.; IPCC: Geneva, Switzerland, 2023; pp. 35–115. [CrossRef]
3. Lopez-Toledo, L.; Prieto-Torres, D.A.; Barros, F.D.V.; Ribeiro, N.; Pennington, R.T. Seasonally dry tropical forests: New insights for their knowledge and conservation. *Front. Glob Change* **2024**, *6*, 1350375. [CrossRef]
4. Hasselquist, N.J.; Allen, M.F.; Santiago, L.S. Water relations of evergreen and drought-deciduous trees along a seasonally dry tropical forest chronosequence. *Oecologia* **2010**, *164*, 881–890. [CrossRef] [PubMed]
5. Aguirre-Gutiérrez, J.; Rifai, S.W.; Deng, X.; Steege, H.t.; Thomson, E.; Corral-Rivas, J.J.; Guimaraes, A.F.; Muller, S.; Klipel, J.; Fauset, S.; et al. Canopy functional trait variation across Earth's tropical forests. *Nature* **2025**, *641*, 129–136. [CrossRef] [PubMed]
6. Ortega, M.A.; Cayuela, L.; Griffith, D.M.; Camacho, A.; Coronado, I.M.; del Castillo, R.F.; Figueroa-Rangel, B.L.; Fonseca, W.; Garibaldi, C.; Kelly, D.L.; et al. Climate Change Increases threat to Plant Diversity in Tropical Forests of Central America and Southern Mexico. *PLoS ONE* **2024**, *19*, e0297840. [CrossRef]
7. Anderegg, W.R.L.; Konings, A.G.; Trugman, A.T.; Yu, K.; Bowling, D.R.; Gabbitas, R.; Karp, D.S.; Pacala, S.; Sperry, J.S.; Sulman, B.N.; et al. Hydraulic diversity of forests regulates ecosystem resilience during drought. *Nature* **2018**, *561*, 538–541. [CrossRef] [PubMed]
8. Méndez-Alonzo, R.; Paz, H.; Zuluaga, R.C.; Rosell, J.A.; Olson, M.E. Coordinated Evolution of Leaf and Stem Economics in Tropical Dry Forest Trees. *Ecology* **2012**, *93*, 2397–2406. [CrossRef]
9. De Guzman, M.E.; Acosta-Rangel, A.; Winter, K.; Meinzer, F.C.; Bonal, B.; Santiago, L.S. Hydraulic traits of Neotropical canopy liana and tree species across a broad range of wood density: Implications for predicting drougth mortality with models. *Tree Physiol.* **2021**, *41*, 24–34. [CrossRef]
10. Markesteijn, L.; Poorter, L.; Bongers, F.; Paz, H.; Sack, L. Hydraulics and Life History of Tropical Dry Forest Tree Species: Coordination of Species' Drought and Shade Tolerance. *New Phytol.* **2011**, *191*, 480–495. [CrossRef]
11. Ávila-Lovera, E.; Urich, R.; Coronel, I.; Tezara, W. Ecophysiological traits change Little along a successional gradient in a tropical dry deciduous woodland from Margarita Island, Venezuela. *Front. For. Glob. Change* **2023**, *6*, 1043574. [CrossRef]
12. Flo, V.; Martínez-Vilalta, J.; Mencuccini, M.; Granda, V.; Anderegg, W.R.; Poyatos, R. Climate and functional traits jointly mediate tree water-use strategies. *New Phytol.* **2021**, *231*, 617–630. [CrossRef]
13. Fagundes, M.V.; Souza, A.F.; Oliveira, R.S.; Ganade, G. Functional traits above and below ground allow species with distinct ecological strategies to coexist in the largest seasonally dry tropical forest in the Americas. *Front. For. Glob. Change* **2022**, *5*, 930099. [CrossRef]
14. Smith-Martin, C.M.; Muscarella, R.; Hammond, W.M.; Jansen, S.; Brodribb, T.J.; Choat, B.; Johnson, D.M.; Vargas-G, G.; Uriarte, M. Hydraulic variability of tropical forests is largely independent of water availability. *Ecol. Lett.* **2023**, *26*, 1829–1839. [CrossRef] [PubMed]

15. Borchert, R.; Pockman, W.T. Water storage capacitance and xylem tension in isolated branches of temperate and tropical trees. *Tree Physiol.* **2005**, *25*, 457–466. [CrossRef] [PubMed]
16. Lavorel, S.; Garnier, E. Predicting Changes in Community Composition and Ecosystem Functioning from Plant Traits: Revisiting the Holy Grail. *Funct. Ecol.* **2002**, *16*, 545–556. [CrossRef]
17. Valdez-Hernández, M.; Andrade, J.L.; Jackson, P.C.; Rebolledo-Vieyra, M. Phenology of five tree species of a tropical dry forest in Yucatan, Mexico: Effects of environmental and physiological factors. *Plant Soil* **2010**, *329*, 155–171. [CrossRef]
18. Palomo-Kumul, J.; Valdez-Hernández, M.; Islebe, G.A.; Cach-Pérez, M.J.; Andrade, J.L. El Niño-Southern Oscillation affects the water relations of tree species in the Yucatan Peninsula, Mexico. *Sci. Rep.* **2021**, *11*, 10451. [CrossRef]
19. Adams, R.E.; West, J.B. Functional Groups Mask Inter- and Intraspecific Variation in Water Use Strategies in a Seasonally Dry Tropical Forest. *Front. Water* **2022**, *4*, 950346. [CrossRef]
20. Jackson, P.C.; Andrade, J.L.; Reyes-García, C.; Hernández-González, O.; McElroy, T.; Us-Santamaría, R.; Simá, J.L.; Dupuy, J.M. Physiological responses of species to microclimate help explain population dynamics along succession in a tropical dry forest of Yucatan, Mexico. *Forests* **2018**, *9*, 411. [CrossRef]
21. Liu, C.; Huang, Y.; Wu, F.; Liu, W.; Ning, Y.; Huang, Z.; Tang, S.; Liang, Y. Plant adaptability in karst regions. *J. Plant Res.* **2021**, *134*, 889–906. [CrossRef]
22. Oliveira, R.S.; Eller, C.B.; Barros, F.D.V.; Hirota, M.; Brum, M.; Bittencourt, P. Linking plant hydraulics and the fast–slow continuum to understand resilience to drought in tropical ecosystems. *New Phytol.* **2021**, *230*, 904–923. [CrossRef] [PubMed]
23. Li, F.; He, X.; Sun, Y.; Zhang, X.; Tang, X.; Li, Y.; Yi, Y. Distinct endophytes are used by diverse plants for adaptation to karst regions. *Sci. Rep.* **2019**, *9*, 5246. [CrossRef] [PubMed]
24. Ford, D.; Williams, P. *Karst Hydrogeology and Geomorphology*; John Willey & Sons: Sussex, UK, 2007.
25. Geekiyanage, N.; Goodale, U.M.; Cao, K.; Kitajima, K. Plant ecology of tropical and subtropical karst ecosystems. *Biotropica* **2019**, *51*, 626–640. [CrossRef]
26. Estrada-Medina, H.; Santiago, L.S.; Graham, R.C.; Allen, M.F.; Jimenez-Osornio, J. Source water, phenology and growth of two tropical dry forest tree species growing on shallow karst soils. *Trees* **2013**, *27*, 1297–1307. [CrossRef]
27. Narvaez-Montoya, C.; Mondragón Bonilla, R.; Goldscheider, N.; Mahlknecht, J. Groundwater salinization patterns in the Yucatan Peninsula reveal contamination and vulnerability of the karst aquifer. *Commun. Earth Environ.* **2025**, *6*, 468. [CrossRef]
28. Hernández-Flores, G.; Gutiérrez-Aguirre, M.A.; Cervantes-Martínez, A.; Marín-Celestino, A.E. Historical analysis of a karst aquifer: Recharge, water extraction, and consumption dynamics on a tourist island (Cozumel, Mexico). In *Annales de Limnologie-International Journal of Limnology*; EDP Sciences: Les Ulis, France, 2021; Volume 57, p. 16. [CrossRef]
29. Valdez-Hernández, M.; González-Salvatierra, C.; Reyes-García, C.; Jackson, P.C.; Andrade, J.L. Physiological Ecology of Vascular Plants. In *Biodiversity and Conservation of the Yucatán Peninsula*; Islebe, G., Calmé, S., León-Cortés, J., Schmook, B., Eds.; Springer: Cham, Switzerland, 2015. [CrossRef]
30. Thien, L.; Bradburn, A.S.; Welden, A.L. *The Woody Vegetation of Dzibilchaltún. A Maya Archeological Site in Northwest Yucatán, México*; Middle American Research Institute: New Orleans, LA, USA, 1982; pp. 1–24.
31. Valdez-Hernández, M.; Sánchez, O.; Islebe, G.A.; Snook, L.K.; Negreros-Castillo, P. Recovery and early succession after experimental disturbance in a seasonally dry tropical forest in Mexico. *For. Ecol. Manag.* **2014**, *334*, 331–343. [CrossRef]
32. Bautista, F.; Palacio, G.; Ortiz-Pérez, M.; Batllori-Sampedro, E.; Castillo-González, M. El origen y el manejo maya de las geoformas, suelos y aguas en la Península de Yucatán. In *Caracterización y Manejo de los Sue los de la Península de Yucatán: Implicaciones Agropecuarias, Forestales y Ambientales*; Zúñiga, F.B., Ed.; Universidad Autónoma de Campeche: Campeche, Mexico; Universidad Autónoma de Yucatán: Mérida, Mexico, 2005; pp. 21–32.
33. Chave, J.; Coomes, D.; Jansen, S.; Lewis, S.L.; Swenson, N.G.; Zanne, A.E. Towards a Worldwide Wood Economics Spectrum. *Ecol. Lett.* **2009**, *12*, 351–366. [CrossRef]
34. Mo, L.; Zhang, Y.; Li, X.; Johnson, D.J.; Fortunel, C.; Lin, D.; Swenson, N.G.; Wright, S.J.; Xu, H.; He, N. The Global Distribution and Drivers of Wood Density. *Nat. Plants* **2024**, *10*, 1120–1132. [CrossRef]
35. Koide, R.T.; Robichaux, R.H.; Morse, S.R.; Smith, C.M. Plant water status, hydraulic resistance and capacitance. In *Plant Physiological Ecology*; Pearcy, R.W., Ehleringer, J.R., Mooney, H.A., Rundel, P.W., Eds.; Springer: Dordrecht, The Netherlands, 1989. [CrossRef]
36. Schneider, C.A.; Rasband, W.S.; Eliceiri, K.W. NIH Image to ImageJ: 25 years of image analysis. *Nat. Methods* **2012**, *9*, 671–675. [CrossRef]
37. Bucci, S.J.; Scholz, F.G.; Goldstein, G.; Meinzer, F.C.; Arce, M.E. Soil Water Availability and Rooting Depth as Determinants of Hydraulic Architecture of Patagonian Woody Species. *Oecologia* **2009**, *160*, 631–641. [CrossRef]
38. StatSoft, Inc. *STATISTICA*, Version 12. Data Analysis Software System. StatSoft, Inc.: Tulsa, OK, USA, 2013.
39. McCune, B.; Mefford, M.J. *PC-ORD*, Version 5.10. Multivariate Analysis of Ecological Data. MjM Software: Gleneden Beach, OR, USA, 2006.

40. Wei, Z.; Kou, J.; Miao, L.; Hu, F.; Li, L.; Wu, X.; Li, S.; Meng, L. Exploring diurnal variation in soil moisture via sub-daily estimates reconstruction. *J. Hydrol.* **2025**, *662*, 134005. [CrossRef]
41. Hacke, U.G.; Sperry, J.S.; Pockman, W.T.; Davis, S.D.; McCulloh, K.A. Trends in wood density and structure are linked to prevention of xylem implosion by negative pressure. *Oecologia* **2001**, *126*, 457–461. [CrossRef]
42. Gleason, S.M.; Westoby, M.; Jansen, S.; Choat, B.; Hacke, U.G.; Pratt, R.B.; Bhaskar, R.; Brodribb, T.J.; Bucci, S.J.; Cao, K.-F.; et al. Weak tradeoff between xylem safety and xylem-specific hydraulic efficiency across the world's woody plant species. *New Phytol.* **2016**, *209*, 123–136. [CrossRef]
43. Rao, P.S.; Saraswathyamma, C.K.; Sethuraj, M.R. Studies on the relationship between yield and meteorological parameters of para rubber tree (*Hevea brasiliensis*). *Agr. Forest Meteorol.* **1998**, *90*, 235–245. [CrossRef]
44. García, E.G.; Di Stefano, J.F. Fenología de árbol *Sideroxylon capiri* (Sapotaceae) en el Bosque Seco Tropical de Costa Rica. *Rev. Biol. Trop.* **2005**, *53*, 5–14. [PubMed]
45. Vijayakumar, K.R.; Dey, S.K.; Chandrasekhar, T.R.; Devakumar, A.S.; Mohankrishna, T.; Sanjeeva Rao, P.; Sethuraj, M.R. Irrigation requirement of rubber trees (*Hevea brasiliensis*) in the subhumid tropics. *Agric. Water Manag.* **1998**, *35*, 245–259. [CrossRef]
46. Dugelby, B. Mecanismos gubernamentales y tradicionales que norman la extracción del látex del chicle en El Petén Guatemala. In *La Selva Maya Conservación y Desarrollo*; Primack, R.B., Bray, D., Galletti, H.A., Ponciano, I., Eds.; Siglo XXI Editores Mexico: Mexico City, Mexico, 1999; pp. 197–220.
47. Querejeta, J.I.; Estrada-Medina, H.; Allen, M.F.; Jiménez-Osornio, J.J. Water Source Partitioning Among Trees Growing on Shallow Karst Soils in a Seasonally Dry Tropical Climate. 44. *Oecologia* **2007**, *152*, 26–36. [CrossRef]
48. Reyes-García, C.; Andrade, J.L.; Luis Simá, J.; Us-Santamaría, R.; Jackson, P.C. Sapwood to heartwood ratio affects whole-tree water use in dry forest legume and non-legume trees. *Trees* **2012**, *26*, 1317–1330. [CrossRef]
49. Borchert, R. Soil and Stem Water Storage Determine Phenology and Distribution of Tropical Dry Forest Trees. *Ecology* **1994**, *75*, 1437–1449. [CrossRef]
50. Bucci, S.J.; Goldstein, G.; Meinzer, F.C.; Scholz, F.G.; Franco, A.C.; Bustamante, M. Functional Convergence in Hydraulic Architecture and Water Relations of Tropical Savanna Trees: From Leaf to Whole Plant. *Tree Physiol.* **2004**, *24*, 891–899. [CrossRef]
51. Singh, K.P.; Kushwaha, C.P. Emerging paradigms of tree phenology in dry tropics. *Curr. Sci.* **2005**, *89*, 964–975.
52. Stratton, L.; Goldstein, G.; Meinzer, F.C. Stem water storage capacity and efficiency of water transport: Their functional significance in a Hawaiian dry forest. *Plant Cell Environ.* **2000**, *23*, 99–106. [CrossRef]
53. Olivares, E.; Medina, E. Water and nutrient relations of woody perennials from tropical dry forests. *J. Veg. Sci.* **1992**, *3*, 383–392. [CrossRef]
54. Goldstein, G.; Sarmiento, G.; Meinzer, F. Patrones diarios y estacionales en las relaciones hídricas de árboles siempreverdes de la sabana tropical. *Acta Oecologica* **1986**, *7*, 107–119.
55. Borchert, R. Phenology and Flowering Periodicity of Neotropical Dry Forest Species: Evidence from Herbarium Collections. *J. Trop. Ecol.* **1996**, *12*, 65–80. [CrossRef]
56. Worbes, M.; Blanchart, S.; Fichtler, E. Relations between water balance, wood traits and phenological behavior of tree species from a tropical dry forest in Costa Rica—A multifactorial study. *Tree Physiol.* **2013**, *33*, 527–536. [CrossRef]
57. Johnson, D.M.; Katul, G.; Domec, J.C. Catastrophic hydraulic failure and tipping points in plants. *Plant Cell Environ.* **2022**, *45*, 2231–2266. [CrossRef]
58. Borchert, R. Responses of Tropical Trees to Rainfall Seasonality and Its Long-Term Changes. *Clim. Change* **1998**, *39*, 381–393. [CrossRef]
59. Valladares, F.; Vilagrosa, A.; Peñuelas, J.; Ogaya, R.; Camarero, J.J.; Corcuera, L.; Sisó, S.; Gil-Pelegrín, E. Estrés hídrico: Ecofisiología y escalas de la sequía. In *Ecología del Bosque Mediterráneo en un Mundo Cambiante*, 2nd ed.; Valladares, F., Ed.; Naturaleza y Parques Nacionales, Ministerio de Medio Ambiente: Madrid, Spain, 2004; pp. 165–192.
60. Wu, L.; Bai, X.; Li, C.; Li, H.; Cao, Y.; Ran, C.; Zhang, S.; Xiong, L.; Du, C.; Luo, G.; et al. Assessment of carbon sinks caused by the chemical weathering of carbonate rocks under the influence of exogenous acids: Methods, progress, and prospects. *Sci. China Earth Sci.* **2025**, *68*, 1785–1804. [CrossRef]
61. ICRAF 2019. Tree Functional Attributes and Ecological Database. Available online: https://worldagroforestry.org/tree-knowledge/type-of-resource/tree-databases (accessed on 25 June 2025).

Disclaimer/Publisher's Note: The statements, opinions and data contained in all publications are solely those of the individual author(s) and contributor(s) and not of MDPI and/or the editor(s). MDPI and/or the editor(s) disclaim responsibility for any injury to people or property resulting from any ideas, methods, instructions or products referred to in the content.

forests

MDPI

Article

Effect of Lead on the Physiological Parameters and Elemental Composition of *Pinus sylvestris* L. and *Picea abies* (L.) H. Karst Seedlings

Andrea Pogányová [1], Djordje P. Božović [2], Martin Bačkor [1,3], Michal Goga [1,4], Marián Tomka [3] and Marko S. Sabovljević [1,2,*]

[1] Department of Plant Biology, Institute of Biology and Ecology, Faculty of Science, Pavol Jozef Šafárik University in Košice, Mánesova 23, 041 67 Košice, Slovakia
[2] Institute of Botany and Botanical Garden, Faculty of Biology, University of Belgrade, Takovska 43, 11000 Belgrade, Serbia
[3] Department of Biochemistry and Biotechnology, Institute of Biotechnology, Faculty of Biotechnology and Food Sciences, Slovak University of Agriculture, 949 76 Nitra, Slovakia
[4] Center for Interdisciplinary Biosciences, Technology and Innovation Park, Pavol Jozef Šafárik University in Košice, Jesenná 5, 041 54 Košice, Slovakia
* Correspondence: marko@bio.bg.ac.rs

Abstract: Lead (Pb) pollution poses a long-term threat to forest ecosystems, particularly in mountainous areas affected by atmospheric deposition. This study examined the physiological and biochemical responses of juvenile *Pinus sylvestris* L. and *Picea abies* (L.) H. Karst seedlings to low concentrations of lead nitrate during early development. Treatments simulated environmentally relevant Pb exposure and focused on pigment composition, oxidative stress markers, soluble protein and proline levels, and elemental content. Both species exhibited hormetic stimulation of photosynthetic pigments at lower Pb concentrations. In *P. sylvestris*, this effect declined at the highest dose, whereas *P. abies* maintained pigment levels, suggesting stronger regulatory control. Pb exposure reduced soluble proteins and induced species-specific alterations in MDA and proline levels. Correlation analysis revealed a well-integrated stress response in *P. abies*, while *P. sylvestris* showed a more fragmented pattern. Elemental analysis confirmed Pb accumulation primarily in roots, with higher levels in *P. sylvestris*. Both species experienced reduced root Mg, K, and Mn, indicating ionic imbalance due to Pb^{2+} interference. Zn content increased in *P. sylvestris* but decreased in *P. abies*, possibly reflecting differences in uptake regulation. These species-specific responses support the hypothesis that *P. abies* activates more effective defense mechanisms against Pb toxicity, while *P. sylvestris* exhibits a stronger physiological stress response.

Keywords: biochemical markers; lead tolerance; micronutrient interactions; pinaceae; stress responses

1. Introduction

The advancing level of technology in most areas of industry, mining, and manufacturing has not eliminated the long-term issue of environmental contamination by heavy metals. Even today, many countries experience significant contamination from heavy metals released through fossil fuel combustion, with lead being one of the key pollutants entering the environment through this process. Contamination with lead is caused by emissions from industrial processes, exhaust gases, mining, or the burning of fossil

fuels [1–3]. The problem is not only the initial contamination with lead but also the further fate of this element [4,5]. Lead is characterized by low mobility, and as a result, its particles often remain on the soil surface or in water sediments [6–8]. This can lead to the gradual accumulation of this element in the environment [9,10]. Many studies have confirmed increased deposition of lead in areas affected by prevailing wind flow in the downwind direction from the original source of pollution [11–13]. High concentrations of lead are often found in mountainous areas, which act as a natural barrier to long-distance air flows [14–16]. This causes, on the windward side, a long-term contamination effect of the natural environment and forest stands [14,17,18]. Plants, including trees such as pine (*Pinus sylvestris* L.) and spruce (*Picea abies* (L.) H. Karst), absorb lead through their roots from the soil surface [19–21]. The presence of lead is toxic to plants and can cause many changes, like the disruption of nutrient uptake and water transport [22,23]. Lead also damages photosynthesis by inhibiting chlorophyll synthesis, destroying chloroplasts [24,25], and affecting the production of healthy pollen grains [26,27]. Therefore, the impact of lead in forest stands can lead to reduced tree growth, lower biomass accumulation, and diminished forest productivity [28,29]. The condition of forests is also influenced by other effects of the presence of lead, such as changes in soil microbial diversity [30,31]. Ecosystem contamination is a complex process influenced by various factors, such as site altitude, soil characteristics, organic matter content, forest litter [32–34] pH, temperature, and precipitation [35,36]. These factors affect the presence and bioavailability of lead (Pb) in forest ecosystems, as well as its direct impact on individual trees [37–39]. At lower concentrations, signs of contamination may not always be evident, as many species can adapt to prolonged exposure to these contaminants [38,40,41]. This study focuses on the contamination of juvenile stages of forest tree species from the *Pinaceae* family. Pine and spruce are key species in European woodlands, making up a significant proportion of forest stands [42,43]. Here, we simulated Pb contamination in forest stands, which could occur through long-term exposure to polluted precipitation [44]. The concentrations used in this study exceed the permissible limit for lead in surface waters in Europe [45], as well as the average Pb content typically found in precipitation across Europe [46,47]. However, long-term exposure to low concentrations of Pb can have a cumulative effect, resulting in increased Pb levels in topsoil and the ecosystem [48,49]. The concentrations used were thus chosen to reflect potential impacts on physiological processes in plants without causing immediate toxic effects. Here, we aimed to determine the basic impact of Pb on the physiological processes of juvenile conifer individuals germinating from seeds during the first two months of growth in Pb-contaminated forest stands.

The main hypothesis of this study is that juveniles of the two tested coniferous species express different sensitivity to variously lead-loaded sites. The results can be further used in the selection of reforestation practices at lead-loaded sites. The choice of not only plant species but also plant developmental stage can be made based on the results obtained, i.e., seeds, juveniles, or young trees.

2. Materials and Methods

2.1. Growth Conditions and Pb Treatments

The experiment was performed using seeds of *Pinus sylvestris* and *Picea abies* (Forests of the Slovak Republic, state enterprise, Semenoles, Slovakia, 2023). Only visually healthy seeds of average size that were free of abnormalities in size, shape, and color were selected for the study. In total, 1920 seeds were used—80 seeds per group, with 24 groups in total, including replicates. The seeds were placed in uncovered plastic containers (20 × 15 × 10 cm), with each group assigned to one container. The containers were filled with a perlite substrate (Perlite substrate, Forestina s.r.o., Mnichov, Czech Republic) and maintained under

controlled conditions with a 16 h light/8 h dark photoperiod, a temperature of 23 ± 2 °C, and a relative humidity of 60 ± 5%. The samples were watered exclusively with distilled water, with no additional nutrients or treatments. For the first three weeks after sowing, the seeds were left untreated with Pb. After this period, 0.5 L of metal solution was applied five times at seven-day intervals (except in the control groups). The treatments included lead nitrate ($Pb(NO_3)_2$) at concentrations of 0.5 mg/L, 1 mg/L, and 2 mg/L. These solutions were applied directly to the substrate during watering for both species. Following the final treatment, the plants remained in the containers for an additional seven days before the experiment was terminated. The total duration of the experiment was nine weeks. After removal from the substrate, the plants were immediately rinsed with water and frozen in liquid nitrogen to preserve tissue integrity. The aboveground and below-ground parts were then separated and stored at −80 °C until further analysis.

2.2. Pigments

Before all analyses, plant samples from each treatment group (averaging 50 individuals per group) were homogenized in a frozen state to ensure uniformity for subsequent analyses. For pigment analysis, 25 mg of plant tissue (FW) was incubated in 15 mL of dimethyl sulfoxide (DMSO) at 65 °C for 60 min. After incubation, absorbance was measured using a multimode microplate spectrophotometer (Synergy HT, BioTek, Hudson, NY, USA) at wavelengths of 665, 649, 480, 435, and 415 nm for chlorophylls and carotenoids and 663, 647, and 537 nm for anthocyanins. The concentrations of chlorophylls a and b, total chlorophyll (a + b), and total carotenoids were calculated according to Wellburn's method [50]. Anthocyanin concentration (μmol/mL) was determined using the formula: $0.08173 \times A537 - 0.00697 \times A647 - 0.00228 \times A663$ [51]. Pigment analyses were performed only on the aboveground photosynthetic tissues of the plants, with each sample analyzed in triplicate.

2.3. MDA Analysis

Malondialdehyde (MDA) content was evaluated using the method of Heath and Packer [52]. A total of 100 mg (FW) of homogenized plant tissue was ground in a pestle and mortar with 1.0 mL of 0.1% trichloroacetic acid (TCA) extract and then centrifuged at ±4 °C. After removing the supernatant, the samples were incubated with a mixture of 20% TCA and 0.5% thiobarbituric acid (TBA) at 90 °C. Following immediate cooling on ice, the samples were analyzed using the same spectrometer (Synergy HT, BioTek) as used in pigment analysis at wavelengths of 532 and 600 nm. MDA concentration (μg/mg FW) was calculated using the following formula: $[(A_{532} - A_{600})/155] \times 1000 \times Volextract/Volaliquot \times 1/FW$. MDA analyses were performed only on the aboveground photosynthetic tissues of the plants, with each sample analyzed in triplicate.

2.4. Soluble Protein Quantification

For soluble protein quantification, the protocol of Bradford [53] was used. A total of 25 mg (FW) of homogenized tissue was ground in a pestle and mortar with 50 mM phosphate buffer (pH 6.5) and centrifuged at 15,000× g at 4 °C for 20 min. Then, the supernatant was mixed with Bradford solution and measured at an absorbance of 595 nm (Synergy HT, BioTek). Bovine serum albumin was used as the calibration standard. Soluble protein quantification analyses were performed only on the aboveground photosynthetic tissues of the plants, with each sample analyzed in triplicate.

2.5. Proline Analysis

Proline content was analyzed based on the protocol of Ábrahám et al. [54]. A total of 50 mg fresh weight (FW) of tissue per sample was ground in a mortar and pestle with 3% sulfosalicylic

acid (SSA). Samples were centrifuged for 5 min at room temperature, and the supernatants were then incubated in a mixture of 3% SSA, glacial acetic acid, and acidic ninhydrin at 96 °C for 60 min. Subsequently, the samples were extracted with toluene, and absorbance was measured at 520 nm using a spectrometer (Synergy HT, BioTek). Proline concentration was determined using a standard curve and calculated based on fresh weight. Proline analysis was performed only on the aboveground tissues, and each sample was analyzed in triplicate.

2.6. AAS Determination of Elements

A total of 100 mg of dry plant samples was weighed into PTFE digestion vessels. To each sample, 8 mL of HNO_3 and 2 mL of H_2O_2 (trace purity, Sigma-Aldrich Chemie GmbH, Steinheim, Germany) were added. The digestion was performed using a microwave digestion system, ETHOS-One (Milestone Srl., Sarisole, Italy), with the following parameters: first ramp to 200 °C over 20 min, hold at 200 °C for 20 min, followed by a 20 min cooling phase. After mineralization, the digested samples were filtered using quantitative Munktell filter paper No. 390 (Munktell & Filtrak, Bärenstein, Germany) into 50 mL volumetric flasks and filled to the final volume with double deionized water (ddH_2O, 18.2 MΩ·cm^{-1} at 25 °C), prepared using the Simplicity 185 purification system (Millipore SAS, Molsheim, France). The resulting solutions were stored in polyethylene tubes until analysis by ICP-OES. Elemental analysis was carried out using an Agilent 720 ICP-OES spectrometer (Agilent Technologies Inc., Santa Clara, CA, USA) with the axial plasma configuration and an SPS-3 auto-sampler (Agilent Technologies GmbH, Göttingen, Germany). The operating conditions were as follows: RF power of 1.75 kW, plasma gas flow rate of 16.0 L·min^{-1}, auxiliary gas flow of 1.50 L·min^{-1}, nebulizer gas flow of 0.85 L·min^{-1}, and CCD detector temperature set at −35 °C. Signal acquisition time was 3 × 3 s for each of the three replicates. Calibration of the ICP-OES method was conducted using a TraceCert ICP 5 mixed standard (Sigma-Aldrich GmbH, Steinheim, Germany), diluted to three concentration levels: Level I—0.0475 mg·kg^{-1}, Level II—0.0950 mg·kg^{-1}, and Level III—0.190 mg·kg^{-1}. Argon and carbon were used as internal standards. ERM®-CE278k (mussel tissue; IRMM, Geel, Belgium) and procedural blanks were included for quality control. The recovery values, limits of detection (LOD), limits of quantification (LOQ), determination wavelengths, and calibration linearity are presented in the corresponding table in the Results section. For non-certified elements, recoveries were determined using the standard addition method. Elemental concentrations were determined separately for roots and aboveground parts, with each sample analyzed in triplicate.

2.7. Statistical Analysis

Complete statistical analysis was conducted using the R programming language (v. 4.4.1) [55]. For each parameter, a nonparametric factorial ANOVA was performed using the aligned rank transform (ART) procedure [56,57] implemented via the "ARTool" R package [58]. The ART method was applied because it enables analysis of factorial designs while accommodating non-normal data distributions and interaction effects. Factorial models were constructed using the "art" function, followed by an evaluation of the main effects and interactions with the "anova" function. Subsequently, post hoc contrast tests were carried out using the "art.con" function from the same package. In addition, Spearman correlation was performed to assess the relationships between parameters, along with complete-linkage hierarchical clustering using the "pheatmap" R package [59].

3. Results

In this study, the effects of low doses of lead on juvenile individuals of *Pinus sylvestris* and *Picea abies* during the first weeks after germination were shown. The physiological

and biochemical responses of these species to the treatment, as well as the level of lead accumulation in plant tissues and its influence on the content of selected micro- and macroelements, were documented. In pigment content analysis, within the control groups, there were no significant differences between the species for any of the pigment parameters (Figure 1). In both species, chlorophyll a, chlorophyll b, and total chlorophyll concentrations (Figure 1A, Figure 1B, and Figure 1C, respectively) did not differ significantly between the control and the lowest applied lead nitrate concentration (0.5 mg/L). However, significantly higher values were observed in cases of higher applied lead nitrate concentrations (1 and 2 mg/L) compared to the control group ($p < 0.05$), suggesting a stimulatory effect of lead nitrate on chlorophyll content in both species. Lead nitrate treatments had a slightly positive effect on the chlorophyll a/b ratio (Figure 1D) in *P. sylvestris* ($p < 0.05$), while in *P. abies*, only the highest applied concentration (2 mg/L) significantly increased the ratio. Despite these differences, the chlorophyll a/b ratio remained close to 2:1 across all treatments. All applied concentrations significantly increased anthocyanin content in both species ($p < 0.05$) (Figure 1F). Additionally, a similar trend was observed for total carotenoids (Figure 1E), with the exception of *P. abies* treated with the lowest lead nitrate concentration (0.5 mg/L). Factorial ANOVA revealed that the main effects of concentration (C) and the interaction between species and concentration (S × C) were significant for all pigment parameters, indicating that pigment responses varied depending on both treatment intensity and species identity. Additionally, the main effect of species (S) was significant for both the chlorophyll a/b ratio and anthocyanin concentration ($p < 0.05$ and $p < 0.001$, respectively) (Figure 1).

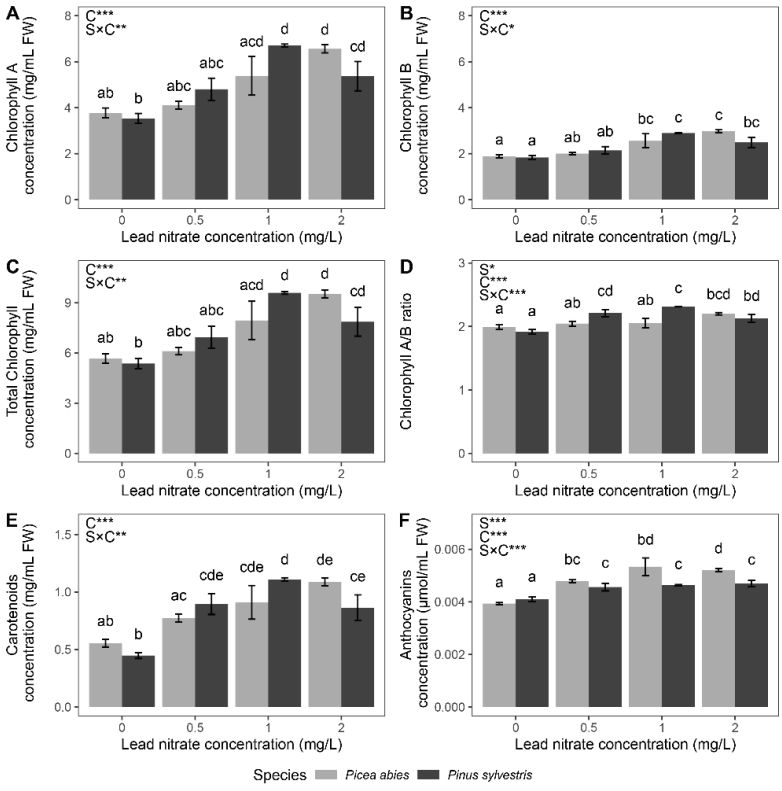


Figure 1. Pigment content in *Picea abies* and *Pinus sylvestris* following exposure to different concentrations of lead nitrate. Values represent mean ± standard error. Significant differences among the groups ($p < 0.05$) are indicated by distinct letters above the bars; groups sharing the same letter do not differ significantly. Asterisks denote significant effects after factorial analysis of variance for species (S), lead nitrate concentration (C), and their interaction (S × C): *** $p < 0.001$, ** $p < 0.01$, * $p < 0.05$. (**A**) chlorophyll A content; (**B**) chlorophyll B content; (**C**) total chlorophyll content; (**D**) chlorophyll A/B ratio; (**E**) content of carotenoids; (**F**) content of anthocyanins.

The highest total protein concentration in both species was recorded in the control group, with no significant difference observed between the species (Figure 2A). Upon lead nitrate treatment, total protein levels significantly decreased in both species compared to their respective controls ($p < 0.05$), suggesting a general suppression of protein synthesis and/or degradation under treatment conditions. Malondialdehyde (MDA) concentrations (Figure 2B) did not differ significantly between species under control conditions. Under lead nitrate exposure, *P. sylvestris* exhibited significantly lower MDA levels compared to the control group ($p < 0.05$). In *P. abies*, MDA concentrations were significantly lower than the control ($p < 0.05$) at lower applied concentrations (0.5 and 1 mg/L), but at the highest applied concentration (2 mg/L), MDA levels returned to values comparable to the control. Proline concentrations (Figure 2C) differed significantly between the species under control conditions ($p < 0.05$), with much lower baseline levels documented in *P. sylvestris.* In *P. abies*, upon treatments, proline levels were significantly lower compared to the control group (Figure 2C), while they grew with the lead nitrate concentration. In *P. sylvestris*, a significant increase in proline concentration was observed only at the highest treatment level. Similar to *P. abies*, the proline concentration significantly increased with treatment concentration ($p < 0.05$). The main effects of species (S), concentration (C), and their interaction (S × C) were statistically significant for all three parameters (Figure 2) ($p < 0.001$), indicating that each species responded differently across the range of concentrations, reflecting distinct response patterns.

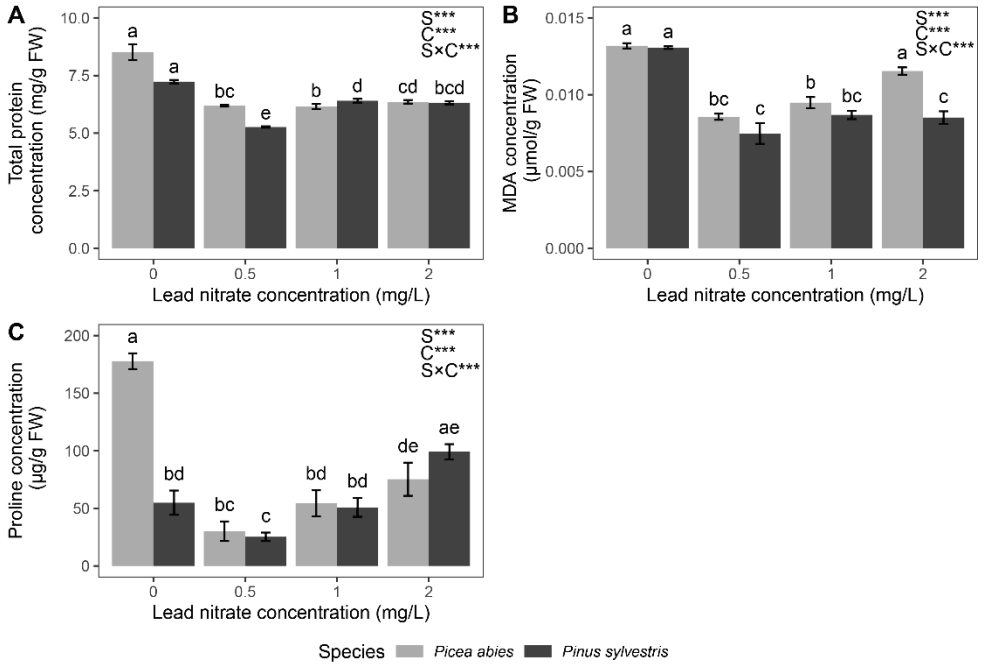


Figure 2. Concentrations of total proteins (**A**), malondialdehyde (MDA) (**B**), and proline (**C**) in *Picea abies* and *Pinus sylvestris* following exposure to different concentrations of lead nitrate. Values represent mean ± standard error. Significant differences among the groups ($p < 0.05$) are indicated by distinct letters above the bars; groups sharing the same letter do not differ significantly. Asterisks denote significant effects after factorial analysis of variance for species (S), lead nitrate concentration (C), and their interaction (S × C): *** $p < 0.001$.

More detailed insight into the relationships among variables is offered by the correlation heatmaps (Figures 3 and 4). The variables are distinctly grouped into two clusters, i.e., biochemical and pigment parameters in both species. Parameters within each cluster show strong positive correlations, particularly in *P. abies* (Figure 3). When comparing inter-cluster correlations in *P. abies*, proline and MDA exhibit weak negative correlations

with pigment parameters (ρ = −0.2), while proteins show a moderate negative correlation (ρ = −0.4). Notably, anthocyanins diverged from this pattern, exhibiting a strong negative correlation with proteins (ρ = −0.8) and moderate correlations with MDA and proline (ρ = −0.4). Inter-cluster analysis revealed divergent relationships between stress markers and pigments in *P. sylvestris* (Figure 4). While MDA and proteins consistently correlated negatively with pigments (ρ = −0.2 to −0.4), proline showed a strong negative association with carotenoids (ρ = −0.6) but no linkage to chlorophylls. Notably, anthocyanins uniquely exhibited a positive correlation with proline (ρ = 0.4), contrasting with their negative associations with MDA and proteins (ρ = −0.4).

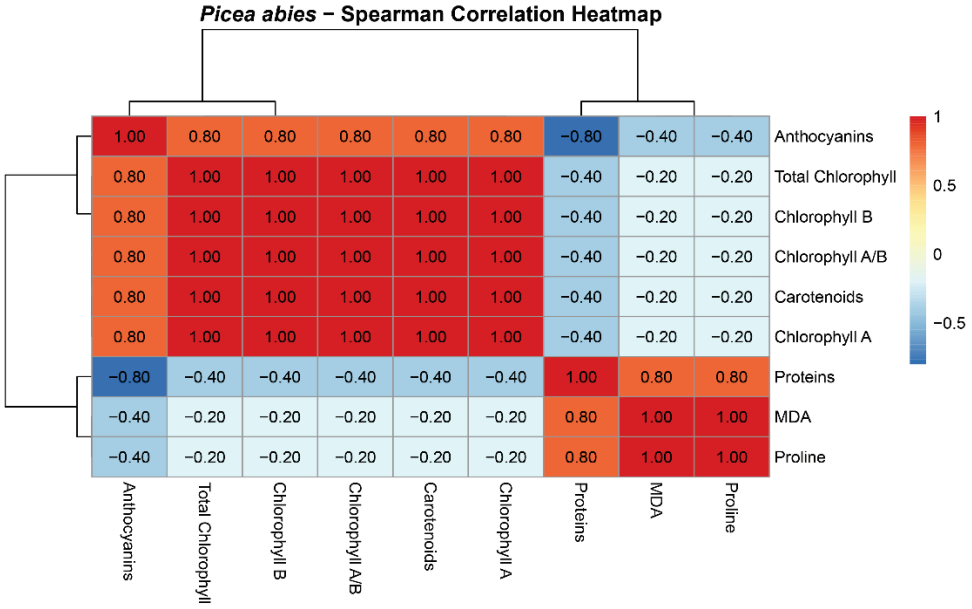


Figure 3. Spearman correlation heatmap of assessed parameters in *Picea abies* treated with various lead nitrate concentrations, with complete-linkage hierarchical clustering dendrogram.

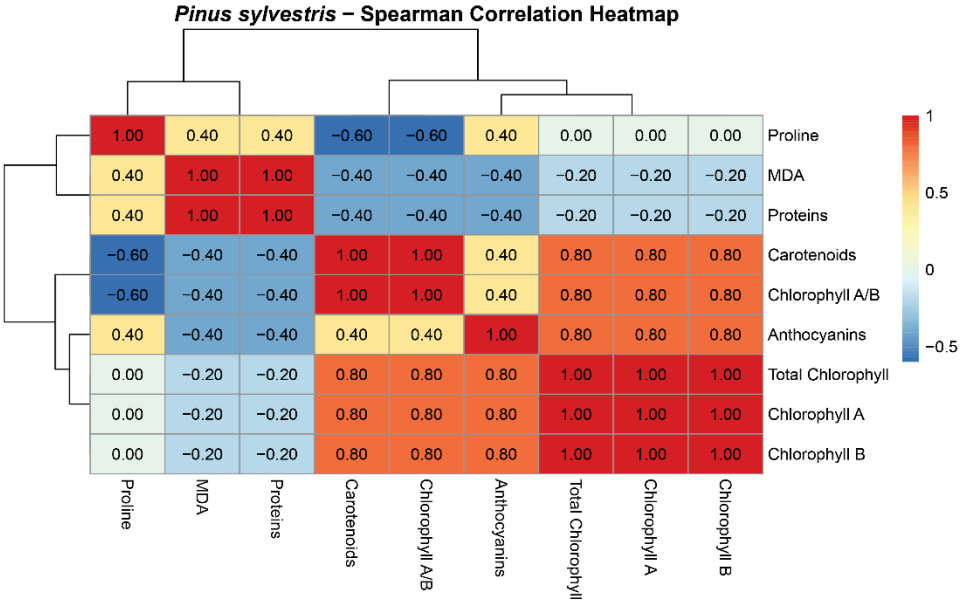


Figure 4. Spearman correlation heatmap of assessed parameters in *Pinus sylvestris* treated with various lead nitrate concentrations, with complete-linkage hierarchical clustering dendrogram.

A final perspective on the processes induced by lead treatment was complemented by the elemental analysis (Table 1). In the control groups, measured lead concentrations

in both root and shoot tissues were below the limit of detection (LOD). In contrast, lead concentrations exceeding the LOD were detected in root tissues of both species following lead nitrate treatments, with generally higher values observed in *P. sylvestris* compared to *P. abies* (Table 1). In *P. abies*, the iron content in the roots decreased from 234.5 to 132.9 mg/kg after treatment, while in *P. sylvestris*, its levels slightly increased following exposure. A pronounced decrease was also observed in manganese—in *P. abies*, root concentrations dropped from 85.8 to 37.4 mg/kg, whereas in *P. sylvestris*, the values were generally lower, and changes were more evident at the highest Pb dose. Magnesium in the roots of *P. abies* declined from 505.2 to 413.4 mg/kg, while in *P. sylvestris*, the pattern was less pronounced. Potassium in *P. abies* showed a marked decrease after treatment, particularly in the roots (from 14,573 to 7089 mg/kg), while in *P. sylvestris*, the changes were less consistent. Copper and zinc contents did not follow a clear trend, although a decrease in Zn was observed in the roots of *P. abies* after treatment, while in *P. sylvestris*, Zn levels slightly increased at the intermediate Pb concentration. Sodium remained relatively stable in both species, with no notable deviations from the control.

Table 1. Element concentrations in shoots and roots of *Picea abies* and *Pinus sylvestris* seedlings exposed to lead nitrate treatments (mg/L). Values are expressed as mean concentrations (mg/kg) ± relative standard deviation (RSD, %). For measurements below the limit of detection (LOD), the LOD value is reported and expressed in mg/kg.

Species	Tissue	$Pb(NO_3)_2$	Pb	Cu	Fe	K	Mg	Mn	Na	Zn
Picea abies	Roots	0	<LOD = 3.49	38.79 ± 0.57	234.55 ± 0.67	14,523.44 ± 0.71	5052.59 ± 0.85	58.86 ± 0.73	4004.57 ± 0.06	136.96 ± 0.26
		0.5	8.37 ± 2.39	15.93 ± 0.59	374.60 ± 1.05	6282.36 ± 1.39	4904.22 ±1.22	35.48 ± 0.94	4277.96 ± 0.34	45.76 ± 0.86
		1	28.16 ± 2.39	20.36 ± 1.29	570.59 ± 2.28	7069.70 ± 1.52	4134.04 ± 1.30	37.46 ± 0.63	4401.02 ± 0.38	61.48 ± 0.36
		2	69.83 ± 1.16	18.94 ± 2.11	322.29 ± 2.07	6962.75 ± 0.77	4599.52 ± 0.98	23.12 ± 0.67	4107.79 ± 0.65	88.47 ± 0.97
	Shoots	0	<LOD = 2.30	20.90 ± 1.00	161.18 ± 5.06	10,830.89 ± 2.70	4561.15 ± 3.00	654.21 ± 0.32	1541.12 ± 0.40	114.00 ± 0.22
		0.5	<LOD = 2.93	6.94 ± 4.75	60.51 ± 6.49	5926.68 ± 2.66	4959.92 ± 2.21	229.73 ± 1.28	2944.83 ± 0.40	81.84 ± 0.08
		1	<LOD = 2.98	8.55 ± 1.56	107.00 ± 3.71	6459.11 ± 3.40	4368.03 ± 3.45	280.80 ± 0.40	3029.08 ± 0.23	82.92 ± 0.26
		2	<LOD = 3.14	7.81 ± 2.08	63.61 ± 1.02	5882.56 ± 1.54	4963.27 ± 2.02	245.15 ± 0.63	4020.92 ± 0.61	60.52 ± 0.03
Pinus sylvestris	Roots	0	<LOD = 2.56	39.22 ± 0.91	163.91 ± 4.10	11,049.32 ± 1.89	4859.56 ± 2.48	43.58 ± 0.85	4184.89 ± 0.17	99.40 ± 0.20
		0.5	21.39 ± 2.01	19.58 ± 1.44	382.99 ± 5.09	8102.72 ± 3.36	3794.21 ± 3.49	14.85 ± 0.51	5609.98 ± 0.11	85.28 ± 1.06
		1	47.73 ± 3.94	21.26 ± 1.38	431.07 ± 0.92	8995.49 ± 1.64	4243.87 ± 1.27	20.06 ± 0.62	7941.17 ± 0.70	109.86 ± 0.62
		2	153.33 ± 1.15	19.21 ± 3.55	211.28 ± 2.80	5586.62 ± 1.88	5377.81 ± 0.79	12.70 ± 1.48	10,104.37 ± 0.39	195.59 ± 0.59
	Shoots	0	<LOD = 3.35	15.45 ± 0.37	215.28 ± 1.28	792.46 ± 0.81	6942.64 ± 0.59	40.57 ± 0.42	3482.70 ± 0.23	149.10 ± 0.02
		0.5	<LOD = 3.49	3.41 ± 4.53	30.58 ± 8.26	8094.84 ± 2.12	4456.62 ± 2.10	80.20 ± 0.87	2900.29 ± 0.08	76.50 ± 0.50
		1	<LOD = 3.78	5.38 ± 7.23	39.11 ± 10.58	8690.26 ± 1.93	5102.89 ± 2.50	135.50 ± 0.48	4529.69 ± 0.30	97.63 ± 0.33
		2	<LOD = 3.75	6.38 ± 1.91	63.50 ± 5.90	5342.98 ± 3.18	5434.18 ± 3.61	181.88 ± 0.34	4573.15 ± 0.33	95.07 ± 0.57

4. Discussion

Both tested species showed stimulation in the production of chlorophyll a and b, anthocyanins, and carotenoids in correlation with the increasing intensity of lead treatment. This finding is particularly interesting, as numerous studies have confirmed that lead toxicity inhibits photosynthesis [7,60]. We assume that this stimulatory effect resulted from the selected concentration, which remained below the level of acute toxicity. This threshold, along with overall sensitivity and stress response to lead exposure, is species-specific [61,62], probably also varying in different developmental stages, genotypes, and ecotypes of tested species. Most detailed scientific studies have focused on crop plants or utilized model species [9,63]. Therefore, the specific effects of lead exposure—and particularly the threshold of acute toxicity—remain understudied in many forest tree species to this day [64].

The fact that low doses of lead may enhance photosynthetic parameters via the activation of hormetic stimulation mechanisms has been confirmed in juvenile maize—*Zea mays* L. [65], as well as in *Vigna radiata* (L.) R. Wilczek [66] and *Vicia faba* L. [67]. The stimulatory effect on pigment production in *P. sylvestris* begins to decline at the highest applied concentration, where pigment levels start to show a downward trend. We assume that this effect would intensify with continued exposure to higher concentrations and would likely become apparent in *Picea abies* as well. These differences also point to the

distinct sensitivity of these species. The sensitivity of pine to lead was thoroughly studied by Belousov et al. [68], who confirmed the first toxic responses at the level of cytogenetic parameters at 5 μM (approximately equivalent to our treatment at 2 mg/L). The response of respiratory stress markers became fully apparent only at 500 μM [69]. Other evaluated markers also suggest rather different physiological responses in these conifers. While *P. abies* showed a gradual increase in MDA levels with increasing treatment concentration, this response was weaker in *P. sylvestris*. In contrast, proline accumulation was more pronounced in *P. sylvestris*. We assume that, under the highest treatment concentration, lead-detoxification within pine cells was insufficient. This interpretation is supported by the findings of Staszak et al. [70], in which germinating *P. sylvestris* seeds exposed to lead exhibited a significant reduction in reduced glutathione (GSH), along with an increase in its oxidized form (GSSG), indicating a rapid depletion of the non-enzymatic antioxidant system and a shift toward compensatory mechanisms. Reduced GSH capacity may trigger enhanced synthesis of alternative stress-related molecules such as proline.

These observations are further supported by correlation heatmaps (Figures 3 and 4), in which *P. abies*, the evaluated parameters formed two coherent clusters—pigment and biochemical—with strong internal correlations, suggesting a well-coordinated stress response, while *P. sylvestris* showed fragmented responses, with weak coordination between proline and pigments. A similar trend was reported in a study by Khan et al. [71], where the sensitive rice cultivar exhibited weakened activation of antioxidant mechanisms, reduced pigment stability, and a less coordinated stress response. Wiszniewska et al. [72] emphasize that a coordinated stress response is crucial for resistance to toxicity, which is well expressed in adapted plants after prolonged exposure.

Furthermore, our elemental analysis (Table 1) shows that lead accumulation in the roots of pine was nearly twice as high as in spruce. This trend has already been observed in the study by Maddah and Moraghebi [73], and overall, *P. sylvestris* is often considered a suitable species for biomonitoring or for managing contaminated sites [19,74,75]. Therefore, increased proline levels do not correlate with more efficient lead exclusion or uptake regulation by the root system, but rather reflect a passive stress response, as also suggested by Hayat et al. [76]. In contrast, *P. abies* likely employs more effective defense mechanisms that limit both the uptake and toxicity of lead. These may include the remodeling of cell wall polysaccharides, which increases the wall's capacity to bind lead and decreases its permeability—a mechanism that, together with the sequestration of toxic metals into vacuoles, has been confirmed in many plant species [77].

When focusing on other elements that play specific roles in plant metabolism, we observe trends similar to those reported in an earlier study by Godbold and Kettner [78], conducted on *Picea abies*. That study documented an increase in iron (Fe) concentrations in root tips at lower Pb concentrations, followed by a decrease as Pb treatment levels increased. This effect of lead on enhanced iron uptake was further detailed in the study by Varga et al. [79]. At the same time, the recorded decrease in Mg and K concentrations in the roots of both species suggests a disruption in ion homeostasis caused by competition between lead and essential cations Mg^{2+} and K^{+} [80]. A study by Shen et al. [81], conducted on *Torreya grandis* Fortune ex Lindl. (Taxaceae), also emphasized the critical role of Mg in these processes. Lamhamdi et al. [82] further reported a reduction in the content of most mineral ions in spinach and wheat even at low lead doses, which is consistent with our observations.

The only exception is the increasing concentration of zinc in the roots in response to higher Pb concentrations. Several studies have reported an antagonistic relationship between lead and zinc contents [83,84]. However, a study by Musielińska et al. [85], conducted on 60 plant species, also highlighted the high species-specific variability in these metabolic interactions. Another important aspect is that Zn plays a protective role against

heavy metal toxicity by activating antioxidant enzymes, stabilizing cellular membranes, and regulating the expression of metal transporter genes [86]. The observed increase in Zn with rising Pb concentrations may thus represent a compensatory response to ionic stress. Since both Pb^{2+} and Zn^{2+} utilize similar transport mechanisms (e.g., transporters from the ZIP or HMA families) [87], it is likely that plants increase Zn uptake in an effort to maintain homeostasis and compensate for functions disrupted by lead toxicity.

Overall, after evaluating all variables, we conclude that *Pinus sylvestris* exhibits a more pronounced stress response with visible signs of toxicity at the highest tested lead-treatment concentration, while *Picea abies* appears to activate more effective regulatory mechanisms and a more coordinated metabolic response. At lower treatment concentrations, a hormetic effect was observed, manifested as a temporary stimulation of photosynthetic pigment production.

However, studies on synergistic/antagonistic effects of numerous environmental variables would be appreciated. Also, further investigations on molecular and microscopic levels could provide new insights and confirm the results achieved here. The mechanisms of lead stress response in the studied species would elucidate the results achieved here.

5. Conclusions

This study highlights species-specific responses to low-level lead exposure during the early developmental stages of conifers. *Picea abies* demonstrated greater physiological stability and more coordinated stress responses compared to *Pinus sylvestris*, suggesting a higher inherent tolerance to lead. Although *P. sylvestris* exhibits a less coordinated physiological response, it accumulates significantly more lead in its tissues, which—provided the plant maintains viability—may prove advantageous for phytoremediation efforts. These differences in metal uptake, pigment metabolism, and osmotic adjustment may not only influence forest regeneration at contaminated sites but also be useful in ecological engineering and metal-loaded site recovery by seeds or seedlings. Understanding such variability among species is critical for assessing ecological risks and guiding reforestation strategies in polluted environments.

Author Contributions: Conceptualization, A.P. and M.G.; methodology, A.P. and M.B.; software, D.P.B.; validation, D.P.B., M.S.S. and A.P. formal analysis, A.P. and D.P.B.; investigation, A.P. and D.P.B.; resources, M.G., M.S.S. and M.B.; data curation, A.P.; writing—original draft preparation, A.P., M.T. and D.P.B.; writing—review and editing, M.S.S.; visualization, D.P.B.; supervision, M.G., M.S.S. and M.B.; project administration, A.P. and M.G.; funding acquisition, M.G., M.S.S. and M.B. All authors have read and agreed to the published version of the manuscript.

Funding: This work was financially supported by the Slovak Research and Development Agency under contract No. APVV-21-0289, Slovak Grant Agency KEGA under contracts No. 008SPU-4/2023 and 009UPJŠ-4/2023, and Slovak Grant Agency VEGA (VEGA 1/0252/24 and 1/0768/25).

Data Availability Statement: The data supporting the findings of this study are available from the corresponding author upon reasonable request.

Acknowledgments: During the preparation of this manuscript, the authors used ChatGPT OpenAI 2024 for English translation, grammar editing, and formatting assistance. The authors have reviewed and edited the output and take full responsibility for the content of this publication.

Conflicts of Interest: The authors declare no conflicts of interest.

References

1. Alloway, B.J. *Heavy Metals in Soils: Trace Metals and Metalloids in Soils and Their Bioavailability*; Springer: Dordrecht, The Netherlands, 2013. [CrossRef]
2. Yang, Q.; Li, Z.; Lu, X.; Duan, Q.; Huang, L.; Bi, J. A review of soil heavy metal pollution from industrial and agricultural regions in China: Pollution and risk assessment. *Sci. Total Environ.* **2018**, *642*, 690–700. [CrossRef] [PubMed]

3. Zhang, L.; Zhu, Y.; Gu, H.; Lam, S.S.; Chen, X.; Sonne, C.; Peng, W. A review of phytoremediation of environmental lead (Pb) contamination. *Chemosphere* **2024**, *342*, 142691. [CrossRef] [PubMed]
4. Yin, K.; Wang, Q.; Lv, M.; Chen, L. Microorganism remediation strategies towards heavy metals. *Chem. Eng. J.* **2019**, *360*, 1553–1563. [CrossRef]
5. Naz, S.; Chatha, A.M.M.; Téllez-Isaías, G.; Ullah, S.; Ullah, Q.; Khan, M.Z.; Kari, Z.A. A Comprehensive Review on Metallic Trace Elements Toxicity in Fishes and Potential Remedial Measures. *Water* **2023**, *15*, 3017. [CrossRef]
6. Tóth, G.; Hermann, T.; Da Silva, M.R.; Montanarella, L. Heavy metals in agricultural soils of the European Union with implications for food safety. *Environ. Int.* **2016**, *88*, 299–309. [CrossRef]
7. Kumar, V.; Parihar, R.D.; Sharma, A.; Bakshi, P.; Sidhu, G.P.S.; Bali, A.S.; Karaouzas, I.; Bhardwaj, R.; Thukral, A.K.; Gyasi-Agyei, Y.; et al. Global evaluation of heavy metal content in surface water bodies: A meta-analysis using heavy metal pollution indices and multivariate statistical analyses. *Chemosphere* **2019**, *236*, 124364. [CrossRef]
8. Xiang, M.; Li, Y.; Yang, J.; Lei, K.; Li, Y.; Li, F.; Zheng, D.; Fang, X.; Cao, Y. Heavy metal contamination risk assessment and correlation analysis of heavy metal contents in soil and crops. *Environ. Pollut.* **2021**, *278*, 116911. [CrossRef]
9. Sharma, P.; Dubey, R.S. Lead toxicity in plants. *Braz. J. Plant Physiol.* **2005**, *17*, 35–52. [CrossRef]
10. Marx, S.K.; Rashid, S.; Stromsoe, N. Global-scale patterns in anthropogenic Pb contamination reconstructed from natural archives. *Environ. Pollut.* **2016**, *213*, 283–298. [CrossRef]
11. Punia, M. *Environmental Changes and Sustainable Development in India: Perspectives from Remote Sensing and GIS*; Springer: Cham, Switzerland, 2021.
12. Yang, Y.; Wang, Y.; Liu, R.; Xue, Y.; Jiang, H.; Wang, X. Lead isotopic composition and pollution source tracing in surface soils of Beijing, China. *J. Geochem. Explor.* **2020**, *210*, 106426. [CrossRef]
13. Kang, M.J.; Kim, K.H.; Szulejko, J.E.; Park, Y.H. Study on the spatial distribution and mobility of heavy metals in soils in a mining complex area. *Environ. Geochem. Health* **2016**, *38*, 665–677. [CrossRef]
14. Qin, Y.; Yang, X.; Wang, Y.; Zhang, S. Assessment of heavy metal pollution and human health risk in soils from the Qilian Mountains, China. *Ecotoxicol. Environ. Saf.* **2023**, *258*, 115002. [CrossRef]
15. Miśkowiec, P. The impact of the mountain barrier on the spread of heavy metal pollution on the example of Gorce Mountains, Southern Poland. *Environ. Monit. Assess.* **2022**, *194*, 663. [CrossRef] [PubMed]
16. Bing, H.; Zhou, J.; Wu, Y.; Luo, X.; Xiang, Z.; Sun, H.; Wang, J.; Zhu, H. Barrier effects of remote high mountain on atmospheric metal transport in the eastern Tibetan Plateau. *Sci. Total Environ.* **2018**, *628*, 687–696. [CrossRef]
17. Liu, H.; Wang, X.; Wu, Y.; Zhang, S.; Zhao, Y.; Gao, J. Source apportionment and risk assessment of heavy metals in the forest soil: A case study of the Yanshan Mountains, China. *Environ. Sci. Pollut. Res.* **2024**, *31*, 11782–11795. [CrossRef]
18. Qin, M.; Jin, Y.; Peng, T.; Zhao, B.; Hou, D. Heavy metal pollution in Mongolian-Manchurian grassland soil and effect of long-range dust transport by wind. *Environ. Int.* **2023**, *177*, 108019. [CrossRef]
19. Świsłowski, P.; Kříž, J.; Rajfur, M. The use of bark in biomonitoring heavy metal pollution of forest areas on the example of selected areas in Poland. *Ecol. Chem. Eng. S* **2020**, *27*, 195–210. [CrossRef]
20. Pająk, M.; Halecki, W.; Gąsiorek, M. Accumulative response of Scots pine (*Pinus sylvestris* L.) and silver birch (*Betula pendula* Roth) to heavy metals enhanced by Pb-Zn ore mining and processing plants: Explicitly spatial considerations of ordinary kriging based on a GIS approach. *Chemosphere* **2017**, *168*, 851–859. [CrossRef]
21. Popović, V.; Šešlija Jovanović, D.; Miletić, Z.; Milovanović, J.; Lučić, A.; Rakonjac, L.; Miljković, D. The evaluation of hazardous element content in the needles of the Norway spruce (*Picea abies* L.) that originated from anthropogenic activities in the vicinity of the native habitats. *Environ. Monit. Assess.* **2023**, *195*, 109. [CrossRef]
22. Andráš, P.; Turisová, I.; Buccheri, G.; de Matos, J.M.X.; Dirner, V. Comparison of heavy-metal bioaccumulation properties in *Pinus* sp. and *Quercus* sp. in selected European Cu deposits. *Web Ecol.* **2016**, *16*, 81–87. [CrossRef]
23. Krupa, Z.; Baszyński, T. Some aspects of heavy metals toxicity towards photosynthetic apparatus: Direct and indirect effects on light and dark reactions. *Environ. Exp. Bot.* **1995**, *35*, 135–149. [CrossRef]
24. Wójcik, M.; Tukiendorf, A. Cadmium uptake, localization and detoxification in *Zea mays*. *Biol. Plant.* **2005**, *49*, 237–245. [CrossRef]
25. Pourrut, B.; Shahid, M.; Dumat, C.; Winterton, P.; Pinelli, E. Lead uptake, toxicity, and detoxification in plants. *Rev. Environ. Contam. Toxicol.* **2011**, *213*, 113–136. [CrossRef]
26. Patra, M.; Sharma, A. Mercury toxicity in plants. *Bot. Rev.* **2000**, *66*, 379–423. [CrossRef]
27. Gregušková, E.K.; Mihálik, D.; Kraic, J.; Mrkvová, M.; Sokol, J.; Gregor, P.; Rafajová, A.; Čupr, P. Genotoxic effects of transboundary pollutants in *Pinus mugo* in the high mountain habitats. *Ecol. Indic.* **2022**, *140*, 109009. [CrossRef]
28. Chropeňová, M.; Gregušková, E.K.; Karásková, P.; Přibylová, P.; Kukučka, P.; Baráková, D.; Čupr, P. Pine needles and pollen grains of *Pinus mugo* Turra—A biomonitoring tool in high mountain habitats identifying environmental contamination. *Ecol. Indic.* **2016**, *66*, 132–142. [CrossRef]
29. Jia, X.; Zhang, C.; Zhao, Y.; Liu, T.; He, Y. Three years of exposure to lead and elevated CO_2 affects lead accumulation and leaf defenses in *Robinia pseudoacacia* L. seedlings. *J. Hazard. Mater.* **2018**, *349*, 215–223. [CrossRef] [PubMed]

30. Singh, R.P.; Agrawal, M. Effects of sewage sludge amendment on heavy metal accumulation and consequent responses of *Beta vulgaris* plants. *Chemosphere* **2007**, *67*, 2229–2240. [CrossRef] [PubMed]
31. Giller, K.E.; Witter, E.; McGrath, S.P. Microbial diversity in soil: Effects of metal contamination. *Soil Biol. Biochem.* **2009**, *41*, 1901–1915. [CrossRef]
32. Chodak, M.; Gołębiewski, M.; Morawska-Płoskonka, J.; Kuduk, K.; Niklińska, M. Diversity of microorganisms from forest soils differently polluted with heavy metals. *Appl. Soil Ecol.* **2013**, *64*, 7–14. [CrossRef]
33. Szopka, K.; Karczewska, A.; Jezierski, P.; Kabała, C. Spatial distribution of lead in the surface layers of mountain forest soils: An example from the Karkonosze National Park, Poland. *Geoderma* **2013**, *192*, 259–268. [CrossRef]
34. Sipos, P.; Németh, T.; Mohai, I.; Dódony, I. Effect of soil composition on adsorption of lead as reflected by a study on a natural forest soil profile. *Geoderma* **2005**, *124*, 363–374. [CrossRef]
35. Ettler, V.; Vaněk, A.; Mihaljevič, M.; Bezdička, P. Contrasting lead speciation in forest and tilled soils heavily polluted by lead metallurgy. *Chemosphere* **2005**, *58*, 1449–1459. [CrossRef] [PubMed]
36. Keresztesi, Á.; Nita, I.A.; Birsan, M.V.; Bodor, Z.; Szép, R. The risk of cross-border pollution and the influence of regional climate on the rainwater chemistry in the Southern Carpathians, Romania. *Environ. Sci. Pollut. Res.* **2020**, *27*, 9382–9402. [CrossRef]
37. Levin, R.; Vieira, C.L.Z.; Mordarski, D.C.; Rosenbaum, M.H. Lead seasonality in humans, animals, and the natural environment. *Environ. Res.* **2020**, *180*, 108797. [CrossRef] [PubMed]
38. Cherednichenko, V.S.; Cherednichenko, A.V.; Zheksenbaeva, A.K.; Madibekov, A.S. Heavy metal deposition through precipitation in Kazakhstan. *Heliyon* **2021**, *7*, e05844. [CrossRef]
39. Kalugina, O.V.; Mikhailova, T.A.; Shergina, O.V. Biochemical adaptation of Scots pine (*Pinus sylvestris* L.) to technogenic pollution. *Contemp. Probl. Ecol.* **2018**, *11*, 79–88. [CrossRef]
40. Doichinova, V.; Zhiyanski, M.; Hursthouse, A.; Bech, J. Study on the mobility and bioavailability of PTEs in soils from urban forest parks in Sofia, Bulgaria. *J. Geochem. Explor.* **2014**, *147*, 222–228. [CrossRef]
41. Angelovičová, L.; Boguská, Z.; Fazekašová, D. Physico-chemical water properties and flora diversity under the old mining load influence (Rudnansky creek, Slovakia). *Pollack Period.* **2015**, *10*, 123–131. [CrossRef]
42. Brunner, I.; Luster, J.; Günthardt-Goerg, M.S.; Frey, B. Heavy metal accumulation and phytostabilisation potential of tree fine roots in a contaminated soil. *Environ. Pollut.* **2008**, *152*, 559–568. [CrossRef]
43. Caudullo, G.; Tinner, W.; de Rigo, D. *Picea abies* in Europe: Distribution, habitat, usage and threats. In *European Atlas of Forest Tree Species*; San-Miguel-Ayanz, J., de Rigo, D., Caudullo, G., Houston Durrant, T., Mauri, A., Eds.; Publications Office of the European Union: Luxembourg, 2016; pp. 114–115.
44. Krakau, U.K.; Liesebach, M.; Aronen, T.; Lelu-Walter, M.A.; Schneck, V. Scots pine (*Pinus sylvestris* L.). In *Forest Tree Breeding in Europe*; Pâques, L., Ed.; Springer: Dordrecht, The Netherlands, 2013; Volume 25, pp. 281–323. [CrossRef]
45. Graney, J.R.; Landis, M.S. Coupling meteorology, metal concentrations, and Pb isotopes for source attribution in archived precipitation samples. *Sci. Total Environ.* **2013**, *448*, 141–150. [CrossRef] [PubMed]
46. European Parliament; Council of the European Union. Directive 2013/39/EU of the European Parliament and of the Council of 12 August 2013 amending Directive 2000/60/EC and 2008/105/EC as regards priority substances in the field of water policy. *Off. J. Eur. Union* **2013**, *L226*, 1–17. Available online: https://eur-lex.europa.eu/legal-content/EN/TXT/?uri=CELEX:32013L0039 (accessed on 2 April 2025).
47. Kozak, K.; Kozioł, K.; Luks, B.; Chmiel, S.; Ruman, M.; Marć, M.; Namieśnik, J.; Polkowska, Ż. The role of atmospheric precipitation in introducing contaminants to the surface waters of the Fuglebekken catchment, Spitsbergen. *Polar Res.* **2015**, *34*, 24207. [CrossRef]
48. Bohlin-Nizzetto, P.; Aas, W.; Halvorsen, H.L.; Nikiforov, V.; Pfaffhuber, K.A. Monitoring of Environmental Contaminants in Air and Precipitation: Annual Report 2020. *NILU Rep.* 2021. Available online: https://www.miljodirektoratet.no/globalassets/publikasjoner/m1736/m1736.pdf (accessed on 2 April 2025).
49. Zhou, J.; Du, B.; Wang, Z.; Zhang, W.; Xu, L.; Fan, X.; Liu, X.; Zhou, J. Distributions and pools of lead (Pb) in a terrestrial forest ecosystem with highly elevated atmospheric Pb deposition and ecological risks to insects. *Sci. Total Environ.* **2019**, *647*, 932–941. [CrossRef] [PubMed]
50. Johansson, K.; Bergbäck, B.; Tyler, G. Impact of atmospheric long range transport of lead, mercury and cadmium on the Swedish forest environment. *Water Air Soil Pollut. Focus* **2001**, *1*, 279–297. [CrossRef]
51. Wellburn, A.R. The spectral determination of chlorophylls a and b, as well as total carotenoids, using various solvents with spectrophotometers of different resolution. *J. Plant Physiol.* **1994**, *144*, 307–313. [CrossRef]
52. Sims, D.A.; Gamon, J.A. Relationships between leaf pigment content and spectral reflectance across a wide range of species, leaf structures and developmental stages. *Remote Sens. Environ.* **2002**, *81*, 337–354. [CrossRef]
53. Heath, R.L.; Packer, L. Photoperoxidation in isolated chloroplasts: I. Kinetics and stoichiometry of fatty acid peroxidation. *Arch. Biochem. Biophys.* **1968**, *125*, 189–198. [CrossRef] [PubMed]

54. Bradford, M.M. A rapid and sensitive method for the quantitation of microgram quantities of protein utilizing the principle of protein-dye binding. *Anal. Biochem.* **1976**, *72*, 248–254. [CrossRef]
55. Ábrahám, E.; Hourton-Cabassa, C.; Erdei, L.; Szabados, L. Methods for determination of proline in plants. In *Plant Stress Tolerance: Methods and Protocols*; Springer: New York, NY, USA, 2010; pp. 317–331. [CrossRef]
56. R Core Team. *R: A Language and Environment for Statistical Computing (Version 4.3.2)*; R Foundation for Statistical Computing: Vienna, Austria, 2024; Available online: https://www.r-project.org/ (accessed on 2 April 2025).
57. Wobbrock, J.O.; Findlater, L.; Gergle, D.; Higgins, J.J. The aligned rank transform for nonparametric factorial analyses using only ANOVA procedures. In Proceedings of the SIGCHI Conference on Human Factors in Computing Systems, Vancouver, BC, Canada, 7–12 May 2011; ACM: New York, NY, USA, 2011; pp. 143–146. [CrossRef]
58. Elkin, L.; Kay, M.; Higgins, J.; Wobbrock, J. An aligned rank transform procedure for multifactor contrast tests. In Proceedings of the 34th Annual ACM Symposium on User Interface Software and Technology, Virtual Event, USA, 10–14 October 2021; Association for Computing Machinery: New York, NY, USA, 2021; pp. 754–768. [CrossRef]
59. Kay, M.; Elkin, L.; Higgins, J.; Wobbrock, J. mjskay/ARTool: ARTool 0.11.0, (v0.11.0). Zenodo. 2021. Available online: https://zenodo.org/records/4721941 (accessed on 20 December 2022). [CrossRef]
60. Kolde, R. pheatmap: Pretty heatmaps (R Package Version 1.0.12). 2018. Available online: https://github.com/raivokolde/pheatmap (accessed on 2 April 2025).
61. Mitra, A.; Chatterjee, S.; Voronina, A.V.; Walther, C. Lead toxicity in plants: A review. In *Lead in Plants and the Environment*; Gupta, D., Chatterjee, S., Walther, C., Eds.; Springer: Cham, Switzerland, 2020; pp. 161–194. [CrossRef]
62. Khodaverdiloo, H.; Ghorbani, D.S.; Rezapour, S. Lead and cadmium accumulation potential and toxicity threshold determined for land cress and spinach. *J. Plant Prod.* **2011**, *5*, 275–282.
63. Cunha, A.R.D.; Ambrósio, A.D.S.; Wolowski, M.; Westin, T.B.; Govêa, K.P.; Carvalho, M.; Barbosa, S. Negative effects on photosynthesis and chloroplast pigments exposed to lead and aluminum: A meta-analysis. *Cerne* **2020**, *26*, 232–237. [CrossRef]
64. Jia, M.; Li, W.; Wang, Z.; Lu, C.; Wang, J. Effects of Pb on photosynthesis and antioxidant system in model plants: A comparative study. *Ecotoxicol. Environ. Saf.* **2022**, *239*, 113649. [CrossRef]
65. Erofeeva, M. Hormesis and adaptive responses to low-dose stress factors in woody plants. *Environ. Res.* **2023**, *216*, 114473. [CrossRef]
66. Małkowski, E.; Sitko, K.; Szopiński, M.; Gieroń, Ż.; Pogrzeba, M.; Kalaji, H.M.; Zieleźnik-Rusinowska, P. Hormesis in plants: The role of oxidative stress, auxins and photosynthesis in corn treated with Cd or Pb. *Int. J. Mol. Sci.* **2020**, *21*, 2099. [CrossRef]
67. Sengar, R.S.; Gautam, M.; Garg, S.K.; Chaudhary, R.; Sengar, K. Effect of lead on seed germination, seedling growth, chlorophyll content and nitrate reductase activity in mung bean (*Vigna radiata*). *Res. J. Phytochem.* **2008**, *2*, 61–68. [CrossRef]
68. Wang, Y.; Yang, Z.M. Nitric oxide reduces oxidative stress induced by paraquat in the leaves of *Phaseolus vulgaris*. *Biol. Plant.* **2010**, *54*, 104–109. [CrossRef]
69. Belousov, M.V.; Mashkina, O.S.; Popov, V.N. Cytogenetic response of Scots pine (*Pinus sylvestris* Linnaeus, 1753) (Pinaceae) to heavy metals. *Comp. Cytogenet.* **2012**, *6*, 93. [CrossRef] [PubMed]
70. Belousov, M.V.; Zemlyanukhina, O.A. Nitrate lead influence on cytogenetic and some biochemical parameters of scotch pine seedlings. *Vestn. Tambov. Univ. Ser. Nat. Tech. Sci.* **2011**, *16*, 1321–1324.
71. Staszak, A.M.; Małecka, A.; Ciereszko, I.; Ratajczak, E. Differences in stress defence mechanisms in germinating seeds of *Pinus sylvestris* exposed to various lead chemical forms. *PLoS ONE* **2020**, *15*, e0238448. [CrossRef]
72. Khan, M.N.; Khan, Z.; Mobin, M.; Abbas, Z.K.; Alamri, S.A.; Alyemeni, M.N. Assessment of lead induced oxidative stress and alteration in antioxidant defense system in rice (*Oryza sativa* L.) genotypes. *Sci. Rep.* **2021**, *11*, 4532. [CrossRef]
73. Wiszniewska, A.; Muszyńska, E.; Kołton, A.; Kamińska, I.; Hanus-Fajerska, E. *In vitro* acclimation to prolonged metallic stress is associated with modulation of antioxidant responses in a woody shrub *Daphne jasminea*. *Plant Cell Tissue Organ Cult.* **2019**, *139*, 339–357. [CrossRef]
74. Maddah, A.; Moraghebi, F. The accumulation of heavy metals in Scots pine (*Pinus sylvestris*) grown on contaminated soils and their effect on biomass and growth. *Environ. Monit. Assess.* **2013**, *185*, 251–258. [CrossRef]
75. Alaqouri, H.A.A.; Genc, C.O.; Aricak, B.; Kuzmina, N.; Menshikov, S.; Cetin, M. The possibility of using Scots pine needles as biomonitor in determination of heavy metal accumulation. *Environ. Sci. Pollut. Res.* **2020**, *27*, 20273–20280. [CrossRef] [PubMed]
76. Hayat, S.; Hayat, Q.; Alyemeni, M.N.; Wani, A.S.; Pichtel, J.; Ahmad, A. Role of proline under changing environments: A review. *Plant Signal. Behav.* **2012**, *7*, 1456–1466. [CrossRef]
77. Krzesłowska, M. The cell wall in plant cell response to trace metals: Polysaccharide remodeling and its role in defense strategy. *Acta Physiol. Plant.* **2011**, *33*, 35–51. [CrossRef]
78. Godbold, D.L.; Kettner, C. Lead influences root growth and mineral nutrition of *Picea abies* seedlings. *J. Plant Physiol.* **1991**, *139*, 95–99. [CrossRef]
79. Varga, A.; Záray, G.; Fodor, F.; Cseh, E. Study of interaction of iron and lead during their uptake process in wheat roots by total-reflection X-ray fluorescence spectrometry. *Spectrochim. Acta B* **1997**, *52*, 1027–1032. [CrossRef]

80. Gupta, M.; Dwivedi, V.; Kumar, S.; Patel, A.; Niazi, P.; Yadav, V.K. Lead toxicity in plants: Mechanistic insights into toxicity, physiological responses of plants and mitigation strategies. *Plant Signal. Behav.* **2024**, *19*, 2365576. [CrossRef]
81. Shen, J.; Song, L.; Müller, K.; Hu, Y.; Song, Y.; Yu, W.; Wang, H.; Wu, J. Magnesium alleviates adverse effects of lead on growth, photosynthesis, and ultrastructural alterations of *Torreya grandis* seedlings. *Front. Plant Sci.* **2016**, *7*, 1819. [CrossRef]
82. Lamhamdi, M.; El Galiou, O.; Bakrim, A.; Novoa-Muñoz, J.C.; Arias-Estévez, M.; Aarab, A.; Lafont, R. Effect of lead stress on mineral content and growth of wheat (*Triticum aestivum*) and spinach (*Spinacia oleracea*) seedlings. *Saudi J. Biol. Sci.* **2013**, *20*, 29–36. [CrossRef]
83. Mleczek, M.; Budka, A.; Gąsecka, M.; Budzyńska, S.; Drzewiecka, K.; Magdziak, Z.; Rutkowski, P.; Goliński, P.; Niedzielski, P. Copper, lead and zinc interactions during phytoextraction using *Acer platanoides* L.—A pot trial. *Environ. Sci. Pollut. Res.* **2023**, *30*, 27191–27207. [CrossRef] [PubMed]
84. He, P.P.; Lv, X.Z.; Wang, G.Y. Effects of Se and Zn supplementation on the antagonism against Pb and Cd in vegetables. *Environ. Int.* **2004**, *30*, 167–172. [CrossRef] [PubMed]
85. Musielińska, R.; Kowol, J.; Kwapuliński, J.; Rochel, R. Antagonism between lead and zinc ions in plants. *Arch. Environ. Prot.* **2016**, *42*, 54–61. [CrossRef]
86. Hassan, M.U.; Nawaz, M.; Mahmood, A.; Shah, A.A.; Shah, A.N.; Muhammad, F.; Batool, M.; Rasheed, A.; Jaremko, M.; Abdelsalam, N.R.; et al. The role of zinc to mitigate heavy metals toxicity in crops. *Front. Environ. Sci.* **2022**, *10*, 990223. [CrossRef]
87. Claus, J.; Bohmann, A.; Chavarría-Krauser, A. Zinc uptake and radial transport in roots of *Arabidopsis thaliana*: A modelling approach to understand accumulation. *Ann. Bot.* **2013**, *112*, 369–380. [CrossRef]

Disclaimer/Publisher's Note: The statements, opinions and data contained in all publications are solely those of the individual author(s) and contributor(s) and not of MDPI and/or the editor(s). MDPI and/or the editor(s) disclaim responsibility for any injury to people or property resulting from any ideas, methods, instructions or products referred to in the content.

forests

MDPI

Article

Functional Traits Associated with Drought Tolerance Exhibit Low Variability in 21 Provenances of a Montane Tree Species—*Eucalyptus delegatensis*

Anita Gurung [1], Benjamin Wagner [1,*], Elizabeth C. Pryde [2], Craig R. Nitschke [1] and Stefan K. Arndt [1,*]

[1] School of Agriculture, Food and Ecosystem Sciences, The University of Melbourne, 500 Yarra Boulevard, Richmond, VIC 3121, Australia; me.anitagrg56@gmail.com (A.G.); craign@unimelb.edu.au (C.R.N.)
[2] Greening Australia, 349 Collins Street, Melbourne, VIC 3000, Australia; epryde@greeningaustralia.org.au
* Correspondence: benjamin.wagner@unimelb.edu.au (B.W.); sarndt@unimelb.edu.au (S.K.A.)

Abstract: Elevated temperatures and extended drought periods are driving significant changes in the structure and function of forest ecosystems. High-elevation alpine ash forests (*Eucalyptus delegatensis* R.T. Baker) in Australia are an example of forests that are already impacted by climate change. These obligate seeder forests can shift to non-forest ecosystems following extreme drought and altered fire regimes, raising concern about their adaptation to a rapidly changing environment and long-term forest persistence. Plant functional traits play a major role in determining adaptive mechanisms to environmental conditions. While alpine ash forests are vulnerable to climate change, it is unclear if different provenances have adapted to the climatic conditions in which they grow. We therefore studied the variation in expression of functional traits related to drought tolerance in 21 provenances of alpine ash distributed across an environmental gradient. We investigated if functional traits varied between the provenances and were related to climate of origin in order to identify provenances that may be better adapted to drought. We measured the following traits in a common garden experiment under well-watered conditions: stomatal density, specific leaf area, minimum stomatal conductance and osmotic potential at full turgor. There was very little variation in trait expression between the 21 provenances for all functional traits related to drought tolerance. All provenances had medium-range stomatal density (170–300 stomata mm^2) and specific leaf area (SLA, 50–70 cm^2 g^{-1}), a very low minimum stomatal conductance (2–4 mmol m^2 s^{-1}) and a high osmotic potential at full turgor (−0.6–0.7 MPa). There was no statistically significant correlation of trait expression with the climate of origin. Thus, there is very little evidence for genetically controlled differences in trait expression of drought tolerance traits in this species. It is likely that the high elevation and high rainfall environment of the species' ecological niche has not been subjected to frequent and extensive drought periods that would elicit an evolutionary pressure selecting for drought-tolerant traits. We could not identify provenances that would have different drought-tolerant functional trait responses than others, potentially conferring an adaptive advantage under climate change. This has implications for using climate-adjusted provenancing to improve resilience in alpine ash forests predicted to experience more frequent and severe droughts in the future.

Keywords: plant traits; drought tolerance; provenances; *Eucalyptus*; climate change

1. Introduction

There is growing evidence suggesting that current climatic changes are adversely impacting forest ecosystems [1]. Periods of drought are predicted to increase in incidence and

severity, which can significantly reduce species' survival, distribution and productivity [2]. For instance, extreme drought and heat stress have caused widespread tree mortality in most bioregions in the past two decades [3–6].

The capacity of plant species to adapt to changing climatic conditions has been crucial for ecosystem persistence and countering biodiversity loss [7]. As climate change alters the environment, plant functional traits that determine their adaptive capacity may underpin their survival [8]. Several studies have demonstrated that different functional traits define the drought resistance capacity of the plant. For example, Bartlett et al. (2012) observed a strong correlation between leaf water potential at the turgor loss point and water availability within and across the biomes [9]. Here, the turgor loss point refers to the point at which the leaf cells become flaccid as they dry out. During dry seasons or drought conditions, lowering and maintaining cell turgor facilitates water uptake, increasing the hydraulic safety and drought tolerance capacity of plants [10]. Similarly, plant specific leaf area has been adjusted to adapt to a dry environment [11]. Modulating leaf stomatal density to regulate fluxes of CO_2 uptake and water loss in response to the surrounding environment is another key morphological characteristic of the plants related to drought resilience [12]. Equally, minimum leaf stomatal conductance determines the rate of water loss when stomata are closed [13].

Functional traits related to drought resistance often differ in plant species from arid environments compared to species from wet and/or cold environments [14–18]. Functional traits can also vary within a given species across environmental gradients encompassing a species' geographic range [16,19], indicating an adaptive response of the species to different environmental conditions. Variation between species has been extensively studied in the past, yet recent research indicates that approximately 40% of the functional trait variation also occurs within species [20]. Conversely, some studies have observed little or no variation in the expression of functional traits for different populations within a species [21–23].

The significance of functional trait variations and their plasticity in tree species is becoming increasingly recognised. Understanding the adaptive capacity within tree species populations can provide important information for planned adaptation of vulnerable forests [24], particularly in the context of selecting provenances to include in restoration/revegetation efforts. However, compared to studies on interspecific variations, only a few studies have investigated intraspecific variations in phenotypic plasticity and drought resistance capacity among populations [10,25–27]. Studies conducted on climate-related plasticity among populations have included only a limited number of provenances, which restricts a comprehensive understanding of how the various populations adapt to changing environments [25]. In addition, it is less well-known how the functional traits relate to climate variables within various populations of a single species [28,29].

Over 800 species of *Eucalyptus* occur across a significant portion of the Australian landscape [30]. Many of these species are predicted to face climatic conditions in the future that exceed the ranges they are experiencing in their current natural habitats [31,32]. Alpine ash (*Eucalyptus delegatensis*) is a species under significant threat from climate change [33,34]. It is a fire-sensitive, bradysporous obligate seeder species—regeneration from seed after fire is the primary mode of regeneration—and it typically reaches reproductive maturity after 15 to 20 years [35]. Alpine ash is restricted to southeast Australia, occurring at elevations ranging from 900 m to 1450 m [33]. It has been identified as being highly vulnerable in its regeneration phase to drought [36] and warming winters [37] and frequent, severe and broad-scale fire regimes driven by increased aridity under climate change [33,35,36,38,39]. These bushfires have impacted a substantial proportion of alpine ash forests in the region [35].

Alpine ash occurs across an elevational gradient, suggesting their populations may exhibit a range of trait expressions reflecting localised climate variation. Despite the susceptibility of alpine ash to climate change, the intraspecific variation in the functional trait expression of provenances along a climatic gradient is little known. This lack of knowledge creates uncertainties about which populations may be suited to withstand exacerbated future drought conditions. With rapid anthropogenic climate change and expected detrimental impacts on the alpine ash distribution, there is a growing concern about the species' long-term survival [40].

This study aimed to investigate the variability of drought-adaptive functional traits across different provenances of alpine ash along a climatic gradient. We addressed the following research questions:

1. Is there variability in the expression of functional traits among provenances of alpine ash sourced across a climatic gradient?
2. Do the morphological and physiological traits correlate with each other?
3. Is there any relationship between the expression of functional traits and climate of origin?

Based on trends observed in other species, we hypothesised that: (i) alpine ash provenances will exhibit variability in their functional traits across a climatic gradient, (ii) morpho-physiological traits would be significantly correlated to each other, and (iii), there would be a significant correlation between functional trait expressions and climate of origin.

2. Materials and Methods

2.1. Study Site

The study was conducted at a common garden provenance trial site located at the Burnley Campus of the University of Melbourne, Victoria, Australia (−37.829, 145.024, Figure 1). A common garden is a traditional experimental approach where populations sourced from various locations of a species are planted together in the same environment to observe the differences in the functional traits among provenances [41]. Such experiments are used to test and differentiate the adaptive capacity of populations from different environments [42]. The mean annual rainfall and mean annual temperature of the site are 648 mm and 15 °C, respectively [43].

2.2. Plant Material

Seeds were collected from 21 provenances across the geographic distribution of alpine ash in southeastern Australia (Figure 1). Among them, 15 provenances were from the state of Victoria (VIC), three from Tasmania (TAS) and three from New South Wales (NSW; Appendix A, Table A1). Seeds were germinated at a nursery and planted in the common garden in November 2022 when the seedlings were six months of age. After planting, plants were irrigated every second day for half an hour from late spring to early autumn (May–October) with approximately 2 litres of water per plant. By the time the leaf samples were collected for this study, the plants were about two years old, corresponding to 1.5 years after planting.

2.3. Climatic and Topographic Variables Investigated

The four climatic variables used in this study to investigate climatic adaptation were mean annual temperature (MAT), mean annual precipitation (MAP), elevation and the annual heat moisture index (AHMI). Climate data were sourced from WorldClim [44]. AHMI was subsequently calculated from MAT and MAP (AHMI = [MAT + 10]/[MAP/1000]), which is a measure of the climatic aridity of each provenance location [45,46]. AHMI was chosen for this study because it integrates the interactive impacts of temperature and precipitation, distinguishes warm-dry from cool-wet areas of the landscape, and, therefore,

better quantifies the effects of local climates on plant communities. We further considered elevation, which was sourced from the Shuttle Radar Topography Mission data [47]. All variables were extracted for the location of provenance origin (Appendix A, Table A1).

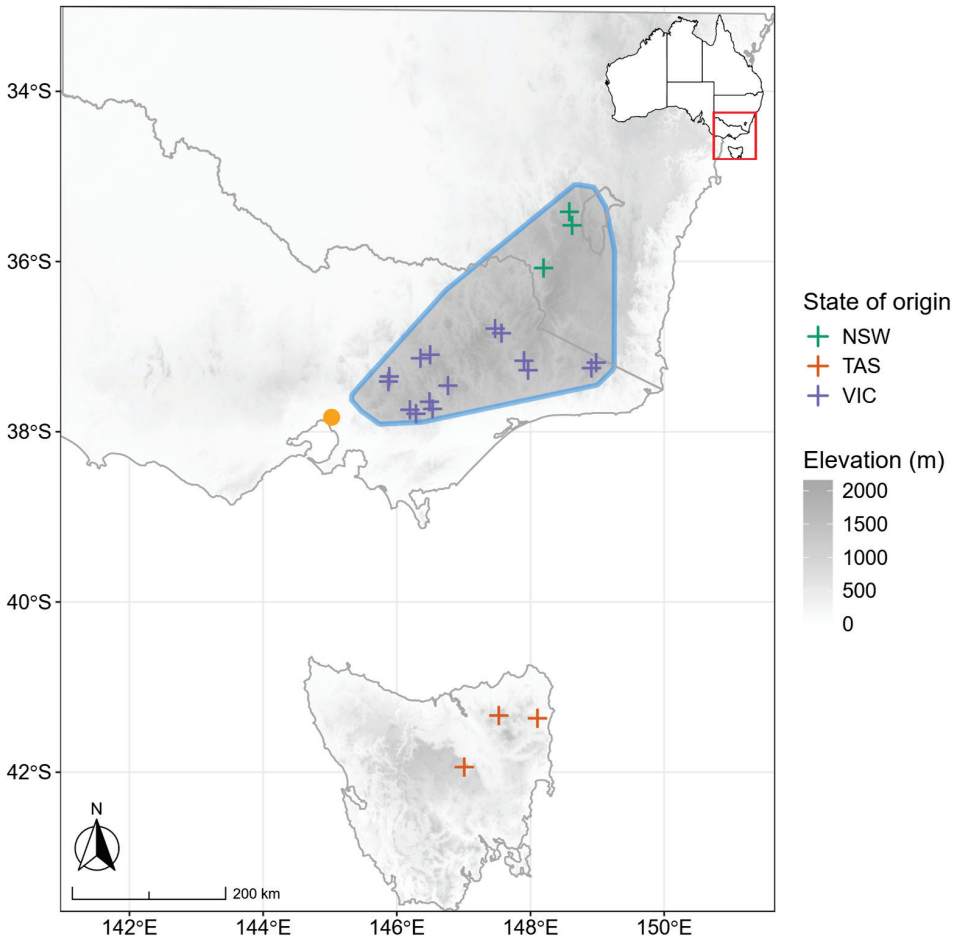


Figure 1. Map showing the locations of seed sources for the 21 provenances of alpine ash (crosses), the geographic extent of alpine ash distribution in mainland Australia (blue outline) with elevation, and the location of the common garden experimental site in Melbourne, Victoria, Australia (orange point).

2.4. Planting Design

Alpine ash seedlings were planted in three replicate plots that each had a uniform spacing of 2.5 m between each plant. The plots were rectangular, measured 35 m × 25 m, and had a total of 165 plants per plot. A specific planting pattern with a matrix of three rows and three columns forming a 3 x 3 grid was created so that the provenances did not neighbour themselves but neighbour the same set of other provenances in a consistent manner (Appendix A, Figure A1).

2.5. Morphological Trait Measurements

2.5.1. Specific Leaf Area (SLA)

From each provenance, five trees were sampled for the measurement of specific leaf area (SLA, n = 105), and five to twenty leaves per tree were collected, depending on leaf quality. We selected fully expanded and hardened leaves. Leaves were scanned digitally, and the area of scanned leaves was subsequently measured using the image analysis software ''ImageJ'' v1.54i [48]. Leaf dry weights were recorded after the samples had been oven-dried at 80 °C for 48 h (until they reached a constant weight). All measurements were averaged to give a single value per sample tree.

2.5.2. Stomatal Density (SD)

For the measurement of stomatal density (SD), nail polish imprints were taken in the middle of the abaxial (lower) surface of leaves, avoiding major veins and edges, which were then observed by light microscope [49]. This part of the leaf region was used because it represents the average value SD across the entire leaf and provides a good proxy for the leaf as a whole [50]. Transparent nail polish was used for the impressions, and imprints were mounted on the microscope slide. The camera field view of the microscope was approximately 0.074825 mm^2 under a 400× magnification. This specific area of the camera view allows for accurate counting of stomata within a defined space, ensuring consistency across all measurements. Thus, to calculate the density, the total number of stomata that fell within the field view was counted and divided by the area of the field view. Three images were taken from each nail polish peel, one peel was taken from each leaf, and two leaves were sampled from each tree. This process was repeated across five trees per provenance (n = 210). Measurements were averaged to give a single value for each sample tree.

2.6. Physiological Trait Measurements

2.6.1. Osmotic Potential at Full Turgor ($\pi_{(100)}$)

Osmotic potential at full turgor of leaves was measured by osmometry of expressed sap [51]. Five trees from each provenance were measured (n = 105), and three leaves were taken from each tree. Collected leaves were rehydrated for at least one hour to compare individuals at full hydration, also known as full turgor ($\pi_{(100)}$). The water potential of each leaf was assessed using a pressure chamber following hydration. A leaf was considered to be at full turgor if the water potential reached greater than −0.1 MPa. Leaf material was then extracted with a cork borer, avoiding the mid-veins, and then placed into a 0.6 mL micro-tube and immediately stored in a freezer. The plant material was kept frozen for a day, thawed and sap extracted by centrifugation. The osmolality of expressed sap was determined using a freezing point osmometer (Osmomat 030, Gonotec, Berlin, Germany) that was calibrated using solutions provided by the manufacturer.

2.6.2. Minimum Stomatal Conductance (g_{min})

Minimum stomatal conductance (g_{min}) was measured by the bench drying method [52,53], with minor modifications. Fully expanded, sun-exposed leaves without visible damage were collected early in the morning. We measured one leaf per tree and five trees per provenance (n = 105). Measurements were conducted for five days, with 21 leaves from 21 provenances measured for each day. Collected leaves were kept in zip-lock bags with a moist tissue paper and then transported to the lab within one hour. Leaves were labelled and then rehydrated with distilled water for one hour before starting the procedure. After fully rehydrating the leaves, petioles were cut and sealed with melted candle wax to prevent moisture loss. The prepared leaves were placed on a drying rack with weather station sensors positioned next to the rack to record climate conditions (temperature, relative humidity and atmospheric pressure). The leaves were weighed at 30 min intervals over a period of 5 h and 30 min, resulting in a total of 12 data points for each leaf sample. At the end of the measurement, leaves were scanned, and the leaf area was calculated using ImageJ software. The recorded data—weighing times, values of leaf mass (g), leaf area (cm^2), temperature (°C), relative humidity (%) and atmospheric pressure (kPa)—were entered into a spreadsheet. Saturated vapour pressure (VPsat in kPa) and mole fraction vapour pressure deficit (mfVPD in mol x mol^{-1}) were calculated based on the temperature and relative humidity values. g_{min} was computed using the last four data points. Since g_{min} can be sensitive to fluctuations in temperature and relative humidity [54], particularly under

extreme conditions, care was taken to ensure stable environmental conditions throughout the measurement.

2.7. Statistical Analyses

All statistical analyses were performed in R, version 4.3.3 [55]. We used linear models to test for significant relationships between traits and climate of origin, as well as inter-trait relationships. One-way analysis of variance (ANOVA) was used to test for differences between the provenances in their morphological and physiological traits and to determine trait variance within the provenances. To further explore which provenance expressions may drive significant differences, we computed Tukey Honest Significant Difference (HSD) tests for pairwise comparisons. Significant relationships were identified using *p*-values (threshold of $p < 0.05$). We used r-squared and variable estimates to assess the strength and direction of these significant relationships. Intraspecific variation within provenances was calculated using the quartile coefficient of variation as it is a more robust metric for calculating the coefficient of variation for traits [56].

3. Results

3.1. Climate of Origin

The distribution of the 21 alpine ash provenance source locations (climate of origin) along an aridity gradient occurred across a relatively narrow range (AHMI values between 10–30), with most provenances originating from areas with AHMI between 12 and 18, indicative of cool and wet conditions in mountainous areas (Figure 2). Provenance origin mean annual temperature ranged from 6.6–11.8 °C and annual precipitation from 813–1847 mm (Appendix A, Figure A2).

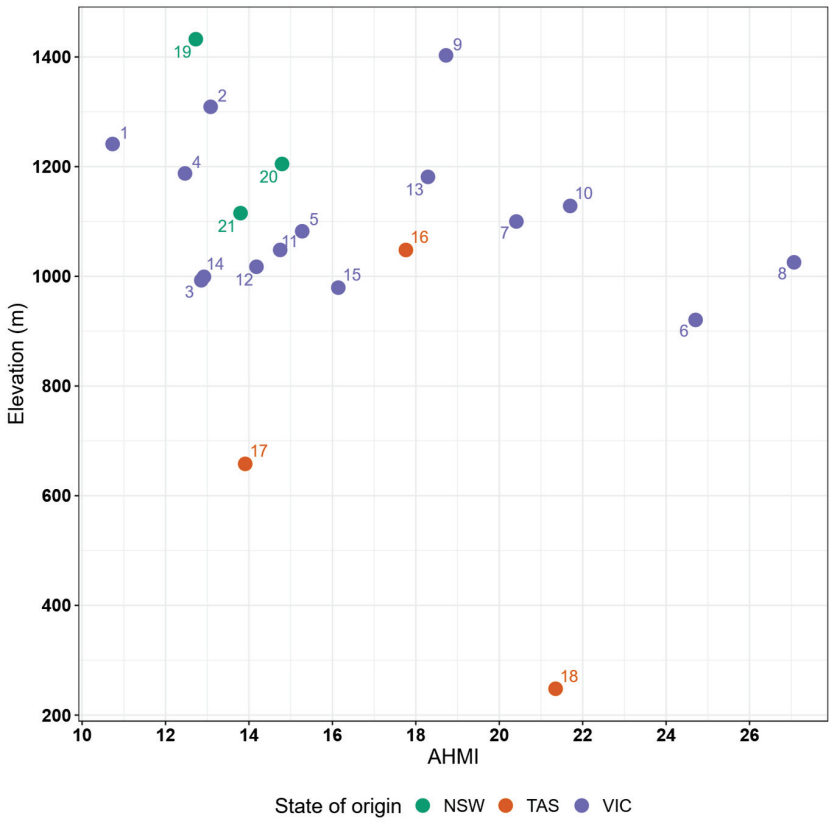


Figure 2. Elevation and average aridity (illustrated via AHMI—annual heat moisture index) of seed source location (climate of origin) for the 21 alpine ash provenances studied.

3.2. Variation in Morpho-Physiological Traits

There was no statistically significant trait variation among the provenances ($p = 0.91$) for any of the four traits (Figure 3). The g_{min} values varied between 2–4 mmol m^2 s^{-1} and the greatest variation within a provenance was detected in provenance 8 (origin Victoria, variance 3.01) and the lowest in provenance 3 (origin Victoria, variance 0.04). Similarly, there was some variation in π_{100} rates within the provenances; however, differences across the provenances were not statistically significant ($p = 0.81$). The highest π_{100} value was observed in provenance 4 (−0.52 MPa) and the lowest in provenance 9 (−0.72, both originating from Victoria). For SD, we observed the highest variation in provenance 13 and least in provenance 10 (both originating from Victoria). We did not find statistically significant differences among the provenances ($p = 0.59$) in SD. Likewise, there were no significant differences among the provenances ($p = 0.07$) in SLA. Provenance 10 had the lowest SLA (41.0 cm^2 g^{-1}), and the highest SLA was observed in provenance 18 (origin Tasmania, 84.8 cm^2 g^{-1}).

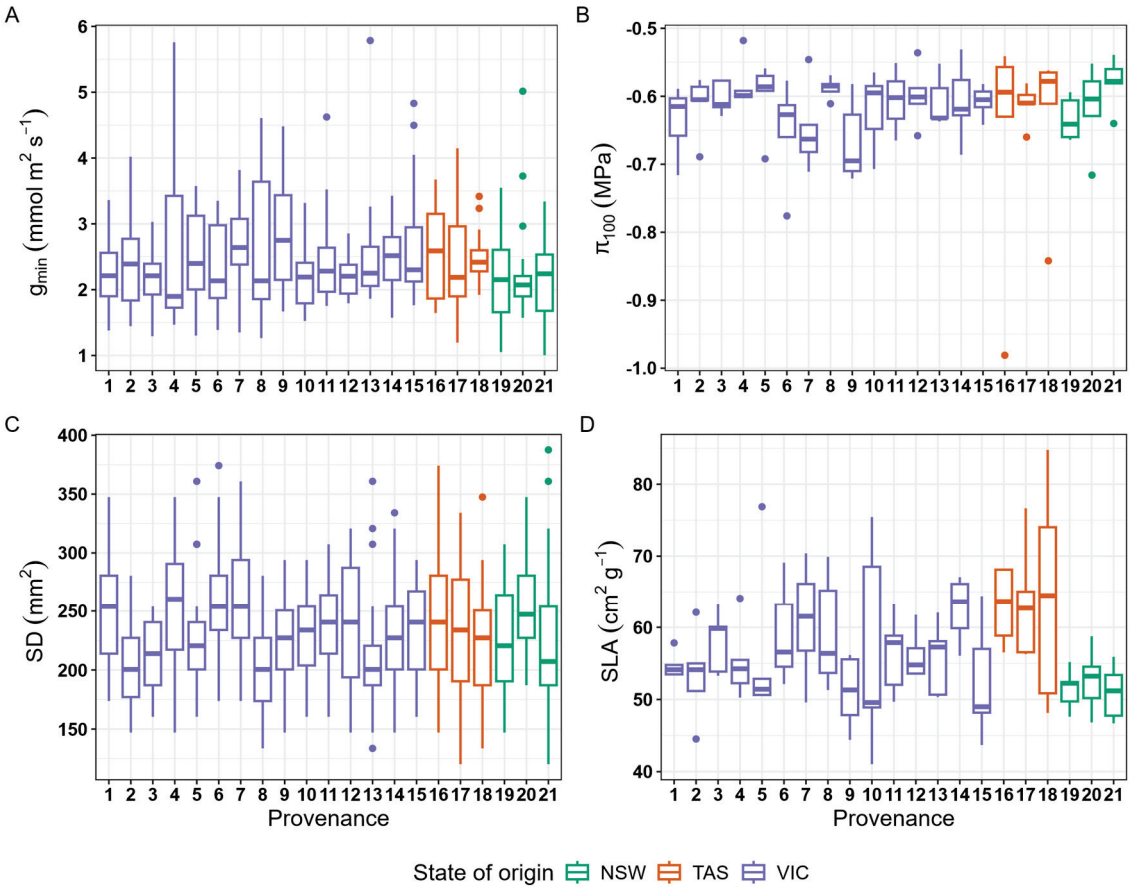


Figure 3. Morpho-physiological trait variation among the 21 provenances of alpine ash. Physiological traits are (**A**) g_{min} (minimum stomatal conductance) and (**B**) π_{100}, (osmotic potential at full turgor), and morphological traits are (**C**) SD (stomatal density) and (**D**) SLA (specific leaf area). Purple box plots indicate provenances from Victoria, orange ones from Tasmania and green ones from New South Wales.

3.3. Correlation Among Morpho-Physiological Traits

We did not determine significant relationships between morphological and physiological traits (Figure 4). While there was some variation observed between osmotic potential and SD (Figure 4C), the relationship was not statistically significant.

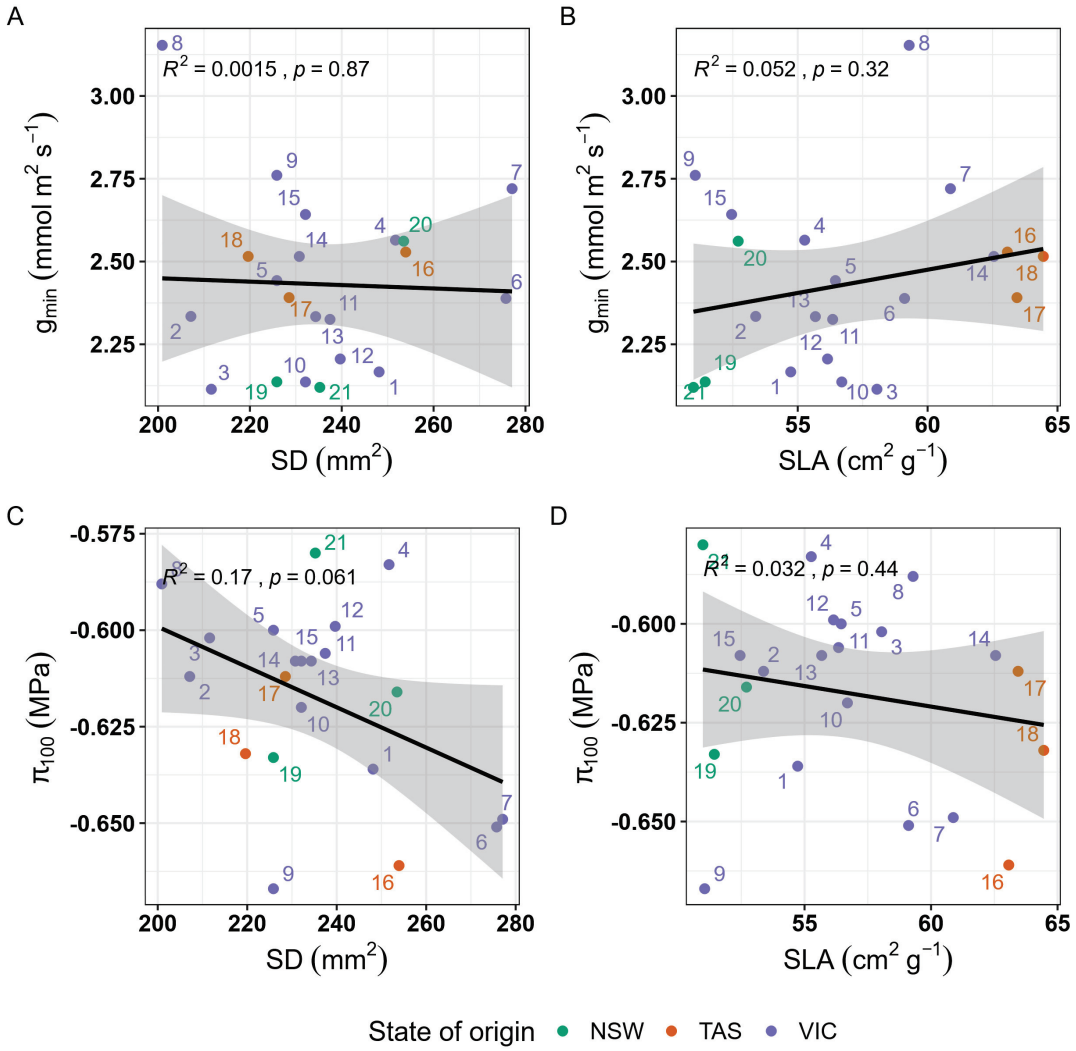


Figure 4. Regressions between morphological and physiological traits. (**A**) g_{min} (minimum stomatal conductance) and SD (stomatal density) (**B**) g_{min} and SLA (specific leaf area) π_{100}, (osmotic potential at full turgor), and morphological traits are (**C**) π_{100} (osmotic potential at full turgor) and SD and (**D**) π_{100} and SLA. Shaded grey area around the line shows the 95% confidence interval of the regression model. None of the regressions were statistically significant.

3.4. Relationship Between Traits and Climate of Origin

Most relationships between climatic variables (AHMI, MAP, MAT) and elevation and morpho-physiological traits were not significant (Table 1). AHMI had a significant positive relationship with g_{min} (Figure 5). There was a significant relationship between MAP and π_{100}, where π_{100} increased with increasing precipitation. The other morphological traits did not show any significant relationship with MAP. There was a highly significant relationship between elevation and SLA, with lower SLA at higher elevation (Figure 5).

Table 1. Summary of results for the relationship between functional trait expressions and climate of origin and elevation. Bold values indicate significant relationships.

Climate Variables (Predictor)	Traits	Values		
		p-Value	Estimate ± S.E.	Adjusted R-Squared
AHMI	g_{min}	**0.011**	0.67 ± 0.08	0.27
	π_{100}	0.22	0.59 ± 0.02	0.03
	SD	0.76	230.41 ± 17.49	−0.05
	SLA	0.07	51.44 ± 3.56	0.07
MAT	g_{min}	0.76	2.30 ± 0.44	−0.05
	π_{100}	0.29	0.66 ± 0.04	0.01
	SD	0.98	236.52 ± 33.25	−0.05
	SLA	0.45	51.50 ± 7.07	−0.02
MAP	g_{min}	0.056	2.90 ± 0.24	0.13
	π_{100}	**0.043**	0.67 ± 0.02	0.16
	SD	0.22	259.27 ± 19.04	0.03
	SLA	0.30	61.26 ± 4.15	0.01
Elevation (DEM)	g_{min}	0.66	2.54 ± 0.26	−0.04
	π_{100}	0.80	0.61 ± 0.02	−0.05
	SD	0.76	229.70 ± 19.37	−0.05
	SLA	**0.0001**	70.01 ± 2.83	0.5

Significance codes for *p*-value: 0 '***' 0.001 '**' 0.01 '*' 0.05.

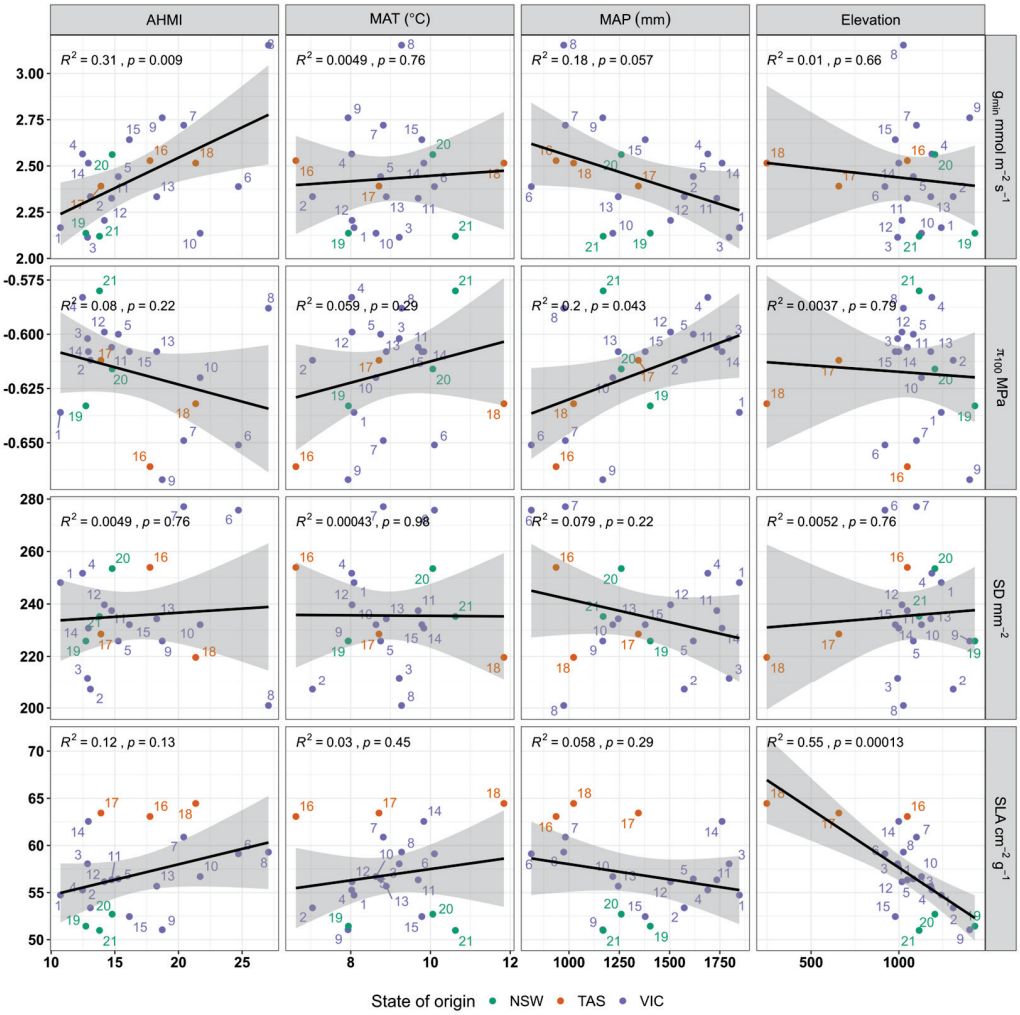


Figure 5. Relationships of morpho-physiological traits with climate (annual heat moisture index (AHMI), mean annual temperature (MAT), mean annual precipitation (MAP)) and topography (elevation above sea level). Shaded grey area around the line shows the 95% confidence interval of the regression model.

3.5. Intraspecific Trait Variation

The variation in trait expression within provenances varied (see Figure 6) between provenances and between traits. The variation of π_{100} was low, ranging from 0.7 to ~6.2%; for SLA, it ranged from 1.2 to 18.5%; for SD, it ranged from 3.8 to 13.4%; and for g_{min}, it ranged from 4.7 to 32.9%. There were significant relationships between the quartile coefficient of variation (QCV) and climate factors for three of the traits: SLA, SD and g_{min} (see Figure 7). For SLA, a multivariate model with AHMI ($p < 0.003$) and mean temperature of the coldest quarter ($p < 0.027$) explained 55% of the variation in QCV. Both climate variables were positively related to QCV, with the model providing moderate to strong evidence that provenances from more arid sites with warmer winters had higher variation in SLA. There was a significant and negative relationship between QCV and mean temperature of the driest quarter for g_{min} ($p < 0.032$; adjusted-r^2: 18%), providing moderate evidence that provenances from warmer sites typically had lower variation in g_{min}. There was weak evidence ($p = 0.068$; adjusted-r^2: 12%) for a positive relationship between QCV of stomatal density and minimum temperature of the coldest month, indicating that sites with colder winters have lower stomatal density. There were no significant relationships between climate of origin and osmotic potential of full turgor (π_{100}).

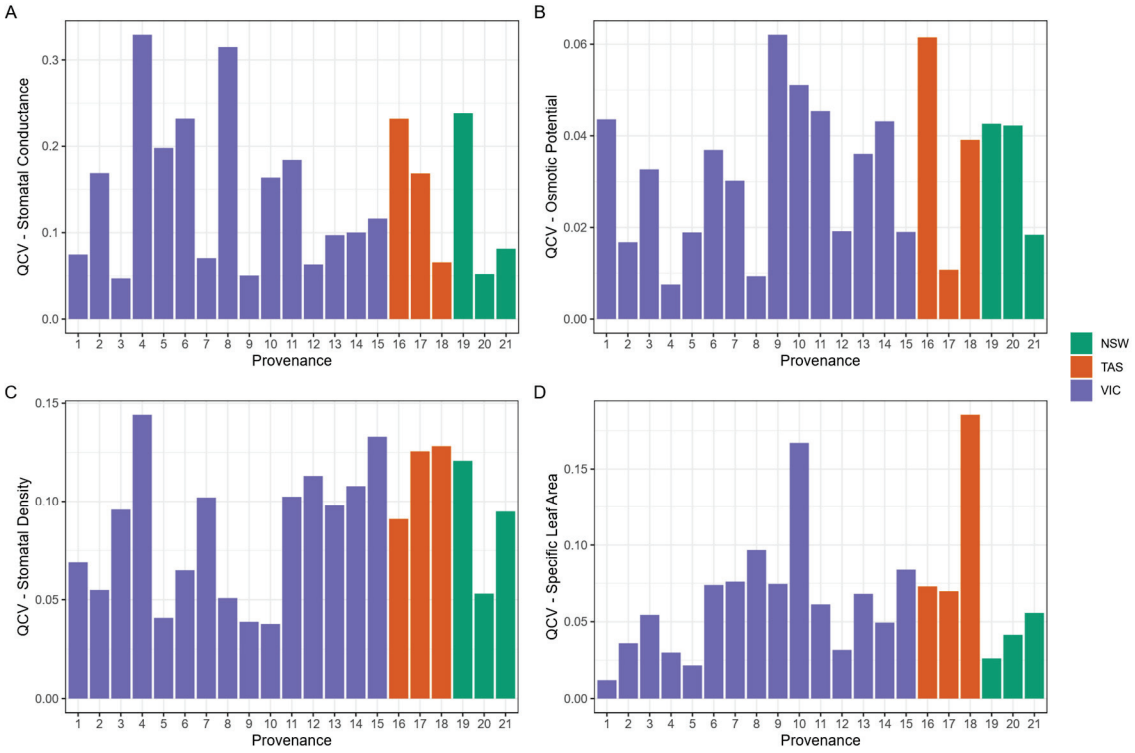


Figure 6. Quartile coefficient of variation (QCV) of morpho-physiological traits: (**A**) minimum stomatal conductance (g_{min}), (**B**) osmotic potential of full turgor (π_{100}), (**C**) stomatal density, and (**D**) specific leaf area (SLA) for each provenance. Provenances are colour coded by state of origin: New South Wales (NSW), Tasmania (TAS), and Victoria (VIC).

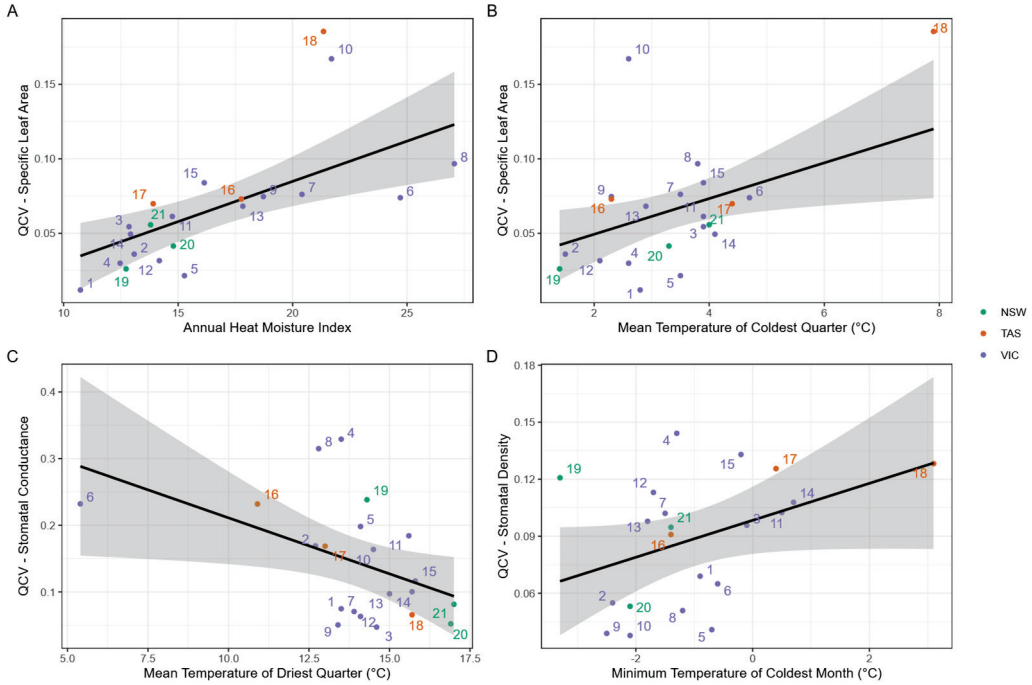


Figure 7. Relationships between the quartile coefficient of variation (QCV) of morpho-physiological traits and climate of origin: (**A**) specific leaf area (SLA) versus the annual heat moisture index (AHMI), (**B**) SLA versus the mean temperature of the coldest quarter, (**C**) minimum stomatal conductance (g_{min}) vs. the mean temperature of the driest quarter; and, (**D**) stomatal density versus minimum temperature of the coldest month. There were no significant relationships for osmotic potential of full turgor (π_{100}). Provenances are colour coded by state of origin New South Wales (NSW), Tasmania (TAS), and Victoria (VIC).

4. Discussion

We did not confirm the hypotheses of this study. There was very little variation in the expression of functional traits across the provenances; there was no trait correlation between morpho-physiological functional traits; only rainfall-related climate of origin influenced functional trait expression of g_{min} and π_{100}; and elevation of origin had an influence on SLA.

4.1. Variability of Functional Traits Across the Climate Gradient

We observed very little variation in trait expression among the 21 different provenances for any of the traits. Minimum stomatal conductance ranged from 2–4 mmol m^2 s^{-1}, which is at the lower range of reported values for g_{min} [57]. This indicates that *E. delegatensis* has very 'tight' leaves that lose very little moisture when stomata are closed. Stomatal density ranged from 170–300 stomata mm^{-1}, which is mid-range stomatal density compared to other tree species globally [58]. Specific leaf area ranged from 50–70 cm^2 g^{-1}, which is mid-range SLA in Australian trees [59] but lower than the SLA values reported for eucalypts from high elevation and high rainfall areas in Victoria [60]. We note that our plants were grown at very low altitude in the common garden (50 m), which could have influenced the SLA compared to the study by Givnish et al. [60], which sampled trees in the field. The osmotic potential of full turgor was very high, with values between −0.6 and 0.7 MPa. This would equate to a water potential at turgor loss (TLP) of −0.9–1.0 MPa when applying a generic conversion factor [61]. These values are higher than turgor loss points reported for other eucalypts in Victoria [62] and high values are usually associated with species that exhibit lower drought tolerance [9].

The low observed correlation between the traits is likely due to the measured traits within provenances responding differently to the environmental conditions of the common garden. When traits within a population diverge in their responses to the environment, then correlations between traits among populations are likely to weaken or disappear [63]. Intraspecific trait variation is the most likely explanation for the decoupling of traits that are typically correlated with each other when compared across populations and species [63].

We found varying relationships between functional traits and climatic/topographic variables. Aridity at climate of origin has a positive influence on g_{min}, and MAP had a positive influence on π_{100}. However, it is important to note that the overall variation of g_{min} and π_{100} was very small and likely of no consequence to the drought tolerance of the population. There was a small decrease in π_{100} with decreasing rainfall, but this would not lead to greater or substantially different drought tolerance of a population. The same is true for g_{min}, which was very low in all populations. There was a significant negative relationship between SLA and elevation of origin. This has been reported before and can largely be explained by the altitude-related temperature gradient [64]. However, in our study, MAT was not related to SLA; it is possible that, in addition to temperature, higher levels of solar irradiation and wind exposure may affect leaf size and SLA [63,65].

4.2. Why Was the Variation of Functional Traits So Small Among Provenances?

The variation of functional traits across environmental gradients has been reported before and is especially prevalent in eucalypts. Eucalypts in more arid environments are shorter, have smaller leaves and smaller SLA [60,66]; they have smaller xylem vessels and greater wood density [16], often have lower turgor loss points [62,67] and a lower vulnerability of xylem vessels to embolism [68]. However, almost all studies that observed these differences investigated eucalypt species from very contrasting environments, often ranging from very arid woodlands to wet forests. The variability of the climate in the distribution of *E. delegatensis* is much smaller as it grows mainly at high altitudes (usually elevation > 1000 m), with high rainfall (900–1800 mm) and low temperatures (MAP 6–12 °C; Appendix A, Table A1). The aridity in the natural environment of *E. delegatensis* is also very low, with AHMI values between 10 and 20, whereas most other eucalypts occur in much more arid environments (AHMI values 20–100; Appendix A, Figure A3). Thus, *E. delegatensis* is occupying a climatic environment that is very uniform and that is also not prone to prolonged periods of very hot and dry conditions.

The very low g_{min} values demonstrate that *E. delegatensis* has very tight leaves and loses very little water when stomata are closed. The very high values of osmotic potential at full turgor, on the other hand, indicate that this is a species that is not well adapted to chronic or extensive drought [69]. It is therefore likely that *E. delegatensis* will respond to periods of drought by transient adjustments such as stomatal closure or maybe even small adjustments of leaf area. Stems of tall trees, such as *E. delegatensis*, can store large amounts of water that can provide 10%–50% of daily transpiration [70], which would provide a water buffer in dry periods. These reversible physiological responses to water deficit are likely sufficient to survive short heat waves and periods of low rainfall. It is therefore likely that the climatic conditions in the natural environment of *E. delegatensis* have not led to evolutionary pressures that would have selected for leaf functional traits that are associated with greater drought tolerance.

4.3. Genetic vs. Environmental Influences of Trait Expression

It is important to note that we studied the expression of functional traits in a common garden experiment under non-stressed conditions. This means that all provenances were exposed to the same environmental conditions. It is therefore expected that trait expres-

sion was mainly controlled by plant genetics, as there would be very little (or similar) environmental influence on trait expression. This will be different in studies that investigate plants along environmental gradients in situ. In these studies, and there are many examples [7,10,16,60,71–73], the trait expression will be influenced by plant genetics and environmental influences that trigger trait plasticity. This was highlighted in a recent study where ten eucalypt species were studied in multiple common gardens along a climatic gradient [74]. Most traits were adaptive across species within gardens, indicating fixed genetic differences, and adaptive within species across gardens, indicating plasticity. For the *E. delegatensis* provenances assessed in this study, it appears that phenotypic coordination was strong within the studied environment. This means that it is entirely possible that *E. delegatensis* may express differences in functional trait expression if we study them across an environmental gradient in the natural environment. It is possible that all four functional traits could exhibit trait plasticity and adjust to local conditions. Yet the environmental conditions in the natural environment, with high elevation, low MAT and high MAP, are not very drought prone. Thus, it is likely that any adjustments would be transient, and drought avoidance responses outlined above are more likely than plasticity-mediated drought tolerance. The functional traits of *E. delegatensis* are typical of a less drought-tolerant species: high π_{100}, low g_{min}, large leaves, tall trees and hydraulic architecture with large xylem vessels enabling efficient water transport—and hydraulic traits in eucalypts appear to be largely genotypic in origin rather than environmentally plastic [16]. Thus, it is unlikely that a eucalypt could become drought-tolerant by means of trait plasticity alone. However, future experiments could explore the drought tolerance of the species in stress experiments to further explore plastic trait responses.

4.4. Intraspecific Trait Variation

Intraspecific trait expression varied between provenances for all traits. This variation is unlikely due to ontogeny effects, as the trees were of the same age, nor due to the influence of within-site variation in environmental factors, such as soil properties, as the trees were sampled across the same gradient of soil properties [63]. The relationship between intraspecific trait variation and climate of origin variables provides evidence of genetic control over three of the traits measured [75]—SLA, g_{min} and SD—which may have shaped trait expression [76]. The greater variation in SLA expression for provenances from warmer and drier climates of origin suggests that these environments could be more variable in their climate, which may have selected for increased plasticity in SLA to enable trees to take advantage of ephemeral pulses of resources to maximise growth [76]. This increase in variation in SLA was counterbalanced by a decrease in the variation of g_{min} at warmer and drier sites which indicates that *E. delegatensis* growing at these sites may be more tightly adapted to their climate of origin, enabling them to reduce water loss at these warmer and drier sites. Our results add novel aspects to the expression of functional traits and climate of origin *within* a species. There is plenty of evidence that traits vary *across species* along environmental gradients (see references above). However, trait variation *within species* that is genetically controlled and not influenced by environmental plasticity appears to be much less common. In *E. camaldulensis*, the most widely distributed eucalypt in Australia, there was no relationship between turgor loss point or SLA and the climate of origin in nine provenances in a glasshouse study [77]. The same was true for subspecies of *Dodonaea viscosa* Jacq., a polymorphic shrub species in Australia that occurs in vastly different environments [27]. A different response was recorded in *Eucalyptus obliqua* L'Her., a eucalypt with a greater environmental distribution than *E. delegatensis* in SE Australia [10]. Several functional traits (TLP, SLA, xylem vulnerability) decreased with lower MAP in the field, and some also changed with summer drought. However, when the provenances were

grown in the glasshouse under identical conditions, TLP, SLA or Huber value were identical among provenances, whereas xylem vulnerability and leaf size still decreased with lower rainfall at origin. This means that some functional traits were under significant genetic control in populations along climatic gradients, whereas others are not. It is important to note that some traits are also much more inherently plastic. For example, the osmotic potential at full turgor (and by extension TLP) is mainly influenced by the concentration of solutes in the leaves, and these will fluctuate between seasons or with stress exposure. Similarly, SLA can change during the season, and HV will change rapidly with leaf loss, a common drought response of many trees. Thus, we need to consider experimental design and influences of genetics and the environment when studying trait variation.

4.5. Management Implications

In the face of fast-paced changes in climatic conditions, restoration (or rather 'renovation' sensu Prober) actions must ensure that the trees that are planted today can persist and adapt into an uncertain future. This necessitates transitioning from the *status quo* of including only locally sourced seeds to inclusion of 'climate analogues': strategic seed sourcing from provenances along the species' distribution that will confer greater adaptive potential to a changing climate [78]. Based on our results, selecting *E. delegatensis* provenances on the basis of their leaf-mediated drought tolerance will not be necessary. In our study, all 21 provenances of *E. delegatensis* that originate from an environmental gradient did not show significant differences in the expression of drought tolerance related functional leaf traits. Overall, the trait expression observed in this study indicates that *E. delegatensis* may be tightly adapted to its environment [79].

Statistical relationships with climate of origin and elevation provide evidence that some traits may be under genetic control. The variability in trait expression within provenances and the influence of climate of origin on intraspecific trait variation could indicate that plasticity may have been selected for across the species range. An exception to this is osmotic potential of full turgor, which had no relationship with climate of origin and very low values of variation, indicating the presence of "constant plasticity" across provenances [80]. This constancy of trait expression is a concern because it can reduce the strength of natural selection and therefore influence local adaptation to a changing climate [79,80]. The results do not indicate that certain provenances would be superior to others in terms of drought tolerance, as they all had very similar trait expressions. This suggests that adopting a more flexible approach to seed sourcing that focuses on cost-effective strategies and practicality rather than adherence to specific provenances could be better. This approach would substantially improve the efficient use of available resources in restoration projects.

5. Conclusions

The selection of provenances that have better adaptation and phenotypic plasticity to adverse climatic conditions, particularly drought, has been an important aspect of forest restoration and management [81]. However, we detected little interspecific variation in drought functional traits among 21 alpine ash provenances collected from an environmental gradient. In addition, the relationship between the morpho-physiological traits was insignificant. While there were some significant relationships between trait expression and climate of origin, the trait variation was very limited among provenances and would be unlikely to have any significant biological consequence for the drought tolerance of a provenance. This lack of variation could be attributed to the species being tightly adapted to its narrow distribution range, which has a narrow range of climatic conditions. The variability of trait expression was related to climate of origin, suggesting that some provenances may be inherently more plastic for some traits; however, the functionality of this plasticity requires

further testing. The highly variable climatic conditions experienced by the species across its range may have exerted selection pressure on other traits that promote regeneration, growth and/or frost tolerance over drought adaptation strategies between the provenances to enable the species to dominate large areas on the montane landscapes of southeastern Australia. This means that there is likely no 'superior' provenance to be selected based on drought-adapted traits. The influence of provenance on other key traits related to regeneration, growth and reproduction requires investigation to determine the importance of genetics, plasticity and ontogeny on trait expression in these key processes.

Author Contributions: A.G., B.W., E.C.P., C.R.N. and S.K.A. conceptualized the research; B.W., E.C.P., C.R.N. and S.K.A. designed the common garden experiment and supported planting and site maintenance; A.G. carried out field and laboratory work; A.G. analyzed the data with support by B.W. and S.K.A.; A.G. drafted the manuscript; B.W., E.C.P., C.R.N. and S.K.A. revised the manuscript and supported the writing process; B.W. and S.K.A. finalized the submitted version of the manuscript for publication with support from A.G. All authors have read and agreed to the published version of the manuscript.

Funding: Funding for this research was generously provided by Greening Australia Ltd. and the Minderoo Foundation for the project Minderoo Climate Future Plots 25-8333.

Data Availability Statement: Datasets used in this research are publicly available on github via https://github.com/BennyWag/ashtraits.

Acknowledgments: We thank Melinda Pickup (Greening Australia Ltd.) for project facilitation and support and Rebecca Du (The University of Melbourne) for laboratory training and support.

Conflicts of Interest: Author Elizabeth C. Pryde was employed by the company Greening Australia Ltd. The remaining authors declare that the research was conducted in the absence of any commercial or financial relationships that could be construed as a potential conflict of interest.

Appendix A

Appendix A.1. Figures

Total Reps	9	8	9	9	8	8	9	9	8	9	9	8	8	9	9
Reps - buffer	6	6	5	5	6	6	5	6	6	5	5	6	6	5	6
Distance (m)	0	2.5	5	7.5	10	12.5	15	17.5	20	22.5	25	27.5	30	32.5	35
0	1	16	10	4	19	13	7	1	16	10	4	19	13	7	1
2.5	2	17	11	5	20	14	8	2	17	11	5	20	14	8	2
5	3	18	12	6	21	15	9	3	18	12	6	21	15	9	3
7.5	4	19	13	7	1	16	10	4	19	13	7	1	16	10	4
10	5	20	14	8	2	17	11	5	20	14	8	2	17	11	5
12.5	6	21	15	9	3	18	12	6	21	15	9	3	18	12	6
15	7	1	16	10	4	19	13	7	1	16	10	4	19	13	7
17.5	8	2	17	11	5	20	14	8	2	17	11	5	20	14	8
20	9	3	18	12	6	21	15	9	3	18	12	6	21	15	9
22.5	10	4	19	13	7	1	16	10	4	19	13	7	1	16	10
25	11	5	20	14	8	2	17	11	5	20	14	8	2	17	11

Figure A1. The selected planting design that forms a 3 × 3 grid to avoid neighbouring the same set of provenances.

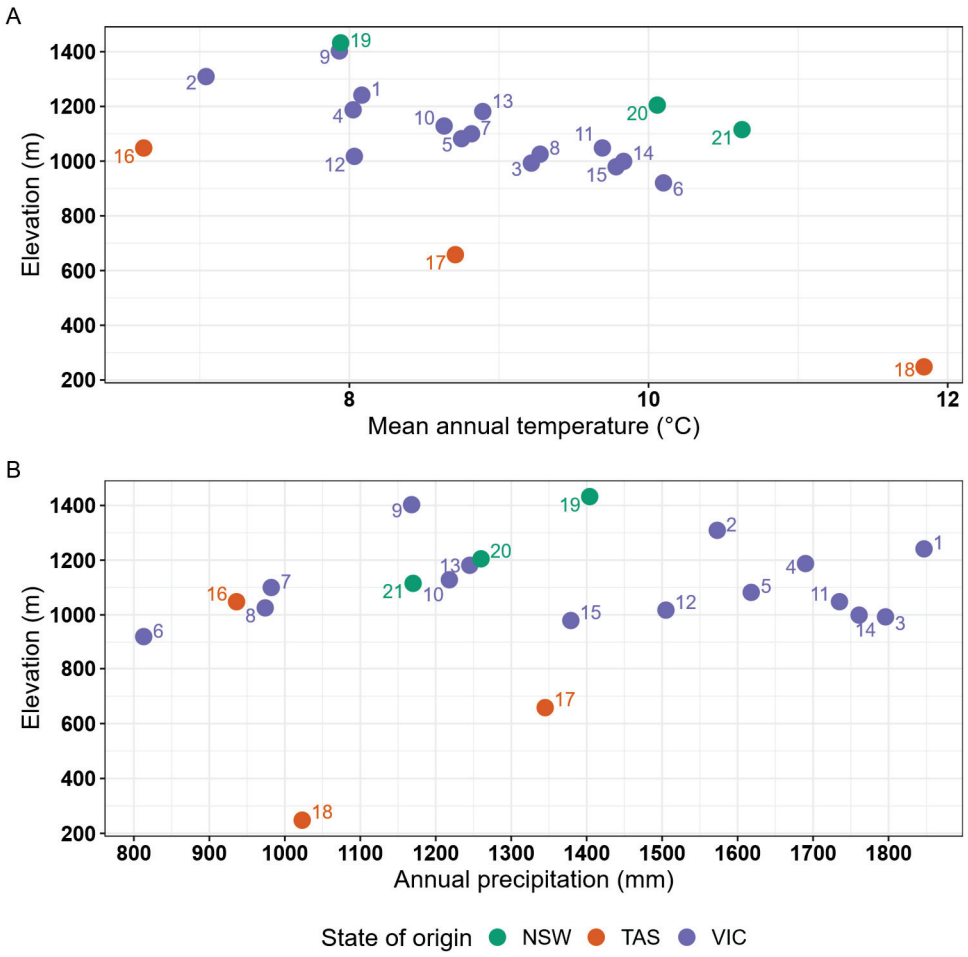


Figure A2. Elevation and climate (mean annual temperature (**A**) and mean annual precipitation (**B**)) of seed source location (climate of origin) for the 21 *Eucalyptus delegatensis* provenances studied.

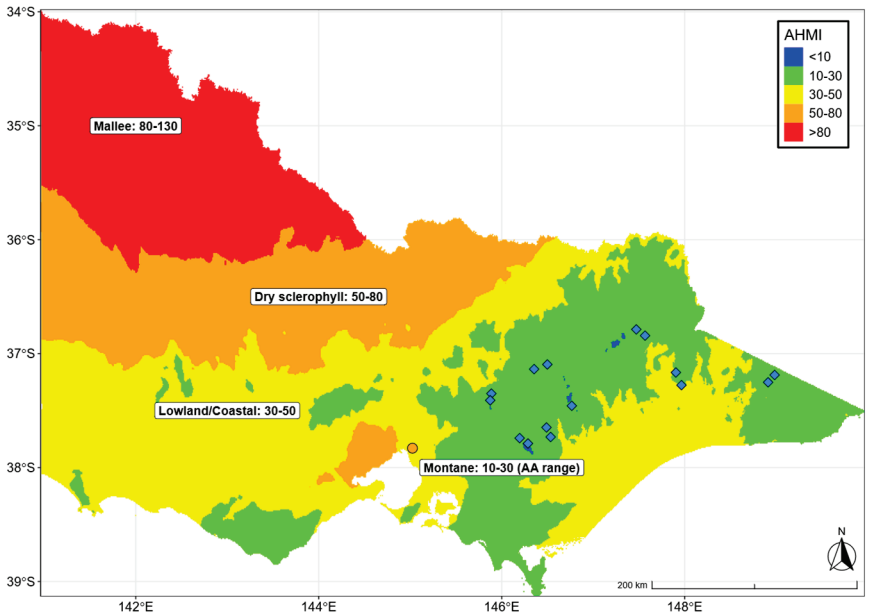


Figure A3. HMI range of *Eucalyptus delegatensis* (*Eucalyptus delegatensis* range, location of origin of Victorian *Eucalyptus delegatensis* provenance shown as blue diamonds) compared with other ecotones and their AHMI ranges in Victoria. The location of the common garden experimental site in Melbourne is shown as an orange point.

Appendix A.2. Tables

Table A1. Locations and climatic conditions of 21 provenances of *Eucalyptus delegatensis* (Alpine ash) across their geographic distribution in southeast Australia (Australian Alps bioregion).

Provenance	State	x-Coordinate	y-Coordinate	AHMI	Elevation (m)	MAT (°C)	MAP (mm)
1	VIC	146.287	−37.789	10.731	1241.250	8.083	1847
2	VIC	146.766	−37.458	13.081	1309.080	7.042	1573
3	VIC	146.196	−37.741	12.857	992.747	9.217	1796
4	VIC	146.489	−37.648	12.467	1187.594	8.025	1690
5	VIC	146.535	−37.731	15.276	1082.156	8.750	1618
6	VIC	148.983	−37.187	24.706	920.500	10.100	813
7	VIC	148.911	−37.252	20.410	1099.987	8.817	982
8	VIC	147.964	−37.277	27.066	1025.535	9.275	974
9	VIC	147.903	−37.165	18.724	1402.855	7.933	1168
10	VIC	147.566	−36.842	21.700	1128.332	8.633	1218
11	VIC	145.887	−37.351	14.748	1048.137	9.692	1735
12	VIC	146.498	−37.095	14.180	1017.419	8.033	1505
13	VIC	147.446	−36.793	18.291	1181.303	8.892	1245
14	VIC	145.874	−37.410	12.921	999.127	9.833	1761
15	VIC	146.354	−37.136	16.141	979.337	9.783	1379
16	TAS	147.009	−41.940	17.762	1048.000	6.625	936
17	TAS	147.526	−41.334	13.910	658.000	8.708	1345
18	TAS	148.104	−41.367	21.351	248.000	11.842	1023
19	NSW	148.623	−35.574	12.726	1432.359	7.942	1404
20	NSW	148.581	−35.416	14.793	1204.887	10.058	1260
21	NSW	148.195	−36.076	13.798	1115.211	10.625	1170

References

1. Anderegg, W.R.L.; Kane, J.M.; Anderegg, L.D.L. Consequences of widespread tree mortality triggered by drought and temperature stress. *Nat. Clim. Change* **2012**, *3*, 30–36. [CrossRef]
2. Engelbrecht, B.M.; Comita, L.S.; Condit, R.; Kursar, T.A.; Tyree, M.T.; Turner, B.L.; Hubbell, S.P. Drought sensitivity shapes species distribution patterns in tropical forests. *Nature* **2007**, *447*, 80–82. [CrossRef] [PubMed]
3. Allen, C.D.; Macalady, A.K.; Chenchouni, H.; Bachelet, D.; McDowell, N.; Vennetier, M.; Kitzberger, T.; Rigling, A.; Breshears, D.D.; Hogg, E.H.; et al. A global overview of drought and heat-induced tree mortality reveals emerging climate change risks for forests. *For. Ecol. Manag.* **2010**, *259*, 660–684. [CrossRef]
4. Kurz, W.A.; Dymond, C.C.; Stinson, G.; Rampley, G.J.; Neilson, E.T.; Carroll, A.L.; Ebata, T.; Safranyik, L. Mountain pine beetle and forest carbon feedback to climate change. *Nature* **2008**, *452*, 987–990. [CrossRef] [PubMed]
5. van Mantgem, P.J.; Stephenson, N.L.; Byrne, J.C.; Daniels, L.D.; Franklin, J.F.; Fule, P.Z.; Harmon, M.E.; Larson, A.J.; Smith, J.M.; Taylor, A.H.; et al. Widespread increase of tree mortality rates in the western United States. *Science* **2009**, *323*, 521–524. [CrossRef]
6. Anderson, N.S.; Fontaine, J.B.; Lewandrowski, W.; Walden, L.; Ruthrof, K.X. Drought and Wildfire Legacies Highlight Vulnerability of a Mediterranean Climate-Type Forest. *Austral Ecol.* **2025**, *50*, e70011. [CrossRef]
7. Ahrens, C.W.; Andrew, M.E.; Mazanec, R.A.; Ruthrof, K.X.; Challis, A.; Hardy, G.; Byrne, M.; Tissue, D.T.; Rymer, P.D. Plant functional traits differ in adaptability and are predicted to be differentially affected by climate change. *Ecol. Evol.* **2020**, *10*, 232–248. [CrossRef]
8. Heilmeier, H. Functional traits explaining plant responses to past and future climate changes. *Flora* **2019**, *254*, 1–11. [CrossRef]
9. Bartlett, M.K.; Scoffoni, C.; Sack, L. The determinants of leaf turgor loss point and prediction of drought tolerance of species and biomes: A global meta-analysis. *Ecol. Lett.* **2012**, *15*, 393–405. [CrossRef]
10. Pritzkow, C.; Williamson, V.; Szota, C.; Trouve, R.; Arndt, S.K. Phenotypic plasticity and genetic adaptation of functional traits influences intra-specific variation in hydraulic efficiency and safety. *Tree Physiol.* **2020**, *40*, 215–229. [CrossRef]
11. Warren, C.R.; Tausz, M.; Adams, M.A. Does rainfall explain variation in leaf morphology and physiology among populations of red ironbark (*Eucalyptus sideroxylon* subsp. tricarpa) grown in a common garden? *Tree Physiol.* **2005**, *25*, 1369–1378. [CrossRef] [PubMed]
12. Bertolino, L.T.; Caine, R.S.; Gray, J.E. Impact of Stomatal Density and Morphology on Water-Use Efficiency in a Changing World. *Front. Plant Sci.* **2019**, *10*, 225. [CrossRef]
13. James, A.T.; Lawn, R.J.; Cooper, M. Genotypic variation for drought stress response traits in soybean. I. Variation in soybean and wild *Glycine* spp. for epidermal conductance, osmotic potential, and relative water content. *Aust. J. Agric. Res.* **2008**, *59*, 656–669. [CrossRef]
14. Choat, B.; Jansen, S.; Brodribb, T.J.; Cochard, H.; Delzon, S.; Bhaskar, R.; Bucci, S.J.; Feild, T.S.; Gleason, S.M.; Hacke, U.G.; et al. Global convergence in the vulnerability of forests to drought. *Nature* **2012**, *491*, 752–755. [CrossRef]
15. Li, X.; Blackman, C.J.; Choat, B.; Duursma, R.A.; Rymer, P.D.; Medlyn, B.E.; Tissue, D.T. Tree hydraulic traits are coordinated and strongly linked to climate-of-origin across a rainfall gradient. *Plant Cell Environ.* **2018**, *41*, 646–660. [CrossRef]

16. Pfautsch, S.; Harbusch, M.; Wesolowski, A.; Smith, R.; Macfarlane, C.; Tjoelker, M.G.; Reich, P.B.; Adams, M.A. Climate determines vascular traits in the ecologically diverse genus *Eucalyptus*. *Ecol. Lett.* **2016**, *19*, 240–248. [CrossRef] [PubMed]
17. Trueba, S.; Pouteau, R.; Lens, F.; Feild, T.S.; Isnard, S.; Olson, M.E.; Delzon, S. Vulnerability to xylem embolism as a major correlate of the environmental distribution of rain forest species on a tropical island. *Plant Cell Environ.* **2017**, *40*, 277–289. [CrossRef]
18. Kibria, M.G.; Tjoelker, M.G.; Marchin, R.M.; Arndt, S.K.; Rymer, P.D. Can species climate niche predict canopy growth, functional traits and phenotypic plasticity in urban trees? *Urban For. Urban Green.* **2024**, *98*, 128417. [CrossRef]
19. Warren, C.R.; Dreyer, E.; Tausz, M.; Adams, M.A. Ecotype adaptation and acclimation of leaf traits to rainfall in 29 species of 16-year-old Eucalyptus at two common gardens. *Funct. Ecol.* **2006**, *20*, 929–940. [CrossRef]
20. Umana, M.N.; Swenson, N.G. Intraspecific variation in traits and tree growth along an elevational gradient in a subtropical forest. *Oecologia* **2019**, *191*, 153–164. [CrossRef]
21. Li, X.; Blackman, C.J.; Choat, B.; Rymer, P.D.; Medlyn, B.E.; Tissue, D.T. Drought tolerance traits do not vary across sites differing in water availability in *Banksia serrata* (Proteaceae). *Funct. Plant Biol.* **2019**, *46*, 624–633. [CrossRef] [PubMed]
22. Lobo, A.; Torres-Ruiz, J.M.; Burlett, R.; Lemaire, C.; Parise, C.; Francioni, C.; Truffaut, L.; Tomaskova, I.; Hansen, J.K.; Kjaer, E.D.; et al. Assessing inter- and intraspecific variability of xylem vulnerability to embolism in oaks. *For. Ecol. Manag.* **2018**, *424*, 53–61. [CrossRef] [PubMed]
23. Maherali, H.; DeLucia, E.H. Xylem conductivity and vulnerability to cavitation of ponderosa pine growing in contrasting climates. *Tree Physiol.* **2000**, *20*, 859–867. [CrossRef] [PubMed]
24. Doherty, M.D.; Lavorel, S.; Colloff, M.J.; Williams, K.J.; Williams, R.J. Moving from autonomous to planned adaptation in the montane forests of southeastern Australia under changing fire regimes. *Austral Ecol.* **2017**, *42*, 309–316. [CrossRef]
25. McLean, E.H.; Prober, S.M.; Stock, W.D.; Steane, D.A.; Potts, B.M.; Vaillancourt, R.E.; Byrne, M. Plasticity of functional traits varies clinally along a rainfall gradient in *Eucalyptus tricarpa*. *Plant Cell Environ.* **2014**, *37*, 1440–1451. [CrossRef]
26. Nicotra, A.B.; Atkin, O.K.; Bonser, S.P.; Davidson, A.M.; Finnegan, E.J.; Mathesius, U.; Poot, P.; Purugganan, M.D.; Richards, C.L.; Valladares, F.; et al. Plant phenotypic plasticity in a changing climate. *Trends Plant Sci.* **2010**, *15*, 684–692. [CrossRef]
27. Xu, G.Q.; Farrell, C.; Arndt, S.K. Climate of origin has no influence on drought adaptive traits and the drought responses of a widely distributed polymorphic shrub. *Tree Physiol.* **2022**, *42*, 86–98. [CrossRef]
28. Ramirez-Valiente, J.A.; Cavender-Bares, J. Evolutionary trade-offs between drought resistance mechanisms across a precipitation gradient in a seasonally dry tropical oak (*Quercus oleoides*). *Tree Physiol.* **2017**, *37*, 889–901. [CrossRef]
29. Walters, M.B.; Gerlach, J.P. Intraspecific growth and functional leaf trait responses to natural soil resource gradients for conifer species with contrasting leaf habit. *Tree Physiol.* **2013**, *33*, 297–310. [CrossRef]
30. Booth, T.H.; Broadhurst, L.M.; Pinkard, E.; Prober, S.M.; Dillon, S.K.; Bush, D.; Pinyopusarerk, K.; Doran, J.C.; Ivkovich, M.; Young, A.G. Native forests and climate change: Lessons from eucalypts. *For. Ecol. Manag.* **2015**, *347*, 18–29. [CrossRef]
31. Hughes, L.; Cawsey, E.M.; Westoby, M. Climatic Range Sizes of Eucalyptus Species in Relation to Future Climate Change. *Glob. Ecol. Biogeogr. Lett.* **1996**, *5*, 23–29. [CrossRef]
32. Westoby, M.; Andrew, S.C.; Gallagher, R.V.; Schrader, J. Species gain and loss per degree Celsius. *Oikos* **2024**, *2024*, e10556. [CrossRef]
33. Bowman, D.M.; Murphy, B.P.; Neyland, D.L.; Williamson, G.J.; Prior, L.D. Abrupt fire regime change may cause landscape-wide loss of mature obligate seeder forests. *Glob. Change Biol.* **2014**, *20*, 1008–1015. [CrossRef]
34. McColl-Gausden, S.C.; Bennett, L.T.; Ababei, D.A.; Clarke, H.G.; Penman, T.D. Future fire regimes increase risks to obligate-seeder forests. *Divers. Distrib.* **2021**, *17*, 542–558. [CrossRef]
35. Fairman, T.A.; Nitschke, C.R.; Bennett, L.T. Too much, too soon? A review of the effects of increasing wildfire frequency on tree mortality and regeneration in temperate eucalypt forests. *Int. J. Wildland Fire* **2016**, *25*, 831–848. [CrossRef]
36. Singh, A.; Baker, P.J.; Kasel, S.; Trouvé, R.; Stewart, S.B.; Nitschke, C.R. The role of climatic variability on Eucalyptus regeneration in southeastern Australia. *Glob. Ecol. Conserv.* **2021**, *32*, e01929. [CrossRef]
37. Mok, H.F.; Arndt, S.K.; Nitschke, C.R. Modelling the potential impact of climate variability and change on species regeneration potential in the temperate forests of South-Eastern Australia. *Global Change Biol.* **2012**, *18*, 1053–1072. [CrossRef]
38. Tng, D.Y.P.; Williamson, G.J.; Jordan, G.J.; Bowman, D. Giant eucalypts—Globally unique fire-adapted rain-forest trees? *New Phytol.* **2012**, *196*, 1001–1014. [CrossRef] [PubMed]
39. Collins, L.; Clarke, H.; Clarke, M.F.; McColl Gausden, S.C.; Nolan, R.H.; Penman, T.; Bradstock, R.; Varner, M. Warmer and drier conditions have increased the potential for large and severe fire seasons across south-eastern Australia. *Global Ecol. Biogeogr.* **2022**, *31*, 1933–1948. [CrossRef]
40. Bassett, O.D.; Prior, L.D.; Slijkerman, C.M.; Jamieson, D.; Bowman, D.M.J.S. Aerial sowing stopped the loss of alpine ash (*Eucalyptus delegatensis*) forests burnt by three short-interval fires in the Alpine National Park, Victoria, Australia. *For. Ecol. Manag.* **2015**, *342*, 39–48. [CrossRef]
41. Mátyás, C. Climatic adaptation of trees: Rediscovering provenance tests. *Euphytica* **1996**, *92*, 45–54. [CrossRef]
42. de Villemereuil, P.; Gaggiotti, O.E.; Mouterde, M.; Till-Bottraud, I. Common garden experiments in the genomic era: New perspectives and opportunities. *Heredity* **2016**, *116*, 249–254. [CrossRef] [PubMed]

43. Stewart, S.B.; Nitschke, C.R. Improving temperature interpolation using MODIS LST and local topography: A comparison of methods in south east Australia. *Int. J. Climatol.* **2017**, *37*, 3098–3110. [CrossRef]
44. Fick, S.E.; Hijmans, R.J. WorldClim 2: New 1-km spatial resolution climate surfaces for global land areas. *Int. J. Climatol.* **2017**, *37*, 4302–4315. [CrossRef]
45. Paudel, S.K.; Waeber, P.O.; Simard, S.W.; Innes, J.L.; Nitschke, C.R. Multiple factors influence plant richness and diversity in the cold and dry boreal forest of southwest Yukon, Canada. *Plant Ecol.* **2016**, *217*, 505–519. [CrossRef]
46. Wang, T.; Hamann, A.; Yanchuk, A.; O'Neill, G.A.; Aitken, S.N. Use of response functions in selecting lodgepole pine populations for future climates. *Global Change Biol.* **2006**, *12*, 2404–2416. [CrossRef]
47. Farr, T.G.; Rosen, P.A.; Caro, E.; Crippen, R.; Duren, R.; Hensley, S.; Kobrick, M.; Paller, M.; Rodriguez, E.; Roth, L. The shuttle radar topography mission. *Rev. Geophys.* **2007**, *45*, 1–33. [CrossRef]
48. Schneider, C.A.; Rasband, W.S.; Eliceiri, K.W. NIH Image to ImageJ: 25 years of image analysis. *Nat. Methods* **2012**, *9*, 671–675. [CrossRef]
49. Camargo, M.A.B.; Marenco, R.A. Density, size and distribution of stomata in 35 rainforest tree species in Central Amazonia. *Acta Amaz.* **2011**, *41*, 205–212. [CrossRef]
50. Beaulieu, J.M.; Leitch, I.J.; Patel, S.; Pendharkar, A.; Knight, C.A. Genome size is a strong predictor of cell size and stomatal density in angiosperms. *New Phytol.* **2008**, *179*, 975–986. [CrossRef]
51. Callister, A.N.; Arndt, S.K.; Adams, M.A. Comparison of four methods for measuring osmotic potential of tree leaves. *Physiol. Plant.* **2006**, *127*, 383–392. [CrossRef]
52. Pearcy, R.W.; Ehleringer, J.R.; Mooney, H.A.; Rundel, P.W. *Plant Physiological Ecology: Field Methods and Instrumentation*; Springer: Berlin/Heidelberg, Germany, 2012.
53. Sack, L.; Cowan, P.D.; Jaikumar, N.; Holbrook, N.M. The 'hydrology' of leaves: Co-ordination of structure and function in temperate woody species. *Plant Cell Environ.* **2003**, *26*, 1343–1356. [CrossRef]
54. Schreiber, L.; Skrabs, M.; Hartmann, K.D.; Diamantopoulos, P.; Simanova, E.; Santrucek, J. Effect of humidity on cuticular water permeability of isolated cuticular membranes and leaf disks. *Planta* **2001**, *214*, 274–282. [CrossRef]
55. R Core Development Team. *R: A Language and Environment for Statistical Computing*; R Foundation for Statistical Computing: Vienna, Austria, 2024.
56. Botta-Dukat, Z. Quartile coefficient of variation is more robust than CV for traits calculated as a ratio. *Sci. Rep.* **2023**, *13*, 4671. [CrossRef] [PubMed]
57. Duursma, R.A.; Blackman, C.J.; Lopez, R.; Martin-StPaul, N.K.; Cochard, H.; Medlyn, B.E. On the minimum leaf conductance: Its role in models of plant water use, and ecological and environmental controls. *New Phytol.* **2019**, *221*, 693–705. [CrossRef] [PubMed]
58. Liu, C.; Sack, L.; Li, Y.; Zhang, J.; Yu, K.; Zhang, Q.; He, N.; Yu, G. Relationships of stomatal morphology to the environment across plant communities. *Nat. Commun.* **2023**, *14*, 6629. [CrossRef]
59. Portelli, A.M.; Windecker, S.M.; Pollock, L.J.; Neal, W.C.; Morris, W.K.; Khot, R.; Vesk, P.A.; Williams, D. From mallees to mountain ash, specific leaf area is coordinated with eucalypt tree stature, resprouting, stem construction, and fruit size. *Aust. J. Bot.* **2023**, *71*, 506–522. [CrossRef]
60. Givnish, T.J.; Wong, S.C.; Stuart-Williams, H.; Holloway-Phillips, M.; Farquhar, G.D. Determinants of maximum tree height inEucalyptusspecies along a rainfall gradient in Victoria, Australia. *Ecology* **2014**, *95*, 2991–3007. [CrossRef]
61. Bartlett, M.K.; Scoffoni, C.; Ardy, R.; Zhang, Y.; Sun, S.; Cao, K.; Sack, L. Rapid determination of comparative drought tolerance traits: Using an osmometer to predict turgor loss point. *Methods Ecol. Evol.* **2012**, *3*, 880–888. [CrossRef]
62. Salvi, A.M.; Smith, D.D.; Adams, M.A.; McCulloh, K.A.; Givnish, T.J. Mesophyll photosynthetic sensitivity to leaf water potential in Eucalyptus: A new dimension of plant adaptation to native moisture supply. *New Phytol.* **2021**, *230*, 1844–1855. [CrossRef]
63. Laughlin, D.C.; Lusk, C.H.; Bellingham, P.J.; Burslem, D.; Simpson, A.H.; Kramer-Walter, K.R. Intraspecific trait variation can weaken interspecific trait correlations when assessing the whole-plant economic spectrum. *Ecol. Evol.* **2017**, *7*, 8936–8949. [CrossRef]
64. Koerner, C.; Bannister, P.; Mark, A.F. Altitudinal variation in stomatal conductance, nitrogen content and leaf anatomy in different plant life forms in New Zealand. *Oecologia* **1986**, *69*, 577–588. [CrossRef] [PubMed]
65. Liu, W.; Zheng, L.; Qi, D. Variation in leaf traits at different altitudes reflects the adaptive strategy of plants to environmental changes. *Ecol. Evol.* **2020**, *10*, 8166–8175. [CrossRef] [PubMed]
66. Anderegg, L.D.L.; Loy, X.; Markham, I.P.; Elmer, C.M.; Hovenden, M.J.; HilleRisLambers, J.; Mayfield, M.M. Aridity drives coordinated trait shifts but not decreased trait variance across the geographic range of eight Australian trees. *New Phytol.* **2021**, *229*, 1375–1387. [CrossRef]
67. Bourne, A.E.; Creek, D.; Peters, J.M.R.; Ellsworth, D.S.; Choat, B. Species climate range influences hydraulic and stomatal traits in Eucalyptus species. *Ann. Bot.* **2017**, *120*, 123–133. [CrossRef]
68. Peters, J.M.R.; Lopez, R.; Nolf, M.; Hutley, L.B.; Wardlaw, T.; Cernusak, L.A.; Choat, B. Living on the edge: A continental-scale assessment of forest vulnerability to drought. *Glob. Change Biol.* **2021**, *27*, 3620–3641. [CrossRef]

69. Sanders, G.J.; Arndt, S.K. Osmotic Adjustment Under Drought Conditions. In *Plant Responses to Drought Stress*; Springer: Berlin/Heidelberg, Germany, 2012; pp. 199–229.
70. Matheny, A.M.; Bohrer, G.; Garrity, S.R.; Morin, T.H.; Howard, C.J.; Vogel, C.S. Observations of stem water storage in trees of opposing hydraulic strategies. *Ecosphere* **2015**, *6*, 1–13. [CrossRef]
71. Larter, M.; Pfautsch, S.; Domec, J.C.; Trueba, S.; Nagalingum, N.; Delzon, S. Aridity drove the evolution of extreme embolism resistance and the radiation of conifer genus *Callitris*. *New Phytol.* **2017**, *215*, 97–112. [CrossRef]
72. Ellis, T.W.; Hatton, T.J. Relating leaf area index of natural eucalypt vegetation to climate variables in southern Australia. *Agric. Water Manag.* **2008**, *95*, 743–747. [CrossRef]
73. Blackman, C.J.; Halliwell, B.; Brodribb, T.J. All together now: A mixed-planting experiment reveals adaptive drought tolerance in seedlings of 10 Eucalyptus species. *Plant Physiol.* **2024**, *197*, kiae632. [CrossRef]
74. Smith, D.D.; Adams, M.A.; Salvi, A.M.; Krieg, C.P.; Ane, C.; McCulloh, K.A.; Givnish, T.J. Ecophysiological adaptations shape distributions of closely related trees along a climatic moisture gradient. *Nat. Commun.* **2023**, *14*, 7173. [CrossRef] [PubMed]
75. Fontes, C.G.; Pinto-Ledezma, J.; Jacobsen, A.L.; Pratt, R.B.; Cavender-Bares, J. Adaptive variation among oaks in wood anatomical properties is shaped by climate of origin and shows limited plasticity across environments. *Funct. Ecol.* **2021**, *36*, 326–340. [CrossRef]
76. Russo, S.E.; Kitajima, K. The Ecophysiology of Leaf Lifespan in Tropical Forests: Adaptive and Plastic Responses to Environmental Heterogeneity. In *Tropical Tree Physiology*; Tree Physiology; Springer: Berlin/Heidelberg, Germany, 2016; pp. 357–383.
77. Aspinwall, M.J.; Blackman, C.J.; Maier, C.; Tjoelker, M.G.; Rymer, P.D.; Creek, D.; Chieppa, J.; Griffin-Nolan, R.J.; Tissue, D.T. Aridity drives clinal patterns in leaf traits and responsiveness to precipitation in a broadly distributed Australian tree species. *Plant Environ. Interact.* **2023**, *4*, 70–85. [CrossRef]
78. Breed, M.F.; Stead, M.G.; Ottewell, K.M.; Gardner, M.G.; Lowe, A.J. Which provenance and where? Seed sourcing strategies for revegetation in a changing environment. *Conserv. Genet.* **2012**, *14*, 1–10. [CrossRef]
79. Rice, K.J.; Emery, N.C. Managing microevolution: Restoration in the face of global change. *Front. Ecol. Environ.* **2003**, *1*, 469–478. [CrossRef]
80. Lopez, R.; Cano, F.J.; Choat, B.; Cochard, H.; Gil, L. Plasticity in Vulnerability to Cavitation of Pinus canariensis Occurs Only at the Driest End of an Aridity Gradient. *Front. Plant Sci.* **2016**, *7*, 769. [CrossRef]
81. Buras, A.; Sass-Klaassen, U.; Verbeek, I.; Copini, P. Provenance selection and site conditions determine growth performance of pedunculate oak. *Dendrochronologia* **2020**, *61*, 125705. [CrossRef]

Disclaimer/Publisher's Note: The statements, opinions and data contained in all publications are solely those of the individual author(s) and contributor(s) and not of MDPI and/or the editor(s). MDPI and/or the editor(s) disclaim responsibility for any injury to people or property resulting from any ideas, methods, instructions or products referred to in the content.

forests

MDPI

Article

Seasonal Variations in the Relationship Between Canopy Solar-Induced Chlorophyll Fluorescence and Gross Primary Production in a Temperate Evergreen Needleleaf Forest

Kaijie Yang [1], Yifei Cai [1], Xiaoya Li [1], Weiwei Cong [2,*], Yiming Feng [1,*] and Feng Wang [1,*]

[1] Institute of Ecological Conservation and Restoration, Chinese Academy of Forestry, Beijing 100091, China; kiss0822@126.com (K.Y.); cyf@caf.ac.cn (Y.C.); lixiaoya@caf.ac.cn (X.L.)
[2] College of Agronomy, Shenyang Agricultural University, Shenyang 110161, China
* Correspondence: vivien8026@syau.edu.cn (W.C.); fengym@caf.ac.cn (Y.F.); wangfeng@caf.ac.cn (F.W.)

Abstract: The temperate evergreen needleleaf forest (ENF), primarily composed of Mongolian Scots pine (*Pinus sylvestris* var. *mongolica*), plays a pivotal role in the "The Great Green Wall" Shelterbelt Project in northern China as a major species for windbreak and sand fixation. Solar-induced chlorophyll fluorescence (SIF) has emerged as a revolutionary remote sensing signal for quantifying photosynthetic activity and gross primary production (GPP) at the ecosystem scale. Meanwhile, eddy covariance (EC) technology has been widely employed to obtain in situ GPP estimates. Although a linear relationship between SIF and GPP has been reported in various ecosystems, it is mainly derived from satellite SIF products and flux-tower GPP observations, which are often difficult to align due to mismatches in spatial and temporal resolution. In this study, we analyzed synchronous high-frequency SIF and EC-derived GPP measurements from a Mongolian Scots pine plantation during the seasonal transition (August–December). The results revealed the following. (1) The ENF acted as a net carbon sink during the observation period, with a total carbon uptake of 100.875 $gC \cdot m^{-2}$. The diurnal dynamics of net ecosystem exchange (NEE) exhibited a "U"-shaped pattern, with peak carbon uptake occurring around midday. As the growing season progressed toward dormancy, the timing of CO_2 uptake and release gradually shifted. (2) Both GPP and SIF peaked in September and declined thereafter. A strong linear relationship between SIF and GPP (R^2 = 0.678) was observed, consistent across both diurnal and sub-daily scales. SIF demonstrated higher sensitivity to light and environmental changes, particularly during the autumn–winter transition. Cloudy and rainy conditions significantly affect the relationship between SIF and GPP. These findings highlight the potential of canopy SIF observations to capture seasonal photosynthesis dynamics accurately and provide a methodological foundation for regional GPP estimation using remote sensing. This work also contributes scientific insights toward achieving China's carbon neutrality goals.

Keywords: temperate evergreen needleleaf forest; gross primary production; solar-induced chlorophyll fluorescence

1. Introduction

Terrestrial ecosystems can absorb up to 33% of total anthropogenic carbon emissions (from both fossil fuel combustion and land use), contributing to the reduction of atmospheric CO_2 levels [1]. Gross primary production (GPP) refers to the amount of CO_2 fixed by terrestrial vegetation per unit time through the reduction of CO_2 into organic compounds

via photosynthesis, representing the primary pathway of carbon input into ecosystems and the fundamental mechanism underlying terrestrial carbon sequestration [2,3]. Accurately characterizing photosynthesis (i.e., GPP) at spatial and temporal scales provides crucial information on the timing, location, and amount of carbon absorbed [4,5]. This is a critical component of terrestrial carbon budgets. Changes in vegetation structure, growing season, and climate-responsive functions across ecosystems indicate that GPP is undergoing global changes [6]. A precise understanding of GPP is fundamental for comprehensively evaluating the role of terrestrial ecosystems in the global carbon cycle and climate change, yet global GPP remains difficult to quantify accurately.

GPP estimation primarily relies on eddy covariance (EC) flux observations and greenness-based remote sensing models. EC flux towers are considered one of the most accurate methods for quantifying canopy-scale biomass productivity [7–9]. By measuring the net ecosystem exchange (NEE) of CO_2 between vegetation and the atmosphere, EC reflects the overall carbon exchange processes within the flux footprint, thereby enhancing our understanding of the terrestrial carbon cycle [10,11]. However, due to the limited number of observation sites and their uneven spatial distribution, the representativeness and coverage of EC flux towers at the global scale are constrained. Greenness models based on remote sensing vegetation indices (e.g., NDVI) serve as an important approach for GPP estimation and have been widely applied in monitoring large-scale carbon fluxes [12–14]. These models estimate potential photosynthetic activity based on the correlation between vegetation indices and photosynthetic capacity, but they are limited in capturing instantaneous photosynthesis or the dynamic nature of actual GPP [15,16]. Moreover, GPP estimations based on light use efficiency (LUE) models are highly dependent on the accuracy of meteorological input data, and uncertainties in model structure and parameterization further limit their applicability in complex ecosystems [17].

In recent years, solar-induced chlorophyll fluorescence (SIF) has gained increasing attention as a physiological indicator of GPP [18]. Unlike reflectance-based vegetation indices, SIF originates directly from the photosynthetic process and can more accurately reflect plant photosynthetic activity [19]. Therefore, SIF is regarded as a more sensitive indicator of vegetation's carbon uptake capacity [20]. With the advancement of satellite remote sensing technologies, large-scale retrieval of SIF has become increasingly feasible. Studies have shown that SIF can be integrated into land surface models to improve GPP estimation, offering a novel pathway for remote-sensing-based GPP monitoring. Early studies using low-spatial-resolution satellite SIF data (tens of kilometers) revealed a strong linear relationship between SIF and GPP [21]. The emergence of high-resolution satellite platforms, such as NASA's Orbiting Carbon Observatory-2 (OCO-2) with a spatial resolution of 1.2 $\times$ 2 km, has made it possible to match satellite-derived SIF data with ground-based EC observations of GPP [22]. Research has demonstrated a high degree of consistency between SIF and GPP across diurnal, seasonal, and interannual timescales, supporting the stability and scalability of SIF as an indicator of GPP [23].

To address the scale mismatch between satellite remote sensing and ground-based observations, an increasing number of studies have focused on the relationship between SIF and GPP at the canopy scale. At this scale, numerous studies have explored the response of SIF to photosynthesis in agricultural systems, such as maize (*Zea mays* L.), rice (*Oryza sativa* L.), and broadleaf tree species, such as beech (*Fagus grandifolia Ehrh*) and red oak (*Quercus rubra*) [24–26]. In ENFs, the relationship between SIF and GPP varies depending on the forest type. A linear relationship has been observed in lodgepole pine (*P. contorta* Douglas ex Loudon) and Engelmann spruce (*Picea engelmannii* Parry ex Engelm) in Colorado [21], whereas a nonlinear relationship has been reported in Korean pine (*Pinus koraiensis* Siebold et. Zucc) ecosystems [27]. These contrasting patterns may be driven by

differences in canopy structure, leaf area index, and environmental conditions, suggesting that the SIF–GPP relationship in ENFs is modulated by a combination of biophysical and ecological factors [28,29]. The Mongolian Scots pine (*Pinus sylvestris* var. *mongolica*), a key afforestation species in China's "The Great Green Wall" Shelterbelt Program, plays an important ecological role in combating desertification. However, as a representative semi-arid evergreen needleleaf ecosystem, its carbon exchange dynamics and seasonal variations in photosynthetic activity remain unclear, and it is still uncertain whether SIF can accurately reflect the temporal dynamics of its GPP.

In this study, we conducted tower-based synchronous SIF and EC observations in a Mongolian Scots pine plantation in northern China and estimated GPP using EC measurements. Our objectives were to (1) evaluate the carbon sequestration capacity in this ENF ecosystem; (2) investigate the relationship between SIF and GPP, with an emphasis on its seasonal dynamics; and (3) examine the environmental drivers of SIF and GPP during seasonal transitions.

2. Materials and Methods

2.1. Study Location

The study site of the Mongolian Scots pine plantation is located at the border between Jianping County, Chaoyang City, Liaoning Province, and the Inner Mongolia Autonomous Region over the period of 1 September to 30 November 2020 (Figure 1a). The dominant landform is low mountainous hills with an elevation of 871 m above sea level. The site is geographically situated at 41°58′169″ N, 119°25′104″ E and lies within a temperate continental monsoon climate zone. The region is characterized by pronounced monsoon activity and prevailing winds of 2–3 on the Beaufort scale. Spring is dry with little rainfall, while winter lasts approximately 140 days, typically from early November to late March of the following year. Summer lasts for about 90 days, and both spring and autumn are relatively short, each lasting less than two months.

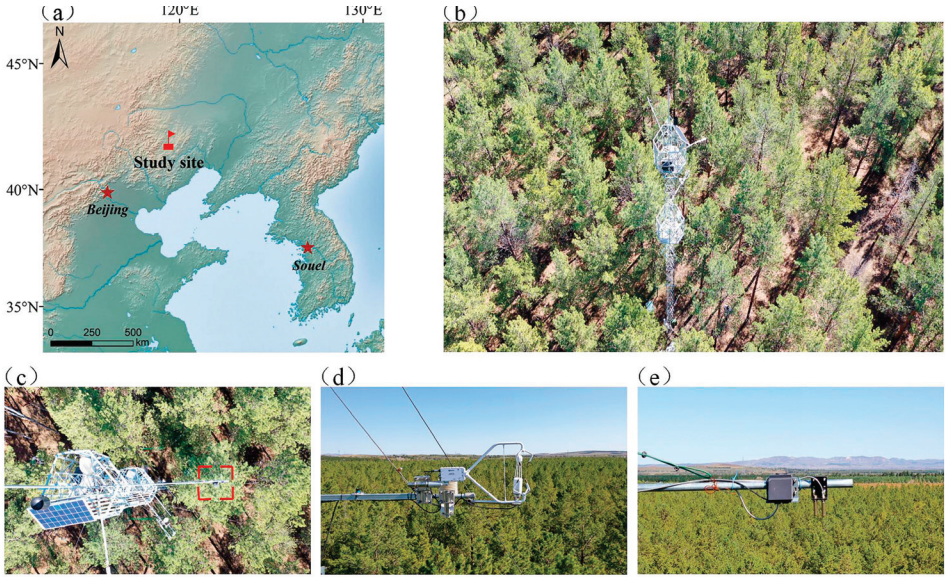


Figure 1. Map of the geographical location, vegetation landscape, and instrument observation overview of the Mongolian Scots pine (*Pinus sylvestris* var. *mongolica*) in Horqin Sandy Land, northeast China ((**a**) geographic location; (**b**) vegetation landscape; (**c**) observation sites; (**d**) flux observation; (**e**) SIF observation).

The annual average temperature is 7.6 °C, with extremes ranging from a minimum of −29 °C to a maximum of 42.2 °C. The region receives approximately 2765 h of sunshine

annually, and the average daily sunshine duration is approximately 7.5 h per day. The mean annual precipitation is 450 mm, with most rainfall concentrated between June and August. The average frost-free period is 138 days per year.

The ENF in the study area is approximately 30 years old, with an average tree height of 10 meters and virtually no understory vegetation (Figure 1b).

2.2. Eddy Covariance (EC) Flux Measurements

Open-path eddy covariance technology measures CO_2 flux by calculating the covariance between fluctuations in vertical wind speed and CO_2 concentration. A three-dimensional sonic anemometer (CSAT 3, Campbell Scientific, Logan, UT, USA; Figure 1d) and an open-path infrared CO_2/H_2O gas analyzer (IRGA; LI-7500A, LI-Cor., Lincoln, NE, USA) were installed at 15 m height on the observation tower. The LI-7500A was configured with a temperature control mode set to 5 °C. Both instruments operated at a sampling frequency of 10 Hz, with data automatically collected and stored by a datalogger (CR2000, Campbell Scientific, Logan, UT, USA).

2.3. Solar-Induced Chlorophyll Fluorescence (SIF) Observations

Canopy-level SIF was monitored using an automated chlorophyll fluorescence observation system (AUTOSIF, Bergson Spectrum Science Limited., Beijing, China). The AUTOSIF system included a high-sensitivity spectrometer (QEPRO, Ocean Optics, Dunedin, FL, USA) for retrieving SIF in the O_2-A absorption band, featuring a signal-to-noise ratio (SNR) of 1000, a wavelength range of 730–785 nm, and a spectral sampling interval of 0.07 nm. A high-throughput optical fiber was installed 5 m above the forest canopy, targeting a circular observation area with a diameter of 4.4 m. The downwelling irradiance was collected using a cosine-corrected optical configuration, while the target surface was observed via a bare optical fiber (Figure 1c,e). The fiber type used in the system was a 600 μm core fiber (Ocean Optics, Dunedin, FL, USA). Radiometric and wavelength calibrations were performed using a mercury calibration lamp (HL-3 Plus, Ocean Optics Inc., Dunedin, FL, USA) and an integrating sphere (LightFluxColor LFC-illumia Plus2., Labsphere, North Sutton, NH, USA), respectively.

2.4. Meteorological Observations

Meteorological data primarily included air temperature (T_{air}) and relative humidity (RH) (HMP45C, Vaisala, Helsinki, Finland), and photosynthetically active radiation (PAR) (LI-190, LI-COR., Lincoln, NE, USA). Data from the conventional meteorological observation system were collected at a sampling frequency of 0.5 Hz using a CR2000 datalogger (Campbell Scientific, Logan, UT, USA), which automatically recorded and stored the measurements.

2.5. Data Processing

2.5.1. CO_2 Flux Correction and Gap Filling

The raw data obtained from flux observations are based on ideal conditions (e.g., flat and homogeneous underlying surfaces) and therefore require further processing, including double coordinate rotation and Webb–Pearman–Leuning (WPL) correction. All of these procedures were performed using EddyPro software (v7.0.6, LI-Cor., LI-COR., Lincoln, NE, USA). Outlier detection was conducted separately for daytime and nighttime data within a 13-day moving window. Nighttime periods were identified using a global solar radiation (R_g) threshold of 20 W/m^2, and day/night segmentation was determined based on R_g.

The R package REddyProc (v1.3.3) [30] was employed to perform u^* filtering with 200 bootstrapped resamplings (default setting). The gap-filling procedure was applied to

data that had already undergone outlier removal, and the Marginal Distribution Sampling (MDS) method was used for flux data interpolation.

2.5.2. NEE Partitioning and GPP Estimation

In this study, photosynthesis is quantified as GPP, which represents the total amount of CO_2 fixed by vegetation at the ecosystem scale. The estimation process was performed in two steps. First, ecosystem respiration (Reco) was estimated by partitioning the NEE based on environmental drivers. Second, GPP was derived by subtracting NEE from Reco.

The NEE data were partitioned based on the light response curve of NEE to R_g, the effect of T_{air} on *Reco*, and the influence of R_g and vapor pressure deficit (*VPD*) on GPP. The temperature sensitivity parameter E_0 was fitted using nighttime NEE and T_{air} data within a 15-day window, with T_0 fixed at −46.02 °C and T_{Ref} at 15 °C. The optimal E_0 was determined as the value corresponding to the smallest standard deviation and used as the annual E_0. Based on the fitted E_0, the reference respiration rate R_{Ref} was calculated using a 7-day moving window with a 4-day step size (3-day overlap). Curve fitting and linear interpolation were used to derive a unique R_{Ref} for each sample [31].

$$NEE = \frac{\alpha\beta R_g}{\alpha R_g + \beta} + R_{Ref} exp\left[E_0\left(\frac{1}{T_{Ref} - T_0} - \frac{1}{T - T_0}\right)\right] \quad (1)$$

$$\beta = \begin{cases} \beta_0\, exp(-k(VPD - VPD_0)) & VPD > VPD_0 \\ \beta = \beta_0 & VPD < VPD_0 \end{cases} \quad (2)$$

In these equations, R_{Ref} is the baseline ecosystem respiration rate at the reference temperature, E_0 is the temperature sensitivity parameter, T_{Ref} is the reference temperature, and T_0 is a constant. α is the canopy light use efficiency (μmolC·m^{-2}·s^{-1}), β is the maximum CO_2 uptake rate (μmolC·m^{-2}·s^{-1}), and the parameter k is fitted using a 4-day window, assuming VPD_0 = 0.

Following the estimation of *Reco*, GPP was calculated based on the following equation [30]:

$$GPP = Reco - NEE \quad (3)$$

where GPP is gross primary production (gC·m^{-2}·day^{-1}), Reco is ecosystem respiration (gC·m^{-2}·day^{-1}), and NEE is net ecosystem carbon exchange (gC·m^{-2}·day^{-1}).

All flux data processing was performed using the REddyProc package in the R environment (v4.5.0) [31].

2.5.3. Solar-Induced Chlorophyll Fluorescence (SIF) Data Processing

The retrieval of SIF signals is based on algorithms derived from the classical Fraunhofer Line Discrimination (FLD) method [32]. In this study, we employed the Spectral Fitting Model (SFM) algorithm. This method performs least-squares fitting using multiple spectral bands over a relatively wide wavelength window based on the natural spectral characteristics of both SIF and surface reflectance to reconstruct a continuous SIF spectral curve. It assumes that surface reflectance and the fluorescence spectrum conform to specific mathematical functions (e.g., linear, polynomial, or Gaussian functions), enabling spectral fitting and inversion of the SIF signal [30,33]):

$$L(\lambda) = \frac{r_{MOD}(\lambda)\cdot E(\lambda)}{\pi} + F_{MOD} + \varepsilon(\lambda) = L_{MOD}(\lambda) + \varepsilon(\lambda) \quad (4)$$

where $r_{MOD}(\lambda)$ is the modeled reflectance, $F_{MOD}(\lambda)$ is the modeled fluorescence, $L_{MOD}(\lambda)$ is the modeled apparent radiance, and $\varepsilon(\lambda)$ is the residual between the observed and modeled values at each wavelength, representing the model fitting error.

The SFM algorithm was adopted as the standard fluorescence retrieval algorithm for the FLEX mission. It was widely used in top-of-atmosphere SIF retrievals in the O_2-A and O_2-B bands, and its performance and accuracy were extensively evaluated. Compared to the FLD family of algorithms, the SFM method had higher spectral resolution requirements but offered the advantage of retrieving full-spectrum fluorescence within the fitting window and greater resistance to noise.

3. Results

3.1. Seasonal Variation in GPP and SIF Under Changing Conditions

In the analysis of meteorological factors, GPP, SIF, PAR, and evapotranspiration (ET) in the study area, we observed distinct seasonal variation patterns in all of these factors. The daily average of R_g closely followed changes in PAR, but, unlike other factors, both R_g and PAR exhibited a steady decline throughout the observation period, reaching approximately half of their values in winter compared to other seasons. Combined with precipitation data, this suggests a higher frequency of cloudy and rainy days during late summer and early autumn (Figure 2b,e), contributing to greater fluctuations prior to the onset of winter. The daily average T_{air} ranged from −13.8 °C to 30.0 °C and dropped below 0 °C on Julian day (DOY) 322 (where DOY represents the day of the year starting from January 1st as DOY 1) (Figure 2a). Similarly, the soil water content (SWC) at a depth of 10 cm exhibited seasonal trends similar to those of radiation and temperature, with significant fluctuations in late summer and autumn, and it remained low and stable during winter (Figure 2h). Distinct from other meteorological variables, VPD showed substantial fluctuations until approximately DOY 320, after which it rapidly decreased and stabilized (Figure 2g). Overall, GPP, SIF, and all meteorological factors exhibited a declining trend from DOY 230 to DOY 360 (Figure 2). During late summer and autumn (DOY 230–270), GPP and SIF fluctuated sharply. Further analysis of rainfall, radiation, soil moisture, and VPD indicated similar fluctuations during the same period. Particularly noteworthy is the transitional period between autumn and winter (DOY 290–310), during which temperature dropped below 0 °C and VPD plummeted from around 10 kPa to near 0, accompanied by sharp declines in SIF, GPP, and ET. Compared to other meteorological factors, ET and SIF exhibited the most synchronized temporal response to seasonal changes (Figure 2d,f), both approaching zero around DOY 293. Notably, SIF declined more rapidly than GPP, leading by approximately 20 days (DOY 285–310), and it approached zero earlier.

In addition to overall seasonal patterns, the diel dynamics of CO_2 fluxes revealed distinct seasonal differences (Figure 3). Because plant respiration emits CO_2, CO_2 fluxes are positive during the day, indicating a carbon source, and negative at night, indicating a carbon sink. From August to December, NEE in the study area was 100.875 $gC \cdot m^{-2}$, suggesting that the ecosystem functioned predominantly as a carbon sink. The only exception occurred in November, where it acted as a carbon source, releasing 0.989 $gC \cdot m^{-2}$.

Trends in GPP and Reco exhibited similar temporal trends, characterized by an initial increase followed by a subsequent decline. The diurnal variation in NEE exhibited a "U-shaped" pattern (Figure 3), with negative values during daylight hours and positive values at night. In August, the minimum NEE reached −7.0 $\mu mol \cdot m^{-2} \cdot s^{-1}$ at approximately 12:00, while in December the minimum dropped only to −3.62 $\mu mol \cdot m^{-2} \cdot s^{-1}$ around 10:00, indicating a significant seasonal decline in photosynthetic capacity.

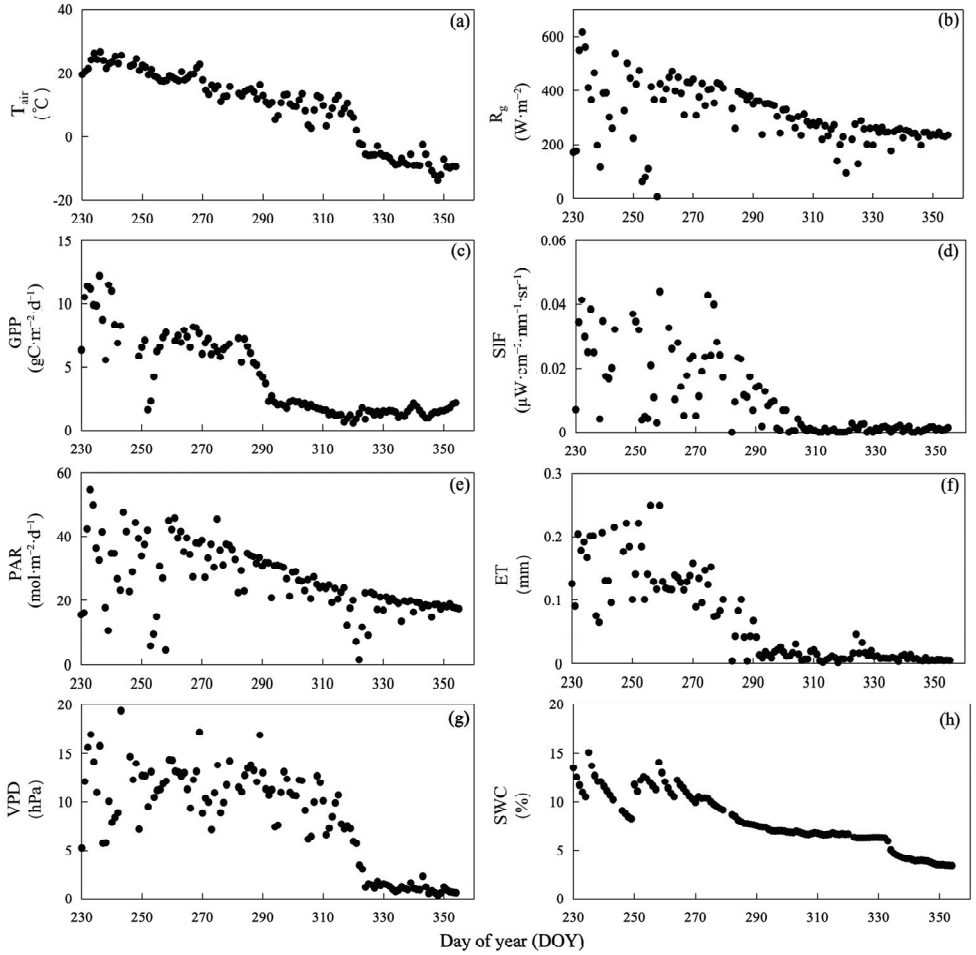


Figure 2. Seasonal variation in ENF. T_{air} (**a**), R_g (**b**), GPP (**c**), SIF (**d**), PAR (**e**), ET (**f**), VPD (**g**) and SWC (**h**) from August to December.

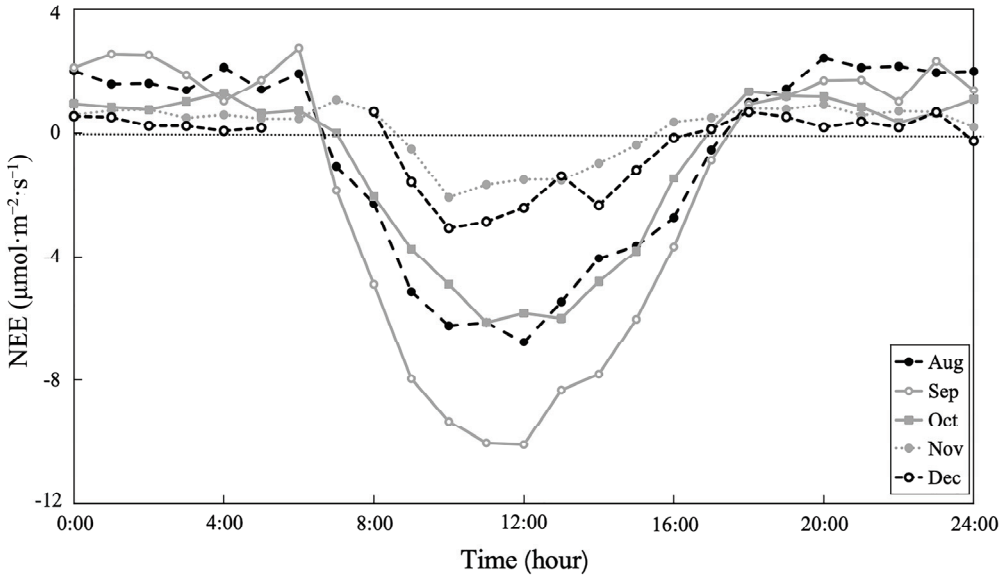


Figure 3. Diurnal variation of CO_2 fluxes by month in ENF from August to December.

From August to December, the timing of the minimum (most negative) NEE advanced from around 12:00 to 10:00, indicating a seasonal decline in photosynthetic capacity. Similarly, the transition from a carbon sink back to a source occurred between 16:30 and 17:30, with later transitions observed closer to the peak of the growing season (Figure 3).

3.2. Variations in the Correlation Between GPP and SIF Under Seasonal Transitions

At the half-hourly scale, both SIF and GPP exhibited strong temporal correspondence across different months (Figure 4). The hourly R^2 values for each month were August—0.698; September—0.748; October—0.884; November—0.452; and December—0.293. Both SIF and GPP exhibited diurnal patterns with values increasing from morning to midday, peaking around 12:00, and declining in the afternoon. However, GPP exhibited a more stable temporal pattern compared to SIF. From August to December, the SIF value at 12:00 decreased from 0.42 to 0.003 $\mu W \cdot cm^{-2} \cdot nm^{-1} \cdot sr^{-1}$, while GPP decreased from 14.35 $gC \cdot m^{-2} \cdot day^{-1}$ to 2.84 $gC \cdot m^{-2} \cdot day^{-1}$. Notably, SIF responded earlier than GPP in terms of both its daily onset and decline. At sunrise (around 6:30), while GPP remained minimal, SIF had already responded to early light conditions. In the afternoon (around 17:00), SIF had nearly dropped to zero, while GPP continued to decline. These observations suggest that weak photosynthetic activity persisted in the ENF during the winter months of November and December.

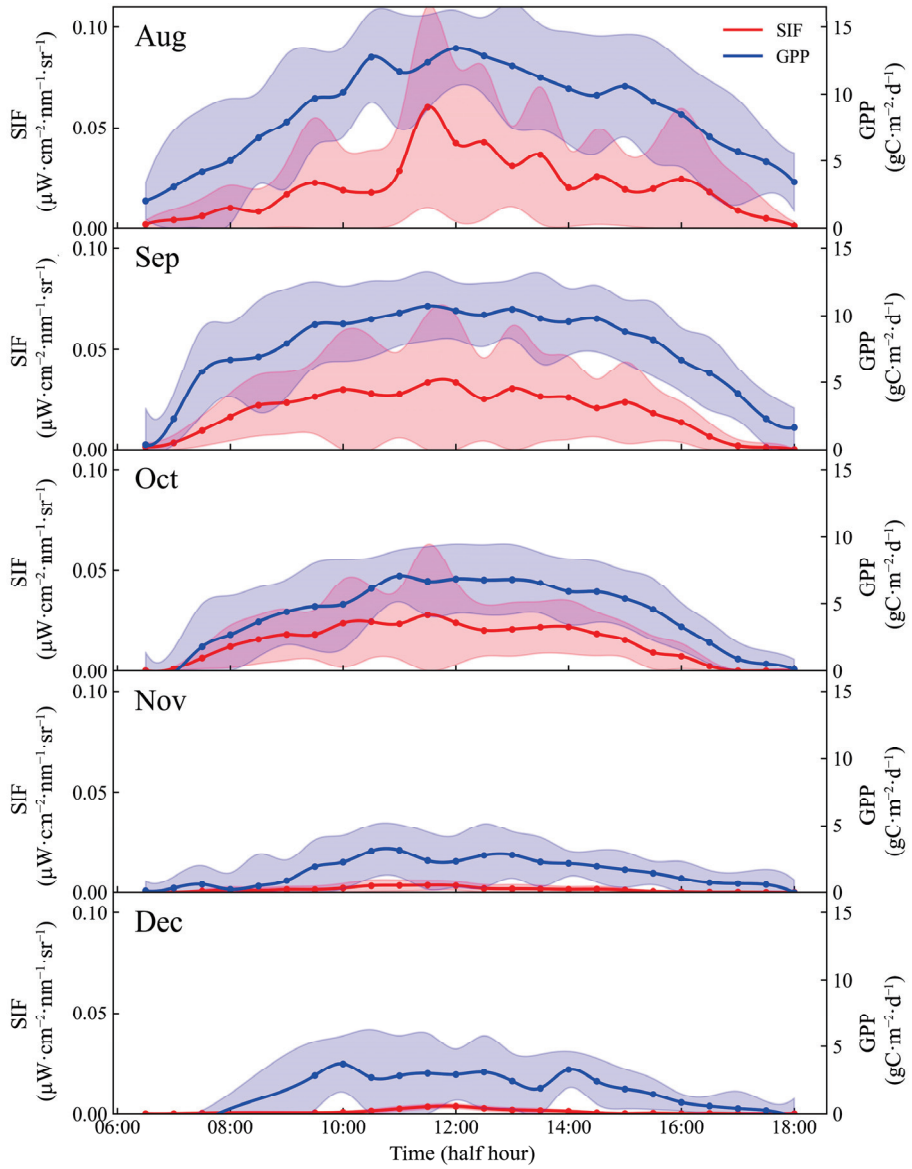


Figure 4. Diurnal variation of SIF and GPP by month in ENF from August to December.

At the daily scale, our results indicated a significant linear relationship between GPP and SIF in the *Pinus sylvestris* var. *mongolica* plantation from August to December, with an

overall coefficient of determination (R^2) of 0.6784 (Figure 5). This relationship was consistently strong at both daily and sub-daily scales (Figure 5). Specifically, the monthly correlations (R^2) between GPP and SIF were August—0.626; September—0.249; October—0.619; November—0.301; and December—0.086. During August and September, the scatter points were densely distributed along the regression line, with daily GPP values ranging from 1.65 to 12.25 $gC \cdot m^{-2} \cdot day^{-1}$ and SIF values from 0.003 to 0.045 $\mu W \cdot cm^{-2} \cdot nm^{-1} \cdot sr^{-1}$, indicating both high photosynthetic activity and strong SIF sensitivity. In contrast, October and November were characterized by low solar radiation and frequent cloudy days, leading to larger scatter in the data and a weakened correlation, with SIF below 0.004 $\mu W \cdot cm^{-2} \cdot nm^{-1} \cdot sr^{-1}$ and GPP rarely exceeding 2.0 $gC \cdot m^{-2} \cdot day^{-1}$.

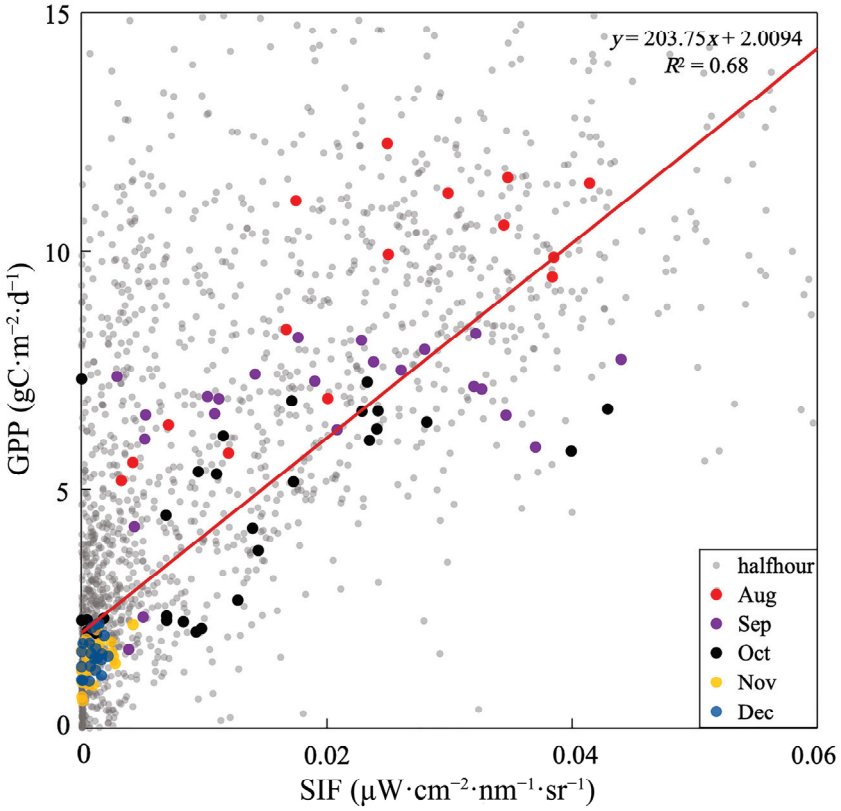


Figure 5. Relationship between SIF and GPP in ENF from August to December. (Gray points represent half-hourly values; colored points indicate daily means. The red regression line is fitted to the daily mean values).

The correlation peaked in October during the seasonal transition from autumn to winter (DOY 290–310), a period of the most pronounced changes in both variables. In contrast, during September—characterized by low radiation and frequent cloudy or rainy days—the SIF–GPP correlation weakened. As winter approached and photosynthetic activity nearly ceased, the relationship became negligible by December.

We analyzed the sensitivity of SIF and GPP to key meteorological factors, including PAR, VPD, ET, R_g, T_{air}, and SWC. Although both SIF and GPP were significantly influenced by environmental factors, their correlation patterns exhibited notable differences (Figure 6).

Both SIF and GPP showed strong positive correlations with most environmental factors, especially with ET, PAR, and SWC. However, there were differences in the strength of these correlations. For instance, the correlation between SIF and ET was 0.78, whereas GPP and ET showed a higher correlation of 0.84, indicating that ET has a more significant impact on GPP. Conversely, SIF was slightly more sensitive to PAR (R^2 = 0.79) compared to GPP (R^2 = 0.72).

Furthermore, the two indicators responded differently to temperature and radiation. SIF exhibited stronger correlations with T_{air} and R_g (R^2 = 0.64 and 0.71), while the correlations between GPP and these factors were slightly lower (R^2 = 0.77 and 0.66). This suggests that SIF, as a proxy for chlorophyll fluorescence, responds more acutely to light and thermal conditions, while GPP—representing broader canopy-level carbon assimilation—is more regulated by the combined effects of temperature and water availability.

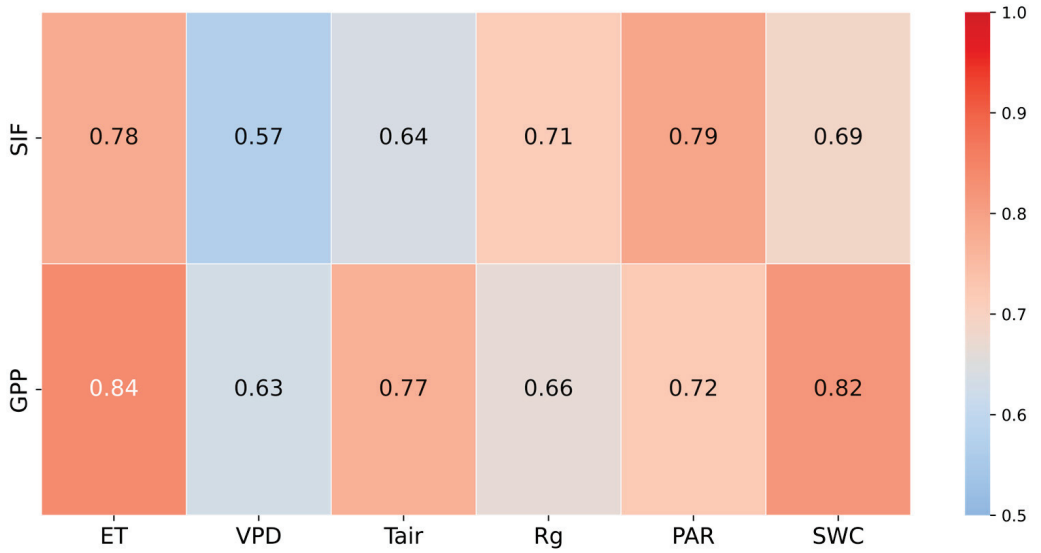


Figure 6. The relationship between SIF, GPP and ET, VPD, T_{air}, R_g, PAR, and SWC.

In summary, although SIF and GPP are both modulated by common environmental factors, SIF appears more sensitive to light-related variables, while GPP is more dependent on moisture and thermal conditions. The differences in the correlation strengths between SIF and GPP provide valuable insights for further understanding how environmental factors influence plant photosynthesis and ecosystem carbon dynamics.

4. Discussion

4.1. Carbon Sequestration Capacity Across Different Ecosystems in Semi-Arid Regions

The NEE of the ENF (*Pinus sylvestris* var. *mongolica*) from August to December was −100.875 gC·m^{-2}, indicating that the ecosystem functioned as a carbon sink. Previous studies have reported relatively high carbon sink capacities in comparable arid ecosystems. For example, the Mojave Desert in the United States exhibited a total NEE ranging from −127 to −102 gC·m^{-2} [34,35], which is higher than that reported for the Tengger Desert in China (−23.4 to −13.9 gC·m^{-2}) [36] and the Fukang Desert ecosystem (−49 gC·m^{-2}) [37]. Other studies have also reported significant variability in the carbon source–sink status, even within the same desert ecosystem. For instance observed that the NEE in the Baja California region of Mexico ranged from −52 to −9 gC·m^{-2} [38].

In comparison, the total NEE of the ENF (*Pinus sylvestris* var. *mongolica*) was higher than that of other semi−arid ecosystems in northern China, such as the desert steppe in Inner Mongolia (−69 to −7.2 gC·m^{-2}) [39] and the semi-arid degraded grassland in Tongyu, Jilin (−73 to 0.32 gC·m^{-2}) [40]. Overall, these results suggest that the ENF, as one of the key afforestation species in China's "The Great Green Wall" Shelterbelt Project, possesses a strong carbon sequestration capacity, highlighting its important role in sand fixation and ecological protection.

4.2. SIF and GPP Relationship and Environmental Drivers

Previous studies have consistently demonstrated a significant linear relationship between GPP and SIF across a variety of ecosystem types. Strong correlations have been observed in deciduous broadleaf forests, such as beech (*Fagus grandifolia Ehrh*) and red oak (*Quercus rubra*), at the Harvard Forest site in the United States [24], as well as in key agricultural systems, including soybean (*Glycine max* L. *Merr*) fields in Iowa [19], rice (*Oryza sativa* L.) paddies in Jurong, China [26], and maize (*Zea mays* L.) fields in both Maryland, USA [25], and Zhangye, China [41].

In agreement with these findings, our study revealed a significant linear correlation between SIF and GPP in the temperate evergreen needleleaf forest (ENF), with a coefficient of determination (R^2) of 0.678. In the ENF, the relationship between SIF and GPP is jointly influenced by absorbed photosynthetically active radiation (APAR), as well as by the distinct stability of the canopy structure and the seasonal dynamics of leaf-level physiology [27]. Compared to crops and deciduous forests, ENFs exhibit minimal seasonal variation in canopy structural parameters, such as leaf area index (LAI), leaf angle distribution, and leaf clumping, leading to a relatively stable canopy escape fraction (f_{esc}) [42]. However, this relationship was not temporally uniform. Seasonal changes in environmental conditions, particularly radiation and precipitation, were found to influence the strength of the SIF–GPP coupling. For example, due to more frequent cloudy and rainy days, the correlation in August was markedly weaker than that observed in September and October, which were characterized by higher radiation levels. In ENFs, seasonal variation in SIF is primarily driven by changes in the chlorophyll fluorescence yield (Φ_F), which is regulated by physiological adjustments in response to environmental stresses. For instance, during winter, ENF trees activate photoprotective mechanisms that increase the carotenoid/chlorophyll ratio, enhancing sustained non-photochemical quenching (Φ_{sNPQ}) to prevent photodamage [43]. As environmental conditions improve in spring, this mechanism is reversed, allowing for higher $\Phi_{PS(II)}$ and reversible NPQ (Φ_{rNPQ}) to dominate energy partitioning [44]. In contrast, GPP is mainly regulated by canopy light use efficiency (LUE_P) and leaf gas exchange. Thus, the SIF–GPP relationship in ENFs reflects a unique coupling between stable canopy structure and seasonally dynamic leaf physiology [21].

These results suggest that the SIF–GPP relationship is modulated by environmental drivers, with SIF and GPP exhibiting different sensitivities to microclimatic factors. While GPP reflects net carbon assimilation and is influenced by both radiative and physiological constraints, SIF is more directly linked to absorbed light and its subsequent dissipation. Our continuous ground-based observations during autumn and early winter provided detailed insight into canopy SIF responses under variable weather conditions. The diurnal patterns of SIF differed seasonally, with stronger signals in autumn and near-zero levels in winter. This is consistent with observations in coniferous forests in Colorado [21].

Notably, SIF exhibited a continuous increase with PAR throughout the growing season, with no evidence of midday depression or saturation. In contrast, GPP was primarily regulated by SWC. This partial decoupling of SIF and GPP under certain conditions is consistent with findings from rice paddies, where SIF showed a stronger correlation with absorbed light than GPP did [45]. The divergence arises from energy allocation mechanisms, as SIF serves as an important non-photochemical dissipation pathway that protects the photosynthetic apparatus under excess light, whereas GPP depends on additional biochemical and water-related constraints.

Furthermore, Chen et al. [46] reported that GPP and SIF tend to decline along a climatic gradient from cold and humid regions to hot and arid regions. Their study also found that under equivalent temperature conditions, increased precipitation can elevate the GPP/SIF ratio. This is consistent with our observations, where frequent precipitation in August likely

disrupted direct coupling between SIF and GPP, leading to a lower correlation compared to the drier months of September and October.

4.3. Limitations and Uncertainties

Although this study benefits from continuous, ground-based observations of both SIF and GPP in a semi-arid evergreen needleleaf forest, several limitations and uncertainties remain that should be addressed in future work.

First, the issue of footprint mismatch between flux and spectral observations may affect the accuracy of the observed SIF–GPP relationship. While both the EC system and the automated tower-based spectral system were installed on the same tower and the SIF field of view was largely within the EC footprint, this does not fully resolve the potential discrepancy in spatial representativeness. In heterogeneous or semi-structured ecosystems, such as semi-arid woodlands, even slight misalignments between the observation footprints can introduce inconsistencies in data interpretation [47,48]. A more detailed analysis of spatial matching, including high-resolution footprint modeling, is recommended to further constrain this source of uncertainty.

Second, this study focused on a single vegetation type within a semi-arid biome. While the ENF ecosystem is a representative afforestation type in northern China, the applicability of our findings to other semi-arid ecosystems, such as desert steppe, shrubland, or mixed savanna, remains unclear. Future studies should consider the deployment of coordinated multi-site observational networks that encompass diverse ecosystem types, thereby enabling cross-site comparisons of SIF–GPP relationships under different structural and climatic regimes.

Third, our results highlight the high sensitivity of SIF to incident radiation, particularly under varying sky conditions. SIF values measured only on clear days may overestimate the seasonal mean value, especially during periods with frequent cloudy or rainy weather. This suggests that solar radiation conditions play a critical role in shaping the observed SIF–GPP relationship, at both diurnal and seasonal scales. As such, future studies should incorporate the classification of sky conditions (e.g., clear vs. overcast) into the analysis framework to better interpret the SIF response. Distinguishing between the influence of diffuse versus direct radiation on SIF could also help reveal mechanisms underlying its variability and decoupling from GPP [49].

Taken together, these limitations suggest that although SIF holds strong potential as a proxy for photosynthetic activity, its interpretation requires careful consideration of the observational scale, ecosystem diversity, and the environmental context. Addressing these uncertainties will be essential for improving the robustness of SIF-based GPP estimation models, particularly in complex, semi-arid landscapes.

5. Conclusions

Based on the study conducted in the ENF (*Pinus sylvestris* var. *mongolica*) plantation, we found the following. (1) From August to December, the total net carbon uptake of the Mongolian Scots pine plantation was 100.875 $gC \cdot m^{-2}$, indicating that the ecosystem functioned overall as a carbon sink. The diurnal variation of CO_2 flux exhibited a "U-shaped" pattern, with the strongest carbon sequestration occurring at 12:00 noon. Under seasonal transition conditions, both GPP and SIF exhibited a gradual decline, with greater fluctuations during autumn and particularly strong responses during the transition from autumn to winter. (2) Meteorological factors in the plantation showed distinct seasonal variation patterns. A clear linear relationship was observed between SIF and GPP (R^2 = 0.678), with high consistency at both daily and sub-daily time scales. The correlation between SIF and GPP was especially strong at the sub-daily scale, and SIF was found to respond to photosyn-

thetic activity earlier than GPP. Their correlation was strongest during the autumn–winter transition period. Both SIF and GPP reached their peak around 12:00 noon, although GPP exhibited a more stable diurnal pattern than SIF. Notably, even during winter months (November and December), weak photosynthetic activity was still detected through both SIF and GPP. Furthermore, both SIF and GPP were closely related to soil water content and total radiation, and their relationship was significantly affected by cloudy and rainy weather conditions.

Author Contributions: Conceptualization, F.W. and K.Y.; methodology, F.W. and K.Y.; investigation, W.C. and K.Y.; data curation, W.C. and K.Y.; writing—original draft preparation, K.Y.; writing—review and editing, Y.C., F.W., and K.Y.; visualization, X.L. and K.Y.; supervision, F.W. and Y.F.; project administration, F.W. All authors have read and agreed to the published version of the manuscript.

Funding: This work was supported by the Fundamental Research Funds of the Chinese Academy of Forestry (Grants No. CAFYBB2020QD002, CAFYBB2021MC002 and CAFYBB2023ZA009), and the National Natural Science Foundation of China (Grant No. 32171875, 32371960).

Data Availability Statement: The original contributions presented in this study are included in the article. Further inquiries can be directed to the corresponding author.

Conflicts of Interest: The authors declare no conflicts of interest.

References

1. Jeong, S.; Park, H. Toward a Comprehensive Understanding of Global Vegetation CO_2 Assimilation from Space. *Glob. Change Biol.* **2021**, *27*, 1141–1143. [CrossRef] [PubMed]
2. Rodda, S.R.; Thumaty, K.C.; Jha, C.S.; Dadhwal, V.K. Seasonal Variations of Carbon Dioxide, Water Vapor and Energy Fluxes in Tropical Indian Mangroves. *Forests* **2016**, *7*, 35. [CrossRef]
3. Mamkin, V.; Varlagin, A.; Yaseneva, I.; Kurbatova, J. Response of Spruce Forest Ecosystem CO_2 Fluxes to Inter-Annual Climate Anomalies in the Southern Taiga. *Forests* **2022**, *13*, 1019. [CrossRef]
4. Han, C.; Li, Y.; Dong, X.; Zhao, C.; An, L. Pinus Tabulaeformis Forests Have Higher Carbon Sequestration Potential Than Larix Principis-Rupprechtii Forests in a Dryland Mountain Ecosystem, Northwest China. *Forests* **2022**, *13*, 739. [CrossRef]
5. Dou, X.; Yang, Y. Modeling and Predicting Carbon and Water Fluxes Using Data-Driven Techniques in a Forest Ecosystem. *Forests* **2017**, *8*, 498. [CrossRef]
6. Park, H.; Jeong, S.; Penuelas, J. Accelerated Rate of Vegetation Green-up Related to Warming at Northern High Latitudes. *Glob. Change Biol.* **2020**, *26*, 6190–6202. [CrossRef]
7. Baldocchi, D. Breathing of the Terrestrial Biosphere: Lessons Learned from a Global Network of Carbon Dioxide Flux Measurement Systems. *Aust. J. Bot.* **2008**, *56*, 1–26. [CrossRef]
8. Anic, M.; Sever, M.Z.O.; Alberti, G.; Balenovic, I.; Paladinic, E.; Peressotti, A.; Tijan, G.; Vecenaj, Z.; Vuletic, D.; Marjanovic, H. Eddy Covariance vs. Biometric Based Estimates of Net Primary Productivity of Pedunculate Oak (*Quercus robur* L.) Forest in Croatia during Ten Years. *Forests* **2018**, *9*, 764. [CrossRef]
9. Ma, X.; Feng, Q.; Yu, T.; Su, Y.; Deo, R.C. Carbon Dioxide Fluxes and Their Environmental Controls in a Riparian Forest within the Hyper-Arid Region of Northwest China. *Forests* **2017**, *8*, 379. [CrossRef]
10. Reichstein, M.; Falge, E.; Baldocchi, D.; Papale, D.; Aubinet, M.; Berbigier, P.; Bernhofer, C.; Buchmann, N.; Gilmanov, T.; Granier, A.; et al. On the Separation of Net Ecosystem Exchange into Assimilation and Ecosystem Respiration: Review and Improved Algorithm. *Glob. Change Biol.* **2005**, *11*, 1424–1439. [CrossRef]
11. Baldocchi, D.D.; Hincks, B.B.; Meyers, T.P. Measuring Biosphere–Atmosphere Exchanges of Biologically Related Gases with Micrometeorological Methods. *Ecology* **1988**, *69*, 1331–1340. [CrossRef]
12. Schimel, D.; Pavlick, R.; Fisher, J.B.; Asner, G.P.; Saatchi, S.; Townsend, P.; Miller, C.; Frankenberg, C.; Hibbard, K.; Cox, P. Observing Terrestrial Ecosystems and the Carbon Cycle from Space. *Glob. Change Biol.* **2015**, *21*, 1762–1776. [CrossRef]
13. Huemmrich, K.F.; Campbell, P.; Landis, D.; Middleton, E. Developing a Common Globally Applicable Method for Optical Remote Sensing of Ecosystem Light Use Efficiency. *Remote Sens. Environ.* **2019**, *230*, 111190. [CrossRef]
14. Tucker, C.J.; Fung, I.Y.; Keeling, C.D.; Gammon, R.H. Relationship between Atmospheric CO_2 Variations and a Satellite-Derived Vegetation Index. *Nature* **1986**, *319*, 195–199. [CrossRef]

15. Guanter, L.; Zhang, Y.; Jung, M.; Joiner, J.; Voigt, M.; Berry, J.A.; Frankenberg, C.; Huete, A.R.; Zarco-Tejada, P.; Lee, J.-E.; et al. Global and Time-Resolved Monitoring of Crop Photosynthesis with Chlorophyll Fluorescence. *Proc. Natl. Acad. Sci. USA* **2014**, *111*, E1327–E1333. [CrossRef]
16. Piao, S.; Fang, J.; Ciais, P.; Peylin, P.; Huang, Y.; Sitch, S.; Wang, T. The Carbon Balance of Terrestrial Ecosystems in China. *Nature* **2009**, *458*, 1009–1013. [CrossRef]
17. Tan, C.; Samanta, A.; Jin, X.; Tong, L.; Ma, C.; Guo, W.; Knyazikhin, Y.; Myneni, R.B. Using Hyperspectral Vegetation Indices to Estimate the Fraction of Photosynthetically Active Radiation Absorbed by Corn Canopies. *Int. J. Remote Sens.* **2013**, *34*, 8789–8802. [CrossRef]
18. Mohammed, G.H.; Colombo, R.; Middleton, E.M.; Rascher, U.; van der Tol, C.; Nedbal, L.; Goulas, Y.; Pérez-Priego, O.; Damm, A.; Meroni, M.; et al. Remote Sensing of Solar-Induced Chlorophyll Fluorescence (SIF) in Vegetation: 50 Years of Progress. *Remote Sens. Environ.* **2019**, *231*, 111177. [CrossRef]
19. He, L.; Magney, T.; Dutta, D.; Yin, Y.; Köhler, P.; Grossmann, K.; Stutz, J.; Dold, C.; Hatfield, J.; Guan, K.; et al. From the Ground to Space: Using Solar-Induced Chlorophyll Fluorescence to Estimate Crop Productivity. *Geophys. Res. Lett.* **2020**, *47*, 12. [CrossRef]
20. Frankenberg, C.; Fisher, J.B.; Worden, J.; Badgley, G.; Saatchi, S.S.; Lee, J.-E.; Toon, G.C.; Butz, A.; Jung, M.; Kuze, A.; et al. New Global Observations of the Terrestrial Carbon Cycle from GOSAT: Patterns of Plant Fluorescence with Gross Primary Productivity. *Geophys. Res. Lett.* **2011**, *38*, L17706. [CrossRef]
21. Magney, T.S.; Bowling, D.R.; Logan, B.A.; Grossmann, K.; Stutz, J.; Blanken, P.D.; Burns, S.P.; Cheng, R.; Garcia, M.A.; Köhler, P.; et al. Mechanistic Evidence for Tracking the Seasonality of Photosynthesis with Solar-Induced Fluorescence. *Proc. Natl. Acad. Sci. USA* **2019**, *116*, 11640–11645. [CrossRef] [PubMed]
22. Sun, Y.; Frankenberg, C.; Wood, J.D.; Schimel, D.S.; Jung, M.; Guanter, L.; Drewry, D.T.; Verma, M.; Porcar-Castell, A.; Griffis, T.J.; et al. OCO-2 Advances Photosynthesis Observation from Space via Solar-Induced Chlorophyll Fluorescence. *Science* **2017**, *6360*, 189. [CrossRef]
23. Köhler, P.; Frankenberg, C.; Magney, T.S.; Guanter, L.; Joiner, J.; Landgraf, J. Global Retrievals of Solar-Induced Chlorophyll Fluorescence with TROPOMI: First Results and Intersensor Comparison to OCO-2. *Geophys. Res. Lett.* **2018**, *45*, 10456–10463. [CrossRef]
24. Lu, X.; Liu, Z.; Zhao, F.; Tang, J. Comparison of Total Emitted Solar-Induced Chlorophyll Fluorescence (SIF) and Top-of-Canopy (TOC) SIF in Estimating Photosynthesis. *Remote Sens. Environ.* **2020**, *251*, 112083. [CrossRef]
25. Yang, P.; van der Tol, C.; Campbell, P.K.E.; Middleton, E.M. Unraveling the Physical and Physiological Basis for the Solar-Induced Chlorophyll Fluorescence and Photosynthesis Relationship Using Continuous Leaf and Canopy Measurements of a Corn Crop. *Biogeosciences* **2021**, *18*, 441–465. [CrossRef]
26. Chou, S.; Chen, B.; Chen, J.M. Multi-Angular Instrument for Tower-Based Observations of Canopy Sun-Induced Chlorophyll Fluorescence. *Instrum. Sci. Technol.* **2020**, *48*, 146–161. [CrossRef]
27. Kim, J.; Ryu, Y.; Dechant, B.; Lee, H.; Kim, H.S.; Kornfeld, A.; Berry, J.A. Solar-Induced Chlorophyll Fluorescence Is Non-Linearly Related to Canopy Photosynthesis in a Temperate Evergreen Needleleaf Forest during the Fall Transition. *Remote Sens. Environ.* **2021**, *258*, 112362. [CrossRef]
28. Liang, J.; Crowther, T.W.; Picard, N.; Wiser, S.; Zhou, M.; Alberti, G.; Schulze, E.-D.; McGuire, A.D.; Bozzato, F.; Pretzsch, H.; et al. Positive Biodiversity–Productivity Relationship Predominant in Global Forests. *Science* **2016**, *354*, aaf8957. [CrossRef] [PubMed]
29. Pan, Y.; Birdsey, R.A.; Fang, J.; Houghton, R.; Kauppi, P.E.; Kurz, W.A.; Phillips, O.L.; Shvidenko, A.; Lewis, S.L.; Canadell, J.G.; et al. A Large and Persistent Carbon Sink in the World's Forests. *Science* **2011**, *333*, 988–993. [CrossRef]
30. Wutzler, T.; Lucas-Moffat, A.; Migliavacca, M.; Knauer, J.; Sickel, K.; Šigut, L.; Menzer, O.; Reichstein, M. Basic and Extensible Post-Processing of Eddy Covariance Flux Data with REddyProc. *Biogeosciences* **2018**, *15*, 5015–5030. [CrossRef]
31. Falge, E.; Baldocchi, D.; Olson, R.; Anthoni, P.; Aubinet, M.; Bernhofer, C.; Burba, G.; Ceulemans, R.; Clement, R.; Dolman, H.; et al. Gap Filling Strategies for Defensible Annual Sums of Net Ecosystem Exchange. *Agric. For. Meteorol.* **2001**, *107*, 43–69. [CrossRef]
32. Plascyk, J.A.; Gabriel, F.C. The Fraunhofer Line Discriminator MKII—An Airborne Instrument for Precise and Standardized Ecological Luminescence Measurement. *IEEE Trans. Instrum. Meas.* **1975**, *24*, 306–313. [CrossRef]
33. Cogliati, S.; Verhoef, W.; Kraft, S.; Sabater, N.; Alonso, L.; Vicent, J.; Moreno, J.; Drusch, M.; Colombo, R. Retrieval of Sun-Induced Fluorescence Using Advanced Spectral Fitting Methods. *Remote Sens. Environ.* **2015**, *169*, 344–357. [CrossRef]
34. Jasoni, R.L.; Smith, S.D.; Arnone, J.A., III. Net Ecosystem CO_2 Exchange in Mojave Desert Shrublands during the Eighth Year of Exposure to Elevated CO_2. *Glob. Change Biol.* **2005**, *11*, 749–756. [CrossRef]
35. Wohlfahrt, G.; Fenstermaker, L.F.; Arnone Iii, J.A. Large Annual Net Ecosystem CO_2 Uptake of a Mojave Desert Ecosystem. *Glob. Change Biol.* **2008**, *14*, 1475–1487. [CrossRef]
36. Gao, Y.; Li, X.; Liu, L.; Jia, R.; Yang, H.; Li, G.; Wei, Y. Seasonal Variation of Carbon Exchange from a Revegetation Area in a Chinese Desert. *Agric. For. Meteorol.* **2012**, *156*, 134–142. [CrossRef]

37. Liu, R.; Li, Y.; Wang, Q.-X. Variations in water and CO_2 fluxes over a saline desert in western China. *Hydrol. Process.* **2012**, *26*, 513–522. [CrossRef]
38. Hastings, S.J.; Oechel, W.C.; Muhlia-Melo, A. Diurnal, Seasonal and Annual Variation in the Net Ecosystem CO_2 Exchange of a Desert Shrub Community (Sarcocaulescent) in Baja California, Mexico. *Glob. Change Biol.* **2005**, *11*, 927–939. [CrossRef]
39. Yang, F.; Zhou, G.; Hunt, J.E.; Zhang, F. Biophysical Regulation of Net Ecosystem Carbon Dioxide Exchange over a Temperate Desert Steppe in Inner Mongolia, China. *Agric. Ecosyst. Environ.* **2011**, *142*, 318–328. [CrossRef]
40. Du, Q.; Liu, H.; Feng, J.; Wang, L.; Huang, J.; Zhang, W.; Christian, B. Carbon Dioxide Exchange Processes over the Grassland Ecosystems in Semiarid Areas of China. *Sci. China Earth Sci.* **2012**, *55*, 644–655. [CrossRef]
41. Cui, T.; Sun, R.; Qiao, C.; Zhang, Q.; Yu, T.; Liu, G.; Liu, Z. Estimating Diurnal Courses of Gross Primary Production for Maize: A Comparison of Sun-Induced Chlorophyll Fluorescence, Light-Use Efficiency and Process-Based Models. *Remote Sens.* **2017**, *9*, 1267. [CrossRef]
42. Lee, H.; Park, J.; Cho, S.; Lee, M.; Kim, H.S. Impact of Leaf Area Index from Various Sources on Estimating Gross Primary Production in Temperate Forests Using the JULES Land Surface Model. *Agric. For. Meteorol.* **2019**, *276–277*, 107614. [CrossRef]
43. Míguez, F.; Fernández-Marín, B.; Becerril, J.M.; García-Plazaola, J.I. Activation of Photoprotective Winter Photoinhibition in Plants from Different Environments: A Literature Compilation and Meta-Analysis. *Physiol. Plant.* **2015**, *155*, 414–423. [CrossRef] [PubMed]
44. Porcar-Castell, A. A High-Resolution Portrait of the Annual Dynamics of Photochemical and Non-Photochemical Quenching in Needles of Pinus Sylvestris. *Physiol. Plant.* **2011**, *143*, 139–153. [CrossRef]
45. Yang, K.; Ryu, Y.; Dechant, B.; Berry, J.A.; Hwang, Y.; Jiang, C.; Kang, M.; Kim, J.; Kimm, H.; Kornfeld, A.; et al. Sun-Induced Chlorophyll Fluorescence Is More Strongly Related to Absorbed Light than to Photosynthesis at Half-Hourly Resolution in a Rice Paddy. *Remote Sens. Environ.* **2018**, *216*, 658–673. [CrossRef]
46. Chen, A.; Mao, J.; Ricciuto, D.; Lu, D.; Xiao, J.; Li, X.; Thornton, P.E.; Knapp, A.K. Seasonal Changes in GPP/SIF Ratios and Their Climatic Determinants across the Northern Hemisphere. *Glob. Change Biol.* **2021**, *27*, 5186–5197. [CrossRef]
47. Qiu, R.; Han, G.; Ma, X.; Sha, Z.; Shi, T.; Xu, H.; Zhang, M. CO_2 Concentration, A Critical Factor Influencing the Relationship between Solar-Induced Chlorophyll Fluorescence and Gross Primary Productivity. *Remote Sens.* **2020**, *12*, 1377. [CrossRef]
48. Liu, X.; Liu, L.; Hu, J.; Du, S. Modeling the Footprint and Equivalent Radiance Transfer Path Length for Tower-Based Hemispherical Observations of Chlorophyll Fluorescence. *Sensors* **2017**, *17*, 1131. [CrossRef]
49. Cogliati, S.; Rossini, M.; Julitta, T.; Meroni, M.; Schickling, A.; Burkart, A.; Pinto, F.; Rascher, U.; Colombo, R. Continuous and Long-Term Measurements of Reflectance and Sun-Induced Chlorophyll Fluorescence by Using Novel Automated Field Spectroscopy Systems. *Remote Sens. Environ.* **2015**, *164*, 270–281. [CrossRef]

Disclaimer/Publisher's Note: The statements, opinions and data contained in all publications are solely those of the individual author(s) and contributor(s) and not of MDPI and/or the editor(s). MDPI and/or the editor(s) disclaim responsibility for any injury to people or property resulting from any ideas, methods, instructions or products referred to in the content.

forests

MDPI

Article

The Effects of Inoculation with Rhizosphere Phosphate-Solubilizing Bacteria on the Growth and Physiology of *Reaumuria soongorica* Seedlings Under NaCl Stress

Xueying Wang, Peifang Chong *, Xinguang Bao and Feng Zhang

College of Forest, Gansu Agriculture University, Lanzhou 730030, China; 107332202196@st.gsau.edu.cn (X.W.); baoxg@st.gsau.edu.cn (X.B.); 107332202194@st.gsau.edu.cn (F.Z.)
* Correspondence: zhongpf@gsau.edu.cn; Tel.: +86-139-1923-5069

Abstract: Soil salinization significantly exacerbates the deficiency in plant-available phosphorus in the soil, thereby adversely affecting plant growth and development. Through various processes, phosphate-solubilizing bacteria in the rhizosphere significantly increase soil-soluble phosphorus content, boosting plant development and stress resistance. This study focused on annual *R. soongorica* seedlings to examine how rhizosphere phosphate-solubilizing bacteria enhance growth under NaCl-induced stress conditions. This study isolated and characterized rhizosphere phosphate-solubilizing bacteria, evaluating their phosphate solubilization capacity and effects on *R. soongorica* seedling growth and physiology under NaCl stress through pot experiments, with potential applications in saline soil improvement and desert ecosystem restoration. This study used four treatment groups (control group, NaCl treatment group, bacterial inoculation treatment group, and bacterial and NaCl mixed-treatment group) with twelve treatments and four replicates per treatment. The experimental results demonstrated that five phosphate-solubilizing bacterial strains exhibited a significant phosphate solubilization capacity, accompanied by a notable reduction in pH within the inorganic phosphorus medium. Compared to the NaCl treatment, the net growth of the plant height of *R. soongorica* seedlings inoculated with strains J23, J24, and M1 under NaCl stress increased significantly ($p < 0.05$), and all of them more than doubled, and the net growth of the stem diameter of *R. soongorica* seedlings inoculated with strain J24 increased significantly by 144.17%. The physiological characteristics of *R. soongorica* seedlings demonstrated significant alterations following inoculation with the five phosphate-solubilizing bacterial strains. The inoculation of *R. soongorica* seedlings with the five phosphate-solubilizing bacterial resulted in a statistically significant increase in both foliar total phosphorus content and available phosphorus levels within the rhizosphere soil ($p < 0.05$). Additionally, under NaCl stress conditions, *R. soongorica* seedlings inoculated with the five phosphate-solubilizing bacterial strains exhibited varying degrees of salt tolerance, with the following descending order of effectiveness: J24 > P2 > J23 > P3 > M1. In conclusion, the rhizosphere phosphate-solubilizing bacteria J24 represents a potentially valuable microbial resource for saline soil amelioration, demonstrating the most pronounced enhancement in both the growth parameters and salt tolerance of *R. soongorica* seedlings under 300 mmol·L^{-1} NaCl stress.

Keywords: *Reaumuria soongorica*; NaCl stress; phosphate-solubilizing bacteria; growth-promoting effect; salt tolerance

1. Introduction

Salinized soil is found throughout China with a total area of 3.69×107 hm^2 and comes in various forms. It is particularly prevalent in arid and semi-arid regions, where it significantly negatively influences the long-term viability of forestry and agriculture [1]. Soil salinization occurs when soluble salts accumulate excessively in the soil, driven by human activities and climatic factors. Key contributors include inappropriate tillage techniques, the misuse of chemical fertilizers, and climatic conditions such as high evaporation and precipitation. NaCl is the most prevalent of them [2]. Similar to other forms of abiotic stress, the excessive accumulation of soluble salts adversely affects plant growth, development, physiology, and biochemical processes. These effects include osmotic stress, ion homeostasis disruption, and reduced plant nutrient uptake [3]. Therefore, soil salinization remediation is crucial to enhancing soil usage and maintaining ecosystem stability.

Over the long-term evolution process, numerous halophytes have emerged in nature, capable of thriving in high-salinity environments and mitigating salt stress damage through diverse defence mechanisms [4]. On the one hand, plants can alleviate salt stress by maintaining cellular ion homeostasis. On the other hand, plants employ both non-enzymatic antioxidants and antioxidant enzymes to synergistically reduce the accumulation of reactive oxygen species (ROS). Additionally, the accumulation of osmoregulatory substances supports plant cell expansion and maintains adequate water uptake [5]. Furthermore, various growth-promoting bacteria in the rhizosphere may also relate to salt tolerance. Phosphate-solubilizing bacteria (PSB), a group within plant growth-promoting rhizobacteria (PGPR) in halophytes, can solubilize insoluble phosphate or mineralize organic phosphorus [6]. They enhance plants' absorption and utilization of soluble phosphorus while preventing the re-fixation of the released soluble phosphorus [7]. Additionally, they promote plant growth and improve stress tolerance through various pathways, including the production of organic acids, iron carriers, auxin, and other beneficial substances [8]. The phosphate-solubilizing bacterium *Curtobacterium luteum* has been isolated from a saline–alkali seagrass meadow. In quantitative analysis, the phosphate-solubilizing amount of the strain was 208.41 μg/mL. By inoculating three crops under saline–alkali stress, the results showed that it promoted the growth of the three crops, and the soil available phosphorus content increased significantly by 67.23%, 37.61%, and 7.47% [9]. Additionally, phosphate-solubilizing bacteria enhance the decomposition of soil insoluble or fixed phosphorus by actively participating in soil phosphorus cycling. A study inoculated MWP-1 (*Pseudomonas poae*), a highly efficient phosphorus-solubilizing bacterium, into the high-altitude Muli mining area of Qinghai Province to investigate its effects on soil properties and nutrient cycling. The results showed that the strain was able to significantly increase soil quick-acting phosphorus content by over 50%. Additionally, it altered the relative abundance of genes regulating phosphorus uptake, transport, and inorganic phosphorus solubilization within the bacterial community [10]. Therefore, rhizosphere phosphate-solubilizing bacteria in halophytes hold significant potential for mitigating soil salinization.

Phosphorus, an essential mineral nutrient for plant growth and development, plays a critical role in metabolic processes such as photosynthesis, respiration, signal transduction, and energy transfer. It is also vital for improving plant resistance to abiotic stress [11]. Under conditions of excessive salt accumulation, phosphorus is essential for maintaining the functional diversity of soil ecosystems and supporting normal plant growth. Wu Yang demonstrated a strong correlation between soil multifunctionality under salt stress and the functional diversity of soil phosphorus [12]. At the same salt concentration, reductions in treatment levels led to declines in the phosphorus content, chlorophyll content, plant height, and dry weight of *Sorghum bicolor* 'Dochna' leaves [13]. Although phosphorus is abundant in natural soil, plants can only absorb and utilize a small amount. Simultaneously, excessive

soil salt accumulation causes osmotic stress and ion toxicity, impairing plant phosphorus absorption and transport. This leads to phosphorus fixation and mineralization in the soil due to cation interactions and competition with phosphate, disrupting plant phosphorus transport, absorption, and utilization and exacerbating the deficiency in plant-available phosphorus [14]. Studies show that treating *Medicago sativa* with a certain quantity of NaCl considerably decreases its phosphorus content [15]. Consequently, improving plants' phosphorus absorption and utilization is crucial to increase their salt tolerance.

R. soongorica is a *Tamaricaceae* shrub that is highly xerophytic and stress-resistant. It serves as a key constructive and dominant species in the arid and semi-arid regions of Northwest China, playing a vital role in ecological protection and vegetation restoration in desert and grassland areas [16]. *R. soongorica* possesses a unique salt gland structure, enabling it to transport internal salts to large vesicles under salt stress, which are then excreted through the secretory cells' external membranes [17]. Some studies have found that *R. soongorica*, which belongs to salt-secreting plants, can secrete salt through its leaves to alleviate salt stress [16]. Despite its strong salt tolerance, *R. soongorica* has weak seedling resistance and slow growth, limiting its widespread use in large-scale desert vegetation restoration. The research on *R. soongorica* is predominantly focused on three main aspects: physiological characteristics [18], the influence of exogenous substances on stress resistance [19], and the screening of resistance genes. There are relatively few studies on the characteristics of bacterial community composition in the rhizosphere of *R. soongorica* and the effect of rhizosphere phosphate-solubilizing bacteria on the salt tolerance of *R. soongorica*. How does the inoculation of rhizosphere phosphate-solubilizing bacteria affect *R. soongorica*'s growth and physiological characteristics when exposed to NaCl stress? How has the phosphorus content of its rhizosphere soil and leaves changed? A series of problems, such as salt tolerance, can be improved by inoculating phosphate-solubilizing bacteria. Therefore, this paper took *R. soongorica* seedlings as the research object, analysed the effects of phosphate-solubilizing bacteria on the growth and physiological characteristics of the seedlings by applying NaCl and phosphate-solubilizing bacteria, and explored the effects of inoculating rhizosphere phosphate-solubilizing bacteria on the phosphorus content of *R. soongorica*. This study aimed to establish a scientific foundation for enhancing *R. soongorica*'s resistance to salt and to serve as a guide for improving saline soil.

2. Materials and Methods

2.1. Experimental Materials

2.1.1. Overview of the Study Area and Soil Sample Collection

Soil samples were collected in the Qingtu Lake area of Minqin County, Gansu Province, with an average annual temperature of about 7.6 °C and an average annual precipitation of 113.2 mm. The latitude and longitude of the sampling site is 39°8′10.65″ N, 103°30′19.60″ E, and the altitude is 1030.2 m. The area experiences low rainfall, extensive evaporation, and a significant temperature difference between day and night, characteristic of a typical temperate continental desert climate [20]. The dominant vegetation is mainly herbaceous plants and drought-tolerant shrubs, including herbaceous plants such as *Limonium aureum* and *Agriophyllum pungens* and shrubs such as *R. soongorica* and *Haloxylon ammodendron* [21].

In April 2023, in this area, three sample plots with *R. soongorica* populations as the dominant population or a single population were set up as standard sample plots with a size of 100 m × 100 m. Within the standard sample plots set, five small sample plots with a size of 10 m × 10 m were selected using the five-point method, and then five plants of *R. soongorica* with the same growth and no pests or diseases were randomly selected in the small sample plots. The debris on the soil's surface was scooped away, the soil was dug up around the roots, and *R. soongorica* roots in the 0–20 cm soil layer were

collected. After shaking off the loose soil block from the root surface, a small brush was used to lightly brush the soil attached to the root surface of about 2 mm as rhizosphere soil. The researchers sterilized all experimental tools to avoid contamination during sample collection. After completing the sampling, the rhizosphere soil obtained from the small sample was evenly put into sterile bags and then transported back to the laboratory at a low temperature and stored in a refrigerator at −80 °C for subsequent separation and screening of phosphate-solubilizing bacterial strains.

2.1.2. Testing Material

The rhizosphere soil obtained from the small sample was sampled evenly. The seeds of *R. soongorica* used in the experiment were collected from the Qingtu Lake area of Minqin County, Wuwei City, Gansu Province, in November 2022 and preserved by low-temperature drying, and the annual *R. soongorica* seedlings were cultivated artificially for the test.

The phosphate-solubilizing bacteria used in the experiment were isolated from the rhizosphere soil of *R. soongorica* in the Qingtu Lake area. After 16S rRNA sequencing, combined with Gram staining and phylogenetic analysis, five strains of phosphate-solubilizing bacteria were finally identified as P2 (*Bacillus pumilus*), P3 (*Enterobacter mori*), J23 (*Enterobacter cloacae*), J24 (*Bacillus safensis*), and M1 (*Bacillus megaterium*).

The medium used in the experiment was LB liquid medium: tryptone 10 $g \cdot L^{-1}$, yeast extract 5 $g \cdot L^{-1}$, NaCl 10 $g \cdot L^{-1}$, and pH = 7.2 (solid medium with agar 10–15 $g \cdot L^{-1}$); inorganic phosphorus liquid medium: glucose 10 $g \cdot L^{-1}$, $(NH_4)_2SO_4$ 0.5 $g \cdot L^{-1}$, yeast extract 0.5 $g \cdot L^{-1}$, NaCl 0.3 $g \cdot L^{-1}$, KCl 0.3 $g \cdot L^{-1}$, $MgSO_4 \cdot 7H_2O$ 0.3 $g \cdot L^{-1}$, $FeSO_4 \cdot 7H_2O$ 0.03 $g \cdot L^{-1}$, $MnSO_4 \cdot H_2O$ 0.03 $g \cdot L^{-1}$, $Ca_3(PO_4)_2$ 5 $g \cdot L^{-1}$, and pH = 7.2 (solid medium with agar 10–15 $g \cdot L^{-1}$).(The above reagents are from Haibo Biology in Qingdao, Shandong Province, China)

2.2. Determination Indexes and Methods

2.2.1. Isolation and Identification of Phosphate-Solubilizing Bacteria

The 16S rRNA sequencing technology was used to determine the taxonomic status of the selected dephosphorylated strains, and the genes of the strains were amplified by PCR using 27F (5′-AGAGAGTTTGATCCTGGGCTCAG-3′) and 1492R (5′-TACGGGYTACCTTGTTAYGACTT-3′) as the primers. The reaction conditions were as follows: pre-denaturation at 95 °C for 2 min; denaturation at 95 °C for 15 s, annealing at 53 °C for 15 s, extension at 72 °C for 15 s, and the repetition of this cycle 31 times; and total extension at 72 °C for 5 min. The PCR products were detected by agarose gel electrophoresis with 1% agarose to ensure that the concentration was up to the standard, and then, the resulting amplified genes were sent to Guangdong Meige Genetic Science and Technology Co. The obtained sequences were compared and analysed with the NCBI database using the Blast program, and the gene sequences of standard strains with high similarity were selected. A phylogenetic tree was constructed using the MEGA 11 neighbour-joining method. The above methods were used to determine the classification status of the strains.

The dilution-coated plate method and plate scribing method were used to isolate and purify the phosphate-solubilizing bacteria from *R. soongorica* rhizosphere soil. In total, 1 g of *R. soongorica* rhizosphere soil was weighed into a triangular vial containing 100 mL of sterile water, placed in a 150 $rpm \cdot min^{-1}$ shaker for 30 min, and then subjected to gradient dilution (10^{-2}–10^{-6}), with three replicates set for each gradient. Then, 0.1 mL soil dilutions of different gradients were spread on LB solid medium and inverted in an incubator at a constant temperature of 28 °C for 24 h–72 h. Different morphological colonies growing well on the medium were labelled and numbered, and single colonies were picked with inoculation rings. Subsequently, the LB solid medium was delineated by the trichotomous

delineation method and inverted in a constant-temperature incubator at 28 °C for 24 h. After three rounds of purified delineation, the resulting purified strains were placed in 25%–30% glycerol tubes and stored in a refrigerator at −80 °C for spare use [22].

2.2.2. Functional Characteristics of Phosphate-Solubilizing Bacteria

The isolation and purification of phosphate-solubilizing bacteria from the rhizosphere soil of *R. soongorica* were conducted by the dilution-coated plate and plate streaking methods. The selected phosphate-solubilizing bacteria were inoculated in an LB liquid medium and placed on a shaker at 28 °C and 180 rpm·min^{-1} for 24 h to produce a bacterial suspension with an OD600 = 0.8–1. The fermentation broth was inoculated into the inorganic phosphorus-dissolving liquid medium with 1% inoculation amount, and the inorganic phosphorus liquid medium without inoculation was used as the control. It was placed on a shaker at 28 °C and 180 rpm·min^{-1} for 7 days. The fermentation broth was taken on the 1st, 3rd, 5th, and 7th days. The researchers determined the available phosphorus content using molybdenum–antimony resistance colorimetry and measured the pH with a pH meter (German Sartorius PB10, Gottingen, Germany) [22].

2.2.3. Pot Experiments

The experiment was conducted at the science and technology base on the Gansu Agricultural University campus, with good ventilation, sufficient light, and an artificial rain shelter. Before seedling cultivation, the full, uniform, and pest-free *R. soongorica* seeds were soaked in 75% alcohol for 1 min and then rinsed with sterile distilled water 3–5 times to complete seed disinfection. The substrate used in the experiment was composed of peat soil, vermiculite, and perlite mixed according to the volume ratio of 3:1:1. Seedlings began to grow in the tray on 17 April 2023 and were transplanted on 17 June 2023 into uniformly sized pots filled with about 5.2 kg of substrate per pot. When the plant height reached 10–12 cm, the researchers selected *R. soongorica* seedlings with uniform growth for the experiment and placed two plants in each pot.

The experiment was set up with four treatment groups, which included a total of twelve treatments, with each treatment replicated four times for a total of 48 pots, as follows: (1) control group (CK); (2) NaCl treatment group (concentration 300 mmol·L^{-1}); (3) phosphate-solubilizing bacteria treatment group (P2, P3, J23, J24, M1); and (4) phosphate-solubilizing bacteria and salt mixed-treatment group (P2 + NaCl, P3 + NaCl, J23 + NaCl, J24 + NaCl, M1 + NaCl). The previous research results of the research group have shown that when NaCl reaches 300 mmol·L^{-1}, it can slightly inhibit the growth of *R. soongorica* seedlings, so the authors selected to use this concentration of NaCl to treat *R. soongorica*. A progressive salt application method was used to treat the *R. soongorica* seedlings with NaCl to prevent acute salt damage to seedlings. The experiment started with 50 mmol·L^{-1} NaCl solution per day and gradually increased the target concentration, reaching 50 mmol·L^{-1} NaCl solution daily [23]. We irrigated each pot with 1500 mL of water each time and added the same amount of sterile water without NaCl treatment. The inoculation of plants with phosphate-solubilizing bacteria was conducted after 7 days of NaCl treatment. Five strains of phosphate-solubilizing bacteria were inoculated in LB liquid medium at 1% and placed on a shaker at 28 °C and 180 rpm·min^{-1} for 24 h. After centrifugation at 6000 rpm·min^{-1} for 6 min to collect phosphate-solubilizing bacteria, the OD600 was adjusted to 0.8–1 with sterile saline (0.9% NaCl) to obtain a phosphate-solubilizing bacterial suspension. *R. soongorica* was inoculated with 100 mL phosphate-solubilizing bacterial suspension per pot by the root-drenching method. After 14 days, the same process was used for secondary inoculation, and the same amount of sterile normal saline was added to the non-

inoculated treatment. Seven days after the last treatment, the plant seedling heights and stem thicknesses were measured, and plant and rhizosphere soil samples were collected.

After collecting plant samples, the physiological characteristics and phosphorus content were determined. Superoxide dismutase (SOD), catalase (CAT), and peroxidase (POD) were determined by the nitrogen blue tetrazolium (NBT) method, ultraviolet absorption method, and guaiacol method, respectively. The contents of soluble sugar, soluble protein, and free proline were determined by the anthrone colorimetry method, Coomassie brilliant blue method, and acid ninhydrin colorimetry, respectively [24]. The content of available phosphorus in rhizosphere soil and total phosphorus in plant leaves was determined by the 0.5 mol·L^{-1} $NaHCO_3$ method and molybdenum–vanadium yellow colorimetric method, respectively [25]. (The above reagents are from Shanghai Sinopharm Group, Shanghai, China)

2.3. Data Statistics and Analysis

We used Microsoft Excel 2010 and SPSS 26.0 software to complete the statistical data analysis. We also used Pearson correlation analysis of soluble phosphorus content and pH of phosphate-solubilizing bacteria in the rhizosphere soil of *R. soongorica*. One-way ANOVA was used to compare the growth characteristics, physiological characteristics, and phosphorus content of *R. soongorica* seedlings under different treatments. The ability of phosphorus-solubilizing bacteria to improve the salt tolerance of *R. soongorica* was compared by membership function analysis. Origin 2021 software was used for mapping.

3. Results

3.1. Determination of Phosphorus-Solubilizing Capacity of Phosphate-Solubilizing Bacteria

3.1.1. Phosphate-Solubilizing Ability of Different Strains

Figures 1 and 2 shows the phylogenetic evolutionary tree of five strains of phosphate-solubilizing bacteria, combined with 16S rRNA to determine the taxonomic status of the strains. Table 1 shows the phosphate-solubilizing effects of five strains of phosphate-solubilizing bacteria, P2, P3, J23, J24, and M1, in inorganic phosphorus-solubilizing solid medium. The colony diameters ranged from 0.39 to 0.74 cm, the diameters of solubilized phosphorus circles ranged from 0.42 to 1.44 cm, and the solubilizing index (SI) ranged from 2.08 to 3.55. Among them, the phosphorus solubilization index of the P2 strain was the highest, and the phosphorus solubilization index of the J24 strain was the lowest. The preliminary conclusion is that these five strains can dissolve inorganic phosphorus.

Table 1. The effect of different phosphorus-solubilizing bacteria in solid inorganic phosphorus-solubilizing medium.

Bacterial Strain Number	Name of the Bacterial Strain	Colony Diameter, D (cm)	Diameter of Dissolved Phosphorus Ring, d (cm)	Solubilizing Index, SI(D + d/D)
P2	*Bacillus pumilus*	0.53 ± 0.01 c	1.35 ± 0.04 b	3.55 ± 0.01 a
P3	*Enterobacter mori*	0.74 ± 0.01 a	1.14 ± 0.00 c	2.53 ± 0.02 b
J23	*Enterobacter cloacae*	0.62 ± 0.05 b	1.44 ± 0.00 a	3.33 ± 0.20 a
J24	*Bacillus safensis*	0.39 ± 0.02 d	0.42 ± 0.03 e	2.08 ± 0.00 c
M1	*Bacillus megaterium*	0.51 ± 0.00 c	0.89 ± 0.02 d	2.75 ± 0.01 b

Note: Different letters showed significant difference in phosphate-solubilizing effect among different phosphate-solubilizing strains ($p < 0.05$).

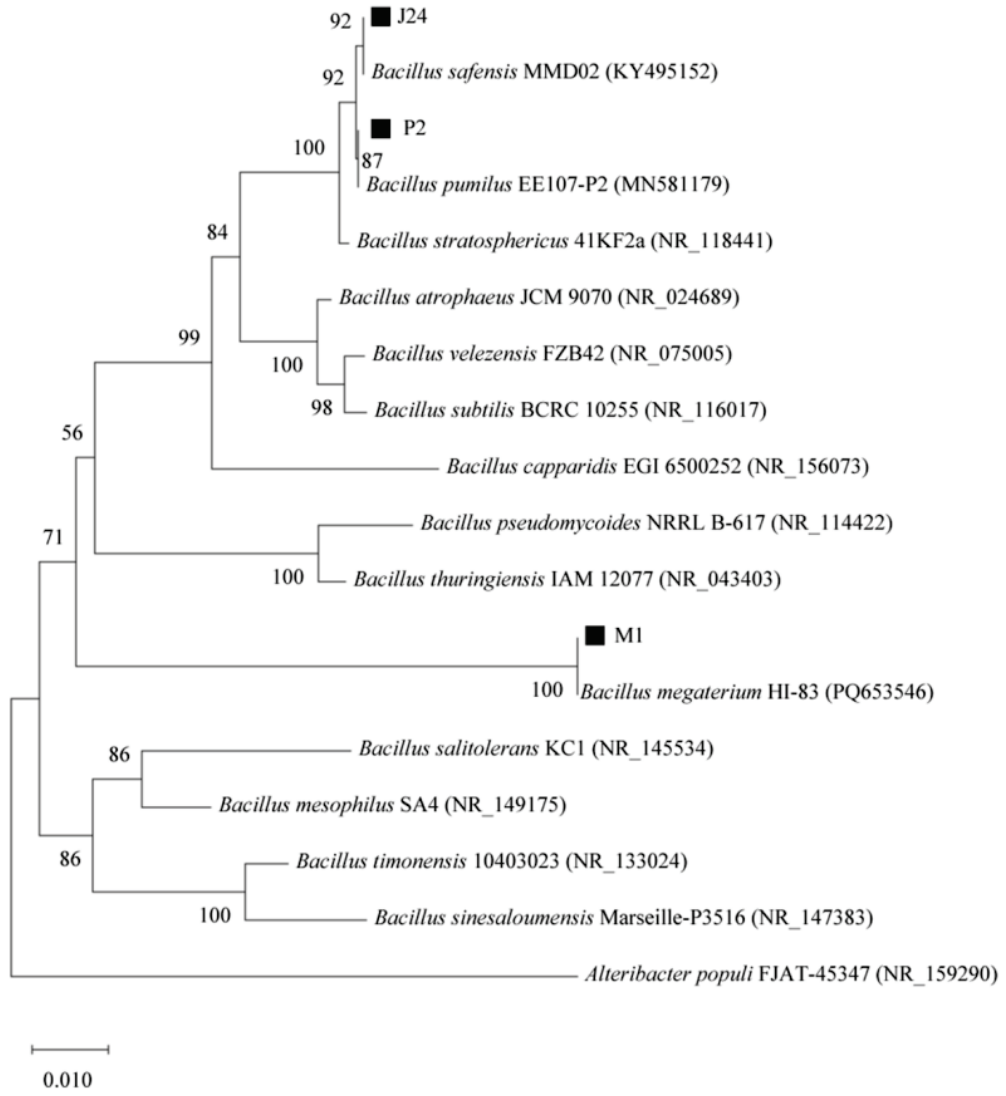


Figure 1. The phylogenetic tree of phosphate-solubilizing bacteria (strains P2, J24, M1) in the rhizosphere of *Bacillus* was constructed based on 16S rRNA gene sequence.

3.1.2. Growth Dynamics of Phosphate-Solubilizing Bacteria During Phosphate-Solubilizing Process

Five strains of phosphate-solubilizing bacteria were inoculated in an inorganic phosphorus medium containing $Ca_3(PO_4)_2$ as the sole inorganic phosphorus source, without bacteria as the control (CK). The dissolved phosphorus content and pH were measured during the incubation period, as illustrated in Figure 3. The five strains could solubilize inorganic phosphorus compared to the CK. As the culture time increased, the phosphorus solubilization capacities of strains P2, P3, and J23 reached the maximum on the first day of culture, which were 126.53 mg·L^{-1}, 58.74 mg·L^{-1}, and 26.47 mg·L^{-1}, respectively, before declining with further incubation. The soluble phosphorus content of the M1 strain increased with the rise in culture time, reached the maximum value of 44.15 mg·L^{-1} on the fifth day, and then decreased with the increase in culture time. The soluble phosphorus content of the J24 strain increased with the rise in culture time, and the maximum soluble phosphorus content reached 1.71 mg·L^{-1} on the seventh day. During the culture time, the pH value of the inorganic phosphorus-solubilizing medium inoculated with five strains of phosphorus-solubilizing bacteria was lower than that of the CK, and the changing trend of different strains was different.

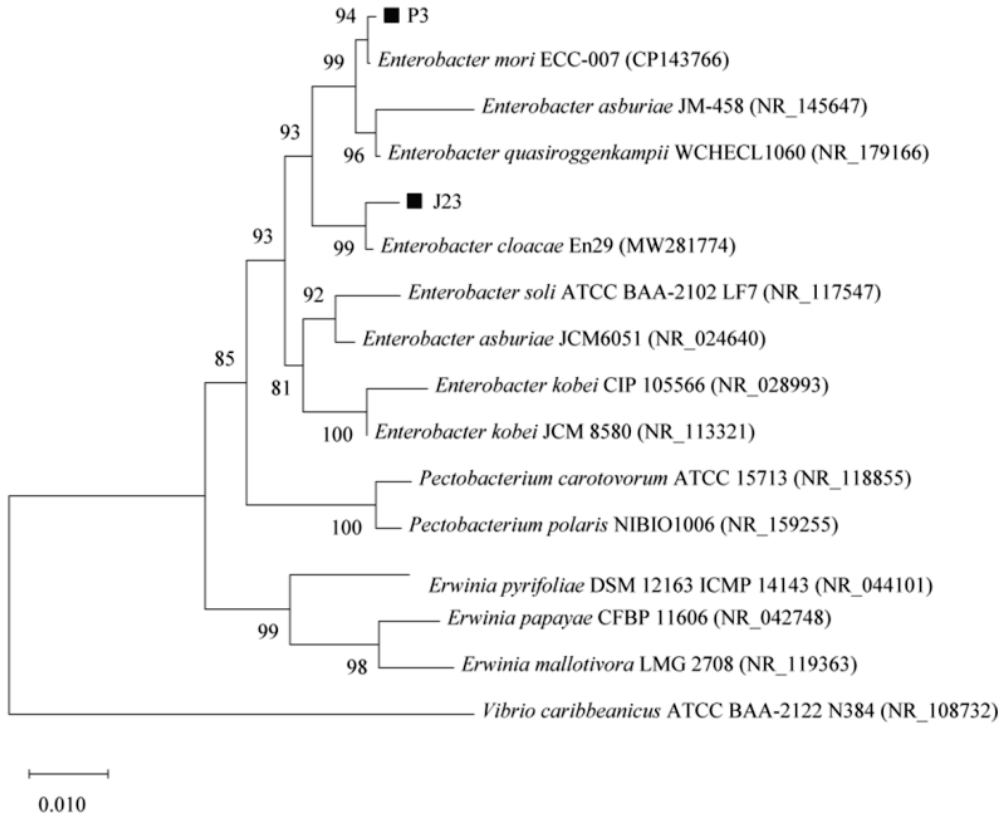


Figure 2. The phylogenetic tree of phosphate-solubilizing bacteria (strains P3 and J23) in the rhizosphere of *Enterobacter* was constructed based on 16S rRNA gene sequence.

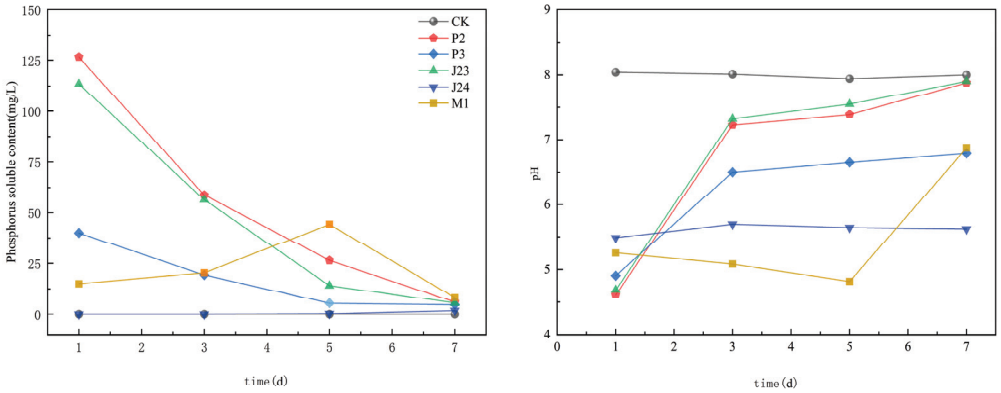


Figure 3. Changes in soluble phosphorus content and pH in inorganic phosphorus medium under different treatments of phosphate-solubilizing bacteria.

In contrast, the pH value of the CK did not significantly change and stabilized at about 8.0. The pH value of the inorganic phosphorus-solubilizing medium of the P2, P3, and J23 strains was the smallest on the first day of inoculation, which was 4.61, 4.91, and 4.69, respectively, and then increased rapidly. After three days of inoculation, the rise rate slowed until it was close to the CK on the seventh day. The pH value of the J24 strain minimized to 5.49 on the first day of inoculation, then increased until it decreased slowly after three days. The pH of the M1 strain decreased after one day of inoculation until the third day when the pH reached a minimum value of 5.09 and then increased rapidly.

Table 2 shows the results of the correlation analysis between the available phosphorus content and pH in the inorganic phosphorus medium under different phosphate-solubilizing bacteria treatments. There was a significant negative correlation between the available phosphorus content and pH in the inoculated inorganic phosphorus medium of

strains P2, P3, and J23 ($p < 0.01$) and a significant negative correlation between the available phosphorus content and pH of strain M1 ($p < 0.05$).

Table 2. Correlation analysis of dissolved phosphorus content and pH in inorganic phosphorus medium treated with different phosphate-solubilizing bacteria.

Bacterial Strain Number	Name of the Bacterial Strain	pH
P2	*Bacillus pumilus*	−0.965 **
P3	*Enterobacter mori*	−0.952 **
J23	*Enterobacter cloacae*	−0.945 **
J24	*Bacillus safensis*	0.177
M1	*Bacillus megaterium*	−0.728 *

The data used in the correlation analysis are the average values, indicating an extremely significant correlation at the 0.01 level and an extremely significant correlation at the 0.05 level. The data used in the correlation analysis are the average of the values. ** indicates extremely significant correlation at the 0.01 level, * indicates extremely significant correlation at the 0.05 level.

3.2. Effect of Phosphate-Solubilizing Bacteria on Growth of R. soongorica

Figure 4 shows that inoculation with different phosphate-solubilizing bacteria significantly affected the growth characteristics of *R. soongorica* seedlings ($p < 0.05$). Under the NaCl stress treatment, there were substantial differences in the plant height net growth and root biomass compared with the CK ($p < 0.05$), which decreased by 42.65% and 43.68%, respectively. In contrast, inoculation with different phosphate-solubilizing bacteria had various positive effects on the growth of *R. soongorica* seedlings under NaCl stress. The net growth in the plant height of *R. soongorica* seedlings inoculated with the J23, J24, and M1 strains under NaCl stress increased significantly ($p < 0.05$) compared to the NaCl treatment, which was more than doubled. The net growth of the base diameter of *R. soongorica* seedlings inoculated with the J24 strain increased significantly by 144.17%. The total biomass of *R. soongorica* seedlings inoculated with the P2 and J23 strains significantly increased by 7.35% and 21.01%, respectively. The root biomass of *R. soongorica* inoculated with five strains increased significantly, by 124.37%, 33.04%, 106.88%, 63.35%, and 40.34%. The biomass of *R. soongorica* seedling leaves inoculated with the J23 strain increased significantly by 11.03%.

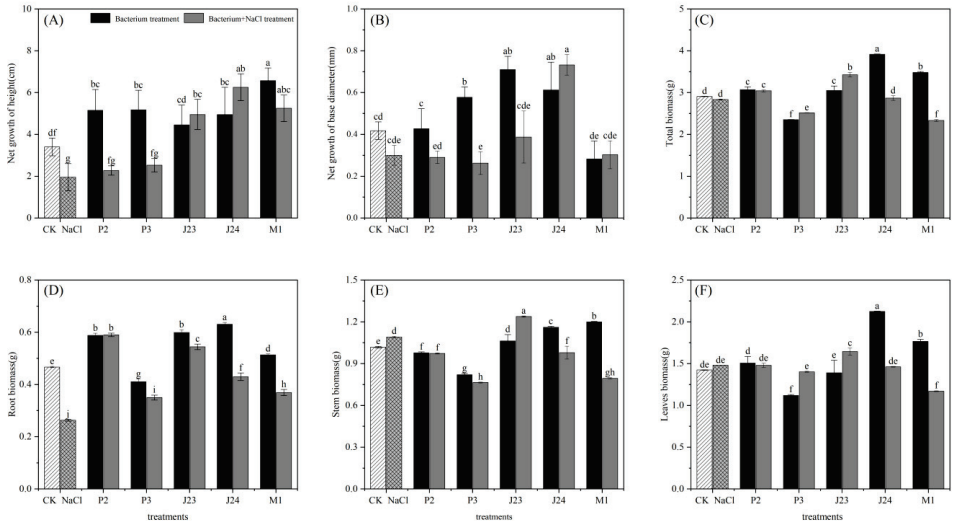


Figure 4. Effects of different treatments on growth indexes of *R. soongorica* seedlings. Different letters show significant difference in *R. soongorica* seedling growth between treatments ($p < 0.05$). (**A**) is net growth height, (**B**) is net growth of diameter, (**C**) is total biomass, (**D**) is root biomass, (**E**) is stem biomass, (**F**) is leaves biomass.

3.3. Effect of Phosphate-Solubilizing Bacteria on Antioxidant Enzyme Activity of R. soongorica Seedlings

As shown in Figure 5, the POD activity of *R. soongorica* seedlings increased significantly by 42.53% compared with the CK under NaCl stress, indicating that the 300 mmol·L^{-1} NaCl treatment inhibited the growth of *R. soongorica* seedlings. Under NaCl stress, the SOD activity of *R. soongorica* seedlings inoculated with the P3 and M1 strains was significantly different from that of the NaCl treatment ($p < 0.05$), in which the SOD activity of *R. soongorica* seedlings inoculated with the M1 strain increased by 30.13%. The difference in the POD activity of *R. soongorica* seedlings inoculated with the P3, J24, and M1 strains under NaCl stress was significant ($p < 0.05$) compared with the NaCl treatment, and the POD activity of *R. soongorica* seedlings inoculated with the J24 strain increased by 87.55%. There was no significant difference in the CAT activity between *R. soongorica* inoculated with P3 and seedlings inoculated with the J24 strain ($p > 0.05$).

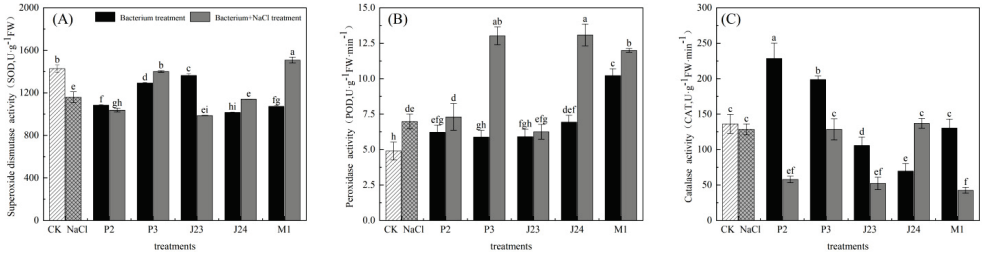


Figure 5. Effect of different treatments on antioxidant enzyme activities of *R. soongorica* seedlings. Different letters show significant difference in *R. soongorica* seedling growth between treatments ($p < 0.05$). (**A**) is superoxide dismutase activity(SOD), (**B**) is peroxidase cetivity(POD), (**C**) is catalase activity(CAT).

3.4. Effect of Phosphate-Solubilizing Bacteria on Osmotic Adjustment Substance of R. soongorica Seedlings

As shown in Figure 6, the NaCl stress treatment significantly reduced the soluble sugar content of *R. soongorica* seedlings by 35.69%, and the soluble protein and proline contents were different from the CK ($p < 0.05$), increasing by 70.98% and 9.46%, respectively. The soluble sugar content of *R. soongorica* seedlings inoculated with the P2, J23, and M1 strains under NaCl stress was significantly reduced by 24.91%, 45.55%, and 22.91%, respectively, compared with the NaCl stress treatment. The soluble protein of *R. soongorica* seedlings inoculated with the P2, P3, J23, and M1 strains under NaCl stress was significantly different from that under NaCl stress ($p < 0.05$) and more than three times higher. The proline content of *R. soongorica* seedlings inoculated with the P3 and J23 strains under NaCl stress significantly differed from that under NaCl stress ($p < 0.05$), increasing by 27.06% and 19.67%, respectively.

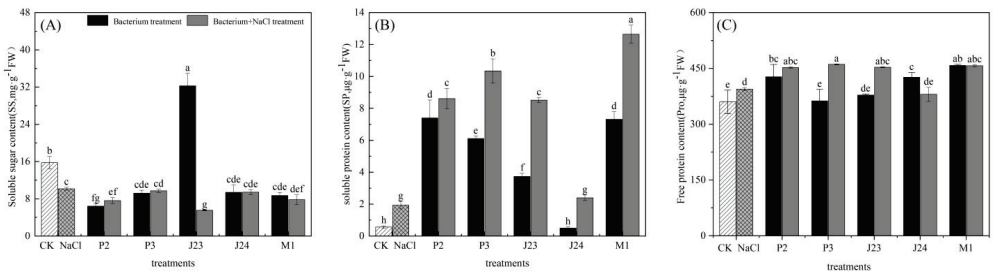


Figure 6. Effects of different treatments on osmoregulatory substances in *R. soongorica* seedlings. Different letters show significant difference in *R. soongorica* seedling growth between treatments ($p < 0.05$). (**A**) is soluble sugar content(ss), (**B**) is soluble protein(SP), (**C**) is free protein(SP).

3.5. Effects of Phosphate-Solubilizing Bacteria on Phosphorus Content in Leaves and Rhizosphere Soil of R. soongorica Seedlings

As shown in Figure 7, the contents of total phosphorus in the leaves and available phosphorus in the rhizosphere soil of *R. soongorica* seedlings under NaCl stress were significantly different from those of the CK ($p < 0.05$), decreasing by 60.65% and 45.86%, respectively. The total phosphorus content of *R. soongorica* seedling leaves inoculated with five strains under NaCl stress was significantly increased compared with the NaCl stress treatment ($p < 0.05$), and the total phosphorus content of *R. soongorica* seedling leaves inoculated with the J24 strain increased by more than four times. The content of available phosphorus in the rhizosphere soil of *R. soongorica* seedlings inoculated with the P2, J23, J24, and M1 strains was significantly increased compared with that under NaCl stress ($p < 0.05$), and the content of available phosphorus in the rhizosphere soil of *R. soongorica* seedlings increased by more than five times following inoculation with P2.

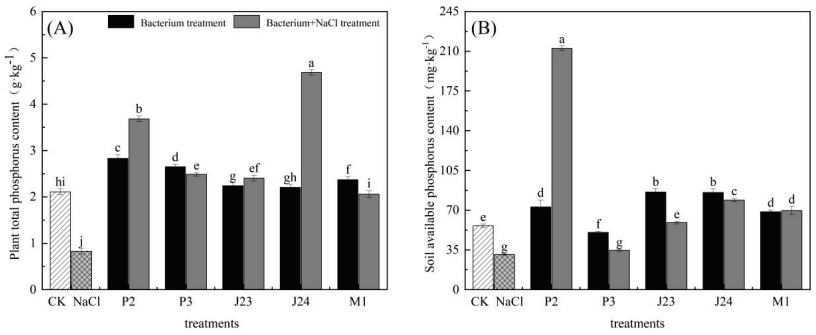


Figure 7. Effects of different treatments on total phosphorus content and rhizosphere soil available phosphorus content of *R. soongorica* seedlings. Different letters show significant difference in *R. soongorica* seedling growth between treatments ($p < 0.05$). (**A**) is plant total phosphorus content (TP), (**B**) is soil available phosphrus content (AP).

3.6. Comprehensive Evaluation of Effects of Different Phosphate-Solubilizing Bacteria on Salt Tolerance of R. soongorica Seedlings Under NaCl Stress

As shown in Figure 8, a correlation analysis of 14 indexes of *R. soongorica* seedlings inoculated with phosphate-solubilizing bacteria under NaCl stress was carried out. The total biomass had a negative correlation with SOD; TP had a negative correlation with SP; the net stem gross growth had a negative correlation with proline and SP. SS had a positive correlation with POD, and SP had a positive correlation with proline. Many of the indicators are significantly associated, and the evaluation information overlaps. Therefore, it is necessary to use principal component analysis to further screen the key factors affecting the growth and physiological characteristics of *R. soongorica* seedlings under NaCl stress.

As shown in Table 3, we performed principal component analysis on 14 individual indicators of *R. soongorica* seedlings inoculated with phosphate-solubilizing bacteria under NaCl stress. The contribution rates of the first four comprehensive indicators are 44.515%, 34.894%, 12.778%, and 7.812%. The cumulative contribution rate was greater than 85%, and the eigenvalue was more significant than 1. The data show that the eigenvalue of the first principal component was 6.232, and the coefficients of total biomass, root biomass, and stem biomass were more significant in the first principal component. The eigenvalue of the second principal component was 4.885, and the coefficients of net stem thickness growth, TP, and CAT were more prominent in the second principal component. The eigenvalue of the third principal component was 1.789, and AP, TP, and soluble sugar had significant coefficients in the third principal component. The characteristic value of the fourth principal component was 1.094, and the coefficients of CAT, leaf biomass, and total biomass were more extensive in the fourth principal component. This exhaustive

evaluation selected the first four comprehensive indicators as independent indicators. We calculated the relevant, comprehensive index values based on the standardized values of the four individual indexes under NaCl stress and the eigenvector coefficients of each comprehensive index.

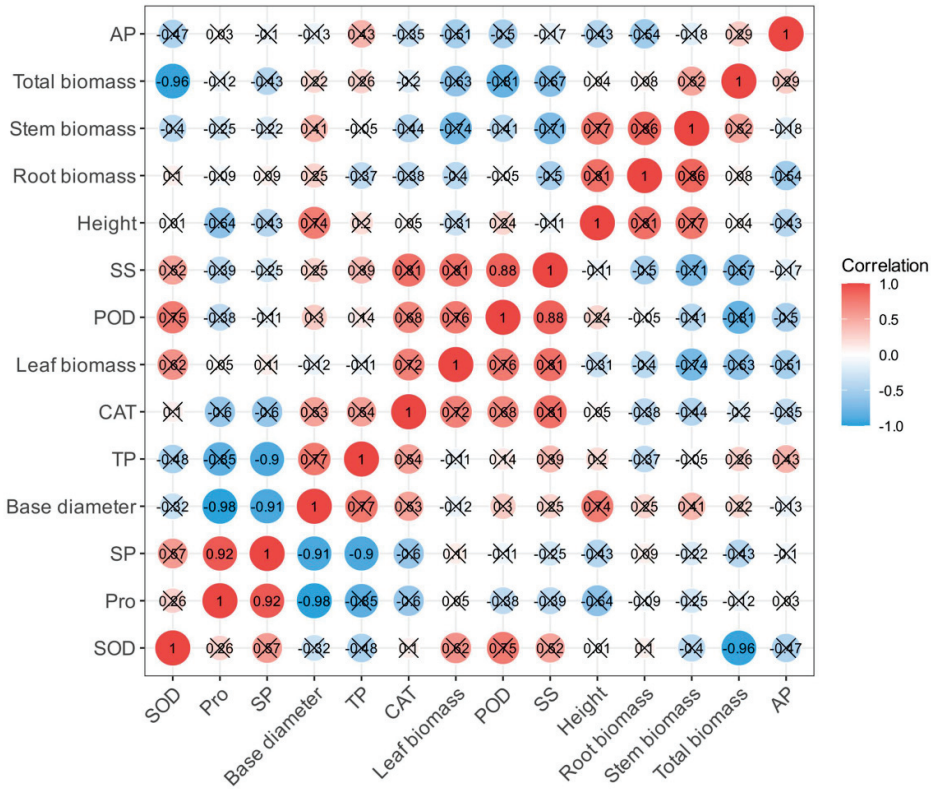


Figure 8. The correlation heatmap of every single index.

Table 3. Principal component analysis of growth and physiological indexes of *R. soongorica* seedlings inoculated with different phosphate-solubilizing bacteria under NaCl stress.

Variable	Principal Component 1	Principal Component 2	Principal Component 3	Principal Component 4
Net growth of height	0.006	0.110	−0.420	−0.351
Net growth of ground diameter	0.036	0.191	−0.126	−0.150
Total biomass	0.157	0.003	−0.053	0.178
Root biomass	0.149	−0.042	0.146	−0.140
Stem biomass	0.150	0.006	−0.197	0.070
Leaf biomass	0.137	0.028	−0.006	0.458
Superoxide dismutase activity, SOD	−0.157	−0.031	−0.067	−0.084
Catalase activity, CAT	−0.048	0.160	0.120	0.459
Peroxidase activity, POD	−0.136	0.108	−0.004	0.029
Free protein content, Pro	−0.023	−0.198	0.032	0.189
Soluble sugar content, SS	−0.110	0.115	0.243	0.141
Soluble protein content, SP	−0.069	−0.184	−0.044	−0.025
Plant total phosphorus content, TP	0.053	0.167	0.241	−0.177
Soil available phosphorus content, AP	0.074	−0.033	0.406	−0.442
Eigenvalue	6.232	4.885	1.789	1.094
Contribution/%	44.515	34.894	12.778	7.812
Cumulative contribution/%	44.515	79.409	92.188	100.000

The effects of different phosphate-solubilizing bacteria on the salt tolerance of *R. soongorica* seedlings under NaCl stress were evaluated by the membership function

method. As shown in Table 4, according to the comprehensive evaluation D value of each index, the effect of five strains of phosphate-solubilizing bacteria on the salt tolerance of *R. soongorica* seedlings under 300 mmol·L^{-1} NaCl stress was J24 > P2 > J23 > P3 > M1.

Table 4. Comprehensive Evaluation of the Effects of Inoculating Different Phosphate-Solubilizing Bacteria on the Salt Tolerance of *R. soongorica* Seedlings under NaCl Stress.

Bacterial Strain Number	Name of the Bacterial Strain	D-Value	Rank
P2	*Bacillus pumilus*	0.522	2
P3	*Enterobacter mori*	0.231	4
J23	*Enterobacter cloacae*	0.518	3
J24	*Bacillus safensis*	0.651	1
M1	*Bacillus megaterium*	0.022	5

4. Discussion

4.1. Functional Characteristics of Rhizosphere Phosphorus-Solubilizing Bacteria

Phosphate-solubilizing bacteria drive the soil phosphorus cycle and can increase the soil's phosphorus concentration. Plants can utilize this enhanced phosphorus in multiple ways to improve the soil's ecological environment [26,27]. However, the distribution of phosphate-solubilizing bacteria is influenced by various factors, including soil environmental conditions, plant species, and diversity. Researchers have not thoroughly studied the resources of phosphate-solubilizing bacteria in the rhizosphere of desert plants. In this study, the five strains of phosphate-solubilizing bacteria isolated from the rhizosphere soil of the desert plant *R. soongorica* belong to *Bacillus* and *Enterobacter*. Their maximum inorganic phosphorus-solubilizing content was 126.53 mg·L^{-1}, 58.74 mg·L^{-1}, 26.47 mg·L^{-1}, 44.15 mg·L^{-1}, and 1.71 mg·L^{-1}. Some researchers have isolated phosphate-solubilizing bacteria from the rhizosphere soil of *Phragmites australis* in saline and alkaline areas, mainly *Bacillus*, *Enterobacter*, and *Pseudomona*, and the phosphorus-solubilizing amount ranged from 55.8 to 722.3 mg·L^{-1} [28], which is similar to the phosphate-solubilizing bacteria groups screened from the rhizosphere saline–alkali soil of plants in different regions, and the amount of inorganic phosphorus-solubilizing content is different between them. Therefore, we speculated that *Bacillus* and *Enterobacter* are necessary phosphorus-solubilizing bacterial resources widely distributed in desert saline–alkali soil environments, which can better adapt to the extreme climate of the desert. However, due to the different types of phosphate-solubilizing bacterial strains and culture environments, the amount of inorganic phosphorus-solubilizing content will also be different.

Furthermore, phosphate-solubilizing bacteria dissolve insoluble phosphorus through processes such as acidification, proton secretion, and enzymatic hydrolysis. The acidification principle is mainly based on producing organic acid-chelating cations or releasing hydrogen ions [29]. This study found that inoculating the inorganic phosphorus-solubilizing medium with the P2, P3, J23, and M1 strains resulted in a lower pH value compared to the CK during the culture time, and the soluble phosphorus content showed a significant negative correlation with pH. Studies have shown that *Burkholderia cepacia* and *Bacillus pumilus* contain different kinds of organic acids in the supernatant [30]. The combined application of phosphate-solubilizing bacteria and phosphate fertilizer significantly enhances rhizosphere phosphatase activity and organic acid content in wheat [31]. We therefore hypothesize that different phosphate-solubilizing bacteria secrete varying types and concentrations of organic acids or H^+ during respiration and fermentation, et cetera, leading to differing degrees of pH reduction in the medium [32]. The pH of strain J24 was lower than that of the blank control. However, the correlation between its soluble phosphorus content

and pH was weak, likely because this strain dissolves phosphorus not only through acid production but also via extracellular phosphatase secretion and other mechanisms.

4.2. Effects of Phosphate-Solubilizing Bacteria on Growth and Physiological Characteristics of R. soongorica Seedlings Under NaCl Stress

Increased soil salinity leads to the accumulation of soluble ions such as Na^+ and Cl^- in plants roots, adversely affecting plant growth and development, ion toxicity, reactive oxygen species accumulation, osmotic stress, and other mechanisms [33]. Phosphate-solubilizing bacteria in the rhizosphere play a crucial role in the root environment, producing beneficial compounds such as IAA, hydrolases, and siderophores, which positively influence plant growth. They enhance plant salt tolerance by promoting plant growth, increasing antioxidant enzyme activity, accumulating osmoregulatory substances, and boosting plant available phosphorus content, with phosphate solubilization being the most beneficial function [34]. When researchers subject plants to salt stress, growth indicators such as plant height and stem diameter can intuitively reflect the effects on their appearance. *Bacillus amyloliquefaciens* and *Bacillus* pumilus can improve the salt tolerance of *Cicer Argentum* by increasing plant height, root length, and leaf phosphorus content [35]. This study found that inoculating *R. soongorica* seedlings with five different strains of phosphate-solubilizing bacteria enhanced growth under NaCl stress, increasing the net growth of the plant height, the net growth of the stem diameter, and biomass. However, the effects varied among strains, likely due to differences in their phosphate-solubilizing capacity and environmental adaptability.

Under salt stress, changes in antioxidant enzymes and osmoregulatory substances help scavenge accumulated reactive oxygen species (ROS) and regulate osmotic balance, mitigating salt-induced damage. These changes are key indicators of plant salt tolerance. Inoculating phosphorus-solubilizing bacteria with a growth-promoting ability could improve plant salt tolerance [36]. This study found that SOD and POD in *R. soongorica* seedlings inoculated with phosphate-solubilizing bacteria under NaCl stress increased to varying degrees compared with the NaCl treatment. We speculated that phosphate-solubilizing bacteria alleviate salt stress in *R. soongorica* by enhancing SOD and POD activity, maintaining ion homeostasis, and reducing reactive oxygen species (ROS) accumulation. Additionally, inoculation with five phosphate-solubilizing bacterial strains increased the soluble protein levels in *R. soongorica* seedlings under NaCl stress to varying degrees. In comparison, the soluble sugar content of *R. soongorica* seedlings inoculated with five strains of phosphate-solubilizing bacteria decreased to varying degrees, which was inconsistent with the results for *Oryza sativa* inoculated with *Bacillus subtilis* under salt stress [37]. We suggest that under 300 $mmol \cdot L^{-1}$ NaCl stress, soluble sugars in *R. soongorica* leaves may act as energy sources or secondary metabolites in plant metabolism, while soluble proteins and proline function as osmoregulatory substances to enhance seedling salt tolerance.

4.3. Effects of Rhizosphere Phosphate-Solubilizing Bacteria on Phosphorus Content of R. soongorica Seedlings Under NaCl Stress

In arid and semi-arid regions, soil salinization exacerbates the fixation of soluble phosphorus, impairing root nutrient absorption and worsening phosphorus deficiency. In [38], it was shown that adding an appropriate amount of phosphate fertilizer could enhance the salt tolerance of two varieties of *Medicago sativa*. However, excess phosphorus fertilizer added to saline soils is adsorbed and fixed, forming insoluble phosphates that plants cannot absorb or utilize. Studies have shown that rhizosphere phosphate-solubilizing bacteria exhibit functional traits such as phosphorus solubilization and IAA secretion. Generally, they lower soil pH and chelate metal ions by producing small-molecule organic acids like gluconic and acetic acid while also secreting phosphatases to decompose insoluble

phosphorus [39]. Meanwhile, it was found that *Bacillus anthracis*, *B. licheniformis*, and *B. cereus*, which have a phosphate-solubilizing function, were all able to produce IAA [40]. Additionally, they stimulate plant roots, induce root secretions, and indirectly enhance plant growth. Thus, applying phosphate-solubilizing bacteria to increase soil-soluble phosphorus content significantly improves saline soil. This study found that inoculating *R. soongorica* seedlings with five phosphate-solubilizing bacterial strains under NaCl stress significantly increased leaf total phosphorus and rhizosphere soil available phosphorus content compared to NaCl stress alone ($p < 0.05$). In conclusion, phosphate-solubilizing bacteria enhance soluble phosphorus content in saline soils and improve plant phosphorus absorption and utilization efficiency.

4.4. Comprehensive Evaluation of Effect of Rhizosphere Phosphate-Solubilizing Bacteria on Salt Tolerance of R. soongorica Seedlings Under NaCl Stress

Plants respond to environmental stress through changes in multiple growth and physiological indicators; thus, resistance evaluation should not rely solely on all indicators or a single indicator [41]. This study employed correlation analysis, principal component analysis, and membership function analysis to comprehensively evaluate the impact of phosphate-solubilizing bacteria on *R. soongorica* seedling salt tolerance, using total biomass, organ biomass, stem net growth, CAT activity, soluble sugars, proline, leaf total phosphorus, and rhizosphere soil available phosphorus as indicators. This experimentation result is consistent with the evaluation index of the salt tolerance of *Melia azedarach*, *Ulmus pumila*, and *Robinia pseudoacacia* [42]. Finally, the membership function values indicated that the effectiveness of the five phosphate-solubilizing bacterial strains in enhancing *R. soongorica* seedling salt tolerance under NaCl stress followed the order J24 > P2 > J23 > P3 > M1. J24 phosphate-solubilizing bacteria enhance *R. soongorica* seedling growth and salt tolerance under stress by regulating antioxidant enzyme activity, accumulating osmoregulatory substances, and increasing available phosphorus.

5. Conclusions

The five rhizosphere phosphate-solubilizing bacteria lower medium pH and solubilize phosphate, enhancing *R. soongorica* seedling salt tolerance through improvements in growth, physiology, phosphorus content, and rhizosphere soil enzyme activity. The comprehensive evaluation revealed that seedlings inoculated with J24 exhibited the strongest salt tolerance, while those inoculated with M1 showed the weakest. These findings offer valuable insights for desert ecological restoration and saline soil improvement.

Author Contributions: Conceptualization, data curation, visualization, review, and editing, X.W.; funding acquisition, investigation, supervision, review, and editing, P.C.; investigation, review, and editing, X.B.; data curation, investigation, and methodology, F.Z. All authors have read and agreed to the published version of the manuscript.

Funding: This work was supported by the National Natural Foundation of China, grant number 32160407, the Major Special Project of Gansu Provincial Science and Technology Plan—International Cooperation Field—grant number 25ZDWA007, and the Gansu Provincial Key Research and Development Program, grant number 23YFFA0065.

Data Availability Statement: The original contributions presented in this study are included in the article; further inquiries can be directed to the corresponding author.

Acknowledgments: The authors are thankful to the National Natural Foundation of China (32160407) for providing financial support. The authors are also thankful to the Gansu Provincial Key Research and Development Program (23YFFA0065) for providing financial support. The authors are thank-

ful to the Major Special Project of Gansu Provincial Science and Technology Plan—International Cooperation Field (25ZDWA0070).

Conflicts of Interest: The authors declare no conflicts of interest.

References

1. Su, T.; Wang, X.; Ning, S.; Sheng, J.; Jiang, P.; Gao, S.; Yang, Q.; Zhou, Z.; Cui, H.; Li, Z. Enhancing Soil Salinity Evaluation Accuracy in Arid Regions: An Integrated Spatiotemporal Data Fusion and AI Model Approach for Arable Lands. *Land* **2024**, *13*, 1837. [CrossRef]
2. Potestio, S.; Giannelli, G.; Degola, F.; Vamerali, T.; Fragni, R.; Cocconi, E.; Sandei, L.; Visioli, G. Salt stress mitigation and improvement in fruit nutritional characteristics of tomato plants: New opportunities from the exploitation of a halotorelant Agrobacterium strain. *Plant Stress* **2024**, *13*, 100558.
3. Chang, W.; Zhang, Y.; Ping, Y.; Li, K.; Qi, D.-D.; Song, F.-Q. Label-free quantitative proteomics of arbuscular mycorrhizal Elaeagnus angustifolia seedlings provides insights into salt-stress tolerance mechanisms. *Front. Plant Sci.* **2023**, *13*, 1098260.
4. Al-Huqail, A.A.; Aref, N.M.A.; Khan, F.; Sobhy, S.E.; Hafez, E.E.; Khalifa, A.M.; Saad-Allah, K.M. Azolla filiculoides extract improved salt tolerance in wheat (*Triticum aestivum* L.) is associated with prompting osmostasis, antioxidant potential and stress-interrelated genes. *Sci. Rep.* **2024**, *14*, 11100.
5. Banzouzi Bouzika, V.J.; Chong, P.-f.; Jia, X.-y.; Lu, W.-t.; Tin, Y.-l. Effects of foliar-spraying nitric oxide on the carbon metabolism enzymes activities and nutrients in leaves and roots of *Reaumuria soongorica* (pall.) maxim seedlings under NaCl stress. *Plant Stress* **2022**, *5*, 100096.
6. Teles, E.A.P.; Xavier, J.F.; Arcênio, F.S.; Amaya, R.L.; Gonçalves, J.V.S.; Rouws, L.F.M.; Zonta, E.; Coelho, I.S. Characterization and evaluation of potential halotolerant phosphate solubilizing bacteria from *Salicornia fruticosa* rhizosphere. *Front. Plant Sci.* **2024**, *14*, 1324056.
7. Bakki, M.; Banane, B.; Marhane, O.; Esmaeel, Q.; Hatimi, A.; Barka, E.A.; Azim, K.; Bouizgarne, B. Phosphate solubilizing Pseudomonas and Bacillus combined with rock phosphates promoting tomato growth and reducing bacterial canker disease. *Front. Microbiol.* **2024**, *15*, 1289466.
8. Cheng, Y.; Yuan, J.; Wang, G.; Hu, Z.; Luo, W.; Zhao, X.; Guo, Y.; Ji, X.; Hu, W.; Li, M. Phosphate-solubilizing bacteria improve the antioxidant enzyme activity of *Potamogeton crispus* L. and enhance the remediation effect on Cd-contaminated sediment. *J. Hazard. Mater.* **2024**, *470*, 134305.
9. Saranya, K.; Sundaramanickam, A.; Manupoori, S.; Kanth, S.V. Screening of multi-faceted phosphate-solubilising bacterium from seagrass meadow and their plant growth promotion under saline stress condition. *Microbiol. Res.* **2022**, *261*, 127080. [CrossRef]
10. Wu, Y.; Yang, W.; Kou, J.; Li, Q.; Liu, J.; Chi, L.; Zhang, Y.; Liu, Q.; Yu, Y. Impacts of phosphate-solubilizing bacterium strain MWP-1 on vegetation growth, soil characteristics, and microbial communities in the Muli coal mining area, China. *Front. Microbiol.* **2024**, *15*, 1500070.
11. Wang, J.; Qin, Q.; Pan, J.; Sun, L.; Sun, Y.; Xue, Y.; Song, K. Transcriptome analysis in roots and leaves of wheat seedlings in response to low-phosphorus stress. *Sci. Rep.* **2019**, *9*, 19802.
12. Wu, Y. *Effects of High Salt Stress on Soil Carbon, Nitrogen, and Phosphorus Metabolism and Its Microbiological Mechanism*; Northwest Agriculture and Forestry University: Xi'an, China, 2023.
13. Zhang, X.J. *Effect of Low Phosphorus on Light Energy Utilization of Sorghum Bicolor 'Dochna' Under Salt Stress*; Shandong Normal University: Jinan, China, 2021.
14. Ibeas, M.A.; Salinas-Grenet, H.; Johnson, N.R.; Pérez-Díaz, J.; Vidal, E.A.; Alvarez, J.M.; Estevez, J.M. Filling the gaps on root hair development under salt stress and phosphate starvation using current evidence coupled with a meta-analysis approach. *Plant Physiol.* **2024**, *196*, 2140–2149. [PubMed]
15. Zhao, L.; Su, R.; He, H. Effects of soil salt stress on phosphorus utilization of Medicago sativa. *J. Soil Water Conserv.* **2019**, *38*, 414–422.
16. He, F.-L.; Bao, A.-K.; Wang, S.-M.; Jin, H.-X. NaCl stimulates growth and alleviates drought stress in the salt-secreting xerophyte *Reaumuria soongorica*. *Environ. Exp. Bot.* **2019**, *162*, 433–443.
17. Liu, H.; Chong, P.; Yan, S.; Liu, Z.; Bao, X.; Tan, B. Transcriptome and Proteome Association Analysis to Screen Candidate Genes Related to Salt Tolerance in *Reaumuria soongorica* Leaves under Salt Stress. *Plants* **2023**, *12*, 3542. [CrossRef]
18. Yan, S.; Chong, P.; Zhao, M.; Liu, H. Physiological response and proteomics analysis of *Reaumuria soongorica* under salt stress. *Sci. Rep.* **2022**, *12*, 2539.
19. Shan, L.; Yang, C.; Li, Y.; Duan, Y.; Geng, D.; Li, Z.; Zhang, R.; Duan, G.; Васильевич, Ж.А. Effects of drought stress on root physiological traits and root biomass allocation of *Reaumuria soongorica*. *Acta Ecol. Sin.* **2015**, *35*, 155–159.
20. Zhang, S.; Zhao, J.; Yang, J.; Xie, J.; Sun, Z. Feature Selection and Regression Models for Multisource Data-Based Soil Salinity Prediction: A Case Study of Minqin Oasis in Arid China. *Land* **2024**, *13*, 877. [CrossRef]

21. Wang, T.; Zhang, S.; Zhang, S.; Shao, M.; Ding, Z.; Zhou, Y.; Su, C. The Process of Soil Carbon Sequestration in Different Ecological Zones of Qingtu Lake in the Arid–Semi-Arid Region of Western China. *Microorganisms* **2024**, *12*, 2122. [CrossRef]
22. Zeng, Q.; Tang, L.; Zhang, Y.; Shao, Y.; Wu, W.; Wang, J.; Ding, X.; Han, X.; Bilal, M. Isolation and characterization of phosphate-solubilizing bacteria from rhizosphere of poplar on road verge and their antagonistic potential against various phytopathogens. *BMC Microbiol.* **2023**, *23*, 221.
23. Liu, H.; Chong, P.; Liu, Z.; Bao, X.; Tan, B. Exogenous hydrogen sulfide improves salt stress tolerance of *Reaumuria soongorica* seedlings by regulating active oxygen metabolism. *PeerJ* **2023**, *11*, e15881.
24. Gao, J.F. *Plant Physiology Experiment Instruction*; Higher Education Press: Beijing, China, 2006.
25. Bao, S.D. *Soil Agrochemical Analysis*; China Agriculture Press: Beijing, China, 2000.
26. Janati, W.; Mikou, K.; El Ghadraoui, L.; Errachidi, F. Growth stimulation of two legumes (*Vicia faba* and *Pisum sativum*) using phosphate-solubilizing bacteria inoculation. *Front. Microbiol.* **2023**, *14*, 1212702.
27. Pan, L.; Cai, B. Phosphate-Solubilizing Bacteria: Advances in Their Physiology, Molecular Mechanisms and Microbial Community Effects. *Microorganisms* **2023**, *11*, 2904. [CrossRef]
28. Wang, J.L.; Wang, D.L.; Zhou, Q.; Zhang, T.; Li, M.Y. Screening and growth-promoting characteristics of phosphate-solubilizing strains from the rhizosphere of Phragmites australis in saline-alkali soil. *Jiangsu J. Agric.* **2024**, *40*, 64–74.
29. Wei, Y.; Zhao, Y.; Shi, M.; Cao, Z.; Lu, Q.; Yang, T.; Fan, Y.; Wei, Z. Effect of organic acids production and bacterial community on the possible mechanism of phosphorus solubilization during composting with enriched phosphate-solubilizing bacteria inoculation. *Bioresour. Technol.* **2018**, *247*, 190–199. [PubMed]
30. Luo, Y.H.; Ke, Z.B.; Zhong, C.; Chen, Y.J. Isolation, identification, and characteristics of phosphate-solubilizing bacteria from mangrove soil. *China Environ. Sci.* **2020**, *40*, 2664–2673.
31. Khourchi, S.; Elhaissoufi, W.; Ibnyasser, A.; Haddine, M.; Ghani, R.; Zeroual, Y.; Delaplace, P.; Bargaz, A. Integrated use of polyphosphate and P-solubilizing bacteria enhanced P use efficiency and growth performance of durum wheat. *Front. Microbiol.* **2023**, *14*, 1211397.
32. Cheng, Y.; Narayanan, M.; Shi, X.; Chen, X.; Li, Z.; Ma, Y. Phosphate-solubilizing bacteria: Their agroecological function and optimistic application for enhancing agro-productivity. *Sci. Total Environ.* **2023**, *901*, 166468. [CrossRef]
33. Nurrahma, A.H.I.; Harsonowati, W.; Putri, H.H.; Iqbal, R. Current Research Trends in Endophytic Fungi Modulating Plant Adaptation to Climate Change-associated Soil Salinity Stress. *J. Soil Sci. Plant Nutr.* **2024**, *24*, 6446–6466. [CrossRef]
34. Wael, D.; El-Amier, Y.; Saber, W.I.A.; Elsayed, A. Plant-associated halotolerant bacteria improving growth of *Vicia faba* L. Mariout-2 under salinity conditions. *Sci. Rep.* **2024**, *14*, 16737. [CrossRef]
35. Rahimi Chegeni, A.; Fatehi, F.; Ebrahimi, A.; Maleki, M. Phosphate-Solubilizing Bacteria Modulated Salinity Stress in the Presence of Phosphorous through Improving Growth, Biochemical Properties, and Gene Expression of Chickpea (*Cicer arientnum* L.). *J. Soil Sci. Plant Nutr.* **2023**, *23*, 4450–4462.
36. AbuQamar, S.F.; El-Saadony, M.T.; Saad, A.M.; Desoky, E.-S.M.; Elrys, A.S.; El-Mageed, T.A.A.; Semida, W.M.; Abdelkhalik, A.; Mosa, W.F.A.; Al Kafaas, S.S.; et al. Halotolerant plant growth-promoting rhizobacteria improve soil fertility and plant salinity tolerance for sustainable agriculture—A review. *Plant Stress* **2024**, *12*, 100482.
37. Siddika, A.; Rashid, A.A.; Khan, S.N.; Khatun, A.; Karim, M.M.; Prasad, P.V.V.; Hasanuzzaman, M. Harnessing plant growth-promoting rhizobacteria, *Bacillus subtilis* and B. aryabhattai to combat salt stress in rice: A study on the regulation of antioxidant defense, ion homeostasis, and photosynthetic parameters. *Front. Plant Sci.* **2024**, *15*, 1419764.
38. Su, R.; Zhang, Z.; Chang, C.; Peng, Q.; Cheng, X.; Pang, J.; He, H.; Lambers, H. Interactive effects of phosphorus fertilization and salinity on plant growth, phosphorus and sodium status, and tartrate exudation by roots of two alfalfa cultivars. *Ann. Bot.* **2022**, *129*, 53–64.
39. Koczorski, P.; Furtado, B.U.; Baum, C.; Weih, M.; Ingvarsson, P.; Hulisz, P.; Hrynkiewicz, K. Large effect of phosphate-solubilizing bacteria on the growth and gene expression of *Salix* spp. at low phosphorus levels. *Front. Plant Sci.* **2023**, *14*, 1218617.
40. Khosravi, M.; Heydari, M.; Alikhani, A.H. Mitigating negative impacts of drought on oak seedlings performances through plant growth-promoting rhizobacteria. *J. Environ. Manag.* **2025**, *375*, 124163.
41. Yan, S.; Chong, P.F.; Zhao, M. Effect of salt stress on the photosynthetic characteristics and endogenous hormones, and: A comprehensive evaluation of salt tolerance in *Reaumuria soongorica* seedlings. *Plant Signal. Behav.* **2022**, *17*, 2031782.
42. Gan, H.H.; Gong, S.; Liu, H.; Chu, J.M. Evaluation of salt tolerance of seedlings of three afforestation tree species in China and screening of indicators. *For. Sci. Res.* **2024**, *37*, 156–168.

Disclaimer/Publisher's Note: The statements, opinions and data contained in all publications are solely those of the individual author(s) and contributor(s) and not of MDPI and/or the editor(s). MDPI and/or the editor(s) disclaim responsibility for any injury to people or property resulting from any ideas, methods, instructions or products referred to in the content.

forests

MDPI

Article

Variations in Leaf Photosynthesis and Its Limitations at Different Canopy Positions in Mature Camphor Trees

Hanbing Leng *, Lingyan Zhou and Wei Yan

Shanghai Botanical Garden, Longwu Road 1111, Shanghai 200231, China; zhoulingyan@fudan.edu.cn (L.Z.); yanw816@163.com (W.Y.)
* Correspondence: 008slhb@163.com

Abstract: Urban forests play important roles in carbon sequestration and climate change mitigation. However, their adaptive mechanisms and limitations on photosynthesis throughout the canopy are poorly understood. This study takes the most widely distributed 50-year-old camphor plantations (*Cinnamomum camphora*) in Shanghai as the research objects. We investigated the variations in leaf morphology and photosynthetic physiology and biochemistry at six different canopy positions during a summer and an autumn period. We discovered that on account of leaf nitrogen loss and water deficit, light-saturated photosynthesis (A_{max}) declined in upper sunlit leaves despite being exposed to high sunlight in the same fashion as stomatal and mesophyll conductance (g_{sw}, g_m), photochemical quenching coefficient and actual photochemical efficiency of PSII (Φ_{PSII}, q_P), and maximum rate of electron transport and carboxylation (J_{max}, V_{cmax}) during the growing season. Although seasonal change had little effect on A_{max}, the relative importance of limitations varied temporally. Mesophyll and biochemical limitation were the major contributors to the decline in the A_{max} in upper sunlit leaves between summer and autumn, respectively. Our study highlights the constraints of carbon fixation capacity in dense stands of mature camphor trees and offers technical support for the accurate prediction of canopy photosynthesis and the enhancement of carbon sequestration management in urban forests.

Keywords: light heterogeneity of canopy; photosynthetic traits; resource allocation; mesophyll conductance; *Cinnamomum camphora*

1. Introduction

The forest canopy, as the main place of photosynthesis, is the primary functional interface for matter and energy exchange between trees and the atmosphere [1]. In the canopy, light availability—which is affected by stand structure and foliage distribution—often differs more than 50-fold from the top of the canopy to the bottom [2]. Concomitantly, air and leaf temperatures, humidity, and vapor pressure deficits also vary dramatically along the canopy [3,4]. This environmental variability generates strong gradients in canopy leaf anatomical, morphological, and functional traits [5]. Thus, the distinct phenomenon of sun leaves and shade leaves is produced, driving leaf carbon gain dynamics in the whole tree [6]. Compared with leaves grown in shade, sun leaves have been found to have thicker palisade tissue, higher leaf mass per area (*LMA*) and area-based nitrogen content (N_a), as well as greater rate of photosynthesis (A_n) [7,8], yet they also suffer more sun exposure stress due to excessive light absorption [9,10].

The scaling up of photosynthesis from leaves to the canopy is often simulated and performed using the biochemical model established by Farquhar et al. [11]. The initial

optimality model (i.e., big leaf model) proposed that the photosynthetic capacity and *N* distribution is proportional to the light extinction coefficient in the canopy so that canopy carbon gain could be maximized [12,13]. Nevertheless, the actual *N* distribution in the canopy has been shown to be much less steep than the light gradient [14]. And also the photosynthetic rate usually levels off at 30%–50% of above-canopy light, implying a certain limit for high–light acclimation [15,16]. Peltoniemi et al. [17] developed a simple 'toy' two-leaf canopy model, which suggests that hydraulic constraints to water supply can explain shallow *N* gradients in the canopy. The hydraulic limitation theory states that the hydraulic conductance of the soil–leaf pathway is inversely related to the length of the water transport path. Thus, the sun leaves of the upper canopy have lower water potentials than the shaded ones of the lower canopy which may lead to lower *N* allocation in the upper leaves [18,19], but more *N* is partitioned to Calvin–Benson cycle enzymes to accelerate the photosynthetic capacity [20]. However, there is also evidence that plants can overcome this path-length limitation and can even construct superior water transport efficiency in sun branches at the top canopy as a plastic response of xylem anatomy to the light environment [21,22]. Since high photosynthetic capacity tends to be sustained by high stomatal conductance and high hydraulic conductance, the distribution optimization of hydraulic conductance and photosynthetic nitrogen within the canopy could achieve the maximization of tree primary production in the whole canopy [23]. As a matter of fact, better additional structural, chemical, and physiological constraints can be likewise used to introduce more reality into optimality models like *LMA* and g_{sw} [17]. Whether these factors are included depends on their roles in the regulation of photosynthesis. But to date, there is very limited evidence on physiological and biochemical factors incorporated into canopy models of photosynthesis in urban forests of subtropical region.

Under saturated light, photosynthetic rates in terrestrial C_3 plants are limited by CO_2 diffusion resistance and by CO_2 fixation velocity (i.e., biochemical limitaion), which are expressed by stomatal and mesophyll conductances (g_s and g_m), and by maximum rates of Ribulose-1,5-Bisphosphate (RuBP) carboxylation and regeneration in the Calvin cycle (V_{cmax} and J_{max}), respectively [24,25]. Generally, g_s and g_m are found to be constrained by the leaf anatomical structure and biochemical factors, such as aquaporins and carbonic anhydrase [26,27], while V_{cmax} and J_{max} are mainly associated with *N* concentration and the amount (and activity) of the relevant enzymes [28,29]. Any decrease in CO_2 diffusion or utilization would lead to a direct reduction in the photosynthesis rate [24]. g_s, g_m, V_{cmax}, and J_{max} vary temporally and spatially under the influence of species, leaf ontogeny, and environment conditions, e.g., light, CO_2, temperature, as well as water and nutrition supply [26,30–32]. Thus, the relative importance of these photosynthetic limitations may be highly responsive to both the intra-canopy resource gradient and seasonal variability. Several studies have reported on limitations to carbon uptake throughout the canopy. For instance, in mature *Eucalytus tereticornis* trees, Crous et al. [33] found stronger electron transport and carboxylation limitations to photosynthesis in lower shading leaves, while Campany et al. [34] suggested that the lower A_n in shade leaves was primarily associated with reduced g_m. It was further discovered that seasonal changes impacted the relative importance of limitations across the entire canopy. According to Cano et al. [35], moderate summer drought lowered A_n in upper and lower beech leaves and in lower oak leaves by reducing the g_s and g_m. These discrepancies may be determined by the degree of variability in biochemical demand and CO_2 supply among canopy positions. The preceding studies, however, did not investigate how these inequalities throughout the canopy vary with the changing seasons, especially with regard to temperature and sunlight, and a lack of empirical data hinders us from interpreting their coupled effects on the diffusive and biochemical components.

Cinnamomum camphora is one of the most important urban tree species in the subtropical region of China and is commonly cultivated as dense pure plantations. Currently, its application frequency has been found to be as high as 80% in Shanghai [36]. However, very little is understood about the adaptive mechanisms that regulate photosynthesis in the canopy of *C. camphora* grown in the urban greenery. Here, we conducted a field study in monospecific camphor stands in a subtropical monsoon climate to assess the effects of canopy position on key leaf photosynthetic characteristics and associated functional traits at two times during the growing season. We further investigated the correlation of leaf photosynthetic capacity with resource partition and physiological and biochemical components, as well as the seasonal variability of quantitative limitations on photosynthesis along the canopy. Several questions were asked: Do photosynthetic traits increase as light increases in the canopy? Are there significant differences in photosynthetic physiology and biochemistry in the canopy between the two growing seasons? Which components significantly affect canopy photosynthesis? The present study aims to predict canopy photosynthesis more accurately using optimality-based models and guide the carbon sequestration management in urban forests.

2. Materials and Methods

2.1. Study Site

This study was conducted in the adult stand of *C. camphora* located at Shanghai Botanical Garden (81.86 hm^2) in the central region of Shanghai (31°08′44.40″ N, 121°26′50.12″ E). The garden is characterized by various broad-leaved evergreen and deciduous plantations, and *C. camphora* is one of the main tree species, covering an area of around 4 hm^2, with 774 individuals in total. The mean annual temperature is 17.8 °C, and the mean annual precipitation is 1660.8 mm. The soil is silty clay loamy sand with an average pH value of 7.7. The total organic matter, nitrogen, and phosphorous contents in the topsoil are 16.80, 2.67, and 1.05 $g \cdot kg^{-1}$, respectively. Two sample camphor plots, with an area of 100 m^2 each and with trees spaced 2–3 m apart (dense stand), were established. Three approximately 50-year-old sample trees were selected in each plot, for a total of six study trees with a mean height of 17.9 m and a mean diameter at breast height of 40.5 cm.

2.2. Experimental Design

In accordance with canopy height, a three-storied bamboo platform with a height of about 14 m was built to provide access to the leaves of the three sample trees in each plot (Figure S1). Leaf–gas exchange measurements were performed during two measurement campaigns through the 2023 growing season, from 22 August to 7 September (summer) and from 17 October to 31 October (autumn). The same measurement protocol was followed during each campaign. Measurements were taken at three canopy layers: upper, corresponding to the outer edge of the canopy within three meters from the top; middle, corresponding to the mid-canopy (the halfway up the canopy, 11~12 m high); lower, corresponding to the lowest living branch (6~7 m high). At the same time, each layer within the canopy was divided into southern and northern faces, resulting in six distinct canopy positions, i.e., the southern and northern faces of the upper (US and UN), middle (MS and MN), and lower (LS and LN) layers. According to the developing locations of branches, the leaves located at the middle and lower layers were sampled on the secondary branches of the inner canopy, while the leaves at the upper layer were sampled on the branch apex. Fully expanded and undamaged current-year leaves were selected from the same branch for gas exchange measurements. Leaf–gas exchange and chlorophyll fluorescence were measured simultaneously on sunny days between 9:00 and 12:00 a.m. Over the two dates, we completed 60 A_n versus CO_2 concentration in the intercellular air

space (C_i) response curves (A_n/C_i curves) in total. On each date, we made four to six A_n/C_i curves at each canopy position. Following the gas exchange measurement on the first date, leaves attached to the same branch were collected, with one portion of leaves used to analyze the pigment concentration and the other to determine the carbon and nitrogen contents.

2.3. Environmental Measurements

Prior to gas exchange measurement on each date, the photosynthetic active radiation (*PAR*) incident on the selected leaves was measured with a handheld quantum sensor (Li-250A, LI-COR Inc., Lincoln, NE, USA) at each canopy position for the sample trees. *PAR* was performed on sunny days every two hours between 8:00 and 16:00. The daily *PAR* (PAR_{sum}) was calculated by the integral area of the diurnal light curves. Data on air temperature and precipitation were gathered by the microclimate station (DJ-6595A, DIANJIANG TECH Inc., Shanghai, China) located in the Shanghai Botanical Garden.

2.4. Gas Exchange and Chlorophyll Fluorescence Measurements

A_n/C_i curves were established from gas exchange measurements using an open gas exchange system (LI-6400XT and LI-6400-40, LI-COR Inc., Lincoln, NE, USA). The conditions inside the cuvette during the measurements were as follows: *PAR* of 1800 $\mu mol \cdot m^{-2} \cdot s^{-1}$ (saturating-light condition from previous trials, 90% red and 10% blue light), CO_2 concentration of 400 $\mu mol \cdot mol^{-1}$, leaf temperature at prevailing levels (33–40 °C and 26–32 °C at two measurement times, respectively), relative humidity of 40%–60%, and air flow rate of 300 $\mu mol \cdot m^{-2} \cdot s^{-1}$. A_n/C_i curve measurements were initiated when A_n and g_{sw} (stomatal conductance to H_2O) had stabilized under these conditions (usually within 30min after clamping onto the leaf). A series of adjustments were made to the ambient CO_2 concentration (C_a) inside the chamber: 400, 300, 250, 200, 150, 100, 50, 400, 600, 800, 1000, 1200, 1500, 1800 $\mu mol \cdot mol^{-1}$. The parameters were recorded when a steady state was reached for both gas exchange and chlorophyll fluorescence.

At each C_a step, chlorophyll fluorescence was measured simultaneously. Steady-state fluorescence (F_s) was recorded under actinic light of 1800 $\mu mol \cdot m^{-2} \cdot s^{-1}$ from light-emitting diodes and maximal fluorescence (F_m') was recorded during a light-saturated pulse of ca. 8000 $\mu mol \cdot m^{-2} \cdot s^{-1}$ at 630 nm by the multiphase flash protocol. Far-red light of 5 $\mu mol \cdot m^{-2} \cdot s^{-1}$ was applied at 740 nm without actinic light to obtain minimal fluorescence in the light-adapted leaf (F_o'). The photochemical quenching coefficient of PSII (q_P) and the actual photochemical efficiency of PSII (Φ_{PSII}) were calculated according to the gas exchange system: $q_P = (F_m' - F_s)/(F_m' - F_o')$, $\Phi_{PSII} = (F_m' - F_s)/F_m'$. Electron transport rate (*ETR*) was calculated as $\Phi_{PSII} \times PAR \times \alpha \times \beta$, where α is the leaf absorbance (taken as 0.85) [37] and β is the distribution of light between PSI and PSII (taken as 0.5).

Finally, light-saturated gas exchange (A_{max}, g_{sw}, and C_i) and chlorophyll fluorescence parameters (q_P, Φ_{PSII}, *ETR*) were determined at a C_a of 400 $\mu mol \cdot mol^{-1}$ and a *PAR* of 1800 $\mu mol \cdot m^{-2} \cdot s^{-1}$, which were used in the following calculations and analyses.

2.5. Estimation of Mesophyll Conductance and Biochemical Parameters

The maximum carboxylation rate ($V_{cmax}(C_i)$), potential maximum electron transport rate at saturating-light levels ($J_{max}(C_i)$), and mitochondrial respiration rate in the light (R_{day}) were estimated based on A_n/C_i curves according to Farquhar et al. [11].

Mesophyll conductance (g_m) was estimated by combining gas exchange and chlorophyll fluorescence measurements via the variable *J* method of Harley et al. [38], as follows:

$$g_m = \frac{A_n}{C_i - \frac{\Gamma^* \times \left(ETR + 8\left(A_n + R_{day}\right)\right)}{ETR - 4\left(A_n + R_{day}\right)}}$$

where g_m was judged to be reliable only when C_i ranged from 100 to 300 μmol·mol^{-1} [38]. Hence, the values of A_n, C_i, and ETR at C_a of 400 μmol·mol^{-1} were taken from the gas exchange and chlorophyll fluorescence measurements. R_{day} was calculated and derived for the A_n/C_i curve. Γ^* represents the CO_2 compensation point in the absence of R_{day}, taken from Bernacchi et al. [39]. The CO_2 concentration at the site of carboxylation (C_c) was calculated following Fick's law, which can be described as $C_c = C_i - A_n/g_m$. Therefore, using estimates of g_m, A_n/C_i curves could be converted to A_n/C_c curves. The values of $V_{cmax}(C_c)$ and $J_{max}(C_c)$ were calculated from A_n/C_c curves and then standardized to 25 °C using the temperature-dependent equation reported by Bernacchi et al. [40]. As the effects of temperature on g_m are controversial—a positive effect was observed until 35 °C in *Nicotiana* while an obvious decline was observed from 26.9 °C to 40 °C in beech trees [30,35]—g_m estimates were not scaled with temperature. C_c-based V_{cmax} and J_{max} estimates at 25 °C were used in the subsequent analyses and comparisons. This method has stronger operability and higher reliability, which is conducive to the observation and analysis of multi-processing and multi-repetitive samples in our study.

2.6. Quantitative Limitation to the Light-Saturated Photosynthesis(A_{max})

According to Grassi and Magnani [30], the contributions to the decreased A_{max} were partitioned into g_{sc} (stomatal conductance to CO_2), g_m, and V_{cmax}. The photosynthesis limitations were determined as follows:

$$\frac{dA_n}{A_n} = S_L + M_L + B_L = l_s \times \frac{dg_{sc}}{g_{sc}} + l_m \times \frac{dg_m}{g_m} + l_b \times \frac{dV_{cmax}}{V_{cmax}}$$

$$l_s = \frac{g_{tot}/g_{sc} \times \partial A_n/\partial C_c}{g_{tot} + \partial A_n/\partial C_c}$$

$$l_m = \frac{g_{tot}/g_m \times \partial A_n/\partial C_c}{g_{tot} + \partial A_n/\partial C_c}$$

$$l_b = \frac{g_{tot}}{g_{tot} + \partial A_n/\partial C_c}$$

where S_L, M_L, and B_L are the contributions of g_{sc}, g_m, and V_{cmax} to dA/A, respectively. l_s, l_m, and l_b are the corresponding relative limitations to photosynthesis, respectively. g_{sc} is calculated as $g_{sc} = g_{sw}/1.6$. g_{tot} is total conductance to CO_2 between the leaf surface and carboxylation site ($1/g_{tot} = 1/g_{sc} + 1/g_m$). $\partial A_n/\partial C_c$ was determined as the slope of A_n/C_c curve at C_c = 50–120 μmol·mol^{-1}.

To investigate how the canopy position limits A_{max} between the two seasons, we compared the contributions of g_{sc}, g_m, and V_{cmax} to the reduced A_{max} (i.e., S_L, M_L, and B_L). The maximum values of A_{max}, g_{sc}, g_m, and V_{cmax} were regarded as reference values, regardless of the season in which they occurred.

2.7. Concentration of Foliar Carbon, Nitrogen, and Photosynthetic Pigments

At each canopy position of sample trees in each plot, around 20 leaves were collected, scanned to measure surface area (cm^2) using a leaf area meter (Scan Maker i800 plus, MICROTEK Inc., Shanghai, China), oven-dried at 80 °C for 48 h, and subsequently weighed to determine the leaf dry mass (g). Then, the leaf mass per area (LMA, g·m^{-2}) was calculated. Afterward, the leaf samples were milled to assess the carbon (C_m, %) and nitrogen contents (N_m, %) using an organic element analyzer (Vario EL Cube, Elementar Inc., Hanau, Germany). Leaf nitrogen per area (N_a, g·m^{-2}) was calculated by using the leaf LMA.

Similarly, four leaves were collected, cut into small pieces with scissors (avoiding the main vein of the leaves), and soaked in 80% acetone for 48 h until whitened. The absorbance of the extract was measured at 470, 646, and 663 nm using an ultraviolet–visible

spectrophotometer (L6S (765), INESA Inc., Shanghai, China) following Lichtenthaler and Wellburn [41]. The concentration of leaf chlorophyll a (Chl_a, mg·g^{-1}), chlorophyll b (Chl_b, mg·g^{-1}), and carotenoid (Car, mg·g^{-1}) were determined.

2.8. Statistical Analysis

All analyses and graphics were performed using SPSS18.0 and Origin Pro 9.1, respectively. Before analysis, Shapiro–Wilk's and Levene's tests were conducted to check normality and homogeneity. The variables that did not meet the assumption were log-transformed. Repeated measures analysis of variance with Duncan's post hoc test were performed to test the effects of canopy position and date. The relationships among photosynthetic traits were assessed using linear regressions. Curve fitting analyses were performed to assess the correlation between PAR_{sum} and leaf physiological characteristics. Effects were considered significant at 0.05. All data were represented as mean ± SE (standard error).

3. Results

3.1. Growth Environment

Precipitation and air temperature varied significantly between the summer and autumn periods. The mean daily maximum temperature was 30.57 °C and 25.43 °C, and the total precipitation was 98.2 mm and 1.2 mm, respectively (Figure 1a). The first campaign experienced higher temperatures but more rainfall, which suggests that camphor trees did not suffer from summer drought stress.

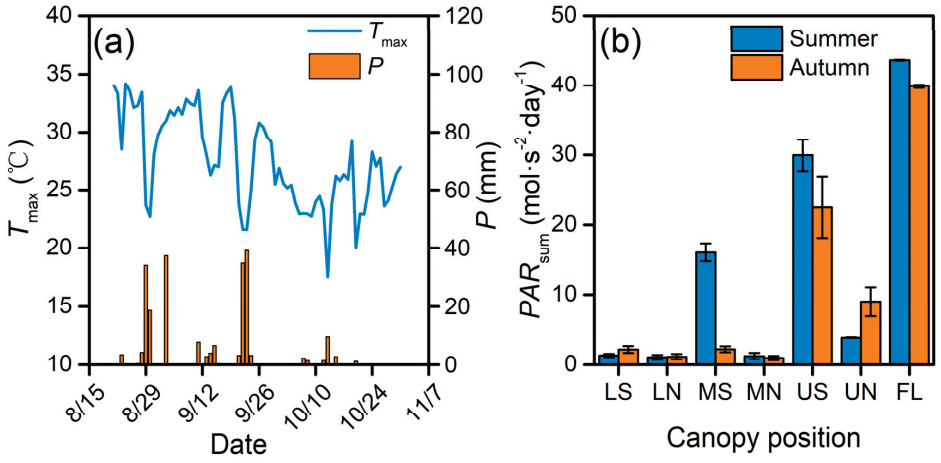


Figure 1. (**a**) Maximum air temperature (T_{max}) and daily precipitation (P) during measurement dates from late August to November of 2023. (**b**) Daily photosynthetic active radiation (PAR_{sum}) across camphor canopy positions during two campaigns. US and UN, MS and MN, LS and LN represent the southern and northern faces at the upper, middle, and lower canopy layers, respectively. FL represents full light above the canopy.

The diurnal variations in PAR in the canopy of camphor trees were measured above the canopy and at each canopy position on typical sunny days (Figure S2). The maximal daily PAR (PAR_{sum}) throughout the canopy was observed on the southern side of the upper layer (US position, 29.94 mol·m^{-2}·day^{-1} in summer and 22.49 mol·m^{-2}·day^{-1} in autumn), accounting for 68.56% and 56.41% of above-canopy light (full light), respectively (Figure 1b). A close second was the southern side of the middle layer in summer (MS position, 16.05 mol·m^{-2}·day^{-1} of PAR_{sum}; Figure 1b). Affected by solar elevation angle and crown profile, there was an obvious effect of seasonality on PAR_{sum} incident in leaves developing at the MS positions, where light availability was 7.32-fold higher in summer than in autumn, respectively. At other canopy positions, PAR_{sum} was relatively lower

over both seasons (<10 mol·m^{-2}·day^{-1}; Figure 1b). Therefore, the leaves grown at the US position were considered upper sunlit leaves.

3.2. Effect of Canopy Position and Season on Leaf Photosynthetic Traits

Between the two campaigns, g_{sw}, g_m, C_i, and J_{max} showed significant date effects (Table 1). Mean g_{sw} and C_i were reduced by 12.32% and 7.84%, respectively, and mean g_m and J_{max} increased by 19.89% and 44.79%, respectively, from summer to autumn (Figures 2c–h and 3c,d). Seasonal variation was more marked in the g_{sw} of leaves grown in the MS position, in the g_m at the lower layer, and in the C_i and J_{max} in most positions except for US and MN positions, respectively (Figures 2c–h and 3c,d). Other variables did not vary seasonally (Table 1). Meanwhile, no date effects were detected along with the fluctuation pattern of all photosynthetic traits throughout the canopy (Table 1).

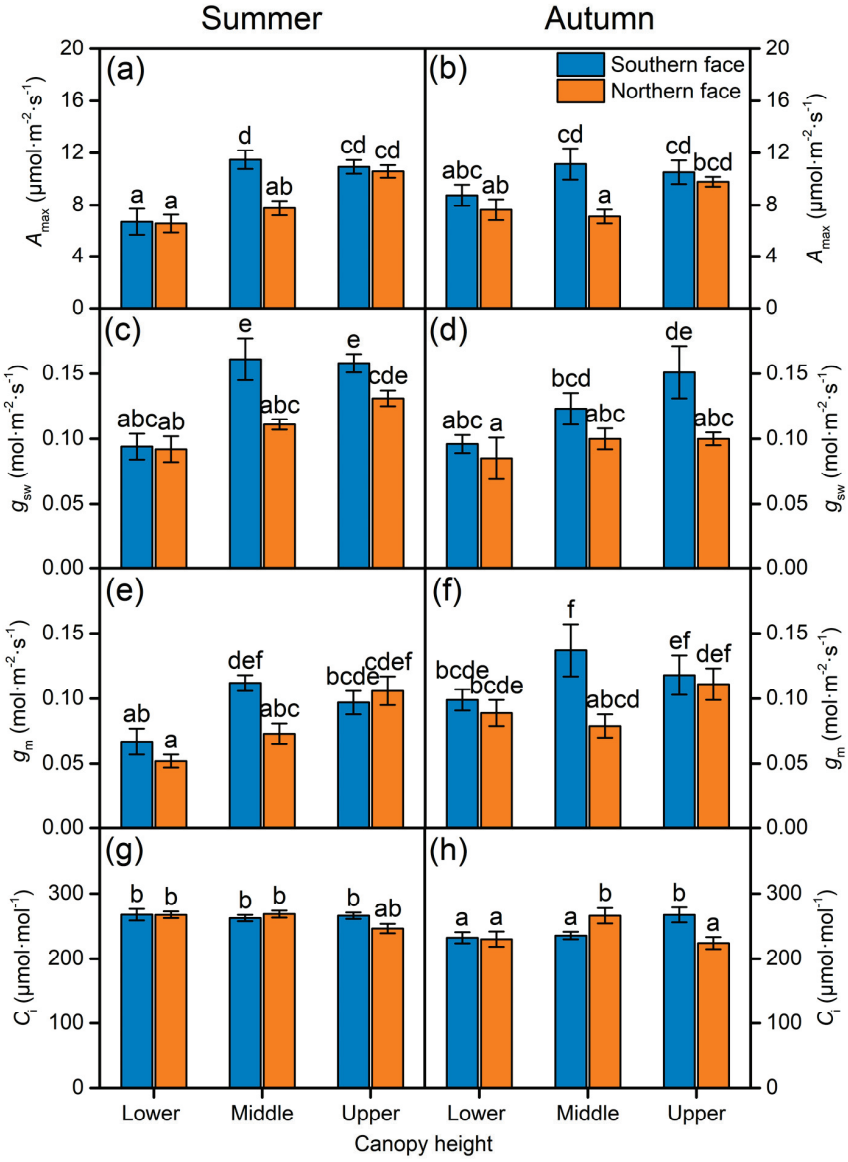


Figure 2. Effects of canopy position and season on gas exchange parameters for mature *C. camphora* trees. (**a**,**b**) Light-saturated photosynthesis (A_{max}), (**c**,**d**) stomatal conductance (g_{sw}), (**e**,**f**) mesophyll conductance (g_m), and (**g**,**h**) CO_2 concentration in the intercellular air spaces (C_i) are given as mean ± SE (n = 4–6). Letters represent a significant difference across canopy positions and seasons according to Duncan's test (α = 0.05).

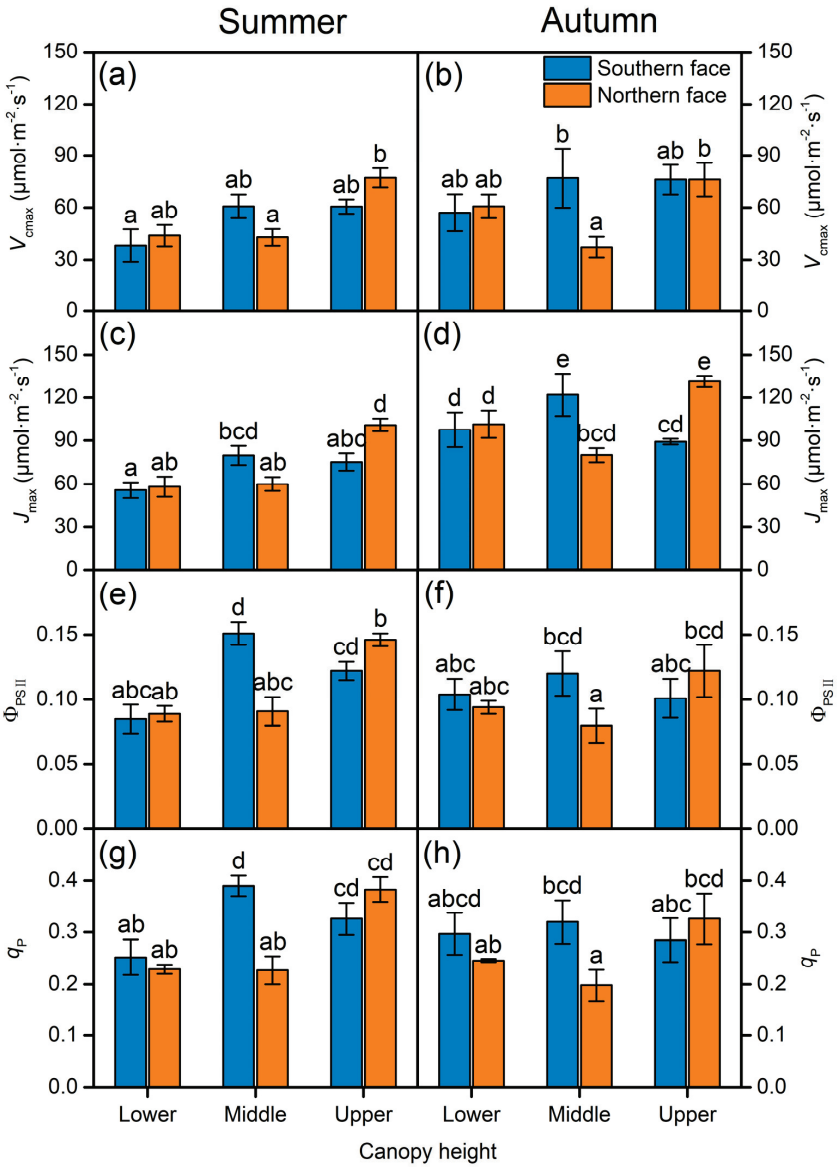


Figure 3. Effects of canopy position and season on biochemical traits for mature *C. camphora* trees. (**a**,**b**) Maximum carboxylation rate at 25 °C (V_{cmax}), (**c**,**d**) potential maximum electron transport rate at 25 °C (J_{max}), (**e**,**f**) actual photochemical efficiency of PSII (Φ_{PSII}), and (**g**,**h**) photochemical quenching coefficient of PSII (q_P) are given as mean ± SE (n = 4–6). Letters represent a significant difference across canopy positions and seasons according to Duncan's test (α = 0.05).

Significant effects of both canopy height and orientation on the A_{max}, g_{sw}, g_m, and q_P were observed across canopy positions, while the V_{cmax}, J_{max}, and Φ_{PSII} only exhibited prominent differences across canopy heights (Table 1). Accordingly, most leaf photosynthetic traits (except for g_{sw} and C_c) showed significant interactive effects (Table 1). Contrasting two canopy orientations over two seasons, the A_{max}, g_m, V_{cmax}, J_{max}, Φ_{PSII}, and q_P all increased pronouncedly as height increased but only for the north-facing canopy. The south-facing leaves instead showed a tendency to decline at the upper layer relative to the middle layer (Figures 2a,b,e,f and 3a–h). Nevertheless, this pattern only occurred for the g_{sw} in summer, while the value increased significantly with height for both-side leaves in the autumn (Figure 2c,d). In summary, the highest photosynthetic traits were shown in leaves grown in the MS or UN position rather than the US position, which implies that the scaling of photosynthetic traits with the PAR_{sum} was not linear. In terms of the C_i, conspicuous increases of 16.03% and 15.44% from summer to autumn were shown in the

US and MN positions, respectively, whereas no disparities existed among canopy positions at the first sampling (Figure 2g,h). In addition, no change was detected in the C_c across heights or orientations over the two campaigns (Table 1).

Table 1. *F* statistics from full-factorial mixed effect ANOVA for a main effect and interactions of canopy position and season on photosynthetic physiology and biochemistry. Variables analyzed were: light-saturated photosynthesis (A_{max}), stomatal conductance (g_{sw}), mesophyll conductance (g_m), CO_2 concentration in the intercellular air spaces (C_i), CO_2 concentration at the site of carboxylation (C_c), maximum carboxylation rate at 25 °C (V_{cmax}), potential maximum electron transport rate at 25 °C (J_{max}), actual photochemical efficiency of PSII (Φ_{PSII}), and photochemical quenching coefficient of PSII (q_P).

	Date	Canopy Height	Canopy Orientation	H × O	D × H × O
A_{max}	0.07	11.73 ***	13.53 **	6.06 **	0.32
g_{sw}	6.41 *	10.34 **	12.94 **	1.74	1.98
g_m	13.23 **	5.78 *	8.29 **	3.91 *	1.13
C_i	10.55 **	2.75	0.27	14.60 ***	1.22
C_c	0.50	0.65	0.49	3.25	0.83
C_i-C_c	15.08 **	0.28	0.01	0.04	1.63
V_{cmax}	0.60	4.81 *	0.54	11.39 ***	0.14
J_{max}	45.81 ***	9.19 **	0.06	25.65 ***	0.49
Φ_{PSII}	4.11	4.93 *	2.37	10.15 **	1.79
q_P	2.95	5.23 *	4.48 *	8.03 **	1.62

Significance is noted as * $p < 0.05$, ** $p < 0.01$, and *** $p < 0.001$ in the table. H, O, and D represent canopy height, canopy orientation, and measuring date, respectively.

Figure 4 illustrates the PAR_{sum} responses of gas exchange and chlorophyll fluorescence parameters at the first measuring with higher light intensity. A quadratic polynomial was applied and well-fitted the A_{max}, g_{sw}, g_m, Φ_{PSII}, and q_P vs. PAR_{sum} correlation ($R^2 = 0.573$, $p = 0.022$; $R^2 = 0.725$, $p = 0.003$; $R^2 = 0.556$, $p = 0.026$; $R^2 = 0.486$, $p = 0.049$; $R^2 = 0.516$, $p = 0.038$; Figure 4a–c), but it was not able to fit the relationships of V_{cmax} and J_{max} with PAR_{sum} ($p > 0.05$; Figure 4d). Still, these photosynthetic traits all followed similar trends, that is, an initial increase within a certain range of PAR_{sum} and a decline after reaching the apex.

Figure 5 and Table S1 illustrate comparisons among canopy positions in other leaf functional traits. The *LMA* was positively related to the PAR_{sum} ($R^2 = 0.589$, $p = 0.018$) and increased with height; hence, upper-canopy leaves showed a higher *LMA* than mid and lower leaves (Figure 5a). With regard to leaf stoichiometry, there were significant effects of height and height × orientation interaction on *N* content (including N_m and N_a; Figure 5c,e). The N_m and N_a both varied along the canopy in the same fashion as the gas exchange and chlorophyll fluorescence (i.e., there was a decline in the US position of the canopy), but only did the N_m show a significant quadratic correlation with the PAR_{sum} ($R^2 = 0.831$, $p < 0.001$; Figure 5c). In contrast to the N_m, the C_m followed a shallower gradient throughout the canopy (only 0.91% of dispersion coefficient), though significant effects of canopy height and orientation were observed (Table S1). As a result, a significant quadratic correlation was also found between the ratio of C_m to N_m (*C*:*N*) and the PAR_{sum} (Figure 5f). As for pigment concentrations, chlorophyll (Chl_{a+b}) decreased markedly as canopy height increased, and they were lower in leaves growing on the southern face than on the northern face, similar to the variation in *Car* (Figure 5b,d). Finally, the PAR_{sum} had a significantly negative power relationships with Chl_{a+b} and *Car* ($R^2 = 0.648$, $p = 0.017$; $R^2 = 0.662$, $p = 0.001$). The gradual drop in the chlorophyll to carotenoid ratio (Chl_{a+b}:*Car*) was observed as canopy height increased on account of more dramatic changes in Chl_{a+b}, though there was no response to the PAR_{sum} (Table S1).

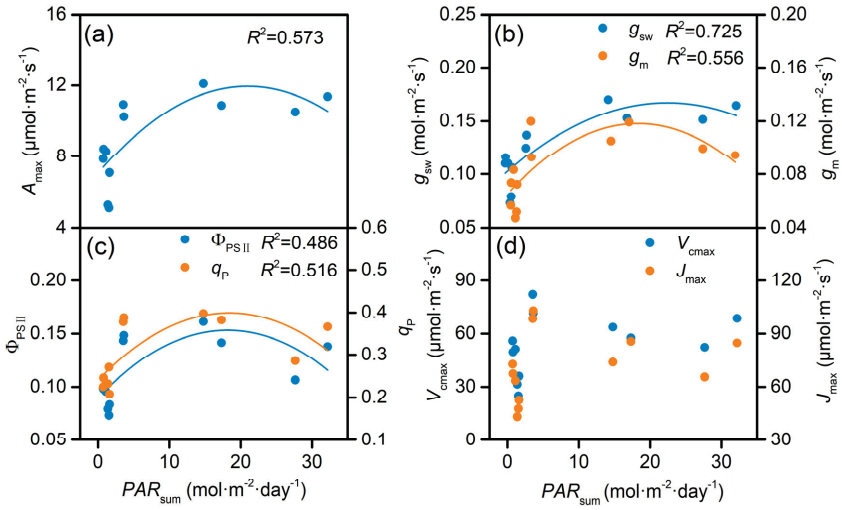


Figure 4. Correlations of daily photosynthetic active radiation (PAR_{sum}) with (**a**) light-saturated photosynthesis (A_{max}), (**b**) stomatal conductance (g_{sw}), (**b**) mesophyll conductance (g_m), (**c**) actual photochemical efficiency of PSII (Φ_{PSII}), (**c**) photochemical quenching coefficient of PSII (q_P) throughout the camphor tree canopy, (**d**) maximum carboxylation rate at 25 °C (V_{cmax}), and (**d**) potential maximum electron transport rate at 25 °C (J_{max}). Regression lines are only shown for significant relationships ($p < 0.05$). Blue circles indicate A_{max}, g_{sw}, Φ_{PSII}, and V_{cmax} of canopy leaves, and orange circles indicate g_m, q_P, and J_{max}.

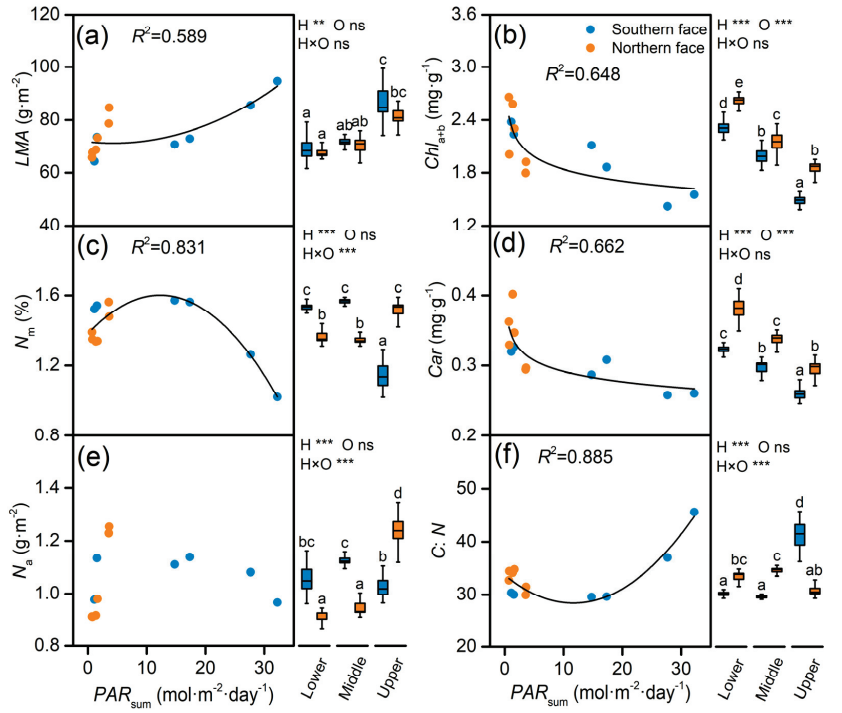


Figure 5. Correlations of daily photosynthetic active radiation (PAR_{sum}) with (**a**) leaf dry mass per area (LMA), (**b**) chlorophyll concentration (Chl_{a+b}), (**c**,**e**) mass- (N_m) and area-based (N_a) nitrogen content, (**d**) carotenoid concentration (Car), and (**f**) ratio of C_m to N_m (C:N) throughout the camphor tree canopy. Blue and orange circles represent the southern and northern faces of the canopy, respectively. Regression lines are only shown for significant relationships ($p < 0.05$). The boxplots of the leaf traits are included on the right side of the scatter subplots, and both share the same Y-axis. Lowercase letters represent a significant difference across canopy heights and orientations according to Duncan's test ($\alpha = 0.05$). Capital letters represent canopy height (H), orientation (O), and their interaction (H × O), whose significance is noted as ns $p > 0.05$, ** $p < 0.01$, and *** $p < 0.001$. All values are mean ± SE (n = 6).

3.3. Correlations Among A_{max} and Other Photosynthetic Traits

Across canopy positions and sampling times, the A_{max} correlated significantly with the g_{sw}, g_m, V_{cmax}, J_{max}, Φ_{PSII}, and q_P ($R^2 = 0.664$, $p < 0.001$; $R^2 = 0.634$, $p < 0.001$; $R^2 = 0.630$, $p < 0.001$; $R^2 = 0.330$, $p = 0.001$; $R^2 = 0.755$, $p < 0.001$; $R^2 = 0.636$, $p < 0.001$; Figure 6a). Meanwhile, the g_m related negatively to the C_i-C_c drawdown and Chl_{a+b} ($R^2 = 0.278$, $p = 0.008$; $R^2 = 0.519$, $p = 0.008$; Figure S3a), and there was also a strong positive relationship between the V_{cmax} and the J_{max} ($R^2 = 0.650$, $p < 0.001$; Figure S3b). Additionally, the N_a was positively associated with the g_m, J_{max}, Φ_{PSII}, and q_P ($R^2 = 0.369$, $p = 0.036$; $R^2 = 0.364$, $p = 0.038$; $R^2 = 0.346$, $p = 0.044$; $R^2 = 0.545$, $p = 0.006$; Figure 6b,c) but had no relationships with the V_{cmax} ($p > 0.05$; Figure 6c).

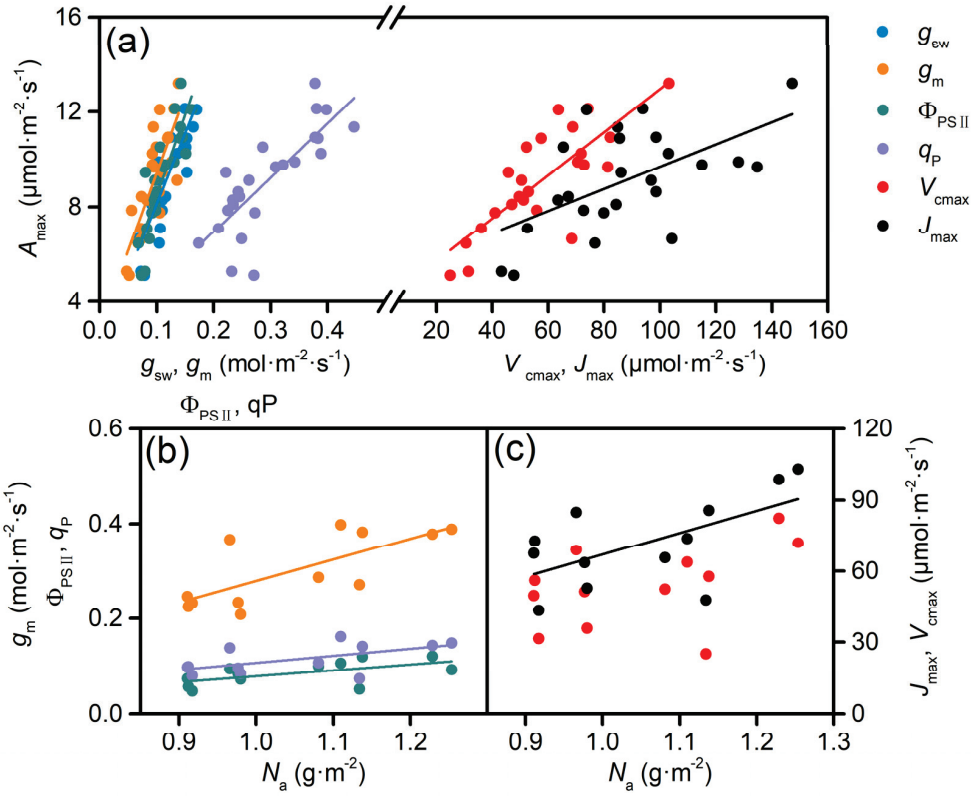


Figure 6. Linear regression relationships (**a**) between light-saturated photosynthesis (A_{max}) and stomatal conductance (g_{sw}), mesophyll conductance (g_m), actual photochemical efficiency of PSII (Φ_{PSII}) and photochemical quenching coefficient of PSII (q_P), maximum carboxylation rate at 25 °C (V_{cmax}), potential maximum electron transport rate at 25 °C (J_{max}). (**b**,**c**) Between nitrogen content on an area basis (N_a) and Φ_{PSII}, q_P, g_m, V_{cmax}, and J_{max} across canopy positions during the summer and autumn seasons (or only during summer period). Regression lines are only shown for significant relationships ($p < 0.05$).

3.4. Quantitative Limitation to Photosynthesis Throughout the Canopy

Figure 7 presents the contribution of stomatal (S_L), mesophyll (M_L), and biochemical (B_L) limitations to relative changes in the A_{max} throughout the canopy from August to October. MS position leaves reached the maximum A_{max} with the lowest total limitation, and upper leaves were close behind, limited to a certain extent by the photosynthetic process. The weaker light decreased photosynthesis to a greater extent. In summer, g_m was the main contributor to photosynthetic limitations throughout the canopy, including for US position leaves (Figure 7a). But during the autumn period, the decline in the A_{max} was primarily triggered by stomatal and biochemical limitations due to the up-regulation in g_m.

B_L explained the major relative changes in the A_{max} of upper sunlit leaves in particular (US position; Figure 7b).

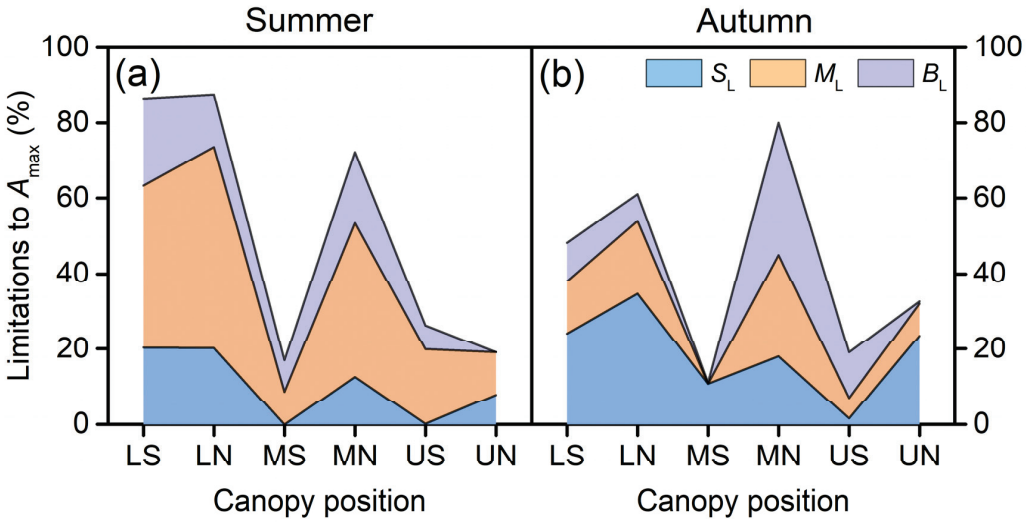


Figure 7. Quantitative limitation to light-saturated photosynthesis (A_{max}) among canopy positions during summer (**a**) and autumn (**b**). US and UN, MS and MN, LS and LN represent the southern and northern faces at the upper, middle, and lower canopy layers, respectively. S_L, M_L, and B_L represent the contribution of stomatal, mesophyll, and biochemical limitations, respectively.

4. Discussion

4.1. Foliar Physiological and Biochemical Traits Regulated by Light Availability

Our research investigated changes in leaf functional traits, such as the *LMA*, *C* and *N* contents, and pigment concentrations along the canopy of mature *C. camphora*. We found that the *LMA* was closely related to the amount of incident light, increasing significantly as canopy height increased, in accordance with previous research [35]. Conversely, the N_m was notably constrained in the sunlit leaves of the upper canopy and showed a substantial decline. While some studies suggested that the N_m remained constant regardless of spatial irradiance heterogeneity within the canopy [42], the leaves with higher *LMA*—as characterized by thicker, denser structures with more palisade layers—tended to 'dilute' the N_m. This reveals a greater investment in leaf structure (such as cell wall development) rather than in photosynthesis (such as prevention of mesophyll damage from intense light and enhancing leaf resilience), as supported by our observation of a higher *C*:*N* ratio in corresponding canopy position leaves [43,44]. In contrast, the N_a did not respond to light, primarily due to a counteracted effect of variations in the *LMA* and N_m. It was contrary to the views of Kenichi [8] and Jin et al. [45], who found that leaf *LMA* increased and N_m remained unchanged with the canopy height in natural forests, leading to the positive correlation between light and N_a. This discrepancy may be attributed to species–specific differences in canopy structure and nitrogen distribution acclimating to their respective environments. We also observed an apparent intra-canopy light gradient to which pigments were responding. In line with previous studies on forest-grown trees, irradiance had significantly negative relationships with Chl_{a+b} and *Car* [46], thus indicating that shaded leaves require more light capture to improve photosynthetic efficiency [47,48]. In the upper-canopy leaves that were exposed to high light, more *Car* was invested than Chl_{a+b} (resulting in lower Chl_{a+b}:*Car*) so as to dissipate excess light energy and to protect the photosynthetic machinery [49,50].

Photosynthetic physiological and biochemical characteristics strongly varied with the light gradient, which are predetermined to scale up from the bottom to the top of

canopy [51,52]. Contrary to our expectation, however, we observed that the A_{max} peaked in the south-facing leaves of the mid canopy, and it failed to acclimate to high light as full as the *LMA* in the upper sunlit leaves. Other photosynthetic parameters, such as the g_{sw}, g_m, Φ_{PSII}, q_P, V_{cmax}, and J_{max}, simultaneously exhibited similar patterns to the A_{max}, declining in leaves at the corresponding position, and had a positive linear correlation with the A_{max} along the light gradient. Most parameters showed quadratic correlations with light, whereas the V_{cmax} and J_{max} did not follow this pattern, mainly because the maximum values in leaves occurred under lower light conditions to avoid photoinhibition [53]. The decrease in the g_{sw} and g_m reflects the limitation of CO_2 diffusion resistance on the photosynthetic rate in leaves. Since the photosynthetic biochemistry acts as the core driver of photosynthesis, the reduced energy conversion and transport efficiency (i.e., Φ_{PSII}, q_P, and J_{max}) and limited RuBisCO (RuBP carboxylase) amount and activity (i.e., V_{cmax}) would also weaken photosynthetic efficiency. The upper sunlit canopy, as the 'engine' of light capture, determines the level of the whole canopy productivity. Any slight decline in photosynthetic capacity can be gradually amplified through resource allocation imbalance and hormone signal disorder, ultimately manifested as decreased biomass accumulation and abnormal growth of the plant [5].

4.2. Strategies of Canopy Resource Allocation to Photosynthetic Traits

The photosynthetic progress needs to be supported by sufficient nutrients, and leaf nitrogen is assumed to be crucial for the regulation of synthesis and the activity of photosynthetic organs [54,55]. The amount of RuBisCO that predominantly determines the V_{cmax} accounts for a large fraction of the total *N* in leaves, while *N* is allocated to electron transport system including cytochrome f and coupling factor [56,57]. The V_{cmax} and J_{max} are closely coordinated to ensure that the energy supply from light harvesting and electron transport meets the carboxylation demand [29]. Our data suggests that both the V_{cmax} and J_{max} were constrained by *N* loss in the sunlit leaves of the upper canopy due to their simultaneous decreases, which resulted in reduced energy demand for the Calvin cycle, and paralleled descents in the Φ_{PSII} and q_P as a crucial protective strategy for the photosystem reaction center. Since the J_{max} decreased more significantly than the V_{cmax} did, the lowered J_{max} to V_{cmax} ratio displayed the imbalance between light-driven electron transport and RuBisCO carboxylation capacity, and contributed to avoiding photoinhibition under high light conditions [58]. However, we found a positive relationship of N_a with the J_{max}, Φ_{PSII}, and q_P, but not with the V_{cmax}. This may be due to intra-canopy gradients in other environmental conditions (not light availability) that also influence the V_{cmax} [4,59]. Furthermore, total *N* in leaves is also used for non-photosynthetic opponents (e.g., cell walls), which further complicates the relationship between *N* concentration and the V_{cmax} [60]. Additionally, total *N* likewise impacts the g_m through the changes in anatomical structure and relative gene expression that regulate transmembrane transport [61–63], which concurs with our finding of a strong coupling between the N_a and g_m.

According to the hydraulic limitation hypothesis, as trees grow in stature, leaf water stress increases due to gravity and path-length resistance. Upper-canopy leaves are most suitable for absorbing sunlight, but they are also more prone to suffering from sun exposure, temperature, and wind stress especially in summer, exhibiting the greatest demand for water [42]. In our study, the upper sunlit leaves in camphor trees had a lower A_{max} and g_{sw} compared with southern leaves of mid canopy, indicating that they are probably subject to a water deficit (i.e., the reduced leaf water potential) driven by both a high transpiration rate and insufficient water availability [17,27], as the g_{sw} is regulated by hydraulic conductance [64]. Eventually, leaf growth and photosynthesis are restricted, even if the soil humidity is adequate [65]. The overgrowth in camphor tree height in overly dense

stands (up to nearly 20 m high) intensifies the burden of hydraulic transport to upper leaves and accelerate water transpiration through stomata. In light of the trade-off between xylem hydraulic efficiency and safety, the sun leaves in the upper canopy could close stomata and mitigate the water loss to prevent cavitation or embolism of the branch xylem, albeit at the expense of reduced photosynthesis [65–67]. In conclusion, the concomitant decrease of the g_{sw} and N_m in top canopy leaves reveals the optimal co-allocation of leaf nitrogen and hydraulic conductance in plant canopies, as the waste of excess nitrogen investment under the condition of hydraulic supply shortage can be avoided [17].

4.3. Effect of Season on Canopy Photosynthesis and Its Limitations

The seasonal effects on leaf photosynthetic traits can be highlighted through a comparison of the summer and autumn periods, which could be characterized as a modest growing season and a near-dormant season, respectively. The notable disparities were observed only in the g_{sw}, g_m, C_i, and J_{max}, whereas the A_{max} remained unchanged. It was primarily due to no change in the CO_2 supply in the carboxylation site (i.e., C_c) and the RuBisCO carboxylation rate that Calvin cycle was limited (i.e., V_{cmax}) in spite of the significant increase of the g_m and J_{max}. Many studies have documented a marked decrease in photosynthetic traits in woody species throughout the whole growing season due to leaf ontogeny and the severity of summer drought [35,53,68]. Our study, nonetheless, only focused on the current-year mature leaves of camphor trees, a broad-leaved evergreen species, which did not suffer from leaf senescence prior to defoliation nor from obvious summer drought from August to October. We therefore speculate that the seasonal fluctuations in the g_{sw}, g_m, C_i, and J_{max} may be ascribed to the different rates (i.e., time scale) at which these photosynthetic traits acclimated to changes in the temperature and *PAR*, consistent with the findings of Yu et al. [60]. Actually, distinguishing between the contributions of leaf ontogenetic development and of climatic impacts at the seasonal scale remains a challenge because of their mutual dependence [69].

In our study, the g_{sw} declined in camphor tree leaves as the air cooled, and this has also been reported by some researchers who have proposed that stomata close at lower temperatures to prevent water loss and energy consumption [70]. Because mid-canopy leaves are better protected from temperature and wind extremes and can transport water more effectively, some researchers have suggested that their increased g_{sw} outperforms upper sunlit leaves, particularly when exposed to sunflecks [34,71]. This finding is corroborated by our results, where this phenomenon occurred during the summer period when apparent sunflecks persisted 2–4 h from mid-morning to noon each day (Figure S2). As the sunflecks diminished in autumn, due to the decreasing solar zenith angle, a corresponding stronger stomatal closure was observed. Our observations display the adaptability and sensitivity of stomata in camphor leaves to high-light conditions across a certain seasonal temperature range.

The g_m is influenced by leaf anatomical traits (e.g., cell wall thickness and chloroplast surface area exposed to intercellular air space, S_c) and biochemical mechanisms (e.g., the quantity and activity of aquaporins, AQPs, and carbonic anhydrase, CA) [26]. AQPs, located in the chloroplast envelope and plasma membrane, facilitate CO_2 diffusion into the stroma, whereas CA regulates pH value inside the chloroplast by interconversion between CO_2 and HCO_3^- to enhance CO_2 diffusion to the carboxylation site [72,73]. Previous studies suggest that the *LMA* increases gradually as season progresses, and a higher *LMA* could lead to an increased cell wall thickness and a reduced g_m [74]. Instead, our study revealed the marked enhancement in g_m from summer to autumn, indicating that membrane permeabilities and cytosol probably dominate the variation in g_m [75,76]. Bernacchi [39] suggested that the g_m gradually declined at temperatures over 35 °C in *Nicotiana*, whereas other researchers

found the reduced g_m from around 27–29 °C to 40 °C in tree species [77–79]. Although our measurements were conducted at a mean maximum air temperature of 30.38 °C in summer, many sampling leaves were subjected to leaf temperatures exceeding 35 °C inside the cuvette, which may generate the deactivation of AQPs and CA proteins and finally lead to the significant reduction in g_m of canopy leaves. The lower leaves with thicker chloroplasts were more prone to the decline in CA activity [80], consistent with our finding of the negative link between g_m and Chl_{a+b} (Figure S3a).

In terms of photosynthetic biochemical capacity, we found that only the J_{max} was significantly suppressed along the camphor canopy profile in summer, whereas the V_{cmax} did not vary seasonally. It indicates that the electron transport chain is more sensitive to high temperatures, thereby causing ATP shortage and RuBP regeneration limitation. In other words, the J_{max} is more susceptible to environmental changes than the V_{cmax}, as was also supported by Kumarathunge [81]. The value of C_i is determined by an equilibrium between the CO_2 supply from the atmosphere and the CO_2 demand in the chloroplast. Its dependence on the simultaneous changes in stomatal opening (e.g., g_{sw}) and photosynthetic capacity (e.g., J_{max}) thereby accounts for the differences observed between the two seasons.

Based on the observations above, a quantitative limitation analysis was conducted to assess the effects of canopy position and seasonal climate on stomatal (S_L), mesophyll (M_L), and biochemical limitations (B_L) to the A_{max} in camphor trees. It was found that the limitation to photosynthesis decreased with within-canopy light intensity. However, the relative contributions were distinct between summer vs. autumn periods, though small differences were observed in the A_{max}. During the summer, characterized by higher temperatures, the g_m was the main contributor to the reduction in the A_{max} of canopy leaves, whereas S_L and B_L became predominant when the weather grew cooler in autumn because of the rising g_m. With regard to the decline in A_{max} of upper sunlit leaves, M_L and B_L could explain the main cause in summer and autumn, respectively. Bachofen et al. [4] reported stomatal limitation of photosynthesis in top European beech canopy leaves during spring, while Cano et al. [35] identified both the g_s and g_m as the key limitations during summer. Instead, Crous et al. [33] did not detect canopy differences in the g_m and g_s of mature eucalyptus leaves. It is possible that the differences in photosynthetic limitations along the canopy can be attributed to species-specific physiological responses to climate.

5. Conclusions

Here, we showed the significant effect that canopy position and season have on most of the leaf photosynthetic properties during the summer and autumn seasons in dense stands of mature camphor trees (*Cinnamomum camphora*). Different from the variations in the *LMA* and C content, the key gas exchange and chlorophyll fluorescence parameters increased along the canopy merely within a certain range of irradiance. In spite of being exposed to high light, the upper sunlit leaves exhibited a limited photosynthetic process (i.e., lower A_{max}, g_{sw}, g_m, q_P, Φ_{PSII}, J_{max} and V_{cmax}), which was generated by nitrogen loss and water deficit. On the other hand, despite the significant differences in the g_{sw}, C_i, g_m, and J_{max} between two seasons, the A_{max} did not respond to seasonality due to there being no variation in CO_2 supply in the carboxylation site (C_c) and RuBisCO carboxylation rate that limits the Calvin cycle (V_{cmax}). From the perspective of quantitative limitation analysis, our findings highlight that mesophyll and biochemical limitation contribute the most to the A_{max} decrease in summer and autumn, respectively. It is recommended to conduct the moderate regulation and management of stand density for mature forests. These findings are vital for the accurate prediction of carbon sink capacity of urban vegetation in the region.

Supplementary Materials: The following supporting information can be downloaded at: https://www.mdpi.com/article/10.3390/f16040581/s1, Figure S1: Bamboo experimental platform established in Shanghai Botanical Garden; Figure S2: Diurnal variation in photosynthetic active radiation (*PAR*) across canopy positions between summer and autumn. US and UN, MS and MN, LS and LN represent the southern and northern faces at the upper, middle, and lower canopy layers, respectively. FL represents full light above the canopy; Figure S3: Linear regression relationships (a) between mesophlly conductance (g_m) and the CO_2 concentration difference from stomatal cavity to carboxylation site (C_i-C_c), chlorophyll content (Chl_{a+b}), and (b) between maximum carboxylation rate of RuBisCO at 25 °C (V_{cmax}) and potential maximum electron transport rate at 25 °C (J_{max}) across canopy positions during summer and autumn seasons (or only during summer period); Table S1: Leaf morphology, stoichiometry and pigment across different canopy positions for mature *C. camphor* trees.

Author Contributions: Conceptualization, L.Z. and H.L.; methodology, L.Z. and H.L.; formal analysis, H.L.; data curation, H.L.; writing—original draft preparation, H.L.; writing—review and editing, H.L., L.Z. and W.Y.; visualization, H.L. and W.Y.; supervision, W.Y.; project administration, W.Y.; funding acquisition, W.Y. All authors have read and agreed to the published version of the manuscript.

Funding: The study has been funded by the Natural Science Foundation of Shanghai (22ZR1461000) and the National Natural Science Foundation of China (32471683, 31600352).

Data Availability Statement: The data that underlie this study are available upon request.

Acknowledgments: We thank Zhang Chao for helpful suggestions on the manuscript. Special thanks to Guo Jiankang for providing meteorological data. Finally, we thank Jiang Kai for English editing.

Conflicts of Interest: The authors declare no conflicts of interest.

References

1. Ozanne, C.M.P.; Anhuf, D.; Boulter, S.L.; Keller, M.; Kitching, R.L.; Ko, C.; Meinzer, F.C.; Mitchell, A.W.; Nakashizuka, T.; Dias, P.L.S.; et al. Biodiversity meets the atmosphere: A global view of forest canopies. *Science* **2003**, *301*, 183–186. [CrossRef] [PubMed]
2. Valladares, F. Light heterogeneity and plants: From ecophysiology to species coexistence and biodiversity. In *Progress in Botany*; Esser, K., Lüttge, U., Beyschlag, W., Hellwig, F., Eds.; Springer: Berlin/Heidelberg, Germany, 2003; pp. 439–471.
3. Niinemets, Ü.; Anten, N.P.R. Packing the photosynthesis machinery: From leaf to canopy. In *Photosynthesis in Silico*; Laisk, A., Nedbal, L., Govindjee, Eds.; Springer: Berlin/Heidelberg, Germany, 2009; pp. 363–399.
4. Bachofen, C.; D'Odorico, P.; Buchmann, N. Light and VPD gradients drive foliar nitrogen partitioning and photosynthesis in the canopy of European beech and silver fir. *Oecologia* **2020**, *192*, 323–339. [CrossRef] [PubMed]
5. Niinemets, Ü. Photosynthesis and resource distribution through plant canopies. *Plant Cell Environ.* **2007**, *30*, 1052–1071. [CrossRef]
6. Iio, A.; Fukasawa, H.; Nose, Y.; Kato, S.; Kakubari, Y. Vertical, horizontal and azimuthal variations in leaf photosynthetic characteristics within a *Fagus crenata* crown in relation to light acclimation. *Tree Physiol.* **2005**, *25*, 533–544. [CrossRef]
7. Hanba, Y.T.; Kogami, H.; Terashima, I. The effect of growth irradiance on leaf anatomy and photosynthesis in Acer species differing in light demand. *Plant Cell Environ.* **2002**, *25*, 1021–1030. [CrossRef]
8. Kenichi, Y. Irradiance heterogeneity within crown affects photosynthetic capacity and nitrogen distribution of leaves in Cedrela sinensis. *Plant Cell Environ.* **2010**, *33*, 750–758. [CrossRef]
9. Thomas, S.C.; Winner, W.E. Photosynthetic differences between saplings and adult trees: An integration of field results by meta-analysis. *Tree Physiol.* **2002**, *22*, 117–127. [CrossRef]
10. Valladares, F.; Pearcy, R.W. The functional ecology of shoot architecture in sun and shade plants of *Heteromeles arbutifolia* M. Roem., a Californian chaparral shrub. *Oecologia* **1998**, *114*, 1–10. [CrossRef]
11. Farquhar, G.D.; von Caemmerer, S.; Berry, J.A. A biochemical model of photosynthetic CO_2 assimilation in leaves of C_3 species. *Planta* **1980**, *149*, 78–90. [CrossRef]
12. Field, C. Allocating leaf nitrogen for the maximization of carbon gain: Leaf age as a control on the allocation program. *Oecologia* **1983**, *56*, 341–347. [CrossRef]
13. Lloyd, J.; Wong, S.; Styles, J.M.; Batten, D.; Priddle, R.; Turnbull, C.; McConchie, C. Measuring and modelling whole-tree gas exchange. *Funct. Plant Biol.* **1995**, *22*, 987–1000. [CrossRef]
14. Hirtreiter, J.N.; Potts, D.L. Canopy structure, photosynthetic capacity and nitrogen distribution in adjacent mixed and monospecific stands of *Phragmites australis* and *Typha latifolia*. *Plant Ecol.* **2012**, *213*, 821–829. [CrossRef]

15. Niinemets, Ü.; Keenan, T.F.; Hallik, L. A worldwide analysis of within-canopy variations in leaf structural, chemical and physiological traits across plant functional types. *New Phytol.* **2015**, *205*, 973–993. [CrossRef]
16. Niinemets, Ü. Variation in leaf photosynthetic capacity within plant canopies: Optimization, structural, and physiological constraints and inefficiencies. *Photosyn Res.* **2023**, *158*, 131–149. [CrossRef]
17. Peltoniemi, M.S.; Duursma, R.A.; Medlyn, B.E. Co-optimal distribution of leaf nitrogen and hydraulic conductance in plant canopies. *Tree Physiol.* **2012**, *32*, 510–519. [CrossRef] [PubMed]
18. Aasamaa, K.; Sõber, A.; Hartung, W.; Niinemets, Ü. Drought acclimation of two deciduous tree species of different layers in a temperate forest canopy. *Trees* **2004**, *18*, 93–101. [CrossRef]
19. Sellin, A.; Õunapuu, E.; Kupper, P. Effects of light intensity and duration on leaf hydraulic conductance and distribution of resistance in shoots of silver birch (*Betula pendula*). *Physiol. Plant.* **2008**, *134*, 412–420. [CrossRef]
20. Evans, J.R.; Poorter, H. Photosynthetic acclimation of plants to growth irradiance: The relative importance of specific leaf area and nitrogen partitioning in maximizing carbon gain. *Plant Cell Environ.* **2001**, *24*, 755–767. [CrossRef]
21. Sellin, A.; Kupper, K. Effects of light availability versus hydraulic constraints on stomatal responses within a crown of silver birch. *Oecologia* **2005**, *142*, 388–397. [CrossRef]
22. Sellin, A.; Kupper, K. Effects of enhanced hydraulic supply for foliage on stomatal responses in little-leaf linden (*Tilia cordata* Mill). *Eur. J. For. Res.* **2007**, *126*, 241–251. [CrossRef]
23. Niinemets, Ü. Optimization of foliage photosynthetic capacity in tree canopies: Towards identifying missing constraints. *Tree Physiol.* **2012**, *32*, 505–509. [CrossRef] [PubMed]
24. Xiong, D.L.; Douthe, C.; Flexas, J. Differential coordination of stomatal conductance, mesophyll conductance and leaf hydraulic conductance in response to changing light across species: Coordination of CO_2 diffusion and H_2O transport inside leaves. *Plant Cell Environ.* **2017**, *41*, 436–450. [CrossRef] [PubMed]
25. Ubierna, N.; Gandin, A.; Cousins, A. The response of mesophyll conductance to short-term variation in CO_2 in the C_4 plants *Setaria viridis* and *Zea mays*. *J. Exp. Bot.* **2018**, *69*, 1159–1170. [CrossRef] [PubMed]
26. Flexas, J.; Ribas-Carbo, M.; Diaz-Espejo, A.; Galmés, J.; Medrano, H. Mesophyll conductance to CO_2: Current knowledge and future prospects. *Plant Cell Environ.* **2008**, *31*, 602–621. [CrossRef]
27. Li, S.L.; Tan, T.T.; Fan, Y.F.; Muhammad Ali, R.; Wang, Z.L.; Wang, B.B.; Zhang, J.W.; Tan, X.M.; Chen, P.; Iram, S.; et al. Responses of leaf stomatal and mesophyll conductance to abiotic stress factors. *J. Integr. Agric.* **2022**, *21*, 2787–2804. [CrossRef]
28. Grassi, G.; Meir, P.; Cromer, R.; Tompkins, D.; Jarvis, P.G. Photosynthetic parameters in seedlings of *Eucalyptus grandis* as affected by rate of nitrogen supply. *Plant Cell Environ.* **2002**, *25*, 1677–1688. [CrossRef]
29. Bachofen, C.; Hülsmann, L.; Revil, A.; Buchmann, N.; D'Odorico, P. Accounting for foliar gradients in V_{cmax} and J_{max} improves estimates of net CO_2 exchange of forests. *Agric. For. Meteorol.* **2022**, *314*, 108771. [CrossRef]
30. Grassi, G.; Magnani, F. Stomatal, mesophyll conductance and biochemical limitations to photosynthesis as affected by drought and leaf ontogeny in ash and oak trees. *Plant Cell Environ.* **2005**, *28*, 834–849. [CrossRef]
31. Walker, A.P.; Quaife, T.; van Bodegom, P.M.; de Kauwe, M.G.; Keenan, T.F.; Joiner, J.; Lomas, M.R.; MacBean, N.; Xu, C.; Yang, X.; et al. The impact of alternative trait-scaling hypotheses for the maximum photosynthetic carboxylation rate (V_{cmax}) on global gross primary production. *New Phytol.* **2017**, *215*, 1370–1386. [CrossRef]
32. Guo, J.M.; Beverly, D.P.; Ewers, B.E.; Williams, D.G. Stomatal, mesophyll and biochemical limitations to photosynthesis and their relationship with leaf structure over an elevation gradient in two conifers. *Photosyn Res.* **2023**, *157*, 85–101. [CrossRef]
33. Crous, K.Y.; Campany, C.; López, R.; Cano, F.J.; Ellsworth, D.S. Canopy position affects photosynthesis and anatomy in mature Eucalyptus trees in elevated CO_2. *Tree Physiol.* **2020**, *41*, 206–222. [CrossRef]
34. Campany, C.E.; Tjoelker, M.G.; von Caemmerer, S.; Duursma, R.A. Coupled response of stomatal and mesophyll conductance to light enhances photosynthesis of shade leaves under sunflecks. *Plant Cell Environ.* **2016**, *39*, 2762–2773. [CrossRef] [PubMed]
35. Cano, F.J.; Sánchez-Gómez, D.; Rodríguez-Calcerrada, J.; Warren, C.R.; Gil, L.; Aranda, I. Effects of drought on mesophyll conductance and photosynthetic limitations at different tree canopy layers. *Plant Cell Environ.* **2013**, *36*, 1961–1980. [CrossRef]
36. Zhong, J.J.; Li, X.M.; Wang, B.Y.; Xu, X.B.; Yan, W. Investigation and Analysis of the Woody Plants in Shanghai Parks. *Chin. Landsc. Archit.* **2019**, *35*, 123–127. (In Chinese) [CrossRef]
37. Evans, J.R.; Loreto, F. Acquisition and diffusion of CO_2 in higher plant leaves. In *Photosynthesis: Physiology and Metabolism*; Leegood, R.C., Sharkey, T.D., von Caemmerer, S., Eds.; Kluwer Academic: Dordrecht, The Netherland, 2000; pp. 321–351.
38. Harley, P.C.; Loreto, F.; Dimarco, G.; Sharkey, T.D. Theoretical considerations when estimating the mesophyll conductance to CO_2 flux by analysis of the response of photosynthesis to CO_2. *Plant Physiol.* **1992**, *98*, 1429–1436. [CrossRef] [PubMed]
39. Bernacchi, C.J.; Portis, A.R.; Nakano, H.; von Caemmerer, S.; Long, S.P. Temperature response of mesophyll conductance. Implications for the determination of Rubisco enzyme kinetics and for limitations to photosynthesis in vivo. *Plant Physiol.* **2002**, *130*, 1992–1998. [CrossRef]
40. Bernacchi, C.J.; Pimentel, C.; Longi, S.P. In vivo temperature response functions of parameters required to model RuBP-limited photosynthesis. *Plant Cell Environ.* **2003**, *26*, 1419–1430. [CrossRef]

41. Lichtenthaler, H.K.; Wellburn, A.R. Determinations of total carotenoids and chlorophylls a and b of leaf extracts in different solvents. *Biochem. Soc. Trans.* **1983**, *11*, 591–592. [CrossRef]
42. Schmiege, S.C.; Griffin, K.L.; Boelman, N.T.; Vierling, L.A.; Bruner, S.G.; Min, E.; Maguire, A.J.; Jensen, J.; Eitel, J.U.H. Vertical gradients in photosynthetic physiology diverge at the latitudinal range extremes of white spruce. *Plant Cell Environ.* **2022**, *46*, 45–63. [CrossRef]
43. Warren, C.R.; Adams, M.A. Evergreen trees do not maximize instantaneous photosynthesis. *Trends Plant Sci.* **2004**, *9*, 270–274. [CrossRef]
44. González-Zurdo, P.; Escudero, A.; Babiano, J.; García-Ciudad, A.; Mediavilla, S. Costs of leaf reinforcement in response to winter cold in evergreen species. *Tree Physiol.* **2016**, *36*, 273–286. [CrossRef] [PubMed]
45. Jin, D.; Cao, X.; Ma, K. Leaf functional traits vary with the adult height of plant species in forest communities. *J. Plant Ecol.* **2014**, *7*, 68–76. [CrossRef]
46. Gardner, A.; Ellsworth, D.S.; Pritchard, J.; MacKenzie1, A.R. Are chlorophyll concentrations and nitrogen across the vertical canopy profile affected by elevated CO_2 in mature Quercus trees? *Trees* **2022**, *36*, 1797–1809. [CrossRef]
47. Sharwood, R.E.; Crous, K.Y.; Whitney, S.M.; Ellsworth, D.S.; Ghannoum, O. Linking photosynthesis and leaf N allocation under future elevated CO_2 and climate warming in *Eucalyptus globulus*. *J. Exp. Bot.* **2017**, *68*, 1157–1167. [CrossRef]
48. Lennon, A.M.; Lewis, V.R.; Farrell, A.D.; Umaharan, P. Photochemical responses to light in sun and shade leaves of *Theobroma cacao* L. (West African Amelonado). *Sci. Hortic.* **2021**, *276*, 109747. [CrossRef]
49. Ruban, A.V. Evolution under the sun: Optimizing light harvesting in photosynthesis. *J. Exp. Bot.* **2015**, *66*, 7–23. [CrossRef]
50. Magney, T.S.; Eitel, J.U.H.; Griffin, K.L.; Boelman, N.T.; Greaves, H.E.; Prager, C.M.; Logan, B.A.; Zheng, G.; Ma, L.; Fortin, E.A.; et al. LiDAR canopy radiation model reveals patterns of photosynthetic partitioning in an *Arctic shrub*. *Agric. For. Meteorol.* **2016**, *221*, 78–93. [CrossRef]
51. Crous, K.Y.; Ellsworth, D.S. Canopy position affects photosynthetic adjustments to long-term elevated CO_2 concentration (FACE) in aging needles in a mature Pinus taeda forest. *Tree Physiol.* **2004**, *24*, 961–970. [CrossRef] [PubMed]
52. Rogers, A.; Medlyn, B.E.; Dukes, J.S.; Bonan, G.; von Caemmerer, S.; Dietze, M.C.; Zaehle, S. A roadmap for improving the representation of photosynthesis in Earth system models. *New Phytol.* **2017**, *213*, 22–42. [CrossRef]
53. Bauerle, W.L.; McCullough, C.; Iversen, M.; Hazlett, M. Leaf age and position effects on quantum yield and photosynthetic capacity in Hemp crowns. *Plants* **2020**, *9*, 271. [CrossRef]
54. Warren, J.M.; Jensen, A.M.; Medlyn, B.E.; Norby, R.J.; Tissue, D.T. Carbon dioxide stimulation of photosynthesis in *Liquidambar styracifua* is not sustained during a 12-year field experiment. *AoB Plants* **2015**, *7*, plu074. [CrossRef] [PubMed]
55. Xiong, D.L.; Liu, X.; Liu, L.; Douthe, C.; Li, Y.; Peng, S.B.; Liang, H.J. Rapid responses of mesophyll conductance to changes of CO_2 concentration, temperature and irradiance are affected by N supplements in rice. *Plant Cell Environ.* **2015**, *38*, 2541–2550. [CrossRef] [PubMed]
56. Quebbeman, J.A.; Ramirez, J.A. Optimal allocation of leaf-level nitrogen: Implications for covariation of V_{cmax} and J_{max} and photosynthetic downregulation. *J. Geophys. Res. Biogeosci.* **2016**, *121*, 2464–2475. [CrossRef]
57. Rajsnerová, P.; Klem, K.; Holub, P.; Novotná, K.; Večeřová, K.; Kozáčiková, M.; Rivas-Ubach, A.; Sardans, J.; Marek, M.V.; Peñuelas, J.; et al. Morphological, biochemical and physiological traits of upper and lower canopy leaves of European beech tend to converge with increasing altitude. *Tree Physiol.* **2015**, *35*, 47–60. [CrossRef]
58. Walker, A.P.; Beckerman, A.P.; Gu, L.; Kattge, J.; Cernusak, L.A.; Domingues, T.F.; Scales, J.C.; Wohlfahrt Georg Wullschleger, S.D.; Woodward, F.I. The relationship of leaf photosynthetic traits -V_{cmax} and J_{max}- to leaf nitrogen, leaf phosphorus, and specific leaf area: A meta-analysis and modeling study. *Ecol. Evol.* **2014**, *4*, 3218–3235. [CrossRef]
59. Buckley, T.N. Optimal carbon partitioning helps reconcile the apparent divergence between optimal and observed canopy profiles of photosynthetic capacity. *New Phytol.* **2021**, *230*, 2246–2260. [CrossRef]
60. Yu, L.; Luo, X.; Croft, H.; Rogers, C.A.; Chen, J.M. Seasonal variation in the relationship between leaf chlorophyll content and photosynthetic capacity. *Plant Cell Environ.* **2024**, *47*, 3953–3965. [CrossRef]
61. Bown, H.E.; Watt, M.S.; Mason, E.G.; Cliton, P.W.; Whitehead, D. The influence of nitrogen and phosphorus supply and genotype on mesophyll conductance limitations to photosynthesis in *Pinus radiata*. *Tree Physiol.* **2009**, *29*, 1143–1151. [CrossRef]
62. Hacke, U.G.; Plavcová, L.; Almeida-Rodriguez, A.; King-Jones, S.; Zhou, W.; Cooke, J.E.K. Influence of nitrogen fertilization on xylem traits and aquaporin expression in stems of hybrid poplar. *Tree Physiol.* **2010**, *30*, 1016–1025. [CrossRef]
63. Ligaba, A.; Katsuhara, M.; Shibasaka, M.; Djira, G. Abiotic stresses modulate expression of major intrinsic proteins in barley (*Hordeum vulgare*). *C R. Biol.* **2011**, *334*, 127–139. [CrossRef]
64. Flexas, J.; Scoffoni, C.; Gago, J.; Sack, L. Leaf mesophyll conductance and leaf hydraulic conductance: An introduction to their measurement and coordination. *J. Exp. Bot.* **2013**, *64*, 3965–3981. [CrossRef]
65. Ryan, M.J.; Yoder, B.J. Hydraulic limits to tree height and tree growth. *BioSci.* **1997**, *47*, 235–242. [CrossRef]
66. Domec, J.C.; Lachenbruch, B.; Meinzer, F.C.; Woodruff, D.R.; Warren, J.M.; McCulloh, K.A. Maximum height in a conifer is associated with conflicting requirements for xylem design. *Proc. Natl. Acad. Sci. USA* **2008**, *105*, 12069–12074. [CrossRef]

67. Givnish, T.J.; Wong, S.C.; Stuart-Williams, H.; Holloway-Phillips, M.; Farquhar, G.D. Determinants of maximum tree height in Eucalyptus species along a rainfall gradient in Victoria, Australia. *Ecology* **2014**, *95*, 2991–3007. [CrossRef]
68. Wright, I.J.; Leishman, M.R.; Read, C.; Westoby, M. Gradients of light availability and leaf traits with leaf age and canopy position in 28 Australian shrubs and trees. *Funct. Plant Biol.* **2006**, *33*, 407–419. [CrossRef] [PubMed]
69. Yamashita, N.; Koike, N.; Ishida, A. Leaf ontogenetic dependence of light acclimation in invasive and native subtropical trees of different successional status. *Plant Cell Environ.* **2002**, *25*, 1341–1356. [CrossRef]
70. Urban, J.; Ingwers, M.; McGuire, M.A.; Teskey, R. Increase in leaf temperature opens stomata and decouples net photosynthesis from stomatal conductance in *Pinus taeda* and *Populus deltoides*×*nigra*. *J. Exp. Bot.* **2017**, *68*, 1757–1767. [CrossRef]
71. Buckley, T.N.; Martorell, S.; Diaz-Espejo, A.; Tomàs, M.; Medrano, H. Is stomatal conductance optimized over both time and space in plant crowns? A field test in grapevine (*Vitis vinifera*). *Plant Cell Environ.* **2014**, *37*, 2707–2712. [CrossRef]
72. Uehlein, N.; Sperling, H.; Heckwolf, M.; Kaldenhoff, R. The *Arabidopsis* aquaporin PIP1;2 rules cellular CO_2 uptake. *Plant Cell Environ.* **2012**, *35*, 1077–1083. [CrossRef]
73. Momayyezi, M.; Guy, R.D. Substantial role for carbonic anhydrase in latitudinal variation in mesophyll conductance of *Populus trichocarpa* Torr. & Gray. *Plant Cell Environ.* **2017**, *40*, 138–149. [CrossRef]
74. Tomás, M.; Flexas, J.; Copolovici, L.; Galmés, J.; Hallik, L.; Medrano, H.; Ribas-Carbó, M.; Tosens, T.; Vislap, V.; Niinemets, Ü. Importance of leaf anatomy in determining mesophyll diffusion conductance to CO_2 across species: Quantitative limitations and scaling up by models. *J. Exp. Bot.* **2013**, *64*, 2269–2281. [CrossRef] [PubMed]
75. Boex-Fontvieille, E.; Jossier, M.; Davanture, M.; Zivy, M.; Hodges, M.; Tcherkez, G. Differential protein phosphorylation regulates chloroplast movement in response to strong light and darkness in *Arabidopsis thaliana*. *Plant Mol. Biol. Rep.* **2014**, *32*, 987–1001. [CrossRef]
76. Ouyang, W.; Struik, P.; Yin, X.; Yang, J. Stomatal conductance, mesophyll conductance, and transpiration efficiency in relation to leaf anatomy in rice and wheat genotypes under drought. *J. Exp. Bot.* **2017**, *68*, 5191–5205. [CrossRef]
77. Pons, T.L.; Welschen, R.A.M. Midday depression of net photosynthesis in the tropical rainforest tree *Eperua grandiflora*: Contributions of stomatal and internal conductances, respiration and Rubisco functioning. *Tree Physiol.* **2003**, *23*, 937–947. [CrossRef] [PubMed]
78. Warren, C.R.; Dreyer, E. Temperature response of photosynthesis and internal conductance to CO_2: Results from two independent approaches. *J. Exp. Bot.* **2006**, *57*, 3057–3067. [CrossRef] [PubMed]
79. Montpied, P.; Granier, A.; Dreyer, E. Seasonal time-course of gradients of photosynthetic capacity and mesophyll conductance to CO_2 across a beech (*Fagus sylvatica* L.) canopy. *J. Exp. Bot.* **2009**, *60*, 2407–2418. [CrossRef]
80. Tosens, T.; Niinemets, Ü.; Vislap, V.; Eichelmann, H.; Castro Díez, P. Developmental changes in mesophyll diffusion conductance and photosynthetic capacity under different light and water availabilities in Populus tremula: How structure constrains function. *Plant Cell Environ.* **2012**, *35*, 839–856. [CrossRef]
81. Kumarathunge, D.P.; Medlyn, B.E.; Drake, J.E.; Tjoelker, M.G.; Aspinwall, M.J.; Battaglia, M.; Cano, F.J.; Carter, K.R.; Cavaleri, M.A.; Cernusak, L.A.; et al. Acclimation and adaptation components of the temperature dependence of plant photosynthesis at the global scale. *New Phytol.* **2019**, *222*, 768–784. [CrossRef]

Disclaimer/Publisher's Note: The statements, opinions and data contained in all publications are solely those of the individual author(s) and contributor(s) and not of MDPI and/or the editor(s). MDPI and/or the editor(s) disclaim responsibility for any injury to people or property resulting from any ideas, methods, instructions or products referred to in the content.

forests

MDPI

Article

Mycorrhization of *Quercus dentata* Seedlings with *Laccaria bicolor* Enhances Salt Tolerance of Plants Only Under Relatively Moderate Soil Salinity Level

Wenlong Sun [1], Luyu Qi [1], Haonan Chen [1], Yixin Song [1], Jiaqi Jiang [1], Puyi Zhang [1], Bojian Wang [2], Qiang Wang [2], Gaode Meng [1], Tianyu Ji [1], Xinke Sun [1], Weihua Guo [1], Ning Du [1,*] and Janusz J. Zwiazek [3]

[1] Qingdao Key Laboratory of Ecological Protection and Restoration, School of Life Sciences, Shandong University, 72 Binhai Road, Qingdao 266237, China; qingyuansanren@163.com (W.S.); jiaqijiang123@126.com (J.J.)
[2] Shandong Provincial Forestry Protection and Development Service Center, 5948 Second Ring East Road, Jinan 250100, China
[3] Department of Renewable Resources, University of Alberta, 442 Earth Sciences Building, Edmonton, AB T6G 2E3, Canada; jzwiazek@ualberta.ca
* Correspondence: duning_sdu@126.com; Tel.: +86-135-7314-6471

Abstract: Soil salinization is a growing global concern in many ecosystems. Although ectomycorrhizal fungi have been shown to alleviate the effects of salinity in some tree species, uncertainties persist concerning their effectiveness when plants are exposed to different salinity levels that are commonly present in salt-affected soils. *Quercus dentata* seedlings either non-inoculated (mycorrhizal control) or inoculated with the ectomycorrhizal fungus *Laccaria bicolor* were then treated with three NaCl concentrations (0, 0.4%, and 0.8%). The physiological, stoichiometric, and growth characteristics of the plants were examined. NaCl significantly affected seedling growth and physiology. However, the impact of *L. bicolor* on *Q. dentata* seedlings could shift in response to varying salt concentrations. Under moderate salinity, inoculation of *L. bicolor* increased root biomass by 4.55% and leaf chlorophyll concentrations by 46.8%, and decreased leaf Na^+ concentrations and the Na^+/K^+ ratios. Under high salinity, *L. bicolor* decreased leaf water content and fluorescence parameters, and increased leaf Na^+ concentrations. The effect of ectomycorrhizal fungus *L. bicolor* on *Q. dentata* seedlings was dependent on NaCl concentration, and our results indicate that the use of *L. bicolor* in afforestation efforts with *Q. dentata* would only be effective under relatively low soil salinity levels.

Keywords: *Quercus dentata*; *Laccaria bicolor*; salt tolerance; phytoremediation; ectomycorrhiza

1. Introduction

Increasing soil salinization is one of the major and widespread soil factors that threatens plant survival and affects their growth and yield in many ecosystems [1,2]. Combined with progressing global climate changes and human activity, major disturbances of the ecosystems could be expected to cause a catastrophic collapse of the ecosystem states and services [3]. To achieve sustainability of agricultural production and stability of ecosystems, it is essential to prevent further salinization of soils and to develop the knowledge required to manage salt-affected sites to restore their productivity [4,5]. It is generally recognized that phytoremediation and revegetation of salinized land are appropriate but challenging tasks that can mitigate soil salinization [6,7]. For the revegetation processes, species

selection and remediation methods are especially critical and may be combined with an enhancement of plant salt tolerance by beneficial microorganisms [8,9].

Plant species commonly used in saline phytoremediation are mainly halophytes [10–12], which have been employed to restore landscapes damaged by a variety of contaminants and disturbances [13,14]. However, other salt-tolerant plant species have also been considered for their suitability of restoration of moderately saline areas. *Quercus* is considered to be a tree genus with a successful evolutionary history of adaptation to changing and complex environments [15,16]. Studies have shown that some species of *Quercus*, including *Quercus robur* [17], *Q. virginiana* [18], and *Q. ilex* [19], exhibit tolerance of moderate salt levels. Therefore, the oak should be considered a potential tree species for the restoration of salt-affected areas.

In addition to selecting halophytes with superior salt tolerance [7,10], appropriate management techniques corresponding to soil regeneration are also required to improve ecosystem stability [20]. Phytoremediation with mycorrhizal fungi that can live in symbiosis with their host plants is one of the effective and sustainable methods for ecosystem stability. Mycorrhizal fungi have long been known to contribute to the stress tolerance of plants, including salinity in various plants [21–24] including oak species [25,26]. Studies have shown that inoculation with ectomycorrhizal fungi (EMF) can alleviate the toxic effects of salinity in *Q. mongolica* seedlings by promoting the uptake of K^+ and Ca^{2+}, which helps regulate ionic balance by increasing K^+/Na^+ and Ca^{2+}/Na^+ ratios [27]. Seedling height increased following inoculation, but the magnitude of the effect of different species of EMF varied [27]. Another study has also shown that inoculation with EMF improved salt tolerance in *Q. mongolica* seedlings by increasing in plants the contents of soluble sugars, soluble proteins, and chlorophyll, in addition to enhancing leaf stomatal conductance (gs) and intercellular CO_2 concentrations (Ci), suggesting that different species of EMF may improve salt tolerance in the *Quercus* species via different mechanisms [28].

Within the range of salt stresses tolerated by the fungi, the host plants could be able to survive better. And the stabilization of the cooperation in mutualism might be limited by the severity of environmental stress. Fungi themselves vary in salt tolerance [29]. For example, there has been research published for different ectomycorrhizal fungi cultivated on plates [30]. Then, if salt stress in the environment is exacerbated, the survival of the fungus is bound to suffer. The contested point we need to focus on is if mycorrhizas will offer any protection to plants when they are exposed to moderate and high salt concentrations. Also, maintaining mycorrhizas is costly to the plant since the fungi drain the plant of its carbon resources. The question is, then, if the plants are severely stressed with salt, will the fungus still be helpful or will it become a burden for the plant weakened by the salt.

In the present study, we examined the effects of the ectomycorrhizal fungus *Laccaria bicolor* on the responses of the Daimyo oak (*Quercus dentata*) to relatively moderate (0.4% soil DW) and high (0.8% soil DW) NaCl concentrations. *Q. dentata* is a common temperate deciduous tree of medium size. Its fruit is a nut, usually encased in a cup-shaped shell hopper. The scales of the cupule are short, about 0.5–1.0 cm in length. *Q. dentata* has been reported to have high genetic differentiation and diversity [31], as well as superior salt tolerance even at the seedling stage [32]. The trees of this species are broadly distributed across the temperate zone of the northern hemisphere [16], and form symbiotic relationships with a wide range of ectomycorrhizal fungi [25]. *Q. dentata* has been widely used for vegetation restoration in fragile environments, especially in temperate regions [33]. Since ectomycorrhizal fungi vary in their effectiveness in enhancing salt tolerance to trees, the choice of an appropriate fungal species for mycorrhization of *Q. dentata* could help with improving the restoration efforts of areas affected by salinity. As the first sequenced

ectomycorrhizal fungus [34], *L. bicolor* forms ectomycorrhizal associations with a wide range of host tree species and has been successfully used to improve salinity tolerance in multiple host plants [29,35,36]. A series of effector-type small, secreted proteins (SSPs) are induced to initiate phenotypical or physiological changes in ectomycorrhizal fungi or host plants during mutualistic symbiosis, by which, *L. bicolor* can strive for an increase in the infestation success [37]. *L. bicolor*, therefore, can form symbioses with multiple host plants including oaks [38]. However, most studies have examined the effects of mycorrhization on plant responses to relatively low salinity levels, and it is presently little known how effective the ectomycorrhizal fungi are in enhancing salt tolerance in plants facing the salinity levels in the soils that are classified as saline. We, therefore, carried out experiments with *Q. dentata* seedlings that were either non-inoculated or inoculated with the ectomycorrhizal fungus *L. bicolor* and exposed the seedlings to relatively moderate and high soil NaCl levels. We hypothesized that an inoculation of *Q. dentata* seedlings with *L. bicolor* will improve the salt tolerance of seedlings under both relatively moderate and high soil salinity conditions, but the effectiveness of the mycorrhization will be more pronounced under the lower level of soil salinity.

2. Materials and Methods

2.1. Seed Collection and Germination

Q. dentata acorns were collected from Zhongshan Park in Tsingtao, Shandong province, China and stored at 4 °C until Spring. Large, healthy acorns were selected and soaked in 5% H_2O_2 for 5 min, washed with water, and germinated in sand in a greenhouse (70% light transmittance, 25.1 °C average temperature, 80.4% average relative humidity during the experimental period). The growth substrate was composed of equal volumes of river sand and organic cultivation soil; after that, thoroughly mixed and homogenized growth substrate had been sterilized twice using high-pressure steam (121 °C, 20 min). The pH of the growth substrate is in the range of 6.5 to 7.5, and the organic matter content is $\geq$30%. After germination, the seedlings with a radicle of approximately the same length (2–3 cm) were selected and transferred into the pots (24 × 26 cm (diameter × height) filled with 5 kg soil) and watered daily to sustain vigorous growth.

2.2. Fungal Culture and Inoculation

The fungal strain *L. bicolor* UAMH8232 provided by the University of Alberta, Microfungus Collection and Herbarium, Edmonton, Canada, was cultured with modified Melin–Norkrans medium (MMN medium) [29]. After 2 weeks of cultivation in a shaking incubator (25 °C, 120 rpm), the filtered and homogenized mycelia were diluted with distilled water to 0.5 mg dry mycelia/mL [35] to make an inoculum.

One week after germination, the potted plants were divided into two equal groups. The mycorrhizal group was inoculated with *L. bicolor* by adding 10 mL of mycelial suspension to the soil (*L.b*). The soil of the second group was injected with 10 mL distilled water to serve as mycorrhizal control (CK). For the inoculation, four holes were made in the soil near the plants and the inoculum (2.5 mL) was added to each hole. The inoculation treatments were repeated every other week for a total of four times.

2.3. NaCl Treatments

NaCl treatments started two months after the root mycorrhizal inoculation. According to the results obtained from the previous study, *Q. dentata* seedlings were able to maintain overall growth and demonstrated a certain salt stress tolerance in 1% NaCl concentration, but above 1% concentration, plant growth would be significantly limited and could not survive normally [32]. Thus, the NaCl concentration of the experimental design is not

suitable for exceeding its own salt stress tolerance ability. However, the seedlings in the previous study [32] grew to a certain stage before salt addition, whereas our NaCl treatment was for relatively early seedlings, so the salt concentration should be relatively reduced. Referring to the classification criteria of saline soils in China, soil salinity over 0.6% is classified as saline soil [39]. Therefore, in addition to the NaCl control (0% NaCl), we subjected the seedlings to two NaCl soil concentrations below (0.4% NaCl, moderate salinity treatment) and above (0.8% NaCl, high salinity treatment) this level. To avoid seedling shock response, the salt solution was added gradually to the soil. Overwatering and spilling were avoided during watering over the one month of the treatment duration to ensure that the NaCl did not leach from the soil. There were ten replicated seedlings in each treatment group (one seedling per pot), for a total of sixty seedlings (two inoculation treatments × three salinity levels × ten replicates) in the experiment.

2.4. Mycorrhizal Colonization Rate Determination

After one month of NaCl treatments, three seedlings were randomly selected from each treatment group. The first-order fine roots were carefully excised, washed with slow running water, and cut into ~1 cm long root segments. A total of 20 root segments were randomly selected from each seedling to examine for the presence of fungal hyphae and mycorrhizal structures. The roots were stained [40] and examined under the light microscope. The proportion of mycorrhizal root segments in the total number of observed roots was considered as the mycorrhizal colonization rate.

2.5. Plant Measurements

At the end of the NaCl treatments, plant heights (H) and base stem diameters (BD) were measured. Plant height was measured between the base of the plant and the shoot tip, and base stem diameter was measured with a Vernier caliper 1 cm above the soil surface.

Before harvest, mature and fully expanded functional leaves were selected for instantaneous measurements of gas exchange parameters using a portable gas exchange measurement system (Li-6800, Li-Cor, Lincoln, NE, USA). Measurements were taken between 9:00 and 12:00 h on a sunny day. Net photosynthetic rate (A), transpiration rate (E), and stomatal conductance (gs) were measured, and instantaneous water use efficiency (iWUE) was calculated as the ratio of A to E. Leaf chamber parameters were maintained as follows: leaf temperature, 28 °C; relative air humidity, 70%; light intensity, 1000 $\mu mol \cdot m^{-2} \cdot s^{-1}$; and CO_2 concentration, 400 $\mu mol \cdot mol^{-1}$.

Chlorophyll fluorescence parameters and P700 were measured simultaneously using a portable chlorophyll fluorometer (Dual-PAM-100, Walz, Effeltrich, Germany) set to dual-channel mode. After allowing leaves to adapt to the dark for 30 min, original fluorescence (Fo) was measured, then a saturating pulse (20,000 $\mu mol \cdot m^{-2} \cdot s^{-1}$) was performed to obtain the maximum fluorescence (Fm) and the maximum absorption change (Pm) in the dark-adapted state. After that, actinic light (400 $\mu mol \cdot m^{-2} \cdot s^{-1}$) was turned on to drive photosynthesis for 40 s, following which, a saturation pulse was performed to record the maximum fluorescence intensity of PSII (Fm') and the maximum absorption change of PSI (Pm'). The steady-state fluorescence intensity (Ft) of PSII and steady-state absorption changes of PSI were recorded under continuous background light. Next, maximum quantum yield of PS II (Fv/Fm), photochemical quenching (qP), electron transport rate (ETR), and actual quantum yield (Y) of photosystem I and II were calculated according to the following formulae [41,42]:

$$Fo' = 1/(1/Fo - 1/F_M + 1/F_M') \quad (1)$$

$$Fv/F_M = (F_M - Fo)/F_M \quad (2)$$

$$qp = (F_M' - Ft)/(F_M' - Fo') \quad (3)$$

$$Y(II) = 1 - Y(NPQ) - Y(NO) = (F_M' - F)/F_M' \quad (4)$$

$$Y(I) = 1 - Y(ND) - Y(NA) \quad (5)$$

$$ETR(I) = 0.5 \times Y(I) \times 0.84 \times PAR \quad (6)$$

$$ETR(II) = 0.5 \times Y(II) \times 0.84 \times PAR \quad (7)$$

where Y(NPQ) and Y(NO) correspond to the quantum yield of regulatory and non-regulatory energy dissipation, they can be obtained by the following formulae:

$$Y(NPQ) = F/F_M' - F/F_M \quad (8)$$

$$Y(NO) = F/F_M \quad (9)$$

Y(ND) corresponds to the fraction of P700 that is already oxidized by actinic light; Y(NA) corresponds to the fraction of P700 that are closed owing to acceptor side limitation, they can be obtained by the following formulae:

$$Y(ND) = P700_{OX}/P_M \quad (10)$$

$$Y(NA) = P_M/P_M' \quad (11)$$

An amount of 0.5 is the fraction of absorbed light reaching PSI or PSII; and PAR is photosynthetically active radiation, we take 0.84 of the PAR as the absorbed irradiance.

The leaf blades were collected as above for the chlorophyll concentration measurements. The leaf samples were weighed to determine fresh weights and soaked in 10 mL of 95% ethanol in the dark until the chlorophyll was fully leached out. The absorbance value of the extract was then determined by an ultraviolet-visible spectrophotometer (UV-9000s, Shanghai Metash Instruments Co., Ltd., Shanghai, China) at wavelengths of 649 and 665 nm, with 95% ethanol used as a blank control. The chlorophyll content was calculated using the following formulae [43]:

$$\text{Chlorophyll a concentration (Chl a)} = 13.95 \times D665 - 6.88 \times D649 \quad (12)$$

$$\text{Chlorophyll b concentration (Chl b)} = 24.96 \times D649 - 7.32 \times D665 \quad (13)$$

$$\text{Chlorophyll content} = (Chl \times V_{\text{leach liquor}})/\text{fresh weight} \quad (14)$$

$$\text{Total chlorophyll content (Chl t)} = \text{Chl a content} + \text{Chl b content} \quad (15)$$

where D649 and D665 correspond to the absorbance value of the extract measured at 649 and 665 nm wavelengths, respectively.

Harvested plant material was sorted into leaves, stems, and roots. Leaf fresh weight was recorded and the leaf area of 10 mature and fully unfolded leaves was measured using a scanner (LiDE120, Canon, Tokyo, Japan). Leaf dry weight was measured after drying and used to calculate the specific leaf area (SLA; leaf area/leaf dry weight) and the leaf water content (LWC; (leaf fresh weight − leaf dry weight)/leaf dry weight). We present these two indicators together, rather than separately, in the growth indicators section.

All plant fractions were heat treated at 105 °C for 30 min and oven-dried at 65 °C for 48 h, after which dry weight was collected for each portion. Seedling biomass allocation was assessed as the proportion of each part to total biomass, and included root mass ratio (RMR), stem mass ratio (SMR), and leaf mass ratio (LMR). The root–shoot ratio (R/S) was calculated as the ratio of below and above ground plant dry weight.

Next, all dried leaf, stem, and root tissues were powdered and packaged. An amount of 0.2 g from each fraction was digested by mixing with 30 mL $HClO_4$ and HNO_3 solution (v/v = 1:5) and heated to 70 °C for 10 min, followed by 40 min at 153 °C and 70 min at 190 °C. After smoke in the digestion tubes had dispersed and the liquid had cooled, the transparent liquid was transferred to a 100 mL volumetric flask and diluted to volume with deionized water. CsCl solution was added to determine the concentration of sodium and potassium ions, and $LaCl_3$ solution was added to determine concentrations of calcium and magnesium ions. Ion concentrations were measured using an atomic absorption spectrophotometer (AA-7000, Shimadzu, Kyoto, Japan) and calculated according to corresponding dilution ratios.

Nitrogen content was determined for each fraction using the Kjeldahl method. An amount of 0.2 g of each fraction was mixed with a catalyst ($CuSO_4$, 0.2 g; K_2SO_4, 3 g) and 8 mL concentrated sulfuric acid, after which it was digested by heating to 200 °C for 40 min followed by 400 °C for 40 min. The liquid was transferred to a 100 mL volumetric flask and diluted with deionized water to volume. An amount of 10 mL of the liquid under the test was taken to determined total nitrogen content of each part of the plant organs by a Kjeldahl apparatus (K9860, Hanon, Jinan, China). Another 5 mL liquid under the test was transferred to a volumetric flask (50 mL) and diluted to volume in order to determine the phosphorus content using a spectrophotometer (UV-9000s, Metash, Shanghai, China) by ascorbic acid–molybdophosphate blue method.

2.6. Statistical Analysis

A normality test and a variance homogeneity test were performed on all data before testing analysis. The effects of fungal inoculation and salt treatment on plant physiological and growth indexes of *Q. dentata* seedlings were analyzed by two-way analysis of variance (ANOVA) using SPSS 25.0 (SPSS Inc., Chicago, IL, USA). The responses of seedlings to different treatment combinations were analyzed by one-way analysis of variance (ANOVA). Before ANOVA analysis, data were tested for normality and homogeneity of variance first, and were log- or sqrt-transformed when necessary. Multiple comparisons were performed with a chi-squared test in order to effectively test the independence of fungal infestation and salinity stresses, and the significance levels were set at $\alpha = 0.05$. There were five to six biological replicates for each measurement. Plotting was performed using Origin 2019 (OriginLab Corp., Northampton, MA, USA).

3. Results

3.1. Inoculation and Mycorrhiza Formation

There were no ectomycorrhizal structures or hyphae detected in the control group (CK). The root colonization rates were similar in the NaCl control and the 0.4% NaCl treatment. However, the root colonization rate was drastically reduced by the 0.8 NaCl treatment (Table 1).

Table 1. Root colonization of *Q. dentata* seedlings in control group (CK) and inoculated seedlings (*L.b*) subjected to treatments with different NaCl concentrations. Different letters indicate significant differences between treatments ($p < 0.05$, $n = 3$) determined by a chi-squared test.

Treatment	Soil Salinity	Root Colonization Rate (%)
CK	0	0
	0.4% NaCl	0
	0.8% NaCl	0
L.b	0	48 ± 8 a
	0.4% NaCl	50 ± 5 a
	0.8% NaCl	22 ± 3 b

3.2. Effects of *L. bicolor* Inoculation on Growth Indicators Under Salt Stress

Prior to multiple comparisons, the effects of fungal inoculation, salt treatment, and the interactions between the two were assessed using two-way ANOVA (Table A1). Multiple comparison revealed that there was no significant difference in H and BD of the fungus-inoculated and non-inoculated seedlings under different salt stress conditions (Figure 1a,b). The leaf water content of both the inoculated and the CK seedlings under salt stress was significantly lower than that of the CK without salt stress, and leaf water content decreased by more than 50% under high salt stress (Figure 1c). Compared to the CK, the leaf water content of the inoculated seedlings was significantly lower under high salt stress, but was not significantly different compared to the other salt treatments (Figure 1c). Specific leaf area (SLA) increased with increasing salinity in both the inoculated and non-inoculated seedlings. SLA was higher in the inoculated group compared to the non-inoculated group, but this difference was only significant under moderate salt stress conditions (Figure 1d).

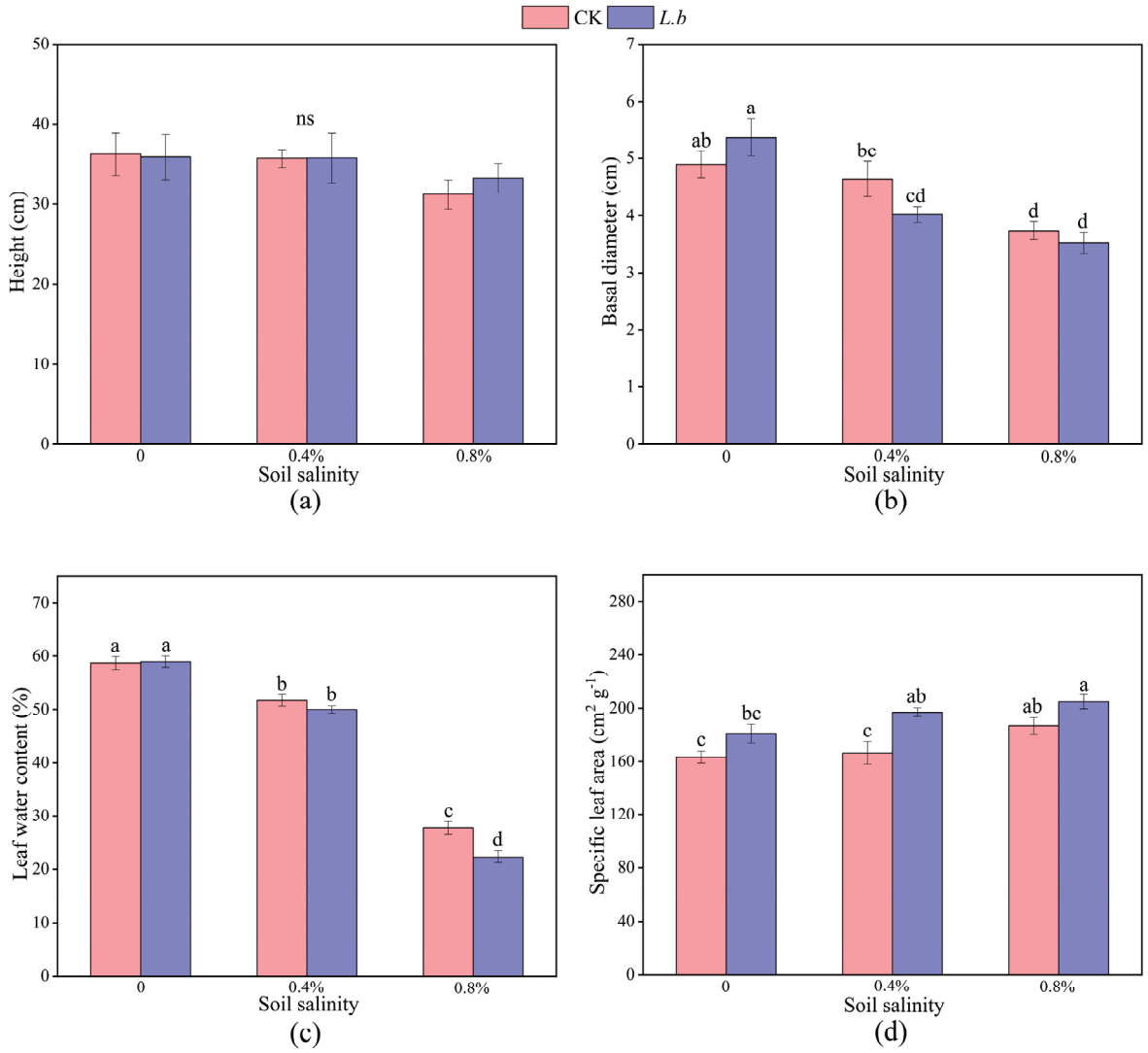


Figure 1. (**a**) hight, (**b**) basal diameter, (**c**) leaf water content and (**d**) specific leaf area of *Q. dentata* seedlings in the control (CK) and inoculation (*L.b*) groups subjected to different NaCl treatment concentrations. Bars represent means of six replicates (±SE). For each parameter, bars with different letters indicate significant differences among treatments ($p \leq 0.05$) determined by one-way analysis of variance (ANOVA).

Generally, root, stem, leaf, and total plant biomass decreased with increasing salinity in both the inoculated and non-inoculated seedlings. The inoculated seedlings under no

salt stress showed an increase in root biomass by 44.5%, whereas under moderate salt stress, the root biomass of the inoculated seedlings increased by 27.8%. There was no significant difference in the root biomass between the inoculated and uninoculated seedlings under high salt stress (Figure 2a). Inoculation did not affect the stem or leaf biomass under different salt stress treatments (Figure 2b,c). Total seedling biomass increased by 29.8% in the inoculated group under no salt stress, but the difference was not significant (Figure 2d). Increased biomass in the inoculated group under no salt stress was mainly due to differences in the root biomass.

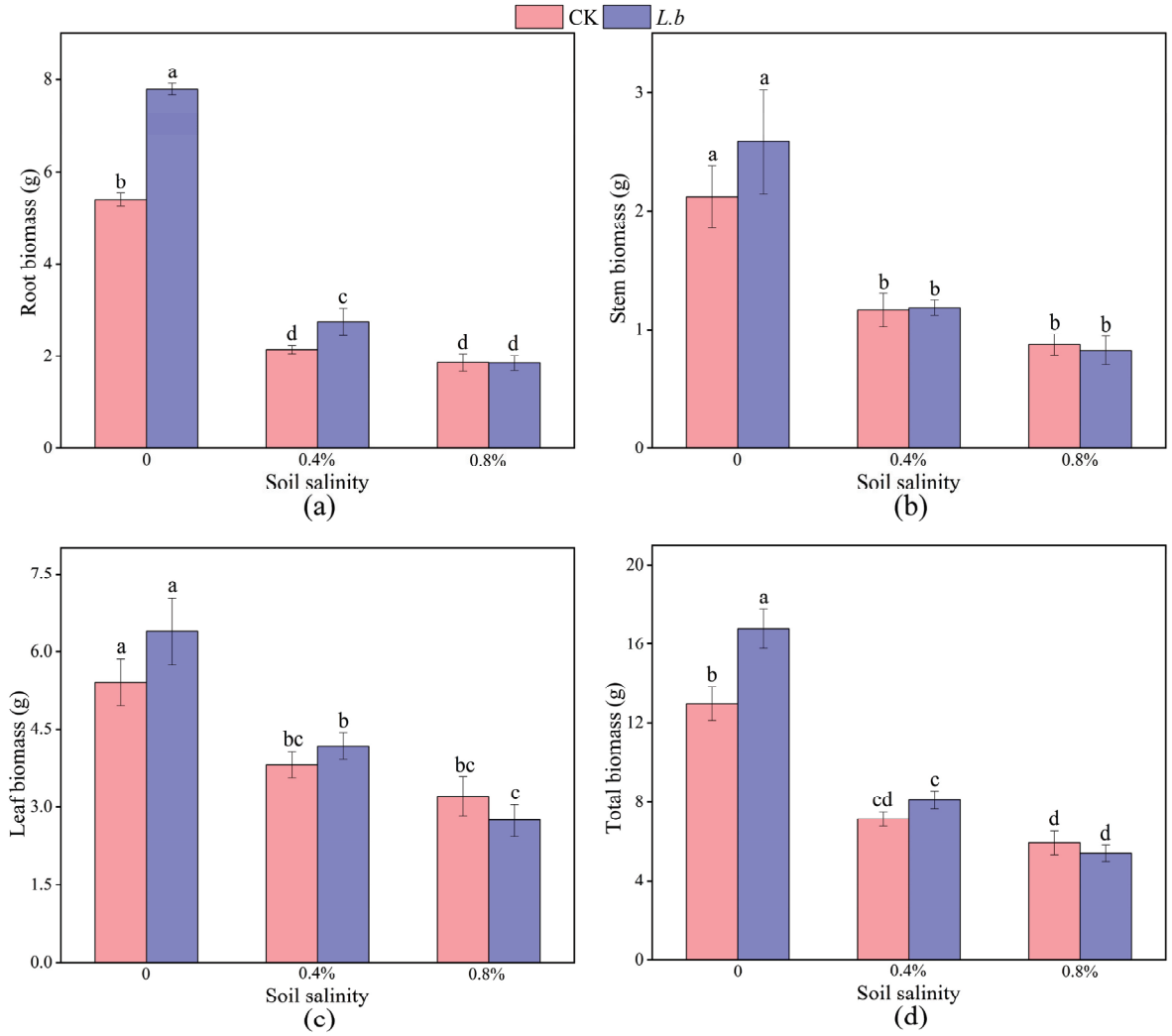


Figure 2. (**a**) root biomass, (**b**) stem biomass, (**c**) leaf biomass and (**d**) total biomass of *Q. dentata* seedlings in the control (CK) and inoculation (*L.b*) groups subjected to different NaCl treatment concentrations. Bars represent means of six replicates (±SE). For each parameter, bars with different letters indicate significant differences among treatments ($p \leq 0.05$) determined by one-way ANOVA.

Root mass ratio (RMR) decreased in both the control and the inoculated seedlings under salt stress. Inoculation increased RMR significantly, but only under no salt stress (Figure 3a). Neither inoculation nor NaCl treatment had a significant impact on seedling stem mass ratio (SMR) (Figure 3b). In contrast to RMR, leaf mass ratio (LMR) was significantly higher under salt stress, but inoculation did not have an effect, regardless of salt stress treatment (Figure 3c). Root–shoot ratio (R/S) followed the same trend as RMR, and inoculation significantly increased the root–shoot ratio of the seedlings, but only those in the no salt stress group (Figure 3d).

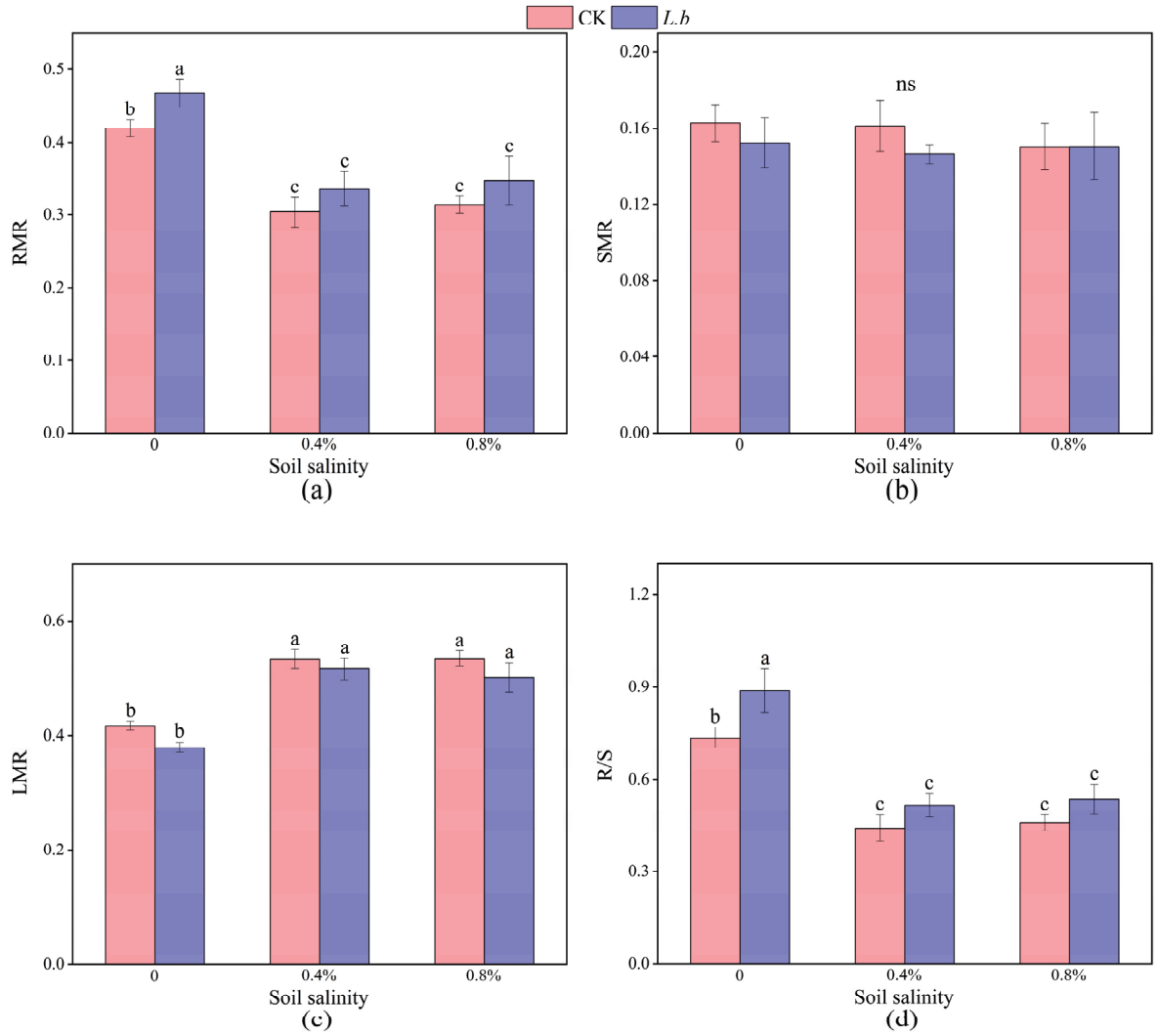


Figure 3. Biomass allocation of *Q. dentata* seedlings in the control (CK) and inoculation (*L.b*) groups subjected to different NaCl treatment concentrations: (**a**) root mass ratio, (**b**) stem mass ratio, (**c**) leaf mass ratio, (**d**) root–shoot ratio. Bars represent means of six replicates (±SE). For each parameter, bars with different letters indicate significant differences among treatments ($p \leq 0.05$) determined by one-way ANOVA.

3.3. Effects of L. bicolor on Physiological Indicators Under Salt Stress

Two-way ANOVA revealed that inoculation did not significantly affect gas exchange parameters in seedlings (Table A1), while salt stress significantly affected most gas exchange parameters (Figure 4a,b,d). Our findings suggest that plant physiological activity was increasingly restricted as salinity increased. We also note that iWUE did not exhibit the same degree of change with increasing salinity as other gas exchange parameters (Figure 4c). Inoculation reduced stomatal conductance only in the no salt stress group (Figure 4d).

Salt treatment significantly reduced chlorophyll a and total chlorophyll content. Both increased in the inoculated seedlings, but this increase was significant only in the moderate salt stress treatment group (Figure 5a,c). Under salt stress, chlorophyll b content of the inoculated seedlings was slightly higher than that of the non-inoculated control group, but the difference was not significant (Figure 5b). Furthermore, inoculation did not have a significant effect on the seedlings' chlorophyll a/b under different levels of salt stress. Chlorophyll a/b decreased with increasing soil salinity in both the inoculated and control groups (Figure 5d).

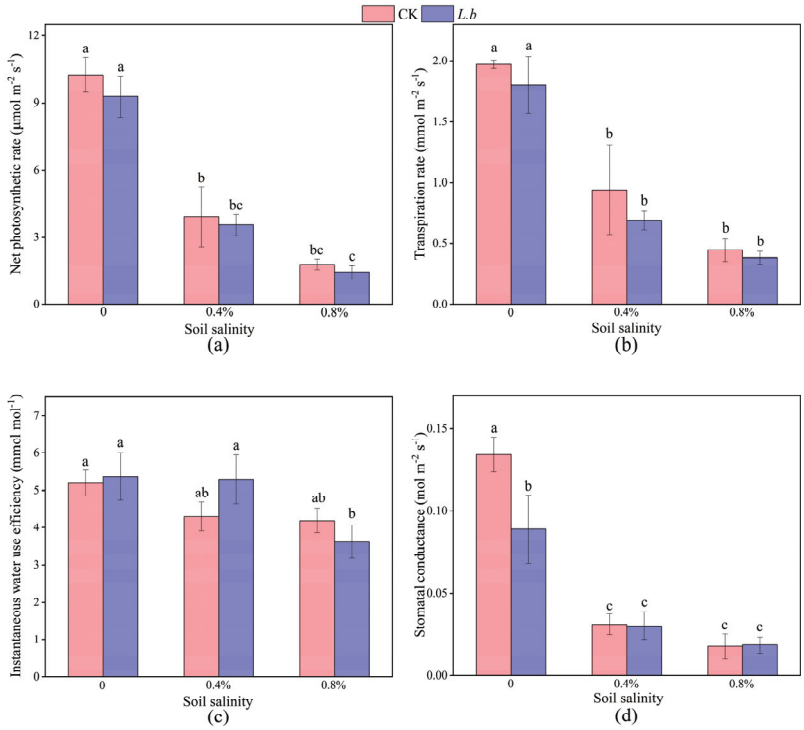


Figure 4. Gas exchange parameters of *Q. dentata* seedlings in the control (CK) and inoculation (*L.b*) groups subjected to different NaCl treatment concentrations: (**a**) net photosynthetic rate, (**b**) transpiration rate, (**c**) instantaneous water use efficiency, (**d**) stomatal conductance. Bars represent means of five replicates (±SE). For each parameter, bars with different letters indicate significant differences among treatments ($p \leq 0.05$) determined by one-way ANOVA.

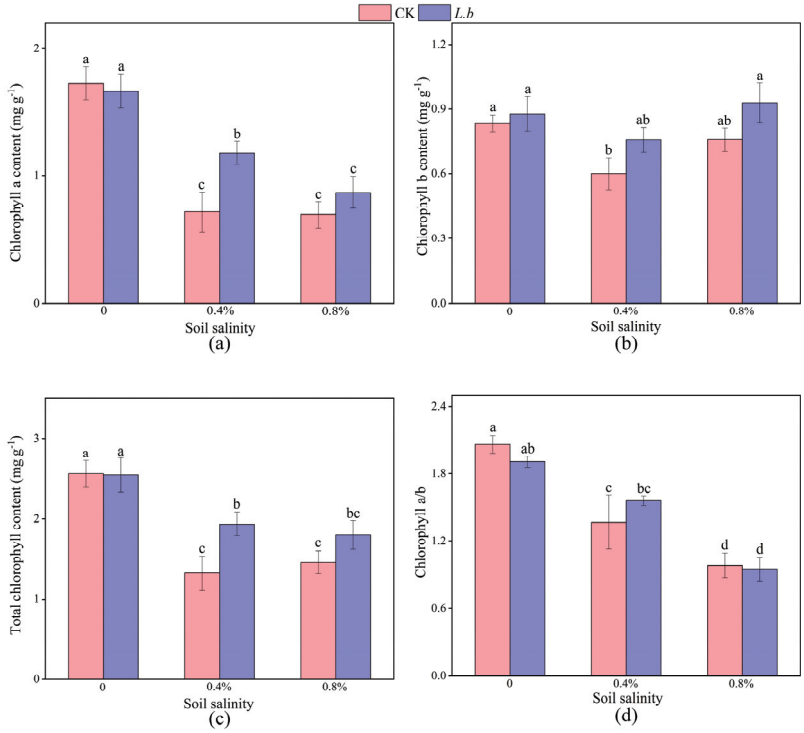


Figure 5. Leaf chlorophyll content of *Q. dentata* seedlings in the control (CK) and inoculation (*L.b*) groups subjected to different NaCl treatment concentrations: (**a**) chlorophyll a content, (**b**) chlorophyll b content, (**c**) total chlorophyll content, (**d**) chlorophyll a/b. Bars represent means of five replicates (±SE). For each parameter, bars with different letters indicate significant differences among treatments ($p \leq 0.05$) determined by one-way ANOVA.

The ETR and Y varied similarly. The ETR and Y of PS II were not significantly affected by inoculation, but gradually decreased with increasing salinity (Figure 6c,d). The ETR(I) and Y(I) both declined with increasing salinity, but the decline was exacerbated by inoculation under high-salt conditions (Figure 6a,b). Whereas Fv/Fm and qP declined only under high salt stress and, an effect that was exacerbated by inoculation, there were no significant changes in no-salt and low-salt environments (Figure 6e,f).

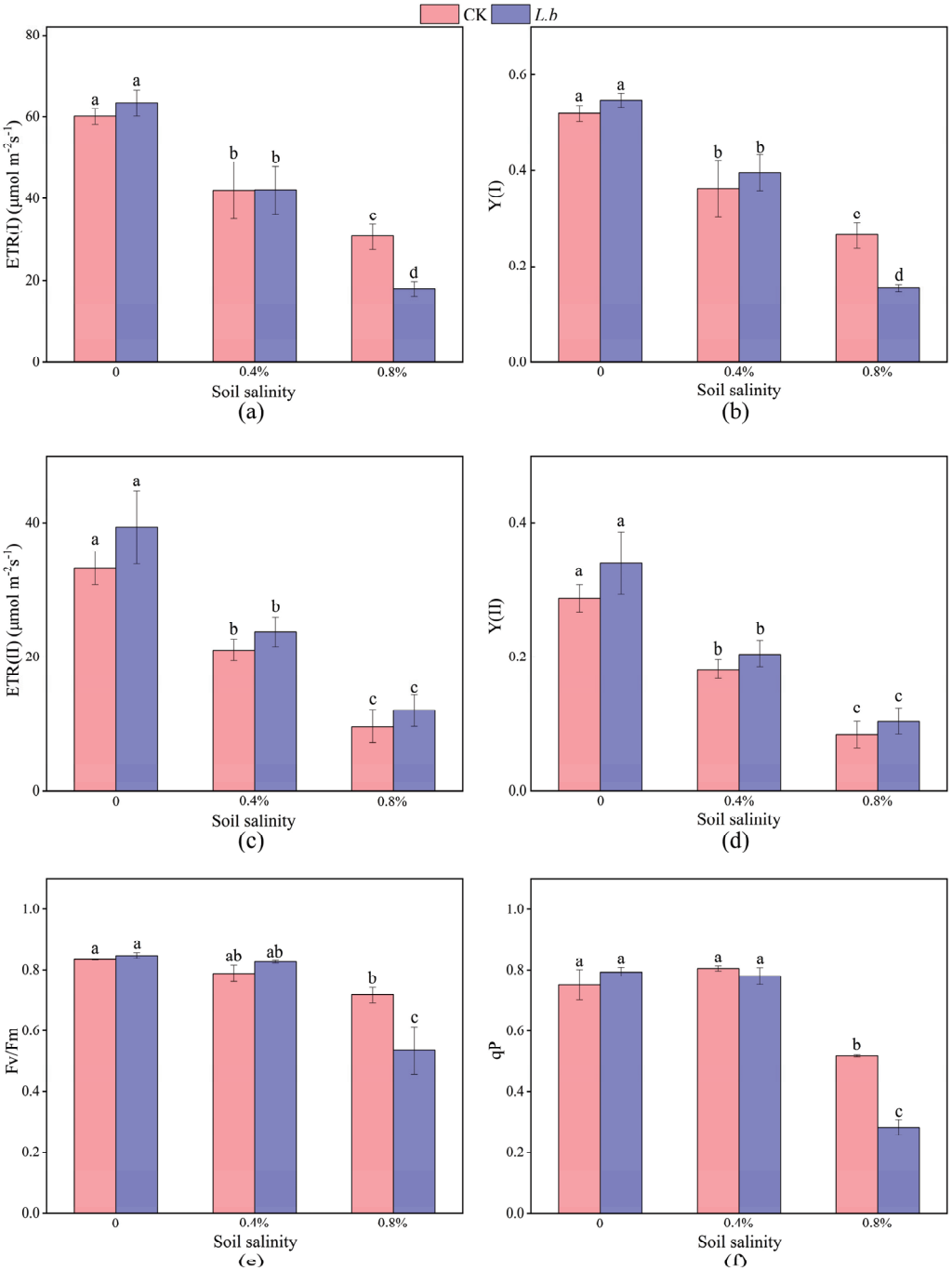


Figure 6. Chlorophyll fluorescence parameters of *Q. dentata* seedlings in the control (CK) and inoculation (*L.b*) groups subjected to different NaCl treatment concentrations: (**a**) ETR(I), (**b**) Y(I), (**c**) ETR(II), (**d**) Y(II), (**e**) Fv/Fm and (**f**) qP. Bars represent means of five replicates (±SE). For each parameter, bars with different letters indicate significant differences among treatments ($p \leq 0.05$) determined by one-way ANOVA.

With increasing soil salinity, Na^+ content of all seedling organs increased significantly. Inoculation did not significantly affect the root and stem Na^+ content; compared to the CK, however, the leaf Na^+ content was significantly lower under moderate salt stress and significantly higher under high salt stress conditions (Figure 7a).

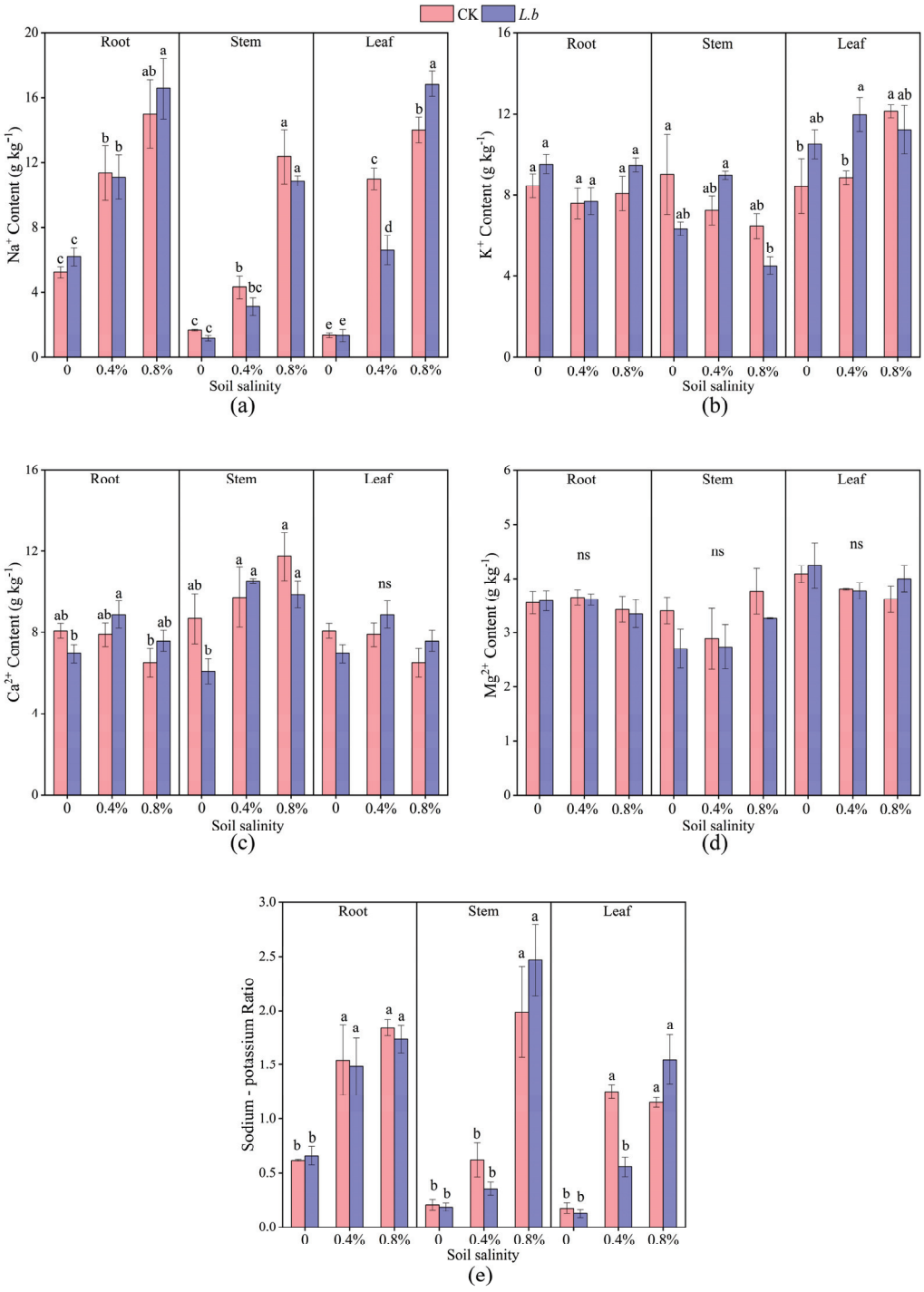


Figure 7. Metal ion content and ratio of *Q. dentata* seedlings in the control (CK) and inoculation (*L.b*) groups subjected to different NaCl treatment concentrations: (**a**) Na^+ content, (**b**) K^+ content, (**c**) Ca^{2+} content, (**d**) Mg^{2+} content and (**e**) sodium-potassium ratio. Bars represent means of five replicates (±SE). For each parameter, bars with different letters indicate significant differences among treatments ($p \leq 0.05$) determined by one-way ANOVA.

Salt stress did not have a significant effect on the root K^+ content; the stem K^+ decreased with increasing salinity, while the leaf K^+ content increased (Figure 7b). Fungal inoculation

did not affect the root or stem K^+ content, but increased the leaf K^+ content significantly under moderate salt stress conditions (Figure 7b). The Na^+/K^+ ratios increased with increasing salinity in all organs, and fungal inoculation lowered the leaf Na^+/K^+ ratios significantly only in low-salt environments (Figure 7e). There was no significant difference in the root, stem, or leaf Ca^{2+} and Mg^{2+} content between the inoculated and control seedlings under different salt treatments. The stem Ca^{2+} only increased significantly in inoculated seedlings (Figure 7c,d).

Except for the root N concentration, which increased in the CK seedlings but decreased in inoculated seedlings in high salt environments, neither salt treatment nor fungal inoculation had a significant effect on the plant organ N (Figure 8a,c,e). The plant organ P content did not change significantly in response to the NaCl treatment or fungal inoculation (Figure 8b,d,f).

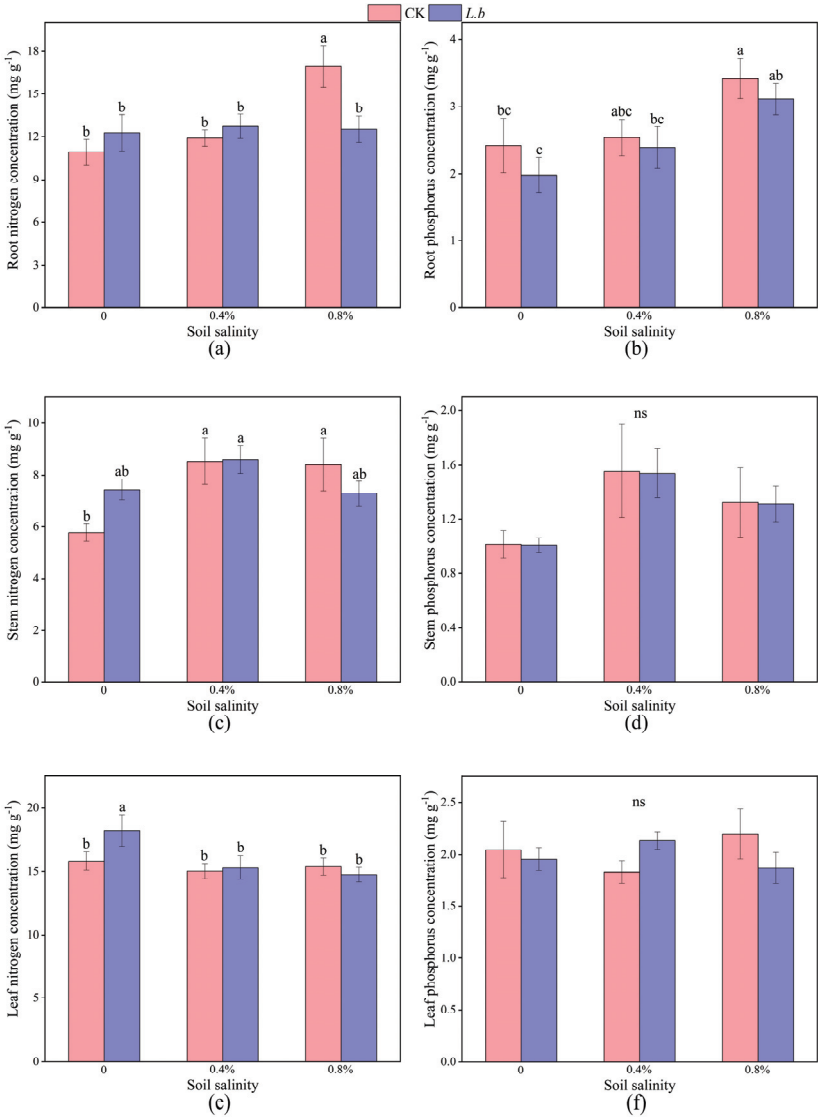


Figure 8. Nutrient concentration of *Q. dentata* seedlings in the control (CK) and inoculation (*L.b*) groups subjected to different NaCl treatment concentrations: (**a**) root nitrogen content, (**b**) root phosphorus content, (**c**) stem nitrogen content, (**d**) stem phosphorus content, (**e**) leaf nitrogen content and (**f**) leaf phosphorus content. Bars represent means of five replicates (±SE). For each parameter, bars with different letters indicate significant differences among treatments ($p \leq 0.05$) determined by one-way ANOVA.

4. Discussion

4.1. Response of Q. dentata Seedlings to NaCl Treatment

The NaCl treatment appeared to have a greater impact on *Q. dentata* seedlings than inoculation with *L. bicolor* (Table A1), both in terms of growth and physiological indicators. Most parameters change monotonically with increasing salinity. Results also show that one-year old *Q. dentata* seedlings were resistant to relatively low salt stress and that increasing concentrations of NaCl exacerbated negative effects on seedling growth (Figure 9). This is consistent with previous work reporting salt tolerance in oaks, even at the seedling stage [18,19]. Other research has found that *Q. dentata* is also resistant to NaCl stress within a certain range [32]. Whether they were inoculated or not, seedlings were able to survive in saline environments (0%–0.8%), exhibiting intermediate and considerable NaCl tolerance compared with salt-tolerant species planted in afforestation projects, such as *Q. virginiana*, *Q. acutissima* [18], and *Robinia pseudoacacia* [44]. Our findings showing that *Q. dentata* has a certain degree of salt tolerance is promising for saline–alkaline land restoration.

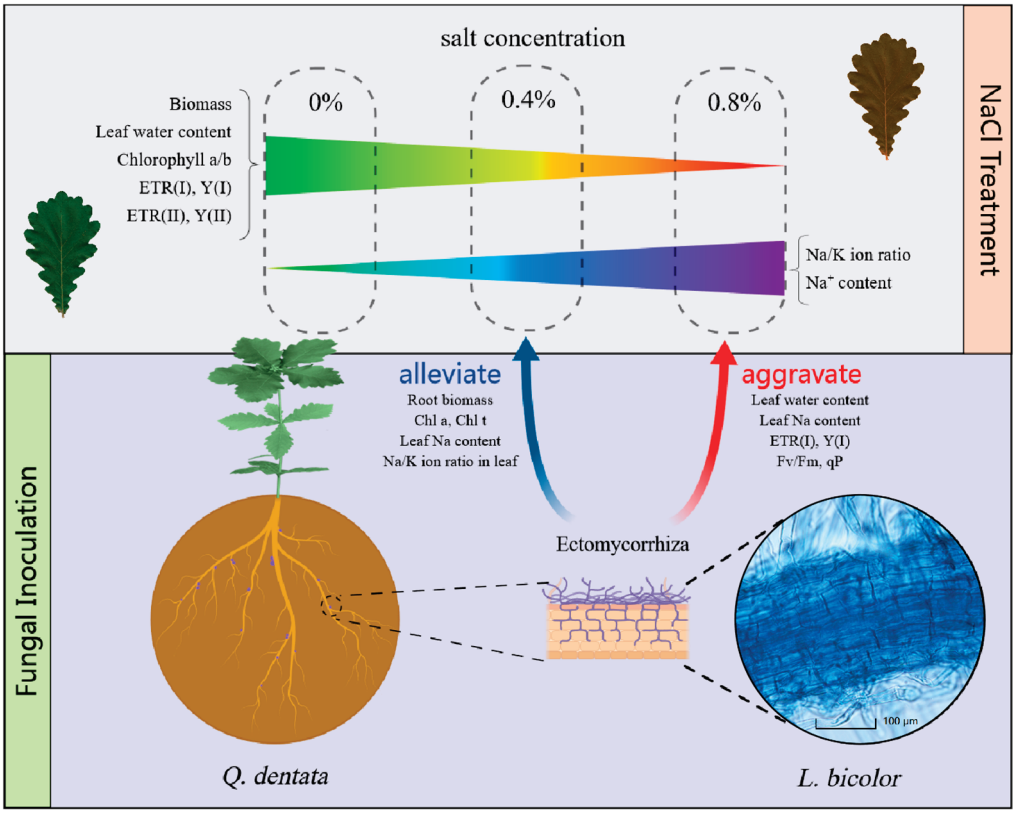


Figure 9. Conceptual model summarizing the effects of *L. bicolor* inoculation on *Q. dentata* seedlings under saline conditions.

With increasing salinity (0.4%), the negative effects of NaCl on seedling growth caused a decrease in plant biomass (Figure 2). Seedlings altered the nutrient and biomass distribution ratios by increasing the leaf biomass ratio and by decreasing the root biomass ratio and root–shoot ratio (Figure 3) to reduce salt uptake and upward transport by the roots and to prioritize resource allocation to the leaves for photosynthesis. This pattern of biomass distribution has also been observed in *Ceriops tagal* [45], a mangrove halophyte. An opposite, upward trend has been reported in *Picea glauca* and *Pinus banksiana* [29], even in individuals inoculated with *L. bicolor*. As soil salt content increases further (0.8%), sodium ion toxicity occurs, plant water–salt balance is disrupted, leaf tissue water loss is more

serious, and leaves wither or senesce [46–48]. As a result, osmotic stress and ionic toxicity become stronger.

Total chlorophyll content declined significantly under increasing salt stress (Figure 5c), likely attributable to two mechanisms: (1) Na^+ accumulation-induced ion toxicity impairs chlorophyll–protein binding and disrupts the chloroplast ultrastructure through thylakoid membrane degradation [49]; (2) salt-activated chlorophyllase accelerates chlorophyll a catabolism via ROS-mediated pathways [50]. The observed parallel reduction in chlorophyll a and total chlorophyll (Figure 5), coupled with decreased chlorophyll a/b ratios, demonstrates greater the salt sensitivity of chlorophyll a compared to chlorophyll b in seedlings [51].

In addition, salt stress significantly impaired photosynthetic capacity, evidenced by reduced chlorophyll content, stomatal limitations, and disrupted electron transport (Figures 4 and 6) [8,52]. Declines in net photosynthetic rate, stomatal conductance, and transpiration rate were directly correlated with salinity levels, suggesting heightened photosynthetic sensitivity to soil salinity. Mechanistically, osmotic stress-induced leaf water deficits reduced guard cell turgor pressure, driving stomatal closure [51,53,54]. Concurrently, salt-induced thylakoid membrane destabilization restricted intersystem electron flow between PSII and PSI [55]. Progressive decreases in the ETR and quantum yields (Y) under elevated salinity indicated impaired light energy conversion and reaction center dysfunction [56]. While PSII maintained photosynthetic conversion capacity (qP, Fv/Fm) at moderate salinity, severe salt stress caused significant photodamage and functional impairment [57]. This dual-phase response highlights threshold-dependent salt tolerance mechanisms in photosynthetic apparatus.

4.2. Positive Effects of L. bicolor on Q. dentata Seedlings Under Moderate Salinity

EMF partner with many woody plants and usually maintain reciprocal symbiosis [58]. Plants provide fungi with a portion of the carbohydrate fixed by photosynthesis and fungi help the plant absorb water and nutrients in return, improving resilience [59]. Here, inoculation worked in *Q. dentata* seedlings and played a beneficial role in non-hypersaline environments.

Our findings indicate a complex interaction between salinity and fungal symbiosis. We found that inoculation under salt-free conditions significantly increased the root biomass of the *Q. dentata* seedlings, resulting in higher total biomass for the inoculated group compared to the CK. The root–shoot ratio was also significantly higher among the inoculated seedlings, indicating that colonization by EMF promotes root growth in *Q. dentata* seedlings and increases the proportion of resources allocated below ground, enhancing plant uptake and storage of water and nutrients [60]. In addition, we also found that symbiosis with *L. bicolor* improves seedling salt tolerance under moderate salinity. Under relatively low NaCl stress, *L. bicolor* induced the host plants to expand their roots (Figure 2a) to alleviate the osmotic stress and to supply the leaves with adequate water (Figure 1c), representing a trade-off between its own water absorption capacity and the osmotic pressure caused by salt stress. Likewise, ion toxicity to plant leaves decreased proportionally with decreasing sodium–potassium ratios in relation to sodium ion concentrations (Figure 7a,e), which resulted from the increased water supply to the leaves. As a result, the total chlorophyll content of *Q. dentata* seedlings increased with increasing chlorophyll a content under relatively low salt stress (Figure 5a,c) to mitigate the degradative effects of salt stress [61]. This is consistent with previous research, and is probably due to the fact that the symbiotic fungus secretes growth regulators, such as cytokinins, thereby increasing leaf chlorophyll content [62]. Our findings suggest that symbiosis with *L. bicolor* has a positive effect on *Q. dentata* seedling growth and can promote seedling growth under moderate salt stress.

4.3. Negative Effects of L. bicolor on Q. dentata Seedlings Under High Salinity

Symbiotic relationships between mycorrhizal fungi and host plants are not unbreakable [63], and cooperation becomes uneven when resource exchange is diminished or stops in response to environmental stress [64,65]. As soil salinity gradually exceeds the normal tolerance range of plants, the relationship between symbiotic mycorrhiza and the host plant becomes more subtle [66,67]. The effects of EMF inoculation on various indicators, like tissue biomass, gas exchange parameters, chlorophyll content, chlorophyll fluorescence parameters, and sodium–potassium ratio, were weaker under high salt stress. Regardless, the mycorrhizal association did not provide any benefit to the host plants when the seedlings were unable to withstand the damage caused by salt stress (Figure 9). At the same time, we found that moderate NaCl promotes the growth of *L. bicolor* mycelium (Table A2), consistent with previous research demonstrating the salt tolerance of the *L. bicolor* [68]. As salinity increases, the ability of the fungus to generate its own growth as well as its vigor to colonize and live in symbiosis with the host plant decreases; in particular, mycorrhizal colonization rates are significantly lower under high salt conditions than they are under no-salt and medium-salt conditions (Table 1). The high salinity environment could raise the threshold of fungal competitiveness to the host plants; *L. bicolor* that colonize *Q. dentata* seedlings not only become less numerous but play a negative role in plant growth.

In relatively harsh environments, where fungus is restricted in its own growth and its protective effect on plants from NaCl is lost, the limited available resources made by the seedlings face intense competition from both the fungus and the host plant, and the fungus will rob the survival resources from the plants thereby inhibiting their growth. Thus, host plants are unable to meet the mycorrhizal demand for resources, which remain high under saline conditions, and exacerbated nutrient and water stress reduce root nitrogen (Figure 8a) and the leaf water content (Figure 1c). As the main photosynthetic organ, leaves accumulate sodium when water is lost [69] and experience worsening ion toxicity (Figure 7a). Chlorophyll fluorescence parameters, which are sensitive to ion penetration and water–salt balance, also decrease (Figure 6).

Notably, our results suggest that leaf Na^+ content is a sensitive and critical indicator of fungal colonization under different salt stress conditions. That is, when plant growth is limited primarily by environmental salt stress, the physiological changes induced by a plant's association with symbiotic mycorrhizal fungi are most obvious in the leaf Na^+ content (Figure 7). Inoculation with *L. bicolor* reduces photosystem efficiency in highly saline soil. Moreover, the effect of salt stress on photosynthetic efficiency is most apparent in changes in the ETR and Y of photosystem I, which are more sensitive to the effects of fungal inoculation than those of photosystem II (Figure 6). Severe salinity decreases PSII stability and donor side intactness [55] which were maintained under relatively low salt stress (Figure 6e,f). Fungal inoculation further jeopardizes the stability of the photosynthetic apparatus under high salt conditions (Figure 6). These results indicate that mycorrhizal association with *L. bicolor* can help *Q. dentata* seedlings maintain photosynthesis and mitigate oxidative damage under moderate salt stress, although the symbiotic system becomes ineffective at elevated salt stress concentrations. Consequently, the inclusion of mycorrhizal symbiosis in afforestation strategies for saline–alkali soils necessitates the monitoring of key physiological and biochemical parameters, particularly chlorophyll fluorescence indices and ionic homeostasis markers, to optimize symbiotic efficacy in challenging edaphic conditions.

4.4. Implications for Afforestation Activities in Saline Areas

Many oak species are tolerant to salt stress and have potential applications in land afforestation in saline–alkali soil [19,70]. Research conducted in the Basianshan National

Nature Reserve has shown that *Q. dentata* plays a crucial pioneering role in the early stages of forest restoration, contributing to the formation of stable dominant populations and improving community structure and diversity [33].

Moreover, the genome-wide identification and expression analysis of the ZIP gene family in *Q. dentata* have revealed its capability in heavy metal transport, particularly zinc, which underscores its potential in the phytoremediation of contaminated soils [71]. This genetic insight aligns with the findings that *Q. dentata* can effectively absorb and transport essential trace elements, thereby mitigating soil pollution and enhancing soil health [72].

Ecologically, *Q. dentata* contributes to the improvement of soil enzyme activities and nutrient cycling, which are essential for maintaining soil fertility and promoting plant growth under stress conditions such as drought and nitrogen enrichment [72]. The ability of this species to adapt to various environmental stresses and improve soil conditions makes it a valuable asset in ecological restoration projects.

Mycorrhizal fungi have a strong regulatory effect on root exudation and nitrogen uptake in temperate tree species [73]. Afforestation studies suggest that EMF symbiosis during silviculture can enhance carbon sequestration and improve soil properties [74,75]. Although it is possible that afforestation, combined with carefully selected EMF symbionts, can improve saline–alkali soil [76,77], the mechanisms underpinning these improvements and the potential use of EMF, including *L. bicolor*, are still poorly understood.

It appears that, in this study, *L. bicolor* was effective only under the moderate salinity level because the fungus itself could not tolerate higher salt concentrations, as shown by a reduction in root colonization under the high salt concentration (Table 1). It is proved that the survival and mycelial extension of *L. bicolor* cultured in vitro were not significantly affected under higher salt concentration (Table A2). It is a fact that *L. bicolor* is one kind of mycorrhizal fungi with strong saline–alkali tolerance [78] and even certain salinity could promote the proliferation of fungi in vitro (Table A2), while the higher salinity level might restrict the inoculation of EMF, as shown by less colonization density on the same individual (Table 1). Because of the decline in co-benefits, the probability of *L. bicolor* to refuse to inoculate plants increases under high salinity concentrations. Therefore, the effectiveness of the fungus in conferring salt tolerance to plants can be only up to the salt concentration that the fungus can tolerate itself. It is the salt concentration in vitro that may not only be too high for the mycorrhizal fungi combined with plants in afforestation to be survival, but determines the activeness and effectiveness in conferring salt protection to the plants. Therefore, it is necessary to consider the effect of fungal cooperative afforestation according to the requirements and adaptability of applied fungi to the soil environment. Furthermore, a deeper understanding is needed of the long-term effects of salinity on *Q. dentata–L. bicolor* symbionts and the underlying mechanisms.

5. Conclusions

In our study, mycorrhization with *L. bicolor* had either a positive or a negative impact on plant responses to NaCl depending on the soil salt. Here, this association helped plants cope with salt stress by promoting the root growth, increasing the light capture area, promoting chlorophyll accumulation, and regulating the ion balance under moderate salt stress. By contrast, EMF association under high salt stress exacerbated nutrient stress, water stress, and Na^+ toxicity, leading to a decrease in plant photosynthetic activity, rate, and yield. Therefore, mycorrhizal seedlings inoculated with EMF can be considered for vegetation restoration in mildly saline soil, which supports *Quercus* growth. However, when the soil salinity is high beyond a certain range, it is necessary to fully consider not only the salt tolerance of *Quercus* themselves, but the survival of the symbiotic fungi in saline environments and the actual effect of mycorrhizal symbiosis, under which mycorrhizal

means may not be applicable. Collectively, afforestation with *Q. dentata* seedlings combined with symbiosis with *L. bicolor* is a reasonable choice with broad application prospects. The symbiont of *L. bicolor* and *Q. dentata*, with its remarkable adaptability and multifunctional benefits, holds significant potential for real-world applications, particularly in afforestation projects and soil remediation initiatives. Its ability to enhance forest community stability and diversity makes it an ideal candidate for partnerships in large-scale afforestation projects. However, additional research investigating the genetic and molecular mechanisms driving enhanced salt tolerance is needed to maximize the benefits of the interaction between *L. bicolor* and *Q. dentata*.

Author Contributions: All authors contributed to the study conception and design. Material preparation, data collection, and analysis were performed by W.S., H.C., Y.S. and L.Q. The first draft of the manuscript was written by W.S. and all authors commented on previous versions of the manuscript. All authors have read and agreed to the published version of the manuscript.

Funding: This study was funded by the Natural Science Foundation of Shandong Province, China (No. ZR2020MC035, No. ZR2024MC012), Shandong Province "Double-Hundred Talent Plan" Project (No. WSG2018023), Seed funding for International Scientific Research Cooperation of Shandong University (No. SD202015), and Key Research and Development Program of Shandong Province, China (No. 2021CXGC010803).

Data Availability Statement: Data will be made available from the corresponding author on reasonable request.

Acknowledgments: We thank Chengjia Zhang and Nannan Dong of the Core Facilities for Life and Environmental Sciences, State Key laboratory of Microbial Technology of Shandong University for metal ion assay and analysis.

Conflicts of Interest: The authors declare no conflicts of interest.

Abbreviations

The following abbreviations are used in this manuscript:

EMF	Ectomycorrhizal fungi
SLA	Specific leaf area
RMR	Root mass ratio
SMR	Stem mass ratio
LMR	Leaf mass ratio

Appendix A

Appendix A.1

Table A1. Two-way analysis of variance (ANOVA) on all measured indicators of *Q. dentata* seedlings under fungus inoculation and salt treatment.

Plant Traits	F Value and Its Significance		
	Fungus Inoculation	Soil Salinity	Interaction Effects
Height (cm)	0.094	1.798	0.161
Basal diameter (mm)	0.661	17.46 ***	2.733
Leaf water content (%)	5.547 *	485.198 ***	3.277
SLA ($cm^2\ g^{-1}$)	16.562 ***	6.131 **	0.652
Total biomass (g)	8.486 ***	115.954 ***	6.165 ***
Root biomass (g)	31.085 ***	251.122 ***	14.307 ***
Stem biomass (g)	1.096	38.333 ***	1.185
Leaf biomass (g)	0.952	29.783 ***	1.934

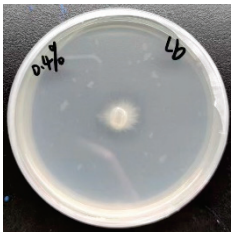
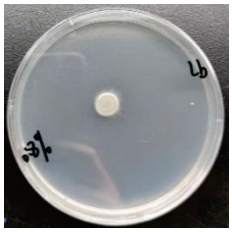
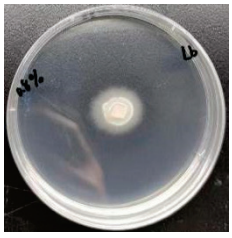
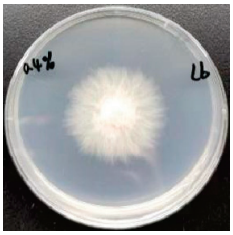
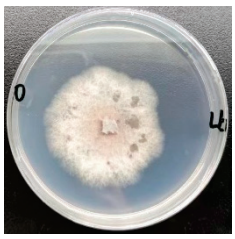
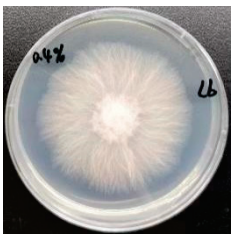
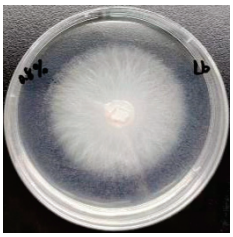
Table A1. *Cont.*

Plant Traits	F Value and Its Significance		
	Fungus Inoculation	**Soil Salinity**	**Interaction Effects**
RMR	4.305 *	17.907 ***	0.070
SMR	0.663	0.163	0.194
LMR	4.096	30.781 ***	0.173
R/S	5.920 ***	24.919 ***	0.383
Net photosynthetic rate (μmol m^{-2} s^{-1})	0.568	40.001 ***	1.506
Transpiration rate (mmol m^{-2} s^{-1})	0.375	40.475 ***	0.573
Instantaneous water use efficiency (mmol mol^{-1})	0.381	3.000	1.003
Stomatal conductance (mol m^{-2} s^{-1})	1.668	54.428 ***	1.571
Chlorophyll a (mg g^{-1})	3.391 *	31.083 ***	2.083
Chlorophyll b (mg g^{-1})	4.534 *	3.657 *	0.501
Total chlorophyll (mg g^{-1})	4.428 *	17.895 ***	1.508
Chlorophyll a/b	0.486	34.169 ***	0.419
Maximum quantum yield of photosystem II	1.353	11.559 ***	1.705
Photochemical quenching	12.054 **	140.885 ***	15.256 ***
Relative electron transport rate of photosystem I (μmol m^{-2} s^{-1})	1.259	51.444 **	2.002
Actual quantum yield of photosystem I	1.292	51.809 ***	1.995
Relative electron transport rate of photosystem II (μmol m^{-2} s^{-1})	0.441	42.891 ***	0.093
Actual quantum yield of photosystem II	0.447	42.682 ***	0.093
Root Na^+ content	0.393	23.507 ***	0.197
Stem Na^+ content	2.779	93.984 ***	0.198
Leaf Na^+ content	19.099 **	219.260 ***	5.476 *
Root K^+ content	2.749	2.621	0.539
Stem K^+ content	1.616	4.605 *	3.282
Leaf K^+ content	3.831	3.138	2.795
Root Ca^{2+} content	0.453	2.890	2.382
Stem Ca^{2+} content	2.239	6.655 *	1.624
Leaf Ca^{2+} content	0.338	2.890	1.367
Root Mg^{2+} content	0.031	0.819	0.043
Stem Mg^{2+} content	2.165	1.771	0.277
Leaf Mg^{2+} content	0.748	1.560	0.374
Sodium–potassium ratio	0.061	43.960 ***	1.858
Root nitrogen content	1.130	4.922 *	4.541 *
Root phosphorus content	2.221	6.621 **	0.025
Stem nitrogen content	0.140	4.511 *	2.253
Stem phosphorus content	0.004	3.489	0.040
Leaf nitrogen content	0.571	2.949	1.756
Leaf phosphorus content	0.569	0.237	2.136

The abbreviations in the table represent as follows: specific leaf area (SLA), root mass ratio (RMR), stem mass ratio (SMR), leaf mass ratio (LMR), root–shoot ratio (R/S). The significance of each effect is indicated by *: * indicates $p < 0.05$, ** indicates $p < 0.01$, and *** indicates $p < 0.001$.

Appendix A.2

Table A2. Growth changes of *L. bicolor* in solid culture under different salt stress.

Growth Time	NaCl Content in the Culture Medium		
	0	0.4%	0.8%
One day			
Three days			
Five days			
Seven days			

References

1. Kopittke, P.M.; Menzies, N.W.; Wang, P.; McKenna, B.A.; Lombi, E. Soil and the intensification of agriculture for global food security. *Environ. Int.* **2019**, *132*, 105078. [CrossRef] [PubMed]
2. Singh, A. Soil salinization management for sustainable development: A review. *J. Environ. Manag.* **2021**, *277*, 111383. [CrossRef] [PubMed]
3. Negacz, K.; Malek, Z.; de Vos, A.; Vellinga, P. Saline soils worldwide: Identifying the most promising areas for saline agriculture. *J. Arid Environ.* **2022**, *203*, e104775. [CrossRef]
4. Ullah, S.; Dahlawi, S.; Naeem, A.; Rengel, Z.; Naidu, R. Biochar application for the remediation of salt-affected soils: Challenges and opportunities. *Sci. Total. Environ.* **2017**, *625*, 320–335.
5. Mukhopadhyay, R.; Sarkar, B.; Jat, H.S.; Sharma, P.C.; Bolan, N.S. Soil salinity under climate change: Challenges for sustainable agriculture and food security. *J. Environ. Manag.* **2021**, *280*, 111736. [CrossRef]
6. Crooks, S.; Sutton-Grier, A.E.; Troxler, T.G.; Herold, N.; Bernal, B.; Schile-Beers, L.; Wirth, T. Coastal wetland management as a contribution to the US National Greenhouse Gas Inventory. *Nat. Clim. Change* **2018**, *8*, 1109–1112. [CrossRef]
7. Litalien, A.; Zeeb, B. Curing the earth: A review of anthropogenic soil salinization and plant-based strategies for sustainable mitigation. *Sci. Total Environ.* **2020**, *698*, 134235. [CrossRef]
8. Van Zelm, E.V.; Zhang, Y.X.; Testerink, C. Salt tolerance mechanisms of plants. *Annu. Rev. Plant Biol.* **2020**, *71*, 403–433. [CrossRef]
9. Hao, S.H.; Wang, Y.R.; Yan, Y.X.; Liu, Y.H.; Wang, J.Y.; Chen, S. A review on plant responses to salt stress and their mechanisms of salt resistance. *Horticulturae* **2021**, *7*, 132. [CrossRef]

10. Ruan, C.J.; de Silva, J.A.T.; Mopper, S.; Qin, P.; Lutt, S. Halophyte improvement for a salinized world. *Crit. Rev. Plant Sci.* **2010**, *29*, 329–359. [CrossRef]
11. Manousaki, E.; Kalogerakis, N. Halophytes—An emerging trend in phytoremediation. *Int. J. Phytoremediat* **2011**, *13*, 959–969. [CrossRef] [PubMed]
12. Stavi, I.; Thevs, N.; Priori, S. Soil salinity and sodicity in drylands: A review of causes, effects, monitoring, and restoration measures. *Front. Environ. Sci.* **2021**, *9*, 712831. [CrossRef]
13. Manousaki, E.; Kalogerakis, N. Halophytes present new opportunities in phytoremediation of heavy metals and saline soils. *Ind. Eng. Chem. Res.* **2011**, *50*, 656–660. [CrossRef]
14. Liang, L.C.; Liu, W.T.; Sun, Y.B.; Huo, X.H.; Li, S.; Zhou, Q.X. Phytoremediation of heavy metal contaminated saline soils using halophytes: Current progress and future perspectives. *Environ. Rev.* **2017**, *25*, 269–281. [CrossRef]
15. Kremer, A.; Hipp, A.L. Oaks: An evolutionary success story. *New Phytol.* **2019**, *226*, 987–1011. [CrossRef]
16. Sork, V.L.; Cokus, S.J.; Fitz-Gibbon, S.T.; Zimin, A.V.; Puiu, D.; Garcia, J.A.; Gugger, P.F.; Henriquez, C.L.; Zhen, Y.; Lohmueller, K.E.; et al. High-quality genome and methylomes illustrate features underlying evolutionary success of oaks. *Nat. Commun.* **2022**, *13*, 2047. [CrossRef]
17. Alaoui-Sossé, B.; Sehmer, L.; Barnola, P.; Dizengremel, P. Effect of NaCl salinity on growth and mineral partitioning in *Quercus robur* L. a rhythmically growing species. *Trees* **1998**, *12*, 424–430. [CrossRef]
18. Wang, S.F.; Hu, Y.X.; Sun, H.J.; Shi, X.; Pan, H.W.; Chen, Y.T. Effects of salt stress on growth and root development of two oak seedlings. *Acta. Ecol. Sin.* **2014**, *34*, 1021–1029.
19. Gugliuzza, G.; Gentile, C.; Scuderi, D.; Palazzolo, E.; Farina, V. Effects of salt stress on growth of *Quercus ilex* L. seedlings. *Open Agric.* **2023**, *8*, 20220211. [CrossRef]
20. Jesus, J.M.; Danko, A.S.; Fiúza, A.; Borges, M.T. Phytoremediation of salt-affected soils: A review of processes, applicability, and the impact of climate change. *Environ. Sci. Pollut. R.* **2015**, *22*, 6511–6525. [CrossRef]
21. Muhsin, T.M.; Zwiazek, J.J. Colonization with *Hebeloma crustuliniforme* increases water conductance and limits shoot sodium uptake in white spruce (*Picea glauca*) seedlings. *Plant Soil* **2002**, *238*, 217–225. [CrossRef]
22. Begum, N.; Qin, C.; Ahanger, M.A.; Raza, S.; Khan, M.I.; Ashraf, M.; Ahmed, N.; Zhang, L.X. Role of Arbuscular Mycorrhizal Fungi in Plant Growth Regulation: Implications in Abiotic Stress Tolerance. *Front. Plant Sci.* **2019**, *10*, 1068. [CrossRef] [PubMed]
23. Klinsukon, C.; Lumyong, S.; Kuyper, T.W.; Boonlue, S. Colonization by arbuscular mycorrhizal fungi improves salinity tolerance of eucalyptus (*Eucalyptus camaldulensis*) seedlings. *Sci. Rep.* **2021**, *11*, 4362. [CrossRef] [PubMed]
24. Peng, Z.C.; Zulfiqar, T.; Yang, H.C.; Wang, M.; Zhang, F.H. Effect of Arbuscular Mycorrhizal Fungi (AMF) on photosynthetic characteristics of cotton seedlings under saline-alkali stress. *Sci. Rep.* **2024**, *14*, 8633. [CrossRef]
25. Arai, H.; Tamai, Y.; Yajima, T.; Obase, K.; Miyamato, T. Ectomycorrhizal fungal communities associated with *Quercus dentata* in a coastal broadleaf forest. *Mycosphere* **2017**, *8*, 561–567. [CrossRef]
26. Guerrero-Galán, C.; Calvo-Polanco, M.; Zimmermann, S.D. Ectomycorrhizal symbiosis helps plants to challenge salt stress conditions. *Mycorrhiza* **2019**, *29*, 291–301. [CrossRef]
27. Guo, W.; Hao, H.; Zhang, W.H.; Hu, Z.H.; Leng, P.S. Ectomycorrhizal fungi enhance salt tolerance of *Quercus mongolica* by regulating ion balance. *Chin. J. Appl. Ecol.* **2022**, *33*, 3303–3311.
28. Bai, X.N.; Hao, H.; Hu, Z.H.; Leng, P.S. Ectomycorrhizal inoculation enhances the salt tolerance of *Quercus mongolica* seedlings. *Plants* **2021**, *10*, 1790. [CrossRef]
29. Bois, G.; Bigras, F.J.; Bertrand, A.; Piché, Y.; Fung, M.Y.P.; Khasa, D.P. Ectomycorrhizal fungi affect the physiological responses of *Picea glauca* and *Pinus banksiana* seedlings exposed to an NaCl gradient. *Tree Physiol.* **2006**, *26*, 1185–1196. [CrossRef]
30. Tang, M.; Sheng, M.; Chen, H.; Zhang, F.F. In vitro salinity resistance of three ectomycorrhizal fungi. *Soil Biol. Biochem.* **2009**, *41*, 948–953. [CrossRef]
31. Zhou, B.F.; Shi, Y.; Chen, X.Y.; Yuan, S.; Liang, Y.Y.; Wang, B.S. Linked selection, ancient polymorphism, and ecological adaptation shape the genomic landscape of divergence in *Quercus dentata*. *J. Syst. Evol.* **2022**, *60*, 1344–1357. [CrossRef]
32. Hao, H.; Cao, L.; Chen, W.N.; Hu, Z.H.; Leng, P.S. Effects of salt stress on the ion balance and physiological-biochemical characteristics of *Quercus dentata* seedlings. *Acta. Ecol. Sin.* **2020**, *40*, 6897–6904.
33. Qiu, Z.L.; Zhang, M.; Wang, K.F.; Shi, F.C. Vegetation community dynamics during naturalized developmental restoration of *Pinus tabulaeformis* plantation in North warm temperate zone. *J. Plant Ecol.* **2023**, *16*, rtac102. [CrossRef]
34. Martin, F.; Aerts, A.; Ahrén, D.; Brun, A.; Danchin, E.G.J.; Duchaussoy, F.; Gibon, J.; Kohler, A.; Lindquist, E.; Pereda, V.; et al. The genome of *Laccaria bicolor* provides insights into mycorrhizal symbiosis. *Nature* **2008**, *452*, 88–92. [CrossRef] [PubMed]
35. Polanco, M.C.; Zwiazek, J.J.; Voicu, M.C. Responses of ectomycorrhizal American elm (*Ulmus americana*) seedlings to salinity and soil compaction. *Plant Soil* **2008**, *308*, 189–200. [CrossRef]
36. Xu, H.; Kemppainen, M.; El Kayal, W.; Lee, S.H.; Pardo, A.G.; Cooke, J.E.K.; Zwiazek, J.J. Overexpression of *Laccaria bicolor* aquaporin JQ585595 alters root water transport properties in ectomycorrhizal white spruce (*Picea glauca*) seedlings. *New Phytol.* **2015**, *205*, 757–770. [CrossRef]

37. Plett, J.M.; Kemppainen, M.; Kale, S.D.; Kohler, A.; Legué, V.; Brun, A.; Tyler, B.M.; Pardo, A.G.; Martin, F. A secreted effector protein of *Laccaria bicolor* is required for symbiosis development. *Curr. Biol.* **2011**, *21*, 1197–1203. [CrossRef]
38. Shi, N.N.; Guo, C.; Zheng, Y.; Guo, L.D. Effects of ectomycorrhizal fungal identity and diversity on subtropical tree competition. *J. Plant Ecol.* **2017**, *10*, 47–55. [CrossRef]
39. Wang, Z.Q. *Saline Soils in China*, 1st ed.; Science Press: Beijing, China, 1993; pp. 133–139.
40. Phillips, J.M.; Hayman, D.S. Improved procedures for clearing roots and staining parasitic and vesicular-arbuscular mycorrhizal fungi for rapid assessment of infection. *Trans. Br. Mycol. Soc.* **1970**, *55*, 158–160. [CrossRef]
41. Lu, C.M.; Zhang, J.H. Effects of water stress on photosystem II photochemistry and its thermostability in wheat plants. *J. Exp. Bot.* **1999**, *50*, 1199–1206. [CrossRef]
42. Maxwell, K.; Johnson, G.N. Chlorophyll fluorescence—A practical guide. *J. Exp. Bot.* **2000**, *51*, 659–668. [CrossRef] [PubMed]
43. Lichtenthaler, H.K.; Wellburn, A.R. Determinations of total carotenoids and chlorophylls a and b of leaf extracts in different solvents. *Biochem. Soc. T.* **1983**, *11*, 591–592. [CrossRef]
44. Mao, P.L.; Zhang, Y.J.; Cao, B.H.; Guo, L.M.; Shao, H.B.; Cao, Z.Y.; Jiang, Q.K.; Wang, X. Effects of salt stress on eco-physiological characteristics in *Robinia pseudoacacia* based on salt-soil rhizosphere. *Sci. Total Environ.* **2016**, *568*, 118–123. [CrossRef] [PubMed]
45. Patel, N.T.; Gupta, A.; Pandey, A.N. Strong positive growth responses to salinity by Ceriops tagal, a commonly occurring mangrove of the Gujarat coast of India. *AoB. Plants* **2010**, *2010*, pjq011. [CrossRef]
46. Horie, T.; Hauser, F.; Schroeder, J.I. HKT transporter-mediated salinity resistance mechanisms in Arabidopsis and monocotcrop plants. *Trends Plant Sci.* **2009**, *14*, 660–668. [CrossRef]
47. Hammer, E.C.; Nasr, H.; Pallon, J.; Olsson, P.A.; Wallander, H. Elemental composition of arbuscular mycorrhizal fungi at high salinity. *Mycorrhiza* **2011**, *21*, 117–129. [CrossRef]
48. Heng, T.; He, X.L.; Yang, G.; Tian, L.J.; Li, F.D.; Yang, L.L.; Zhao, L.; Feng, Y.; Xu, X. Growth and nitrogen status of cotton (*Gossypium hirsutum* L.) under salt stress revealed using 15N-labeled fertilizer. *J. Plant Ecol.* **2022**, *15*, 1213–1226. [CrossRef]
49. Pardo, J.M. Biotechnology of water and salinity stress tolerance. *Curr. Opin. Biotech.* **2010**, *21*, 185–196. [CrossRef]
50. Li, J.M.; Hu, L.P.; Zhang, L.; Pan, X.B.; Hu, X.H. Exogenous spermidine is enhancing tomato tolerance to salinity–alkalinity stress by regulating chloroplast antioxidant system and chlorophyll metabolism. *BMC Plant Biol.* **2015**, *15*, 303. [CrossRef]
51. Akram, M. Effects of nitrogen application on chlorophyll content, water relations, and yield of maize hybrids under saline conditions. *Commun. Soil Sci. Plan.* **2014**, *45*, 1336–1356. [CrossRef]
52. Sudhir, P.; Murthy, S.D.S. Effects of salt stress on basic processes of photosynthesis. *Photosynthetica* **2004**, *42*, 481–486. [CrossRef]
53. Bose, J.; Munns, R.; Shabala, S.; Gilliham, M.; Pogson, B.; Tyerman, S. Chloroplast function and ion regulation in plants growing on saline soils: Lessons from halophytes. *J. Exp. Bot.* **2017**, *68*, 3129–3143. [CrossRef]
54. Tombesi, S.; Nardini, A.; Frioni, T.; Soccolini, M.; Zadra, C.; Farinelli, D.; Poni, S.; Palliotti, A. Stomatal closure is induced by hydraulic signals and maintained by ABA in drought-stressed grapevine. *Sci. Rep.* **2015**, *5*, 12449. [CrossRef] [PubMed]
55. Zahra, N.; Al Hinai, M.S.; Hafeez, M.B.; Rehman, A.; Wahid, A.; Siddique, K.H.M.; Farooq, M. Regulation of photosynthesis under salt stress and associated tolerance mechanisms. *Plant Physiol. Bioch.* **2022**, *178*, 55–69. [CrossRef] [PubMed]
56. Gururani, M.A.; Venkatesh, J.; Tran, L.P. Regulation of photosynthesis during abiotic stress-induced photoinhibition. *Mol. Plant* **2015**, *8*, 1304–1320. [CrossRef] [PubMed]
57. Humeed, A.; Ahmed, M.Z.; Hussain, T.; Aziz, I.; Ahmad, N.; Gul, B.; Nielsen, B.L. Effects of salinity stress on chloroplast structure and function. *Cells* **2021**, *10*, 2023. [CrossRef]
58. Genre, A.; Lanfranco, L.; Perotto, S.; Bonfante, P. Unique and common traits in mycorrhizal symbioses. *Nat. Rev. Microbiol.* **2020**, *18*, 649–660. [CrossRef]
59. Bahadur, A.; Batool, A.; Nasir, F.; Jiang, S.J.; Qin, M.S.; Zhang, Q.; Pan, J.B.; Liu, Y.J.; Feng, H.Y. Mechanistic insights into arbuscular mycorrhizal fungi-mediated drought stress tolerance in plants. *Int. J. Mol. Sci.* **2019**, *20*, 4199. [CrossRef]
60. Wang, R.Z.; Chen, L.; Bai, Y.G.; Xiao, C.W. Seasonal dynamics in resource partitioning to growth and storage in response to drought in a perennial rhizomatous grass, *Leymus chinensis*. *J. Plant Growth Regul.* **2008**, *27*, 39–48. [CrossRef]
61. Al-Khaliel, A.S. Effect of salinity stress on mycorrhizal association and growth response of peanut infected by *Glomus mosseae*. *Plant Soil Environ.* **2010**, *56*, 318–324. [CrossRef]
62. Tilak, K.V.B.R.; Ranganayaki, N.; Manoharachari, C. Synergistic effects of plant-growth promoting rhizobacteria and Rhizobium on nodulation and nitrogen fixation by pigeonpea (*Cajanus cajan*). *Eur. J. Soil Sci.* **2006**, *57*, 67–71. [CrossRef]
63. Douglas, A.E. Conflict, cheats and the persistence of symbioses. *New Phytol.* **2008**, *177*, 849–858. [CrossRef] [PubMed]
64. Bonfante, P.; Genre, A. Mechanisms underlying beneficial plant–fungus interactions in mycorrhizal symbiosis. *Nat. Commun.* **2010**, *1*, 48. [CrossRef] [PubMed]
65. Kiers, E.T.; Duhamel, M.; Beesetty, Y.; Mensah, J.A.; Franken, O.; Verbruggen, E.; Fellbaum, C.R.; Kowalchuk, G.A.; Hart, M.M.; Bago, A. Reciprocal rewards stabilize cooperation in the mycorrhizal symbiosis. *Science* **2011**, *333*, 880–882. [CrossRef] [PubMed]
66. Johnson, N.C.; Graham, J.H.; Smith, F.A. Functioning of mycorrhizal associations along the mutualism-parasitism continuum. *New Phytol.* **1997**, *135*, 575–585. [CrossRef]

67. Kaldorf, M.; Koch, B.; Rexer, K.H.; Kost, G.; Varma, A. Patterns of interaction between *Populus* Esch5 and *Piriformospora indica*: A transition from mutualism to antagonism. *Plant Biol.* **2005**, *7*, 210–218. [CrossRef]
68. Bois, G.; Bertrand, A.; Piche, Y.; Fung, M.; Khasa, D.P. Growth, compatible solute and salt accumulation of five mycorrhizal fungal species grown over a range of NaCl concentrations. *Mycorrhiza* **2006**, *16*, 99–109. [CrossRef]
69. Flowers, T.J.; Munns, R.; Colmer, T.D. Sodium chloride toxicity and the cellular basis of salt tolerance in halophytes. *Ann. Bot.* **2015**, *115*, 419–431. [CrossRef]
70. Li, Z.P.; Zhang, W.H.; Cui, Y.C. Effects of NaCl and Na2CO3 stresses on seed germination and seedling growth of *Quercus variabilis*. *Acta. Ecol. Sin.* **2015**, *35*, 742–751.
71. Zhang, Z.; Wang, M.J.; Zhang, X.J.; Wang, W.B.; He, X.F.; Wang, R.; Wang, C.; Leng, P.S.; Mladenov, P.; Wang, W.H.; et al. Genome-wide identification and expression analysis of the ZIP gene family in *Quercus dentata*. *Curr. Plant Biol.* **2023**, *35–36*, 100291. [CrossRef]
72. Zhao, Z.P.; Xie, B.; Wang, X.N.; Wang, Q.; Guo, C.; Zhang, F.; Wang, H.R.; Zhang, R.J.; Zhang, C. Adaptive growth strategies of *Quercus dentata* to drought and nitrogen enrichment: A physiological and biochemical perspective. *Front. Plant Sci.* **2024**, *15*, 1479563. [CrossRef] [PubMed]
73. Liese, R.; Lübbe, T.; Albers, N.W.; Meier, I.C. The mycorrhizal type governs root exudation and nitrogen uptake of temperate tree species. *Tree Physiol.* **2018**, *38*, 83–95. [CrossRef] [PubMed]
74. Hong, S.B.; Piao, S.L.; Chen, A.P.; Liu, Y.W.; Liu, L.L.; Peng, S.S.; Sardans, J.; Sun, Y.; Peñuelas, J.; Zeng, H. Afforestation neutralizes soil pH. *Nat. Commun.* **2018**, *9*, 520. [CrossRef] [PubMed]
75. Yuan, C.X.; Wu, F.Z.; Peng, Y.; Wu, Q.Q.; Zhu, G.Q.; Zhao, Z.M.; Wang, Y.Q.; An, N.N.; Ni, X.Y.; Yue, K. Pain or gain: The dual role of afforestation effects on soil pH at the global scale. *Plant Soil* **2023**, *493*, 617–628. [CrossRef]
76. Huang, Y.; Mónica, C.P.; Michael, D.M.; Janusz, J.Z. Responses of ectomycorrhizal *Populus tremuloides* and *Betula papyrifera* seedlings to salinity. *Environ. Exp. Bot.* **2008**, *62*, 357–363.
77. Qin, Y.; Pan, X.Y.; Kubicek, C.; Druzhinina, I.; Chenthamara, K.; Labbé, J.; Yuan, Z.L. Diverse plant-associated pleosporalean fungi from saline areas: Ecological tolerance and nitrogen-status dependent effects on plant growth. *Front. Microbiol.* **2017**, *8*, 158. [CrossRef]
78. Kernaghan, G.; Hambling, B.; Fung, M.; Khasa, D.J.R.E. In vitro selection of boreal ectomycorrhizal fungi for use in reclamation of saline-alkaline habitats. *Restor. Ecol.* **2002**, *10*, 43–51. [CrossRef]

Disclaimer/Publisher's Note: The statements, opinions and data contained in all publications are solely those of the individual author(s) and contributor(s) and not of MDPI and/or the editor(s). MDPI and/or the editor(s) disclaim responsibility for any injury to people or property resulting from any ideas, methods, instructions or products referred to in the content.

MDPI AG
Grosspeteranlage 5
4052 Basel
Switzerland
Tel.: +41 61 683 77 34

Forests Editorial Office
E-mail: forests@mdpi.com
www.mdpi.com/journal/forests



Disclaimer/Publisher's Note: The title and front matter of this reprint are at the discretion of the Guest Editors. The publisher is not responsible for their content or any associated concerns. The statements, opinions and data contained in all individual articles are solely those of the individual Editors and contributors and not of MDPI. MDPI disclaims responsibility for any injury to people or property resulting from any ideas, methods, instructions or products referred to in the content.





Academic Open
Access Publishing

mdpi.com

ISBN 978-3-7258-8992-1